รายงานวิจัยฉบับสมบูรณ์

ทุนส่งเสริมกลุ่มวิจัย สกว.

ชื่อโครงการ

การประยุกต์ใช้โปรตีโอมิกส์ในการศึกษาโรคที่พบบ่อยในเมืองไทย

DISEASE PROTEOMICS: APPLICATIONS TO COMMON DISEASES IN THAILAND

โดย

ศาสตราจารย์นายแพทย์ วิศิษฏ์ ทองบุญเกิด

หน่วยโปรตีโอมิกส์การแพทย์ สถานส่งเสริมการวิจัย

คณะแพทยศาสตร์ศิริราชพยาบาล มหาวิทยาลัยมหิดล

เสร็จสิ้นโครงการเมื่อ เดือนสิงหาคม พ.ศ. 2556

(ระยะเวลาดำเนินการตั้งแต่วันที่ 1 กันยายน 2553 ถึงวันที่ 31 สิงหาคม 2556)

สัญญาเลขที่ RTA5380005

รายงานวิจัยฉบับสมบูรณ์

ทุนส่งเสริมกลุ่มวิจัย สกว.

ชื่อโครงการ

การประยุกต์ใช้โปรตีโอมิกส์ในการศึกษาโรคที่พบบ่อยในเมืองไทย

DISEASE PROTEOMICS: APPLICATIONS TO COMMON DISEASES IN THAILAND

โดย

ศาสตราจารย์นายแพทย์ วิศิษฏ์ ทองบุญเกิด

หน่วยโปรตีโอมิกส์การแพทย์ สถานส่งเสริมการวิจัย

คณะแพทยศาสตร์ศิริราชพยาบาล มหาวิทยาลัยมหิดล

สนับสนุนโดยสำนักงานกองทุนสนับสนุนการวิจัย

(ความเห็นในรายงานนี้เป็นความเห็นของผู้วิจัย สกว. ไม่จำเป็นต้องเห็นด้วยเสมอไป)

สารบัญ

	หน้า
บทคัดย่อ	1
Abstract	1
หน้าสรุปโครงการ (Executive Summary)	2
ชื่อโครงการ	2
ทีมวิจัย	2
ความสำคัญและที่มาของปัญหา	3
วัตถุประสงค์หลัก	3
โครงการย่อย	3
สรุปผลการดำเนินงานวิจัยในแต่ละช่วง 6 เดือนตลอดระยะเวลาโครงการ 3 ปี	5
ผลผลิต/ผลลัพธ์ (Output/Outcome) ที่ได้จากโครงการ	7
เนื้อหางานวิจัย	9
Materials and Instruments	9
Common Methods for All Subprojects	9
Specific Methods for Individual Subprojects	11
ผลผลิต/ผลลัพธ์ (Output/Outcome) ที่ได้จากโครงการ	18
ผลงานตีพิมพ์ (Publications)	18
เครือข่ายวิจัย (Networking)	24
การผลิตนักวิจัยรุ่นใหม่ (Training)	25
การนำผลงานไปใช้ประโยชน์ในเชิงพาณิชย์ เชิงสาธารณะ หรือเชิงนโยบาย	25
วิทยากรรับเชิญในการประชุมที่สำคัญระดับชาติและระดับนานาชาติ	26
รางวัลที่ได้รับระหว่างรับทุนส่งเสริมกลุ่มวิจัย	31
นักวิจัยในโครงการที่ได้รับรางวัลหรือได้รับทุนวิจัยอื่นในระหว่างที่รับทุนส่งเสริมกลุ่มวิจัย	32
รายชื่อกลุ่มวิจัยและสถานภาพปัจจุบัน	35
ภาคผนวก	40
ผลงานตีพิมพ์ในวารสารวิชาการระดับนานาชาติและหนังสือ	40

บทคัดย่อ

โปรตีโอมิกส์ (การวิเคราะห์ชนิด ปริมาณ และหน้าที่ของโปรตีนหลายชนิดพร้อมกันอย่างเป็นระบบ) เป็นวิทยาศาสตร์แขนงใหม่ที่สำคัญและแพร่หลายอย่างรวดเร็วในยุคหลังจีโนมในการนำไปศึกษาถึงปัญหาที่สำคัญทางชีววิทยาและทางการแพทย์ เป้าหมายสูงสุดของการประยุกต์ใช้โปรตีโอมิกส์ คือ 1) เพื่อเข้าใจถึงชีววิทยาและสรีรวิทยาของเซลล์ เนื้อเยื่อ และอวัยวะต่างๆ ในภาวะปกติ 2) เพื่อเข้าใจถึงกลไกการเกิดและพยาธิสรีรวิทยาของโรคต่างๆ 3) เพื่อค้นหาตัวบ่งชี้โรคและเป้าการรักษาใหม่ และ 4) เพื่อค้นหายาและวัคซีนชนิดใหม่ โครงการนี้จึงประยุกต์เอาเทคโนโลยีทางด้านโปรตีโอมิกส์มาศึกษาโรคที่พบบ่อยในประเทศไทย ได้แก่ โรคนิ่วในไต เบาหวาน ธาลัสซีเมีย และไตอักเสบลูปัสในคน รวมทั้งโรคหัวเหลืองในกุ้งซึ่งเป็นสัตว์เศรษฐกิจที่สำคัญของไทย ข้อมูลและองค์ความรู้ที่ได้จากโครงการนี้อาจนำมาสู่ความรู้ความเข้าใจโรคที่ดีขึ้น การดูแลรักษาและป้องกันโรคที่มีประสิทธิภาพมากขึ้น โครงการนี้ยังได้ริเริ่มการสร้างเครือข่ายวิจัยทางด้านโปรตีโอมิกส์ภายในประเทศอีกด้วย นอกจากนี้โครงการ/เครือข่ายวิจัยนี้ยังได้สร้าง/ผลิตนักวิจัยรุ่นใหม่จำนวนหนึ่งที่มีศักยภาพในด้านการวิเคราะห์เชิงโปรตีโอมิกส์อีกด้วย

คำหลัก

1) โปรตีโอมิกส์ 2) โปรตีน 3) กลไกการเกิดโรค 4) ตัวบ่งชี้ 5) โรคนิ่วในไต 6) เบาหวาน 7) ธาลัสซีเมีย 8) ลูปัส 9) โรคหัวเหลือง

Abstract

Proteomics (systematic analysis of proteins for their identities, quantities and functions) has recently become an important field of modern sciences in the post-genomic era. It has been widely used to address many biological and medical problems. Applications of proteomics will ultimately lead to: 1) better understanding of biology and physiology of normal cells, tissues or organs; 2) unraveling the complexity of pathogenic mechanisms and pathophysiology of diseases; 3) identification of novel biomarkers and new therapeutic targets; and finally 4) drug and vaccine discovery. This project has applied proteomics to investigate common diseases in Thailand including kidney stone disease, diabetes mellitus, thalassemia and lupus nephritis in humans, as well as yellowhead disease in shrimps. The data and knowledge obtained from this project may lead to better understanding, proper management, and effective prevention of these common diseases. In addition, this project has initiated collaborative efforts and networking among scientists and clinicians in Thailand who are interested in proteomics. Moreover, this project/network has generated a number of young Thai scientists who are skillful in proteomic analysis.

Keywords

1) Proteomics 2) Proteins 3) Disease mechanisms 4) Biomarkers 5) Kidney stone 6) Diabetes 7) Thalassemia 8) Lupus 9) Yellowhead disease

หน้าสรุปโครงการ (Executive Summary)

1. ชื่อโครงการ

(ภาษาไทย) **การประยุกต์ใช้โปรตีโอมิกส์ในการศึกษาโรคที่พบบ่อยในเมืองไทย**

(ภาษาอังกฤษ) **Disease Proteomics: Applications to Common Diseases in Thailand**

2. ทีมวิจัย

2.1. ที่ปรึกษาโครงการ

ศ.ดร.มรว. ชิษณุสรร สวัสดิวัตน์ (Prof.MR. Jisnuson Svasti, PhD)

(คณะวิทยาศาสตร์ มหาวิทยาลัยมหิดล และสถาบันวิจัยจุฬาภรณ์)

2.2. หัวหน้าโครงการ

นพ. วิศิษฎ์ ทองบุญเกิด (Visith Thongboonkerd, MD)

(สถานส่งเสริมการวิจัย คณะแพทยศาสตร์ศิริราชพยาบาล มหาวิทยาลัยมหิดล)

2.3. ผู้ร่วมโครงการ

2.3.1. รศ.ดร. รัชนีกร กัลล์ประวิทธ์ (Assoc.Prof. Ruchaneekorn Kalpravidh, PhD)

(ภาควิชาชีวเคมี คณะแพทยศาสตร์ศิริราชพยาบาล มหาวิทยาลัยมหิดล)

2.3.2. รศ.นพ. ยิ่งยศ อวิหิงสานนท์ (Assoc.Prof. Yingyos Avihingsanon, MD)

(ภาควิชาอายุรศาสตร์ คณะแพทยศาสตร์ จุฬาลงกรณ์มหาวิทยาลัย)

2.3.3. รศ.ดร.พญ. ณัฏฐิยา หิรัญกาญจน์ (Assoc.Prof. Nattiya Hirankarn, MD, PhD)

(ภาควิชาจุลชีววิทยา คณะแพทยศาสตร์ จุฬาลงกรณ์มหาวิทยาลัย)

2.3.4. รศ.นพ. วิทูรย์ ประสงค์วัฒนา (Assoc.Prof. Vitoon Prasongwatana, MD)

(ภาควิชาชีวเคมี คณะแพทยศาสตร์ มหาวิทยาลัยขอนแก่น)

2.3.5. รศ.ดร. ชาติชาย กฤตนัย (Assoc.Prof. Chartchai Krittanai, PhD)

(สถาบันชีววิทยาศาสตร์โมเลกุล มหาวิทยาลัยมหิดล)

2.3.6. ผศ.ดร.นพ. ชัชวาลย์ ศรีสวัสดิ์ (Assist.Prof. Chatchawan Srisawat, MD, PhD)

(ภาควิชาชีวเคมี คณะแพทยศาสตร์ศิริราชพยาบาล มหาวิทยาลัยมหิดล)

2.3.7. นพ.ดร. สมชาย ชุติพงศ์ธเนศ (Somchai Chutipongtanate, MD, PhD)

(สถานส่งเสริมการวิจัย คณะแพทยศาสตร์ศิริราชพยาบาล มหาวิทยาลัยมหิดล)

2.3.8. ดร. รัตติยาภรณ์ กัลยา (Rattiyaporn Kanlaya, PhD)

(สถานส่งเสริมการวิจัย คณะแพทยศาสตร์ศิริราชพยาบาล มหาวิทยาลัยมหิดล)

2.3.9. ดร.พญ. จารุภา สูงสถิตานนท์ (Jarupa Soongsathitanon, MD, PhD)

(ภาควิชาวิทยาภูมิคุ้มกัน คณะแพทยศาสตร์ศิริราชพยาบาล มหาวิทยาลัยมหิดล)

2.3.10. ดร. ราตรี ทวิชากรตระกูล (Ratree Tavichakorntrakool, PhD)

(คณะเทคนิคการแพทย์ มหาวิทยาลัยขอนแก่น)

2.3.11. นาย ศักดิเทพ ไชยฤทธิ์ (Sakdithep Chaiyarit, PhD Candidate)

(สถานส่งเสริมการวิจัย คณะแพทยศาสตร์ศิริราชพยาบาล มหาวิทยาลัยมหิดล)

3. ความสำคัญและที่มาของปัญหา

After the completion of the Human Genome Project, there was an immediate flooding of human genome information obtained from the high-throughput genomic approach. This big leap has led to the development and/or improvement of several biotechnologies to utilize the genomic information to explain biology and (patho)physiology of cells, tissue or organs during normal and abnormal (diseased) states. One of such post-genomic studies is proteomics, which can simultaneously examine a large number (or a set) of proteins encoded by the genome (proteome). Proteomics has been recently defined as “the systemic analysis of proteins for their identity, quantity and function”. With its high-throughput capability and other advantages that overcome limitations in conventional methods, proteomics has become one of the most powerful tools for biomedical research. The ultimate goals of a classical proteomics study include: 1) better understanding of biology and physiology of normal cells, tissues or organs; 2) unraveling the complexity of pathogenic mechanisms and pathophysiology of diseases; 3) identification of novel biomarkers and new therapeutic targets; and finally 4) drug and vaccine discovery. This project applied proteomics to investigate common diseases in Thailand including kidney stone disease, diabetes mellitus, thalassemia and lupus nephritis in humans, as well as yellowhead disease in shrimps that causes a remarkable loss of production and export value for our country.

4. วัตถุประสงค์หลัก

4.1. To establish a proteomics network in Thailand.

4.2. To apply proteomic technologies to the study of common diseases in Thailand including kidney stone disease, diabetes mellitus, thalassemia and lupus nephritis in humans, as well as yellowhead disease in shrimps.

4.3. To offer training opportunities on proteomic analysis for PhD and MSc students.

5. โครงการย่อย

5.1. Proteomic analysis of changes in mitochondrial proteome in distal renal tubular cells induced by COM crystal adhesion

(PI: Dr. Visith Thongboonkerd)

Specific Aim(s):

- To examine alterations in mitochondrial proteome in renal tubular cells induced by CaOx crystal adhesion.

5.2. Proteomic identification of COM crystal-binding proteins on apical membranes of distal renal tubular cells

(PI: Dr. Visith Thongboonkerd)

Specific Aim(s):

- To globally identify COM crystal-binding proteins on apical membranes of distal renal tubular cells.

5.3. Characterizations of secretome from distal renal tubular cells and its COM-crystal binding components

(PI: Dr. Somchai Chutipongtanate)

Specific Aim(s):

- To globally identify secretome from distal renal tubular cells and its COM-crystal binding components.

5.4. Insights into preventive mechanisms of green tea extract against oxalate-induced renal fibrosis: a proteomics approach

(PI: Dr. Rattiyaporn Kanlaya)

Specific Aim(s):

- To characterize changes in distal renal tubular cells induced by oxalate that could be reversible by green tea catechin treatment.

5.5. Evaluation of altered proteome in macrophages in response to basolateral secretion of renal tubular epithelial cells treated with COM crystals

(PI: Sakdithep Chaiyarit)

Specific Aim(s):

- To define altered proteome profile of monocytes and macrophages in response to basolateral secretion of COM crystal treated renal tubular epithelial cells.

5.6. Proteomic analysis of Trimethoprim/Sulfamethoxazole-resistance *Escherichia coli* isolated from kidney stone

(PI: Dr. Ratree Tavichakorntrakool & Dr. Vitoon Prasongwatana)

Specific Aim(s):

- To identify differentially expressed proteins in Trimethoprim/Sulfamethoxazole-resistance vs. Trimethoprim/Sulfamethoxazole-susceptible *Escherichia coli* isolated from kidney stone.

5.7. Biology of interactions between natural killer (NK) cells and dendritic cells in the pathogenesis of atherosclerosis in diabetes

(PI: Dr. Jarupa Soongsathitanon)

Specific Aim(s):

- To determine alterations of dendritic cell and NK cellular proteomes in high glucose environment.

5.8. Proteomics of lupus nephritis: A biomarker validation project

(PI: Dr. Yingyos Avihingsanon & Dr. Nattiya Hirankarn)

Specific Aim(s):

- To validate selected biomarkers in a well-designed clinical trial. The selected proteins discovered from our previous study will be validated in an independent set of samples. There will be two groups of patients including responders and non-responders to the treatment. All these patients were from a randomized-controlled multi-center clinical trial in Thailand.
- To define a protein map of filtered plasma from severe lupus patients. A preliminary protocol will be developed from 2-D PAGE followed by MS/MS approach.

5.9. Changes in plasma proteome of β-thalassemia/HbE patients treated with anti-oxidant cocktail

(PI: Dr. Ruchaneekorn Kalpravidh & Dr. Chatchawan Srisawat)

Specific Aim(s):

- To identify altered plasma proteins in β-thalassemia/HbE patients after anti-oxidant cocktail treatment.

5.10. Development of 2-D Blue Native PAGE for protein interaction analysis in viral infected shrimp hemocytes

(PI: Dr. Chartchai Krittanai)

Specific Aim(s):

- To develop 2-D Blue Native PAGE for an analysis of protein interaction in shrimp semi-granular cells during yellowhead disease.

6. สรุปผลการดำเนินงานวิจัยในแต่ละช่วง 6 เดือนตลอดระยะเวลาโครงการ 3 ปี

Period	Research activities	Outputs
Month 1-6	- Clinical sample collection and preparation. - Cultivation of various cells. - Cell intervention/treatment. - Isolation of apical membranes. - Isolation of mitochondria.	- Kidney stones, urine, and blood were collected from patients. - Various cells were maintained and ready for subsequent experiments. - The cells were treated with various conditions for subsequent analyses. - Apical membranes were successfully isolated from the cells. - Mitochondria were successfully isolated from the cells.
Month 7-12	- Validation of the experimental models. - Isolation of *E. coli* from kidney stones. - TMP/SMX susceptibility test. - 2-D PAGE. - Spot matching and intensity analysis. - Preparation and submission of 1-2 manuscripts. - First annual meeting.	- Various experimental models were successfully validated and ready for proteomic analysis. - *E. coli* isolates were identified and ready for subsequent tests. - TMP/SMX susceptibility was complete. - Some 2-D gel images were obtained and analyzed. - Spot matching and intensity analysis were done on some samples or entirely in a couple of subprojects. - A number of manuscripts were submitted and published in international journals with Impact Factor. - The first annual meeting was organized.
Month 13-18	- 2-D PAGE (cont.). - Spot matching and intensity analysis (cont.).	- More 2-D gel images were obtained and analyzed.

	- Optimization of 2-D Blue Native PAGE. - Mass spectrometric analyses. - Preparation and submission of 1-2 more manuscripts.	- Spot matching and intensity analysis were done on more samples or entirely in more subprojects. - 2-D Blue Native PAGE was tried. - Some protein spots/bands were successfully identified. - A number of manuscripts were submitted and published in international journals with Impact Factor.
Month 19-24	- 2-D PAGE (cont.). - Spot matching and intensity analysis (cont.). - Optimization of 2-D Blue Native PAGE (cont.). - Mass spectrometric analyses (cont.). - Validation of proteomic data by Western blot analysis or ELISA. - Preparation and submission of 1-3 more manuscripts. - Second annual meeting.	- All 2-D gel images were obtained and analyzed. - Spot matching and intensity analysis were done on all samples and entirely in all subprojects. - 2-D Blue Native PAGE were optimized. - More protein spots/bands were successfully identified. - Some proteomic data were successfully confirmed by Western blot analysis or ELISA. - A number of manuscripts were submitted and published in international journals with Impact Factor. - The second annual meeting was organized.
Month 25-30	- Mass spectrometric analyses (cont.). - Validation of proteomic data by Western blot analysis or ELISA (cont.). - Analysis of protein interactions or networks based on the identified proteins. - Preparation and submission of 1-3 more manuscripts.	- More protein spots/bands were successfully identified. - More proteomic data were successfully confirmed by Western blot analysis or ELISA. - Networks of protein interactions based on the identified proteins were obtained. - A number of manuscripts were submitted and published in international journals with Impact Factor.
Month 31-36	- Validation of urinary biomarker candidates in LN patients in a large number of independent samples. - Summary of all data. - Preparation and submission of 2-4 more manuscripts - Third annual meeting	- Urinary biomarkers for LN were validated. - All the data were summarized. - A number of manuscripts were submitted and published in international journals with Impact Factor. - The third annual meeting was organized.

7. ผลผลิต/ผลลัพธ์ (Output/Outcome) ที่ได้จากโครงการ

7.1. Publications

A total of 30 research articles and 1 book chapter were published in high-impact international journals/book after the completion of the project. These include:

- 5 articles in Journal of Proteome Research (2011 IF = 5.113) (2012 IF = 5.056) (2013 IF = 5.001)
- 4 articles in Journal of Proteomics (2011 IF = 4.878) (2012 IF = 4.088) (2013 IF = 3.929)
- 3 articles in Proteomics Clinical Applications (2011 IF = 1.970) (2012 IF = 2.926)
- 2 articles in Molecular BioSystems (2011 IF = 3.534) (2012 IF = 3.350)
- 2 articles in Talanta (2012 IF = 3.498)
- 2 articles in Biochemical and Biophysical Research Communications (2011 IF = 2.484) (2012 IF = 2.406)
- 1 article in Scientific Reports (2013 IF = 5.078)
- 1 article in Clinical Science (2013 IF = 4.859)
- 1 article in Nephrology Dialysis Transplantation (2012 IF = 3.371)
- 1 article in European Journal of Clinical Investigation (2012 IF = 3.365)
- 1 article in Journal of Biological Inorganic Chemistry (2013 IF = 3.164)
- 1 article in Clinical Chemistry and Laboratory Medicine (2012 IF = 3.009)
- 1 article in European Journal of Pharmacology (2012 IF = 2.592)
- 1 article in World Journal of Gastroenterology (2013 IF = 2.433)
- 1 article in Annals of Hematology (2013 IF = 2.396)
- 1 article in Microbial Pathogenesis (2011 IF = 1.938)
- 1 article in Monoclonal Antibodies in Immunodiagnosis and Immunotherapy (2013 IF = 0.244)
- 1 article in Journal of Analytical Science and Technology (ยังไม่มี IF)
- 1 chapter in an international book series, Contributions to Nephrology

7.2. Proteomics Network in Thailand

This project is a great opportunity to create a proteomics network in Thailand. This network has been joined by several scientists and clinicians, as well as their associates and students who are interested in proteome science. This network offers collaboration, consultation and discussion on trouble shootings in proteomics to enhance the rapid progress of proteomics in Thailand. In practical, this network has regular activities, at least as an annual meeting, as part of the annual meeting of the Protein Society of Thailand.

7.3. International Proteomics Networks

7.3.1. Human Kidney and Urine Proteome Project (HKUPP), Human Proteome Organisation (HUPO)

HKUPP is an international collaborative network officially approved by the HUPO as one of its initiatives. The mission of HKUPP is to encourage and facilitate applications of proteomics to better understand renal (patho)physiology and to define urinary biomarkers for kidney diseases and related

disorders. Dr. Visith is a key member of HKUPP responsible for several projects, especially determination of standards and guidelines for kidney and urine proteome analyses.

7.3.2. European Network for Kidney and Urine Proteomics (EuroKUP)

EuroKUP has been established after HKUPP and focuses its activities within European countries. From approximately 50 participating PIs from almost all European countries, Dr. Visith is one among four members from outside Europe and has joined many EuroKUP projects. He is also responsible for determination of standards and guidelines for kidney and urine proteome analyses.

7.3.3. Institute of Biological Chemistry and Genomic Research Center, Academia Sinica, Taipei, Taiwan (Prof. Shui-Tein Chen, PhD)

With a long-term collaboration, Prof. Chen is one of the key members in our network that are always helpful. Not only us, Prof. Chen has collaborated with many Thai scientists from various institutions.

7.3.4. Department of Medicine I, Charles University Medical School, Pilsen, Czech Republic

7.3.5. The University of Hong Kong, Hong Kong

7.3.6. Mosaiques Diagnostics and Therapeutics AG, Hannover, Germany

7.3.7. Nephrology and Rheumatology UMG, Georg-August University Goettingen, Germany

7.3.8. Biomedical Research Foundation Academy of Athens, Greece

7.3.9. Institute of Nephrology, Niigata University Graduate School of Medical and Dental Sciences, Niigata, Japan

7.3.10. Institut National de la Santé et de la Recherche Médicale (INSERM), U858, Toulouse, France and Université Toulouse III Paul-Sabatier, Institut de Médecine Moléculaire de Rangueil, Equipe n°5, IFR150, Toulouse, France

7.3.11. University of Alabama at Birmingham, Birmingham, Alabama, USA

7.4. Training

This study has offered training opportunities on proteomic analysis for a total of 2 post-docs, 7 research associates, 11 PhD students, and 8 MSc students. For all of the students, their thesis works were related to disease proteomics. They have obtained basic knowledge of methodologies in quantitative and qualitative proteomics and biochemical techniques to examine pathogenic mechanisms of diseases. Specifically, they are able to perform cell culture, cellular fractionation, sample preparation for proteomic analysis, 2-D PAGE, spot matching, quantitative intensity analysis, protein identification by mass spectrometry, and 1-D/2-D Western blotting. These knowledge and skills will make them be able to perform other proteomic studies independently. These really are opportunities to make this new biotechnology more widely used and applied in other areas with a high efficacy.

เนื้อหางานวิจัย

1. Materials and Instruments

- MDCK (Madin-Darbin Canine Kidney) cells, which represent renal tubular epithelial cells of distal nephron, human monocytes (U937), and macrophage cells (PMA-activated U937 cells)
- Permeable polycarbonate membrane inserts
- Scanning electron microscope
- Transmission electron microscope
- Flow cytometer
- Laser scanning confocal/fluorescence microscope
- 2-D PAGE apparati
- Typhoon laser scanner
- 2-D image analysis software
- Q-TOF mass spectrometer

2. Common Methods for All Subprojects

2.1. Protein extraction

For cellular proteome analysis, the cells were harvested and washed three times with PBS. Cell pellets were resuspended in a 2-D lysis buffer containing 7 M urea, 2 M thiourea, 4% 3-[(3-cholamidopropyl) dimethyl-ammonio]-1-propanesulfonate (CHAPS), 120 mM dithiothreitol (DTT), 2% ampholytes (pH 3-10) and 40 mM Tris-HCl, and further incubated at 4°C for 30 min. Unsolubilized nuclei, cell debris, and particulate matters were removed by centrifugation at 12,000 rpm for 2 min. Protein concentrations were determined using the Bradford method.

For urine and secretome analysis, proteins in the urine and culture supernatants were subjected to precipitation using organic solvents. The recovered pellets were then resuspended in 2-D lysis buffer as aforementioned. Protein concentrations were determined using the Bradford method.

2.2. 2-D PAGE

Immobilized pH gradient (IPG) strips, nonlinear pH 3-10 (GE Healthcare), were rehydrated overnight with 100-200 µg proteins using rehydration buffer containing 8 M urea, 2% CHAPS, 0.01 M DTT, 2% ampholytes and bromophenol blue. The first dimensional separation (IEF) were then performed in Ettan IPGphor II Isoelectric Focusing Unit (GE Healthcare) at 20ºC, using stepwise mode to reach 9,083 volt.hours. After completion of the IEF, the samples were equilibrated with a buffer containing 6 M urea, 130 mM DTT, 30% glycerol, 112 mM Tris base, 4% sodium dodecyl sulfate (SDS), 0.002% bromophenol blue and acetic acid, and then with another buffer containing 6 M urea, 135 mM iodoacetamide, 30% glycerol, 112 mM Tris base, 4% SDS, 0.002% bromophenol blue and acetic acid. The focused IPG strips were then transferred onto 12% acrylamide slab gel and the second dimensional separation was performed in Hoefer miniVE system (GE Healthcare) with the current of 20 µA/gel for 1.5 h. The resolved

protein spots were then visualized by Coomassie Brilliant Blue or fluorescence dyes and 2-D gel images were captured by Typhoon laser scanner (GE Healthcare).

2.3. Quantitative intensity analysis

Image Master 2D Platinum (GE Healthcare) software was used for matching and analysis of protein spots on gels. A reference gel was created from an artificial gel combining all of the spots presenting in different gels into one image. The intensity volume in pixel unit (or summation of optical densities of each spot), which represented protein concentration or the amount of protein per spot, was used for quantification. Average mode of background subtraction was performed to normalize the intensity volume of each spot for the compatibility of intensity units across different gels. The reference gel was then used for determination of existence and difference of protein expression among different gels.

2.4. Statistical analysis

Unless indicated otherwise, there were at least 5 gels derived from 5 individual samples per each group for comparative proteomic analysis. Although several proteins were examined simultaneously, each protein spot was analyzed individually to define "*differential protein expression*". Our hypothesis was not to define that expression levels of all proteins were different among each individual sample but we wished to examine whether there was (were) any protein(s) that was (were) differentially expressed between the two different groups. Unpaired t-test was performed to determine differences in intensity volume of each corresponding spot between two groups of samples, whereas ANOVA with multiple comparisons was performed for comparative analysis among three or more groups. P values less than 0.05 were considered statistically significant.

2.5. Mass spectrometry

Proteins spots (from 2-D gels) or bands (from 1-D gels) were identified by quadrupole time-of-flight (Q-TOF) mass spectrometry (MS) and/or tandem MS (MS/MS) analyses. Briefly, the proteins were trypsinized and then premixed 1:1 with the matrix solution containing 5 mg/ml α-cyano-4-hydroxycinnamic acid (CHCA) in 50% ACN, 0.1% (v/v) TFA and 2% (w/v) ammonium citrate and deposited onto the 96-well MALDI target plate. The samples were analyzed by the Q-TOF Ultima^{TM} mass spectrometer (Micromass; Manchester, UK), which was fully automated with predefined probe motion pattern and the peak intensity threshold for switching over from MS survey scanning to MS/MS, and from one MS/MS to another. Within each sample well, parent ions that met the predefined criteria (any peak within the m/z 800 – 3,000 range with intensity above 10 count ± include/exclude list) were selected for CID MS/MS using argon as the collision gas and a mass dependent ± 5 V rolling collision energy until the end of the probe pattern was reached. The MS and MS/MS data were extracted and outputted as the searchable .txt and .pkl files, respectively, for independent searches using the MASCOT search engine (http://www.matrixscience.com), assuming that peptides were monoisotopic. Fixed modification was carbamidomethylation at cysteine residues, whereas variable modification was oxidation at

methionine residues. Only one missed trypsin cleavage was allowed, and peptide mass tolerances of 100 and 50 ppm were allowed for peptide mass fingerprinting and MS/MS ions search, respectively.

2.6. Western blot analysis

A total of 10-30 µg proteins extracted from each sample were resolved by SDS-PAGE at 150 V for approximately 2 h using SE260 mini-Vertical Electrophoresis Unit (GE Healthcare). After the completion of SDS-PAGE, proteins were transferred onto a nitrocellulose membrane and non-specific bindings were blocked with 5% milk in PBS for 1 h. The membrane was then incubated with primary antibody at 4°C overnight. After washing, the membrane was further incubated respective secondary antibody conjugated with horseradish peroxidase at room temperature (RT) for 1 h. Reactive protein bands were then visualized by a chemiluminescence substrate and autoradiography.

3. Specific Methods for Individual Subprojects

3.1. Subproject #1: Proteomic analysis of changes in mitochondrial proteome in distal renal tubular cells induced by COM crystal adhesion

3.1.1. Cell culture and binding of CaOx crystals to renal tubular epithelial cells

MDCK cells were cultivated with complete Eagle's minimum essential medium (MEM) containing 10% fetal bovine serum (FBS), 1.2% penicillinG/ streptomycin and 2 mM glutamine in 75 cm^2 tissue culture flask. The cultured cells were maintained in a humidified incubator at 37°C with 5% CO_2 in presence or absence of COM crystals in culture medium (100 µg crystals/ml culture medium). The cells were incubated for a further 48 h and then harvested.

3.1.2. Mitochondrial isolation

Mitochondria were isolated from MDCK cells by subcellular fractionation. Briefly, the harvested cells were resuspended with ice-cold homogenized buffer (HB) (0.25 M sucrose, 1 mM EDTA, 10 mM HEPES; pH 7.5). The cell suspension was then disrupted. After disruption, the homogenate was centrifuged at 1,000 *g* for 10 min. The supernatant was collected and further centrifuged at 20,000 *g* for 25 min. The pellet was resuspended with fresh isolation buffer (HB without EDTA) and centrifuged at 20,000 *g* for 25 min. Purity of the isolated mitochondria was confirmed by Janus Green B staining, Western analysis and transmission electron microscopy.

The isolated mitochondria from COM-treated versus controlled cells were subjected to comparative proteomic analysis as detailed in ***Section 2***.

3.2. Subproject #2: Proteomic identification of COM crystal-binding proteins on apical membranes of distal renal tubular cells

3.2.1. Cultivation of polarized renal tubular epithelial cells

MDCK cells were seeded at a density of 5-7.5 x 10^4 cells/ml on permeable polycarbonate membrane (0.4 mm pore size) and cultivated for 4 days. The cells were grown in MEM supplemented with 10% FBS, 1.2% penicillinG/streptomycin and 2 mM L-glutamine. The cultured cells were maintained in humidified incubator at 37°C with 5% CO_2. The medium was changed every

other day. The polarization of renal tubular epithelial cells was confirmed by confocal microscopic examination to evaluate expression of Na^+/K^+-ATPase and ZO1, which represented basolateral membrane and tight junction, respectively. The expression of these three markers was examined to confirm the polarization.

3.2.2. Isolation of apical membranes and COM crystal binding

Confluent polarized MDCK cells on the permeable polycarbonate membrane insert were rinsed twice with ice-cold PBS and then harvested. The cells were washed again with ice-cold PBS and the cell pellet (collected using centrifugation at 2,500 rpm for 5 min) was resuspended in a buffer containing 250 mM sucrose, 12 mM Tris-HCl and 5 mM EDTA (pH 7.4). The cells were then lyzed by sonication and $MgCl_2$ was added to a final concentration of 12 mM. After incubation on ice for 10 min, the resuspension was centrifuged at 2,000 *g* for 15 min and the supernatant was further centrifuged at 21,000 *g* for 30 min. The resulting pellet was resuspended in a buffer containing 125 mM sucrose, 6 mM Tris-HCl and 2.5 mM EDTA (pH 7.4). $MgCl_2$ was added to a final concentration of 12 mM and these isolation methods based on differential centrifugal steps were repeated one more cycle. The purified apical membrane pellet was finally resuspended in a buffer containing 50 mM NaCl and 10 mM Tri-HCl (pH 7.4) and saved at -70°C until use.

3.2.3. Binding of CaOx crystals to apical membrane proteins and subsequent dissociation

The purified apical membranes were solubilized in 20 mM n-octyl-β-D-glucopyranoside. After removal of debris, COM crystals were added to the protein solution and the mixture was then incubated overnight at 4°C with a continuous rocker. The crystal-proteins complexes were isolated using centrifugation at 5,000 *g* for 10 min. The pellet was washed twice with ice-cold PBS and the adhered proteins were dissociated from crystals by adding 0.5 M EDTA (pH 8.0) with an overnight incubation at 4°C.

The resulting proteins were subjected to SDS-PAGE and mass spectrometric analysis as detailed in ***Section 2.5***.

3.3. Subproject #3: Characterizations of secretome from distal renal tubular cells and its COM-crystal binding components

MDCK cells were cultivated with MEM supplemented with 10% FBS, 1.2% penicillinG/ streptomycin and 2 mM glutamine in 75 cm^2 tissue culture flask. The cultured cells were maintained in a humidified incubator at 37°C with 5% CO_2 until confluent. Culture supernatants were collected and subjected to sample preparation as detailed in ***Section 2.1***. The recovered proteins were resolved in SDS-PAGE and identified by mass spectrometry. In a parallel experiment, culture supernatants were incubated with COM crystals (1 mg crystals/ml supernatant) for 1 h. After several washes with PBS, the bound proteins were eluted by a lysis buffer and subjected to SDS-PAGE and mass spectrometric analysis as detailed in ***Section 2.5***.

3.4. Subproject #4: Insights into preventive mechanisms of green tea extract against oxalate-induced renal fibrosis: a proteomics approach

MDCK cells were cultivated with MEM supplemented with 10% FBS, 1.2% penicillinG/ streptomycin and 2 mM glutamine in 75 cm^2 tissue culture flask. The cultured cells were maintained in a humidified incubator at 37°C with 5% CO_2. Thereafter, the cells were seeded into 6-well plate to reach 40% confluency and were maintained in a growth medium for 24 h. Prior to treatment, cells were washed with serum-free medium and then pretreated with 25 µM EGCG in maintenance medium for 1 h, followed by 500 µM sodium oxalate to complete 24-h incubation.

Cell morphology was observed under a phase contrast microscope (Olympus CKX41; Tokyo, Japan) at the beginning and 24 h after treatment. For immunofluorescence study, the cells were stained with vimentin, cytokeratin, ZO-1 and F-actin. Briefly, cells were washed once with PBS and then fixed with 3.7% formaldehyde/PBS at RT for 10 min and permeabilized with 1% triton x-100/PBS at RT for 10 min. After washing step, the cells were incubated with appropriated primary antibody at 37°C for 1 h. The cells were extensively washed with PBS and incubated at RT for 1 h with respective secondary antibody conjugated with Cy3 or other labels. After washing, images were captured under a fluorescence microscope (Nikon; Tokyo, Japan).

Subsequently, cellular proteomes of the cells with or without EGCG pretreatment were subjected to comparative proteomic analysis as detailed in ***Section 2***.

3.5. Subproject #5: Evaluation of altered proteome in macrophages in response to basolateral secretion of renal tubular epithelial cells treated with COM crystals

3.5.1. Cultivation of polarized renal tubular epithelial cells with and without COM crystals

Polarized MDCK cells were maintained as detailed in ***Section 3.2.1***. These cells were treated with or without COM crystals (100 µg crystals/ml culture medium) for 48 h. Culture supernatant in the basolateral compartment was collected and used for treatment of macrophages.

3.5.2. Cultivation of macrophages

U937 cells (with a cell density of $1x10^6$ cells/ml) were seeded in each 75 cm^2 tissue culture flask and cultured in RPMI 1640 for 24 h. Then, the cells were maintained in 100 ng/ml phorbol 12-myristate 13-acetate (PMA)-containing medium for 48 h. Thereafter, the culture medium was replaced with RPMI 1640 fresh medium and the cells were further incubated for 48 h.

3.5.3. Treatment of macrophages

The resulting macrophages were treated with culture supernatant from basolateral compartment obtained from the COM-treated cells for 6-14 h, whereas those exposed to the basolateral supernatant obtained from the untreated cells served as the controls (See more details in ***Section 3.5.1.***).

The treated and controlled macrophages were subjected to comparative cellular proteome analysis as detailed in ***Section 2***.

3.6. Subproject #6: Proteomic analysis of Trimethoprim/Sulfamethoxazole-resistance Escherichia coli isolated from kidney stone

The proteomes of *Escherichia coli* isolated from kidney stone were studied. A total of 100 kidney stone patients who were born and had been living in Northeastern Thailand were recruited. Kidney stones were collected from the subjects within 12-h after surgical removal and stored at 4°C. All kidney stones were identified for *E. coli* and tested for Trimetoprim/Sulfamethoxazole (TMP/SMX) susceptibility. Stones were washed with sterile saline solution and crushed under aseptic condition. The resulting powder were cultivated in blood and MacConkey agar and incubated overnight at 37°C. Identification of *E. coli* isolates from kidney stone was done by colony morphology, Gram staining and standard biochemical tests. All *E. coli* isolates were subjected to disc diffusion for TMP/SMX susceptibility on Mueller-Hinton agar and incubated at 37°C.

Thereafter, the analyzed microbes were divided into two groups: TMP/SMX-susceptible and TMP/SMX-resistance groups. Both groups of bacterial samples were subjected to comparative proteomic analysis as detailed in ***Section 2***.

3.7. Subproject #7: Biology of interactions between natural killer (NK) cells and dendritic cells in the pathogenesis of atherosclerosis in diabetes

3.7.1. Co-cultivation of KG-1 and NK92 cells

KG-1 cells were co-cultivated with NK92 cells in the presence of normal physiologic glucose or high glucose for 96 h in round-bottomed 96-well plates.

3.7.2. Determination of cell surface molecules

Flow cytometric analysis of surface molecules of KG-1 and NK92 cells were performed using monoclonal antibodies specific to the maturation and activation markers, adhesion molecules and chemokine receptors of DCs, activating and inhibitory receptors of NK cells.

3.7.3. Cytokine assay

To investigate the impact of DC on the cytokine production by NK cells and the influence of NK cells on cytokine secretion by DC, KG-1 cells and NK92 cells were co-cultivated in 24-well plates in the presence or absence of a separating porous membrane. Supernatants were collected and concentrations of IFN-γ, IL-12 and IL-10 were determined using a commercial ELISA kit.

3.7.4. NK cell toxicity assay

After 96 h of co-cultivation, NK92 cells were separated from KG-1 cells and cytotoxic activity of NK92 cells were analyzed against target cells K562. Percentages of dead K562 cells were determined by flow cytometry.

3.7.5. Comparative proteomic analysis

This part was performed as detailed in ***Section 2***.

3.8. Subproject #8: Proteomics of lupus nephritis: A biomarker validation project

3.8.1. Criteria of active nephritis

Renal involvement was documented by having one of the following criteria:

(1) A total urinary protein level of more than 0.5 g/day.

(2) An increment of serum creatinine levels of more than 0.5 mg/dl during 1 month period of follow-up.

(3) The presence of pyuria, hematuria, or urinary cast by microscopic examination.

3.8.2. Criteria of response to therapy

Therapeutic response was defined either by the improvement of pathological scores of activity and chronicity based on repeated kidney biopsies, or by the following clinical criteria, including:

(1) Stabilization or improvement in renal function.

(2) Decrease in hematuria to less than 10 RBC per high-power field.

(3) Significant reduction in proteinuria (decrease to less than 3 g/day if baseline nephrotic range, or less than 1 g/day if baseline non-nephrotic) for at least 3 months.

3.8.3. Criteria of a loss of renal function

A loss of renal function was determined by doubling of serum creatinine calculated from the renal biopsy date or end-stage renal disease (ESRD). The criteria of ESRD include having a calculated MDRD-GFR below 15 ml/min or initiation of renal replacement therapy (dialysis or transplantation).

3.8.4. Urine collection and preparation

Mid-stream urine samples were collected from normal healthy individuals and LN patients (inactive, active, response, and non-response). The sample was centrifuged at 1,000 *g*, 4°C for 5 min to clear debris. The supernatant was stored at -80°C until further protein isolation procedures as detailed in ***Section 2.1***. Comparative proteomic analysis was performed as detailed in ***Section 2***. Potential biomarkers were validated by ELISA or other immunological methods in a large number of prospective urine samples.

3.8.5. Blood collection and preparation

Peripheral blood samples (10 ml) were collected in EDTA tubes and then centrifuged within 30 min at 1,500 *g* and RT for 10 min. The supernatant was collected and transferred into 15-ml tubes. For platelet removal, plasma samples were centrifuged at 2,500 *g* and RT for 15 min. The resulting supernatants were transferred into 1.5-ml microtubes on ice and kept at -80°C until use. For protein precipitation, 750 µl of 100% ethanol was added into 150 µl plasma samples and mixed. The mixtures were incubated on ice for 10 min and then centrifuged at 12,000 rpm for 10 min. The pellets were saved and then dissolved with a lysis buffer. Protein concentration of each sample was measured by spectrophotometry using the Bradford method.

3.9. Subproject #9: Changes in plasma proteome of β-thalassemia/HbE patients treated with anti-oxidant cocktail

3.9.1. Subject screening

Subjects were recruited from the project "Effect of antioxidant cocktail in β-thalassemia/HbE patients", which was extended to this study. The subjects were divided into 2 groups:

(1) Patients who received daily dose of vitamin E 400 IU, N-acetylcysteine 200 mg, and deferiprone 50 mg/kg (n=10)

(2) Patients who received daily dose of curcuminoids 500 mg, N-acetylcysteine 200 mg, and deferiprone 50 mg/kg (n=10)

3.9.2. Inclusion criteria

Hb typing is $\beta^{0/+}\beta^{E}$ with age between 18-50 years, Hb level at steady state 6-9 g/dL, non-splenectomized, no blood transfusion or iron chelation within 3 months before recruitment, and WHO performance status grade 0-2. All subjects had signed the informed consent.

3.9.3. Exclusion criteria

Pregnancy or lactation, administration of other drugs (except only for folic acid) within 30 days before recruitment, and presence of any severe diseases.

3.9.4. Blood collection and preparation

At the beginning of the study, fasting peripheral blood was collected in EDTA-coated tube and centrifuged at 1,500 *g* and 4°C for 10 min. The separated plasma was re-centrifuged at 3,000 *g* and 4°C for 10 min to obtain platelet-poor plasma for proteomic study. Platelet-poor plasma was aliquoted and kept at -80°C until used. All patients received anti-oxidant cocktail daily for 12 months. Platelet-poor plasma for proteomics study was prepared at baseline (0), 6, and 12 months after the treatment. The high-abundant proteins in plasma were eliminated using optimized technique including ultracentrifugation or affinity chromatography. The remaining low-abundant protein fractions were dialyzed, freeze-dried, rehydrated, and measured for protein concentrations using the Bradford method.

Comparative proteomic analysis was performed as detailed in ***Section 2***.

3.10. Subproject #10: Development of 2-D Blue Native PAGE for protein interaction analysis in viral infected shrimp hemocytes

3.10.1. Sample preparation

Shrimp hemolymph was collected from 25-30 g SPF *P. monodon* rearing in artificial sea water. The total hemocytes in AC-1 anti-coagulant were loaded in Percoll gradient centrifugation to obtain the purified population for each hemocytic cell types. The isolated semi-granular cells were confirmed under microscopic examination and then subjected to protein extraction in lysis buffer, protein clean-up by precipitation and determination for protein concentration. Samples were collected from SPF shrimps in the controlled and disease groups, which were injected by buffer and purified Yellow Head Virus (YHV), respectively.

3.10.2. 2-D Blue Native PAGE

Optimization of buffers and lysis systems were required to obtain the suitable solubility and stabilization of the extracted hemocytic protein complexes. Various combinations of specific detergents such as digitonin and dodecylmaltoside were used and tested for optimal quantity and quality of protein samples in 1-D Blue Native PAGE. Once the condition was obtained, the extracted protein complexes were analyzed further by 2-D Blue Native PAGE. The first dimensional separation was done in a non-denaturing condition to keep protein complexes soluble and stabilized. The second separation was performed using a denaturing SDS-PAGE condition. Protein samples were examined in comparison between those extracted from controlled and from YHV infected cells. A series of time course for YHV infection was also investigated to monitor differential changes in their proteomic profiles as well as the changes in protein interaction patterns. Protein spots were stained either by silver staining method or by Colloidal Coomassie Blue to visualize the protein spots and mark for spot excision.

ผลผลิต/ผลลัพธ์ (Output/Outcome) ที่ได้จากโครงการ

1. ผลงานตีพิมพ์ (Publications)

Output จากนักวิจัยในโครงการที่ **acknowledge สกว.** (แสดงตัวหนาที่ชื่อของหัวหน้าโครงการและทีมวิจัย) โดยค่า Impact Factor เป็นค่าในปีที่ผลงานได้รับการตีพิมพ์

1.1. ผลงานตีพิมพ์ในวารสารวิชาการระดับนานาชาติ (* = Corresponding author)

1.1.1. **Chutipongtanate S**, **Thongboonkerd V***.
Ceftriaxone crystallization and its potential role in kidney stone formation.
Biochem. Biophys. Res. Commun. 406(3): 396-402, 2011
(2011 IF = 2.484)

1.1.2. **Chiangjong W**, Sinchaikul S, Chen ST, **Thongboonkerd V***.
Calcium oxalate dihydrate crystal induced changes in glycoproteome of distal renal tubular epithelial cells.
Mol. Biosyst. 7(6): 1917-1925, 2011
(2011 IF = 3.534)

1.1.3. Poungsawai J, Pattanakitsakul SN, **Thongboonkerd V***.
Subcellular localizations and time-course expression of dengue envelope and non-structural 1 proteins in human endothelial cells.
Microb. Pathog. 51(3): 225-229, 2011
(2011 IF = 1.938)

1.1.4. Zürbig P, Dihazi H, Metzger T, **Thongboonkerd V**, Vlahou A.
Urine proteomics in kidney and urogenital diseases: Moving towards clinical applications.
Proteomics Clin. Appl. 5(5-6): 256-268, 2011
(2011 IF = 1.970)

1.1.5. Mischak H, **Thongboonkerd V**, Schanstra JP, Vlahou A.
Renal and urinary proteomics.
Proteomics Clin. Appl. 5(5-6): 211-213, 2011
(2011 IF = 1.970)

1.1.6. Wongkamchai S, **Chiangjong W**, Sinchaikul S, Chen ST, Choochote W, **Thongboonkerd V***.
Identification of *Brugia malayi* immunogens by an immunoproteomics approach.
J. Proteomics 74(9): 1607-1613, 2011
(2011 IF = 4.878)

1.1.7. **Fong-ngern K**, Sinchaikul S, Chen ST, **Thongboonkerd V***.
Large-scale identification of calcium oxalate monohydrate crystal-binding proteins on apical membrane of distal renal tubular epithelial cells.
J. Proteome Res. 10(10): 4463-4477, 2011
(2011 IF = 5.113)

1.1.8. Thanomsridetchai N, **Singhto N**, Tepsumethanon V, Shuangshoti S, Wacharapluesadee S, Sinchaikul S, Chen ST, Hemachudha T, **Thongboonkerd V***.
Comprehensive proteome analysis of hippocampus, brainstem and spinal cord from paralytic and furious dogs naturally infected with rabies.
J. Proteome Res. 10(11): 4911-4924, 2011
(2011 IF = 5.113)

1.1.9. **Thongboonkerd V***.
Proteomics in dengue virus infection: Host response in human endothelial cells.
J. Anal. Sci. Technol. 2(Suppl A): A46-A51, 2011
(2011 IF = Not applicable)

1.1.10. **Tavichakorntrakool R**, **Prasongwattana V**, Sungkeeree S, Saisud P, Sribenjalux P, Pimratana C, Bovornpadungkitti S, Sriboonlue P, **Thongboonkerd V***.
Extensive characterizations of bacteria isolated from catheterized urine and stone matrices in patients with nephrolithiasis.
Nephrol. Dial. Transplant. 27(11): 4125-4130, 2012
(2012 IF = 3.371)

1.1.11. **Somparn P**, **Hirankarn N**, Leelahavanichkul A, Khovidhunkit W, **Thongboonkerd V**, **Avihingsanon Y**.
Urinary proteomics revealed prostaglandin H2D-isomerase, not Zn-α2-glycoprotein, as a biomarker for active lupus nephritis.
J. Proteomics 75(11): 3240-3247, 2012
(2012 IF = 4.088)

1.1.12. **Chaiyarit S**, **Thongboonkerd V***.
Changes in mitochondrial proteome of renal tubular cells induced by calcium oxalate monohydrate crystal adhesion and internalization are related to mitochondrial dysfunction.
J. Proteome Res. 11(6): 3269–3280, 2012
(2012 IF = 5.056)

1.1.13. Mischak H, Ioannidis JP, Argiles A, Attwood TK, Bongcam-Rudloff E, Broenstrup M, Charonis A, Chrousos GP, Delles C, Dominiczak A, Dylag T, Ehrich J, Egido J, Findeisen P, Jankowski J, Johnson RW, Julian BA, Lankisch T, Leung H, Maahs D, Magni F, Manns MP, Manolis E, Mayer G, Navis G, Novak J, Ortiz A, Persson F, Peter K, Riese HH, Rossing P, Sattar N, Spasovski G, **Thongboonkerd V**, Vanholder R, Schanstra JP, Vlahou A.
Implementation of proteomic biomarkers: Making it work.
Eur. J. Clin. Invest. 42(9): 1027-1036, 2012
(2012 IF = 3.365)

1.1.14. **Chutipongtanate S, Fong-ngern K, Peerapen P, Thongboonkerd V***.
High calcium enhances calcium oxalate crystal binding of renal tubular cells via increased surface ANXA1, but impairs their proliferation and healing.
J. Proteome Res. 11(7): 3650–3663, 2012

(2012 IF = 5.056)

1.1.15. **Chutipongtanate S, Chaiyarit S, Thongboonkerd V*.**

Citrate, not phosphate, can dissolve calcium oxalate monohydrate crystals and detach these crystals from renal tubular cells.

Eur. J. Pharmacol. 689(1-3): 219-225, 2012

(2012 IF = 2.592)

1.1.16. Polprasert C**, Chiangjong W, Thongboonkerd V*.**

Marked changes in red cell membrane proteins in hereditary spherocytosis: A proteomics approach.

Mol. Biosyst. 8(9): 2312-2322, 2012

(2012 IF = 3.350)

1.1.17. **Roop-ngam P, Chaiyarit S, Pongsakul N, Thongboonkerd V*.**

Isolation and characterizations of oxalate-binding proteins in the kidney.

Biochem. Biophys. Res. Commun. 423(3): 629-634, 2012

(2012 IF = 2.406)

1.1.18. **Thongboonkerd V*.**

The variability in tissue proteomics.

Proteomics Clin. Appl. 6(7-8): 340-342, 2012

(2012 IF = 2.926)

1.1.19. **Chutipongtanate S,** Watcharatanyatip K**, Homvises T, Jaturongkakul K, Thongboonkerd V*.**

Systematic comparisons of various spectrophotometric and colorimetric methods to measure concentrations of protein, peptide and amino acid: Detectable limits, linear dynamic ranges, interferences, practicality and unit costs.

Talanta 98: 123-129, 2012

(2012 IF = 3.498)

1.1.20. **Chutipongtanate S, Thongboonkerd V*.**

Phosphate inhibits calcium oxalate crystal growth and crystallization through reducing free calcium ions: A morphological analysis and calcium consumption assay.

Clin. Chem. Lab. Med. 50(9): 1697-1698, 2012

(2012 IF = 3.009)

1.1.21. Chaichompoo P, Kumya P, Khowawisetsut L, **Chiangjong W, Chaiyarit S, Pongsakul N,** Sirithanaratanakul N, Fucharoen S, **Thongboonkerd V*,** Pattanapanyasat K.

Characterizations and proteome analysis of platelet-free plasma-derived microparticles in β-thalassemia/hemoglobin E patients.

J. Proteomics 76: 239-250, 2012

(2012 IF = 4.088)

1.1.22. **Chiangjong W, Thongboonkerd V*.**

A novel assay to evaluate promoting effects of proteins on calcium oxalate crystal invasion through extracellular matrix based on plasminogen/plasmin activity.

Talanta 101: 240-245, 2012

(2012 IF = 3.498)

1.1.23. **Thongboonkerd V***.

The promise and challenge of systems biology in translational medicine.

Clin. Sci. (Lond) 124(6): 389-390, 2013

(2013 IF = 4.859)

1.1.24. **Hatairaktham S, Srisawat C,** Siritanaratkul N, **Chiangjong W,** Fucharoen S, **Thongboonkerd V, Kalpravidh RW**.

Differential plasma proteome profiles of mild versus severe β-thalassemia/Hb E.

Ann. Hematol. 92(3): 365-377, 2013

(2013 IF = 2.396)

1.1.25. **Peerapen P, Thongboonkerd V***.

p38 MAPK mediates calcium oxalate crystal-induced tight junction disruption in distal renal tubular epithelial cells.

Sci. Rep. 3: 1041, 2013

(2013 IF = 5.078)

1.1.26. **Chutipongtanate S, Sutthimethakorn S, Chiangjong W, Thongboonkerd V***.

Bacteria can promote calcium oxalate crystal growth and aggregation.

J. Biol. Inorg. Chem. 18(3): 299-308, 2013

(2013 IF = 3.164)

1.1.27. **Kanlaya R, Fong-Ngern K, Thongboonkerd V***.

Cellular adaptive response of distal renal tubular cells to high-oxalate environment highlights surface alpha-enolase as the enhancer of calcium oxalate monohydrate crystal adhesion.

J. Proteomics 80C: 55-65, 2013

(2013 IF = 3.929)

1.1.28. Chanmee T, Phothacharoen P, **Thongboonkerd V,** Kasinrerk W, Kongtawelert P.

Characterization of monoclonal antibodies against a human chondrocyte surface antigen.

Monoclon. Antib. Immunodiagn. Immunother. (*Formerly Hybridoma*) 32(3):180-186, 2013

(2013 IF = 0.244)

1.1.29. **Singhto N, Sintiprungrat K, Thongboonkerd V***.

Alterations in macrophage cellular proteome induced by calcium oxalate crystals: the association of HSP90 and F-actin is important for phagosome formation.

J. Proteome Res. 12(8): 3561-3572, 2013

(2013 IF = 5.001)

1.1.30. Kuakarn S, **SomParn P**, Tangkijvanich P, Mahachai V, **Thongboonkerd V, Hirankarn N**.

Serum proteins in chronic hepatitis B patients treated with peginterferon alfa-2b.

World J Gastroenterol. 19(31): 5067-5075, 2013

(2013 IF = 2.433)

1.2. ผลงานตีพิมพ์ในวารสารวิชาการระดับนานาชาติได้รับการคัดเลือกขึ้นปกของวารสาร

Journal of Proteome Research (Volume 10, Issue 11, November 2011) (2011 IF = 5.113)

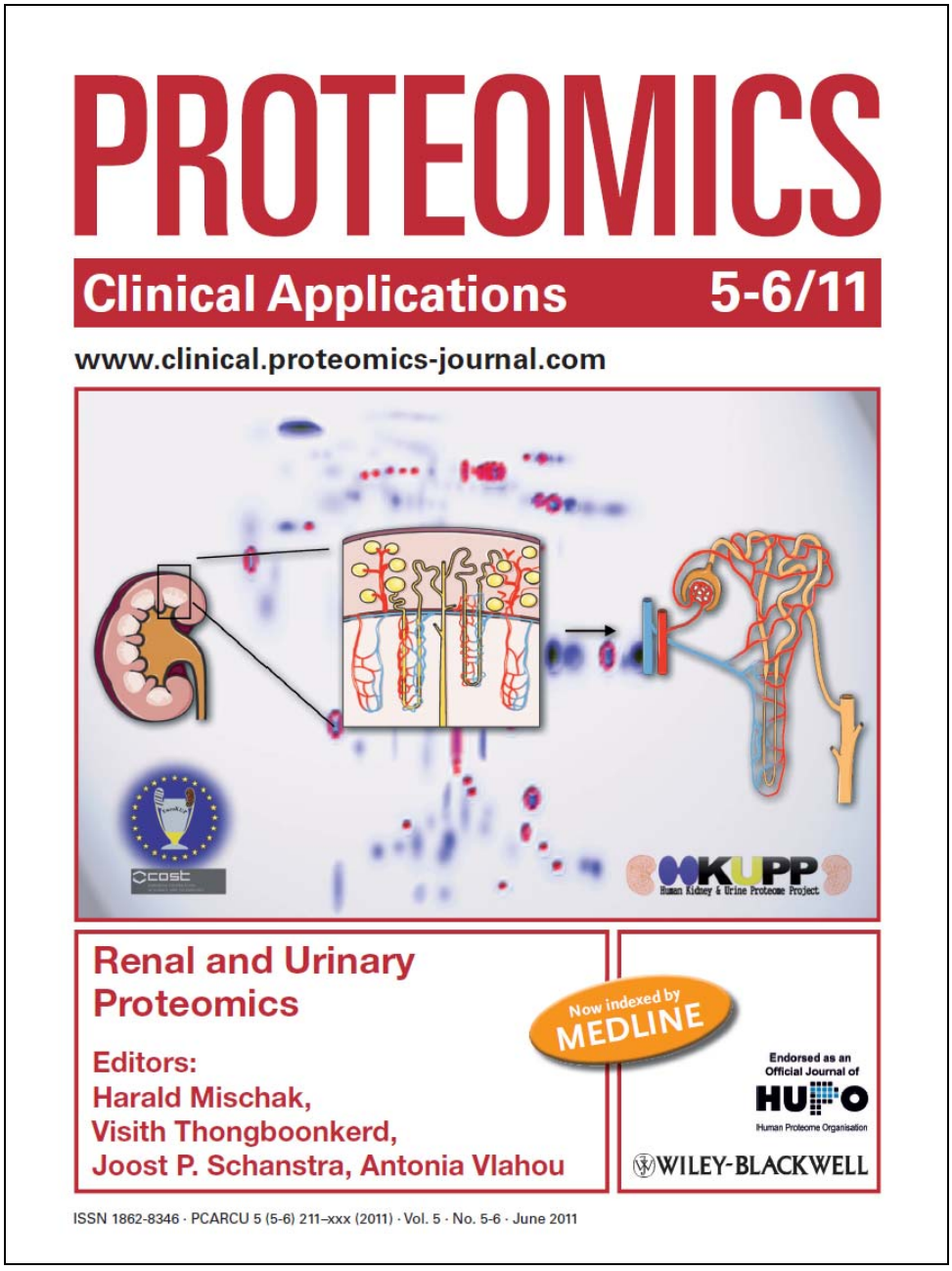


Cover Figure Caption:

"Calcium oxalate monohydrate (COM) crystal adhesion to apical surface of renal tubular epithelial cells can lead to kidney stone formation. Research published in the journal identified COM crystal-binding proteins using a large-scale approach. Depicted on the cover are Madin-Darby Canine Kidney cells which were used in immunofluorescence experiments in this study. Image courtesy of Fong-Ngern, K.; Peerapen, P.; Sinchaikul, S.; Chen, S. T.; **Thongboonkerd, V**. *J. Proteome Res. 2011, 10, 4463–4477*."

1.3. Invited Guest Editor

ศ.นพ. วิศิษฏ์ ทองบุญเกิด ได้รับเชิญ จากสำนักพิมพ์ Wiley-VCH เป็น Guest Editor ร่วมกับนักวิจัยโปรตีโอมิกส์ชั้นแนวหน้าของโลก สำหรับ Special Issue เรื่อง “Renal and Urinary Proteomics” ของวารสาร PROTEOMICS – Clinical Applications ฉบับที่ 5-6 ปี 2011



1.4. บทความในหนังสือนานาชาติ (สำนักพิมพ์ ต่างประเทศ)

1.4.1. **Thongboonkerd V***.

Study of diabetic nephropathy in the proteomic era.

In: Diabetes and the Kidney (Contrib. Nephrol. vol 170)

Edited by Lai KN, Tang SC; Basel, Karger, pp. 172-183, 2011

2. เครือข่ายวิจัย (Networking)

2.1. Proteomics Network in Thailand

This project is a great opportunity to create a proteomics network in Thailand. This network has been joined by several scientists and clinicians, as well as their associates and students who are interested in proteome science. This network offers collaboration, consultation and discussion on trouble shootings in proteomics to enhance the rapid progress of proteomics in Thailand. In practical, this network has regular activities, at least an annual meeting, as part of the annual meeting of the Protein Society of Thailand.

หน่วยงานภายในประเทศที่มีความร่วมมือกันทำวิจัยทางด้านโปรตีโอมิกส์

2.1.1. คณะแพทยศาสตร์ศิริราชพยาบาล มหาวิทยาลัยมหิดล

2.1.2. คณะวิทยาศาสตร์ มหาวิทยาลัยมหิดล

2.1.3. คณะทันตแพทยศาสตร์ มหาวิทยาลัยมหิดล

2.1.4. คณะแพทยศาสตร์ จุฬาลงกรณ์มหาวิทยาลัย

2.1.5. คณะแพทยศาสตร์ มหาวิทยาลัยธรรมศาสตร์

2.1.6. คณะแพทยศาสตร์ มหาวิทยาลัยขอนแก่น

2.1.7. คณะแพทยศาสตร์ มหาวิทยาลัยศรีนครินทรวิโรฒ

2.1.8. คณะแพทยศาสตร์ มหาวิทยาลัยเชียงใหม่

2.1.9. คณะเทคนิคการแพทย์ มหาวิทยาลัยขอนแก่น

2.1.10. สถาบันชีววิทยาศาสตร์โมเลกุล มหาวิทยาลัยมหิดล

2.1.11. สถาบันจีโนม สำนักงานพัฒนาวิทยาศาสตร์และเทคโนโลยีแห่งชาติ (สวทช.)

2.1.12. ศูนย์ปฏิบัติการกลางด้านชีววิทยาศาสตร์คอมพิวเตอร์เพื่อการวิจัยแบบบูรณาการ มหาวิทยาลัยมหิดล

2.1.13. ศูนย์วิจัยด้านธาลัสซีเมีย มหาวิทยาลัยมหิดล

2.2. International Proteomics Networks

2.2.1. Human Kidney and Urine Proteome Project (HKUPP), Human Proteome Organisation (HUPO)

HKUPP is an international collaborative network officially approved by the HUPO as one of its initiatives. The mission of HKUPP is to encourage and facilitate applications of proteomics to better understand renal (patho)physiology and to define urinary biomarkers for kidney diseases and related disorders. Dr. Visith is a key member of HKUPP responsible for several projects, especially determination of standards and guidelines for kidney and urine proteome analyses.

2.2.2. European Network for Kidney and Urine Proteomics (EuroKUP)

EuroKUP has been established after HKUPP and focuses its activities within European countries. From approximately 50 participating PIs from almost all European countries, Dr. Visith is one among four members from outside Europe and has joined many EuroKUP projects. He is also responsible for determination of standards and guidelines for kidney and urine proteome analyses.

2.2.3. Institute of Biological Chemistry and Genomic Research Center, Academia Sinica, Taipei, Taiwan (Prof. Shui-Tein Chen, PhD)

With a long-term collaboration, Prof. Chen is one of the key members in our network that are always helpful. Not only us, Prof. Chen has collaborated with many Thai scientists from various institutions.

2.2.4. Department of Medicine I, Charles University Medical School, Pilsen, Czech Republic

2.2.5. The University of Hong Kong, Hong Kong

2.2.6. Mosaiques Diagnostics and Therapeutics AG, Hannover, Germany

2.2.7. Nephrology and Rheumatology UMG, Georg-August University Goettingen, Germany

2.2.8. Biomedical Research Foundation Academy of Athens, Greece

2.2.9. Institute of Nephrology, Niigata University Graduate School of Medical and Dental Sciences, Niigata, Japan

2.2.10. Institut National de la Santé et de la Recherche Médicale (INSERM), U858, Toulouse, France and Université Toulouse III Paul-Sabatier, Institut de Médecine Moléculaire de Rangueil, Equipe n°5, IFR150, Toulouse, France

2.2.11. University of Alabama at Birmingham, Birmingham, Alabama, USA

3. การผลิตนักวิจัยรุ่นใหม่ (Training)

This study has offered training opportunities on proteomic analysis for a total of 2 post-docs, 7 research associates, 11 PhD students, and 8 MSc students. For all of the students, their thesis works were related to disease proteomics. They have obtained basic knowledge of methodologies in quantitative and qualitative proteomics and biochemical techniques to examine pathogenic mechanisms of diseases. Specifically, they are able to perform cell culture, cellular fractionation, sample preparation for proteomic analysis, 2-D PAGE, spot matching, quantitative intensity analysis, protein identification by mass spectrometry, and 1-D/2-D Western blotting. These knowledge and skills will make them be able to perform other proteomic studies independently. These really are opportunities to make this new biotechnology more widely used and applied in other areas with a high efficacy.

4. การนำผลงานไปใช้ประโยชน์ในเชิงพาณิชย์ เชิงสาธารณะ หรือเชิงนโยบาย

ยังไม่มี เนื่องจากกลุ่มวิจัยเน้นงานวิจัยเชิงลึกเพื่อให้ได้มาซึ่งองค์ความรู้ใหม่สำหรับต่อยอดนำผลงานไปใช้ประโยชน์ในเชิงพาณิชย์ หรือเชิงสาธารณะ หรือเชิงนโยบายในอนาคต

5. วิทยากรรับเชิญในการประชุมที่สำคัญระดับชาติและระดับนานาชาติ

5.1. งานประชุมวิชาการระดับนานาชาติ

Sep 19-23, 2010 **Thongboonkerd V**

Title: "Proteomics for the Investigation of Host Responses in Dengue Virus Infection"

In: HUPO 9th Annual World Congress, Sydney, AUSTRALIA

By: Human Proteome Organisation (HUPO)

Jun 21-23, 2011 **Thongboonkerd V**

Title: "Plasma proteome for early diagnosis of sepsis"

In: 9th Annual ISF Colloquium on: The Systems Biology of Sepsis, Genomics and Beyond, Rockefeller University, New York, USA

By: International Sepsis Forum (ISF)

Nov 15-17, 2011 **Thongboonkerd V**

Title: "Proteomics in dengue virus infection"

In: International Symposium on Analytical Science and Technology, Daejeon, KOREA

By: Korea Basic Science Institute (KBSI)

April 6-8, 2012 **Thongboonkerd V**

Title: "Proteomics in PD"

In: 5th Asian Chapter Meeting of International Society for Peritoneal Dialysis (ISPD) 2011, Pattaya, THAILAND

By: The International Society for Peritoneal Dialysis (ISPD) and The Nephrology Society of Thailand

May 5-7, 2012 **Thongboonkerd V**

Title: "Applications of proteomics to kidney stone disease"

In: AOHUPO 6th Congress, Beijing, CHINA

By: Asia-Oceania Human Proteome Organisation (AOHUPO)

5.2. งานประชุมวิชาการภายในประเทศ

29 กันยายน 2553 **ศ.นพ. วิศิษฏ์ ทองบุญเกิด**

หัวข้อ: “Proteomics in Medicine”

ใน: Biomedical and Technological Sciences Seminar (BTS’s seminar)

จัดโดย: คณะแพทยศาสตร์ มหาวิทยาลัยสงขลานครินทร์

สถานที่: ห้องประชุมอดิเรก ณ ถลาง อาคารเรียนรวมและห้องสมุดคณะแพทยศาสตร์ มหาวิทยาลัยสงขลานครินทร์

เวลา: 13.00-15.00

21 ตุลาคม 2553 **ศ.นพ. วิศิษฏ์ ทองบุญเกิด**

หัวข้อ: “How to write an effective review article?”

ใน: การอบรมเพื่อพัฒนานักวิจัยสาขาวิทยาศาสตร์ชีวภาพและการแพทย์ (ในโครงการจัดกิจกรรมเพื่อ เฉลิมพระเกียรติพระบาทสมเด็จพระจุลจอมเกล้าเจ้าอยู่หัวในโอกาสครบรอบ 100 ปี การสวรรคต “พระปิยมหาราชรำลึก 2553”)

จัดโดย: คณะแพทยศาสตร์ จุฬาลงกรณ์มหาวิทยาลัย

สถานที่ ห้องประชุม 230/1 ชั้น 2 อาคารแพทยพัฒน์ คณะแพทยศาสตร์ จุฬาลงกรณ์มหาวิทยาลัย

เวลา: 11.30-12.00

21 ตุลาคม 2553 **ศ.นพ. วิศิษฏ์ ทองบุญเกิด**

หัวข้อ: “How to write and get your work published (researcher view)?”

ใน: การอบรมเพื่อพัฒนานักวิจัยสาขาวิทยาศาสตร์ชีวภาพและการแพทย์ (ในโครงการจัดกิจกรรมเพื่อ เฉลิมพระเกียรติพระบาทสมเด็จพระจุลจอมเกล้าเจ้าอยู่หัวในโอกาสครบรอบ 100 ปี การสวรรคต “พระปิยมหาราชรำลึก 2553”)

จัดโดย: คณะแพทยศาสตร์ จุฬาลงกรณ์มหาวิทยาลัย

สถานที่: ห้องประชุม 230/1 ชั้น 2 อาคารแพทยพัฒน์ คณะแพทยศาสตร์ จุฬาลงกรณ์มหาวิทยาลัย

เวลา: 13.00-16.00

26 ตุลาคม 2553 **ศ.นพ. วิศิษฏ์ ทองบุญเกิด**

หัวข้อ: “Medical proteomics: The new hope for disease diagnostics, therapeutics and prevention”

ใน: การประชุมวิชาการวิทยาศาสตร์และเทคโนโลยีแห่งประเทศไทย ครั้งที่ 36

จัดโดย: สมาคมวิทยาศาสตร์แห่งประเทศไทยในพระบรมราชูปถัมภ์ ร่วมกับคณะวิทยาศาสตร์และเทคโนโลยี มหาวิทยาลัยธรรมศาสตร์

สถานที่: ห้อง EH102 ศูนย์นิทรรศการและการประชุมไบเทค กรุงเทพฯ

เวลา: 14.00-17.00

1 ธันวาคม 2553 **ศ.นพ. วิศิษฏ์ ทองบุญเกิด**

หัวข้อ: “แพทย์ไทยสู่นักวิจัยโลก”

จัดโดย: โรงเรียนมหิดลวิทยานุสรณ์

สถานที่: หอประชุมพระอุบาลีคุณูปมาจารย์ (ปัญญา อินทปญโญ)โรงเรียนมหิดลวิทยานุสรณ์ ต. ศาลายา จ.นครปฐม

เวลา: 12.00-14.20

9 ธันวาคม 2553 **ศ.นพ. วิศิษฏ์ ทองบุญเกิด**

หัวข้อ: “สถานภาพงานวิจัยด้าน Protein Markers ที่เกี่ยวข้องกับโรคไต”

ใน: การประชุมหารือทิศทางงานวิจัยโรคไต

จัดโดย: สำนักงานพัฒนาวิทยาศาสตร์และเทคโนโลยีแห่งชาติ (สวทช.)

สถานที่: ห้องประชุม 720 ชั้น 7 อาคาร สวทช. – โยธี กระทรวงวิยาศาสตร์ ถนนพระรามหก กรุงเทพฯ

เวลา: 9.35-11.00

17 ธันวาคม 2553 **ศ.นพ. วิศิษฏ์ ทองบุญเกิด**

หัวข้อ: “Proteomics and Kidney Disease”

ใน: การประชุมวิชาการนานาชาติ Mahidol – Kyoto Universities International Symposium 2010

จัดโดย: มหาวิทยาลัยมหิดล ร่วมกับ Kyoto University

สถานที่: ห้องประชุมจุฬาภรณ์ ชั้น 2 ตึกสยามมินทร์ คณะแพทยศาสตร์ศิริราชพยาบาล

เวลา: 11.55-12.20

5 มกราคม 2554 **ศ.นพ. วิศิษฏ์ ทองบุญเกิด**

หัวข้อ: “งานวิจัยส่งเสริมอาชีพแพทย์สู่ความสำเร็จได้อย่างไร”

จัดโดย: คณะแพทยศาสตร์ มหาวิทยาลัยขอนแก่น

สถานที่: ห้องบรรยาย 1 อาคารเตรียมวิทยาศาสตร์คลินิก ชั้น 2 คณะแพทยศาสตร์ มหาวิทยาลัยขอนแก่น

เวลา: 14.00-16.00

21 มกราคม 2554 **ศ.นพ. วิศิษฏ์ ทองบุญเกิด**

หัวข้อ: “From Nephrologist To Scientist”

ใน: การสัมมนาโครงการผลิตอาจารย์แพทย์ และอาจารย์ทันตแพทย์ ครั้งที่ 10

จัดโดย: มหาวิทยาลัยมหิดล

สถานที่: อีสเทิร์นแกรนด์พาเลซ พัทยา จังหวัดชลบุรี

เวลา: 11.15-12.15

8 มีนาคม 2554 **ศ.นพ. วิศิษฏ์ ทองบุญเกิด**

หัวข้อ: “Molecular Tools in Hematology”

ใน: การประชุมวิชาการประจำปี สมาคมโลหิตแห่งประเทศไทย ครั้งที่ 39

จัดโดย: สมาคมโลหิตแห่งประเทศไทย

สถานที่: ห้องเวิลด์บอลล์รูม ชั้น 23 โรงแรมเซ็นทาราแกรนด์ เซ็นทรัลวิลด์ กรุงเทพฯ

เวลา: 15.30-17.00

7 เมษายน 2554 **ศ.นพ. วิศิษฏ์ ทองบุญเกิด**

หัวข้อ: “Proteomics”

ใน: 3rd Biochemistry and Molecular Biology “From Basic to Translational Research for Better Life”

จัดโดย: สมาคมวิทยาศาสตร์แห่งประเทศไทยในพระบรมราชูปถัมภ์ ร่วมกับคณะแพทยศาสตร์ มหาวิทยาลัยเชียงใหม่

สถานที่: ห้องประชุม โรงแรมดิเอ็มเพลสเชียงใหม่ จังหวัดเชียงใหม่

เวลา: 13.00-13.30

15 มิถุนายน 2554 **ศ.นพ. วิศิษฏ์ ทองบุญเกิด**

หัวข้อ: “Medical Proteomics: A Primer”

ใน: งานประชุมวิชาการร่วมระหว่างคณะแพทยศาสตร์สามสถาบัน พ.ศ. 2554: จุฬาฯ – รามาฯ – ศิริราช

จัดโดย: คณะแพทยศาสตร์ จุฬาลงกรณ์มหาวิทยาลัย คณะแพทยศาสตร์โรงพยาบาลรามาธิบดี และ คณะแพทยศาสตร์ศิริราชพยาบาล มหาวิทยาลัยมหิดล

สถานที่: อาคารอิมแพ็คคอนเวนชั่น เซ็นเตอร์ ศูนย์ประชุมอิมแพ็คเมืองทองธานี จังหวัดนนทบุรี

เวลา: 8.00-12.15

16 มิถุนายน 2554 **ศ.นพ. วิศิษฏ์ ทองบุญเกิด**

หัวข้อ: “Disease Proteomics”

ใน: งานประชุมวิชาการร่วมระหว่างคณะแพทยศาสตร์สามสถาบัน พ.ศ. 2554: จุฬาฯ – รามาฯ – ศิริราช

จัดโดย: คณะแพทยศาสตร์ จุฬาลงกรณ์มหาวิทยาลัย คณะแพทยศาสตร์โรงพยาบาลรามาธิบดี และ คณะแพทยศาสตร์ศิริราชพยาบาล มหาวิทยาลัยมหิดล

สถานที่: อาคารอิมแพ็คคอนเวนชั่น เซ็นเตอร์ ศูนย์ประชุมอิมแพ็คเมืองทองธานี จังหวัดนนทบุรี

เวลา: 8.00-12.15

14 ตุลาคม 2554 **ศ.นพ. วิศิษฏ์ ทองบุญเกิด**

หัวข้อ: “Writing a manuscript: Review article vs. original article”

ใน: โครงการฝึกอบรมเพื่อพัฒนานักวิจัยสาขาวิทยาศาสตร์ชีวภาพและการแพทย์ (เนื่องในวโรกาส “วันปิยมหาราชรำลึก” พุทธศักราช 2554)

จัดโดย: คณะแพทยศาสตร์ จุฬาลงกรณ์มหาวิทยาลัย

สถานที่: ห้องประชุม 230/1 ชั้น 2 อาคารแพทยพัฒน์ คณะแพทยศาสตร์ จุฬาลงกรณ์มหาวิทยาลัย

เวลา: 13.00-15.30

25 มกราคม 2555 **ศ.นพ. วิศิษฏ์ ทองบุญเกิด**

หัวข้อ: “การเขียนผลงานวิจัยให้โดนใจ ไร้การละเมิดทางวรรณกรรม”

ใน: Research Facilitating System

จัดโดย: คณะทันตแพทยศาสตร์ มหาวิทยาลัยมหิดล

สถานที่: ห้องประชุมอาคาร 2 ชั้น 5 คณะทันตแพทยศาสตร์ มหาวิทยาลัยมหิดล

เวลา: 13.00-15.00

28 มกราคม 2555 **ศ.นพ. วิศิษฏ์ ทองบุญเกิด**

หัวข้อ: “Proteomics: Applications in Nephrology”

ใน: New Frontiers in Nephrology

จัดโดย: สมาคมโรคไตแห่งประเทศไทย

สถานที่: ห้องประชุมอาคาร 2 ชั้น โรงแรมบางกอกชฎา ถนนรัชดาภิเษก กรุงเทพฯ

เวลา: 09.00-10.00

29 มีนาคม 2555 **ศ.นพ. วิศิษฏ์ ทองบุญเกิด**

หัวข้อ: “เสวนากับนักวิทยาศาสตร์ระดับชาติ”

ใน: Thai Science Camp ครั้งที่ 4

จัดโดย: สมาคมวิทยาศาสตร์แห่งประเทศไทยในพระบรมราชูปถัมภ์

สถานที่: ห้องยูเรก้า องค์การพิพิธภัณฑ์วิทยาศาสตร์แห่งชาติ (อพวช.) กรุงเทพฯ

เวลา: 14.00-17.00

18 ตุลาคม 2555 **ศ.นพ. วิศิษฏ์ ทองบุญเกิด**

หัวข้อ: From Expression Proteomics to Functional Study

ใน: การประชุมวิชาการวิทยาศาสตร์และเทคโนโลยีแห่งประเทศไทย ครั้งที่ 38

จัดโดย: สมาคมวิทยาศาสตร์แห่งประเทศไทยในพระบรมราชูปถัมภ์ ร่วมกับคณะวิทยาศาสตร์ มหาวิทยาลัยเชียงใหม่

สถานที่: ศูนย์ประชุมนานาชาติเอ็มเพลสเชียงใหม่ จังหวัดเชียงใหม่

เวลา: 8.30-9.00

29 พฤศจิกายน 2555 **ศ.นพ. วิศิษฏ์ ทองบุญเกิด**

หัวข้อ: Adsorption Therapy for ESRD: Large Urmic Toxins by Proteomics

ใน: Renal Diseases & Biotechnology for Blood Purification (RB2012)

จัดโดย: หน่วยโรคไต ภาควิชาอายุรศาสตร์ คณะแพทยศาสตร์ มหาวิทยาลัยเชียงใหม่ ร่วมกับสมาคมโรคไตแห่งประเทศไทย

สถานที่: ศูนย์ประชุมนานาชาติเอ็มเพลสเชียงใหม่ จังหวัดเชียงใหม่

เวลา: 15.00-16.30

15 กุมภาพันธ์ 2556 **ศ.นพ. วิศิษฏ์ ทองบุญเกิด**

หัวข้อ: เทคนิคการเขียนบทความตีพิมพ์ในวารสารวิชาการ

ใน: เทคนิคการเขียนบทความตีพิมพ์ในวารสารวิชาการ

จัดโดย: มหาวิทยาลัยมหิดล

สถานที่: ห้องประชุม ศ.นพ.นที รักษ์พลเมือง

เวลา: 09.00-12.00

3 เมษายน 2556 **ศ.นพ. วิศิษฏ์ ทองบุญเกิด**

หัวข้อ: การนำเทคโนโลยีจีโนมไปประยุกต์ใช้ด้านโปรตีโอมิกส์ทางการแพทย์

ใน: การประชุมวิชาการประจำปี 2556 สวทช.

จัดโดย: สำนักงานพัฒนาวิทยาศาสตร์และเทคโนโลยีแห่งชาติ (สวทช.)

สถานที่: ห้องประชุม BT-127 อาคารไบโอเทค อุทยานวิทยาศาสตร์ประเทศไทย จ. ปทุมธานี

เวลา: 15.00-15.30

6. รางวัลที่ได้รับระหว่างรับทุนส่งเสริมกลุ่มวิจัย

6.1. Awards

2010 TWAS Prize for Young Scientists in Thailand

From: The Academy of Sciences for The Developing World (TWAS), which links to UNESCO and the National Research Council of Thailand (NRCT)

Awardee: **Visith Thongboonkerd**

2010 Outstanding Scientist Award

From: Foundation for the Promotion of Science and Technology under the Patronage of His Majesty the King, Thailand

Awardee: **Visith Thongboonkerd**

2010 Outstanding Researcher Award

From: National Research Council of Thailand (NRCT)

Awardee: **Visith Thongboonkerd**

2010, 11 & 12 Outstanding Staff Award

From: Faculty of Medicine Siriraj Hospital

Awardee: **Visith Thongboonkerd**

6.2. Honors

2010 - Present Invited to serve as a Senior Editor of Proteomics Clinical Applications (2011 IF = 1.970)

2011 - 2015 Invited to serve as an Associate Editor of Journal of Proteome Research (2011 IF = 5.113)

2013 - Present Elected to serve as a HUPO (Human Proteome Organisation) Council Member
A total of 3-consecutive 3-year terms (2007-2009, 2010-2012, 2013-2015)

Editorial Board: Proteomics (2011 IF = 4.505)
Expert Review of Proteomics (2011 IF = 3.685)
Proteome Science (2011 IF = 2.328)
Proteomics Insights
International Journal of Proteomics
Genome Medicine
The Open Spectroscopy Journal
Biomarkers in Medicine (2011 IF = 2.630)
Biomarker Insights
International Journal of Nephrology and Renovascular Disease
International Journal of Artificial Organs (2011 IF = 1.861)
American Journal of Nephrology (2011 IF = 2.539)

Editorial Advisory Board: Clinical Science (2011 IF = 4.317)

7. นักวิจัยในโครงการที่ได้รับรางวัลหรือได้รับทุนวิจัยอื่นในระหว่างที่รับทุนส่งเสริมกลุ่มวิจัย

7.1. รางวัล

2010 Merck Young Scientist Award (2nd Runner Up)
From: Merck Limited
Awardee: **Rattiyaporn Kanlaya**

2011 Outstanding Thesis Award
From: Faculty of Graduate Studies, Mahidol University
Awardee: **Nilubon Singhto**

2011 Outstanding Abstract Award
From: The Protein Society of Thailand
Awardee: **Kitisak Sintiprungrat**

2011 Outstanding Abstract Award
From: The Protein Society of Thailand
Awardee: **Suneerat Hatairaktham**

2011 Merck Young Scientist Award 2011 (Honorable Mention)
From: Merck KGaA
Awardee: **Wararat Chiangjong**

2011 รางวัลหน่วยปฏิบัติการวิจัย (RU) ที่มีผลงานดีเด่น สาขาวิทยาศาสตร์สุขภาพ
From: Chulalongkorn University
Awardee: **Yingyos Avihingsanon**

2011 รางวัลผลงานวิจัยดีมาก
From: Chulalongkorn University
Awardee: **Nattiya Hirankarn**

2011 รางวัลผลงานวิจัยดีเด่นระดับปรีคลินิก
From: Faculty of Medicine Siriraj Hospital
Awardee: **Chatchawan Srisawat**

2012 Outstanding Thesis Award
From: Faculty of Graduate Studies, Mahidol University
Awardee: **Sakdithep Chaiyarit**

2012 AOHUPO2012 Young Scientist Travel Award
From: Asia-Oceania Human Proteome Organisation (AOHUPO)
Awardee: **Nilubon Singhto**

2012 Best Poster Award for New TRF Scholars
From: The Thailand Research Fund (During the TRF Annual Meeting)
Awardee: **Ratree Tavichakorntrakool**

7.2. ทุนวิจัย

รศ.นพ. ยิ่งยศ อวิหิงสานนท์ หัวหน้าโครงการวิจัย
Biomarker Discovery in Lupus Nephritis: Omics approach
แหล่งทุน สำนักงานพัฒนาวิทยาศาสตร์และเทคโนโลยีแห่งชาติ

รศ.นพ. ยิ่งยศ อวิหิงสานนท์ หัวหน้าโครงการวิจัย
การวิจัยทางคลินิกแบบสหสถาบันศึกษาเพื่อทดสอบประสิทธิผลของตัวบ่งชี้ทางชีวภาพที่ใช้ในการติดตามการรักษาและพยากรณ์โรคไตอักเสบลูปัส
แหล่งทุน คณะกรรมการวิจัยวิจัยแห่งชาติ (วช.): เครือข่ายวิจัยกลุ่มสถาบันแพทยศาสตร์แห่งประเทสไทย (UResNet)

รศ.นพ. ยิ่งยศ อวิหิงสานนท์ หัวหน้าโครงการวิจัย
A Multicenter, Randomised, Double blind, Placebo-controlled, Proof of concept study to evaluate efficacy and safety of treatment with CNTO136 administed intravenously in subjects with active lupus nephritis
แหล่งทุน Centocor Research and Development Inc.

รศ.นพ. ยิ่งยศ อวิหิงสานนท์ หัวหน้าโครงการวิจัย
A Multicenter, Randomised, Double blind, Placebo-controlled study to evaluate efficacy and safety of treatement with subcutaneous LY2127399 in subjects with SLE
แหล่งทุน Lilly Research Laboratories

รศ.นพ. ยิ่งยศ อวิหิงสานนท์ หัวหน้าโครงการวิจัย
CRAD 001A2429
แหล่งทุน Novartis Pharma

รศ.ดร.พญ. ณัฏฐิยา หิรัญกาญจน์ หัวหน้าโครงการวิจัย
การค้นหาไคเมริกทรานสคริปจำเพาะที่มีความสัมพันธ์กับภาวะไฮโปเมทิเลชั่น ที่ลำดับเบสของไลน์วันในทีเซลล์ชนิด CD4 และนิวโทรฟิลของผู้ป่วยโรคเอสเอลอี
แหล่งทุน สำนักงานพัฒนาวิทยาศาสตร์และเทคโนโลยีแห่งชาติ

รศ.ดร.พญ. ณัฏฐิยา หิรัญกาญจน์ หัวหน้าโครงการวิจัย
การประเมินประสิทธิภาพของชุดตรวจ อิเล็คซิส แอนติ-เอชซีวี รุ่นที่ 2 (Postlaunch)
แหล่งทุน บริษัท Roche Diagnostics ประเทศเยอรมันนี

ผศ.ดร.นพ. ชัชวาลย์ ศรีสวัสดิ์ หัวหน้าโครงการวิจัย
Nanosecond Pulsed Electric Field (nsPEF) System for Pancreatic Tumor Regression
แหล่งทุน แพทยสมาคมแห่งประเทศไทย ในพระบรมราชูปถัมภ์

ผศ.ดร.นพ. ชัชวาลย์ ศรีสวัสดิ์ หัวหน้าโครงการวิจัย
Targeting aptamers specific to hepatocellular carcinoma

	แหล่งทุน Nanotec-Mahidol University Center of Excellence for Cancer Diagnosis and Treatment
รศ.ดร. ชาติชาย กฤตนัย	หัวหน้าโครงการวิจัย
	แหล่งทุน สกอ.
รศ.ดร. ชาติชาย กฤตนัย	หัวหน้าโครงการวิจัย
	แหล่งทุน มหาวิทยาลัยมหิดล
นพ.ดร. สมชาย ชุติพงศ์ธเนศ	หัวหน้าโครงการวิจัย
	แหล่งทุน ทุนพัฒนาศักยภาพในการทำงานวิจัยของอาจารย์รุ่นใหม่ สกว.
ดร. รัตติยาภรณ์ กัลยา	หัวหน้าโครงการวิจัย
	แหล่งทุน ทุนส่งเสริมนักวิจัยรุ่นใหม่ สกว.
ดร.พญ. จารุภา สูงสถิตานนท์	หัวหน้าโครงการวิจัย
	แหล่งทุน ทุนพัฒนาศักยภาพในการทำงานวิจัยของอาจารย์รุ่นใหม่ สกว.
ดร.พญ. จารุภา สูงสถิตานนท์	หัวหน้าโครงการวิจัย
	แหล่งทุน มหาวิทยาลัยมหิดล
ผศ.ดร. ราตรี ทวิชากรตระกูล	หัวหน้าโครงการวิจัย
	แหล่งทุน ทุนพัฒนาศักยภาพในการทำงานวิจัยของอาจารย์รุ่นใหม่ สกว.
ผศ.ดร. ราตรี ทวิชากรตระกูล	หัวหน้าโครงการวิจัย
	แหล่งทุน มหาวิทยาลัยขอนแก่น
ดร. ศักดิเทพ ไชยฤทธิ์	หัวหน้าโครงการวิจัย
	แหล่งทุน ทุนส่งเสริมนักวิจัยรุ่นใหม่ สกว.
ดร.จุฑาทิพย์ มานิสสรณ์	หัวหน้าโครงการวิจัย
	แหล่งทุน ทุนส่งเสริมนักวิจัยรุ่นใหม่ สกว.
ดร.เกศรินทร์ ฟองเงิน	หัวหน้าโครงการวิจัย
	แหล่งทุน ทุนส่งเสริมนักวิจัยรุ่นใหม่ สกว.

รายชื่อกลุ่มวิจัย เมธีวิจัยอาวุโส สกว. (ศ.นพ. วิศิษฏ์ ทองบุญเกิด)

ชื่อ-นามสกุล	เริ่มเข้าร่วมโครงการ			สถานภาพปัจจุบัน		
	ตำแหน่งวิชาการ	สังกัด	ตำแหน่งในโครงการ	ตำแหน่งวิชาการ	สังกัด	หมายเหตุ
1. ศ.ดร.มรว. ชิษณุสรร สวัสดิวัตน์	ศ.	คณะวิทยาศาสตร์ มหาวิทยาลัยมหิดล และสถาบันวิจัยจุฬาภรณ์	ที่ปรึกษาโครงการ	ศ.	คณะวิทยาศาสตร์ มหาวิทยาลัยมหิดล และสถาบันวิจัยจุฬาภรณ์	
2. ศ.นพ. วิศิษฏ์ ทองบุญเกิด	ศ.	สถานส่งเสริมการวิจัย คณะแพทยศาสตร์ศิริราชพยาบาล มหาวิทยาลัยมหิดล	หัวหน้าโครงการ	ศ.	สถานส่งเสริมการวิจัย คณะแพทยศาสตร์ศิริราชพยาบาล มหาวิทยาลัยมหิดล	
3. รศ.ดร. รัชนีกร กัลล์ประวิทธ์	รศ.	ภาควิชาชีวเคมี คณะแพทยศาสตร์ศิริราชพยาบาล มหาวิทยาลัยมหิดล	ผู้ร่วมโครงการ (Co-investigator)	รศ.	ภาควิชาชีวเคมี คณะแพทยศาสตร์ศิริราชพยาบาล มหาวิทยาลัยมหิดล	
4. รศ.นพ. ยิ่งยศ อวิหิงสานนท์	รศ.	ภาควิชาอายุรศาสตร์ คณะแพทยศาสตร์จุฬาลงกรณ์มหาวิทยาลัย	ผู้ร่วมโครงการ (Co-investigator)	ศ.	ภาควิชาอายุรศาสตร์ คณะแพทยศาสตร์จุฬาลงกรณ์มหาวิทยาลัย	
5. รศ.ดร.พญ. ณัฏฐิยา หิรัญกาญจน์	รศ.	ภาควิชาจุลชีววิทยา คณะแพทยศาสตร์จุฬาลงกรณ์มหาวิทยาลัย	ผู้ร่วมโครงการ (Co-investigator)	ศ.	ภาควิชาจุลชีววิทยา คณะแพทยศาสตร์จุฬาลงกรณ์มหาวิทยาลัย	
6. รศ.นพ. วิทูรย์ ประสงค์วัฒนา	รศ.	ภาควิชาชีวเคมี คณะแพทยศาสตร์มหาวิทยาลัยขอนแก่น	ผู้ร่วมโครงการ (Co-investigator)	รศ.	ภาควิชาชีวเคมี คณะแพทยศาสตร์มหาวิทยาลัยขอนแก่น	
7. รศ.ดร. ชาติชาย กฤตนัย	รศ.	สถาบันชีววิทยาศาสตร์โมเลกุล มหาวิทยาลัยมหิดล	ผู้ร่วมโครงการ (Co-investigator)	รศ.	สถาบันชีววิทยาศาสตร์โมเลกุล มหาวิทยาลัยมหิดล	
8. ผศ.ดร.นพ. ชัชวาลย์ ศรีสวัสดิ์	ผศ.	ภาควิชาชีวเคมี คณะแพทยศาสตร์ศิริราชพยาบาล มหาวิทยาลัยมหิดล	ผู้ร่วมโครงการ (Co-investigator)	รศ.	ภาควิชาชีวเคมี คณะแพทยศาสตร์ศิริราชพยาบาล มหาวิทยาลัยมหิดล	
9. นพ.ดร. สมชาย ชุติพงศ์ธเนศ	อาจารย์	สถานส่งเสริมการวิจัย คณะแพทยศาสตร์ศิริราชพยาบาล	ผู้ร่วมโครงการ (Co-investigator)	อาจารย์	ภาควิชากุมารเวชศาตร์ คณะแพทยศาสตร์โรงพยาบาลรามาธิบดี	

		มหาวิทยาลัยมหิดล			(กำลังศึกษาต่อเฉพาะทาง)	
10. ดร. รัตติยาภรณ์ กัลยา	-	สถานส่งเสริมการวิจัย คณะแพทยศาสตร์ศิริราชพยาบาล มหาวิทยาลัยมหิดล	ผู้ร่วมโครงการ (Co-investigator)	อาจารย์	สถานส่งเสริมการวิจัย คณะแพทยศาสตร์ศิริราชพยาบาล มหาวิทยาลัยมหิดล	
11. ดร.พญ. จารุภา สูงสถิตานนท์	อาจารย์	ภาควิชาวิทยาภูมิคุ้มกัน คณะแพทยศาสตร์ศิริราชพยาบาล มหาวิทยาลัยมหิดล	ผู้ร่วมโครงการ (Co-investigator)	อาจารย์	ภาควิชาวิทยาภูมิคุ้มกัน คณะแพทยศาสตร์ศิริราชพยาบาล มหาวิทยาลัยมหิดล	
12. ดร. ราตรี ทวิชากรตระกูล	อาจารย์	คณะเทคนิคการแพทย์ มหาวิทยาลัยขอนแก่น	ผู้ร่วมโครงการ (Co-investigator)	ผศ.	คณะเทคนิคการแพทย์ มหาวิทยาลัยขอนแก่น	
13. ดร. ศักดิเทพ ไชยฤทธิ์	-	สถานส่งเสริมการวิจัย คณะแพทยศาสตร์ศิริราชพยาบาล มหาวิทยาลัยมหิดล	ผู้ร่วมโครงการ (Co-investigator)	-	สถานส่งเสริมการวิจัย คณะแพทยศาสตร์ศิริราชพยาบาล มหาวิทยาลัยมหิดล	
14. Dr. Janjira Thaipadungpanit	-	สถานส่งเสริมการวิจัย คณะแพทยศาสตร์ศิริราชพยาบาล มหาวิทยาลัยมหิดล	นักวิจัย	-	คณะเวชศาสตร์เขตร้อน มหาวิทยาลัยมหิดล	
15. Dr. Juthatip Manissorn	-	สถานส่งเสริมการวิจัย คณะแพทยศาสตร์ศิริราชพยาบาล มหาวิทยาลัยมหิดล	นักวิจัย	-	สถานส่งเสริมการวิจัย คณะแพทยศาสตร์ศิริราชพยาบาล มหาวิทยาลัยมหิดล	
16. Ms. Nilubon Singhto	-	สถานส่งเสริมการวิจัย คณะแพทยศาสตร์ศิริราชพยาบาล มหาวิทยาลัยมหิดล	ผู้ช่วยวิจัยระดับ ป.โท	-	สถานส่งเสริมการวิจัย คณะแพทยศาสตร์ศิริราชพยาบาล มหาวิทยาลัยมหิดล	-กำลังศึกษาต่อระดับ ป.เอก
17. Ms. Piyachat Roopngam	-	สถานส่งเสริมการวิจัย คณะแพทยศาสตร์ศิริราชพยาบาล มหาวิทยาลัยมหิดล	ผู้ช่วยวิจัยระดับ ป.โท	อาจารย์	คณะเทคนิคการแพทย์ มหาวิทยาลัยเวสเทิร์น	
18. Ms. Wimonwon Komonsubin	-	สถานส่งเสริมการวิจัย คณะ	ผู้ช่วยวิจัยระดับ	-	คณะเวชศาสตร์เขตร้อน	

		แพทยศาสตร์ศิริราชพยาบาล มหาวิทยาลัยมหิดล	ป.โท		มหาวิทยาลัยมหิดล	
19. Ms. Nutkridta Pongsakul	-	สถานส่งเสริมการวิจัย คณะ แพทยศาสตร์ศิริราชพยาบาล มหาวิทยาลัยมหิดล	ผู้ช่วยวิจัยระดับ ป.โท	-	สถานส่งเสริมการวิจัย คณะ แพทยศาสตร์ศิริราชพยาบาล มหาวิทยาลัยมหิดล	
20. Ms. Kewalee Jaturongkakul	-	สถานส่งเสริมการวิจัย คณะ แพทยศาสตร์ศิริราชพยาบาล มหาวิทยาลัยมหิดล	ผู้ช่วยวิจัยระดับ ป.โท	-	สถานส่งเสริมการวิจัย คณะ แพทยศาสตร์ศิริราชพยาบาล มหาวิทยาลัยมหิดล	
21. Ms. Teerada Homvises	-	สถานส่งเสริมการวิจัย คณะ แพทยศาสตร์ศิริราชพยาบาล มหาวิทยาลัยมหิดล	ผู้ช่วยวิจัยระดับ ป.โท	-	สถานส่งเสริมการวิจัย คณะ แพทยศาสตร์ศิริราชพยาบาล มหาวิทยาลัยมหิดล	
22. Ms. Patcharin Keawboonraung	-	สถานส่งเสริมการวิจัย คณะ แพทยศาสตร์ศิริราชพยาบาล มหาวิทยาลัยมหิดล	ผู้ช่วยวิจัยระดับ ป.ตรี	-	คณะแพทยศาสตร์โรงพยาบาลรามาธิบดี มหาวิทยาลัยมหิดล	
23. Ms. Kedsarin Fong-ngern	-	Immunology, Faculty of Medicine Siriraj Hospital, Mahidol University	นักศึกษาระดับ ป.เอก	-	สถานส่งเสริมการวิจัย คณะ แพทยศาสตร์ศิริราชพยาบาล มหาวิทยาลัยมหิดล	-จบการศึกษาแล้ว -ปัจจุบันบรรจุเป็นนักวิจัย ที่ศิริราช
24. Ms. Kitisak Sintiprungrat	-	Immunology, Faculty of Medicine Siriraj Hospital, Mahidol University	นักศึกษาระดับ ป.เอก	-	สถาบันวิจัยจุฬาภรณ์	-จบการศึกษาแล้ว
25. Ms. Paleerath Peerapen	-	Immunology, Faculty of Medicine Siriraj Hospital, Mahidol University	นักศึกษาระดับ ป.เอก	-	สถานส่งเสริมการวิจัย คณะ แพทยศาสตร์ศิริราชพยาบาล มหาวิทยาลัยมหิดล	-จบการศึกษาแล้ว -ปัจจุบันทำงานเป็น นักวิจัยที่ศิริราช
26. Mr. Siripat Aluksanasuwan	-	Immunology, Faculty of Medicine Siriraj Hospital, Mahidol University	นักศึกษาระดับ ป.เอก	-	Immunology, Faculty of Medicine Siriraj Hospital, Mahidol University	-กำลังศึกษา
27. Ms. Taniya Kaewarpai	-	Immunology, Faculty of Medicine	นักศึกษาระดับ	-	Immunology, Faculty of Medicine	-กำลังศึกษา

		Siriraj Hospital, Mahidol University	ป.เอก		Siriraj Hospital, Mahidol University	
28. Ms. Wararat Chiangjong	-	Immunology, Faculty of Medicine Siriraj Hospital, Mahidol University	นักศึกษาระดับ ป.เอก	-	สถานส่งเสริมการวิจัย คณะแพทยศาสตร์ศิริราชพยาบาล มหาวิทยาลัยมหิดล	-จบการศึกษาแล้ว -ปัจจุบันทำงานเป็นนักวิจัยที่ศิริราช
29. Ms. Suchitra Sutthimethakorn	-	Molecular Medicine, Faculty of Science, Mahidol University	นักศึกษาระดับ ป.เอก	-	Molecular Medicine, Faculty of Science, Mahidol University	-กำลังศึกษา
30. Mr. Suparat Taengchaiyaphum	-	Molecular Genetics and Genetics Engineering Program, Institute of Molecular Biosciences, Mahidol University	นักศึกษาระดับ ป.เอก	-	สถาบันชีววิทยาศาสตร์โมเลกุล มหาวิทยาลัยมหิดล	-จบการศึกษาแล้ว
31. Ms. Suneerat Hatairaktham	-	Biochemistry, Faculty of Medicine Siriraj Hospital, Mahidol University	นักศึกษาระดับ ป.เอก	-	ภาควิชาชีวเคมี คณะแพทยศาสตร์ศิริราชพยาบาล มหาวิทยาลัยมหิดล	-จบการศึกษาแล้ว -ปัจจุบันทำงานเป็นนักวิจัยที่ศิริราช
32. Ms. Poorichaya Somparn	-	Multidisciplinary, Faculty of Medicine, Chulalongkorn University	นักศึกษาระดับ ป.เอก	-	ภาควิชาจุลชีววิทยา คณะแพทยศาสตร์จุฬาลงกรณ์มหาวิทยาลัย	-จบการศึกษาแล้ว -ปัจจุบันบรรจุเป็นนักวิจัยที่จุฬาฯ
33. Ms. Pattarin Tangtanatakul	-	Multidisciplinary, Faculty of Medicine, Chulalongkorn University	นักศึกษาระดับ ป.เอก	-	Multidisciplinary, Faculty of Medicine, Chulalongkorn University	-กำลังเตรียมตัวสอบป้องวิทยานิพนธ์
34. Mr. Channarong Changtong	-	Immunology, Faculty of Medicine Siriraj Hospital, Mahidol University	นักศึกษาระดับ ป.โท	-	คณะแพทยศาสตร์โรงพยาบาลรามาธิบดี มหาวิทยาลัยมหิดล	-จบการศึกษาแล้ว
35. Ms. Chompunoot Kapincharanon	-	Immunology, Faculty of Medicine Siriraj Hospital, Mahidol University	นักศึกษาระดับ ป.โท	-	Immunology, Faculty of Medicine Siriraj Hospital, Mahidol University	-กำลังเตรียมตัวสอบป้องวิทยานิพนธ์
36. Mr. Issara Songmahachai	-	Biochemistry, Faculty of Medicine Siriraj Hospital, Mahidol University	นักศึกษาระดับ ป.โท	-	ภาควิชาชีวเคมี คณะแพทยศาสตร์ศิริราชพยาบาล มหาวิทยาลัยมหิดล	-จบการศึกษาแล้ว
37. Ms. Sakuna Siriboonpipattana	-	Biochemistry, Faculty of Medicine	นักศึกษาระดับ	-	ภาควิชาอายุรศาสตร์ คณะ	-จบการศึกษาแล้ว

		Siriraj Hospital, Mahidol University	ป.โท		แพทยศาสตร์ศิริราชพยาบาล มหาวิทยาลัยมหิดล	
38. Mr. Nattapong Veerataveeporn	-	Biochemistry, Faculty of Medicine Siriraj Hospital, Mahidol University	นักศึกษาระดับ ป.โท	-	Biochemistry, Faculty of Medicine Siriraj Hospital, Mahidol University	-จบการศึกษาแล้ว
39. Ms. Suparaporn Onsathit	-	Immunology, Faculty of Medicine Siriraj Hospital, Mahidol University	นักศึกษาระดับ ป.โท	-	Immunology, Faculty of Medicine Siriraj Hospital, Mahidol University	-จบการศึกษาแล้ว
40. Ms. Supatsa Dedsatit	-	Microbiology, Faculty of Medical Technology, Khon Kaen University	นักศึกษาระดับ ป.โท	-	Microbiology, Faculty of Medical Technology, Khon Kaen University	-จบการศึกษาแล้ว
41. Ms. Sunida Kuakarn	-	Multidisciplinary, Faculty of Medicine, Chulalongkorn University	นักศึกษาระดับ ป.โท	-	ภาควิชาจุลชีววิทยา คณะแพทยศาสตร์ จุฬาลงกรณ์มหาวิทยาลัย	-จบการศึกษาแล้ว

ภาคผนวก

ผลงานตีพิมพ์ในวารสารวิชาการระดับนานาชาติและหนังสือ

Biochemical and Biophysical Research Communications 406 (2011) 396–402

Contents lists available at ScienceDirect

Biochemical and Biophysical Research Communications

journal homepage: www.elsevier.com/locate/ybbrc

Ceftriaxone crystallization and its potential role in kidney stone formation

Somchai Chutipongtanate, Visith Thongboonkerd *

Medical Proteomics Unit, Office for Research and Development, Faculty of Medicine Siriraj Hospital, and Center for Research in Complex Systems Science, Mahidol University, Bangkok, Thailand

ARTICLE INFO

Article history:
Received 9 February 2011
Available online 15 February 2011

Keywords:
Ceftriaxone
Crystal adhesion
Crystallization
Kidney stone
Nephrolithiasis

ABSTRACT

Drug-induced nephrolithiasis contributes to 1–2% of the incidence of renal calculi. We examined whether ceftriaxone at therapeutic doses could be crystallized in the urine and also explored its role in kidney stone formation. Crystallization was induced by mixing ceftriaxone sodium at therapeutic urinary excretion levels (0.5–4.0 mg/ml) to calcium chloride at physiologic urinary concentration (5 mM) in deionized (dI) water or artificial urine (AU). The results showed that ceftriaxone was crystallized with free calcium in dose- and time-dependent manner. These ceftriaxone/calcium crystals showed birefringence property under polarized microscope. Individual crystals had needle-shape (5–100 μm in length), whereas the aggregated form had star-burst and irregular-plate shape (40–200 μm in diameter) (note that the crystal sizes were much larger than renal tubular lumens). Calcium-depletion assay revealed that crystallization required free calcium as a substrate. In AU, crystallization remained although it was partially inhibited when compared to that in dI water. Finally, these crystals could tightly adhere onto renal tubular cell surface. Our data demonstrated that ceftriaxone at therapeutic levels could be crystallized with free calcium in the urine under physiologic condition. We hypothesize that tubular occlusion and crystal–cell adhesion may play important role in pathogenic mechanisms of ceftriaxone-induced nephrolithiasis.

© 2011 Elsevier Inc. All rights reserved.

1. Introduction

Nephrolithiasis is an outcome of sophisticated events involving numerous factors; e.g., supersaturation of inorganic salts, underlying genetic/metabolic disorders, and defects in stone modulators [1]. Medication has been considered as one of the pathogenic factors for nephrolithiasis [1,2]. Drug-associated nephrolithiasis contributes to approximately 1–2% of the incidence of renal calculi [2]. This drug adverse event most often affects patients who have received high-dose and/or long-term treatment of some drugs with lithogenic potential [2]. According to mechanisms of calculi formation, lithogenic drugs can be classified into two groups [2]. The first group composes of drugs that induce metabolic abnormalities (e.g., hypercalciuria [3,4] hypocitraturia [5,6], hyperuricosuria [7] and alteration of urine acidity [5,6]), which subsequently provoke formation of metabolic calculi; e.g., calcium-containing stones and uric acid nephrolithiasis [2]. Examples of drugs in the first group include calcium/vitamin D supplement [3], furosemide [4], carbonic anhydrase inhibitors [5], laxatives [6], and uricosuric drugs [7]. The second group composes of drugs that can be crystallized directly in the urine due to their high excretory levels and poor solubility [8–11]. A number of drugs (e.g., triamterine [8], sulfonamides [9], indinavir [10], and silicate-containing drugs [11]) belong to this group. It seems that the second group of lithogenic drugs predominates and causes higher incidence of drug-associated nephrolithiasis [2].

Recently, ceftriaxone (a third-generation cephalosporin with broad-spectrum antibiotic activity) has been recognized as a potentially lithogenic drug [12–14]. Intravenous administration of ceftriaxone is widely used for treatment of microbial infections, particularly organ infection and sepsis. Abnormal ceftriaxone crystallization has been recently recognized as one of its side effects [13–15]. Interestingly, these ceftriaxone-induced calculi can develop within a short period after its administration. Two prospective studies using renal ultrasonography have revealed that 1.4–7.8% of patients had developed renal calculi within 7 days after the standard course of ceftriaxone therapy [13,14]. Although predisposing factors of this drug complication remain unclear, patient's age and some congenital genitourinary anomalies may be involved in the increasing risk of the calculi development [13,14,16]. Most patients with ceftriaxone-associated calculi are asymptomatic [13,14]; however, a number of patients may have colicky pain, gross hematuria, anuria, and uremia [12,16–18].

Compositional analysis has revealed that the calculi obtained from patients receiving ceftriaxone therapy compose mainly of ceftriaxone compound [17], suggesting that the mechanism of calculi formation is based on direct drug crystallization. Nonetheless, unlike other lithogenic medications that are crystallized due to their poor solubility, direct ceftriaxone crystallization has been

* Corresponding author. Address: Medical Proteomics Unit, Office for Research and Development, Siriraj Hospital, Mahidol University, 12th Fl. Adulyadej Vikrom Bldg., 2 Prannok Rd., Bangkoknoi, Bangkok 10700, Thailand. Fax: +66 2 4184793.
E-mail address: thongboonkerd@dr.com (V. Thongboonkerd).

0006-291X/$ - see front matter © 2011 Elsevier Inc. All rights reserved.
doi:10.1016/j.bbrc.2011.02.053

thought to occur by interaction between ceftriaxone (anionic) and free calcium (cationic) [12–14,16,17]. However, this hypothesis has not yet been tested. Additionally, it remains unclear whether ceftriaxone can be crystallized in the urine with its therapeutic urinary excretion levels [19] and physiologic concentration of urinary calcium. Moreover, the mechanisms leading to ceftriaxone crystal retention in the kidney or urinary tract has not been previously elucidated.

The present study was therefore aimed to demonstrate direct interaction between ceftriaxone and calcium. Crystallization of ceftriaxone at therapeutic urinary excretion levels [19] together with calcium at physiologic urinary concentration was first examined in dI water and then evaluated under urinary environment simulated by AU condition. Size and morphology of ceftriaxone crystals were evaluated using phase-contrast and polarized microscopy. Calcium-depletion assay was employed to validate the interacting complex between ceftriaxone and calcium. Furthermore, crystal–cell adhesion was also examined to better understand pathogenic mechanisms of ceftriaxone-induced nephrolithiasis.

2. Materials and methods

2.1. Ceftriaxone crystallization

A previous pharmacokinetic study has demonstrated that approximately 67% of administered ceftriaxone was excreted as unchanged compound via renal clearance; thus, urinary excretion levels of ceftriaxone are directly proportional to the administered dose [19]. After intravenous administration of 0.5, 1.0, and 2.0 g ceftriaxone (which are generally used in clinical practice) for 2 h, urinary ceftriaxone levels were 0.53 ± 0.30, 0.99 ± 0.73, and 2.69 ± 1.40 mg/ml, respectively [19]. Therefore, ceftriaxone concentrations of 0.5–4.0 mg/ml were used in our present study to represent therapeutic urinary excretion levels of ceftriaxone in patients.

Ceftriaxone stock solution was prepared by dissolving ceftriaxone sodium powder (Rocephin®, Roche Pharmaceuticals Inc., NJ) in dI water (18.2 MΩ·cm) to the final concentration of 100 mg/ml and kept at −20 °C until used. This stock solution has clear colorless appearance without any precipitates or undissolved particles remained. Ceftriaxone crystallization was performed in each well of a 24-well polystyrene plate (with lid) (Corning Inc.; Corning, NY) as follows. Various amounts of ceftriaxone stock solution were added into dI water containing 5 mM calcium chloride ($CaCl_2$) (equivalent to 5 mM free calcium, a physiologic urinary calcium concentration) to make the final drug concentration of 0.5, 1.0, 2.0, and 4.0 mg/ml. Each crystallized reaction was further incubated for 2, 6, 12, and 24 h at 25 °C. To investigate ceftriaxone crystallization under urinary environment, AU formula (containing 5 mM $CaCl_2$, 200 mM urea, 4 mM creatinine, 5 mM $Na_3C_6H_5O_7{\cdot}2H_2O$, 54 mM NaCl, 30 mM KCl, 15 mM NH_4Cl, 2 mM $MgSO_4{\cdot}7H_2O$, 9 mM Na_2SO_4, pH 6.2) was used in stead of dI water during the crystallization reaction. This AU formula is very similar (almost identical) to the normal human urine considering physico-chemical properties as concentrations of individual compositions are within their physiologic ranges in the normal human urine [20]. In addition, this AU formula excluded oxalate, phosphate, and uric acid to prevent unwanted crystallization of calcium oxalate, calcium phosphate, and uric acid, respectively. All these experiments were done in triplicate (independently). Ceftriaxone crystals and reaction supernatants were further examined as follows.

2.2. Morphological evaluation of ceftriaxone crystals

Ceftriaxone crystal morphology was evaluated by phase-contrast and polarized microscopic examinations. At 2, 6, 12, and 24 h after crystallization, each reaction well was evaluated for ceftriaxone crystal size and morphology using Olympus CKX41 inverted phase-contrast microscope (Olympus Co. Ltd.; Tokyo, Japan). In addition, to gain further information on birefringence property, ceftriaxone crystals were also examined under crossed polarized light, generating by two polarized filters of Nikon ECLIPSE 80i microscope (Nikon Corp.; Tokyo, Japan).

2.3. Calcium-depletion assay

According to the hypothesis that the interaction between ceftriaxone and calcium led to ceftriaxone crystallization, free calcium ions in the solution would be depleted from the solution because they were consumed into the crystal complex as a substrate. Therefore, direct interaction between ceftriaxone and calcium could be demonstrated by a novel calcium-depletion assay established recently [21]. Briefly, the assay was performed by transferring 3 μl supernatant from each sample well into 200 μl of Arsenazo III reagent (0.2 mM Arsenazo III in a buffer containing 75 mM imidazole, pH 6.5) (BioSystems S.A.; Barcelona, Spain) in 96-well polystyrene plate (Corning Inc.; Corning, NY). The samples were gently mixed and then incubated for 5 min at 25 °C. The reaction intensity was measured using Anthos HTII Microplate Reader (Anthos Labtec Instruments; Salzburg, Austria) using a λ620 nm filter to measure the color intensity, which reflected AIII-calcium reaction and level of free calcium ions. All measurements were normalized by subtraction with the intensity background obtained from the blank AIII reagent (because the 620 nm light could be partially absorbed by AIII reagent). The standard curve was generated by using $CaCl_2$ at the following concentrations: 0, 0.312, 0.625, 1.250, 2.500, and 5.000 mM. The concentration of free calcium ions (Free Ca^{2+}) in each sample well was calculated using the following equation:

$$\text{Free } Ca^{2+}(\text{mM}) = \frac{(A_{620} - \text{Constant of the standard curve})}{\text{Slope of the standard curve}}$$

Where A_{620} was the absorbance of the sample at λ620 nm.

All these experiments were done in triplicate (three independent experiments).

2.4. Renal tubular cell culture and crystal–cell adhesion

Approximately 1×10^5 Madin–Darby Canine Kidney (MDCK) cells, which represent cells derived from distal nephron [22], were inoculated in each well of a 24-well, polystyrene, disposable cell culture cluster (with lid) (Corning Inc.) containing complete Eagle's minimum essential medium (MEM) (GIBCO, Invitrogen Corporation; Green Island, NY) supplemented with 10% fetal bovine serum (FBS), 1.2% penicillinG/streptomycin, and 2 mM glutamine. The cultured cells were maintained in a humidified incubator at 37 °C with 5% CO_2 for 24 h. Thereafter, the culture medium in each well was replaced with 1 ml of AU (containing compositions as aforementioned) to simulate intraluminal urinary environment *in vivo*. Various amounts of ceftriaxone stock solution were added into each culture well to the final concentrations of 0.5, 1.0, 2.0, and 4.0 mg/ml, and the cells were then further incubated in a humidified incubator at 37 °C with 5% CO_2 for 2 h. Thereafter, the cells were vigorously washed three times with isotonic phosphate buffered saline (PBS) to remove non-adhered crystals before visualization using an inverted phase-contrast microscope (Olympus Co. Ltd.). All these experiments were done in triplicate (three independent experiments).

2.5. Statistical analysis

All the quantitative data are reported as mean ± SEM. Multiple comparisons were performed using ANOVA with Tukey's post

hoc test (SPSS, version 11.5). *P* values < 0.05 were considered statistically significant.

3. Results

3.1. Ceftriaxone crystal morphology

Size and morphology of ceftriaxone crystals were revealed under phase-contrast and crossed polarized light microscopes. Ceftriaxone crystals were present as individual crystals and also as the aggregates. Individual crystals had needle-shape with a size of approximately 5–100 μm in length (Fig. 1; panel A). Under crossed polarized light, the individual crystals showed birefringence property. The aggregated crystals had two morphological patterns; including star-burst (Fig. 1; panels B and C) and irregular-plate shape (Fig. 1; panels D–F). Size of the aggregated crystals varied in the range of 40–200 μm in diameter or length, which was much larger than the individual crystals. Under crossed polarized light, the aggregated crystals also exhibited birefringence property.

3.2. Factors determining degree of ceftriaxone crystallization

To determine whether ceftriaxone at therapeutic urinary excretion levels could be crystallized together with physiologic urine level of free calcium, various concentrations of 0.5, 1.0, 2.0, and 4.0 mg/ml ceftriaxone were crystallized with 5 mM $CaCl_2$ in dI water. Fig. 2A demonstrates that these concentrations of ceftriaxone could be crystallized with free calcium to form the aggregates in the time- and dose-dependent manner. Both number and size of crystals were directly proportional to drug concentration and incubation time, consistent to the simple rule of chemical reaction.

Also, various concentrations of ceftriaxone were added into AU containing 5 mM $CaCl_2$ to evaluate ceftriaxone crystallization under human urine environment *in vitro*. Our present study selected AU instead of fresh human urine as to reduce inter- and intra-individual variability of urinary components. Additionally, in contrast to the fresh human urine, this AU had no oxalate, phosphate and uric acid; therefore, unwanted crystallization of calcium oxalate, calcium phosphate and uric acid could be excluded from this study. Fig. 2B demonstrates that ceftriaxone could be crystallized in the AU environment, but with the less extent as compared to crystallization in dI water (Fig. 2A). In AU, ceftriaxone crystals were observed only with high doses (2.0 and 4.0 mg/ml), but number and size of the crystals were fewer and smaller, respectively, as compared to crystallization in dI water. These results implicated that AU had some inhibitory effects against ceftriaxone crystallization.

3.3. Ceftriaxone crystallization required free calcium as a substrate

Consumption of free calcium during crystallization was validated using a calcium-depletion assay. Fig. 3A demonstrates calcium depletion after ceftriaxone crystallization in dI water. Degree of calcium depletion was dose- and time-dependent. While the lower doses (0.5 and 1.0 mg/ml) showed minimal degree of calcium depletion, the higher doses (2.0 and 4.0 mg/ml) were accompanied with marked decrease in free calcium levels. At 24 h after crystallization in dI water using 0.5, 1.0, 2.0, and 4.0 mg/ml ceftriaxone, remaining levels of free calcium were 4.54 ± 0.26, 3.63 ± 0.13, 2.00 ± 0.10, and 0.10 ± 0.05 mM, respectively (significantly reduced from the basal level of 5 mM). This data indicated that ceftriaxone crystallization required free calcium as a substrate.

Fig. 3B demonstrates calcium depletion after ceftriaxone crystallization in AU. Degree of calcium depletion was dose- and time-dependent. However, as expected, degree of calcium depletion in AU was lower than that in dI water at all doses and time-points. At the dose of 0.5 mg/ml, there was no calcium depletion observed, whereas there was only minimal degree of calcium-depletion observed at the dose of 1.0 mg/ml. However, calcium depletion was more obvious using higher doses (2.0 and 4.0 mg/ml) ceftriaxone. These data were consistent with the microscopic findings shown in Fig. 2B. At 24 h after crystallization in AU using 0.5, 1.0, 2.0, and 4.0 mg/ml ceftriaxone, remaining levels of free calcium were 4.90 ± 0.15, 4.13 ± 0.24, 3.01 ± 0.14, and 1.60 ± 0.11 mM, respectively. These data also suggested that AU might have some inhibitory effects against ceftriaxone crystallization.

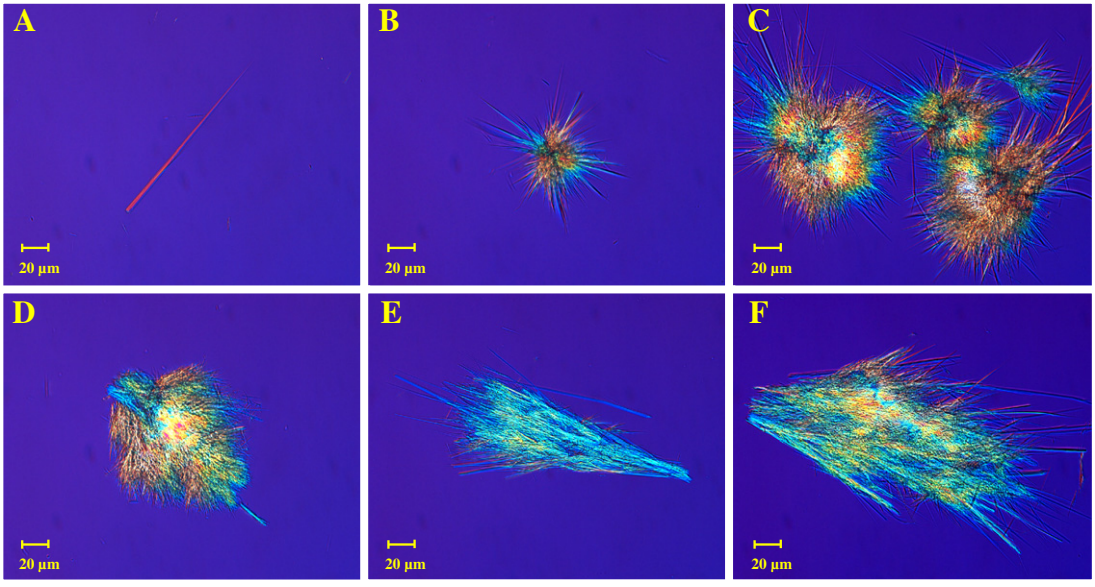


Fig. 1. Ceftriaxone crystal morphology. Crystals were generated by mixing 2.0 mg/ml ceftriaxone with 5 mM $CaCl_2$ in dI water. After 2 h incubation, the crystals were subjected to evaluation by phase-contrast and polarized microscopy. Individual crystals were present with needle shape (panel A), whereas the aggregated forms had star-burst pattern (panels B and C) and irregular-plate shape (panels D–F). Original magnification = 400× for all panels.

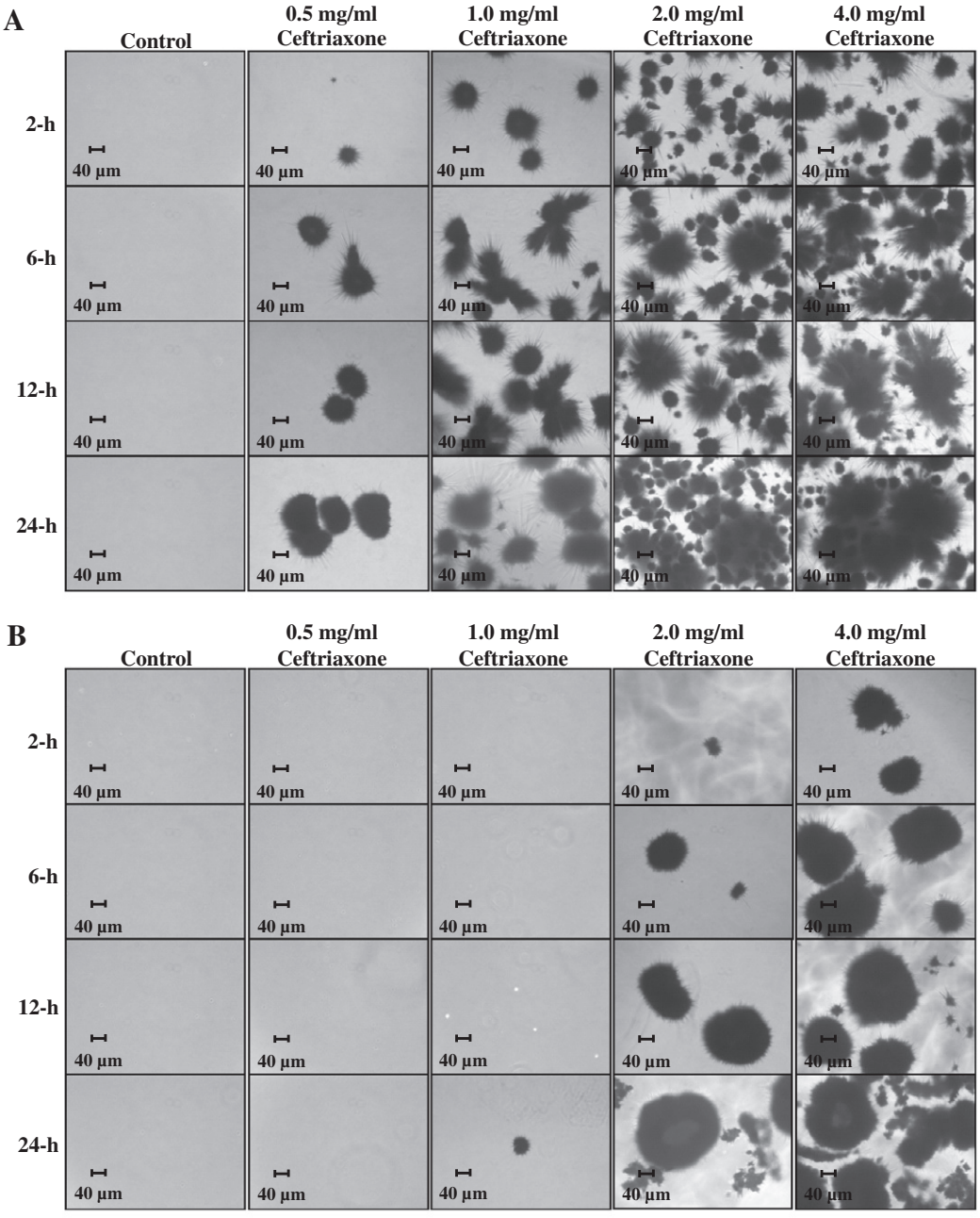


Fig. 2. Ceftriaxone crystallization with varying doses and incubation periods. Ceftriaxone at 0.5, 1.0, 2.0, and 4.0 mg/ml were mixed with 5 mM $CaCl_2$ in dI water (A) or AU (B). The mixtures were then incubated for 2, 6, 12, and 24 h at 25 °C, and crystal images were taken by phase-contrast microscopy. Original magnification = 200× for all panels.

3.4. Ceftriaxone crystals tightly adhered onto MDCK cell surface

Crystal adhesion is considered as one of the most crucial pathogenic mechanisms of renal calculi because this cell–crystal interaction leads to crystal retention in the kidney [23]. Previously, there was no evidence demonstrating that crystal adhesion plays any roles in drug-associated nephrolithiasis. We thus examined the interaction between ceftriaxone crystals and renal tubular (MDCK) cells under simulated urine environment. Fig. 4 shows that ceftriaxone/calcium crystals tightly adhered onto MDCK cell surface as the crystals remained after vigorous washing, particularly when higher doses (2.0 and 4.0 mg/ml) of ceftriaxone were used. As this experiment was performed under the AU environment, crystal adhesion was not obvious when lower doses (0.5–1.0 mg/ml) were used, consistent with the inhibitory effects of AU on ceftriaxone crystallization as also shown in Figs. 2B and 3B. Our data suggested that adhesion of ceftriaxone crystals onto renal tubular cell surface may promote crystal aggregation and crystal retention in the kidney.

4. Discussion

It has been proposed that ceftriaxone-induced nephrolithiasis is a result of direct interaction between ceftriaxone and free calcium in the urine [12–14,16,17]. However, it was unclear in the past whether ceftriaxone could be crystallized with calcium, particularly under physiologic urinary condition. The results in our

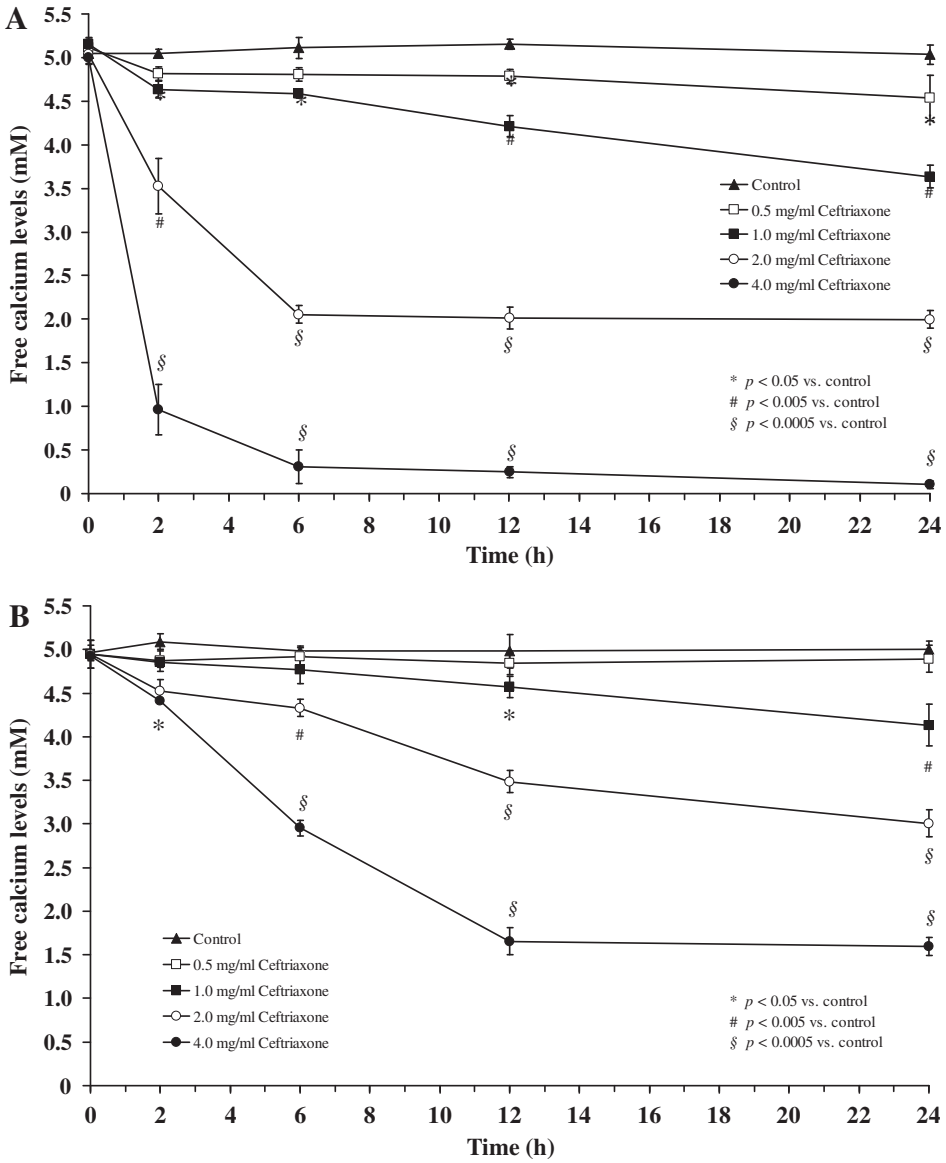


Fig. 3. Calcium-depletion assay. The consumption of free calcium during ceftriaxone crystallization was validated by calcium-depletion assay. Calcium depletion (which reflected consumption of free calcium) was monitored in each crystallization reaction performed in dI water (A) or AU (B) (detailed in Section 2). Each data point was derived from three independent experiments and the data are reported as mean ± SEM.

present study clearly demonstrated that ceftriaxone at therapeutic urinary excretion levels [19] could directly interact with free calcium at physiologic urinary concentration to generate ceftriaxone/calcium crystals. Several factors including drug concentration and incubation time are very important for determining the degree of ceftriaxone/calcium crystallization (Fig. 2A and B). According to our data, ceftriaxone crystallization was dose- and time-dependent reaction. Therefore, high-dose ceftriaxone administration (which leads to increasing urinary ceftriaxone levels) and urinary stasis by any causes (which leads to retention of ceftriaxone crystals in urinary tract, allowing crystal growth and aggregation) may aggravate ceftriaxone calculi formation.

Another interesting factor that may be involved in the pathogenic mechanisms of ceftriaxone-induced nephrolithiasis is urinary environment. Our present study has demonstrated that AU exhibited some degree of inhibitory effects on ceftriaxone crystallization (Figs. 2B and 3B). It has been hypothesized that some substances in AU (e.g., citrate and magnesium) may be responsible for these inhibitory effects. Citrate may bind to free calcium to reduce the remaining free calcium, which is the substrate for ceftriaxone crystallization. In addition to citrate and magnesium, other anionic and cationic urinary composition [24,25] may also act as the modulators to prevent ceftriaxone crystallization. Nevertheless, it still occurs when the high doses of ceftriaxone is administered. Further studies are required to elucidate this hypothesis.

Similar to several other lithogenic drugs [2], the data in this study also suggested that ceftriaxone/calcium calculi may be developed after tubular occlusion. The size of ceftriaxone crystal aggregates was approximately 40–200 μm in diameter (Figs. 1 and 2), whereas the luminal diameters of proximal tubules, distal tubules and collecting ducts are approximately 50–60, 20–30, and 50–60 μm, respectively, which are much smaller than ceftriaxone/calcium crystals. Therefore, the ceftriaxone crystal aggregates can easily obstruct renal tubules, leading to tubular occlusion and ceftriaxone calculi formation.

Furthermore, we have also demonstrated that crystal–cell adhesion may play significant roles in the pathogenic mechanisms of ceftriaxone-induced nephrolithiasis. Our findings showed that

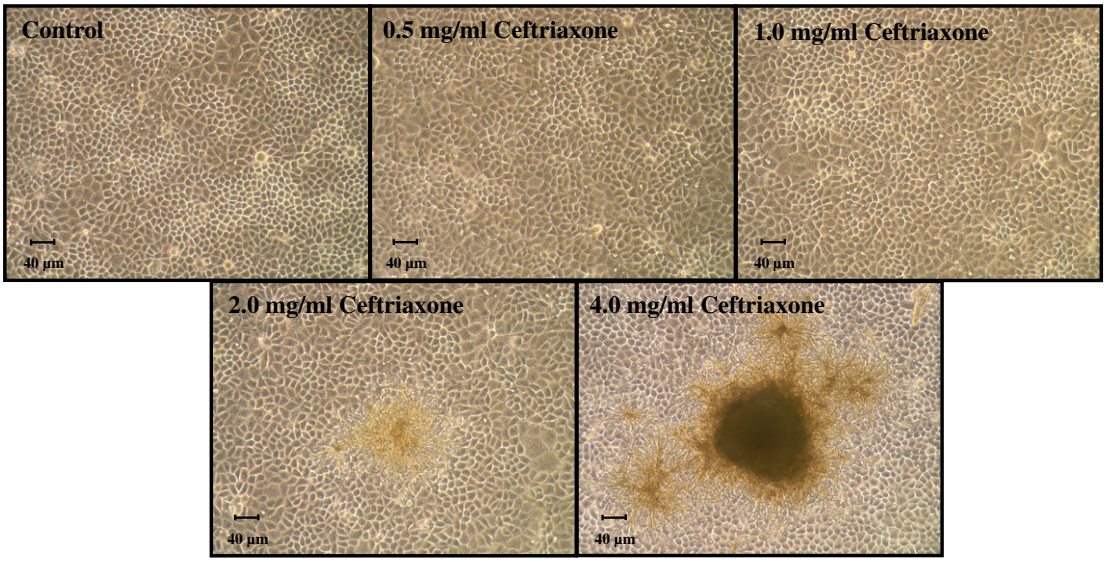


Fig. 4. Adhesion of ceftriaxone crystals onto renal tubular cell surface. Ceftriaxone crystallization was performed in MDCK cell culture well containing AU (detailed in Section 2). After 2 h incubation, the cells were vigorously washed three times with isotonic PBS solution. The remainings were then imaged using a phase-contrast microscope. Original magnification = 200× for all panels. All experiments were done in triplicate.

ceftriaxone crystals could tightly adhere onto renal tubular cell surface (Fig. 4), suggesting the high adhesive force between ceftriaxone crystals and renal tubular cell surfaces. Although the mechanism for such crystal–cell adhesion is still unknown, one possibility is that ceftriaxone/calcium crystals may adhere onto cell surface via ionic interaction and/or hydrogen bond, similar to other calcium-containing crystals (e.g., calcium oxalate, calcium phosphate) [26]. Another possibility is that MDCK cell surface may present some (unknown) receptors for ceftriaxone crystals. These hypotheses should be further elucidated.

Although our data clearly demonstrated that ceftriaxone could be crystallized in the urine at physiologic condition, only a few numbers of patients receiving ceftriaxone therapy have been reported to develop ceftriaxone-containing calculi in routine clinical practice. One explanation is that most of patients with ceftriaxone-induced nephrolithiasis have asymptomatic calculi and thus this complication has been neglected by patients or overlooked by clinicians until severe clinical symptoms are present. This explanation is also supported by a prospective clinical study [13]. In this study, all patients were investigated with renal ultrasonography before and after ceftriaxone therapy to demonstrate the presence or absence of renal calculi. After 50 mg/kg/day intramuscular administration and 100 mg/kg/day intravascular injection of ceftriaxone for 7 days, 7.4% and 8.3%, respectively, of patients developed novel episode of renal calculi [13]. Interestingly, all calculi-affected patients were asymptomatic and had spontaneous recovery with stone passage after conservative treatments. Without renal ultrasonography, these asymptomatic calculi would not be recognized and ceftriaxone-induced nephrolithiasis remains under-investigated. According to this evidence, the accurate incidence of ceftriaxone-associated nephrolithiasis may be higher than that was initially anticipated from clinical experience. Because ceftriaxone is one of the most commonly used drugs in clinical practice, the occurrence of this drug-induced stone should be concerned to avoid or prevent inevitable renal complications (e.g., renal failure) in some cases.

In summary, our present study has shown that ceftriaxone could be crystallized in the urine under physiologic condition. The size of ceftriaxone crystal aggregates was much larger than the diameter of renal tubular lumens, implicating that tubular occlusion may be the major mechanism for subsequent development of ceftriaxone calculi. In addition, crystal adhesion onto renal tubular cell surface may also play important role for the initiation of ceftriaxone-induced nephrolithiasis.

5. Conflict of interest

Both authors declare no conflicts of interest and have no financial relationships with companies that make products relevant to the paper.

Acknowledgments

This study was supported by Office of the Higher Education Commission and Mahidol University under the National Research Universities Initiative, and The Thailand Research Fund to VT and SC (VT is a Senior TRF Research Scholar, whereas SC is a New TRF-CHE Research Scholar). Both SC and VT are also supported by "Chalermphrakiat" Grant, Faculty of Medicine Siriraj Hospital.

References

[1] F.L. Coe, A. Evan, E. Worcester, Kidney stone disease, J. Clin. Invest. 115 (2005) 2598–2608.
[2] M. Daudon, P. Jungers, Drug-induced renal calculi: epidemiology, prevention and management, Drugs 64 (2004) 245–275.
[3] C.Y. Pak, K. Sakhaee, T.I. Hwang, G.M. Preminger, J.A. Harvey, Nephrolithiasis from calcium supplementation, J. Urol. 137 (1987) 1212–1213.
[4] H.N. Noe, J.F. Bryant, S. Roy III, F.B. Stapleton, Urolithiasis in pre-term neonates associated with furosemide therapy, J. Urol. 132 (1984) 93–94.
[5] C. Ahlstrand, H.G. Tiselius, Urine composition and stone formation during treatment with acetazolamide, Scand. J. Urol. Nephrol. 21 (1987) 225–228.
[6] W.H. Dick, J.E. Lingeman, G.M. Preminger, L.H. Smith, D.M. Wilson, W.L. Shirrell, Laxative abuse as a cause for ammonium urate renal calculi, J. Urol. 143 (1990) 244–247.
[7] D.A. McLain, F.J. Garriga, O.S. Kantor, Adverse reactions associated with ticrynafen use, JAMA 243 (1980) 763–764.
[8] R.W. Grunberg, S.J. Silberg, Triamterene-induced nephrolithiasis, JAMA 245 (1981) 2494–2495.
[9] L.A. Farina, R.J. Palou, T.G. Chechile, Reversible acute renal failure due to sulfonamide-induced lithiasis in an AIDS patient, Arch. Esp. Urol. 48 (1995) 418–419.
[10] M. Daudon, L. Estepa, J.P. Viard, D. Joly, P. Jungers, Urinary stones in HIV-1-positive patients treated with indinavir, Lancet 349 (1997) 1294–1295.
[11] J.H. Farrer, J. Rajfer, Silicate urolithiasis, J. Urol. 132 (1984) 739–740.

[12] G. Feher, A. Benczik, E. Szabo, I. Rethy, M. Berenyi, Renal gravel formation inducing renal insufficiency as a side-effect of ceftriaxon, Orv. Hetil. 140 (1999) 769–771.

[13] Z. Avci, A. Koktener, N. Uras, F. Catal, A. Karadag, O. Tekin, H. Degirmencioglu, E. Baskin, Nephrolithiasis associated with ceftriaxone therapy: a prospective study in 51 children, Arch. Dis. Child. 89 (2004) 1069–1072.

[14] M. Mohkam, A. Karimi, A. Gharib, H. Daneshmand, A. Khatami, N. Ghojevand, M. Sharifian, Ceftriaxone associated nephrolithiasis: a prospective study in 284 children, Pediatr. Nephrol. 22 (2007) 690–694.

[15] E. Steadman, D.W. Raisch, C.L. Bennett, J.S. Esterly, T. Becker, M. Postelnick, J.M. McKoy, S. Trifilio, P.R. Yarnold, M.H. Scheetz, Evaluation of a potential clinical interaction between ceftriaxone and calcium, Antimicrob. Agents Chemother. 54 (2010) 1534–1540.

[16] V. Stojanovic, V.G. Djuric, Nephrolithiasis caused by ceftriaxone in a 3-year-old child with ureteropelvic junction obstruction, Case Rep. Med. 2009 (2009) 365962.

[17] R.A. de Moor, A.C. Egberts, C.H. Schroder, Ceftriaxone-associated nephrolithiasis and biliary pseudolithiasis, Eur. J. Pediatr. 158 (1999) 975–977.

[18] V. Tasic, A. Sofijanova, V. Avramoski, Nephrolithiasis in a child with acute pyelonephritis. Ceftriaxone-induced nephrolithiasis and biliary pseudolithiasis, Pediatr. Nephrol. 20 (2005) 1510–1513.

[19] I.H. Patel, S. Chen, M. Parsonnet, M.R. Hackman, M.A. Brooks, J. Konikoff, S.A. Kaplan, Pharmacokinetics of ceftriaxone in humans, Antimicrob. Agents Chemother. 20 (1981) 634–641.

[20] S. Chutipongtanate, V. Thongboonkerd, Systematic comparisons of artificial urine formulas for in vitro cellular study, Anal. Biochem. 402 (2010) 110–112.

[21] S. Chutipongtanate, V. Thongboonkerd, Establishment of a novel colorimetric assay for high-throughput analysis of calcium oxalate crystal growth modulation, Analyst 135 (2010) 1309–1314.

[22] M.H. Saier Jr., Growth and differentiated properties of a kidney epithelial cell line (MDCK), Am. J. Physiol. 240 (1981) C106–C109.

[23] J.C. Lieske, S. Deganello, Nucleation, adhesion, and internalization of calcium-containing urinary crystals by renal cells, J. Am. Soc. Nephrol. 10 (Suppl 14) (1999) S422–S429.

[24] R.L. Ryall, Glycosaminoglycans, proteins, and stone formation: adult themes and child's play, Pediatr. Nephrol. 10 (1996) 656–666.

[25] V. Thongboonkerd, S. Chutipongtanate, T. Semangoen, P. Malasit, Urinary trefoil factor 1 is a novel potent inhibitor of calcium oxalate crystal growth and aggregation, J. Urol. 179 (2008) 1615–1619.

[26] Y.I. Rabinovich, M. Esayanur, S. Daosukho, K.J. Byer, H.E. El Shall, S.R. Khan, Adhesion force between calcium oxalate monohydrate crystal and kidney epithelial cells and possible relevance for kidney stone formation, J. Colloid Interf. Sci. 300 (2006) 131–140.

Journal of Analytical Science & Technology (2011) 2 (Suppl A), A46-A51
Proceeding www.jastmag.org
DOI 10.5355/JAST.2011.A46

Session I – Bioanalysis I **Open Access**

Proteomics in Dengue Virus Infection: Host Response in Human Endothelial Cells

Visith Thongboonkerd[1,2*]

[1]Medical Proteomics Unit, Office for Research and Development, Faculty of Medicine Siriraj Hospital, Mahidol University, Bangkok, Thailand
[2]Center for Research in Complex Systems Science, Mahidol University, Bangkok, Thailand

***Corresponding author:**
Visith Thongboonkerd, Email: thongboonkerd@dr.com (or) vthongbo@yahoo.com

From 2011 International Symposium on Analytical Science and Technology (ISAST)
Daejeon, Republic of Korea, 15-17 November, 2011

Abstract

This mini-review highlights important findings obtained from a series of our recent proteomic studies of human endothelial cells in response to dengue virus infection, which remains common in tropical/subtropical countries. These findings shed light onto mechanisms of vascular leakage, which is a fatal complication of this disease.

Key words: Dengue; Endothelial cell; Proteome; Proteomics; Vascular leakage

Introduction

Dengue virus (DENV) infection remains a common disease in tropical and subtropical regions with periodic outbreaks. The World Health Organization (WHO) has recently estimated that there are more than 2 billion people worldwide who are at risk of DENV infection and there may be 50-100 million individuals infected with DENV annually (among these, approximately 500,000 patients require hospitalization) [1].

The DENV-infected individuals may or may not have symptoms, which vary from mild to severe. The severe or fatal forms of DENV infection include dengue hemorrhagic fever (DHF) and dengue shock syndrome (DSS) with the hallmarks of vascular leakage, bleeding and shock. However, pathogenic mechanisms of vascular leakage in DHF and DSS remain unclear. Our group therefore performed a series of proteomic studies to address expression and functional changes of human endothelial cells in response to DENV infection [2,3]. The important findings obtained from these studies are highlighted as follows.

Results and Discussion

The optimal condition of DENV infection for proteome analysis of host response in human endothelial cells was carefully defined. This condition should provide the high percentage of infectivity but on the other hand should have the minimal degree of cell death, because the study focused mainly to early responses of the infected cells, not the changes caused by cell death. After obtaining such optimal condition, expression proteome analysis was performed followed by highly focused functional studies to address functional significance of the expression data (Fig. 1).

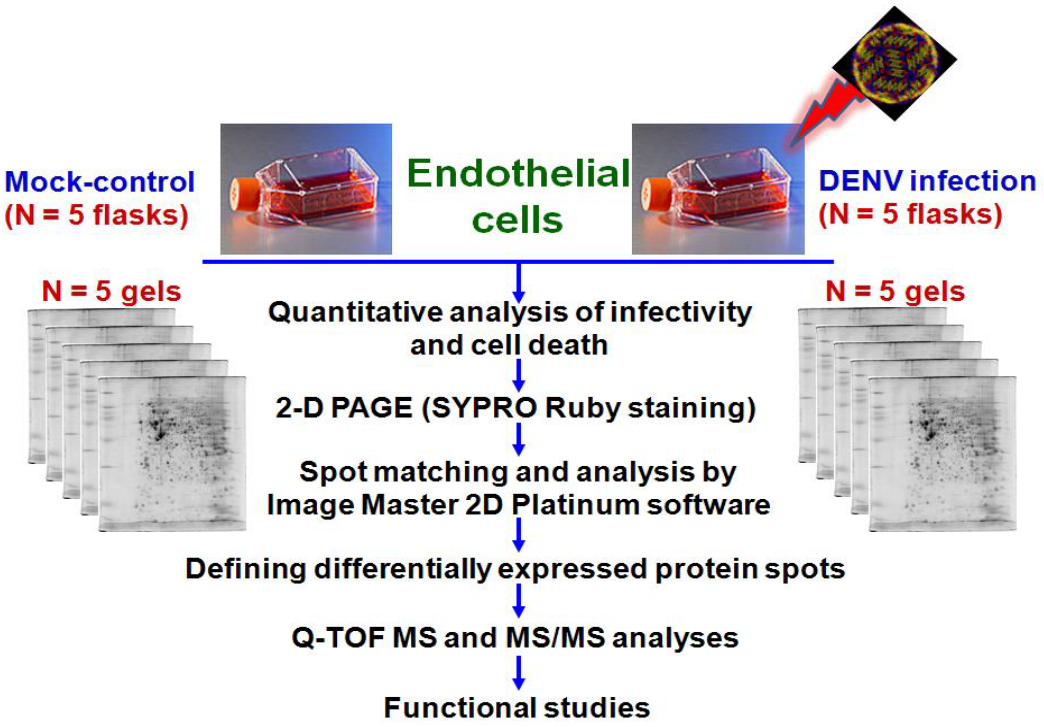


Fig. 1. Schematic summary of analytical approach

Human endothelial cells (EA.hy926) were challenged with DENV at various multiplicities of infection (MOI; or proportional amount of the viral particles per number of cells) (at 1, 5 and 10) for 2 h with 12, 24 and 48 h post-infection incubation periods. Non-infected (mock) cells served as the controls. The infectivity was quantitated by flow cytometric analysis of DENV envelope protein.

The results showed that the cells had the highest percentage of infection at 24 h post-infection with the MOI of 10, whereas prolonged incubation to 48 h did not significantly increase the infectivity. Morphological examination revealed that the DENV-infected cells at 12 and 24 h post-infection had similar morphology to the mock-control cells without any obvious changes regardless of the MOI used. However, at 48 h post-infection, particular with the MOI of 5 and 10, the infected cells showed characteristics of cell death, including cellular detachment and rounding. Quantitative analysis of cell death by flow cytometry using annexin V/propidium iodide co-staining showed that total cell death (early/late apoptosis and necrosis) at 24 h post-infection with the MOI of 10 was not increased significantly. Based on these infectivity and cell death data, the MOI of 10 with 24 h post-infection period was used for all subsequent proteome analyses [2].

Cellular proteins were extracted, resolved by two-dimensional polyacrylamide gel electrophoresis (2-D PAGE), and visualized by SYPRO Ruby fluorescence stain. Comparative proteomics was performed by spot matching and intensity analysis, which revealed 15 protein spots, whose levels were significantly altered by DENV infection. All of them were successfully identified by quadrupole time-of-flight (Q-TOF) mass spectrometry (MS) and tandem mass spectrometry (MS/MS) (Fig. 2) [2].

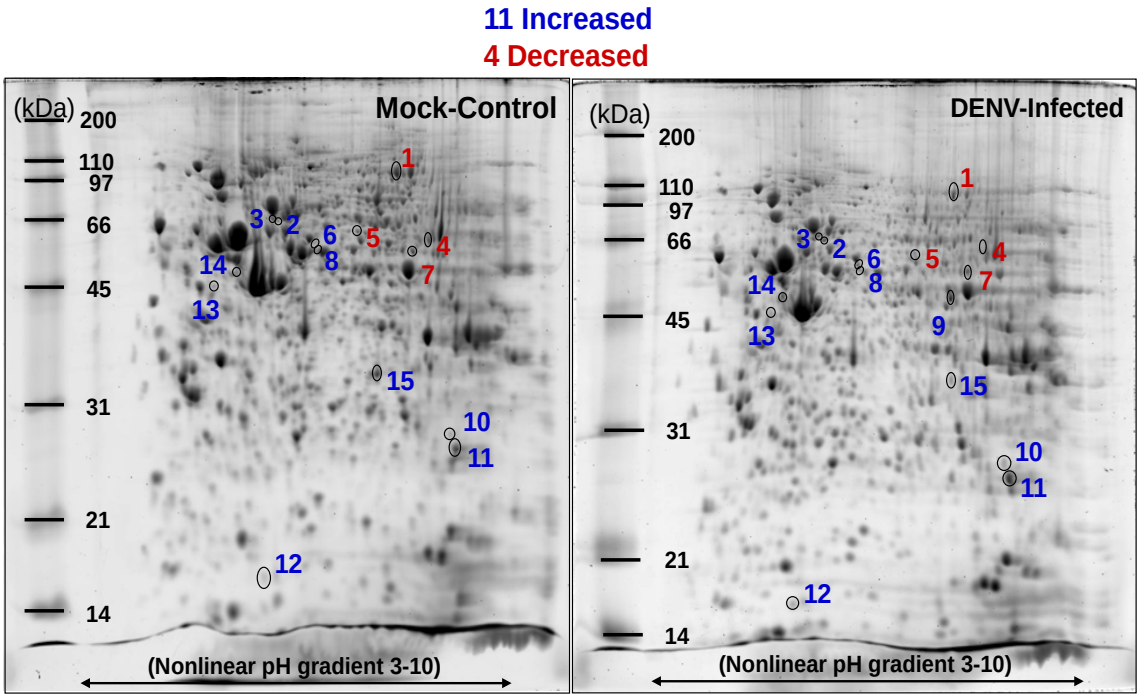


Fig. 2. The proteome map of significantly altered proteins in human endothelial cells in response to DENV infection (n = 5 gels per group derived from 5 individual culture flasks). Modified from Ref [2]. with permission from the American Chemical Society (ACS).

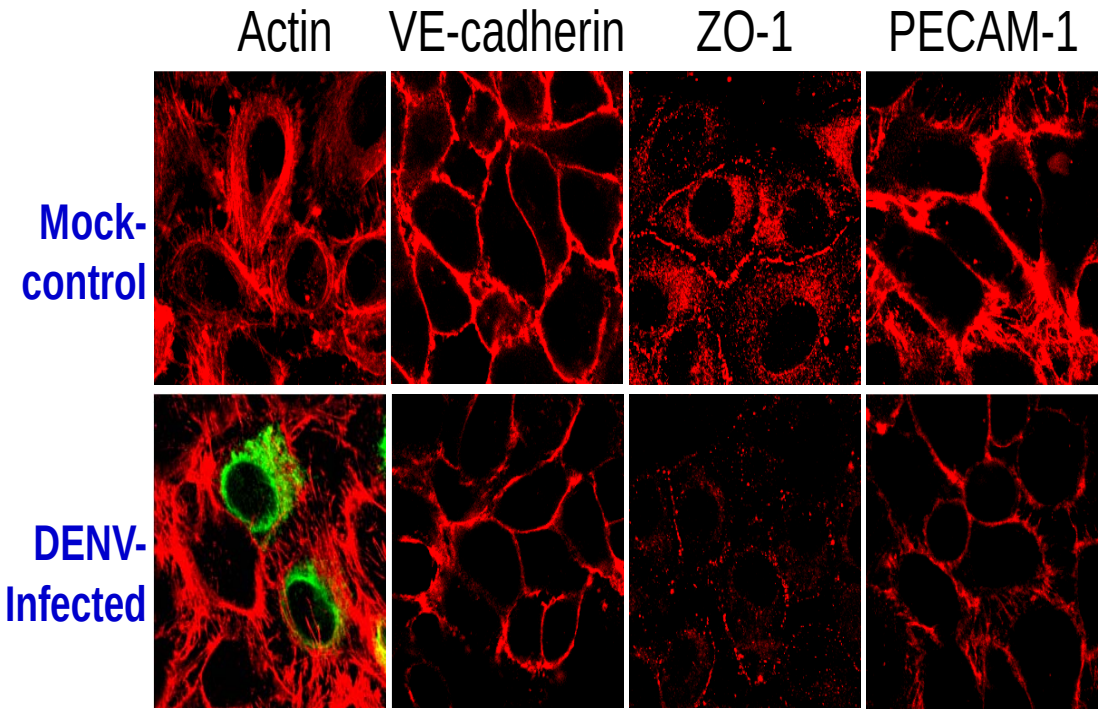


Fig. 3. Expression and organization of actin, VE-cadherin, ZO-1 and PECAM-1 upon DENV infection (showed in red, whereas DENV envelope protein is illustrated in green). Modified from Ref.[2] with permission from the American Chemical Society (ACS).

Among the 15 significantly altered proteins, level of actin was decreased. Actin plays a critical role in cellular structure and integrity of the cells, and is related to tight junction and adhesion molecules, which are crucial for controlling vascular permeability [4]. Actin cytoskeletal assembly and expression of junctional protein complex [5], which includes vascular endothelial cadherin (VE-cadherin), zonula occludens-1 (ZO-1) and platelet-endothelial cell adhesion molecule-1 (PECAM-1), were then evaluated. Laser-scanning confocal microscopic examination revealed decreased expression and re-organization of actin filament in the DENV-infected cells. Moreover, the results showed markedly reduced expression of VE-cadherin, ZO-1 and PECAM-1 (Fig. 3). This is the first proteome dataset to demonstrate the defects in cytoskeletal assembly and junctional protein complex induced by DENV infection [2].

To further address the significance of these findings, alterations in actin and junctional proteins during transendothelial migration of leukocytes, which frequently occurs in DENV infection, were investigated. The transendothelial migration event, particularly at the step of PECAM-1 engagement, was simulated by PECAM-1 cross-linking. The data showed that PECAM-1 cross-linking had the synergistic effects with DENV infection on the decreases of actin, VE-cadherin and ZO-1, strengthening the important role of transendothelial migration of leukocytes in vascular leakage observed in DHF and DSS (Fig. 4) [2].

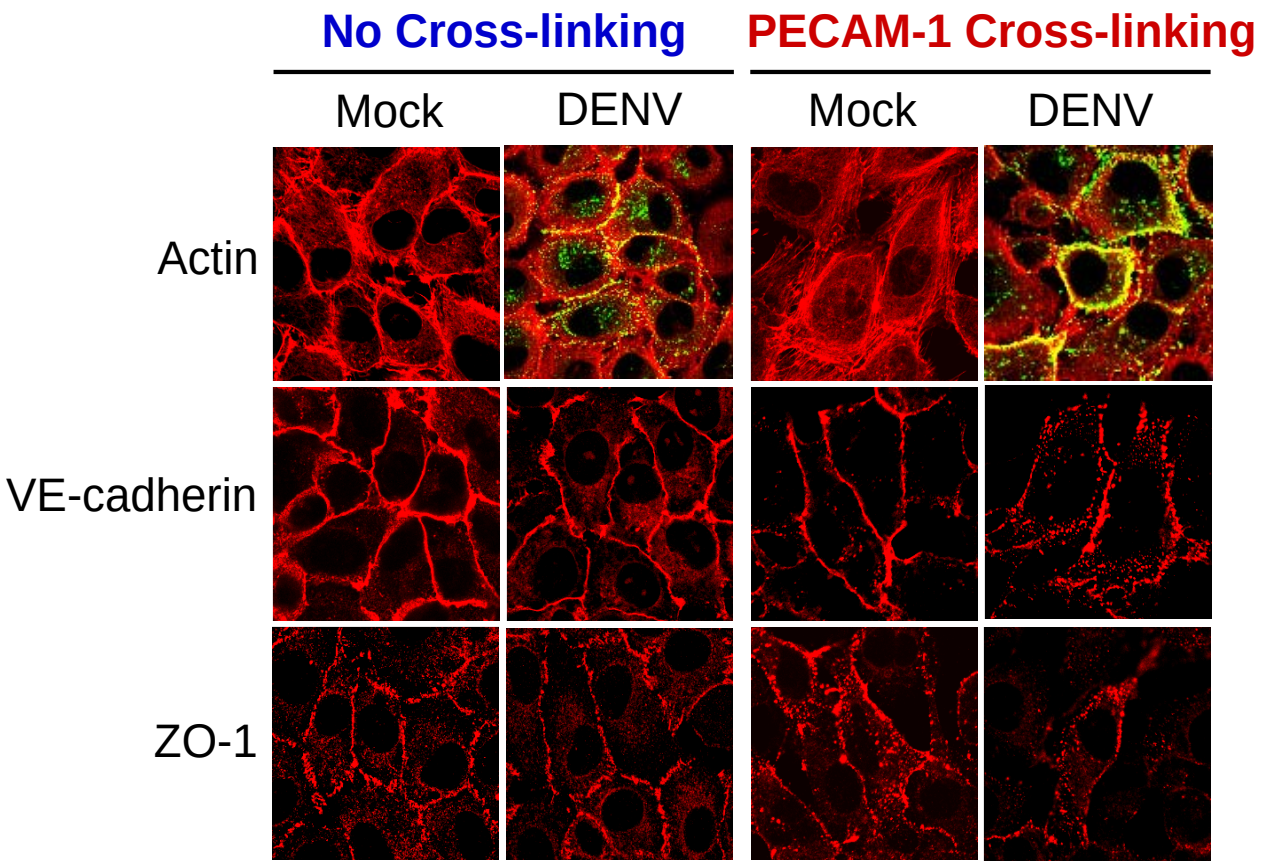


Fig. 4. Expression and organization of actin, VE-cadherin and ZO-1 (showed in red, whereas DENV envelope protein is illustrated in green) after PECAM-1 engagement. Modified from Ref.[2] with permission from the American Chemical Society (ACS).

On the other hand, five forms of heterogeneous nuclear ribonucleoproteins (hnRNPs) were increased. The functional significance of these proteins in response to DENV infection was addressed by functional proteomics study to identify hnRNPs-interacting proteins in the DENV-infected endothelial cells.

Immunoprecipitation followed by 2-D PAGE and Q-TOF MS and MS/MS analyses revealed 18 and 13 interacting partners of hnRNP C1/C2 and hnRNP K, respectively [3]. Among these interacting proteins, interestingly, vimentin was a common partner for both hnRNPs. The interaction between vimentin and these hnRNPs was confirmed by reciprocal immuno-precipitation followed by Western blot analysis. In addition, this interaction was also confirmed by double immunofluorescence co-staining and confocal microscopic examination. Moreover, disruption of vimentin filament by sub-lethal dose of acrylamide caused dissociation of this protein complex [3].

Not only host-host but also host-virus protein-protein interactions were observed. Double immuno-fluorescence co-staining showed that vimentin was strongly associated with DENV nonstructural protein-1 (NS1). The disruption of vimentin filament by sub-lethal dose of acrylamide dissociated this host-virus protein complex and also reduced DENV NS1 protein expression. More importantly, the disruption of vimentin filament by sub-lethal dose of acrylamide markedly reduced both replication and release of DENV (Fig. 5) [3]

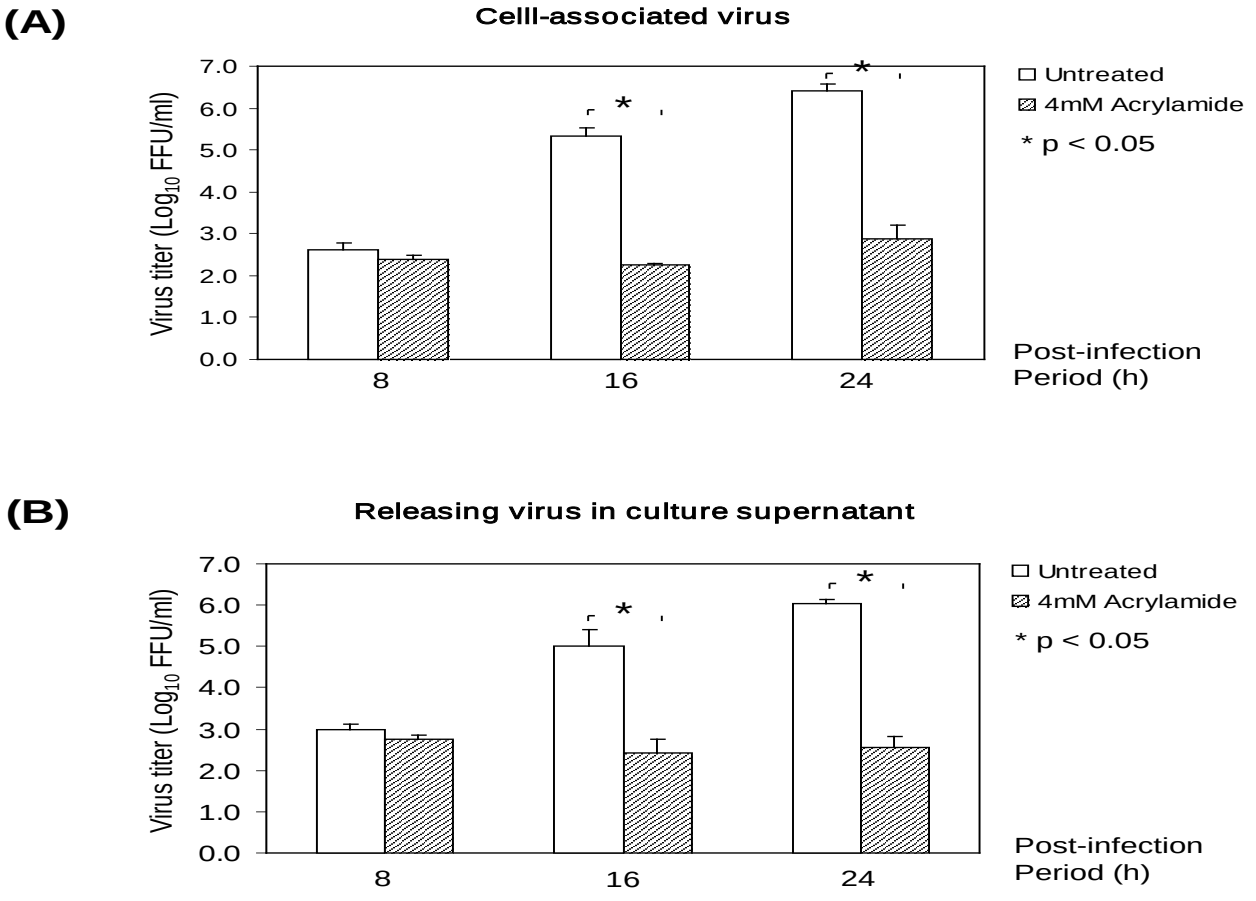


Fig. 5. Effects of vimentin disruption on DENV replication (A) and release (B). Modified from Ref.[3] with permission from the Royal Society of Chemistry (RSC).

In summary, the data obtained from this series of the study indicate that:

- DENV infection causes defects in tight junction (ZO-1), adherens junction (VE-cadherin) and adhesion molecule (PECAM-1) of human endothelial cells.

- Vimentin in human endothelial cells interacts with hnRNPs and DENV NS1 protein. These interactions are important for DENV replication and release.

- These findings provide novel insights into responses of human endothelial cells to DENV infection and better understanding of the pathogenic mechanisms of vascular leakage in DHF and DSS.

Acknowledgement

This work was supported by The Thailand Research Fund (RTA5380005), Office of the Higher Education Commission and Mahidol University under the National Research Universities Initiative. The author is also supported by “Chalermphrakiat” Grant.

References

1. Halstead, S. B. Dengue. *Lancet* **2007**, *370*, 1644-1652.
2. Kanlaya, R.; Pattanakitsakul, S. N.; Sinchaikul, S.; Chen, S. T.; Thongboonkerd, V. Alterations in actin cytoskeletal assembly and junctional protein complexes in human endothelial cells induced by dengue virus infection and mimicry of leukocyte transendothelial migration. *J Proteome. Res.* **2009**, *8*, 2551-2562.
3. Kanlaya, R.; Pattanakitsakul, S. N.; Sinchaikul, S.; Chen, S. T.; Thongboonkerd, V. Vimentin interacts with heterogeneous nuclear ribonucleoproteins and dengue nonstructural protein 1 and is important for viral replication and release. *Mol. Biosyst.* **2010**, *6*, 795-806.
4. Basu, A.; Chaturvedi, U. C. Vascular endothelium: the battlefield of dengue viruses. *FEMS Immunol. Med. Microbiol.* **2008**, *53*, 287-299.
5. Vandenbroucke, E.; Mehta, D.; Minshall, R.; Malik, A. B. Regulation of endothelial junctional permeability. *Ann. N. Y. Acad Sci* **2008**, *1123*, 134-145.

Journal of proteome research

ARTICLE

pubs.acs.org/jpr

Large-scale Identification of Calcium Oxalate Monohydrate Crystal-binding Proteins on Apical Membrane of Distal Renal Tubular Epithelial Cells

Kedsarin Fong-ngern,[†,‡] Paleerath Peerapen,[†,‡] Supachok Sinchaikul,[§] Shui-Tein Chen,[§] and Visith Thongboonkerd*[,†,∥]

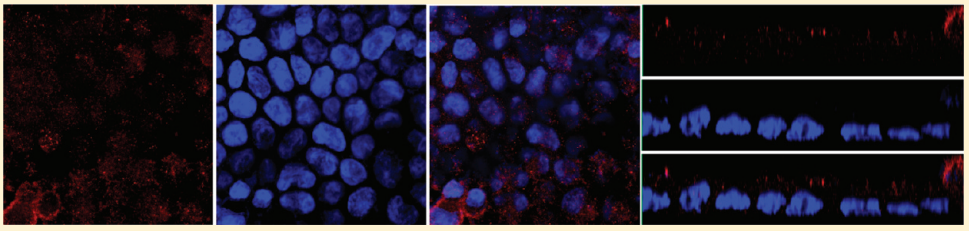
[†]Medical Proteomics Unit, Office for Research and Development, Faculty of Medicine Siriraj Hospital, Mahidol University, Bangkok, Thailand

[‡]Department of Immunology and Immunology Graduate Program, Faculty of Medicine Siriraj Hospital, Mahidol University, Bangkok, Thailand

[§]Institute of Biological Chemistry and Genomic Research Center, Academia Sinica, Taipei, Taiwan

[∥]Center for Research in Complex Systems Science, Mahidol University, Bangkok, Thailand

ABSTRACT:



Adhesion of calcium oxalate monohydrate (COM) crystals onto apical surface of renal tubular epithelial cells is a crucial mechanism for crystal retention, leading to kidney stone formation. Various proteins on apical membrane may bind to COM crystals; however, these crystal-binding proteins remained unidentified. The present study therefore aimed to identify COM crystal-binding proteins on apical membrane of distal renal tubular epithelial cells. Madin-Darby Canine Kidney (MDCK) cells were cultivated to be polarized epithelial cells and apical membrane was isolated from these cells using a peeling method established recently. Enrichment and purity of isolated apical membrane were confirmed by Western blot analysis for specific markers of apical (gp135) and basolateral (Na^+/K^+-ATPase) membranes. Proteins derived from the isolated apical membrane were then resuspended in artificial urine and incubated with COM crystals. The bound proteins were eluted, resolved by SDS-PAGE, and analyzed by Q-TOF MS and MS/MS, which identified 96 proteins. Among these, expression and localization of annexin II on apical surface of MDCK cells were confirmed by Western blot analysis, immunofluorescence staining, and laser-scanning confocal microscopic examination. Finally, the function of annexin II as the COM crystal-binding protein was successfully validated by COM crystal-binding assay. This large data set offers many opportunities for further investigations of kidney stone disease and may lead to the development of new therapeutic targets.

KEYWORDS: apical membrane, calcium oxalate, crystal adhesion, crystal-binding protein, kidney stone, nephrolithiasis, proteomics, renal tubular cells

INTRODUCTION

Kidney stone disease (nephrolithiasis) remains a common disease with a high recurrent rate (approximately 50% within 5−10 years and 75% within 20 years after surgical removal).[1] The recurrent rate is even higher after the first recurrence.[2] The initial processes of kidney stone formation include crystallization and crystal retention. The former occurs by supersaturation of ionic compounds in renal tubular fluid, whereas the latter develops thereafter by adhesion of causative crystals (mainly calcium oxalate monohydrate or COM, which is most commonly found in kidney stone matrices) onto apical or luminal surface of epithelial cells lining along renal tubules. Crystal adhesion can cause many downstream cascades of renal cellular responses.[3−6] Moreover, crystal adhesion can also enhance the adhesion of additional crystals, leading to crystal aggregation and retention inside renal tubules, and finally stone formation.[7,8]

In many previous studies using rat models, hyperoxaluria and calcium oxalate crystalluria were induced in rats by intraperitoneal injection of sodium oxalate[9] or oral administration of 0.75% ethylene glycol through drinking water.[10] Their kidney tissues were then investigated under polarized light or scanning electron microscope (SEM). The results showed that many calcium oxalate crystals were initially attached on renal tubular cell surface

Received: March 17, 2011
Published: August 22, 2011

ACS Publications © 2011 American Chemical Society

in association with microvilli. Thereafter, some of those crystals were found in the intercellular space, whereas some were internalized into the cells.[9,10] In a human study, kidney tissues were obtained from patients with calcium oxalate nephrolithiasis.[9] From these, approximately 50% of the specimens had crystals adhered on renal tubular epithelial cells and some of them were seen inside the cells.[9] These findings strengthen the crucial role of crystal adhesion in kidney stone disease.

The mechanisms underlying COM crystal adhesion on the cell surface are quite complicated. Surface charge is an important factor mediating crystal adhesion as the data obtained from previous studies revealed that COM crystals adhered to the cell surface at anionic sites and could be blocked by specific cations.[11] Adhesive property, electrostatic binding and specific interactions are also believed to be other important factors mediating crystal adhesion. During the past decade, several studies had attempted to identify surface molecules on renal tubular cells that might serve as the receptors for COM crystal adhesion with the ultimate goal to inhibit or block these bindings for disease prevention. Indeed, the apical membrane of renal tubular cells comprises various types of membrane proteins.[12] Many of these apical membrane proteins are expected to play a role in facilitating crystal-cell adhesion. However, only a small number of calcium oxalate crystal-binding proteins have been identified, including sialic acid-containing proteins,[8] annexin II,[13] nucleolin-related protein,[14,15] osteopontin,[16] and surface receptor CD44.[16,17] However, there should be many more calcium oxalate crystal-binding proteins, which remained unidentified.

The present study therefore aimed to identify all of potential COM crystal-binding proteins on apical membrane of distal renal tubular epithelial cells using a proteomics approach. Polarized MDCK cells were maintained and their apical membranes were isolated using a peeling method established recently.[18] Purity of apical membrane isolation was checked and proteins were then solubilized from the purified apical membranes. After an overnight incubation with COM crystals, the unbound proteins were discarded, whereas the bound proteins were resolved with SDS-PAGE and identified by Q-TOF MS and MS/MS analyses. The proteomic data were then confirmed by Western blot analysis, immunofluorescence staining, and laser-scanning confocal microscopic examination.

MATERIALS AND METHODS

Cultivation and Polarization

MDCK cells were grown in Eagle's minimum essential medium (MEM) (GIBCO, Invitrogen Corporation; Grand Island, NY) supplemented with 10% fetal bovine serum (FBS), 1.2% penicillinG/streptomycin and 2 mM L-glutamine and maintained in a humidified incubator with 5% CO_2 at 37 °C. For polarization, MDCK cells at a density of approximately 5.0−7.5 × 10^4cells/mL were seeded and grown on prewetted collagen-coated permeable polycarbonate membrane in Transwells (0.4 μm pore size; Corstar; Cambridge, MA) for four days. The culture medium was refreshed every other day. Polarization was confirmed by immunofluorescence staining and laser-scanning confocal microscopy (described with more details below).

Isolation of Apical Membrane and Solubilization of Apical Membrane Proteins

Apical membrane of the polarized MDCK cells was isolated by a peeling method established recently.[18] Briefly, after the cells were maintained in Transwells for four days, the culture medium was removed and the polarized cells were rinsed twice with ice-cold membrane preserving buffer (1 mM $MgCl_2$ and 0.1 mM $CaCl_2$ in PBS). Thereafter, Whatman filter paper (0.18-mm-thick, Whatman International Ltd.; Maidstone, U.K.) prewetted with deionized water was placed onto the polarized cell monolayer. After a 5-min incubation period, the filter paper was peeled out and the apical membranes retained at the filter paper surface were harvested by rehydration in deionized water and gentle scrapping. The apical membrane-enriched fraction was then lyophilized. Dried apical membrane was solubilized in 1× Laemmli's buffer and then dialyzed against deionized water at 4 °C overnight with three changes of deionized water. After lyophilization, apical membrane protein powder was stored at −80 °C until used. Enrichment and purity of isolated apical membrane were confirmed by Western blot analysis for specific markers of apical (gp135) and basolateral (Na^+/K^+-ATPase) membranes (described with more details below).

Preparation of COM Crystals

COM crystals were prepared as previously described.[19] Briefly, 10 mM calcium chloride dihydrate ($CaCl_2 \cdot 2H_2O$) was mixed with 10 mM sodium oxalate ($Na_2C_2O_4$) in Tris buffer containing 90 mM NaCl (pH 7.4) to make their final concentrations to 5 mM and 0.5 mM, respectively. The mixture was incubated at 25 °C overnight and COM crystals were harvested by a centrifugation at 3000 rpm for 5 min. Supernatant was discarded and the crystals were resuspended in methanol. After another centrifugation at 3000 rpm for 5 min, methanol was discarded and the crystals were dried at 37 °C overnight.

COM Crystal Adhesion and Separation of COM Crystal-Binding Proteins

Apical membrane protein powder was resuspended into 1 mL protein-free artificial urine (containing 5 mM $CaCl_2$, 200 mM urea, 4 mM creatinine, 5 mM $Na_3C_6H_5O_7 \cdot 2H_2O$, 54 mM NaCl, 30 mM KCl, 15 mM NH_4Cl, 2 mM $MgSO_4 \cdot 7H_2O$, and 9 mM Na_2SO_4; pH = 6.2 and osmolality = 446 mOsm/kg).[20] Thereafter, 5 mg COM crystals were added and apical membrane proteins were allowed to interact with COM crystals in the artificial urine on a continuous rotator at 4 °C overnight. The crystal-protein complexes were then collected by a centrifugation at 3000 rpm for 5 min at 4 °C and the unbound proteins were discarded. Thereafter, the crystal-protein complexes were washed three times with PBS and other three times with 4 mM EDTA in PBS. After the final wash with PBS, COM crystal-binding proteins were eluted by 1× Laemmli's buffer and separated in 12% SDS-PAGE gel. The resolved COM crystal-binding proteins were visualized by Coomassie Brilliant Blue G-250 stain. All the procedures in this step are summarized in Figure 1.

In-Gel Tryptic Digestion

A total of 40 gel slices were excised from the whole lane of COM crystal-binding proteins in a preparative gel derived from 6 × 10^7 cells. The excised gel slices were washed twice with 200 μL of 50% acetonitrile (ACN)/25 mM NH_4HCO_3 buffer (pH 8.0) at room temperature for 15 min, and then washed once with 200 μL of 100% ACN. After washing, the solvent was removed and the gel pieces were dried by a SpeedVac concentrator (Savant; Holbrook, NY). The dried gel plugs were then rehydrated with 10 μL of 1% (w/v) trypsin (Promega; Madison, WI) in 25 mM NH_4HCO_3. After rehydration, the gel pieces were crushed with siliconized blue stick and incubated at 37 °C for at least 16 h. Peptides were subsequently extracted twice with 50 μL

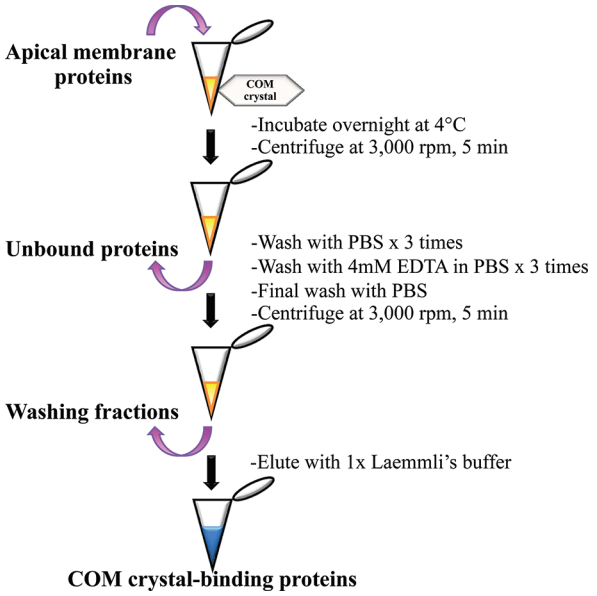


Figure 1. Schematic summary of methodologies to prepare COM crystal-binding proteins. Apical membrane proteins were incubated with COM crystals overnight at 4 °C. After centrifugation, unbound proteins were excluded and the remaining COM crystal-binding proteins were vigorously washed with PBS and 4 mM EDTA. Finally, COM crystal-binding proteins were eluted with 1× Laemmli's buffer.

of 50% ACN/5% trifluoroacetic acid (TFA); the extracted solutions were then combined and dried with the SpeedVac concentrator. The peptide pellets were resuspended with 10 μL of 0.1% TFA and purified using ZipTip$_{C18}$ (Millipore; Bedford, MA). The peptide solution was drawn up and down in the ZipTip$_{C18}$ 10 times and then washed with 10 μL of 0.1% formic acid by drawing up and expelling the washing solution three times. The peptides were finally eluted with 5 μL of 75% ACN/0.1% formic acid.

Quadrupole Time-of-Flight Mass Spectrometry and Tandem Mass Spectrometry (Q-TOF MS and MS/MS)

The trypsinized samples were premixed 1:1 with the matrix solution containing 5 mg/mL α-cyano-4-hydroxycinnamic acid in 50% ACN, 0.1% (v/v) TFA and 2% (w/v) ammonium citrate, and deposited onto the 96-well MALDI (matrix-assisted laser desorption/ionization) target plate. The samples were analyzed by Q-TOF Ultima mass spectrometer (Micromass; Manchester, U.K.), which was fully automated with predefined probe motion pattern and the peak intensity threshold for switching over from MS survey scanning to MS/MS, and from one MS/MS to another. Within each sample well, parent ions that met the predefined criteria (any peak within the m/z 800−3000 range with intensity above 10 count ± include/exclude list) were selected for CID MS/MS using argon as the collision gas and a mass dependent ±5 V rolling collision energy until the end of the probe pattern was reached. The instrument was externally calibrated to less than 5 ppm accuracy over the mass range of m/z 800−3000 using a sodium iodide and PEG 200, 600, 1000, and 2000 mixtures and further adjusted with Glu-Fibrinopeptide B as the near-point lock mass calibrant during data processing. At a laser firing rate of 10 Hz, individual spectra from 5 s integration period acquired for each of the MS survey and MS/MS performed were combined, smoothed, deisotoped (fast option) and centroided using the Micromass ProteinLynxT Global Server (PGS) 2.0 data processing software. The procedure was processed according to the instruction of Micromass data processing software. The combined peptide mass fingerprinting (PMF) and MS/MS ion meta data were searched in concert against the specified protein database within the PGS 2.0 workflow. Additionally, the MS and MS/MS ions data were extracted and outputted as MASCOT-searchable .txt and .pkl files for independent searches using the publicly available MASCOT search engine (http://www.matrixscience.com) to query to the NCBI mammalian protein database, assuming that peptides were monoisotopic. Fixed modification was carbamidomethylation at cysteine residues, whereas variable modification was oxidation at methionine residues. Only one missed trypsin cleavage was allowed, and peptide mass tolerances of 100 and 50 ppm were allowed for PMF and MS/MS ions search, respectively.

Western Blot Analysis

To evaluate the yield and purity of enrichment or isolation of apical membrane, Western blot analysis for specific markers of apical (gp135) and basolateral (Na^+/K^+-ATPase) membranes was performed. Proteins derived from whole cell lysate and purified apical membrane (with an equal amount of 20 μg) were resolved in 12% SDS-PAGE and then transferred onto a nitrocellulose membrane (Whatman; Dassel, Germany) using a semidry transfer apparatus (Bio-Rad; Milano, Italy) at 75 mA for 1-h. Nonspecific bindings were blocked with 5% skim milk in PBS at room temperature for 1-h. The membrane was then incubated with rabbit polyclonal anti-gp135 (Santa Cruz Biotechnology; Santa Cruz, CA) (1:200 in 5% skim milk/PBS) or mouse monoclonal anti-Na^+/K^+-ATPase-α1 subunit (Santa Cruz Biotechnology) (1:1000 in 5% skim milk/PBS) at 4 °C overnight. Thereafter, the membrane was washed three times with PBS and further incubated with respective secondary antibody conjugated with horseradish peroxidase (1:2000 in 5% skim milk/PBS) at room temperature for 1 h. The immunoreactive bands were then visualized by SuperSignal West Pico chemiluminescence substrate (Pierce Biotechnology, Inc.; Rockford, IL) and autoradiography.

To confirm the presence of annexin II in apical membrane and COM crystal-binding fractions, an equal amount (20 μg) of proteins derived from whole cell lysate, purified apical membrane, and COM-binding fraction was loaded in each lane and resolved by 12% SDS-PAGE. Western blot analysis was performed as aforementioned using goat polyclonal antiannexin II (Santa Cruz Biotechnology) (1:1000 in 5% skim milk/PBS) as the primary antibody.

Immunofluorescence Staining and Laser-Scanning Confocal Microscopy

To confirm polarization of MDCK cells, the polarized MDCK monolayer was washed with membrane preserving buffer (1 mM $MgCl_2$ and 0.1 mM $CaCl_2$ in PBS), and then fixed with 3.7% formaldehyde in PBS at 25 °C for 10 min and permeabilized with 0.1% Triton X-100 at 25 °C for 10 min. After extensive washing with membrane preserving buffer, MDCK cells were incubated with mouse monoclonal antibody against zonula occludens-1 (ZO-1) (tight junction marker) (Invitrogen/Molecular Probes; Camarillo, CA), mouse monoclonal anti-Na^+/K^+-ATPase-α1 subunit (basolateral membrane marker) (Santa Cruz Biotechnology), or rabbit polyclonal anti-gp135 (apical membrane marker) (Santa Cruz Biotechnology) (all with a dilution of 1:50 in 1% BSA/PBS) at 37 °C for 1 h. The cells were then rinsed with PBS three times and then incubated with respective secondary antibody conjugated

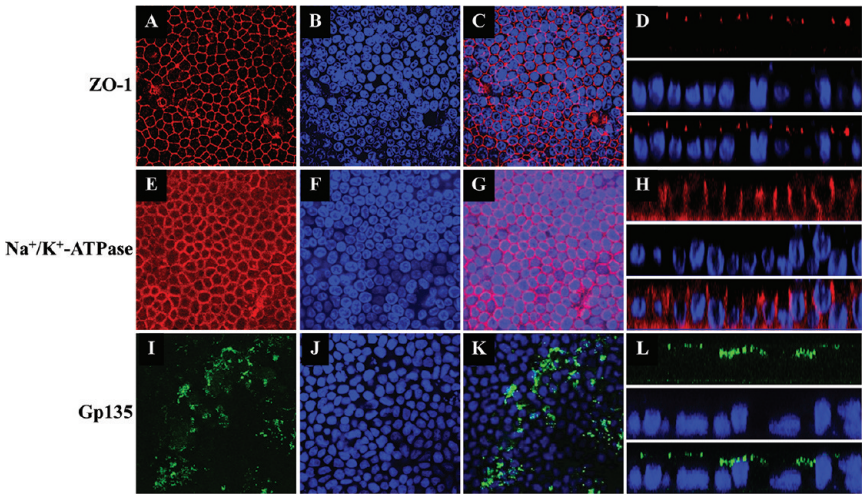


Figure 2. Confirmation of polarization of MDCK cells. Immunofluorescence study was performed to stain markers for (A−D) tight junction (ZO-1), (E−H) basolateral membrane (Na^+/K^+-ATPase α-subunit), and (I−L) apical membrane (gp135). These markers were then visualized and images were taken by laser-scanning confocal microscopy in both horizontal (the first three columns) and sagittal (the last column; panels D, H and L) views. Expression of ZO-1 and Na^+/K^+-ATPase is shown in red, whereas that of gp135 is in green. Blue illustrates nuclei stained with Hoechst dye. Original magnification powers were 400× in the first three columns and 630× in the last column (D, H and L).

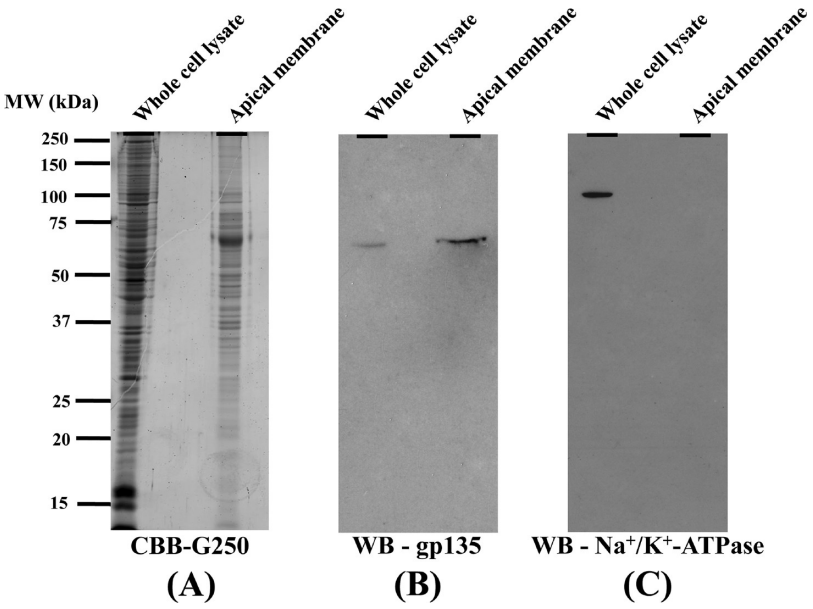


Figure 3. Yield of enrichment and purity of apical membrane isolation. (A) In total, 20 μg of proteins derived from MDCK whole cell lysate and isolated apical membrane were resolved by 12% SDS-PAGE and visualized by Coomassie Brilliant Blue G-250 stain. The resolved proteins were then transferred onto a nitrocellulose membrane and subjected to Western blot analysis using (B) rabbit polyclonal anti-gp135 (apical membrane marker) or (C) mouse monoclonal anti-Na^+/K^+-ATPase-α1 subunit (basolateral membrane marker).

with rhodamine or AlexaFluor-488 (Invitrogen/Molecular Probes) (1:5000 in 1% BSA/PBS) containing 0.1 μg/mL Hoechst dye (DNA staining for nuclear localization) (Invitrogen/Molecular Probes) at 37 °C for 1 h. Thereafter, the cells were examined by a laser-scanning confocal microscope equipped with an LSM5 Image Browser (LSM 510 Meta, Carl Zeiss; Jena, Germany).

To confirm the apical surface expression of annexin II, polarized MDCK cells were rinsed with membrane preserving buffer and then fixed with 3.7% formaldehyde in PBS at 25 °C for 15 min. After extensive washing with membrane preserving buffer, MDCK cells were incubated with goat polyclonal antiannexin II (Santa Cruz Biotechnology) (1:50 in 1% BSA/PBS) at 37 °C for 1 h. The cells were then rinsed with PBS three times and then incubated with rhodamine-conjugated antigoat IgG antibody (Invitrogen/Molecular Probes) (1:5000 in 1% BSA/PBS) containing 0.1 μg/mL Hoechst dye (Invitrogen/Molecular Probes) at 37 °C for 1 h. Thereafter, the cells were examined by a laser-scanning confocal microscope equipped with an LSM5 Image Browser (LSM 510 Meta, Carl Zeiss; Jena, Germany).

COM Crystal-Binding Assay

This set of experiments was performed in cell culture incubator at 37 °C with 5% CO_2. After MDCK cells were confluent, culture medium was removed and the cells were rinsed twice with

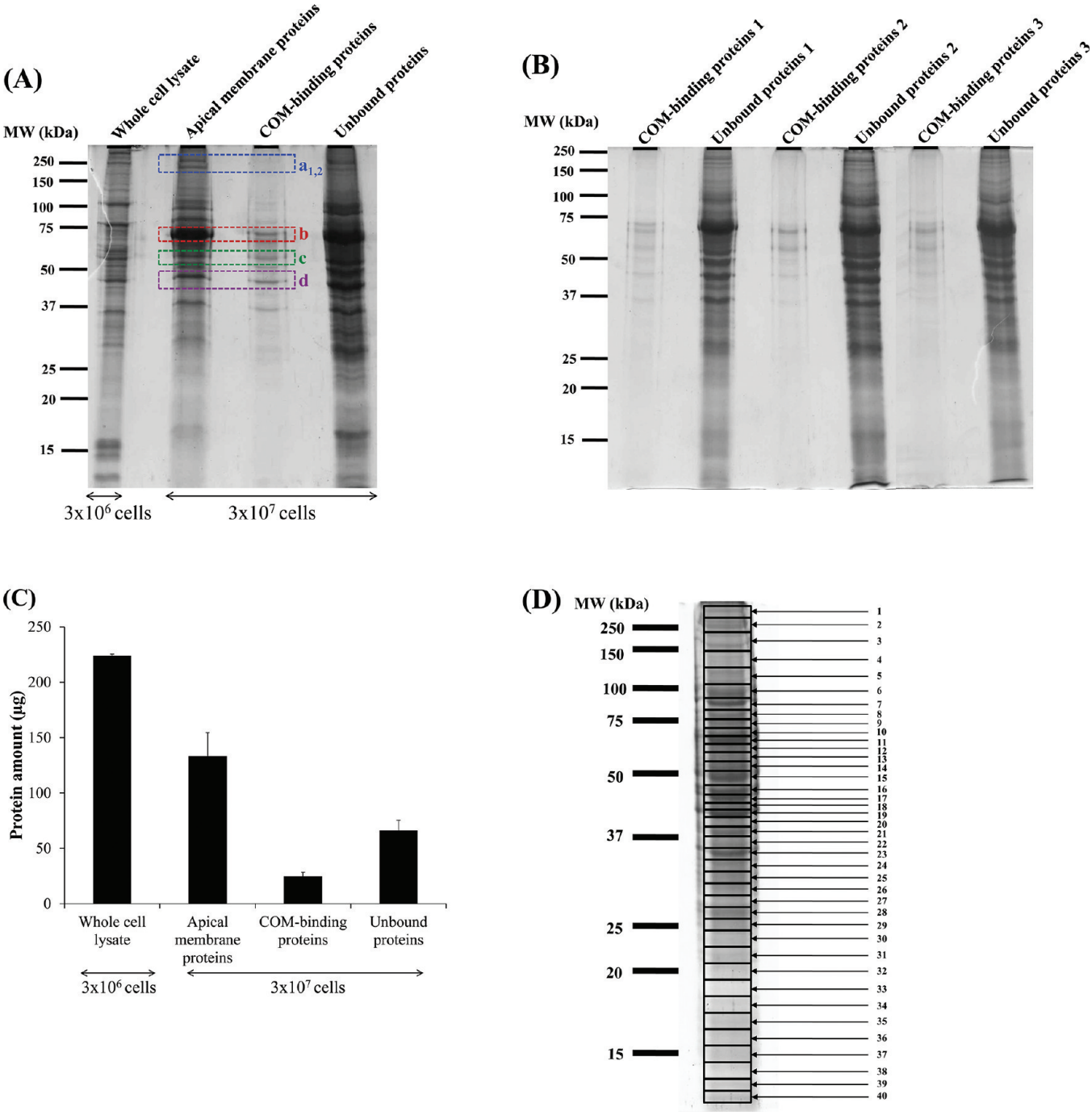


Figure 4. Isolation of COM crystal-binding proteins from apical membrane of polarized renal tubular epithelial cells. (A) COM crystal-binding proteins derived from 3×10^7 cells obtained from methodologies detailed in Figure 1 were resolved in 12% SDS-PAGE gel compared to purified apical membrane proteins and the unbound proteins derived from 3×10^7 cells, as well as whole cell lysate derived from 3×10^6 cells. The highlighted bands a, b, c, and d illustrate the selectivity of COM crystal binding of the COM crystal-binding proteins, as compared to the starting apical membrane fraction. (B) Reproducibility of isolation of COM crystal-binding proteins was confirmed in additional three independent experiments. (C) Amount of proteins derived from each fraction was quantitated. (D) COM crystal-binding proteins derived from 6×10^7 cells were resolved in a preparative gel. A total of 40 gel slices were excised and identified by Q-TOF MS and MS/MS (see also Table 1).

membrane preserving buffer. Nonspecific bindings were then blocked with 1% BSA in membrane preserving buffer for 15 min. Thereafter, the blocking solution was discarded and the cells were washed with membrane preserving buffer four times. MEM supplemented with 10% FBS was then added to the cells without (control) or with 0.2 μg/mL goat polyclonal antiannexin II (Santa Cruz Biotechnology) or goat IgG (nonspecific antibody) (Santa Cruz Biotechnology) for 30 min. Thereafter, the cells were rinsed with membrane preserving buffer four times and further incubated with COM crystals (100 μg/mL in MEM supplemented with 10% FBS) for 1 h. The unbound crystals were then removed by rigorous wash five times with PBS.

dx.doi.org/10.1021/pr2006878 |J. Proteome Res. 2011, 10, 4463–4477

Table 1. Summary of COM Crystal-Binding Proteins Derived from Isolated Apical Membranes Identified by Q-TOF MS and/or MS/MS Analyses[a]

band no.	protein name	NCBI ID	identified by	identification scores (MS, MS/MS)	%cov (MS, MS/MS)	no. of matched peptides (MS, MS/MS)	p*I*	MW (kDa)	BLAST link report[b]
1	Microtubule-actin cross-linking factor 1 isoform 1	gi|194207660	MS	96, NA	8, NA	34, NA	5.20	673.37	
1	Man1a2-prov protein	gi|149633134	MS	73, NA	25, NA	10, NA	6.55	53.52	
2	Protein C9orf55 isoform 1	gi|73971036	MS	78, NA	11, NA	15, NA	6.11	212.96	DENN/MADD domain containing 4C isoform 1
2	Spectrin, beta, nonerythrocytic 1 isoform 2	gi|109102947	MS	72, NA	12, NA	20, NA	5.34	251.96	
3	Hypothetical protein isoform 2	gi|114576746	MS	72, NA	22, NA	14, NA	9.53	109.76	
3	Membrane protein, palmitoylated 5 isoform 1	gi|73963296	MS	56, NA	18, NA	10, NA	5.80	77.47	
4	Hypothetical protein	gi|149632550	MS	82, NA	24, NA	10, NA	5.76	56.08	Temporarily Assigned Gene name family member (tag-278) isoform 7
4	Adenylosuccinate lyase 1	gi|126338737	MS	75, NA	30, NA	10, NA	8.49	56.824	
4	Glutamate receptor 3 isoform flip precursor isoform 2	gi|74008280	MS	50, NA	17, NA	12, NA	8.77	101.74	
5	Dedicator of cytokinesis protein 1 (180 kDa protein downstream of CRK) (DOCK180) isoform 1	gi|109463063	MS	71, NA	16, NA	17, NA	6.40	183.48	
5	Plasma membrane calcium ATPase 2 isoform b isoform 6	gi|73984626	MS	67, NA	15, NA	13, NA	5.75	132.79	
5	Hypothetical protein XP_539070	gi|73973961	MS	66, NA	22, NA	12, NA	5.33	95.16	BEN domain-containing protein 3
5	Ephrin type-B receptor 1 precursor (Tyrosine-protein kinase receptor EPH-2) (NET) (HEK6) (ELK)	gi|194663612	MS	71, NA	14, NA	12, NA	6.34	109.10	
6	Alpha-actinin 4	gi|126329095	MS	105, NA	20, NA	16, NA	5.12	104.98	
6	Centrobin (LYST-interacting protein 8), partial	gi|149438417	MS	74, NA	26, NA	10, NA	5.99	47.25	
6	Acyl-CoA thioesterase 9	gi|31980998	MS	77, NA	29, NA	11, NA	8.74	50.81	
7	Heat shock protein 1, alpha isoform 3	gi|73964029	MS, MS/MS	135, 219	35, 9	17, 4	5.15	71.04	
7	Hypothetical protein	gi|6807647	MS	183, NA	35, NA	21, NA	5.26	85.19	Heat shock protein HSP 90-beta
7	rCG43497, isoform CRA_a	gi|149069299	MS	147, NA	34, NA	17, NA	4.79	69.22	Heat shock protein HSP 90-alpha (HSP 86) isoform 2

dx.doi.org/10.1021/pr2006878 |*J. Proteome Res.* 2011, 10, 4463–4477

Table 1. Continued

band no.	protein name	NCBI ID	identified by	identification scores (MS, MS/MS)	%cov (MS, MS/MS)	no. of matched peptides (MS, MS/MS)	p*I*	MW (kDa)	BLAST link report[b]
7	Protein C9orf55 isoform 1	gi|73971036	MS	95, NA	11, NA	15, NA	6.11	212.96	DENN/MADD domain containing 4C isoform 1
8	Adenomatous polyposis coli protein (APC protein) isoform 1	gi|73951984	MS	58, NA	10, NA	17, NA	8.54	248.71	
8	Ezrin (p81) (Cytovillin) (Villin-2) isoform 3	gi|73945732	MS/MS	NA, 87	NA, 4	NA, 2	9.04	32.76	
8	Acyl-CoA thioesterase 9	gi|31980998	MS	86, NA	35, NA	12, NA	8.74	50.81	
9	78 kDa glucose-regulated protein precursor (GRP 78) (Immunoglobulin heavy chain binding protein) (BiP) (Endoplasmic reticulum lumenal Ca(2+) binding protein grp78) isoform 4	gi|73968068	MS, MS/MS	117, 58	34, 2	16, 1	5.06	66.33	
10	Heat shock protein 8 isoform 3	gi|73954621	MS, MS/MS	102, 58	34, 5	15, 2	5.42	64.01	
10	rCG57965, isoform CRA_b	gi|149041392	MS	100, NA	39, NA	14, NA	6.16	48.62	Heat shock 70 kDa protein 8 isoform 2 isoform 2
11	RAB5B protein	gi|114644159	MS	76, NA	36, NA	8, NA	9.33	32.63	
11	Flotillin-1 isoform 2	gi|73972128	MS	45, NA	25, NA	8, NA	6.71	47.54	
12	Golgi autoantigen, golgin subfamily a, 4 variant	gi|62088966	MS	79, NA	17, NA	20, NA	5.47	153.03	
12	Retinoblastoma-associated protein 140 isoform 4	gi|73985236	MS	73, NA	11, NA	17, NA	5.70	183.46	
12	Hypothetical protein LOC302773	gi|157820041	MS	72, NA	15, NA	17, NA	6.53	143.14	
12	mCG142584	gi|148688105	MS	82, NA	26, NA	12, NA	9.32	68.89	Four and a half LIM domains protein 1 isoform 6
13	Unidentified	NA	NA	NA, NA	NA, NA	NA, NA	NA	NA	
14	Vimentin isoform 9	gi|73948972	MS	145, NA	37, NA	20, NA	5.08	52.84	
14	Protein C9orf55 isoform 1	gi|73971036	MS	74, NA	12, NA	16, NA	6.11	212.96	DENN/MADD domain containing 4C isoform 1
14	Talin 2 isoform 5	gi|74000359	MS	57, NA	17, NA	10, NA	5.35	237.27	
15	Tubulin, beta 2	gi|109069453	MS	89, NA	33, NA	13, NA	4.64	47.83	
15	Crocc protein	gi|114584353	MS	87, NA	13, NA	20, NA	8.08	222.12	
16	MHC class I antigen	gi|259017317	MS	76, NA	50, NA	8, NA	5.53	20.98	

dx.doi.org/10.1021/pr2006878 |*J. Proteome Res.* 2011, 10, 4463–4477

Table 1. Continued

band no.	protein name	NCBI ID	identified by	identification scores (MS, MS/MS)	%cov (MS, MS/MS)	no. of matched peptides (MS, MS/MS)	p*I*	MW (kDa)	BLAST link report[b]
16	Alpha enolase (2-phospho-D-glycerate hydro-lyase) (Non-neural enolase) (NNE) (Enolase 1) (Phosphopyruvate hydratase) (C-myc promoter-binding protein) (MBP-1) (MPB-1) (Plasminogen-binding protein) isoform 14	gi|73956740	MS, MS/MS	96, 108	40, 5	13, 1	5.78	43.23	
16	Unknown (protein for MGC:38398)	gi|23271726	MS	87, NA	13, NA	20, NA	5.90	74.10	
16	S100 calcium binding protein, zeta	gi|73952378	MS	56, NA	10, NA	16, NA	6.03	35.71	
17	MIF4G domain containing, isoform CRA_c	gi|119609671	MS	84, NA	37, NA	7, NA	5.23	25.83	
18	MHC class II antigen	gi|4210492	MS	77, NA	63, NA	6, NA	5.33	10.25	
18	Immunoglobulin heavy chain variable region	gi|112700066	MS	71, NA	60, NA	5, NA	8.56	11.08	
19	Beta-actin	gi|118419975	MS, MS/MS	90, 174	39, 15	12, 4	5.66	40.94	
19	Gamma-actin	gi|809561	MS	84, NA	41, NA	10, NA	5.56	41.34	
19	Dynamin-like protein Dymple isoform	gi|3126874	MS	73, NA	28, NA	11, NA	6.27	78.58	
20	PDZ domain actin binding protein Shroom	gi|6467990	MS	82, NA	13, NA	19, NA	8.62	216.84	
20	Dynein heavy chain at 16F CG7092-PA	gi|109103632	MS	75, NA	9, NA	25, NA	5.71	457.18	
21	Dynein, axonemal, heavy chain 5, isoform CRA_a	gi|148676944	MS	88, NA	9, NA	31, NA	5.80	532.76	
21	Mitochondrial uncoupling protein 4 (UCP 4) (Solute carrier family 25, member 27)	gi|73973081	MS	59, NA	37, NA	10, NA	9.43	36.20	
22	Acyl-CoA thioesterase 9	gi|31980998	MS	77, NA	29, NA	10, NA	8.74	50.81	
22	Hypothetical protein	gi|149641845	MS	71, NA	25, NA	10, NA	7.74	55.66	Tumor necrosis factor type 1 receptor associated protein
23	Annexin A2	gi|119597993	MS	73, NA	43, NA	8, NA	5.93	32.45	
23	Glyceraldehyde-3-phosphate dehydrogenase	gi|50978862	MS, MS/MS	69, 166	42, 13	9, 4	8.20	36.07	
24	F-box and WD-40 domain protein 10	gi|162951862	MS	73, NA	21, NA	15, NA	9.45	117.41	
25	Hypothetical protein	gi|109093687	MS	80, NA	56, NA	8, NA	8.88	19.90	
26	Annexin A8 (Annexin VIII) (Vascular anticoagulant-beta) (VAC-beta) isoform 3	gi|73953205	MS	72, NA	37, NA	11, NA	5.17	32.86	
26	ART5 protein	gi|9998891	MS	70, NA	38, NA	6, NA	9.40	20.26	

dx.doi.org/10.1021/pr2006878 |*J. Proteome Res.* 2011, 10, 4463–4477

Table 1. Continued

band no.	protein name	NCBI ID	identified by	identification scores (MS, MS/MS)	%cov (MS, MS/MS)	no. of matched peptides (MS, MS/MS)	p*I*	MW (kDa)	BLAST link report[b]
26	Hypothetical protein	gi|149254381	MS	78, NA	36, NA	8, NA	9.90	31.55	
26	Hypothetical protein isoform 2	gi|114576746	MS	72, NA	27, NA	13, NA	9.53	109.76	
26	Protein C9orf55 isoform 1	gi|73971036	MS	67, NA	8, NA	12, NA	6.11	212.96	DENN/MADD domain containing 4C isoform 1
27	Unidentified	NA	NA	NA, NA	NA, NA	NA, NA	NA	NA	
28	Phosphoglycerate mutase 1 (Phosphoglycerate mutase isozyme B) (PGAM-B) (BPG-dependent PGAM 1) isoform 2	gi|73998120	MS, MS/MS	86, 137	42, 9	10, 2	5.93	26.00	
28	Protein C9orf55 isoform 1	gi|73971036	MS	90, NA	10, NA	14, NA	6.11	212.96	DENN/MADD domain containing 4C isoform 1
28	Unnamed protein product	gi|194379894	MS	71, NA	26, NA	8, NA	4.42	21.66	Synapse-associated protein 1
29	Triosephosphate isomerase (TIM) (Triose-phosphate isomerase) isoform 5	gi|73997316	MS, MS/MS	122, 59	61, 9	11, 1	8.29	23.18	
29	Hypothetical protein	gi|149638196	MS	73, NA	24, NA	10, NA	4.81	54.40	Androgen receptor associated protein 54
29	256 kD golgin	gi|1236759	MS	75, NA	12, NA	23, NA	5.34	256.67	
29	MTA1	gi|126290061	MS	73, NA	20, NA	14, NA	9.36	85.80	
29	MHC class II antigen	gi|186703093	MS	105, NA	80, NA	7, NA	5.80	10.02	
29	Hypothetical protein isoform 2	gi|114576746	MS	87, NA	22, NA	15, NA	9.53	109.76	
30	Heterogeneous nuclear ribonucleoprotein A1	gi|112421201	MS	83, NA	35, NA	12, NA	9.50	34.31	
30	mCG117968	gi|148682805	MS	72, NA	29, NA	11, NA	9.44	34.02	
30	Protein C9orf55 isoform 1	gi|73971036	MS	66, NA	12, NA	16, NA	6.11	212.96	DENN/MADD domain containing 4C isoform 1
31	Peroxiredoxin 2 (Thioredoxin peroxidase 1) (Thioredoxin-dependent peroxide reductase 1) (Thiol-specific antioxidant protein) (TSA) (PRP) (Natural killer cell enhancing factor B) (NKEF-B) isoform 1	gi|73986497	MS	60, NA	38, NA	6, NA	5.23	22.11	
31	mCG1051031	gi|148691331	MS	71, NA	26, NA	8, NA	5.66	31.33	MHC class I antigen
32	Hypothetical protein	gi|149258923	MS	75, NA	68, NA	6, NA	11.92	8.81	
32	Isopentenyl-diphosphate delta isomerase 2	gi|109505998	MS	77, NA	32, NA	6, NA	8.53	17.68	
33	Unidentified	NA	NA	NA, NA	NA, NA	NA, NA	NA	NA	

dx.doi.org/10.1021/pr2006878 |*J. Proteome Res.* 2011, 10, 4463–4477

Table 1. Continued

band no.	protein name	NCBI ID	identified by	identification scores (MS, MS/MS)	%cov (MS, MS/MS)	no. of matched peptides (MS, MS/MS)	p*I*	MW (kDa)	BLAST link report[b]
34	Adenylosuccinate lyase 1	gi|126338737	MS	77, NA	25, NA	9, NA	8.49	56.82	
35	Sulfotransferase family, cytosolic, 1C, member 2	gi|71896574	MS	79, NA	39, NA	11, NA	8.17	34.96	
35	Glucosamine-6-phosphate deaminase 2 isoform 1	gi|73974964	MS	65, NA	30, NA	9, NA	6.41	31.35	
35	MHC class II antigen	gi|186703093	MS	74, NA	80,NA	5, NA	5.80	10.02	
36	Peptidylprolyl isomerase A (cyclophilin A)	gi|28189771	MS, MS/MS	83, 57	66, 20	10, 2	8.46	17.09	
36	TRIMCyp	gi|76576111	MS	70, NA	54, NA	8, NA	8.26	18.19	
36	Vav-3 protein	gi|73959967	MS	66, NA	20, NA	13, NA	6.22	96.55	
36	Acyl-CoA thioesterase 9	gi|31980998	MS	74, NA	26, NA	10, NA	8.74	50.81	
36	Peptidyl-Pro cis trans isomerase isoform 1	gi|119902257	MS	73, NA	50, NA	7, NA	7.68	18.06	
37	rCG21715	gi|149063079	MS	90, NA	32, NA	9, NA	11.98	26.54	
37	Leucine rich repeat containing 42 isoform 1	gi|73956299	MS	65, NA	19, NA	6, NA	8.49	52.34	
38	Nestin	gi|2209202	MS	74, NA	70, NA	5, NA	8.50	6.56	
39	Acyl-CoA thioesterase 9	gi|31980998	MS	74, NA	25, NA	10, NA	8.74	50.81	
39	Hypothetical protein isoform 2	gi|114576746	MS	74, NA	19, NA	13, NA	9.53	109.76	
40	Rims2 protein	gi|111600267	MS	73, NA	16, NA	20, NA	9.39	175.87	
40	Leucine rich repeat containing 42 isoform 1	gi|73956299	MS	67, NA	28, NA	10, NA	8.49	52.34	
40	GDP dissociation inhibitor 1	gi|50978936	MS	78, NA	24, NA	9, NA	5.00	51.06	
40	Dynamin 1-like, isoform 4	gi|126338701	MS	73, NA	23, NA	12, NA	8.89	82.32	

[a] NCBI = National Center for Biotechnology Information; %cov = %sequence coverage [(number of the matched residues/total number of residues in the entire sequence) × 100%; NA = Not applicable.
[b] Only proteins with ≥80% identities are included.

dx.doi.org/10.1021/pr2006878 |*J. Proteome Res.* 2011, 10, 4463–4477

Table 2. Functional Classification of the Identified COM Crystal-Binding Proteins

function	protein name
Calcium-dependent phospholipid-binding	Annexin A2[a,b]
	Annexin A8 (Annexin VIII) (Vascular anticoagulant-beta) (VAC-beta) isoform 3[a,b]
Calcium ion-binding	Man1a2-prov protein[a,b]
	S100 calcium binding protein, zeta[b]
Cell cycle	MTA1
	Centrobin (LYST-interacting protein 8), partial
Cellular structure	Microtubule-actin cross-linking factor 1 isoform 1[b]
	Spectrin, beta, nonerythrocytic 1 isoform 2
	Adenomatous polyposis coli protein (APC protein) isoform 1
	Ezrin (p81) (Cytovillin) (Villin-2) isoform 3[a]
	Vimentin isoform 9
	Crocc protein[a]
	Talin 2 isoform 5[a]
	Tubulin, beta 2
	Beta-actin
	Gamma-actin
	PDZ domain actin binding protein Shroom[a]
	Leucine rich repeat containing 42 isoform 1[a]
	Nestin
	Dynein heavy chain at 16F CG7092-PA
	Dynein, axonemal, heavy chain 5, isoform CRA_a
Immune response	MHC class I antigen[a]
	MHC class II antigen[a]
	Immunoglobulin heavy chain variable region
	Tumor necrosis factor type 1 receptor associated protein
Ion transporter	Plasma membrane calcium ATPase 2 isoform b isoform 6[a,b]
	Mitochondrial uncoupling protein 4 (UCP 4) (Solute carrier family 25, member 27)[a,b]
Metabolism	Alpha enolase (2-phospho-D-glycerate hydro-lyase) (Non-neural enolase) (NNE) (Enolase 1) (Phosphopyruvate hydratase) (C-myc promoter-binding protein) (MBP-1) (MPB-1) (Plasminogen-binding protein) isoform 14[a,b]
	Glyceraldehyde-3-phosphate dehydrogenase[a]
	Phosphoglycerate mutase 1 (Phosphoglycerate mutase isozyme B) (PGAM-B) (BPG-dependent PGAM 1) isoform 2
	Triosephosphate isomerase (TIM) (Triose-phosphate isomerase) isoform 5[a]
	Sulfotransferase family, cytosolic, 1C, member 2
	Glucosamine-6-phosphate deaminase 2 isoform 1
mRNA processing	Heterogeneous nuclear ribonucleoprotein A1
	Peptidyl-Pro cis trans isomerase isoform 1
Protein and vesicular transport	DENN/MADD domain containing 4C isoform 1[a]
	Alpha-actinin 4[b]
	RAB5B protein[a]
	Golgi autoantigen, golgin subfamily a, 4 variant[a]
	Rims2 protein[a]
	GDP dissociation inhibitor 1
	Flotillin-1 isoform 2[a]
	Dynamin-like protein Dymple isoform[a]
	256 kD golgin[a]
	Dynamin 1-like, isoform 4[a]
Protein folding and protein biosynthesis	TRIMCyp
Receptor	Glutamate receptor 3 isoform flip precursor isoform 2[a]

Table 2. Continued

function	protein name
	Ephrin type-B receptor 1 precursor (Tyrosine-protein kinase receptor EPH-2) (NET) (HEK6) (ELK)[a]
Signal transduction	Vav-3 protein
Stress response	Heat shock protein HSP 90-beta[a,b]
	Heat shock protein HSP 90-alpha (HSP 86) isoform 2[a,b]
	Heat shock protein 1, alpha isoform 3[a,b]
	78 kDa glucose-regulated protein precursor (GRP 78) (Immunoglobulin heavy chain binding protein) (BiP) (Endoplasmic reticulum lumenal Ca(2+) binding protein grp78) isoform 4[a,b]
	Heat shock 70 kDa protein 8 isoform 2 isoform 2[a,b]
	Heat shock protein 8 isoform 3[a,b]
	Peroxiredoxin 2 (Thioredoxin peroxidase 1) (Thioredoxin-dependent peroxide reductase 1) (Thiol-specific antioxidant protein) (TSA) (PRP) (Natural killer cell enhancing factor B) (NKEF-B) isoform 1
Miscellaneous	Membrane protein, palmitoylated 5 isoform 1[a]
	Dedicator of cytokinesis protein 1 (180 kDa protein downstream of CRK) (DOCK180) isoform 1[a]
	Temporarily Assigned Gene name family member (tag-278) isoform 7
	BEN domain-containing protein 3
	Adenylosuccinate lyase 1
	Acyl-CoA thioesterase 9
	ART5 protein[a]
	Hypothetical protein isoform 2
	Peptidylprolyl isomerase A (cyclophilin A)
	Retinoblastoma-associated protein 140 isoform 4
	Four and a half LIM domains protein 1 isoform 6
	Hypothetical protein LOC302773
	Unknown (protein for MGC:38398)
	MIF4G domain containing, isoform CRA_c
	F-box and WD-40 domain protein 10
	Isopentenyl-diphosphate delta isomerase 2
	mCG117968
	rCG21715
	Androgen receptor associated protein 54
	Synapse-associated protein 1
	Hypothetical protein[c]

[a] Cell membrane localization. [b] Calcium-binding activity. [c] Has 3 different GI numbers (gi|109093687, gi|149254381 and gi|149258923).

The remained COM crystals on MDCK apical surface were counted in random 15 high power fields (HPF) under phase contrast microscope (Olympus CKX41; Olympus Co. Ltd., Tokyo, Japan).

Statistical Analysis

The quantitative data are presented as mean ± SEM. Comparisons among groups were performed by one-way analysis of variance (ANOVA) with Tukey's posthoc test (SPSS; version 13.0). P values <0.05 were considered as statistical significant.

RESULTS AND DISCUSSION

This study aimed to identify all of potential COM crystal-binding proteins on apical membrane of distal renal tubular epithelial cells using a proteomics approach. Renal tubular epithelial cells have characteristics of polarization, in which plasma membranes are divided to apical and basolateral portions by a function of tight junction. These two different membrane compartments have unique sets of proteins and lipids according to their differential cellular functions. Apical or luminal membrane is exposed to renal tubular fluid where COM crystals are formed. Madin-Darby Canine Kidney (MDCK) cells, which were derived from distal nephron and used widely as the representing cells of distal renal tubules,[21,22] were used in our present study because the distal nephron is considered as an originating site for COM kidney stone formation.[23,24] We focused our attention to identification of COM-binding proteins only on apical membrane because of their biological relevance *in vivo*—only apical membrane, not basolateral membrane and intracellular compartments, contacts to luminal COM crystals.

The polarization of MDCK epithelial cells was confirmed by immunofluorescence staining of markers for tight junction (ZO-1), basolateral membrane (Na^+/K^+-ATPase α-subunit), and apical membrane (gp135). The data showed the presence of these markers in respective locales and thus confirmed the full polarization of MDCK cells (Figure 2). Apical membrane was then isolated using a recently established peeling method, of

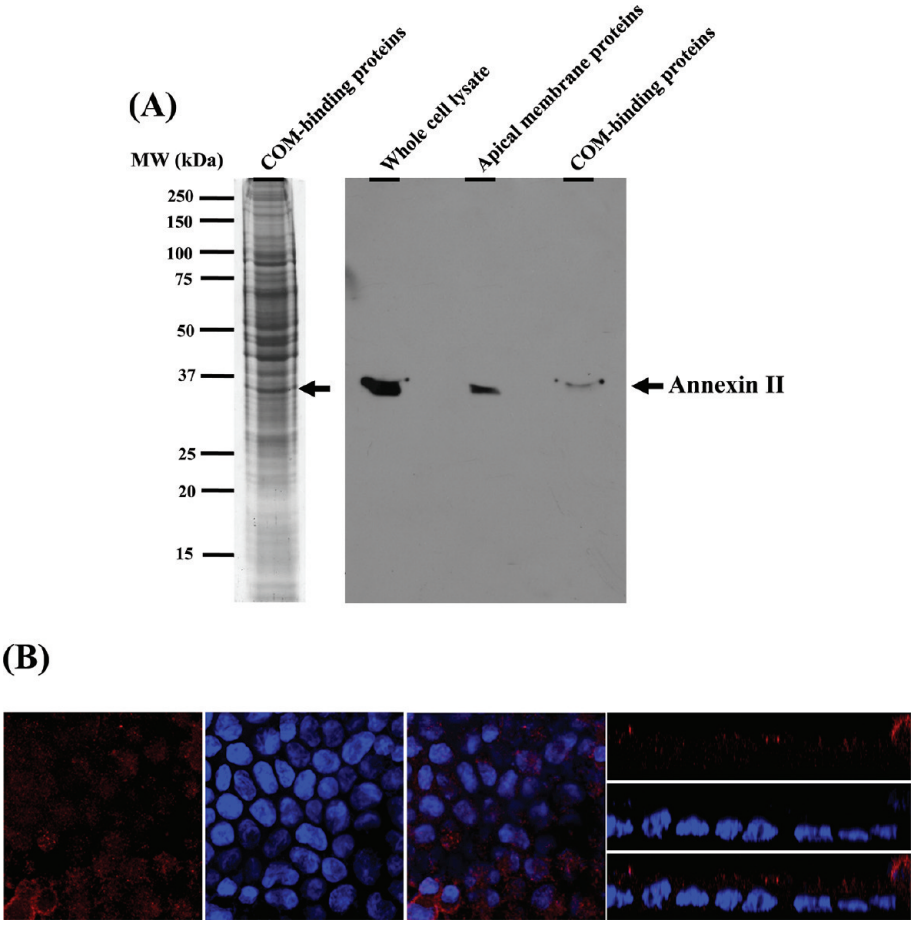


Figure 5. Validation of the expression of annexin II at apical membrane of renal tubular epithelial cells and its role as the COM crystal-binding protein. (A) Proteins derived from whole cell lysate, purified apical membrane, and COM crystal-binding fraction (with an equal amount of 20 μg) were resolved by 12% SDS-PAGE and subjected to Western blot analysis using goat polyclonal antiannexin II as the primary antibody. (B) Immunofluorescence staining of annexin II followed by laser-scanning confocal microscopic examination. The expression of annexin II is illustrated in red, whereas nuclear counter-stain is shown in blue. The confocal micrographs were obtained from both horizontal (first three panels) and sagittal (last three panels) sections. Original magnification = 630× in all panels.

which principle is based on hydrous affinity and/or ionic interaction.[18] Our previous study has demonstrated that this novel method is simple and highly effective for isolation of apical membrane.[18] In the present study, the yield and purity of apical membrane isolation were also evaluated. The results showed that this novel method, based on peeling, was highly effective for enrichment of apical membrane. Figure 3A shows SDS-PAGE profile of the isolated apical membrane proteins, which obviously differed from that of the whole cell lysate. In addition, a typical apical membrane protein (gp135)[25] was effectively enriched by the peeling method as demonstrated by the more prominent gp135 band in Western blot analysis as compared to such band in the sample derived from whole cell lysate (Figure 3B). Moreover, this peeling method also provided the high purity of apical membrane proteins as there was no contamination of basolateral membrane marker (Na^+/K^+-ATPase α-subunit)[26] in the isolated apical membrane fraction (Figure 3C). Therefore, this method would offer a high confident data for the analysis of apical membrane proteins.

Highly purified apical membrane fraction was solubilized with 1× Laemmli's buffer to obtain the mixture of apical membrane proteins. To avoid effects of detergent and reducing agents on crystal-protein interaction/binding, the protein solution was extensively dialyzed against deionized water. After lyophilization, the purified apical membrane proteins were resuspended into the protein-free artificial urine and then incubated with COM crystals overnight. The reason that we used protein-free artificial urine instead of human urine because there are several proteins present in the normal human urine that can interfere with data interpretation (the urinary proteins can also bind to COM crystals). The pH and osmolality of artificial urine used in our present study were 6.2 and 446 mOsm/kg, respectively. Differential levels of pH and osmolality may affect the COM crystal binding capacities of proteins. To demonstrate the selective binding of proteins eluted from COM crystals, the SDS-PAGE profile of COM-binding proteins was examined compared to those of starting apical membrane proteins and unbound fraction (Figure 4A). The data showed that COM crystal-binding proteins had a distinct SDS-PAGE profile that was much different from that of the unbound fraction, which was similar to the profile of the starting apical membrane proteins, indicating the highly selective bindings of proteins in the bound fraction. The reproducibility of isolation of COM crystal-binding proteins was confirmed in additional three independent experiments (Figure 4B), and the amount of proteins derived from each fraction was quantitated (Figure 4C).

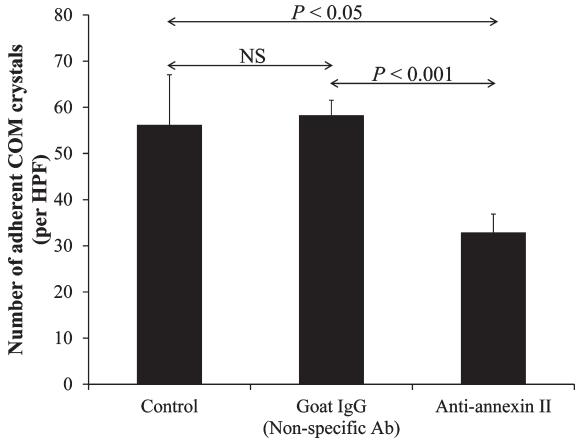


Figure 6. Functional validation of annexin II as the COM crystal-binding protein. COM crystal-binding assay was performed without (control) or with goat polyclonal antiannexin II antibody to neutralize the COM crystal-binding activity of annexin II prior to COM binding. Nonspecific goat IgG served as the treatment control to demonstrate the specificity of neutralization of annexin II activity. $N = 3$ independent experiments.

To identify these COM crystal-binding proteins, the preparative gel derived from 6×10^7 cells was produced. From a total of 40 gel slices (Figure 4D), a total of 96 proteins were identified Q-TOF MS and MS/MS analyses. Their identities, identification numbers, peptide mass fingerprinting and/or MS/MS ions scores, sequence coverage, number of matched peptides, homologues, and other detailed information are summarized in Table 1. The sequences of the identified hypothetical proteins, putative proteins, unnamed protein products, or unknown proteins were also submitted to BLAST search for defining their similarities or homologues, and only proteins with >80% identities are included in Table 1. The actual (experimental) molecular masses of some identified proteins shown in SDS-PAGE gel were not exactly their theoretical (calculated) molecular masses. This is not unexpected as some proteins were the fragmented products of their full lengths, whereas some other might form a tight complex with other proteins in the apical membrane and resisted to reducing agents. All of these identified proteins were classified into various functional categories based on their molecular/cellular functions provided in the UniProt Knowledgebase (UniProtKB) protein database (Table 2). These included calcium-dependent phospholipid-binding, calcium ion-binding, cell cycle, cellular structure, immune response, ion transporter, metabolism, mRNA processing, protein and vesicular transport, protein folding and protein biosynthesis, receptor, signal transduction, stress response, and miscellaneous. Among these identified proteins, many of them were well-known or typical membrane proteins, as well as calcium-binding proteins, convincing that they play important roles in COM crystal binding.

One of the COM crystal-binding proteins identified from apical membrane of renal tubular epithelial cells in our present study is annexin A2 or annexin II (band #23; at approximately 35 kDa), which was also identified as a COM crystal-binding protein in previous study.[13] Western blot analysis was performed to confirm the mass spectrometric identification of annexin II. The data confirmed that annexin II is an apical membrane protein that can bind tightly with COM crystals (Figure 5A). We also performed immunofluorescence staining of annexin II followed by laser-scanning confocal microscopic examination to further confirm our proteomic data. The immunofluorescence data confirmed the expression of annexin II at apical membrane surface (Figure 5B). These consistent data strengthen the role of this well-known calcium-binding protein as the COM crystal-binding protein.

Finally, functional validation of annexin II as the COM crystal-binding protein was performed. The data revealed that preincubation of MDCK cells with antiannexin II antibody significantly reduced (approximately 40%) the number of adherent COM crystals on the apical surface of MDCK cells, whereas preincubation with nonspecific IgG did not affect the number of adherent COM crystals, indicating the specificity of this neutralization by antiannexin II (Figure 6). It should be noted that preincubation or neutralization of the polarized MDCK cells with antiannexin II could not completely abolish COM crystal adhesion on apical surface of the cells. This is not unexpected because annexin II is one among other several COM crystal-binding proteins and blocking only one binding protein definitely cannot inhibit the entire binding capacities of apical surface molecules on epithelial cells.

From the list of the identified proteins (Tables 1 and 2), many of them are able to bind with calcium ion (Ca^{2+}). We found two proteins that are members of the annexin family, including annexin II (A2) and annexin VIII (A8) (band #23 and #26, respectively). Annexins have a conserved COOH-terminal "core" that mediates their membrane localization and calcium-binding properties.[27] Thus, it is not surprising that they were identified as COM crystal-binding proteins in our present study. Several other identified proteins are known to normally express at the apical membrane of renal tubular epithelial cells, for example, plasma membrane calcium ATPase 2 isoform b (PMCA2b) (band #5). This protein is highly enriched in the apical plasma membrane[28] and interacts preferentially with Na^+/H^+ exchanger regulatory factor 2 (NHERF2) to perform the functional assembly of PMCA2b in a multiprotein Ca^{2+} signaling complex and facilitate the integrated cross-talk between local Ca^{2+} influx and efflux.[29] It is possible that PMCA2b binds COM crystals via its Ca^{2+}-binding activity.

We also found some surface receptors that were able to bind with COM crystals, including glutamate receptor 3 isoform flip (band #4) and ephrin (Eph) type-B receptor 1 (band #5). These receptors are type I transmembrane protein and their extracellular regions contain a highly conserved N-terminal domain, which is necessary for ligand binding,[30] whereas their intracellular or cytoplasmic regions contain a highly conserved kinase domain, which catalyzes tyrosine phosphorylation. In addition, the Eph-mediated signaling is restricted to specific membrane microdomains or lipid rafts.[31] Our data report for the first time that these receptors also serve for COM crystal binding.

In summary, we successfully identified several COM crystal-binding proteins from apical membrane of distal renal tubular epithelial cells by a proteomics approach using SDS-PAGE followed by Q-TOF MS and MS/MS analyses. Expression and localization of annexin II on apical surface of MDCK cells were confirmed by Western blot analysis, immunofluorescence staining and laser-scanning confocal microscopic examination. Moreover, its function as the COM crystal-binding protein was validated by a functional study. This large data set offers many opportunities for further investigations of kidney stone disease and may lead to the development of new therapeutic targets.

AUTHOR INFORMATION

Corresponding Author

*Visith Thongboonkerd, MD, FRCPT Professor and Head of Medical Proteomics Unit, Director of Center for Research in Complex Systems Science (CRCSS), Siriraj Hospital, Mahidol University, 12th Floor Adulyadej Vikrom Building, 2 Prannok Road, Bangkoknoi, Bangkok 10700, Thailand. Phone/Fax: +66-2-4184793. E-mail: thongboonkerd@dr.com or vthongbo@yahoo.com.

ACKNOWLEDGMENT

This study was supported by Office of the Higher Education Commission and Mahidol University under the National Research Universities Initiative, and The Thailand Research Fund (RTA5380005) to V.T. K.F. and P.P. are supported by the Royal Golden Jubilee PhD Program of The Thailand Research Fund, whereas V.T. is also supported by "Chalermphrakiat" Grant, Faculty of Medicine Siriraj Hospital.

ABBREVIATIONS:

ACN, acetonitrile; COM, calcium oxalate monohydrate; EDTA, *N*,*N*,*N*′,*N*′-Ethylenediaminetetraacetic acid; Eph, ephrin; gp135, glycoprotein 135; HSP, heat shock protein; MDCK, Madin-Darby Canine Kidney; MS, mass spectrometry; MS/MS, tandem mass spectrometry; NHERF2, Na^+/H^+ exchanger regulatory factor 2; PMCA2b, plasma membrane calcium ATPase 2 isoform b; Q-TOF, quadrupole time-of-flight; TFA, trifluoroacetic acid; ZO-1, Zonula occludens-1

REFERENCES

(1) Trinchieri, A.; Ostini, F.; Nespoli, R.; Rovera, F.; Montanari, E.; Zanetti, G. A prospective study of recurrence rate and risk factors for recurrence after a first renal stone. *J. Urol.* **1999**, *162*, 27–30.

(2) Strauss, A. L.; Coe, F. L.; Deutsch, L.; Parks, J. H. Factors that predict relapse of calcium nephrolithiasis during treatment: a prospective study. *Am. J. Med.* **1982**, *72*, 17–24.

(3) Tsujihata, M. Mechanism of calcium oxalate renal stone formation and renal tubular cell injury. *Int. J. Urol.* **2008**, *15*, 115–120.

(4) Habibzadegah-Tari, P.; Byer, K. G.; Khan, S. R. Reactive oxygen species mediated calcium oxalate crystal-induced expression of MCP-1 in HK-2 cells. *Urol. Res.* **2006**, *34*, 26–36.

(5) Koul, H. K.; Menon, M.; Chaturvedi, L. S.; Koul, S.; Sekhon, A.; Bhandari, A.; Huang, M. COM crystals activate the p38 mitogen-activated protein kinase signal transduction pathway in renal epithelial cells. *J. Biol. Chem.* **2002**, *277*, 36845–36852.

(6) Khan, S. R. Crystal-induced inflammation of the kidneys: results from human studies, animal models, and tissue-culture studies. *Clin. Exp. Nephrol.* **2004**, *8*, 75–88.

(7) Lieske, J. C.; Norris, R.; Swift, H.; Toback, F. G. Adhesion, internalization and metabolism of calcium oxalate monohydrate crystals by renal epithelial cells. *Kidney Int.* **1997**, *52*, 1291–1301.

(8) Kramer, G.; Steiner, G. E.; Prinz-Kashani, M.; Bursa, B.; Marberger, M. Cell-surface matrix proteins and sialic acids in cell-crystal adhesion; the effect of crystal binding on the viability of human CAKI-1 renal epithelial cells. *Br. J. Urol. Int.* **2003**, *91*, 554–559.

(9) Ebisuno, S.; Kohjimoto, Y.; Tamura, M.; Inagaki, T.; Ohkawa, T. Histological observations of the adhesion and endocytosis of calcium oxalate crystals in MDCK cells and in rat and human kidney. *Urol. Int.* **1997**, *58*, 227–231.

(10) Khan, S. R. Calcium oxalate crystal interaction with renal tubular epithelium, mechanism of crystal adhesion and its impact on stone development. *Urol. Res.* **1995**, *23*, 71–79.

(11) Lieske, J. C.; Leonard, R.; Swift, H.; Toback, F. G. Adhesion of calcium oxalate monohydrate crystals to anionic sites on the surface of renal epithelial cells. *Am. J. Physiol.* **1996**, *270*, F192–F199.

(12) Fullekrug, J.; Simons, K. Lipid rafts and apical membrane traffic. *Ann. N.Y. Acad. Sci.* **2004**, *1014*, 164–169.

(13) Kumar, V.; Farell, G.; Deganello, S.; Lieske, J. C. Annexin II is present on renal epithelial cells and binds calcium oxalate monohydrate crystals. *J Am. Soc. Nephrol.* **2003**, *14*, 289–297.

(14) Sorokina, E. A.; Kleinman, J. G. Cloning and preliminary characterization of a calcium-binding protein closely related to nucleolin on the apical surface of inner medullary collecting duct cells. *J. Biol. Chem.* **1999**, *274*, 27491–27496.

(15) Sorokina, E. A.; Wesson, J. A.; Kleinman, J. G. An acidic peptide sequence of nucleolin-related protein can mediate the attachment of calcium oxalate to renal tubule cells. *J. Am. Soc. Nephrol.* **2004**, *15*, 2057–2065.

(16) Asselman, M.; Verhulst, A.; De Broe, M. E.; Verkoelen, C. F. Calcium oxalate crystal adherence to hyaluronan-, osteopontin-, and CD44-expressing injured/regenerating tubular epithelial cells in rat kidneys. *J. Am. Soc. Nephrol.* **2003**, *14*, 3155–3166.

(17) Verhulst, A.; Asselman, M.; Persy, V. P.; Schepers, M. S.; Helbert, M. F.; Verkoelen, C. F.; De Broe, M. E. Crystal retention capacity of cells in the human nephron: involvement of CD44 and its ligands hyaluronic acid and osteopontin in the transition of a crystal binding- into a nonadherent epithelium. *J. Am. Soc. Nephrol.* **2003**, *14*, 107–115.

(18) Fong-ngern, K.; Chiangjong, W.; Thongboonkerd, V. Peeling as a novel, simple, and effective method for isolation of apical membrane from intact polarized epithelial cells. *Anal. Biochem.* **2009**, *395*, 25–32.

(19) Thongboonkerd, V.; Semangoen, T.; Chutipongtanate, S. Factors determining types and morphologies of calcium oxalate crystals: Molar concentrations, buffering, pH, stirring and temperature. *Clin. Chim. Acta* **2006**, *367*, 120–131.

(20) Chutipongtanate, S.; Thongboonkerd, V. Systematic comparisons of artificial urine formulas for in vitro cellular study. *Anal. Biochem.* **2010**, *402*, 110–112.

(21) Rindler, M. J.; Chuman, L. M.; Shaffer, L.; Saier, M. H., Jr. Retention of differentiated properties in an established dog kidney epithelial cell line (MDCK). *J. Cell Biol.* **1979**, *81*, 635–648.

(22) Saier, M. H., Jr. Growth and differentiated properties of a kidney epithelial cell line (MDCK). *Am. J. Physiol.* **1981**, *240*, C106–C109.

(23) Rabinovich, Y. I.; Daosukho, S.; Byer, K. J.; El Shall, H. E.; Khan, S. R. Direct AFM measurements of adhesion forces between calcium oxalate monohydrate and kidney epithelial cells in the presence of Ca2+ and Mg2+ ions. *J. Colloid Interface Sci.* **2008**, *325*, 594–601.

(24) Lieske, J. C.; Deganello, S. Nucleation, adhesion, and internalization of calcium-containing urinary crystals by renal cells. *J Am. Soc. Nephrol.* **1999**, *10* (Suppl 14), S422–S429.

(25) Meder, D.; Shevchenko, A.; Simons, K.; Fullekrug, J. Gp135/podocalyxin and NHERF-2 participate in the formation of a preapical domain during polarization of MDCK cells. *J. Cell Biol.* **2005**, *168*, 303–313.

(26) Hammerton, R. W.; Krzeminski, K. A.; Mays, R. W.; Ryan, T. A.; Wollner, D. A.; Nelson, W. J. Mechanism for regulating cell surface distribution of Na+,K(+)-ATPase in polarized epithelial cells. *Science* **1991**, *254*, 847–850.

(27) Gerke, V.; Moss, S. E. Annexins: from structure to function. *Physiol Rev.* **2002**, *82*, 331–371.

(28) Xiong, Y.; Antalffy, G.; Enyedi, A.; Strehler, E. E. Apical localization of PMCA2w/b is lipid raft-dependent. *Biochem. Biophys. Res. Commun.* **2009**, *384*, 32–36.

(29) DeMarco, S. J.; Chicka, M. C.; Strehler, E. E. Plasma membrane Ca2+ ATPase isoform 2b interacts preferentially with Na+/H+ exchanger regulatory factor 2 in apical plasma membranes. *J. Biol. Chem.* **2002**, *277*, 10506–10511.

(30) Himanen, J. P.; Nikolov, D. B. Eph receptors and ephrins. *Int. J. Biochem. Cell Biol.* **2003**, *35*, 130–134.

(31) Gauthier, L. R.; Robbins, S. M. Ephrin signaling: One raft to rule them all? One raft to sort them? One raft to spread their call and in signaling bind them? *Life Sci.* **2003**, *74*, 207–216.

Journal of proteome research

ARTICLE

pubs.acs.org/jpr

Comprehensive Proteome Analysis of Hippocampus, Brainstem, and Spinal Cord from Paralytic and Furious Dogs Naturally Infected with Rabies

Natthapaninee Thanomsridetchai,[†] Nilubon Singhto,[‡] Veera Tepsumethanon,[§] Shanop Shuangshoti,[∥] Supaporn Wacharapluesadee,[∥] Supachok Sinchaikul,[⊥] Shui-Tein Chen,[⊥] Thiravat Hemachudha,[*,∥] and Visith Thongboonkerd[*,‡,£]

[†]Inter-Department Program of Biomedical Sciences, Faculty of Graduate School, Chulalongkorn University, Bangkok, Thailand

[‡]Medical Proteomics Unit, Office for Research and Development, Faculty of Medicine Siriraj Hospital, Mahidol University, Bangkok, Thailand

[§]Queen Saovabha Memorial Institute, Bangkok, Thailand

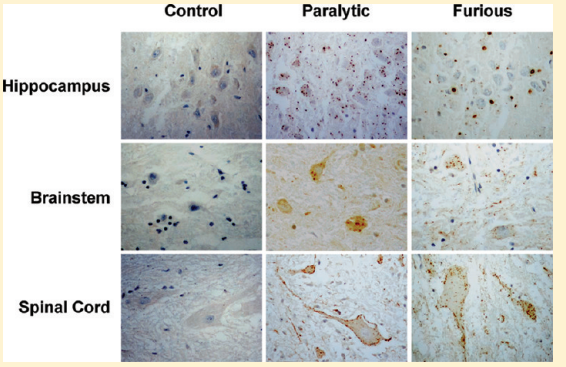
[∥]Faculty of Medicine, Chulalongkorn University and WHO Collaborating Center for Research and Training on Viral Zoonoses, Bangkok, Thailand

[⊥]Institute of Biological Chemistry and Genomic Research Center, Academia Sinica, Taipei, Taiwan

[£]Center for Research in Complex Systems Science, Mahidol University, Bangkok, Thailand

Supporting Information

ABSTRACT: Paralytic and furious forms are unique clinical entities of rabies in humans and dogs. However, molecular mechanisms underlying these disorders remained unclear. We investigated changes in proteomes of the hippocampus, brainstem and spinal cord of paralytic and furious dogs naturally infected with rabies compared to noninfected controls. Proteins were extracted from these tissues and analyzed by two-dimensional gel electrophoresis (2-DE) ($n = 6$ gels/region in each group, a total of 54 gels were analyzed). From >1000 protein spots visualized in each gel, spot matching, quantitative intensity analysis, and ANOVA with Tukey's posthoc multiple comparisons revealed 32, 49, and 67 protein spots that were differentially expressed among the three clinical groups in the hippocampus, brainstem and spinal cord, respectively. These proteins were then identified by quadrupole time-of-flight mass spectrometry and tandem mass spectrometry (Q-TOF MS and MS/MS), including antioxidants, apoptosis-related proteins, cytoskeletal proteins, heat shock proteins/chaperones, immune regulatory proteins, metabolic enzymes, neuron-specific proteins, transcription/translation regulators, ubiquitination/proteasome-related proteins, vesicular transport proteins, and hypothetical proteins. Among these, 13, 17, and 41 proteins in the hippocampus, brainstem and spinal cord, respectively, significantly differed between paralytic and furious forms and thus may potentially be biomarkers to differentiate these two distinct forms of rabies. In summary, we report herein for the first time a large data set of changes in proteomes of the hippocampus, brainstem and spinal cord in dogs naturally infected with rabies. These data will be useful for better understanding of molecular mechanisms of rabies and for differentiation of its paralytic and furious forms.



KEYWORDS: brainstem, furious, hippocampus, paralytic, proteomics, rabies, spinal cord

INTRODUCTION

Rabies remains an important public health problem in some regions as a fatal outcome is expected in almost all cases once symptoms and signs develop. Only three survivors with no or nonsignificant complications have been reported, all of which were associated with bat variants.[1−3] Comparing between dog- and bat-related rabies, patients who are associated with dog variants exhibit more unique clinical manifestations, including paralytic and furious forms. Also, a lesser degree of immune response to rabies virus has been shown in dog-associated cases.[4] None of the patients with dog-associated rabies in Thailand, Cambodia and Africa had a positive test for rabies antibody in cerebrospinal fluid (CSF).[5,6] Additionally, the detection of an antibody against the rabies virus in serum is also unpredictable in dog-associated cases. In contrast, CSF and serum levels of the antirabies antibody appear to be correlated with duration of survival in bat-associated cases.[7]

Received: March 26, 2011
Published: September 26, 2011

ACS Publications © 2011 American Chemical Society

Comparing the two unique forms of rabies, different anatomical involvements of the nervous system have been shown in patients with paralytic versus furious rabies. In the paralytic form, peripheral nerve axonopathy or myelinopathy, not the defect of the motor neuron in the spinal cord, is responsible for muscle weakness.[8] In furious form, although anterior horn cells of spinal cord are affected, clinical deficits from these defective cells are not found and their defects can be detected only by electrophysiological investigations.[8] Innate immune response in the brain of paralytic dogs have been detected with a greater degree as compared to that of furious dogs and is inversely correlated with the viral amount in the brain.[9] Also, disturbance of magnetic resonance imaging (MRI) signals of the brain in the paralytic form is greater than that of furious rabies-infected patients and dogs.[5] The faster time to death is another characteristic of furious rabies. Despite dissimilarity of clinical manifestations, imaging features, clinical courses and the amount of viral load in the brain, they share similar pathologies of the central nervous system (CNS), including scant inflammation.[4,8,10]

Lack of apoptosis in the CNS has been shown to be a marker for virulence of wild-type or street rabies virus in order to escape immune recognition and to facilitate spreading.[11−16] In contrast, fixed virus, such as the challenged virus standard (CVS) strain, induces marked degree of apoptosis in the infected neurons.[17−20] Intriguingly, neurons of different regions display diverse degrees of resistance to cell death. It has been demonstrated that motor neurons of spinal cord resist to apoptosis and cytolysis, and remain functioning several days after CVS infection.[21] However, hippocampal neurons become apoptotic shortly after the infection.[21] Midline CNS structures, that is, thalamus, brainstem, basal ganglia and spinal cord, have been shown to be preferentially infected with rabies in both humans and dogs.[9,10,22] Therefore, the survival of neurons may depend not only on the viral strain but also on differential site-specific responses.

Despite the aforementioned knowledge on rabies, its molecular mechanisms remained unclear. We therefore performed a proteomic study of three regions of the CNS, including the hippocampus, brainstem and spinal cord, of dogs naturally infected with rabies. Proteins were extracted from CNS tissues obtained from paralytic and furious dogs and then subjected to proteomic analysis using two-dimensional gel electrophoresis (2-DE) compared to the noninfected controls.

MATERIALS AND METHODS

Sample Collection

The CNS tissues were taken from paralytic (n = 3) and furious (n = 3) dogs naturally infected with rabies (street strain of genotype 1; sites of the bite were mainly head and face),[9] as well as noninfected controls (n = 6). Each animal was observed at the Quarantine and Rabies Diagnostic Unit of the Queen Saovabha Memorial Institute (QSMI). All of the animals were in late-stage of rabies, and clinical diagnosis of furious and paralytic rabies was achieved using the criteria reported previously.[9] The animals died naturally without receiving any treatment. From each animal, three locales of the CNS tissues, including the hippocampus, brainstem (midbrain, pons and medulla) and spinal cord, were taken and were saved at −70 °C until used.

Immunoperoxidase Staining of Rabies Antigen

The diagnosis of rabies was confirmed by the presence of rabies antigen in the CNS tissues. Paraffin-embedded sections of formalin-fixed tissues (3-μm-thick) were stained with antirabies nucleocapsid polyclonal antibody (Bio-Rad; Marnes-la-Coquette, France) at a dilution of 1:80. After rinsing with PBS, the sections were incubated with a respective secondary antibody conjugated with horseradish peroxidase in the DAKO EnVision-System kit (DAKO Corporation; CA) for 30 min. The slides were then washed with PBS and incubated for 10 min with a peroxidase substrate containing 0.5 mg/mL diaminobenzidine (Sigma; St. Louis, MO), 30% H_2O_2 and 1 M imidazole in Tris-HCl buffer. After rinsing by tap water, the tissues were counterstained with hematoxylin.

Protein Extraction

The tissues were briskly frozen in liquid nitrogen, ground to powder, resuspended in a buffer containing 7 M urea, 2 M thiourea, 4% 3-[(3-cholamidopropyl) dimethyl-ammonio]-1-propanesulfonate (CHAPS), 120 mM dithiothreitol (DTT), 2% (v/v) ampholytes (pH 3−10) and 40 mM Tris-base, and incubated at 4 °C for 30 min. Unsolubilized nuclei, cell debris, and particulate matters were removed by a centrifugation at 10 000 rpm, 4 °C for 5 min. Protein concentrations were determined by the Bradford method using Bio-Rad protein assay (Bio-Rad Laboratories; Hercules, CA).

Two-Dimensional Gel Electrophoresis (2-DE)

For the controlled group, each gel was derived from each sample (n = 6 gels/region). For the paralytic and furious groups, duplicated 2-D gels were derived from each sample to have 6 gels/region in each group. Overall, a total of 54 gels were analyzed in this study. For each 2-D gel, Immobiline DryStrip (nonlinear pH gradient of 3−10, 7 cm long; GE Healthcare, Uppsala, Sweden) was rehydrated overnight with an equal amount of 150 μg of total protein that was premixed with a rehydration buffer containing 7 M urea, 2 M thiourea, 2% CHAPS, 2% (v/v) ampholytes (pH 3−10), 120 mM DTT, 40 mM Tris-base, and bromophenol blue (to make the final volume of 150 μL per strip). The first dimensional separation or isoelectric focusing (IEF) was performed in Ettan IPGphor III System (GE Healthcare) at 20 °C, using a stepwise mode to reach 9083 Vh with limiting current of 50 mA/strip. After completion of the IEF, the strips were first equilibrated for 15 min in an equilibration buffer containing 6 M urea, 130 mM DTT, 112 mM Tris-base, 4% SDS, 30% glycerol and 0.002% bromophenol blue, and then in another similar buffer that replaced DTT with 135 mM iodoacetamide, for a further 15 min. The second dimensional separation was performed in 12% polyacrylamide gel using SE260 mini-Vertical Electrophoresis Unit (GE Healthcare) at 150 V for approximately 2 h. The resolved protein spots were stained with SYPRO Ruby fluorescence dye (Invitrogen/Molecular Probes; Eugene, OR) overnight and then visualized using Typhoon 9200 laser scanner (GE Healthcare).

Spot Matching and Quantitative Intensity Analysis

Image Master 2D Platinum software (GE Healthcare) was used for matching and analysis of protein spots in 2-D gels. Parameters used for spot detection were (i) minimal area = 10 pixels; (ii) smooth factor = 2.0; and (iii) saliency = 2.0. A reference gel was created from an artificial gel combining all of the spots presenting in different gels into one image. The reference gel was then used for determination of existence and difference of protein expression between gels. Background subtraction was performed, and the intensity volume of each spot was normalized with total intensity volume (summation of the

intensity volumes obtained from all spots within the same 2-D gel).

Statistical Analysis

All the quantitative data are reported as mean ± SEM. Intensity volumes of individual spots matched across different gels were compared among groups by multiple comparisons using one-way analysis of variance (ANOVA) with Tukey's posthoc test (SPSS; version 13.0). *P* values less than 0.05 were considered as statistical significant. Significantly different protein spots were subjected to in-gel tryptic digestion and identification by mass spectrometry.

In-Gel Tryptic Digestion

All of the protein spots whose intensity levels significantly differed among groups were excised from 2-D gels, washed twice with 200 μL of 50% acetonitrile (ACN)/25 mM NH_4HCO_3 buffer (pH 8.0) at room temperature for 15 min, and then washed once with 200 μL of 100% ACN. After washing, the solvent was removed, and the gel pieces were dried by a SpeedVac concentrator (Savant; Holbrook, NY) and rehydrated with 10 μL of 1% (w/v) trypsin (Promega; Madison, WI) in 25 mM NH_4HCO_3. After rehydration, the gel pieces were crushed and incubated at 37 °C for at least 16 h. Peptides were subsequently extracted twice with 50 μL of 50% ACN/5% trifluoroacetic acid (TFA); the extracted solutions were then combined and dried with the SpeedVac concentrator. The peptide pellets were resuspended with 10 μL of 0.1% TFA and purified using $ZipTip_{C18}$ (Millipore; Bedford, MA). The peptide solution was drawn up and down in the $ZipTip_{C18}$ 10 times and then washed with 10 μL of 0.1% formic acid by drawing up and expelling the washing solution 3 times. The peptides were finally eluted with 5 μL of 75% ACN/0.1% formic acid.

Protein Identification by Q-TOF MS and MS/MS Analyses

The trypsinized samples were premixed 1:1 with the matrix solution containing 5 mg/mL α-cyano-4-hydroxycinnamic acid (CHCA) in 50% ACN, 0.1% (v/v) TFA and 2% (w/v) ammonium citrate, and deposited onto the 96-well MALDI target plate. The samples were analyzed by Q-TOF Ultima mass spectrometer (Micromass; Manchester, U.K.), which was fully automated with predefined probe motion pattern and the peak intensity threshold for switching over from MS survey scanning to MS/MS, and from one MS/MS to another. Within each sample well, parent ions that met the predefined criteria (any peak within the m/z 800−3000 range with intensity above 10 count ± include/exclude list) were selected for CID MS/MS using argon as the collision gas and a mass dependent ±5 V rolling collision energy until the end of the probe pattern was reached. The MS and MS/MS data were extracted and outputted as the searchable .txt and .pkl files, respectively, for independent searches using the MASCOT search engine (http://www.matrixscience.com), assuming that peptides were monoisotopic. Fixed modification was carbamidomethylation at cysteine residues, whereas variable modification was oxidation at methionine residues. Only one missed trypsin cleavage was allowed, and peptide mass tolerances of 100 and 50 ppm were allowed for peptide mass fingerprinting and MS/MS ions search, respectively.

Western Blot Analysis

Proteins derived from CNS tissues (with an equal amount of 20 μg) were resolved in 12% SDS-PAGE and then transferred onto a nitrocellulose membrane (Whatman; Dassel, Germany) using a semidry transfer apparatus (Bio-Rad; Milano, Italy) at 75 mA for 1 h. Nonspecific bindings were blocked with 5% skim milk in PBS at room temperature for 1 h. The membrane was then incubated with mouse monoclonal antitubulin α1 or anti-HSP90 (Santa Cruz Biotechnology; Santa Cruz, CA) (1:1000 in 5% skim milk/PBS) at 4 °C overnight. Thereafter, the membrane was washed three times with PBS and further incubated with rabbit antimouse IgG conjugated with horseradish peroxidase (DAKO; Glostrup, Denmark) (1:2000 in 5% skim milk/PBS) at room temperature for 1 h. The immunoreactive bands were then visualized by SuperSignal West Pico chemiluminescence substrate (Pierce Biotechnology, Inc.; Rockford, IL) and autoradiography.

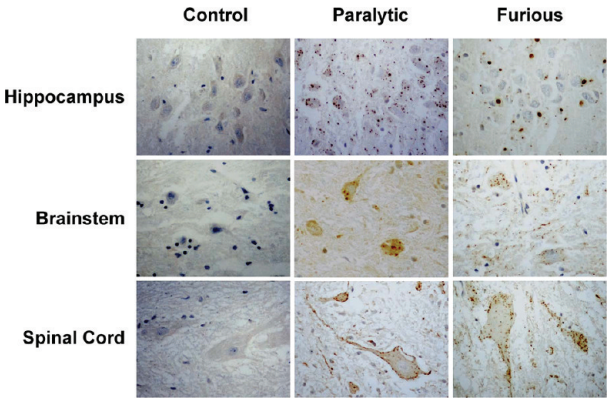


Figure 1. Immunoperoxidase staining of rabies antigen. Hippocampus, brainstem and spinal cord from noninfected dogs and those naturally infected with rabies (both paralytic and furious forms) were subjected to immunohistochemical study for rabies antigen using polyclonal antibody against rabies nucleocapsid as the primary antibody and hematoxylin as the counterstain. Immunoreactive locales of rabies nucleocapsid are shown in brown, whereas nuclei are illustrated in blue.

Global Protein Network Analysis

All of the significantly altered proteins in individual CNS regions of dogs naturally infected with rabies were subjected to global protein network analysis using Ingenuity Pathways Analysis (IPA) tool by Ingenuity Systems (http://www.ingenuity.com) to query each identified protein to other identified proteins and scientific findings curated from the literature relating to genes, cells, diseases, drugs and other biological entities, as described previously.[23] Finally, relevant network(s) or pathway(s) of interacting proteins are reported.

RESULTS

We investigated changes in tissue proteomes of the hippocampus, brainstem and spinal cord of paralytic (n = 3) and furious (n = 3) dogs naturally infected with rabies compared to the noninfected controls (n = 6). Rabies infection was confirmed in paralytic and furious dogs by positive immunoperoxidase staining of rabies nucleocapsid protein in their CNS tissues (as illustrated in brown in Figure 1). Proteins were extracted from these tissues and analyzed by 2-DE (n = 6 gels/region for each group, with or without replication of individual samples; a total of 54 gels were analyzed). From >1000 protein spots visualized in each gel, spot matching, quantitative intensity analysis, and ANOVA with Tukey's posthoc multiple comparisons revealed 32, 49, and 67 protein spots that were differentially expressed among the three clinical groups in the hippocampus (Figure 2),

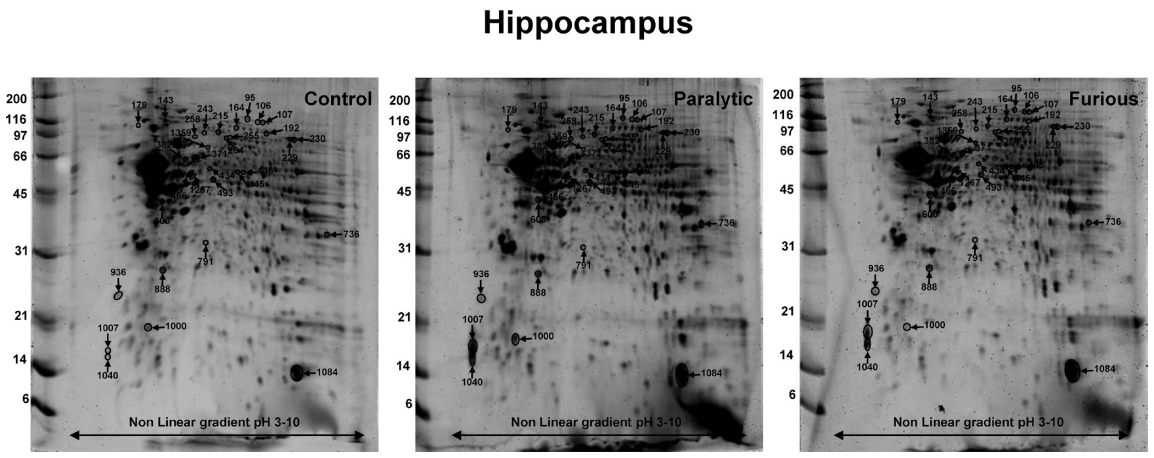


Figure 2. 2-D proteome maps of differentially expressed proteins in hippocampus of dogs naturally infected with rabies. Proteins that significantly differed among groups, including noninfected control, paralytic form of rabies and furious form of rabies, are labeled with numbers that correspond to those reported in Tables 1 and 2, and Supplementary Table S1 (Supporting Information).

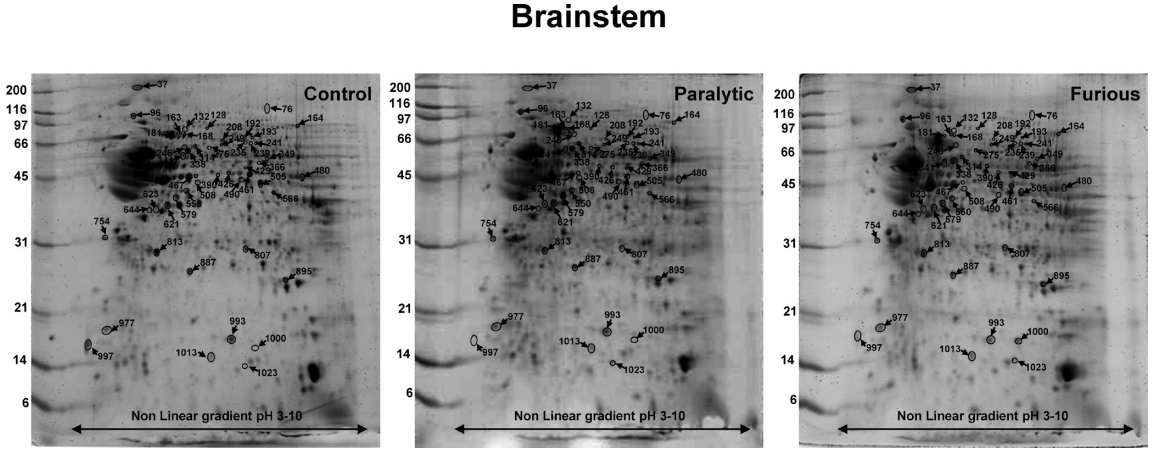


Figure 3. 2-D proteome maps of differentially expressed proteins in brainstem of dogs naturally infected with rabies. Proteins that significantly differed among groups, including noninfected control, paralytic form of rabies and furious form of rabies, are labeled with numbers that correspond to those reported in Tables 1 and 2, and Supplementary Table S2 (Supporting Information).

brainstem (Figure 3) and spinal cord (Figure 4), respectively. These differentially expressed proteins were then identified by Q-TOF MS and/or MS/MS analyses. Their mass spectrometric data (identities, identification scores, sequence coverage, number of matched peptides, isoelectric point or p*I*, molecular weight or MW, etc.), quantitative intensity data, and *p* values obtained from ANOVA as well as Tukey's posthoc multiple comparisons are summarized in Supplementary Tables S1−S3 (Supporting Information), respectively.

These identified proteins were classified into 11 main categories, namely antioxidants, apoptosis-related proteins, cytoskeletal proteins, heat shock proteins/chaperones, immune regulatory proteins, metabolic enzymes, neuron-specific proteins, transcription/translation regulators, ubiquitination/proteasome-related proteins, vesicular transport proteins, and hypothetical proteins (Figure 5). Among these, the top three of most changes (in terms of number of differentially expressed proteins in each functional category) were metabolic enzymes (32%), vesicular transport (20%) and cytoskeletal proteins (15%), respectively (Figure 5). Some proteins were identified as more than one form of the same protein. For example, annexin A2 was identified from spots #1215 and #1408 derived from the spinal cord with a slight difference of their molecular masses in the 2-D proteome map (spot #1215 had a slightly greater molecular mass) (Figure 4). Similarly, annexin A6 was identified from both the hippocampus (spot #258) and brainstem (spot #246) with a slight difference of their molecular masses in the 2-D proteome map (spot #258 had a slightly greater molecular mass) (Figures 2 and 3). These were most likely due to post-translational modifications (PTMs) or cleavage that could alter molecular masses, isoelectric points and cellular function of different forms of the same protein.[24]

Some of differentially expressed proteins identified by proteomic study were validated by Western blot analysis, including significant increase of tubulin α1 in the brainstem of paralytic dogs (Figure 6A), significant increase of heat shock protein 90 (HSP90) in the brainstem of paralytic dogs (Figure 6B), and significant decrease of HSP90 in the spinal cord of furious dogs (Figure 6C). Moreover, all of the significantly altered proteins were subjected to global protein network analysis. Using the Ingenuity Pathway Analysis (IPA) tool, there were four important functional networks detected in differentially expressed proteins in CNS tissues of dogs naturally infected with rabies. These include Network I, Gene expression, cellular development,

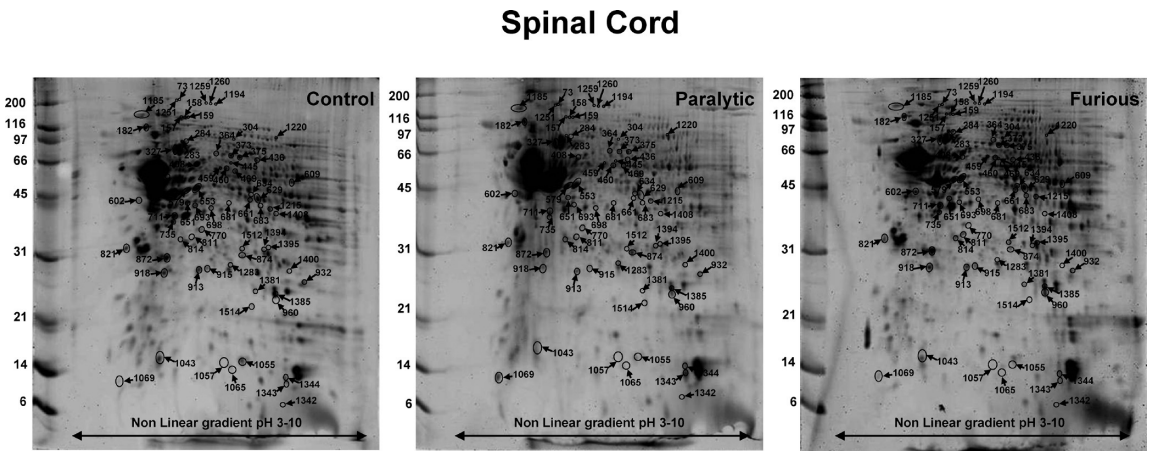


Figure 4. 2-D proteome maps of differentially expressed proteins in spinal cord of dogs naturally infected with rabies. Proteins that significantly differed among groups, including noninfected control, paralytic form of rabies and furious form of rabies, are labeled with numbers that correspond to those reported in Tables 1 and 2, and Supplementary Table S3 (Supporting Information).

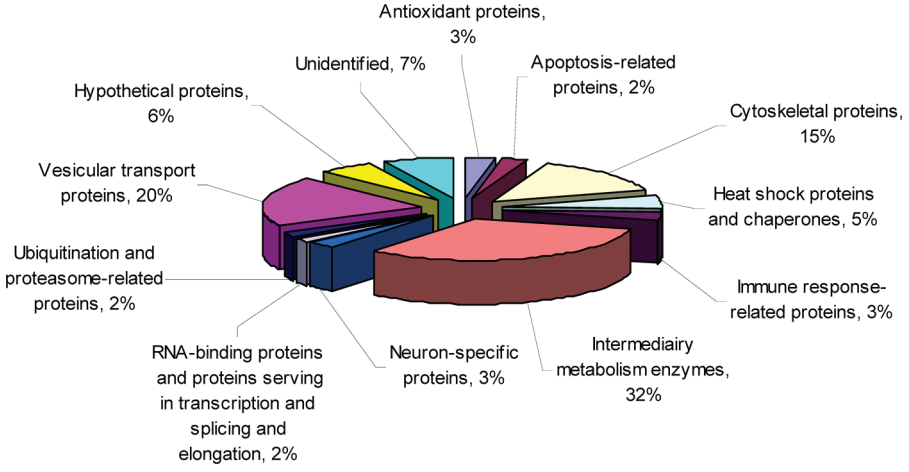


Figure 5. Summary of all differentially expressed proteins in the hippocampus, brainstem and spinal cord of dogs naturally infected with rabies. These significantly differed proteins were classified based on their molecular functions. More details of individual proteins, including mass spectrometric data (identities, identification scores, sequence coverage, number of matched peptides, isoelectric point or pI, molecular weight or MW, etc.), quantitative intensity data, and *p* values obtained from ANOVA as well as Tukey's posthoc multiple comparisons are summarized in Supplementary Tables S1−S3 (Supporting Information).

growth and proliferation (in hippocampus) (Figure 7A); Network II, Drug and lipid metabolism (in brainstem) (Figure 7B); Network III, Genetic disorder and small molecule biochemistry (in spinal cord) (Figure 7C); and Network IV, Neurological disease, energy production and nucleic acid metabolism (in spinal cord) (Figure 7D).

DISCUSSION

Natural infection of rabies virus in dog is an ideal animal model for studying the pathogenesis of rabies.[9] Paralytic and furious manifestations can be found in rabies-infected dogs, resembling those of humans. Our results indicate that paralytic and furious rabies had a marked degree of alterations in their proteome profiles of three different locales of the CNS, including the hippocampus, brainstem and spinal cord, as compared to the noninfected controls. The differentially expressed proteins were involved in many biological processes in response to stress and to the process of rabies viral infection (Figure 5).

Among 11 main functional categories of significantly altered proteins affected by rabies, some functional groups drew our attention as they might be directed to better understanding of the molecular mechanisms of rabies (both paralytic and furious forms). These included: (i) antioxidants, (ii) apoptosis-related proteins; (iii) cytoskeletal proteins; (iv) heat shock proteins/chaperones; (v) immune regulatory proteins; and (vi) neuron-specific proteins (Table 1). Functional significance and potential roles of these proteins are highlighted as follows.

(i). Antioxidants

Oxidative stress has been reported in rabies.[25−27] Jackson and colleagues[28] have demonstrated that rabies virus infection in cultured DRG neurons derived from adult mice caused axonal injury through oxidative stress. Protective proteins (i.e., antioxidants) have been shown to be up-regulated to counteract the oxidative stress induced by rabies infection.[29] *In vivo*, oxidative stress may explain previous observations of the neuronal degeneration processes in the study of transgenic mice.[30] In our present

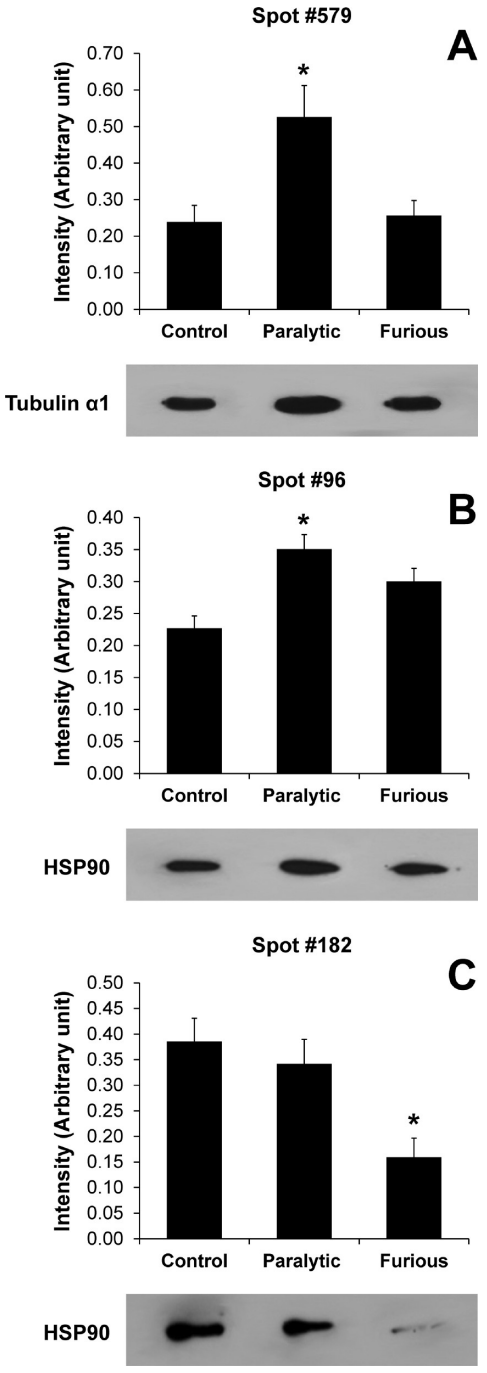


Figure 6. Western blot analysis. Some of the proteomic data were validated by Western blot analysis, including (A) significant increase of tubulin α1 in brainstem of paralytic dogs, (B) significant increase of heat shock protein 90 (HSP90) in brainstem of paralytic dogs, and (C) significant decrease of HSP90 in spinal cord of furious dogs. * = $p < 0.05$ compared to controls. See also Table 1 and Supplementary Tables S1−S3 (Supporting Information).

study, we found both up- and down-regulations of antioxidants in the brainstem and spinal cord of paralytic dogs and down-regulation of one antioxidant protein in the spinal cord of furious dogs (Table 1). These data implicate that the disease process might be at the later stage than antioxidants could handle to protect the CNS from oxidative stress (i.e., irreversible deterioration stage). Analysis of the brains at an earlier stage will be helpful to address this hypothesis.

(ii). Apoptosis-related Proteins

Even with severe clinical entities of both paralytic and furious dogs, there were only 1−2 apoptosis-related proteins that were significantly altered in each region of the CNS, including two forms of annexin A2, two forms of annexin A6, and cytochrome P450 2B12 (CYPIIB12) (Table 1). These data were consistent with previous findings, demonstrating that apoptosis was almost undetectable in wild-type rabies virus infection.[11−15] Interestingly, one form of annexin A2 (spot #1215; full-length) was up-regulated in the spinal cord of paralytic dogs, whereas another form (spot #1408; cleavage or fragmented) was down-regulated in the spinal cord of furious dogs. Similarly, one form of annexin A6 (spot #258; full-length) was up-regulated in the hippocampus of furious dogs, whereas another form (spot #246; cleavage or fragmented) was down-regulated in the brainstem of furious dogs. These disparate results underscore the important role of PTMs and/or cleavage on the functional roles of differential forms of the same protein.[31]

(iii). Cytoskeletal Proteins

Most of cytoskeletal proteins were down-regulated in the CNS of paralytic and furious dogs (Table 1). The decreased amount of cytoskeletal proteins is likely the result of CNS damage by rabies virus infection. These data were consistent with those reported in our previous studies on magnetic resonance imaging of the brains of furious and paralytic dogs during an early stage, which showed tract integrity and macro-structural damage in the brainstem of paralytic rabies and in the cerebral cortex of furious rabies.[32] This process undoubtedly led the animals to further stage with widespread extent of CNS damage, thereby coma and death. In contrast, two forms of glial fibrillary acidic protein (GFAP), tubulin alpha-1 isoform 9, vinculin and xin actin-binding repeat containing 2 isoform 1 were up-regulated. These increases might be due to reorganization of cytoskeletal assembly in the CNS as a part of host response to the CNS infection. However, as there were much fewer up-regulated proteins, this compensatory mechanism failed to cope with the deterioration of CNS damage by rabies virus.

(iv). Heat Shock Proteins/Chaperones

Heat shock proteins or chaperones play important roles in cellular stress responses, protein folding (to ensure the proper protein conformation), and presentation of antigens for the immune system.[33,34] In rabies, heat shock proteins, especially heat shock protein 70 kDa (Hsp70), are known as the functional molecules for replication found in Negri body, working in concert with Toll-like receptor 3 (TLR3) and ubiquitylated proteins.[35−37] Our data showed up-regulation of Hsp70 in spinal cord of paralytic dogs. In addition to Hsp70, there were many heat shock proteins or chaperones that were significantly altered in the CNS tissues of both paralytic and furious dogs. However, their levels were either increased or decreased (Table 1). These disparate results might be due to the balance between deteriorated effects of virus infection and their counter-balances as the compensatory mechanisms of the host to cope with diseases/disorders.

(v). Immune Regulatory Proteins

There were concordant changes in immune regulatory proteins in CNS tissues of both paralytic and furious dogs. These included up-regulation of immunoglobulin heavy chain in the

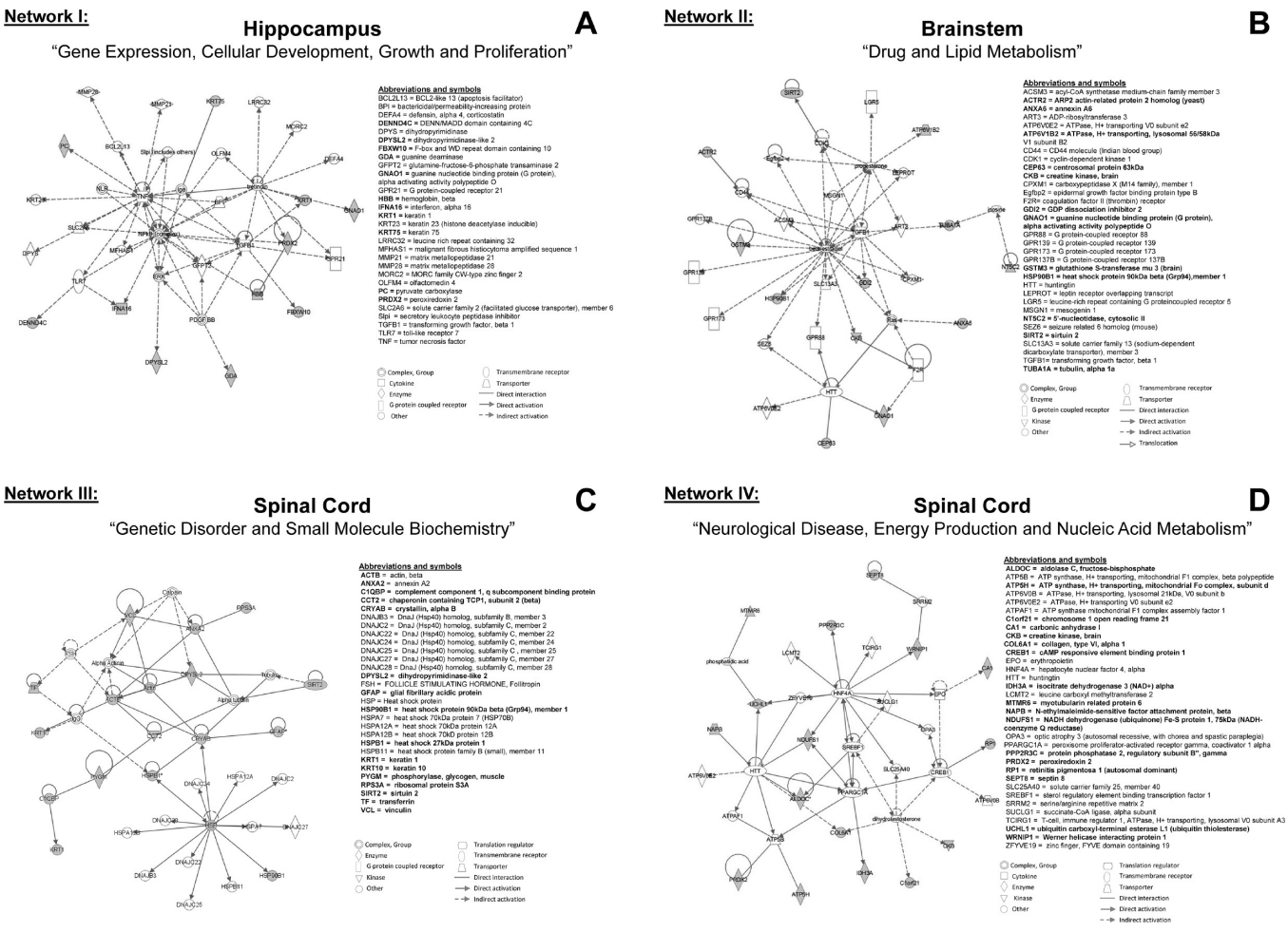


Figure 7. Global protein network analysis. Using the Ingenuity Pathways Analysis (IPA) tool, there were four important functional networks detected in differentially expressed proteins in CNS tissues of dogs naturally infected with rabies. These include (A) Network I, Gene expression, cellular development, growth and proliferation (in hippocampus); (B) Network II, Drug and lipid metabolism (in brainstem); (C) Network III, Genetic disorder and small molecule biochemistry (in spinal cord); and (D) Network IV, Neurological disease, energy production and nucleic acid metabolism (in spinal cord).

brainstem of paralytic dogs and up-regulations of interferon alpha-4 and SARM1 protein in the hippocampus of furious dogs (Table 1). Our data were consistent with the previous findings, indicating the involvement of innate immune response in the brain of rabies-infected dogs.[9]

(vi). Neuron-specific Proteins

Collapsin response mediator proteins (CRMPs) are members of the family of cytosolic phosphoproteins. They are strongly expressed throughout the developing nervous system.[38] CRMP-2 has been shown to bind with tubulin heterodimers and promote microtubule assembly, thereby enhancing axonal growth and branching.[39] CRMP2 can induce neuronal differentiation in hippocampal cultures.[40] In addition, CRMP-2 is also expressed in immune cells and plays a crucial role in T lymphocyte migration as the increased expression of CRMP-2 is associated with the increase in migratory rate of peripheral T lymphocytes.[41] Therefore, CRMP2 expression may serve as an indicator for neuroinflamation.[42] Interestingly, we found that CRMP-2 was down-regulated in the spinal cord of both paralytic and furious forms of rabies but was up-regulated in the brainstem of paralytic dogs (Table 1). These data might be evidence of ingression of activated T cells in the brainstem, consistent with our observation that inflammatory T cells could be demonstrated only in the brainstem of paralytic rabies (Shuangshoti et al., unpublished data).

Global protein network analysis of all differentially expressed proteins in CNS tissues of dogs naturally infected with rabies using the IPA tool revealed four important functional networks detected in these affected tissues. In the hippocampus, Network I associated with gene expression, cellular development, growth and proliferation was observed (Figure 7A), consistent with the data reported in previous studies indicating that several genes involved in cell growth and proliferation are altered in the hippocampus upon rabies virus infection.[43,44] In the brainstem, Network II associated with drug and lipid metabolism was found (Figure 7B). Although a few proteins (e.g., annexin, HSP90, H^+ ATPase) in this network have been found to be altered in rabies-infected CNS tissues in previous genomic/proteomic studies,[44,45] other altered proteins in this network are novel and deserve further investigations to address their functional significance in drug and lipid metabolism upon rabies virus infection. In the spinal cord, two protein networks involved in rabies were identified, including Network III associated with

dx.doi.org/10.1021/pr200276u | J. Proteome Res. 2011, 10, 4911–4924

Table 1. Some Interesting Changes in Furious and Paralytic Dogs Compared to Noninfected Controls[a]

protein name	spot no.	NCBI ID	region	alterations (vs control) paralytic (P)	alterations (vs control) furious (F)
		Antioxidants			
150 kDa oxygen-regulated protein precursor (Orp150) (Hypoxia up-regulated 1)	73	gi|73955046	Spinal cord	↑[b]	NS
Glutathione S-transferase Mu 3 (GSTM3−3) (GST class-mu 3) (hGSTM3−3) isoform 1	807	gi|57088159	Brainstem	↑[b]	NS
Oxygen-regulated protein 1; AltName: Full=Retinitis pigmentosa RP1 protein homologue	157	gi|62900882	Spinal cord	↓[b]	NS
Peroxiredoxin 1	932	gi|4505591	Spinal cord	↓[b]	↓[b]
		Apoptosis-related proteins			
Annexin A2	1215	gi|18645167	Spinal cord	NS	↓[b]
Annexin A2	1408	gi|50950177	Spinal cord	↑[b]	NS
Annexin A6 (Annexin VI) (Lipocortin VI) (P68) (P70) (Protein III) (Chromobindin 20) (67 kDa calelectrin) (Calphobindin-II) (CPB-II) isoform 2	246	gi|73953627	Brainstem	NS	↓[b]
Annexin A6 (Annexin VI) (Lipocortin VI) (P68) (P70) (Protein III) (Chromobindin 20) (67 kDa calelectrin) (Calphobindin-II) (CPB-II) isoform 2	258	gi|73953627	Hippocampus	NS	↑[b]
Cytochrome P450 2B12 (CYPIIB12)	192	gi|62639273	Hippocampus	↓[b]	NS
		Cytoskeletal proteins			
Dynamin	164	gi|181849	Hippocampus	↓[b]	NS
Fascin 1	366	gi|4507115	Brainstem	↓[b]	NS
Glial fibrillary acidic protein, astrocyte (GFAP) isoform 1	459	gi|73965500	Spinal cord	NS	↑[b]
Glial fibrillary acidic protein, astrocyte (GFAP) isoform 1	602	gi|73965500	Spinal cord	NS	↑[b]
Myosin, heavy chain 2, skeletal muscle, adult	208	gi|115947178	Brainstem	↓[b]	NS
Nebulin-related anchoring protein isoform 2	132	gi|114632883	Brainstem	↓[b]	↓[b]
NEFM protein	1185	gi|148342538	Spinal cord	↓[b]	↑[b]
Neurofilament, heavy polypeptide 200 kDa	37	gi|50979202	Brainstem	↓[b]	↓[b]
Septin-8	460	gi|73971156	Spinal cord	↓[b]	↓[b]
TUBB2B protein	1000	gi|133778299	Hippocampus	NS	↓[b]
Tubulin, alpha-1 isoform 9	579	gi|73996547	Brainstem	↑[b]	NS
Tubulin, alpha-2 chain (Alpha-tubulin 2) isoform 7	623	gi|73996522	Brainstem	↓[b]	NS
Vinculin (Metavinculin)	1259	gi|73953587	Spinal cord	↑[b]	↑[b]
Xin actin-binding repeat containing 2 isoform 1	1260	gi|66841385	Spinal cord	↑[b]	NS
		Heat shock proteins/chaperones			
Alpha-Crystallin B chain (Alpha(B)-Crystallin)	960	gi|149716488	Spinal cord	↓[b]	↑[b]
Alpha Crystallin B chain (Alpha(B)-Crystallin) (Rosenthal fiber component) (Heat-shock protein beta-5) (HspB5) isoform 1	895	gi|57085977	Brainstem	NS	↑[b]
Alpha Crystallin B chain (Alpha(B)-Crystallin) (Rosenthal fiber component) (Heat-shock protein beta-5) (HspB5) isoform 1	1385	gi|57085977	Spinal cord	↑[b]	↑[b]
DnaJ (Hsp40) homologue, subfamily C, member 15 (predicted), isoform CRA_b	1055	gi|149050007	Spinal cord	↓[b]	↓[b]
Heat shock cognate 71 kDa protein (Heat shock 70 kDa protein 8)	327	gi|123647	Spinal cord	↑[b]	NS
Heat shock protein 90 kDa beta, member 1	96	gi|50979166	Brainstem	↑[b]	NS
Heat shock protein 90 kDa beta, member 1	182	gi|50979166	Spinal cord	NS	↓[b]
Heat shock protein beta-1	874	gi|50979116	Spinal cord	NS	↑[b]
Heat shock protein beta-1	1512	gi|50979116	Spinal cord	↑[b]	NS

dx.doi.org/10.1021/pr200276u |J. Proteome Res. 2011, 10, 4911–4924

Table 1. Continued

protein name	spot no.	NCBI ID	region	alterations (vs control) paralytic (P)	alterations (vs control) furious (F)
		Immune regulatory proteins			
Immunoglobulin heavy chain variable region	1023	gi|112700066	Brainstem	↑[b]	NS
Interferon alpha 4	107	gi|18767673	Hippocampus	NS	↑[b]
SARM1 protein	1359	gi|114325428	Hippocampus	NS	↑[b]
		Neuron-specific proteins			
Dihydropyrimidinase related protein-2 (DRP-2) (CRMP-2) isoform 6 (Turned on after division, 64 kDa protein) (TOAD-64) (Collapsin response mediator protein 2)	364	gi|73993705	Spinal cord	NS	↓[b]
Dihydropyrimidinase related protein-2 (DRP-2) (Turned on after division, 64 kDa protein) (TOAD-64) (Collapsin response mediator protein 2) (CRMP-2) isoform 6	314	gi|73993705	Brainstem	↑[b]	NS
Dihydropyrimidinase related protein-2 (DRP-2) (Turned on after division, 64 kDa protein) (TOAD-64) (Collapsin response mediator protein 2) (CRMP-2) isoform 4	373	gi|73993699	Spinal cord	↓[b]	↓[b]
Dihydropyrimidinase related protein-2 (DRP-2) (Turned on after division, 64 kDa protein) (TOAD-64) (Collapsin response mediator protein 2) (CRMP-2) isoform 6	375	gi|73993705	Spinal cord	↓[b]	↓[b]
Dihydropyrimidinase related protein-2 (DRP-2) (Turned on after division, 64 kDa protein) (TOAD-64) (Collapsin response mediator protein 2) (CRMP-2) isoform 6	382	gi|73993705	Hippocampus	NS	↑[b]

[a] NCBI = National Center for Biotechnology Information. ↑ = Increased levels as compared to the control (non-infected). ↓ = Decreased levels as compared to the control (non-infected). [b] $p < 0.05$ vs control.

genetic disorder and small molecule biochemistry (Figure 7C) and Network IV associated with neurological disease, energy production and nucleic acid metabolism (Figure 7D). Similar to the findings for Network II, most of the altered proteins in Network III and Network IV are novel and their roles in rabies should be further elucidated.

Interestingly, there were five proteins that were undetectable in spinal cord of the controlled animals, but were detectable in spinal cord of both paralytic and furious forms of rabies, including one form of vinculin (spot #1259), thymopoietin II (spot #1283), hypothetical protein (spot #1342), a form of beta globin (spot #1344), and heat shock protein beta-1 (spot #1512) (Figure 4 and Supplementary Table S3, Supporting Information). These proteins might be involved in the pathogenesis and neurological manifestations of rabies. Furthermore, this phenomenon (the presence of newly expressed proteins in CNS tissues of rabies-infected animals) was observed only in the spinal cord, not in the hippocampus or brainstem.

In addition, we also focused our attention to significant differences between the two forms of rabies in individual CNS tissues, as these data may lead to further identification of tissue biomarkers for differentiation of these two distinct clinical entities of rabies and may also facilitate understanding of factors determining clinical manifestations of rabies. All of these significant differences are summarized in Table 2. A total of 13, 17, and 41 proteins in the hippocampus, brainstem and spinal cord, respectively, significantly differed between paralytic and furious forms. Among these, the most obvious differences were the absence of one form of carbonic anhydrase I (spot #1395), astrocytic GFAP isoform 2 (spot #445), NADH dehydrogenase (ubiquinone) Fe−S protein 1 (75 kDa precursor, isoform 1) (spot #283), and *N*-ethylmaleimide sensitive fusion protein attachment protein beta (spot #735) in the spinal cord of furious dogs and, vice versa, the absence of oxygen-regulated protein 1 (spot #157) and rCG47063 (spot #158) in the spinal cord of paralytic dogs (Figure 4 and Table 2). Again, this phenomenon (the absence of some proteins in CNS tissues of one form of rabies compared to the other form) was observed only in the spinal cord, not in the hippocampus or brainstem. These proteins may potentially be "tissue biomarkers" to differentiate the two distinct forms of rabies. However, for clinical diagnostics, further investigations are needed to validate these "tissue biomarkers" in body fluids (i.e., plasma/serum and cerebrospinal fluid, which are easier to access and obtain from patients) to find the "more practical" biomarkers that can really be used in routine clinical practice.[46]

There is a previous proteomics study on CVS rabies virus infection in mammalian kidney cells.[29] In this previous study, a baby hamster kidney cell line (BHK-21) was infected with CVS rabies virus and alterations in the cellular proteome were identified by 2-DE followed by liquid chromatography (LC) coupled to MS/MS. Limited but significant changes were found

Table 2. Summary of Significant Differences between Furious and Paralytic Rabies[a]

protein name	NCBI ID	spot no.	intensity (mean ± SEM)			ANOVA *p* value	multiple comparisons		
			control [C]	paralytic [P]	furious [F]		P vs C	F vs C	P vs F
			Hippocampus						
Beta globin	gi|57113367	1084	3.2760 ± 0.6120	3.1782 ± 0.2172	5.6296 ± 0.0810	0.0004	NS	0.0014	0.0010
Cytochrome P450 2B12 (CYPIIB12)	gi|62639273	192	0.1120 ± 0.0081	0.0798 ± 0.0014	0.1251 ± 0.0082	0.0008	0.0111	NS	0.0007
Cytokeratin type II	gi|73996498	255	0.0253 ± 0.0055	0.0357 ± 0.0022	0.0173 ± 0.0056	0.0480	NS	NS	0.0390
Dihydropyrimidinase related protein-2 (DRP-2) (Turned on after division, 64 kDa protein) (TOAD-64) (Collapsin response mediator protein 2) (CRMP-2) isoform 3	gi|73993697	371	0.4072 ± 0.1000	0.2610 ± 0.0174	0.5731 ± 0.0446	0.0126	NS	NS	0.0095
FBXW10 protein	gi|20306882	736	0.2409 ± 0.0428	0.2500 ± 0.0288	0.1221 ± 0.0148	0.0182	NS	0.0406	0.0271
Guanine deaminase	gi|73946803	1267	0.0424 ± 0.0139	0.0456 ± 0.0102	0.1045 ± 0.0042	0.0009	NS	0.0018	0.0028
Guanine nucleotide-binding protein G(o), alpha subunit 2 isoform 1	gi|73949832	600	0.1778 ± 0.0254	0.1457 ± 0.0104	0.2802 ± 0.0271	0.0018	NS	0.0141	0.0019
Interferon alpha 4	gi|18767673	107	0.1034 ± 0.0076	0.1106 ± 0.0066	0.1439 ± 0.0101	0.0078	NS	0.0092	0.0313
Keratin 1	gi|160961491	264	0.0330 ± 0.0027	0.0358 ± 0.0050	0.0625 ± 0.0049	0.0004	NS	0.0007	0.0016
Peroxiredoxin 2 (Thioredoxin peroxidase 1) (Thioredoxin-dependent peroxide reductase 1) (Thiol-specific antioxidant protein) (TSA) (PRP) (Natural killer cell enhancing factor B) (NKEF-B) isoform 1	gi|73986497	888	0.2700 ± 0.0363	0.2982 ± 0.0272	0.4202 ± 0.0262	0.0073	NS	0.0084	0.0311
Protein C9orf55 isoform 1	gi|73971036	106	0.0696 ± 0.0106	0.0623 ± 0.0055	0.0964 ± 0.0097	0.0395	NS	NS	0.0410
Pyruvate carboxylase, mitochondrial precursor (Pyruvic carboxylase) (PCB) isoform 1	gi|73982897	95	0.0881 ± 0.0107	0.0907 ± 0.0041	0.0410 ± 0.0185	0.0225	NS	0.0456	0.0346
SARM1 protein	gi|114325428	1359	0.0231 ± 0.0118	0.0180 ± 0.0030	0.0535 ± 0.0116	0.0440	NS	0.0308	0.0204
			Brainstem						
Actin-related protein 2 isoform 4	gi|73969820	490	0.1348 ± 0.0067	0.1785 ± 0.0249	0.1128 ± 0.0063	0.0250	NS	NS	0.0216
Annexin A6 (Annexin VI) (Lipocortin VI) (P68) (P70) (Protein III) (Chromobindin 20) (67 kDa calelectrin) (Calphobindin-II) (CPB-II) isoform 2	gi|73953627	246	0.0739 ± 0.0071	0.0722 ± 0.0074	0.0456 ± 0.0023	0.0078	NS	0.0127	0.0193
ATPase, H+ transporting, V1 subunit B, isoform 2 isoform 2	gi|73993820	338	0.3896 ± 0.0345	0.2466 ± 0.0090	0.5235 ± 0.0593	0.0008	NS	NS	0.0005
ATPase, H+ transporting, V1 subunit B, isoform 2 isoform 2	gi|73993820	341	0.2130 ± 0.0295	0.0973 ± 0.0214	0.2944 ± 0.0141	0.0001	0.0066	NS	0.0001
Centrosomal protein 63 kDa isoform 2	gi|194221623	754	0.1721 ± 0.0061	0.3377 ± 0.0335	0.2202 ± 0.0244	0.0007	0.0006	NS	0.0098
Chain A, Solution Structure Of The Twelfth Cysteine-Rich Ligand- Binding Repeat In Rat Megalin	gi|159164645	128	0.0365 ± 0.0077	0.0699 ± 0.0118	0.0339 ± 0.0044	0.0160	0.0363	NS	0.0241
Creatine kinase B-type (Creatine kinase, B chain) (B-CK) isoform 1	gi|73964131	508	0.0802 ± 0.0087	0.1289 ± 0.0137	0.0846 ± 0.0072	0.0076	0.0115	NS	0.0209

dx.doi.org/10.1021/pr200276u | J. Proteome Res. 2011, 10, 4911–4924

Table 2. Continued

protein name	NCBI ID	spot no.	intensity (mean ± SEM) control [C]	paralytic [P]	furious [F]	ANOVA p value	multiple comparisons P vs C	F vs C	P vs F
Cytosolic purine 5-nucleotidase (5-nucleotidase cytosolic II) isoform 8	gi|73998435	993	0.3931 ± 0.0260	0.6284 ± 0.0636	0.4158 ± 0.0390	0.0041	0.0063	NS	0.0128
GDP dissociation inhibitor 2	gi|50978926	429	0.1042 ± 0.0063	0.0839 ± 0.0096	0.0335 ± 0.0150	0.0011	NS	0.0010	0.0135
Glutathione S-transferase Mu 3 (GSTM3−3) (GST class-mu 3) (hGSTM3−3) isoform 1	gi|57088159	807	0.1705 ± 0.0128	0.2736 ± 0.0398	0.1591 ± 0.0229	0.0186	0.0452	NS	0.0257
GTP-binding protein alpha o	gi|8394152	550	0.1927 ± 0.0220	0.3018 ± 0.0375	0.1850 ± 0.0118	0.0104	0.0164	NS	0.0248
Immunoglobulin heavy chain variable region	gi|112700066	1023	0.2323 ± 0.0192	0.4159 ± 0.0349	0.2525 ± 0.0302	0.0007	0.0012	NS	0.0031
Silent information regulator 2	gi|73697550	566	0.1672 ± 0.0204	0.1711 ± 0.0177	0.0590 ± 0.0072	0.0002	NS	0.0007	0.0005
Tubulin, alpha 1 isoform 9	gi|73996547	579	0.2392 ± 0.0452	0.5260 ± 0.0861	0.2565 ± 0.0414	0.0074	0.0122	NS	0.0018
Unidentified	NA	275	0.0747 ± 0.0070	0.0338 ± 0.0020	0.0627 ± 0.0023	0.0000	0.0000	NS	0.0009
Unidentified	NA	813	0.4906 ± 0.0173	0.3973 ± 0.0308	0.5654 ± 0.0213	0.0006	0.0360	NS	0.0004
Unidentified	NA	1000	0.0931 ± 0.0101	0.1017 ± 0.0117	0.2252 ± 0.0550	0.0216	NS	0.0321	0.0457
			Spinal cord						
40S ribosomal protein S3a (V-fos transformation effector protein) isoform 11	gi|73977917	1394	0.1508 ± 0.0410	0.0887 ± 0.0187	0.2208 ± 0.0126	0.0152	NS	NS	0.0116
Alpha-Crystallin B chain (Alpha(B)-Crystallin)	gi|149716488	960	0.5524 ± 0.0525	0.2190 ± 0.0289	0.7896 ± 0.0898	0.0001	0.0054	0.0452	0.0000
Alpha Crystallin B chain (Alpha(B)-Crystallin) (Rosenthal fiber component) (Heat-shock protein beta-5) (HspB5) isoform 1	gi|57085977	1385	0.0076 ± 0.0076	0.4507 ± 0.0203	0.1978 ± 0.0448	0.0000	0.0000	0.0011	0.0001
ATP synthase, H+ transporting, mitochondrial F0 complex, subunit d isoform a	gi|57108097	913	0.3123 ± 0.0156	0.2056 ± 0.0114	0.2918 ± 0.0095	0.0001	0.0001	NS	0.0009
Carbonic anhydrase I (Carbonate dehydratase I) (CA-I) (Carbonic anhydrase B)	gi|57108007	1395	0.1720 ± 0.0571	0.1475 ± 0.0069	0.0000 ± 0.0000	0.0048	NS	0.0063	0.0178
Chaperonin containing TCP1, subunit 2 isoform 1	gi|73968673	469	0.1049 ± 0.0087	0.0837 ± 0.0081	0.1453 ± 0.0194	0.0173	NS	NS	0.0146
Chromosome 1 open reading frame 27	gi|126306536	711	0.1848 ± 0.0194	0.2134 ± 0.0278	0.3747 ± 0.0224	0.0002	NS	0.0003	0.0013
Collagen, type VI, alpha 1 isoform 1	gi|119887130	1251	0.0041 ± 0.0041	0.0881 ± 0.0190	0.0050 ± 0.0050	0.0006	0.0014	NS	0.0016
Complement component 1, q subcomponent binding protein precursor	gi|73955331	821	0.3736 ± 0.0209	0.2669 ± 0.0160	0.4236 ± 0.0577	0.0270	NS	NS	0.0238
Creatine kinase B-type (Creatine kinase, B chain) (B-CK) isoform 1	gi|73964131	553	0.6536 ± 0.0330	0.6194 ± 0.0661	0.8821 ± 0.0517	0.0110	NS	0.0330	0.0144
Creatine kinase B-type (Creatine kinase, B chain) (B-CK) isoform 1	gi|73964131	579	0.4507 ± 0.0290	0.4179 ± 0.0323	0.6666 ± 0.0596	0.0023	NS	0.0093	0.0033
Cytoplasmic beta-actin isoform 2	gi|73958067	814	0.0935 ± 0.0197	0.1495 ± 0.0279	0.0139 ± 0.0139	0.0037	NS	NS	0.0028
Dihydropyrimidinase-like 2	gi|40254595	408	0.2805 ± 0.0384	0.1761 ± 0.0329	0.3310 ± 0.0298	0.0244	NS	NS	0.0212
Dihydrouridine synthase 1-like (S. cerevisiae)	gi|123288584	1065	0.1881 ± 0.0199	0.1801 ± 0.0299	0.2720 ± 0.0120	0.0329	NS	NS	0.0449
Fructose-bisphosphate aldolase C (Brain-type aldolase) isoform 1	gi|57091277	629	0.4337 ± 0.0392	0.2344 ± 0.0208	0.3765 ± 0.0454	0.0055	0.0050	NS	0.0425

dx.doi.org/10.1021/pr200276u | J. Proteome Res. 2011, 10, 4911–4924

Table 2. Continued

protein name	NCBI ID	spot no.	intensity (mean ± SEM) control [C]	intensity (mean ± SEM) paralytic [P]	intensity (mean ± SEM) furious [F]	ANOVA p value	multiple comparisons P vs C	multiple comparisons F vs C	multiple comparisons P vs F
Fructose-bisphosphate aldolase C (Brain-type aldolase) isoform 2	gi|73966974	634	0.0640 ± 0.0110	0.0090 ± 0.0076	0.0703 ± 0.0200	0.0149	0.0381	NS	0.0207
Glial fibrillary acidic protein, astrocyte (GFAP) isoform 1	gi|73965500	459	0.0620 ± 0.0050	0.0517 ± 0.0032	0.1421 ± 0.0210	0.0003	NS	0.0013	0.0004
Glial fibrillary acidic protein, astrocyte (GFAP) isoform 1	gi|73965500	602	0.0585 ± 0.0379	0.1897 ± 0.1438	4.3635 ± 0.4024	0.0000	NS	0.0000	0.0000
Glial fibrillary acidic protein, astrocyte (GFAP) isoform 2	gi|73965502	445	0.0174 ± 0.0059	0.0371 ± 0.0069	0.0000 ± 0.0000	0.0017	NS	NS	0.0012
Glycogen phosphorylase, muscle form (Myophosphorylase)	gi|1730556	1514	0.0906 ± 0.0323	0.0644 ± 0.0049	0.1619 ± 0.0258	0.0319	NS	NS	0.0304
Heat shock protein 90 kDa beta, member 1	gi|50979166	182	0.3857 ± 0.0451	0.3422 ± 0.0475	0.1595 ± 0.0373	0.0090	NS	0.0101	0.0370
Heat shock protein beta-1	gi|50979116	1512	0.0000 ± 0.0000	0.1178 ± 0.0105	0.0191 ± 0.0191	0.0000	0.0000	NS	0.0003
Hypothetical rhabdomyosarcoma antigen Mu-rms-40.6c	gi|48476968	159	0.0630 ± 0.0070	0.0087 ± 0.0048	0.0411 ± 0.0100	0.0007	0.0005	NS	0.0266
Isocitrate dehydrogenase 3 (NAD+) alpha isoform 2	gi|73951310	651	0.1590 ± 0.0061	0.1092 ± 0.0059	0.2230 ± 0.0127	0.0000	0.0041	0.0005	0.0000
Keratin 1	gi|160961491	698	0.1207 ± 0.0148	0.0849 ± 0.0108	0.1658 ± 0.0247	0.0222	NS	NS	0.0173
Keratin 10 isoform 2	gi|114667513	1381	0.0176 ± 0.0176	0.0756 ± 0.0227	0.3540 ± 0.1066	0.0047	NS	0.0057	0.0205
Heat shock protein beta-1	gi|50979116	874	0.3965 ± 0.0214	0.3070 ± 0.0141	0.6276 ± 0.0376	0.0000	NS	0.0001	0.0000
Myotubularin related protein 6	gi|194672062	811	0.1762 ± 0.0133	0.0835 ± 0.0066	0.1628 ± 0.0140	0.0001	0.0002	NS	0.0009
NADH dehydrogenase (ubiquinone) Fe−S protein 1, 75 kDa precursor isoform 1	gi|57110953	283	0.0410 ± 0.0095	0.0402 ± 0.0048	0.0000 ± 0.0000	0.0005	NS	0.0011	0.0013
N-ethylmaleimide sensitive fusion protein attachment protein beta	gi|62645998	735	0.0988 ± 0.0099	0.1470 ± 0.0457	0.0000 ± 0.0000	0.0155	NS	NS	0.0134
Oxygen-regulated protein 1; AltName: Full=Retinitis pigmentosa RP1 protein homologue	gi|62900882	157	0.0231 ± 0.0035	0.0000 ± 0.0000	0.0214 ± 0.0071	0.0047	0.0076	NS	0.0130
Peroxiredoxin 2 (Thioredoxin peroxidase 1) (Thioredoxin-dependent peroxide reductase 1) (Thiol-specific antioxidant protein) (TSA) (PRP) (Natural killer cell enhancing factor B) (NKEF-B) isoform 1	gi|73986497	918	0.3579 ± 0.0243	0.2140 ± 0.0242	0.4055 ± 0.0460	0.0035	0.0247	NS	0.0035
rCG47063	gi|149028757	158	0.0375 ± 0.0045	0.0000 ± 0.0000	0.0332 ± 0.0095	0.0010	0.0015	NS	0.0042
Septin-8	gi|73971156	460	0.0907 ± 0.0047	0.0126 ± 0.0106	0.0516 ± 0.0047	0.0000	0.0000	0.0118	0.0118
Serotransferrin precursor (Transferrin) (Siderophilin) (Beta-1-metal binding globulin) isoform 1	gi|73990142	1220	0.0647 ± 0.0102	0.1730 ± 0.0231	0.0849 ± 0.0173	0.0033	0.0039	NS	0.0166
Silent information regulator 2	gi|73697550	661	0.1419 ± 0.0139	0.1653 ± 0.0132	0.0792 ± 0.0254	0.0167	NS	NS	0.0158
Thymopoietin II	gi|229542	1283	0.0000 ± 0.0000	0.1248 ± 0.0057	0.1722 ± 0.0153	0.0000	0.0000	0.0000	0.0091
Ubiquitin carboxy-terminal hydrolase L1	gi|73951868	872	0.5050 ± 0.0347	0.3185 ± 0.0398	0.5122 ± 0.0482	0.0105	0.0226	NS	0.0180
Unidentified	NA	436	0.0494 ± 0.0051	0.0468 ± 0.0050	0.0092 ± 0.0060	0.0002	NS	0.0005	0.0009
Werner helicase interacting protein 1, isoform CRA_b	gi|148700412	304	0.0527 ± 0.0031	0.0363 ± 0.0072	0.1077 ± 0.0110	0.0001	NS	0.0008	0.0001
Zinc finger protein 615	gi|197102729	693	0.1327 ± 0.0094	0.1273 ± 0.0073	0.1698 ± 0.0141	0.0316	NS	NS	0.0394

[a] NCBI = National Center for Biotechnology Information. NA = Not applicable. NS = Not statistically significant.

dx.doi.org/10.1021/pr200276u | J. Proteome Res. 2011, 10, 4911–4924

in the expression of viral and host cellular proteins with different functions, including those involved in cytoskeletal assembly, oxidative stress and protein synthesis. Another study was done in rabies-infected mice using 2-DE followed by matrix-assisted laser desorption/ionization time-of-flight (MALDI-TOF) MS.[45] In the latter study, ICR mice were intracerebrally inoculated with attenuated CVS-B2C or wild-type silver-haired bat rabies virus (SHBRV). Animals were sacrificed when they developed severe paralysis and the brains were removed. The expression of host brain proteins, particularly those involved in ion homeostasis and docking and fusion of synaptic vesicles to presynaptic membranes in the CNS, were altered in the animals infected with SHBRV. On the other hand, attenuated rabies virus CVS-B2C up-regulated the expression of proteins involved in the induction of apoptosis. Comparing the data reported in these two aforementioned studies to ours, there were not many identical changes observed. This was not surprising as there were many differences in the study design and models of rabies infection as well as the affected tissues/cells for proteome analysis. Integrative analysis of several models of rabies virus infection at different stages and in different affected organs/tissues or their locales would be very helpful to obtain a larger and clearer picture of the pathophysiology or pathogenic mechanisms of rabies in humans.

In summary, we report herein for the first time a large data set of changes in proteomes of the hippocampus, brainstem and spinal cord in dogs naturally infected with rabies. These data will be useful for better understanding of molecular mechanisms of rabies and for differentiation of its paralytic and furious forms.

■ ASSOCIATED CONTENT

Supporting Information

Table S1. Summary of differentially expressed proteins in hippocampus identified by Q-TOF MS and/or MS/MS analyses. Table S2. Summary of differentially expressed proteins in brainstem identified by Q-TOF MS and/or MS/MS analyses. Table S3. Summary of differentially expressed proteins in spinal cord identified by Q-TOF MS and/or MS/MS analyses. This material is available free of charge via the Internet at http://pubs.acs.org.

■ AUTHOR INFORMATION

Corresponding Author

*Thiravat Hemachudha, Faculty of Medicine, Chulalongkorn University and WHO Collaborating Centre for Research and Training on Viral Zoonoses, Rama 4 Road, Bangkok 10330, Thailand. Phone: +66-2-6523122. Fax: +66-2-6523122. E-mail: fmedthm@gmail.com or th-cu@usa.net. Visith Thongboonkerd, Head of Medical Proteomics Unit, Office for Research and Development, Faculty of Medicine Siriraj Hospital, Mahidol University, 12th Floor Adulyadejvikrom Building, 2 Prannok Rd., Bangkoknoi, Bangkok 10700, Thailand. Phone/Fax: +66-2-4184793. E-mail: thongboonkerd@dr.com or vthongbo@yahoo.com.

■ ACKNOWLEDGMENT

We are grateful to the technical assistance of Phattara-orn Havanapan and Siriwan Mungdee. This work was supported by the National Center for Genetic Engineering and Biotechnology (BIOTEC), the National Science and Technology Development Agency (Thailand); The Thailand Research Fund (DBG5180026 & RTA5380005); The National Research University Project of CHE and the Ratchadaphiseksomphot Endowment Fund (HR1160A); Office of the Higher Education Commission and Mahidol University under the National Research Universities Initiative. V. Thongboonkerd is also supported by "Chalermphrakiat" Grant, Faculty of Medicine Siriraj Hospital.

■ REFERENCES

(1) Hattwick, M. A.; Weis, T. T.; Stechschulte, C. J.; Baer, G. M.; Gregg, M. B. Recovery from rabies. A case report. *Ann. Intern. Med.* **1972**, *76*, 931–942.

(2) Willoughby, R. E., Jr.; Tieves, K. S.; Hoffman, G. M.; Ghanayem, N. S.; Amlie-Lefond, C. M.; Schwabe, M. J.; Chusid, M. J.; Rupprecht, C. E. Survival after treatment of rabies with induction of coma. *N. Engl. J Med.* **2005**, *352*, 2508–2514.

(3) Presumptive abortive human rabies - Texas, 2009. *Morb. Mortal. Wkly. Rep.* **2010**, *59*, 185−190.

(4) Hemachudha, T.; Laothamatas, J.; Rupprecht, C. E. Human rabies: a disease of complex neuropathogenetic mechanisms and diagnostic challenges. *Lancet Neurol.* **2002**, *1*, 101–109.

(5) Hemachudha, T., Mitrabhakdi, E. Rabies. In *Infectious diseases of the nervous;* Davis, L., Kennedy, P. G. E., Eds.; Butterworth-Heinemann: Oxford, 2000; pp 401−444.

(6) Dacheux, L.; Reynes, J. M.; Buchy, P.; Sivuth, O.; Diop, B. M.; Rousset, D.; Rathat, C.; Jolly, N.; Dufourcq, J. B.; Nareth, C.; Diop, S.; Iehle, C.; Rajerison, R.; Sadorge, C.; Bourhy, H. A reliable diagnosis of human rabies based on analysis of skin biopsy specimens. *Clin. Infect. Dis* **2008**, *47*, 1410–1417.

(7) Hemachudha, T. Human rabies: clinical aspects, pathogenesis, and potential therapy. *Curr. Top. Microbiol. Immunol.* **1994**, *187*, 121–143.

(8) Mitrabhakdi, E.; Shuangshoti, S.; Wannakrairot, P.; Lewis, R. A.; Susuki, K.; Laothamatas, J.; Hemachudha, T. Difference in neuropathogenetic mechanisms in human furious and paralytic rabies. *J, Neurol. Sci,* **2005**, *238*, 3–10.

(9) Laothamatas, J.; Wacharapluesadee, S.; Lumlertdacha, B.; Ampawong, S.; Tepsumethanon, V.; Shuangshoti, S.; Phumesin, P.; Asavaphatiboon, S.; Worapruekjaru, L.; Avihingsanon, Y.; Israsena, N.; Lafon, M.; Wilde, H.; Hemachudha, T. Furious and paralytic rabies of canine origin: neuroimaging with virological and cytokine studies. *J, Neurovirol.* **2008**, *14*, 119–129.

(10) Laothamatas, J.; Hemachudha, T.; Mitrabhakdi, E.; Wannakrairot, P.; Tulayadaechanont, S. MR imaging in human rabies. *Am. J Neuroradiol.* **2003**, *24*, 1102–1109.

(11) Yan, X.; Prosniak, M.; Curtis, M. T.; Weiss, M. L.; Faber, M.; Dietzschold, B.; Fu, Z. F. Silver-haired bat rabies virus variant does not induce apoptosis in the brain of experimentally infected mice. *J. Neurovirol.* **2001**, *7*, 518–527.

(12) Sarmento, L.; Li, X. Q.; Howerth, E.; Jackson, A. C.; Fu, Z. F. Glycoprotein-mediated induction of apoptosis limits the spread of attenuated rabies viruses in the central nervous system of mice. *J. Neurovirol.* **2005**, *11*, 571–581.

(13) Suja, M. S.; Mahadevan, A.; Madhusudhana, S. N.; Vijayasarathi, S. K.; Shankar, S. K. Neuroanatomical mapping of rabies nucleocapsid viral antigen distribution and apoptosis in pathogenesis in street dog rabies--an immunohistochemical study. *Clin. Neuropathol.* **2009**, *28*, 113–124.

(14) Jackson, A. C.; Randle, E.; Lawrance, G.; Rossiter, J. P. Neuronal apoptosis does not play an important role in human rabies encephalitis. *J. Neurovirol.* **2008**, *14*, 368–375.

(15) Schnell, M. J.; McGettigan, J. P.; Wirblich, C.; Papaneri, A. The cell biology of rabies virus: using stealth to reach the brain. *Nat. Rev. Microbiol.* **2010**, *8*, 51–61.

(16) Prehaud, C.; Wolff, N.; Terrien, E.; Lafage, M.; Megret, F.; Babault, N.; Cordier, F.; Tan, G. S.; Maitrepierre, E.; Menager, P.; Chopy, D.; Hoos, S.; England, P.; Delepierre, M.; Schnell, M. J.; Buc, H.; Lafon, M. Attenuation of rabies virulence: takeover by the cytoplasmic domain of its envelope protein. *Sci. Signal.* **2010**, *3*, ra5.

(17) Jackson, A. C.; Rossiter, J. P. Apoptosis plays an important role in experimental rabies virus infection. *J. Virol.* **1997**, *71*, 5603–5607.

(18) Jackson, A. C.; Park, H. Apoptotic cell death in experimental rabies in suckling mice. *Acta Neuropathol.* **1998**, *95*, 159–164.

(19) Morimoto, K.; Hooper, D. C.; Spitsin, S.; Koprowski, H.; Dietzschold, B. Pathogenicity of different rabies virus variants inversely correlates with apoptosis and rabies virus glycoprotein expression in infected primary neuron cultures. *J. Virol.* **1999**, *73*, 510–518.

(20) Weli, S. C.; Scott, C. A.; Ward, C. A.; Jackson, A. C. Rabies virus infection of primary neuronal cultures and adult mice: failure to demonstrate evidence of excitotoxicity. *J. Virol.* **2006**, *80*, 10270–10273.

(21) Guigoni, C.; Coulon, P. Rabies virus is not cytolytic for rat spinal motoneurons in vitro. *J. Neurovirol.* **2002**, *8*, 306–317.

(22) Tirawatnpong, S.; Hemachudha, T.; Manutsathit, S.; Shuangshoti, S.; Phanthumchinda, K.; Phanuphak, P. Regional distribution of rabies viral antigen in central nervous system of human encephalitic and paralytic rabies. *J. Neurol. Sci.* **1989**, *92*, 91–99.

(23) Rajagopalan, D.; Agarwal, P. Inferring pathways from gene lists using a literature-derived network of biological relationships. *Bioinformatics* **2005**, *21*, 788–793.

(24) Jensen, O. N. Modification-specific proteomics: characterization of post-translational modifications by mass spectrometry. *Curr. Opin. Chem. Biol.* **2004**, *8*, 33–41.

(25) Koprowski, H.; Zheng, Y. M.; Heber-Katz, E.; Fraser, N.; Rorke, L.; Fu, Z. F.; Hanlon, C.; Dietzschold, B. In vivo expression of inducible nitric oxide synthase in experimentally induced neurologic diseases. *Proc. Natl. Acad. Sci. U.S.A.* **1993**, *90*, 3024–3027.

(26) Hooper, D. C.; Ohnishi, S. T.; Kean, R.; Numagami, Y.; Dietzschold, B.; Koprowski, H. Local nitric oxide production in viral and autoimmune diseases of the central nervous system. *Proc. Natl. Acad. Sci. U.S.A.* **1995**, *92*, 5312–5316.

(27) Shin, T.; Weinstock, D.; Castro, M. D.; Hamir, A. N.; Wampler, T.; Walter, M.; Kim, H. Y.; Acland, H. Immunohistochemical localization of endothelial and inducible nitric oxide synthase within neurons of cattle with rabies. *J. Vet. Med. Sci.* **2004**, *66*, 539–541.

(28) Jackson, A. C.; Kammouni, W.; Zherebitskaya, E.; Fernyhough, P. Role of oxidative stress in rabies virus infection of adult mouse dorsal root ganglion neurons. *J. Virol.* **2010**, *84*, 4697–4705.

(29) Zandi, F.; Eslami, N.; Soheili, M.; Fayaz, A.; Gholami, A.; Vaziri, B. Proteomics analysis of BHK-21 cells infected with a fixed strain of rabies virus. *Proteomics* **2009**, *9*, 2399–2407.

(30) Scott, C. A.; Rossiter, J. P.; Andrew, R. D.; Jackson, A. C. Structural abnormalities in neurons are sufficient to explain the clinical disease and fatal outcome of experimental rabies in yellow fluorescent protein-expressing transgenic mice. *J. Virol.* **2008**, *82*, 513–521.

(31) Oueslati, A.; Fournier, M.; Lashuel, H. A. Role of post-translational modifications in modulating the structure, function and toxicity of alpha-synuclein: implications for Parkinson's disease pathogenesis and therapies. *Prog. Brain Res.* **2010**, *183*, 115–145.

(32) Laothamatas, J.; Sungkarat, W.; Hemachudha, T. Neuroimaging in human rabies. In *Advances in virus research*; Jackson, A. C., Ed.; Academic Press/Elsevier: New York, 2011; Vol. 79, 309−327.

(33) Latchman, D. S. Protective effect of heat shock proteins in the nervous system. *Curr. Neurovasc. Res.* **2004**, *1*, 21–27.

(34) Pockley, A. G. Heat shock proteins as regulators of the immune response. *Lancet* **2003**, *362*, 469–476.

(35) Sagara, J.; Kawai, A. Identification of heat shock protein 70 in the rabies virion. *Virology* **1992**, *190*, 845–848.

(36) Lahaye, X.; Vidy, A.; Pomier, C.; Obiang, L.; Harper, F.; Gaudin, Y.; Blondel, D. Functional characterization of Negri bodies (NBs) in rabies virus-infected cells: Evidence that NBs are sites of viral transcription and replication. *J. Virol.* **2009**, *83*, 7948–7958.

(37) Menager, P.; Roux, P.; Megret, F.; Bourgeois, J. P.; Le Sourd, A. M.; Danckaert, A.; Lafage, M.; Prehaud, C.; Lafon, M. Toll-like receptor 3 (TLR3) plays a major role in the formation of rabies virus Negri Bodies. *PLoS Pathog.* **2009**, *5*, e1000315.

(38) Charrier, E.; Reibel, S.; Rogemond, V.; Aguera, M.; Thomasset, N.; Honnorat, J. Collapsin response mediator proteins (CRMPs): involvement in nervous system development and adult neurodegenerative disorders. *Mol. Neurobiol.* **2003**, *28*, 51–64.

(39) Fukata, Y.; Itoh, T. J.; Kimura, T.; Menager, C.; Nishimura, T.; Shiromizu, T.; Watanabe, H.; Inagaki, N.; Iwamatsu, A.; Hotani, H.; Kaibuchi, K. CRMP-2 binds to tubulin heterodimers to promote microtubule assembly. *Nat. Cell Biol.* **2002**, *4*, 583–591.

(40) Inagaki, N.; Chihara, K.; Arimura, N.; Menager, C.; Kawano, Y.; Matsuo, N.; Nishimura, T.; Amano, M.; Kaibuchi, K. CRMP-2 induces axons in cultured hippocampal neurons. *Nat. Neurosci.* **2001**, *4*, 781–782.

(41) Vincent, P.; Collette, Y.; Marignier, R.; Vuaillat, C.; Rogemond, V.; Davoust, N.; Malcus, C.; Cavagna, S.; Gessain, A.; Machuca-Gayet, I.; Belin, M. F.; Quach, T.; Giraudon, P. A role for the neuronal protein collapsin response mediator protein 2 in T lymphocyte polarization and migration. *J. Immunol.* **2005**, *175*, 7650–7660.

(42) Vuaillat, C.; Varrin-Doyer, M.; Bernard, A.; Sagardoy, I.; Cavagna, S.; Chounlamountri, I.; Lafon, M.; Giraudon, P. High CRMP2 expression in peripheral T lymphocytes is associated with recruitment to the brain during virus-induced neuroinflammation. *J. Neuroimmunol.* **2008**, *193*, 38–51.

(43) Fu, Z. F.; Weihe, E.; Zheng, Y. M.; Schafer, M. K.; Sheng, H.; Corisdeo, S.; Rauscher, F. J.; Koprowski, I. I. I.; Dietzschold, H. B. Differential effects of rabies and borna disease viruses on immediate-early- and late-response gene expression in brain tissues. *J. Virol.* **1993**, *67*, 6674–6681.

(44) Prosniak, M.; Hooper, D. C.; Dietzschold, B.; Koprowski, H. Effect of rabies virus infection on gene expression in mouse brain. *Proc. Natl. Acad. Sci. U.S.A.* **2001**, *98*, 2758–2763.

(45) Dhingra, V.; Li, X.; Liu, Y.; Fu, Z. F. Proteomic profiling reveals that rabies virus infection results in differential expression of host proteins involved in ion homeostasis and synaptic physiology in the central nervous system. *J. Neurovirol.* **2007**, *13*, 107–117.

(46) Thongboonkerd, V. Urinary proteomics: towards biomarker discovery, diagnostics and prognostics. *Mol. Biosyst.* **2008**, *4*, 810–815.

JOURNAL OF PROTEOMICS 74 (2011) 1607–1613



available at www.sciencedirect.com

ScienceDirect

www.elsevier.com/locate/jprot



Identification of *Brugia malayi* immunogens by an immunoproteomics approach

Sirichit Wongkamchai[a], *Wararat Chiangjong*[b], *Supachok Sinchaikul*[c], *Shui-Tein Chen*[c], *Wej Choochote*[d], *Visith Thongboonkerd*[b,e,*]

[a]*Department of Parasitology, Faculty of Medicine Siriraj Hospital, Mahidol University, Bangkok, Thailand*
[b]*Medical Proteomics Unit, Office for Research and Development, Faculty of Medicine Siriraj Hospital, Mahidol University, Bangkok, Thailand*
[c]*Institute of Biological Chemistry and Genomic Research Center, Academia Sinica, Taipei, Taiwan*
[d]*Department of Parasitology, Faculty of Medicine, Chiang Mai University, Chiang Mai, Thailand*
[e]*Center for Research in Complex Systems Science, Mahidol University, Bangkok, Thailand*

ARTICLE INFO

Available online 17 June 2011

Keywords:
Brugia malayi
Diagnostics
Filariasis
Immunogens
Immunoproteomics
Vaccine

ABSTRACT

Filariasis remains a health problem in tropical countries. Identification of immunogens from its causative organism would lead to development of a better diagnostic test, as well as vaccine discovery to effectively prevent this disease. We applied immunoproteomics to define potential immunogens of adult *Brugia malayi* that were recognized by IgM, IgG1 and IgG4 in sera of patients with four distinct clinical spectra of filariasis, including endemic asymptomatic, lymphangitis, elephantiasis and microfilaremia (n=5/group). Sera of healthy individuals (n=5) from non-endemic area served as the negative control. Brugian proteins were resolved by 2-DE and subjected to 2-D Western blot analysis probed with these sera. A total of 30 immunoreactive proteins recognized by IgM, IgG1 and IgG4 in sera from all four filarial groups were identified by Q-TOF MS and MS/MS analyses. Interestingly, only three immunogens were recognized by IgM in lymphangitis, elephantiasis and microfilaremia, but not in endemic asymptomatic group. IgG1 recognized 20 immunogens in endemic asymptomatic, lymphangitis and microfilaremia (mostly in endemic asymptomatic group), but not in elephantiasis, whereas IgG4 recognized 28 immunogens in all four filarial groups (mostly in microfilaremia). This large data set is an important resource for further development of a new diagnostic test and/or vaccine for filariasis.
© 2011 Elsevier B.V. All rights reserved.

1. Introduction

Filariasis remains an important tropical disease. People, who live in endemic areas, are easily infected via mosquito-bite that transmits the causative parasite person-to-person. Patients with filariasis frequently have lymphatic invasion that causes a variety of temporary and permanent disabilities. It is now considered as one of the few infectious diseases that are potentially eliminable [1], and the World Health Organization (WHO) has taken a priority to reduce and finally eliminate lymphatic filariasis by 2020 [2]. Hence, effective diagnostic test becomes crucial for the disease detection. Thick blood smear remains the routine laboratory method used for the diagnosis of lymphatic filariasis. This diagnostic method depends on the detection of microfilaria in peripheral blood (microfilaremia). Due to the diurnal variation of microfilaremic levels in most of endemic areas of lymphatic filariasis, this test requires specimen (blood) collection at night. Furthermore, this method is relatively insensitive and difficult to interpret precisely in the field survey. Serological diagnostic methods exhibit a better sensitivity as

* *Corresponding author at:* Siriraj Hospital, Mahidol University, 12th Floor Adulyadej Vikrom Building, 2 Prannok Road, Bangkoknoi, Bangkok 10700, Thailand. Tel./fax: +66 2 4184793.
E-mail addresses: thongboonkerd@dr.com, vthongbo@yahoo.com (V. Thongboonkerd).

1874-3919/$ – see front matter © 2011 Elsevier B.V. All rights reserved.
doi:10.1016/j.jprot.2011.06.012

compared to the thick blood smear, allowing the detection of subjects with prior infection but are currently non-microfilaremic (endemic asymptomatic). Serological methods also offer opportunity to examine daytime-collected blood samples [3]. Subsequent development of rapid immunochromatographic test (ICT) is a significant advance providing a reliable assay for detection of circulating antigens derived from *Wuchereria bancrofti*[4]. The desirable by-product of this breakthrough enables mapping of endemic areas for the mass drug administration program for eradication of filariasis. However, ICT is specific only for the detection of circulating antigens derived from *W. bancrofti* and is not applicable for the detection of *Brugia malayi*, another common etiologic specifies of filariasis. Apart from the still-imperfect diagnostic tests, there is no effective chemotherapy to completely eradicate lymphatic-dwelling adult filarial parasites that persist in the infected hosts for several years. In addition, there is no vaccine available for effective prevention of filariasis [5]. It is therefore crucial to develop a new diagnostic test that can detect all forms of filariasis and a vaccine that can effectively prevent the disease. Efforts towards these developments seem to be achievable through the characterizations of immune response in patients with filariasis and protective immunity in the exposed population [6].

In the present study, we applied an immunoproteomics approach to define potential immunogens of *B. malayi*. Briefly, proteins derived from adult *B. malayi* were resolved by two-dimensional gel electrophoresis (2-DE) and then subjected to 2-D Western blot analysis probed with sera collected from patients with four clinical entities of filariasis, including endemic asymptomatic, lymphangitis, elephantiasis and microfilaremia. Sera of healthy individuals from non-endemic area served as the negative control. The immunoreactive protein spots detected with anti-IgM, anti-IgG1 and anti-IgG4 antibodies conjugated with horseradish peroxidase were then identified by Q-TOF MS and MS/MS analyses.

2. Materials and methods

2.1. Human subjects and sample collection

A total of 25 human subjects were included in this study. Sera were collected from patients in the endemic area of filariasis in Thailand with various clinical entities, including endemic asymptomatic, lymphangitis, elephantiasis, and microfilaremia ($n=5$ for each group). Other five sera samples were collected from healthy individuals in the non-endemic area (Bangkok, Thailand) and used as the negative control. The study on human subjects was approved by the Institutional Ethical Committee.

2.2. Cultivation of adult stage of *B. malayi* and protein extraction

B. malayi was maintained in *Meriones unguiculatus* gerbils and then harvested from the infected gerbils using a method described by Ash and Riley [7]. The parasites were washed extensively with distilled water and then with 0.1 M phosphate buffer, pH 7.2. They were then ground in distilled water containing protease inhibitors (0.1 M PMSF, 0.1 M TPCK and 0.1 M EDTA) using a glass tissue grinder. The homogenate was then sonicated in an ice box using an ultrasonic sonicator (MSE Scientific Instruments; Sussex, UK) at 20 kilocycle/second and 4 °C for 20 min. The pellet was resuspended in a lysis buffer containing 8 M urea, 2 M thiourea, 4% 3-[(3-cholamidopropyl) dimethyl-ammonio]-1-propanesulfonate (CHAPS), 120 mM dithiothreitol (DTT), 2% (v/v) ampholytes (pH 3–10) and 40 mM Tris-base, and incubated at 4 °C for 30 min. Unsolubilized nuclei, cell debris, and particulate matters were removed by a centrifugation at 10,000 rpm and 4 °C for 5 min. Protein concentration was determined by the Bradford method using Bio-Rad protein assay (Bio-Rad Laboratories; Hercules, CA).

2.3. 2-DE

For each 2-D gel, Immobiline DryStrip (non linear pH gradient of 3–10, 7-cm-long; GE Healthcare, Uppsala, Sweden) was rehydrated overnight with an equal amount of 50 μg total protein that was premixed with a rehydration buffer containing 7 M urea, 2 M thiourea, 2% CHAPS, 2% (v/v) ampholytes (pH 3–10), 120 mM DTT, 40 mM Tris-base, and bromophenol blue (to make the final volume of 150 μl per strip). The first dimensional separation or isoelectric focusing (IEF) was performed in Ettan IPGphor III System (GE Healthcare) at 20 °C, using a stepwise mode to reach 9,083 Vh with limited current of 50 mA/strip. After completion of the IEF, the strip was first equilibrated for 15 min in an equilibration buffer containing 6 M urea, 130 mM DTT, 112 mM Tris-base, 4% SDS, 30% glycerol and 0.002% bromophenol blue, and then in another similar buffer that replaced DTT with 135 mM iodoacetamide, for further 15 min. The second dimensional separation was performed in 12% polyacrylamide gel using SE260 Mini-Vertical Electrophoresis Unit (GE Healthcare) at 150 V for approximately 2 h. The resolved protein spots were either stained with CBB-G250 (USB, Cleveland, OH, USA) or transferred onto a PVDF membrane for subsequent immunoblot analysis.

2.4. 2-D Western blot analysis

Proteins resolved by 2-DE as described above were transferred onto a PVDF membrane using a semi-dry transfer system. After blotting, the membrane was blocked with 5% milk in PBS, pH 7.2 with 0.1% Tween-20 for 30 min and then incubated with the pooled sera of each group at 4 °C overnight. The membrane was washed three times with a washing buffer (containing 2% milk, 0.1% Tween-20 and PBS, pH 7.2) at room temperature and then incubated with mouse monoclonal anti-human IgM, anti-human IgG1 or anti-human IgG4 conjugated with horseradish peroxidase (Invitrogen; Camarillo, CA) diluted 1:10,000 at room temperature for 1 h. The immunoreactive protein spots were then visualized using enhanced chemiluminescence reagent (Pierce Biotechnology; Rockford, IL) followed by autoradiography.

2.5. Intensity analysis and matching of immunoreactive spots with protein spots visualized by CBB-G250 staining

Image Master 2D Platinum (GE Healthcare) software was used for matching and analysis of protein spots on 2-D gels. Parameters used for spot detection were (i) minimal area = 10 pixels,

(ii) smooth factor = 2.0, and (iii) saliency = 2.0. A reference gel was created from an artificial gel combining all of the spots presenting in different gels into one image. The reference gel was then used for matching of corresponding protein spots across different gels.

2.6. *In-gel tryptic digestion*

All the immunoreactive protein spots detected by anti-IgM, anti-IgG1 and anti-IgG4 antibodies were excised from 2-D gels, washed twice with 200 μl of 50% acetonitrile (ACN)/25 mM NH_4HCO_3 buffer (pH 8.0) at room temperature for 15 min, and then washed once with 200 μl of 100% ACN. After washing, the solvent was removed, and the gel pieces were dried by a SpeedVac concentrator (Savant; Holbrook, NY) and rehydrated with 10 μl of 1% (w/v) trypsin (Promega; Madison, WI) in 25 mM NH_4HCO_3. After rehydration, the gel pieces were crushed and incubated at 37 °C for at least 16 h. Peptides were subsequently extracted twice with 50 μl of 50% ACN/5% trifluoroacetic acid (TFA); the extracted solutions were then combined and dried with the SpeedVac concentrator. The peptide pellets were resuspended with 10 μl of 0.1% TFA and purified using $ZipTip_{C18}$ (Millipore; Bedford, MA). The peptide solution was drawn up and down in the $ZipTip_{C18}$ ten times and then washed with 10 μl of 0.1% formic acid by drawing up and expelling the washing solution three times. The peptides were finally eluted with 5 μl of 75% ACN/0.1% formic acid.

2.7. *Protein identification by Q-TOF MS and MS/MS analyses*

The trypsinized samples were premixed 1:1 with the matrix solution containing 5 mg/ml α-cyano-4-hydroxycinnamic acid (CHCA) in 50% ACN, 0.1% (v/v) TFA and 2% (w/v) ammonium citrate, and deposited onto the 96-well MALDI target plate. The samples were analyzed by Q-TOF Ultima™ mass spectrometer (Micromass; Manchester, UK), which was fully automated with predefined probe motion pattern and the peak intensity threshold for switching over from MS survey scanning to MS/MS, and from one MS/MS to another. Within each sample well, parent ions that met the predefined criteria (any peak within the m/z 800–3,000 range with intensity above 10 count ± include/exclude list) were selected for CID MS/MS using argon as the collision gas and a mass dependent ± 5 V rolling collision energy until the end of the probe pattern was reached. The MS and MS/MS data were extracted and outputted as the searchable *.txt* and *.pkl* files, respectively, for independent searches using the MASCOT search engine (http://www.matrixscience.com), assuming that peptides were monoisotopic. Fixed modification was carbamidomethylation at cysteine residues, whereas variable modification was oxidation at methionine residues. Only one missed trypsin cleavage was allowed, and peptide mass tolerances of 100 and 50 ppm were allowed for peptide mass fingerprinting and MS/MS ions search, respectively.

3. Results and discussion

We applied an immunoproteomics approach to identify potential immunogens of adult *B. malayi*, a causative parasite of filariasis. Proteins extracted from *B. malayi* were resolved by 2-DE and subjected to 2-D Western blot analysis probed with pooled sera from five subjects in individual groups, including endemic asymptomatic, lymphangitis, elephantiasis and microfilaremia. The pooled sera from five healthy individuals in non-endemic area served as the negative control. Thereafter, the immunoreactive protein spots were detected by anti-IgM, anti-IgG1 and anti-IgG4 antibodies conjugated with horseradish peroxidase. Combination of 2-DE, immunoblotting and mass spectrometric analysis is a common immunoproteomics approach used for identification of novel antigens [8]. This approach has been proven for characterizing antigens derived from parasitic organisms, e.g. *Toxoplasma gondii*, *Fasciola hepatica*, *Schistosoma japonicum*, *Ascaris suum* and *Neospora caninum*[9]. Using this method, we identified a total of 30 immunoreactive protein spots that were recognized by sera of filarial patients regardless of clinical group and immunoglobulin type examined, whereas none was detected by the negative-control sera (Fig. 1).

Overall, IgM recognized smallest number of antigens, whereas IgG4 recognized greatest number of potential immunogens. Only three immunogens were recognized by IgM, including T-complex protein 1 theta subunit (detectable only in lymphangitis), chaperonin homolog HSP60, mitochondrial precursor (detectable only in elephantiasis) and enolase (detectable only in microfilaremia). There was no IgM-recognized immunogen found in endemic asymptomatic group. IgG1 recognized 20 immunogens in endemic asymptomatic, lymphangitis and microfilaremia (mostly in endemic asymptomatic group), but not in elephantiasis. IgG4 recognized 28 immunogens in all 4 filarial groups (mostly in microfilaremia) (Fig. 1). All of these immunoreactive protein spots were successfully identified by Q-TOF MS and MS/MS analyses. Their mass spectrometric data (identities, identification scores, sequence coverage, number of matched peptides, isoelectric point or pI, molecular weight or MW, etc.) are summarized in Table 1. Moreover, details of their quantitative data, in terms of degree of immune recognition as reflected by intensity volume of the immunoreactive spots recognized by IgM, IgG1 and IgG4, are provided in Table 2.

Indeed, proteomics has previously been applied to filariasis. Hewitson et al. [5] employed 2 parallel proteomic approaches, namely 2-DE and shotgun liquid chromatography (LC) coupled to MS/MS, and successfully identified 80 excretory–secretory proteins and 63 somatic proteins from adult *B. malayi*. In other studies, Moreno and Geary [10] performed 1-DE (SDS-PAGE) followed by LC-MS/MS and identified 228 excretory–secretory proteins derived from adult female, adult male and microfilarial *B. malayi*, whereas Bennuru et al. [11] identified 852 excretory–secretory proteins from various stages of *B. malayi* using microcapillary reverse-phase LC-MS/MS. However, none of the immunogenic proteins were characterized or identified in these studies. Weinkopff et al. [12] identified 18 unique proteins from adult *Brugia pahangi* using 2-DE followed by MALDI-TOF MS. From these 18 identified proteins, 7 were detected as potential immunogens of *B. pahangi*. Among these, only galectin was consistent with our data. The differences might reflect differential species of filarial parasite used in these two studies. In the present study, we have identified, for the first time, potential immunogens of *B. malayi* that could be

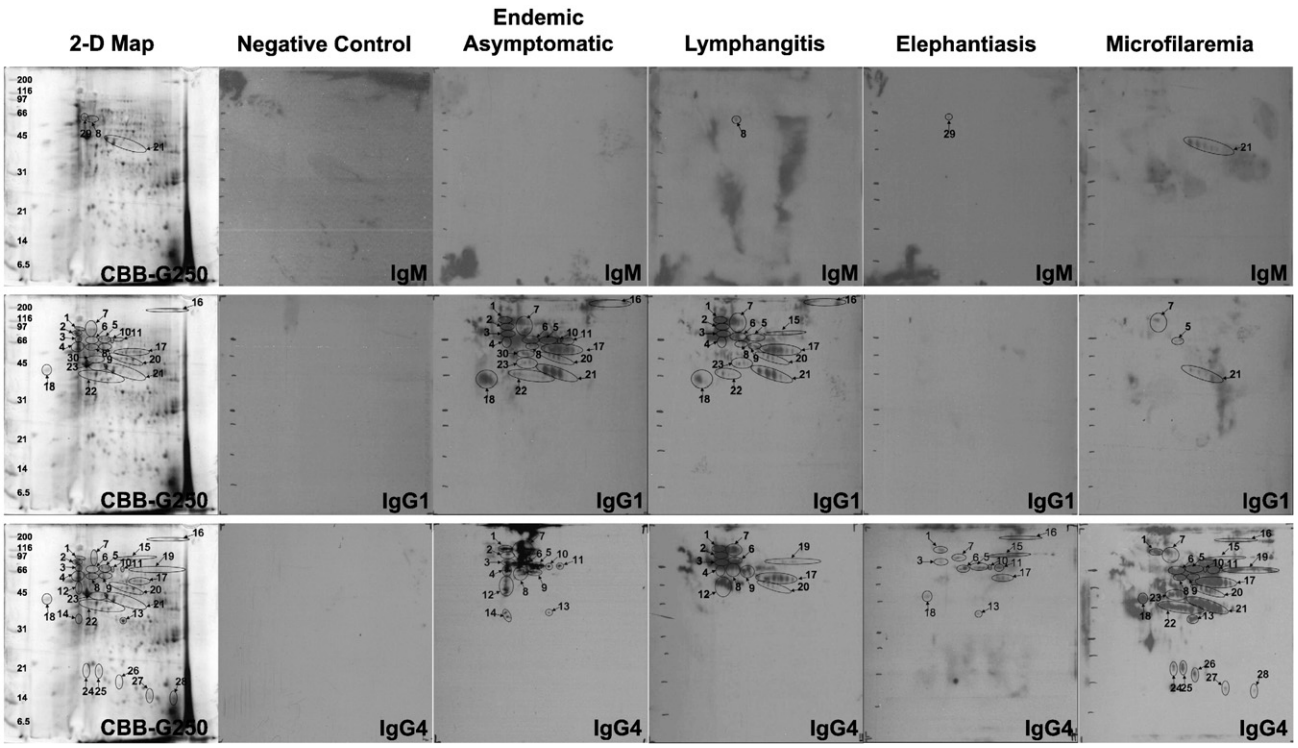


Fig. 1 – 2-D proteome map of all immunoreactive proteins. Proteins derived from adult *B. malayi* (with an equal amount of 50 μg) were resolved in 2-DE and were then either stained with CBB-G250 dye (first column) or subjected to 2-D Western blot analysis (other columns). For the latter, the proteins transferred onto PVDF membranes were probed with pooled sera from patients with different clinical spectra of filariasis, including endemic asymptomatic, lymphangitis, elephantiasis and microfilaremia (sera from healthy individuals in non-endemic area served as the negative control). Immunoreactive protein spots were then detected using horseradish peroxidase-conjugated secondary antibodies against human IgM (first row), IgG1 (second row) and IgG4 (third row). All these immunoreactive proteins were then identified by Q-TOF MS and MS/MS analyses (see also Table 1). The quantitative data of immunoreactivity of these potential immunogens are summarized in Table 2.

recognized by antibodies in sera of patients with different clinical spectra of filariasis. Moreover, another dimension of our data was that we also characterized type of antibodies that recognized such immunogens, including IgM, IgG1 and IgG4.

Among the potential immunogens observed in our present study, actin 1 was identified as multiple isoforms, most likely due to post-translational modifications or cleavage (Table 1). Two of the three isoforms of actin 1 (spots #22, 23) were detected by IgG1 in endemic asymptomatic and lymphangitis, whereas all the three forms (spots #22–24) were detected by IgG4 in microfilaremia (Fig. 1 and Table 2). Actin 1 is a highly conserved protein that is involved in cell motility and is ubiquitously expressed in all eukaryotic cells. Our data were consistent with those reported in a previous study by Sritharan and Piessens [13], demonstrating that actin of *B. malayi* contains a developmentally regulated antigenic epitope. Similarly, two forms of enolase (spots #20, 21) were detected by IgG1 in endemic asymptomatic and lymphangitis, and by IgG4 in microfilaremia (Fig. 1 and Table 2). Enolase has been previously identified in excretory–secretory products of *B. malayi*[5], and been shown as an important antigen in many clinically relevant microbes [14]. These findings strengthen its role as a potential immunogen of *B. malayi*.

Leucine aminopeptidase (spot #6) was a target protein that induced IgG4 response across all clinical spectra of brugian filariasis, and IgG1 response in endemic asymptomatic and lymphangitis (Fig. 1 and Table 2). This aminopeptidase is a phosphorylcholine-containing glycoprotein posing an anti-inflammatory property [15], and has been detected also in excretory–secretory products of *B. malayi* in a previous study [5]. Galectin (spot #13) was identified as a target protein of IgG4 immune response in endemic asymptomatic, elephantiasis and microfilaremic groups (Fig. 1 and Table 2). Strongest immunoreactivity against galectin was observed in microfilaremia. Note that this protein was not detected in lymphangitis group. In a previous proteomic study, galectin has been detected as the major component of *B. malayi* secretome [5]. Galectins are atypical secreted proteins that have been identified from a number of filarial parasites [16,17]. Accumulation of galectins occurs at endothelial interfaces by binding to extracellular proteins and promoting endothelial proliferation [18]. Our data were consistent with those reported by Hewitson et al. [5] demonstrating that galectin Bm1 24940, a protein found in *B. malayi* excretory–secretory products, could bind to IgG with the greatest extent in microfilaremic sera. These data also underscore the significant roles of leucine aminopeptidase and galectin as potential immunogens of *B. malayi*.

In addition, our data also revealed differential responses of human antibodies in different clinical spectra of brugian

Table 1 – Identification of immunoreactive proteins derived from *B. malayi*, detected by IgM, IgG1 and IgG4 in sera of patients with different clinical spectra of filariasis.

Spot no.	Protein name	NCBI ID	Identified by	Identification scores (MS, MS/MS)	%Cov (MS, MS/MS)	No. of matched peptides (MS, MS/MS)	pI	MW (kDa)
1	Endoplasmin precursor	gi|170589273	MS, MS/MS	89, 109	25, 6	17, 3	5.13	90.97
2	Heat shock protein 90	gi|19855062	MS, MS/MS	169, 172	36, 6	23, 4	4.98	83.01
3	Vacuolar ATP synthase catalytic subunit A, osteoclast isoform	gi|170593817	MS, MS/MS	174, 98	41, 5	21, 2	5.10	68.45
4	Tubulin alpha chain	gi|170588855	MS, MS/MS	153, 226	43, 16	17, 5	5.01	50.39
5	Heat shock protein 70	gi|6941872	MS, MS/MS	121, 86	32, 4	18, 2	5.40	70.55
6	Leucyl aminopeptidase	gi|170596311	MS, MS/MS	87, 42	29, 2	10, 1	5.41	45.53
7	Acyl-Coenzyme A oxidase 3, pristanoyl	gi|157073994	MS	94, NA	24, NA	11, NA	8.17	78.68
8	T-complex protein 1 theta subunit	gi|170592683	MS/MS	NA, 53	NA, 5	NA, 2	5.32	600.75
9	Cytoplasmic intermediate filament protein	gi|170596673	MS/MS	NA, 43	NA, 6	NA, 2	5.35	37.43
10	ATP-dependent helicase HrpA	gi|153886738	MS	96, NA	20, NA	19, NA	8.89	150.13
11	Hypothetical protein CHGG_00235	gi|116179214	MS	82, NA	12, NA	20, NA	8.98	223.69
12	Actin 1	gi|170581695	MS, MS/MS	86, 57	33, 7	11, 2	5.30	42.12
13	Galectin	gi|170583137	MS, MS/MS	160, 89	49, 13	17, 3	5.96	31.93
14	Actin 1	gi|170581695	MS/MS	NA, 113	NA, 11	NA, 3	5.30	42.12
15	Carbohydrate phosphorylase	gi|170579084	MS, MS/MS	235, 118	39, 4	31, 3	6.06	96.68
16	Collagen alpha 2(IV) chain precursor	gi|170579429	MS/MS	NA, 95	NA, 1	NA, 2	9.02	168.51
17	Independent phosphoglycerate mutase isoform 1	gi|37681504	MS, MS/MS	141, 104	33, 6	20, 3	6.27	57.97
18	Hypothetical protein MGL_1413	gi|164660214	MS	86, NA	49, NA	8, NA	7.85	19.55
19	Transketolase	gi|170576173	MS, MS/MS	94, 78	24, 7	13, 3	6.12	68.08
20	Enolase	gi|170582775	MS, MS/MS	266, 169	70, 18	28, 5	5.98	47.83
21	Enolase	gi|170582775	MS, MS/MS	90, 26	41, 4	12, 1	5.98	47.83
22	Actin 1	gi|170581695	MS, MS/MS	96, 128	35, 15	14, 4	5.30	42.12
23	Actin 1	gi|170581695	MS, MS/MS	125, 163	37, 12	12, 3	5.30	42.12
24	Actin 1	gi|170581695	MS/MS	NA, 50	NA, 7	NA, 2	5.30	42.12
25	Immunoglobulin heavy chain variable region	gi|112696951	MS	57, NA	51, NA	5, NA	8.91	11.20
26	Putative sigma-54 interacting transcription antiterminator	gi|126699898	MS	74, NA	16, NA	14, NA	5.47	111.54
27	Thymidine kinase	gi|148980443	MS	91, NA	42, NA	8, NA	5.75	22.05
28	Hypothetical protein	gi|118084358	MS	86, NA	14, NA	20, NA	5.89	195.32
29	Chaperonin homolog HSP60, mitochondrial precursor	gi|170576770	MS/MS	NA, 33	NA, 5	NA, 1	4.81	30.54
30	Predicted protein	gi|156362061	MS	87, NA	52, NA	9, NA	9.42	30.32

NCBI = National Center for Biotechnology Information.
%Cov = %Sequence coverage [(number of the matched residues/total number of residues in the entire sequence) × 100%].
NA = not applicable.

Table 2 – Quantitative data of immunoreactivity of potential immunogens detected by IgM, IgG1 and IgG4 in sera of patients with different clinical spectra of filariasis.

Spot no.	Protein name	Intensity volume (×10^4 pixels)														
		Healthy control			Endemic asymptomatic			Lymphangitis			Elephantiasis			Microfilaremia		
		IgM	IgG1	IgG4	IgM	IgG1	IgG4	IgM	IgG1	IgG4	IgM	IgG1	IgG4	IgM	IgG1	IgG4
1	Endoplasmin precursor	0	0	0	0	5.08	5.17	0	11.39	10.18	0	0	0.87	0	0	7.99
2	Heat shock protein 90	0	0	0	0	5.74	1.80	0	6.94	4.53	0	0	0	0	0	0
3	Vacuolar ATP synthase catalytic subunit A, osteoclast isoform	0	0	0	0	4.12	4.81	0	2.36	3.38	0	0	0.55	0	0	0
4	Tubulin alpha chain	0	0	0	0	1.96	3.95	0	2.77	1.88	0	0	0	0	0	0
5	Heat shock protein 70	0	0	0	0	6.56	14.11	0	4.92	0	0	0	3.85	0	1.27	13.45
6	Leucyl aminopeptidase	0	0	0	0	6.46	6.65	0	8.10	7.97	0	0	2.28	0	0	16.27
7	Acyl-Coenzyme A oxidase 3, pristanoyl	0	0	0	0	8.63	35.78	0	8.38	7.99	0	0	1.22	0	1.78	7.68
8	T-complex protein 1 theta subunit	0	0	0	0	8.97	4.09	0.77	5.75	7.25	0	0	0	0	0	4.45
9	Cytoplasmic intermediate filament protein	0	0	0	0	0	6.05	0	2.92	8.05	0	0	0	0	0	6.19
10	ATP-dependent helicase HrpA	0	0	0	0	1.41	1.04	0	0	0	0	0	0.43	0	0	0.33
11	Hypothetical protein CHGG_00235	0	0	0	0	5.69	1.11	0	0	0	0	0	1.13	0	0	12.17
12	Actin 1	0	0	0	0	0	9.97	0	0	15.69	0	0	0	0	0	0
13	Galectin	0	0	0	0	0	0.54	0	0	0	0	0	0.37	0	0	5.56
14	Actin 1	0	0	0	0	0	1.93	0	0	0	0	0	0	0	0	0
15	Carbohydrate phosphorylase	0	0	0	0	0	0	0	7.53	0	0	0	4.53	0	0	10.31
16	Collagen alpha 2(IV) chain precursor	0	0	0	0	14.55	0	0	10.37	0	0	0	4.65	0	0	8.25
17	Independent phosphoglycerate mutase isoform 1	0	0	0	0	15.58	0	0	16.98	15.81	0	0	4.16	0	0	41.58
18	Hypothetical protein MGL_1413	0	0	0	0	12.46	0	0	5.52	0	0	0	1.68	0	0	6.45
19	Transketolase	0	0	0	0	0	0	0	0	3.41	0	0	0	0	0	24.22
20	Enolase	0	0	0	0	6.55	0	0	3.88	2.94	0	0	0	0	0	23.44
21	Enolase	0	0	0	0	20.20	0	0	16.53	0	0	0	0	8.76	10.92	48.37
22	Actin 1	0	0	0	0	20.68	0	0	3.51	0	0	0	0	0	0	53.36
23	Actin 1	0	0	0	0	1.75	0	0	2.13	0	0	0	0	0	0	7.50
24	Actin 1	0	0	0	0	0	0	0	0	0	0	0	0	0	0	2.42
25	Immunoglobulin heavy chain variable region	0	0	0	0	0	0	0	0	0	0	0	0	0	0	3.50
26	Putative sigma-54 interacting transcription antiterminator	0	0	0	0	0	0	0	0	0	0	0	0	0	0	3.94
27	Thymidine kinase	0	0	0	0	0	0	0	0	0	0	0	0	0	0	1.55
28	Hypothetical protein	0	0	0	0	0	0	0	0	0	0	0	0	0	0	0.71
29	Chaperonin homolog HSP60	0	0	0	0	0	0	0	0	0	0.31	0	0	0	0	0
30	Predicted protein	0	0	0	0	3.44	0	0	0	0	0	0	0	0	0	0

filariasis. Among these, IgG4 was the strongest immune response, particularly in microfilaremic subjects, as compared to IgM and IgG1 (Fig. 1 and Table 2). Microfilaremic subjects are the infected individuals who are mostly asymptomatic, despite the presence of circulating microfilaria in the peripheral blood [19]. Its asymptomatic state is perhaps a result of suppression of both Th1 and Th2 responses. This down-regulation of the host immune responses is characterized by impaired proliferation of T cells, increased production of the regulatory cytokine IL-10, and high levels of IgG4 [20]. Thus, the immunoreactive proteins detected by IgG4 may be directed to the discovery of a vaccine for prevention of filariasis, a new therapeutic target, and a novel diagnostic test. On the other hand, filaria-specific IgG1 was far more prominent in endemic asymptomatic and lymphangitis. It is likely that antibody and humeral mechanisms initiated by IgG1 may contribute to the pathology through antibody-dependent cell-mediated cytotoxicity (ADCC) or immune complex formation [21]. Nevertheless, IgG1 is similar to IgG4 in some aspects, e.g. inability to activate complement. The latter may explain why antifilarial IgG1 was also dominantly detected in endemic asymptomatic group.

In summary, we report herein a total of 30 potential immunogens of *B. malayi* identified by an immunoproteomics approach. This large data set is an important resource for further development of a new diagnostic test and/or vaccine for filariasis.

Acknowledgements

This work was supported by The Thailand Research Fund (MRG5080346 to S. Wongkamchai and RTA5380005 to V. Thongboonkerd), Office of the Higher Education Commission and Mahidol University under the National Research Universities Initiative (to V. Thongboonkerd). V. Thongboonkerd is also supported by "Chalermphrakiat" Grant, Faculty of Medicine Siriraj Hospital, whereas W. Chiangjong is supported by the Royal Golden Jubilee PhD Program of The Thailand Research Fund.

REFERENCES

[1] Molyneux DH, Zagaria N. Lymphatic filariasis elimination: progress in global programme development. Ann Trop Med Parasitol 2002;96(Suppl 2):S15–40.

[2] Behbehani K. Candidate parasitic diseases. Bull World Health Organ 1998;76(Suppl 2):64–7.

[3] Ottesen EA. The global programme to eliminate lymphatic filariasis. Trop Med Int Health 2000;5:591–4.

[4] Weil GJ, Lammie PJ, Weiss N. The ICT filariasis test: a rapid-format antigen test for diagnosis of bancroftian filariasis. Parasitol Today 1997;13:401–4.

[5] Hewitson JP, Harcus YM, Curwen RS, Dowle AA, Atmadja AK, Ashton PD, et al. The secretome of the filarial parasite, *Brugia malayi*: proteomic profile of adult excretory–secretory products. Mol Biochem Parasitol 2008;160:8–21.

[6] Ravindran B, Satapathy AK, Sahoo PK, Mohanty MC. Protective immunity in human lymphatic filariasis: problems and prospects. Med Microbiol Immunol 2003;192:41–6.

[7] Ash LR, Riley JM. Development of *Brugia pahangi* in the jird, *Meriones unguiculatus*, with notes on infections in other rodents. J Parasitol 1970;56:962–8.

[8] Kositanont U, Saetun P, Krittanai C, Doungchawee G, Tribuddharat C, Thongboonkerd V. Application of immunoproteomics to leptospirosis: towards clinical diagnostics and vaccine discovery. Proteomics Clin Appl 2007;1:400–9.

[9] Curwen RS, Ashton PD, Johnston DA, Wilson RA. The *Schistosoma mansoni* soluble proteome: a comparison across four life-cycle stages. Mol Biochem Parasitol 2004;138:57–66.

[10] Moreno Y, Geary TG. Stage- and gender-specific proteomic analysis of *Brugia malayi* excretory–secretory products. PLoS Negl Trop Dis 2008;2:e326.

[11] Bennuru S, Semnani R, Meng Z, Ribeiro JM, Veenstra TD, Nutman TB. *Brugia malayi* excreted/secreted proteins at the host/parasite interface: stage- and gender-specific proteomic profiling. PLoS Negl Trop Dis 2009;3:e410.

[12] Weinkopff T, Atwood III JA, Punkosdy GA, Moss D, Weatherly DB, Orlando R, et al. Identification of antigenic *Brugia* adult worm proteins by peptide mass fingerprinting. J Parasitol 2009;95:1429–35.

[13] Sritharan M, Piessens WF. Actin of *Brugia malayi* microfilariae contains a developmentally regulated antigenic epitope. Mol Biochem Parasitol 1997;90:327–30.

[14] Pancholi V. Multifunctional alpha-enolase: its role in diseases. Cell Mol Life Sci 2001;58:902–20.

[15] Grembecka J, Kafarski P. Leucine aminopeptidase as a target for inhibitor design. Mini Rev Med Chem 2001;1:133–44.

[16] Klion AD, Donelson JE. OvGalBP, a filarial antigen with homology to vertebrate galactoside-binding proteins. Mol Biochem Parasitol 1994;65:305–15.

[17] MacKinnon AC, Farnworth SL, Hodkinson PS, Henderson NC, Atkinson KM, Leffler H, et al. Regulation of alternative macrophage activation by galectin-3. J Immunol 2008;180: 2650–8.

[18] Sanford GL, Harris-Hooker S. Stimulation of vascular cell proliferation by beta-galactoside specific lectins. FASEB J 1990;4:2912–8.

[19] Nutman TB, Kumaraswami V. Regulation of the immune response in lymphatic filariasis: perspectives on acute and chronic infection with *Wuchereria bancrofti* in South India. Parasite Immunol 2001;23:389–99.

[20] Hoerauf A, Satoguina J, Saeftel M, Specht S. Immunomodulation by filarial nematodes. Parasite Immunol 2005;27:417–29.

[21] van de Winkel JG, Capel PJ. Human IgG Fc receptor heterogeneity: molecular aspects and clinical implications. Immunol Today 1993;14:215–21.

Author's personal copy

Microbial Pathogenesis 51 (2011) 225–229

Contents lists available at ScienceDirect

Microbial Pathogenesis

journal homepage: www.elsevier.com/locate/micpath

Short Communication

Subcellular localizations and time-course expression of dengue envelope and non-structural 1 proteins in human endothelial cells

Jesdaporn Poungsawai [a,b], Rattiyaporn Kanlaya [a], Sa-nga Pattanakitsakul [c], Visith Thongboonkerd [a,d,*]

[a] Medical Proteomics Unit, Office for Research and Development, Faculty of Medicine Siriraj Hospital, Mahidol University, Bangkok, Thailand
[b] Department of Immunology and Immunology Graduate Program, Faculty of Medicine Siriraj Hospital, Mahidol University, Bangkok, Thailand
[c] Medical Molecular Biology Unit, Office for Research and Development, Faculty of Medicine Siriraj Hospital, Mahidol University, Bangkok, Thailand
[d] Center for Research in Complex Systems Science, Mahidol University, Bangkok, Thailand

ARTICLE INFO

Article history:
Received 22 July 2010
Received in revised form
23 April 2011
Accepted 29 April 2011
Available online 7 May 2011

Keywords:
Dengue
Endothelial cells
Envelope
NS1
Subcellular localization
Viral proteins

ABSTRACT

We performed subcellular fractionation of human endothelial cells (EA.hy926) after a challenge with dengue virus serotype-2 (DEN-2) at multiplicity of infection (MOI) of 10 for 2 h. The cells were fractionated into four fractions including cytosol, membrane/organelle, nucleus and cytoskeleton, and their purity was nicely confirmed by immunofluorescence staining of markers for individual subcellular compartments. Western blot analysis of dengue envelope (E) and non-structural 1 (NS1) proteins showed that E was present only in membrane/organelle fraction, whereas NS1 was present in membrane/organelle, nucleus, and cytoskeleton fractions. Time-course study showed that E was present immediately after the challenge, whereas NS1 was present after 12 h of the challenge. Our data may provide a new roadmap for studying mechanisms of replication of dengue virus and its interactions with host cells.

© 2011 Elsevier Ltd. All rights reserved.

1. Introduction

Dengue virus infection remains an important public health problem worldwide, particularly in tropical and sub-tropical areas [1]. The severe forms of dengue virus infection include dengue hemorrhagic fever (DHF) and dengue shock syndrome (DSS), of which pathogenic mechanisms are still unclear. Like other flaviviruses, dengue virus enters into target cells through receptor-mediated endocytosis using glycosylated envelope (E) protein as a binding ligand to particular receptor(s) [2,3]. After endocytosis, low pH milieu of the endosome triggers E protein to undergo conformational change, exposing a hydrophobic fusion peptide that initiates fusion of virus-host membrane lipid bilayers [4]. The fusion step is crucial for releasing the viral genome to allow successful viral replication in the cytoplasm. Since the genome of dengue virus is a positive-sense RNA strand, the single open reading frame of genome can be translated into single polyprotein, which subsequently undergoes post-translational modification(s) by viral and host proteases. This important step generates three structural proteins including capsid, pre-membrane and E proteins, and seven non-structural (NS) proteins including NS1, NS2A, NS2B, NS3, NS4A, NS4B and NS5. These NS proteins are involved in viral replication, protease activity and RNA polymerase activity. Most of these NS proteins are not packed into viral particles but play important role in viral replication [5].

Generally, RNA viruses do not require any association with the nucleus to induce their replication process. Nevertheless, several lines of evidence have demonstrated the interaction of some RNA viruses with the nuclei of host cells to facilitate viral replication [6,7]. Picornaviruses are the good examples for this association. Through the virus–nucleus interaction, the RNA viruses relocate some nuclear factors regulating transcription of host cell defenses to escape from immunity as well as recruit them to benefit their replication inside the cytoplasm [7]. Some viral proteins, particularly viral proteases, target to the nucleus with their precursor forms containing nuclear localization signal (NLS) to interfere the

Abbreviations: BSA, bovine serum albumin; DEN-2, dengue virus serotype-2; E, envelope protein; ER, endoplasmic reticulum; FBS, fetal bovine serum; hnRNP C1/C2, heterogeneous nuclear ribonucleoprotein C1/C2; MOI, multiplicity of infection; NS1, non-structural 1 protein; RT, room temperature.

* Corresponding author. Medical Proteomics Unit, Director of Center for Research in Complex Systems Science (CRCSS), Siriraj Hospital, Mahidol University, 12th Floor Adulyadej Vikrom Building, 2 Prannok Road, Bangkoknoi, Bangkok 10700, Thailand. Tel./fax: +66 2 4184793.
E-mail addresses: thongboonkerd@dr.com, vthongbo@yahoo.com (V. Thongboonkerd).

0882-4010/$ – see front matter © 2011 Elsevier Ltd. All rights reserved.
doi:10.1016/j.micpath.2011.04.011

Author's personal copy

host transcription process by degrading the cellular transcription machinery [7]. In the case of flaviviruses, active RNA-dependent viral polymerases, including NS3 and NS5, have been found within the nuclei of the cells infected with West Nile virus, Japanese encephalitis virus, and dengue virus [8]. These findings suggest that host cell nucleus also serves as an additional site for active flaviviral replication [8].

Even with the aforementioned information, molecular mechanisms underlying dengue virus replication in the target host cells remain unclear. To better understand such mechanisms, the information of subcellular localizations and time-course expression of viral proteins in infected cells, which are the major targets for dengue virus infection, is crucial. However, such information was under-investigated in previous studies. Therefore, the present study was conducted to obtain such information using subcellular fractionation (based on stepwise extraction by various lysis buffers), Western blot analysis, and immunofluorescence staining.

2. Results & discussion

After 24-h of the challenge with DEN-2 at MOI of 10 for 2 h, the condition of which infectivity was approximately 90% without significant increase of cell death as described in our previous study [9], the cell monolayer was subjected to subcellular fractionation using ProteoExtract Subcellular Proteome Extraction Kit (Mini sPEK). Basically, this kit fractionated subcellular compartments by stepwise extraction using different extraction buffers, of which potency/capacity to solubilize proteins differed (Fig. 1A). Compositions of individual buffers used for differential extraction are provided as Supporting Information. Using this kit, the DEN-2-infected cells were successfully fractionated into four fractions, including cytosol (F1), membrane/organelle (F2), nucleus (F3) and cytoskeleton (F4).

The purity of all these fractions was examined by immunofluorescence staining of markers for individual subcellular

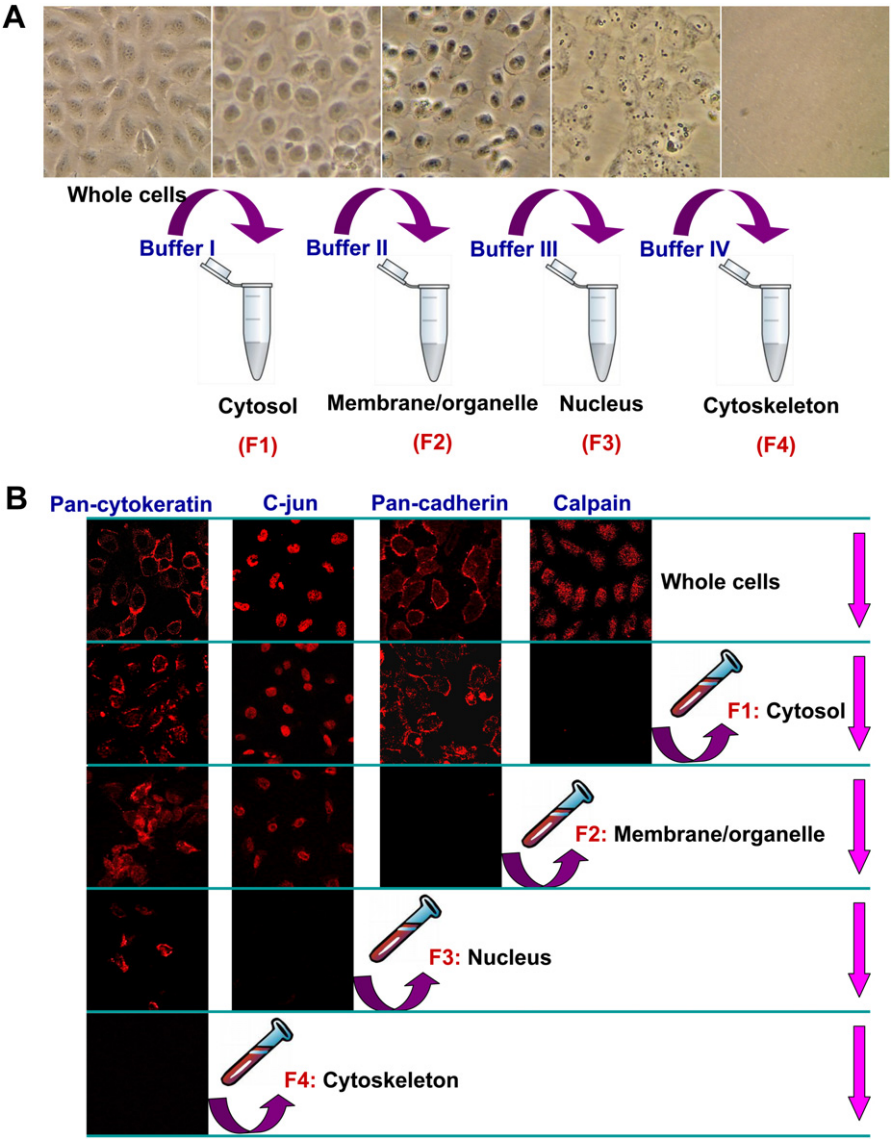


Fig. 1. Subcellular fractionation and its purity. Panel (A) shows schematic summary of basic methods used for subcellular fractionation, based on stepwise extraction by differential buffers of which potency to solubilize proteins differed. Panel (B) demonstrates the purity of subcellular fractionation. Top panels show immunofluorescence staining patterns of markers for cytosol (calpain), membrane/organelle (pan-cadherin), nucleus (c-jun), and cytoskeleton (pan-cytokeratin). After collecting each subcellular fraction, the corresponding marker was absent, whereas the markers for other remaining fractions were still present. Original magnification power was 630X for all panels.

Author's personal copy

compartments. Fig. 1B shows that our fractionation steps yielded highly purified subcellular fractions. Western blot analysis revealed that E protein was present only in membrane/organelle fraction (Fig. 2A), whereas NS1 protein was present in membrane/organelle, nucleus, and cytoskeleton fractions (most prominent in membrane/organelle fraction) (Fig. 2B).

Our results suggested that these dengue proteins may be associated with intracellular organelles, which were used as the cargo for protein translation and/or viral replication. Indeed, this is not surprising as translation and replication of positive-strand viruses, especially dengue virus, have been thought to localize in intracellular membrane structures or endoplasmic reticulum (ER)-associated membranes [10]. E protein is a part of (endosomal) membrane that binds with pre-membrane protein to form a heterodimer for viral assembly during maturation. Therefore, it is reasonable that E protein was identified in the membrane/organelle fraction (Fig. 2A).

NS1 protein has been identified as many different forms; i.e., ER-associated replication complex, membrane-anchored form, and secreted form [11–13]. Our present study identified NS1 at approximately 80 kDa, which was most likely its dimer form. Indeed, newly synthesized NS1 is transiently expressed as a monomer but rapidly forms a homodimer in the ER [14]. The homodimeric NS1 becomes partially hydrophobic and is associated with cellular membranes [12]. Our data showed that NS1 was present predominately in the membrane/organelle fraction, consistent with the findings on characteristics and functional roles of NS1 reported in many previous studies. However, it is surprising to find NS1 in the nucleus and cytoskeleton fractions. This novel finding could be explained by the findings reported in a previous study demonstrating that NS1 interacts with heterogeneous nuclear ribonucleoprotein isoform C1/C2 (hnRNP C1/C2) [15]. Moreover, our recent study clearly demonstrated that NS1 also interacts with vimentin, a cytoskeletal protein that plays significant role in dengue virus replication [16].

We then performed serial analysis of double-immunofluorescence staining of dengue protein (E or NS1) and host pan-cadherin protein (a marker for membrane/organelle) to demonstrate time-course expression of dengue E and NS1 proteins, and to confirm their localization in membrane/organelle compartment. Dengue E protein was observed as early as 0 h after the challenge with DEN-2 (at MOI of 10 for 2 h) (Fig. 3A), whereas NS1 was detectable after 12 h of DEN-2 challenge (Fig. 3B). The intensity of staining was progressively increased when the post-challenge incubation time was prolonged, indicating viral replication. The earlier detection of dengue E protein might be due to its earlier translation based on its locus in the genome or the differential sensitivity of antibody used. We also observed co-localization of both dengue proteins with pan-cadherin (Fig. 3C and D), consistent with the data presented in Fig. 2 demonstrating that E and NS1 were localized predominately in membrane/organelle fraction. Indeed, Fig. 3C and D were derived from 24-h post-challenge time-point, which was the identical condition used in Western blot analysis shown in Fig. 2. However, the co-localization of dengue proteins and pan-cadherin was better illustrated at earlier time-points, which provided a clearer membrane and granular pattern of pan-cadherin, whereas this pattern was flared by overwhelming abundance levels of E and NS1 at 24-h time-point. Interestingly, we did not observe intra-nuclear expression of NS1 protein by immunofluorescence staining, whereas Western blot data clearly demonstrates the expression of NS1 in the nucleus fraction. Whereas there was no doubt on the purity of our subcellular fractionation steps (see Fig. 1B), this contradictory results could be explained that NS1 protein is also expressed at perinuclear, but not intra-nuclear, region to interact with hnRNP C1/C2, which can be shuttled between nucleus and other cellular compartments [17,18].

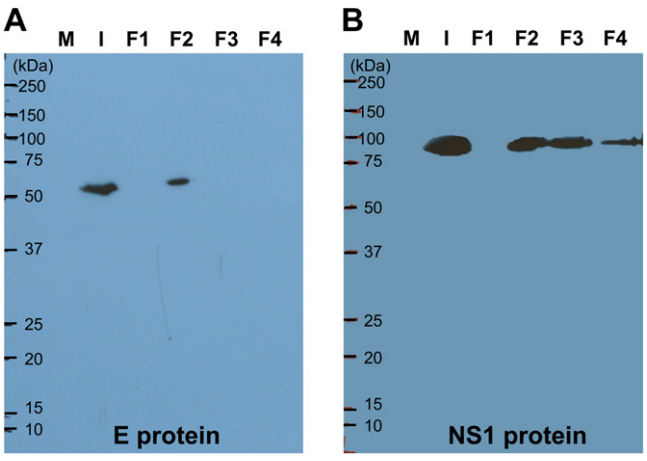


Fig. 2. Western blot analysis of DEN-2 envelope (E) and non-structural 1 (NS1) proteins (panels (A) and (B), respectively). DEN-2-infected EA.hy926 cells (at 24-h after the challenge with DEN-2 at MOI of 10 for 2 h) were fractionated into 4 subcellular fractions, including cytosol (F1), membrane/organelle (F2), nucleus (F3) and cytoskeleton (F4). M and I denote whole cell lysates of mock-control and DEN-2-infected cells, respectively, and served as negative and positive controls, respectively.

In summary, we report herein for the first time subcellular localizations and time-course expression of dengue E and NS1 proteins in human endothelial cells. Our data also demonstrate the strength of fractionation method, which provided highly purified subcellular compartments, and thus is the useful technique for studying mechanisms of viral replication and related intracellular processes. Our data may also offer opportunities to further explore interactions between dengue virus and host cellular proteins, which are involved in viral replication, maturation and assembly.

3. Materials & methods

3.1. Cell cultivation and dengue virus infection

Human endothelial cells (EA.hy926) were cultured in Dulbecco's minimum essential medium/F-12 (DMEM/F-12) (GIBCO; Grand Island, NY) supplemented with 10% heat-inactivated fetal bovine serum (FBS) (GIBCO), 100 U/ml penicillin G and 100 mg/ml streptomycin (SIGMA; St. Louis, MO). The cells were then challenged with dengue virus serotype-2 (DEN-2) (strain 16681) at the multiplicity of infection (MOI) of 10 for 2 h at 37 °C.

3.2. Subcellular fractionation

After 24-h of the challenge with DEN-2, the cell monolayer was subjected to subcellular fractionation using ProteoExtract Subcellular Proteome Extraction Kit (Mini sPEK) (Calbiochem, EMD Biosciences; Darmstadt, Germany) according to the manufacturer's instruction. Buffer I (pH 6.8) contained 10 mM PIPES, 0.02% digitonin, 300 mM sucrose, 15 mM NaCl, and 0.5 mM EDTA; Buffer II (pH 7.4) contained 10 mM PIPES, 0.5% triton X-100, 300 mM sucrose, 15 mM NaCl, and 0.5 mM EDTA; Buffer III (pH 7.4) contained 10 mM PIPES, 1.0% tween-40, 0.5% deoxycholate, 350 mM NaCl, and 500 U/ml benzonase; and Buffer IV (pH 7.4) contained 5% SDS, 10 mM Na_2HPO_4, and 10 mM H_2PO_4.

3.3. Immunofluorescence staining of markers for individual subcellular compartments

The purity of all subcellular fractions was examined by immunofluorescence staining of markers for individual subcellular

Author's personal copy

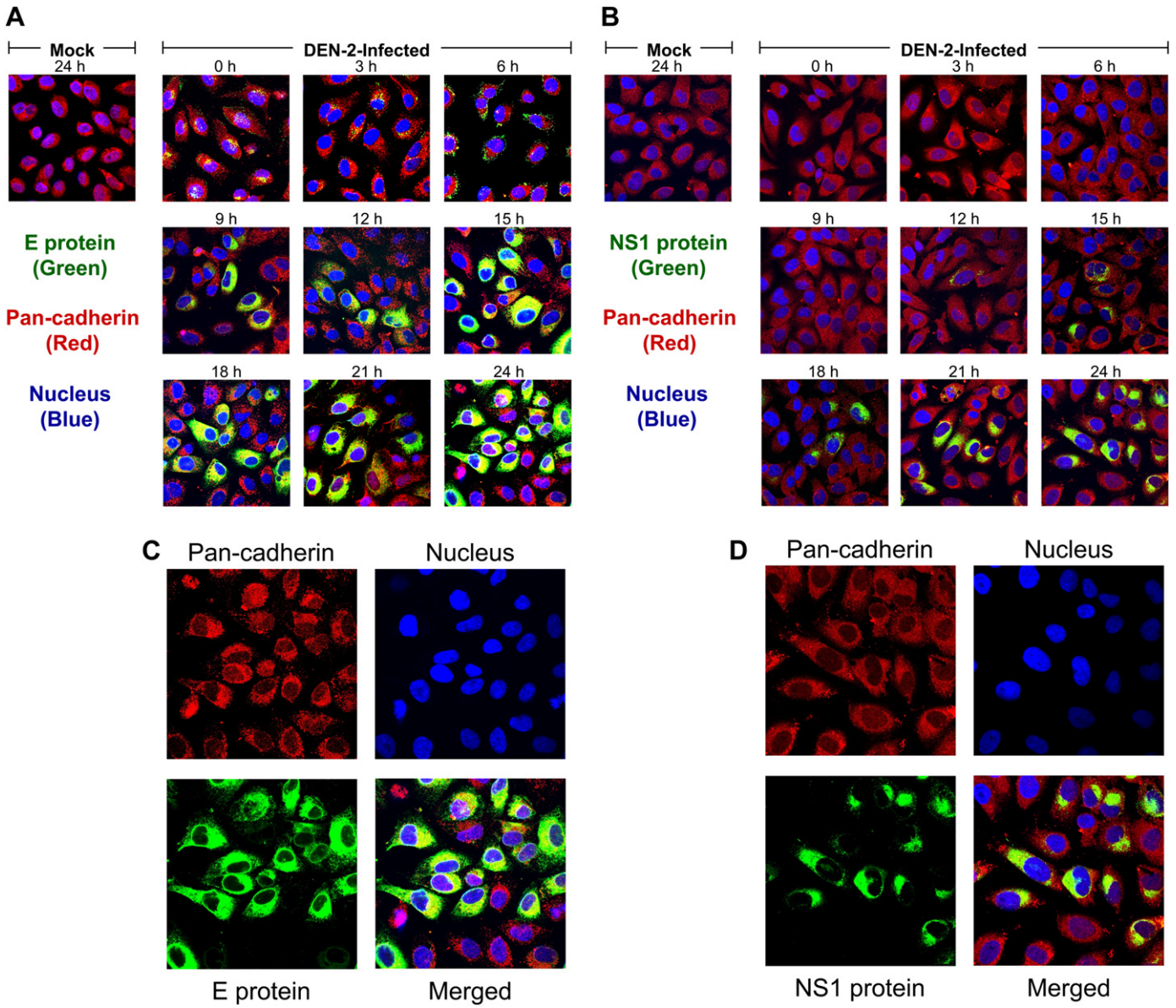


Fig. 3. Time-course double-immunofluorescence staining of dengue proteins (in green) and host pan-cadherin (in red), which is a marker for membrane/organelle. The nucleus was stained by Hoechst dye and is illustrated in blue. Expression of E and NS1 proteins was monitored for up to 24 h after the challenge with DEN-2 (at MOI 10 for 2 h) (panels (A) and (B), respectively). Co-localization of dengue proteins and pan-cadherin is illustrated as yellow. Panels (C) and (D) highlight the co-localization of pan-cadherin with E and NS1 proteins, respectively, at 24-h post-infection (the condition of which was used for Western blot analysis) to confirm the Western blot data presented in Fig. 2. Images were taken by a laser-scanning confocal microscope equipped with LSM5 Image Browser (LSM 510 Meta, Carl Zeiss; Jena, Germany). Original magnification power was 630X for all panels. (For interpretation of the references to colour in this figure legend, the reader is referred to the web version of this article.)

compartments. Briefly, the cells or their remaining compartments of cells were washed with PBS, fixed with 3.7% formaldehyde in PBS for 10 min, permeabilized by 1% triton X-100 in PBS for 10 min, followed by blocking with 1% bovine serum albumin (BSA) in PBS at room temperature (RT) for 1 h. After washing with PBS three times, they were initially incubated at 4 °C overnight with one of the following primary antibodies: rabbit polyclonal anti-calpain (marker for cytosol), mouse monoclonal anti-pan-cadherin (marker for membrane/organelle), mouse monoclonal anti-c-jun (marker for nucleus), and mouse monoclonal anti-pan-cytokeratin (marker for cytoskeleton) (all were purchased from Santa Cruz Biotechnology; Santa Cruz, CA; and all were diluted 1:200 in PBS). After washing with PBS, the cells or their remaining compartments were further incubated with donkey anti-rabbit or goat anti-mouse IgG conjugated with Cy3 (both were purchased from Jackson Immunoresearch Laboratories, Inc.; West Grove, PA, and were diluted 1:10000 in PBS) at RT for 1 h. Images were taken by using a laser-scanning confocal microscope equipped with LSM5 Image Browser (LSM 510 Meta, Carl Zeiss; Jena, Germany).

3.4. Western blot analysis of dengue E and NS1 proteins in individual subcellular fractions

Proteins solubilized in these four fractions were precipitated with ProteoExtract Protein Precipitation Kit (Calbiochem, EMD Biosciences) for concentrating proteins and removal of interfering substances. Protein concentrations were determined by Bio-Rad protein assay (Bio-Rad Laboratories; Hercules, CA) based on Bradford's method [19]. Whole cell lysates derived from mock-control and DEN-2-infected EA.hy926 cells served as negative and

Author's personal copy

positive controls, respectively. Totally 20 μg equally loaded proteins derived from individual subcellular fractions (finally in a buffer containing 50 mM Tris–HCl pH 6.8, 2% SDS, 10% glycerol, and bromophenol blue; without dithiothreitol and mercaptoethanol) were resolved by unheated non-reducing SDS-PAGE (12% acrylamide). The resolved proteins were then transferred onto a nitrocellulose membrane and reacted with mouse monoclonal antibody against dengue E (clone 3H5) or NS1 (clone DN1) (Abcam; Cambridge, UK) (1:200 in 5% skim milk/PBS) at 4 °C overnight, and then with rabbit anti-mouse IgG conjugated with horseradish peroxidase (Santa Cruz Biotechnology; Santa Cruz, CA) (1:1000 in 5% skim milk/PBS) at RT for 1 h. Protein bands were visualized by SuperSignal West Pico chemiluminescence substrate (Pierce Biotechnology, Inc., Rockford, IL) and autoradiograph.

3.5. Time-course study of expression of dengue E and NS1 proteins, and their localization in membrane/organelle compartment

After the challenge with DEN-2 (at the MOI of 10 for 2 h), their expression was monitored for further 0–24 h. Mock EA.hy926 cells cultured in parallel to DEN-2-infected cells (but without DEN-2 infection) served as the negative control. The cell monolayers were washed with PBS, fixed with 3.7% formaldehyde in PBS for 10 min, permeabilized by 1% triton X-100 in PBS for 10 min, followed by blocking with 1% BSA/PBS at RT for 1 h. After washing with PBS three times, they were initially incubated at 4 °C overnight with goat polyclonal anti-pan-cadherin (Santa Cruz Biotechnology) (1:200 in PBS) together with mouse monoclonal antibody against dengue E protein (clone 3H5) or mouse monoclonal anti-NS1 (clone DN1) (Abcam) (1:50 in PBS). Thereafter, all the samples were washed and further incubated at RT for 1 h with donkey anti-goat IgG conjugated with phycoerythrin (Santa Cruz Biotechnology) (1:400 in PBS) together with goat anti-mouse IgG conjugated with Alexa 488 (Invitrogen-Molecular Probes; Eugene, OR) (1:2500 in PBS) and Hoechst dye (Invitrogen-Molecular Probes) (1:1000 in PBS for nuclear stain). Images were then captured using a laser-scanning confocal microscope equipped with LSM5 Image Browser (LSM 510 Meta, Carl Zeiss).

Acknowledgements

We are grateful to Dr. Chunya Puttikhunt for providing cultured supernatant collected from hybridoma clone. This work was supported by the National Center for Genetic Engineering and Biotechnology (BIOTEC) (to SP and VT), Office of the Higher Education Commission and Mahidol University under the National Research Universities Initiative (to VT), and The Thailand Research Fund (RTA5380005) (to VT). JP was supported by Siriraj Graduate Thesis Scholarship, whereas both SC and VT are also supported by "Chalermphrakiat" Grant, Faculty of Medicine Siriraj Hospital.

Appendix. Supplementary material

Supplementary data related to this article can be found online at doi:10.1016/j.micpath.2011.04.011.

References

[1] Halstead SB. Dengue. Lancet 2007;370:1644–52.
[2] Mukhopadhyay S, Kuhn RJ, Rossmann MG. A structural perspective of the flavivirus life cycle. Nat Rev Microbiol 2005;3:13–22.
[3] Anderson R, King AD, Innis BL. Correlation of E protein binding with cell susceptibility to dengue 4 virus infection. J Gen Virol 1992;73(Pt 8):2155–9.
[4] Bressanelli S, Stiasny K, Allison SL, Stura EA, Duquerroy S, Lescar J, et al. Structure of a flavivirus envelope glycoprotein in its low-pH-induced membrane fusion conformation. EMBO J 2004;23:728–38.
[5] Perera R, Kuhn RJ. Structural proteomics of dengue virus. Curr Opin Microbiol 2008;11:369–77.
[6] Hiscox JA. The interaction of animal cytoplasmic RNA viruses with the nucleus to facilitate replication. Virus Res 2003;95:13–22.
[7] Weidman MK, Sharma R, Raychaudhuri S, Kundu P, Tsai W, Dasgupta A. The interaction of cytoplasmic RNA viruses with the nucleus. Virus Res 2003;95:75–85.
[8] Uchil PD, Kumar AV, Satchidanandam V. Nuclear localization of flavivirus RNA synthesis in infected cells. J Virol 2006;80:5451–64.
[9] Kanlaya R, Pattanakitsakul SN, Sinchaikul S, Chen ST, Thongboonkerd V. Alterations in actin cytoskeletal assembly and junctional protein complexes in human endothelial cells induced by dengue virus infection and mimicry of leukocyte transendothelial migration. J Proteome Res 2009;8:2551–62.
[10] Salonen A, Ahola T, Kaariainen L. Viral RNA replication in association with cellular membranes. Curr Top Microbiol Immunol 2005;285:139–73.
[11] Lindenbach BD, Rice CM. Molecular biology of flaviviruses. Adv Virus Res 2003;59:23–61.
[12] Winkler G, Maxwell SE, Ruemmler C, Stollar V. Newly synthesized dengue-2 virus nonstructural protein NS1 is a soluble protein but becomes partially hydrophobic and membrane-associated after dimerization. Virology 1989;171:302–5.
[13] Winkler G, Randolph VB, Cleaves GR, Ryan TE, Stollar V. Evidence that the mature form of the flavivirus nonstructural protein NS1 is a dimer. Virology 1988;162:187–96.
[14] Falgout B, Markoff L. Evidence that flavivirus NS1-NS2A cleavage is mediated by a membrane-bound host protease in the endoplasmic reticulum. J Virol 1995;69:7232–43.
[15] Noisakran S, Sengsai S, Thongboonkerd V, Kanlaya R, Sinchaikul S, Chen ST, et al. Identification of human hnRNP C1/C2 as a dengue virus NS1-interacting protein. Biochem Biophys Res Commun 2008;372:67–72.
[16] Kanlaya R, Pattanakitsakul SN, Sinchaikul S, Chen ST, Thongboonkerd V. Vimentin interacts with heterogeneous nuclear ribonucleoproteins and dengue nonstructural protein 1 and is important for viral replication and release. Mol Biosyst 2010;6:795–806.
[17] Kim JH, Hahm B, Kim YK, Choi M, Jang SK. Protein-protein interaction among hnRNPs shuttling between nucleus and cytoplasm. J Mol Biol 2000;298:395–405.
[18] Pinol-Roma S, Dreyfuss G. Shuttling of pre-mRNA binding proteins between nucleus and cytoplasm. Nature 1992;355:730–2.
[19] Bradford MM. A rapid and sensitive method for the quantitation of microgram quantities of protein utilizing the principle of protein-dye binding. Anal Biochem 1976;72:248–54.

Molecular BioSystems

Dynamic Article Links

Cite this: *Mol. BioSyst.*, 2011, **7**, 1917–1925

www.rsc.org/molecularbiosystems

PAPER

Calcium oxalate dihydrate crystal induced changes in glycoproteome of distal renal tubular epithelial cells†

Wararat Chiangjong,[a] Supachok Sinchaikul,[b] Shui-Tein Chen[bc] and Visith Thongboonkerd*[ad]

Received 8th February 2011, Accepted 23rd March 2011
DOI: 10.1039/c1mb05052d

Calcium oxalate dihydrate (COD) crystals can adhere onto the apical surface of renal tubular epithelial cells. This process is associated with crystal growth and aggregation, resulting in kidney stone formation. Glycoproteins have been thought to play roles in response to crystal adhesion. However, components of the glycoproteome that are involved in this cellular response remain largely unknown. Our present study therefore aimed to identify altered glycoproteins upon COD crystal adhesion onto tubular epithelial cells representing distal nephron, the initiating site of kidney stone formation. Madin-Darby Canine Kidney (MDCK) cells were maintained in culture medium with or without COD crystals for 48 h (n = 5 flasks per group). Cellular proteins were extracted, resolved by 2-DE and visualized by SYPRO Ruby total protein stain, whereas glycoproteins were detected by Pro-Q Emerald glycoprotein dye. Spot matching and quantitative intensity analysis revealed 16 differentially expressed glycoprotein spots, whose corresponding total protein levels were not changed by COD crystal adhesion. These altered glycoproteins were successfully identified by Q-TOF MS and/or MS/MS analyses, and potential glycosylation sites were identified by the GlycoMod tool. For example, glycoforms of three proteasome subunits (which have a major role in regulating cell–cell dissociation) were up-regulated, whereas a glycoform of actin-related protein 3 (ARP3) (which plays an important role in cellular integrity) was down-regulated. These coordinated changes implicate that COD crystal adhesion induced cell dissociation and declined cellular integrity in the distal nephron. Our findings provide some novel insights into the pathogenic mechanisms of kidney stone disease at the molecular level, particularly cell–crystal interactions.

Introduction

Kidney stones are mostly composed of calcium oxalate (CaOx) and are frequently associated with underlying metabolic disorders; *e.g.* hypercalciuria, hyperoxaluria and hypocitraturia.[1] CaOx stone formation generally begins with nucleation, growth and aggregation of CaOx crystals. In addition to these pathogenic mechanisms, the other critical step is adhesion of CaOx crystals onto renal tubular epithelial cells.[2] In human urine, CaOx crystals are predominately in dihydrate form (COD), which can nucleate and adhere directly onto the apical surface of living renal tubular epithelial cells *via* the (100) face under appropriate conditions (*i.e.* decreased levels of inhibitors or, on the other hand, increased levels of promoters).[3,4] The plasma membrane will promote their adhesion due to the nature of crystal-binding sites on the apical surface of the cells.[5,6] The data obtained from previous studies indicate that COD-containing stone is commonly found in patients with high urinary calcium excretion.[7,8]

Although COD crystals are frequently found in human urine and involved in kidney stone formation, a number of macromolecules; *i.e.* urinary glycoproteins (including Tamm–Horsfall protein, bikunin, nephrocalcin, and urinary prothrombin fragment I) can counterbalance the formation of kidney stone by their properties to inhibit crystal growth, aggregation and/or adhesion to renal tubular epithelial cells.[1,9] Deficiency of these inhibitory glycoproteins in the urine has been proposed to enhance the stone formation.

At the apical surface of renal tubular epithelial cells, glycoproteins may aggravate crystal adhesion onto the plasma membrane. However, components of such surface

[a] *Medical Proteomics Unit, Office for Research and Development, Faculty of Medicine Siriraj Hospital, Mahidol University, 12th Fl. Adulyadej Vikrom Bldg., 2 Prannok Rd., Bangkoknoi, Bangkok 10700, Thailand. E-mail: thongboonkerd@dr.com, vthongbo@yahoo.com; Fax: +66-2-4184793; Tel: +66-2-4184793*
[b] *Institute of Biological Chemistry and Genomic Research Center, Academia Sinica, Taipei, Taiwan*
[c] *Institute of Biochemical Sciences, College of Life Science, National Taiwan University, Taipei, Taiwan*
[d] *Center for Research in Complex Systems Science, Mahidol University, Bangkok, Thailand*

† Electronic supplementary information (ESI) available. See DOI: 10.1039/c1mb05052d

glycoproteins are under investigation. Inside renal tubular epithelial cells, glycoproteins play diverse biological functions; *e.g.* cell–cell communications, cellular response and activation, *etc*. However, their role in crystal modulation and processing remains largely unknown. We therefore conducted the present study to explore altered cellular glycoproteome in renal tubular cells derived from distal nephron, the initiating site of kidney stone formation.

Results and discussion

Exposure to 100 μg mL^{-1} COD crystals for 48 h caused adhesion of COD crystals onto MDCK cells, whereas cell death (apoptosis and necrosis) was not changed significantly (these data have been reported in our previous study).[10] Therefore, this treatment condition was suitable for the investigation of early response in MDCK cells during COD crystal adhesion. In the present study, we visualized glycoprotein spots resolved in 2-D gels using a fluorescent hydrazide Pro-Q Emerald 300 dye (Invitrogen—Molecular Probes). In principle, glycols in glycoproteins are oxidized to aldehydes using periodic acid, followed by conjugation with the fluorescent dye, which reacts with aldehyde groups.[11] The efficiency and specificity of Pro-Q Emerald 300 glycoprotein dye for staining carbohydrate residues are satisfactory and have been well addressed in several previous studies.[11] SYPRO Ruby (Invitrogen—Molecular Probes), a bathophenanthroline complex of ruthenium(II) that can interact with cationic amino acid residues on proteins,[12] was used for detection of total proteins within the same gel following the staining by Pro-Q Emerald 300 dye. The total protein staining by SYPRO Ruby on-top of glycoprotein staining by Pro-Q Emerald 300 had no interference because they were detectable by different excitation wavelengths (532 nm for SYPRO Ruby, but 300 nm for Pro-Q Emerald 300). This allowed precise matching of glycoprotein spots to their corresponding total protein spots. With an equal amount (200 μg) of total proteins equally loaded into each gel, 235 ± 22 glycoprotein spots were detected by Pro-Q Emerald 300 dye, whereas 850 ± 19 total protein spots were detected by staining with SYPRO Ruby dye. This result indicated that the high proportion of total proteins were glycosylated, consistent with the data reported previously.[13]

After spot matching using a 2-D gel image analysis software (Image Master 2D Platinum), quantitative intensity analysis revealed significantly altered levels of 16 glycoprotein spots (8 were increased in COD-treated cells, 5 were decreased in COD-treated cells, 2 were present only in COD-treated cells, and 1 was absent after COD adhesion), whose corresponding total protein levels did not change significantly (Fig. 1). These altered glycoproteins were then identified by Q-TOF MS and/or MS/MS analyses. Their identities, quantities and related data are summarized in Table 1, whereas their respective protein levels determined by SYPRO Ruby are shown in Table S1 (ESI†). While our previous study reported changes in levels of some proteins,[10] the present study demonstrated changes in glycosylation status or altered levels of glycoforms of identified proteins, not their total protein levels. As the goal and design of these two studies differed (particularly, changes in total protein levels were excluded from the present study), there were no common changes found in these two studies.

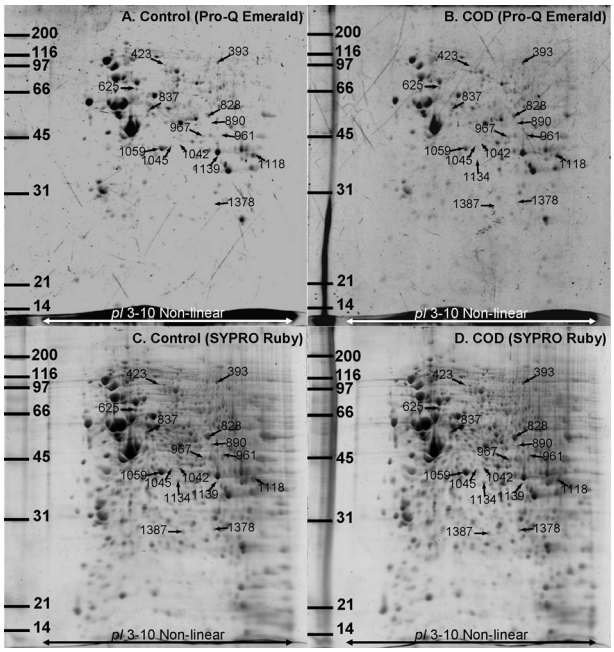


Fig. 1 2-D map of altered glycoproteome in MDCK cells in response to COD crystal adhesion. Proteins derived from whole cell lysate of MDCK cells cultured in the absence (A and C) or presence (B and D) of COD crystals were resolved by 2-DE (non-linear pH gradient of 3–10). The resolved glycoprotein spots were visualized with Pro-Q Emerald 300 glycoprotein stain (A and B). Thereafter, the glycoproteins-stained gels were stained with SYPRO Ruby total protein dye to visualize total protein spots (C and D) (n = 5 gels derived from individual cultured flasks for each set; 200 μg equally loaded into each gel). Significantly differed glycoprotein spots, whose corresponding total protein spots had no significant changes (labeled with numbers in this map), were identified by Q-TOF MS and/or MS/MS analyses (Table 1).

The altered glycoproteins in MDCK tubular cells in response to COD crystal adhesion identified in the present study were related to or involved in many biological processes as summarized in Table 2. Using the GlycoMod tool, many potential *N*-linked glycosylation sites were identified in the altered glycoproteins (Table 3; see also Table S2, ESI†). Potential roles of these glycoproteins in renal tubular epithelial cells in response to COD crystal adhesion are emphasized as follows.

We found increased levels of glycoforms of three unique proteins (one glycoform was increased, whereas the other two glycoforms were observed only in the COD-treated cells), which belong to the proteasome family and have a major role in regulating cell–cell dissociation during cell movement.[14] We also observed decreased level of a glycoform of actin-related protein 3 (ARP3), which plays an important role in cellular integrity.[15] These data implicate that COD crystal adhesion might induce cell dissociation and decline cellular integrity in renal tubular epithelial cells of the distal nephron.

Interestingly, we identified a macrophage scavenger receptor in MDCK cells and its glycoform was increased in the COD-treated cells. In macrophage, it is a membrane glycoprotein

This journal is © The Royal Society of Chemistry 2011

This journal is © The Royal Society of Chemistry 2011

Table 1 Summary of glycoproteins whose levels of glycoforms, not their total protein levels, were significantly altered in MDCK cells during COD crystal adhesion

Spot no.	Protein name	NCBI[a] ID	Identified by	Identification scores (MS, MS/MS)	%Cov[b] (MS, MS/MS)	No. of matched peptides (MS, MS/MS)	pI	MW/kDa	Intensity by Pro-Q Emerald dye (Mean ± SEM)		Ratio (COD/Control)	*p* values
									Control	COD-treated		
Glycoproteins whose levels of glycoforms were significantly increased in COD-treated MDCK cells												
393	Elongation factor 2 (EF-2)	gi|73987435	MS	80, NA	27, NA	13, NA	6.34	78.58	0.0879 ± 0.0540	0.2731 ± 0.0561	3.11	0.045
423	Cytokeratin type II	gi|73996498	MS/MS	NA, 52	NA, 1	NA, 1	6.33	107.86	0.0704 ± 0.0311	0.1784 ± 0.0266	2.54	0.030
890	Macrophage scavenger receptor type I	gi|293746	MS	73, NA	27, NA	10, NA	6.68	50.18	0.0104 ± 0.0104	0.1495 ± 0.0479	14.32	0.022
961	Translocase of outer mitochondrial membrane 40 homolog isoform 2	gi|73947367	MS, MS/MS	58, 65	23, 5	5, 1	8.24	32.59	0.0132 ± 0.0132	0.2655 ± 0.0568	20.11	0.003
967	PIBF1 protein	gi|116283307	MS	72, NA	31, NA	10, NA	6.03	49.82	0.0399 ± 0.0246	0.1902 ± 0.0560	4.77	0.039
1042	Isocitrate dehydrogenase 3 (NAD+) alpha isoform 2	gi|73951310	MS, MS/MS	142, 143	45, 14	12, 4	5.86	35.09	0.0070 ± 0.0070	0.1547 ± 0.0465	22.06	0.014
1045	Protein phosphatase 1, catalytic subunit, alpha	gi|50978728	MS	98, NA	43, NA	11, NA	5.94	38.13	0.0132 ± 0.0132	0.0925 ± 0.0245	6.99	0.022
1378	Proteasome subunit beta type 3 (proteasome theta chain) (proteasome chain 13) (proteasome component C10-II)	gi|57091113	MS	119, NA	58, NA	12, NA	6.15	23.25	0.0538 ± 0.0330	0.2769 ± 0.0275	5.15	0.001
Glycoproteins whose levels of glycoforms were significantly decreased in COD-treated MDCK cells												
625	Heterogeneous nuclear ribonucleo-protein K	gi|55958547	MS, MS/MS	122, 42	38, 2	12, 1	5.43	42.01	0.3117 ± 0.0601	0.0549 ± 0.0341	0.18	0.006
828	Alpha enolase (2-phospho-D-glycerate hydro-lyase) (non-neural enolase) (NNE) (enolase 1) (phosphopyruvate hydratase) (C-myc promoter-binding protein) (MBP-1) (MPB-1) (plasminogen-binding protein) isoform 1	gi|73956716	MS/MS	NA, 196	NA, 15	NA, 4	6.57	45.47	0.4358 ± 0.0495	0.2689 ± 0.0323	0.62	0.022
837	ARP3 actin-related protein 3 homolog	gi|73984196	MS, MS/MS	105, 99	26, 6	12, 3	6.87	64.27	0.4068 ± 0.1093	0.1321 ± 0.0417	0.32	0.047
1059	Annexin A1 (annexin I) (lipocortin I) (calpactin II) (chromobindin 9) (P35) (phospholipase A2 inhibitory protein)	gi|73946797	MS, MS/MS	146, 238	48, 12	14, 3	5.84	38.89	0.6623 ± 0.0752	0.4305 ± 0.0399	0.65	0.026
1118	Heterogeneous nuclear ribonucleo-protein A2/B1 isoform 2	gi|73976124	MS, MS/MS	170, 146	52, 15	15, 3	8.74	32.52	0.9071 ± 0.0476	0.6283 ± 0.0779	0.69	0.016
Glycoproteins whose glycoforms were present only in COD-treated MDCK cells												
1134	Proteasome (prosome, macropain) 26S subunit, non-ATPase, 14 isoform 2	gi|74004396	MS	76, NA	46, NA	8, NA	6.00	33.48	0.0000 ± 0.0000	0.0733 ± 0.0235	#DIV/0	0.014
1387	Proteasome (prosome, macropain) subunit, beta type, 3 isoform 1	gi|109114737	MS, MS/MS	68, 66	37, 8	7, 1	6.15	22.90	0.0000 ± 0.0000	0.2225 ± 0.0645	#DIV/0	0.009
Glycoproteins whose glycoforms were absent in COD-treated MDCK cells												
1139	Annexin A2	gi|50950177	MS, MS/MS	191, 141	51, 12	15, 3	6.92	38.92	0.3483 ± 0.0970	0.0000 ± 0.0000	0.00	0.007

NA = not applicable; #DIV/0 = divided by zero[a] NCBI = National Center for Biotechnology Information; [b] %Cov = %sequence coverage [(number of the matched residues/total number of residues in the entire sequence) × 100%].

Table 2 Subcellular localization, molecular function and biological process of the identified proteins[a]

Spot no.	Protein name	Subcellular localization	Molecular function	Biological process
Glycoproteins whose levels of glycoforms were significantly increased in COD-treated MDCK cells				
393	Elongation factor 2 (EF-2)	Cytoplasm	Elongation factor	Protein biosynthesis
423	Cytokeratin type II	Intermediate filament	Structural molecule activity	Cytoskeleton organization
890	Macrophage scavenger receptor type I	Membrane; single-pass type II membrane protein	Receptor	Endocytosis
961	Translocase of outer mitochondrial membrane 40 homolog isoform 2	Mitochondrion outer membrane; multi-pass membrane protein	Porin	Ion and protein transport
967	PIBF1 protein	NA	Mediator of progesterone	NA
1042	Isocitrate dehydrogenase 3 (NAD+) alpha isoform 2	Mitochondria	Oxidoreductase	Tricarboxylic acid cycle
1045	Protein phosphatase 1, catalytic subunit, alpha	Cytoplasm	Hydrolase, protein phosphatase	Carbohydrate and glycogen metabolism, cell cycle/division
1378	Proteasome subunit beta type 3 (proteasome theta chain) (proteasome chain 13) (proteasome component C10-II)	Cytoplasm, nucleus	Hydrolase, protease, threonine protease	Anaphase-promoting complex-dependent proteasomal ubiquitin-dependent protein catabolic process/mitotic cell cycle
Glycoproteins whose levels of glycoforms were significantly decreased in COD-treated MDCK cells				
625	Heterogeneous nuclear ribonucleoprotein K	Cytoplasm, nucleus	Ribonucleoprotein	mRNA processing/splicing
828	Alpha enolase (2-phospho-D-glycerate hydro-lyase) (non-neural enolase) (NNE) (enolase 1) (phosphopyruvate hydratase) (C-myc promoter-binding protein) (MBP-1) (MPB-1) (plasminogen-binding protein) isoform 1	Cytoplasm, nucleus, cell membrane	Lyase/repressor	Glycolysis, plasminogen activity, translation, translation regulation
837	ARP3 actin-related protein 3 homolog	Cytoplasm	ATP/actin binding	Regulation of actin filament polymerization
1059	Annexin A1 (annexin I) (lipocortin I) (calpactin II) (chromobindin 9) (P35) (phospholipase A2 inhibitory protein)	Nucleus, cytoplasm, basolateral membrane	Phospholipase A2 inhibitor	Anti-apoptosis, cell motion, inflammatory response, cell surface receptor linked signal transduction, calcium ion binding
1118	Heterogeneous nuclear ribonucleoprotein A2/B1 isoform 2	Cytoplasm, nucleus	Ribonucleoprotein	mRNA processing/splicing
Glycoproteins whose glycoforms were present only in COD-treated MDCK cells				
1384	Proteasome (prosome, macropain) 26S subunit, non-ATPase, 14 isoform 2	Cytoplasm	Hydrolase, protease, threonine protease	Anaphase-promoting complex-dependent proteasomal ubiquitin-dependent protein catabolic process/mitotic cell cycle
1387	Proteasome (prosome, macropain) subunit, beta type, 3 isoform 1	Cytoplasm, nucleus	Hydrolase, protease, threonine protease	Anaphase-promoting complex-dependent proteasomal ubiquitin-dependent protein catabolic process/mitotic cell cycle
Glycoproteins whose glycoforms were absent in COD-treated MDCK cells				
1139	Annexin A2	Extracellular matrix, secreted, basement membrane	Calcium ion binding	Calcium-regulated membrane-binding protein, skeleton system development

[a] Obtained from the UnitProt Protein Knowledgeable Database; NA = not applicable.

with an implicated role in the pathologic deposition of low density lipoproteins (LDL) in arterial wall during atherogenesis.[16] Moreover, Type I subunit of this glycoprotein acts as a receptor to mediate endocytosis of a diverse group of macromolecules, including acetylated LDL. In renal tubular cells, its precise role remains unknown but can be postulated to be associated with COD crystal adhesion and internalization into the adherent cells.[2,17]

In metabolic pathways, we identified increased glycoforms of isocitrate dehydrogenase 3 (NAD+) alpha isoform 2 (IDH3α) and protein phosphatase 1 catalytic subunit alpha (PP1α) in the COD-treated cells. These enzymes are generally involved in catalytic activity especially in glycolysis. IDH3α, as a catalytic enzyme belonging to the IDH family, plays a crucial role in oxidative decarboxylation of isocitrate to generate ATP in the tricarboxylic acid cycle, which is regulated by numerous allosteric regulators.[18,19] In addition, the IDH activity is activated by a calcium ion in the presence of isocitrate and adenine nucleotide.[18] PP1α regulates a variety of cellular processes, including carbohydrate and glycogen metabolism, cell division, and protein synthesis. Furthermore, it is required for dephosphorylation of partitioning-defective (Par)-3, which is localized at the apical junctional complex and is essential for formation of an apical–basal polarity and tight junction.[20,21] We hypothesized that the altered levels of their glycoforms were related to altered metabolisms in renal tubular epithelial cells in response to COD crystal adhesion.

Heterogeneous nuclear ribonucleoproteins (hnRNPs) are the major nucleic acid-binding proteins involving in gene

 This journal is © The Royal Society of Chemistry 2011

expression processes; *i.e.* transcriptional regulation, alternative pre-mRNA splicing and processing. We observed changes in glycoforms of hnRNP K and hnRNP A2/B1 induced by COD crystal adhesion. hnRNP K has multiple functions, including pre-mRNA processing and mRNA export from nucleus, and acts as a versatile DNA–RNA binding

Table 3 Potential *N*-linked glycosylation sites identified by the "GlycoMod" tool (peptides containing the motif "N–X–S/T/C" where X was not P)[a]

Spot No.	Protein name	Residues	Sequence	Number of peptide masses identified	Peptide mass with *N*-linked glycosylation	Number of glycoforms
393	Elongation factor 2 (EF-2)	1–10	MV**N**F**T**VDQIR	2	1221.62	17
					1237.61	13
		1–15	MV**N**F**T**VDQIRAIMDK	3	1779.90	1
					1795.90	4
					1811.89	2
		17–32	ANIR**N**M**S**VIAHVDHGK	2	1760.91	6
					1776.91	4
		21–32	**N**M**S**VIAHVDHGK	2	1306.65	12
					1322.64	9
		21–42	**N**M**S**VIAHVDHGKSTLTDSLV CK	4	—	0
		608–641	GHVFEESQVAGTPMFVVKAY LPV**N**E**S**FGFTADLR	2	—	0
		626–641	AYLPV**N**E**S**FGFTADLR	1	1798.89	3
		626–679	AYLPV**N**E**S**FGFTADLRSNTG GQAFPQCVFDHWQILPGDPF D**N**T**S**RPSQVVAETR	4	—	0
		642–679	SNTGGQAFPQCVFDHWQILP GDPFD**N**T**S**RPSQVVAETR	4	—	0
		642–680	SNTGGQAFPQCVFDHWQILP GDPFD**N**T**S**RPSQVVAETRK	4	—	0
423	Cytokeratin type II	82–144	SGFGGRASGGFGAGSGFGYG GAAGGGYGAWGFPVCPPGGI QEVTV**N**Q**S**LLTPLNLQIDPA IQR	4	—	0
		88–144	ASGGFGAGSGFGYGGAAGGG YGAWGFPVCPPGGIQEVTV**N** **Q**S**LLTPLNLQIDPAIQR	4	—	0
		88–146	ASGGFGAGSGFGYGGAAGGG YGAWGFPVCPPGGIQEVTV**N** **Q**S**LLTPLNLQIDPAIQRVR	4	—	0
		286–324	MLFEAELSQMQTQVSDTSVV LSMDN**N**R**S**LDLDSIIAEVK	4	—	0
		325–335	AQYEDIA**N**R**S**R	1	1321.64	8
		454–486	LLEGEECRLSGEGVSPV**N**I**S** IQ**N**S**S**VSVSQGGK	2	—	0
		462–486	LSGEGVSPV**N**I**S**IQ**N**S**S**VSV SQGGK	1	—	0
		462–499	LSGEGVSPV**N**I**S**IQ**N**S**S**VSV SQGGKSFGGSFGGGFGTR	1	—	0
		521–582	ASSGGAGYGLGLGGMGYRAG GAFGGYGFGGGMMSGSAGIQ EVTV**N**Q**S**LLTPLHLEIDPSL QR	4	—	0
		539–582	AGGAFGGYGFGGGMMSGSAG IQEVTV**N**Q**S**LLTPLHLEIDP SLQR	3	—	0
		539–584	AGGAFGGYGFGGGMMSGSAG IQEVTV**N**Q**S**LLTPLHLEIDP SLQRVR	3	—	0
		761–771	AQYEDIA**N**R**S**R	1	1321.64	8
		890–951	LLEGEECRLTGEGVGPV**N**I**S** VVSSSGGTGYSSGGGSLCMT GGGYSSSLGYSSGGGFSSTS GR	6	—	0
		898–951	LTGEGVGPV**N**I**S**VVSSSGGT GYSSGGGSLCMTGGGYSSSL GYSSGGGFSSTSGR	4	—	0
		898–961	LTGEGVGPV**N**I**S**VVSSSGGT GYSSGGGSLCMTGGGYSSSL GYSSGGGFSSTSGR**N**M**S**GSS SSMR	8	—	0
		952–961	**N**M**S**GSSSSMR	3	1042.42	3
					1058.41	5
					1074.41	3
		952–965	**N**M**S**GSSSSMRIISK	3	1483.71	4
					1499.71	3
					1515.70	2
625	Heterogeneous nuclear ribonucleoprotein K	67–86	ALRTDY**N**A**S**VSVPDSSGPER	1	—	0
		70–86	TDY**N**A**S**VSVPDSSGPER	1	—	0
		70–102	TDY**N**A**S**VSVPDSSGPERILS ISADIETIGEILK	1	—	0

Table 3 (*continued*)

Spot No.	Protein name	Residues	Sequence	Number of peptide masses identified	Peptide mass with *N*-linked glycosylation	Number of glycoforms
828	Alpha enolase (2-phospho-D-glycerate hydro-lyase) (non-neural enolase) (NNE) (enolase 1) (phosphopyruvate hydratase) (C-myc promoter-binding protein) (MBP-1) (MPB-1) (plasminogen-binding protein) isoform 1	65–80	AVEHI**N**K**T**IAPALISK	1	1703.99	3
		93–105	LMIEMDGTE**N**K**S**K	3	1494.71	9
					1510.70	9
					1526.70	8
837	ARP3 actin-related protein 3 homolog	1–19	MVEPESL**N**Q**T**IEESHPDQK	2	—	0
		1–26	MVEPESL**N**Q**T**IEESHPDQKL LIGQPR	2	—	0
890	Macrophage scavenger receptor type I	83–101	NCLVCSR**N**T**S**DTSQGPMEK	6	2068.90	1
		90–101	**N**T**S**DTSQGPMEK	2	1309.55	1
		90–110	**N**T**S**DTSQGPMEKE**N**T**S**NVEM R	3	—	0
		102–110	E**N**T**S**NVEMR	2	1078.47	2
					1094.47	2
		102–119	E**N**T**S**NVEMRFTIIMAHMK	4	2199.01	2
		133–151	ADLIDTGRFQ**N**F**S**MATDQR	2	—	0
		141–151	FQ**N**F**S**MATDQR	2	1343.59	1
					1359.59	1
		141–178	FQ**N**F**S**MATDQRLNDILLQLN SLILSVQEHGNSLDAISK	2	—	0
		152–200	LNDILLQLNSLILSVQEHGN SLDAISKSLQSL**N**M**T**LLDVQ LHTETLHVR	2	—	0
		179–200	SLQSL**N**M**T**LLDVQLHTETLH VR	2	—	0
		179–202	SLQSL**N**M**T**LLDVQLHTETLH VRVR	2	—	0
		242–255	QEVRVLN**N**I**T**NDLR	1	1682.91	9
		246–255	VLN**N**I**T**NDLR	1	1170.64	18
		246–257	VLN**N**I**T**NDLRLK	1	1411.82	15
		258–281	DWEHSQTLK**N**I**T**FIQGPPGP QGEK	2	—	0
		267–281	**N**I**T**FIQGPPGPQGEK	1	1581.82	5
		267–284	**N**I**T**FIQGPPGPQGEKGDR	1	1909.97	9
961	Translocase of outer mitochondrial membrane 40 homolog isoform 2	103–139	LTVNKGLSNHFQV**N**H**T**VALS TVGESNYHFGVTYVGTK	1	—	0
		108–139	GLSNHFQV**N**H**T**VALSTVGES NYHFGVTYVGTK	1	—	0
		108–173	GLSNHFQV**N**H**T**VALSTVGES NYHFGVTYVGTKQLSPTEAF PVLVGDMDNSGSLNAQVIHQ LGPGLR	2	—	0
967	PIBF1 protein	11–40	KV**N**I**S**SSLESEDISLETTVP TDDISSSEER	1	—	0
		12–40	V**N**I**S**SSLESEDISLETTVPT DDISSSEER	1	—	0
		12–43	V**N**I**S**SSLESEDISLETTVPT DDISSSEEREGK	1	—	0
		231–239	KNYSEVQIR	1	1135.60	17
		232–239	NYSEVQIR	1	1007.50	16
		232–242	NYSEVQIRCQR	2	1394.67	13
					1451.69	7
		388–400	TNQEIDQLR**N**A**S**R	1	1543.77	5
		397–400	**N**A**S**R	1	446.22	19
		397–405	**N**A**S**REMYER	2	1154.51	5
					1170.51	4
1042	Isocitrate dehydrogenase 3 (NAD+) alpha isoform 2	9–27	APIQWEER**N**V**T**AIQGPGGK	2	—	0
		17–27	**N**V**T**AIQGPGGK	1	1040.56	5
		17–35	**N**V**T**AIQGPGGKWMIPPEAK	4	—	0
		139–150	NNHRS**N**V**T**AVHK	1	1375.71	15
		143–150	S**N**V**T**AVHK	1	854.46	18
		143–155	S**N**V**T**AVHKANIMR	2	1439.77	22
					1455.76	19
1045	Protein phosphatase 1, catalytic subunit, alpha	261–301	RQLVTLFSAP**N**Y**C**GEFDNAG AMMSVDETLMCSFQILKPAD K	12	—	0
		262–301	QLVTLFSAP**N**Y**C**GEFDNAGA MMSVDETLMCSFQILKPADK	12	—	0
		262–303	QLVTLFSAP**N**Y**C**GEFDNAGA MMSVDETLMCSFQILKPADK NK	12	—	0

This journal is © The Royal Society of Chemistry 2011

Table 3 (*continued*)

Spot No.	Protein name	Residues	Sequence	Number of peptide masses identified	Peptide mass with *N*-linked glycosylation	Number of glycoforms
1059	Annexin A1 (annexin I) (lipocortin I) (calpactin II) (chromobindin 9) (P35) (phospholipase A2 inhibitory protein)	None of the peptides obtained by cleavage of protein sequence contains the motif 'N–X–S/T/C (X not P)'.				
1118	Heterogeneous nuclear ribonucleoprotein A2/B1 isoform 2 isoform 22	None of the peptides obtained by cleavage of protein sequence contains the motif 'N–X–S/T/C (X not P)'.				
1134	Proteasome (prosome, macropain) 26S subunit, non-ATPase, 14 isoform 2	224–246	SWMEGLTLQDYSEHCKH**N**E**S** VVK	8	—	0
		240–246	H**N**E**S**VVK	1	811.42	20
		240–253	H**N**E**S**VVKEMLELAK	2	1625.85	9
					1641.84	12
1139	Annexin A2	50–68	GVDEVTIVNILT**N**R**S**NEQR	1	2156.12	2
1378	Proteasome subunit beta type 3 (Proteasome theta chain) (Proteasome chain 13) (Proteasome component C10-II)	None of the peptides obtained by cleavage of protein sequence contains the motif 'N–X–S/T/C (X not P)'				
1387	Proteasome (prosome, macropain) subunit, beta type, 3 isoform 1	None of the peptides obtained by cleavage of protein sequence contains the motif 'N–X–S/T/C (X not P)'				

[a] More details can be found in ESI.†

protein and/or a scaffold protein integrating in signal transduction pathways.[22,23] It is found in nucleus, cytoplasm and mitochondria, and also plays a role in maintaining the cellular ATP level under stress conditions through protection of target mRNAs.[22,24] hnRNP A2/B1 is widely distributed, particularly near nucleoli, and has a well-presented role in RNA processing, especially splicing.[25,26] Moreover, it has a potential role in cell growth but, on the other hand, promotes cell death in transformed and cancer cells.[26,27] However, the mechanistic insights of declined levels of hnRNPs' glycoforms in renal tubular epithelial cells upon COD crystal adhesion remain unknown and should be further investigated.

In summary, we identified altered levels of glycoforms of 16 proteins in MDCK renal tubular epithelial cells in response to COD crystal adhesion. These proteins generally play important roles in many cellular functions. Changes in their glycoforms might be associated with alterations in cellular integrity and metabolisms, as well as COD crystal adhesion and internalization. These findings may provide some novel insights into the pathogenic mechanisms of kidney stone disease.

Materials and methods

Preparation of COD crystals

COD crystals were generated as we previously described.[10] Briefly, 125 mL of 25.08 mM $CaCl_2{\cdot}2H_2O$ was added into 250 mL of a solution containing 19.26 mM $C_6H_5Na_3O_7{\cdot}2H_2O$, 23.1 mM $MgSO_4{\cdot}7H_2O$ and 127.4 mM KCl. When the solution was homogeneously mixed, the pH of the solution was adjusted to 6.5 using HCl and then incubated at 25 °C for 15 min. Thereafter, 125 mL of 6.4 mM $Na_2C_2O_4$ was added into the solution under continuous stirring and further incubated at 25 °C for 15 min. COD crystals were separated from the solution after centrifugation at 2000 × *g* for 5 min. The supernatant was discarded and the crystals were resuspended in absolute methanol. After centrifugation at 2000 × *g* for 5 min, methanol was discarded, whereas the crystals were air-dried at 25 °C overnight. The presence and purity of COD crystals were confirmed by phase-contrast microscopy.

Cell culture

Madin-Darby Canine Kidney (MDCK) cells, which were derived from dog kidney and exhibited distal renal tubule phenotype,[28] were used as a model of mammalian cells derived from distal nephron. Approximately 3×10^6 MDCK cells were cultured in each 75 cm^2 tissue culture flask containing a complete Eagle's minimum essential medium (MEM) (GIBCO, Invitrogen Corporation; Grand Island, NY) supplemented with 10% fetal bovine serum, 1.2% penicillinG/streptomycin, and 2 mM glutamine. The cultured cells were maintained in a humidified incubator at 37 °C with 5% CO_2 for 24 h.

COD crystal adhesion

A total of 10 semi-confluent flasks were then divided into two sets ($n = 5$ each), and the cultured medium was replaced by either COD crystal-containing or crystal-free medium. For the COD crystal-containing medium, after COD crystal generation and harvest, the crystals were decontaminated by UV irradiation for 30 min and then added to MEM to the final concentration of 100 μg of COD crystals per 1 mL of medium. For the crystal-free medium, COD crystals with an equal amount of 100 μg mL^{-1} were added into the medium for 30 min but then removed from the medium to make the identical concentrations of free calcium and oxalate ions in the medium compared to the COD crystal-containing medium. The cells were further maintained for 48 h.

Protein extraction

After cultivation of MDCK cells with or without COD crystals for 48 h, the cells were harvested by scraping, then

removed into the tube containing 0.5 M EDTA in PBS and further incubated at 4 °C for 30 min to dissolve the adherent COD crystals. Thereafter, the cells were washed with PBS three times to remove EDTA, then resuspended in a lysis buffer (7 M urea, 2 M thiourea, 4% 3-[(3-cholamidopropyl) dimethyl-ammonio]-1-propanesulfonate (CHAPS), 120 mM dithiothreitol (DTT), 2% ampholytes (pH 3–10), and 40 mM Tris-HCl), and incubated at 4 °C for 30 min. The suspensions were then centrifuged at 9100 × *g* to remove unsolubilized debris and particulate matter. Protein concentrations were measured by the Bradford assay.

Two-dimensional gel electrophoresis (2-DE)

An equal amount of 200 μg of proteins derived from each sample was mixed with a rehydration buffer (7 M urea, 2 M thiourea, 2% CHAPS, 120 mM DTT, 40 mM Tris-base, 2% ampholytes (pH 3–10), and a trace amount of bromophenol blue) to make the final volume of 150 μL per sample. The samples were then rehydrated onto individual Immobiline DryStrip (nonlinear pH gradient of 3–10, 7 cm long; GE Healthcare, Uppsala, Sweden) at room temperature for 16 h. The isoelectric focusing (IEF) was performed in an Ettan IPGphor III IEF System (GE Healthcare) at 20 °C using a stepwise mode to reach 9083 V h. After the completion of IEF, the strips were equilibrated in an equilibration buffer (6 M urea, 130 mM DTT, 112 mM Tris-base, 4% SDS, 30% glycerol, and 0.002% bromophenol blue) for 15 min at room temperature and then incubated with a similar buffer (where 130 mM DTT was replaced with 135 mM iodoacetamide) for 15 min at room temperature. The proteins on the equilibrated strips were further separated on 13% polyacrylamide gel using a SE260 mini-Vertical Electrophoresis Unit (GE Healthcare) at 150 V for approximately 2 h.

Glycoprotein staining

Glycoproteins separated on 2-D gels were visualized with Pro-Q Emerald 300 glycoprotein gel stain (Invitrogen—Molecular Probes; Eugene, OR). Briefly, the gels were fixed in a fixing solution (50% methanol and 5% acetic acid) for 45 min twice and then washed with 3% glacial acetic acid for 10–20 min twice. The carbohydrates on the gels were oxidized by oxidizing solution (1% (w/v) periodic acid diluted with 3% acetic acid) for 30 min and then washed with 3% glacial acetic acid for 10–20 min three times. Thereafter, the gels were stained with fresh Pro-Q Emerald 300 staining solution (diluting the Pro-Q Emerald 300 stock solution 50-fold into Pro-Q Emerald 300 staining buffer) for 90 min in the dark and then washed with 3% glacial acetic acid for 15–20 min twice. All steps were performed at room temperature with gentle agitation. The gels were scanned using a 300 nm UV transilluminator (the GeneGenius Gel Imaging System-Syngene; Frederick, MD).

Total protein staining

The glycoprotein-stained gels were stained again with SYPRO Ruby total protein gel stain (Invitrogen-Molecular Probes). Briefly, the gels were fixed in a fixing solution (10% methanol and 7% acetic acid) for 30 min and then stained with SYPRO Ruby dye overnight in the dark. After staining, the gels were destained in a destaining solution (10% methanol and 7% acetic acid) for 30 min followed by washing in deionized water for 5 min three times. The gels were scanned using a Typhoon laser scanner (GE Healthcare). Gel images were captured with an excitation of 532 nm and emission of 610 nm band-pass filter. The photo-multiplier tube (PMT) was tuned to 600 V to obtain the resolution at 100 μm pixel size, which produced 100 data points per cm and 200 data lines per grid square.

Matching and analysis of glycoprotein and protein spots

The glycoprotein and total protein spots were detected and matched by Image Master 2D Platinum (GE Healthcare) software. Parameters used for spot detection were (i) minimal area = 10 pixels; (ii) smooth factor = 2.0; and (iii) saliency = 2.0. A reference gel was created as a collection of all gel images. The reference gel was used for matching the glycoprotein and protein spots among gels. Background of each gel was subtracted and the intensity volume of each spot was normalized with the total intensity volume from all spots on individual gels.

Statistical analysis

Intensity levels of individual corresponding (matched) spots across gels were compared between the two sets of the MDCK cells (control *vs*. COD-treated) using unpaired Student's *t*-test. *P*-Values less than 0.05 were considered statistically significant. Only significantly differed glycoprotein spots (stained by Pro-Q Emerald), whose corresponding total protein spots (stained by SYPRO Ruby) had no significant changes, were subjected to in-gel tryptic digestion and identification by quadrupole time-of-flight (Q-TOF) mass spectrometry (MS) and tandem MS (MS/MS).

In-gel tryptic digestion

The differentially expressed glycoprotein spots were excised from 2-D gels, washed twice with 200 μl of 50% acetonitrile (ACN)/25 mM NH_4HCO_3 buffer (pH 8.0) at room temperature for 15 min, and then washed once with 200 μL of 100% ACN. After washing, the solvent was removed and the gel pieces were dried by a SpeedVac concentrator (Savant; Holbrook, NY). The dried gel plugs were then rehydrated with 10 μL of 1% (w/v) trypsin (Promega; Madison, WI) in 25 mM NH_4HCO_3. After rehydration, the gel pieces were crushed with a siliconized blue stick and incubated at 37 °C for at least 16 h. Peptides were subsequently extracted twice with 50 μL of 50% ACN/5% trifluoroacetic acid (TFA); the extracted solutions were then combined and dried with the SpeedVac concentrator. The peptide pellets were resuspended with 10 μL of 0.1% TFA and purified using $ZipTip_{C18}$ (Millipore). The peptide solution was drawn up and down in the $ZipTip_{C18}$ 10 times and then washed with 10 μL of 0.1% formic acid by drawing up and expelling the washing solution three times. The peptides were finally eluted with 5 μL of 75% ACN/0.1% formic acid.

Mass spectrometry (Q-TOF MS and/or MS/MS) and sequence analyses

The trypsinized samples were premixed 1 : 1 with the matrix solution containing 5 mg mL^{-1} α-cyano-4-hydroxycinnamic

This journal is © The Royal Society of Chemistry 2011

acid (CHCA) in 50% ACN, 0.1% (v/v) TFA and 2% (w/v) ammonium citrate, and deposited onto the 96-well MALDI target plate. The samples were analyzed by a Q-TOF Ultima^{TM} mass spectrometer (Micromass; Manchester, UK), which was fully automated with a predefined probe motion pattern and the peak intensity threshold for switching over from MS survey scanning to MS/MS, and from one MS/MS to another. Within each sample well, parent ions that met the predefined criteria (any peak within the m/z 800–3000 range with intensity above 10 count ± include/exclude list) were selected for CID MS/MS using argon as the collision gas and a mass dependent ± 5 V rolling collision energy until the end of the probe pattern was reached. The MS and MS/MS data were extracted and output as the searchable *.txt* and *.pkl* files, respectively, for independent searches using the MASCOT search engine (http://www.matrixscience.com), assuming that peptides were monoisotopic. Fixed modification was carbamidomethylation at cysteine residues, whereas variable modification was oxidation at methionine residues. Only one missed trypsin cleavage was allowed, and peptide mass tolerances of 100 and 50 ppm were allowed for peptide mass fingerprinting and MS/MS ions search, respectively. Thereafter, sequences of the identified proteins were subjected to analyses for their potential functions reported in the UniProt Protein Knowledgeable Database (http://www.uniprot.org) as well as for their potential *N*-linked glycosylation sites using the GlycoMod tool (http://www.expasy.ch/tools/glycomod/).

Abbreviations

2-DE	two-dimensional gel electrophoresis
ACN	acetonitrile
ARP	actin-related protein
CHAPS	3-[(3-cholamidopropyl) dimethyl-ammonio]-1-propanesulfonate
CHCA	cyano-4-hydroxycinnamic acid
COD	calcium oxalate dihydrate
DTT	dithiothreitol
EDTA	*N*,*N*,*N*′,*N*′-ethylenediaminetetraacetic acid
ERK	extracellular signal-regulated kinase
hnRNP	heterogeneous nuclear ribonucleoprotein
IDH	isocitrate dehydrogenase
IEF	isoelectric focusing
MDCK	Madin-Darby Canine Kidney
MEM	minimum essential medium
MS	mass spectrometry
Par	partitioning-defective
PIBF	progesterone-induced blocking factor
PMF	peptide mass fingerprinting
PP1α	protein phosphatase 1 alpha
TFA	trifluoroacetic acid

Acknowledgements

We are grateful to Tistaya Semangoen and Sakdithep Chaiyarit for their technical assistance. We also thank the Core Facilities for Proteomics and Structural Biology Research, Institute of Biological Chemistry, Academia Sinica, Taiwan. This study was supported by Office of the Higher Education Commission and Mahidol University under the National Research Universities Initiative, and The Thailand Research Fund (RTA5380005) (to V. Thongboonkerd). V. Thongboonkerd is also supported by ''Chalermphrakiat'' Grant, Faculty of Medicine Siriraj Hospital, whereas W. Chiangjong is supported by the Royal Golden Jubilee PhD Program of The Thailand Research Fund.

References

1 M. S. Parmar, *BMJ [Br. Med. J.]*, 2004, **328**, 1420–1424.
2 J. C. Lieske and S. Deganello, *J. Am. Soc. Nephrol.*, 1999, **10**(suppl 14), S422–S429.
3 J. C. Lieske, F. G. Toback and S. Deganello, *Kidney Int.*, 2001, **60**, 1784–1791.
4 X. Sheng, M. D. Ward and J. A. Wesson, *J. Am. Soc. Nephrol.*, 2005, **16**, 1904–1908.
5 J. C. Lieske, F. G. Toback and S. Deganello, *Kidney Int.*, 1998, **54**, 796–803.
6 J. C. Lieske, F. G. Toback and S. Deganello, *Calcif. Tissue Int.*, 1996, **58**, 195–200.
7 B. T. Murphy and L. N. Pyrah, *Br. J. Urol.*, 1962, **34**, 129–159.
8 A. Trinchieri, C. Castelnuovo, R. Lizzano and G. Zanetti, *Urol. Res.*, 2005, **33**, 194–198.
9 E. M. Worcester, *Semin. Nephrol.*, 1996, **16**, 474–486.
10 T. Semangoen, S. Sinchaikul, S. T. Chen and V. Thongboonkerd, *J. Proteome Res.*, 2008, **7**, 2889–2896.
11 T. H. Steinberg, K. Pretty On Top, K. N. Berggren, C. Kemper, L. Jones, Z. Diwu, R. P. Haugland and W. F. Patton, *Proteomics*, 2001, **1**, 841–855.
12 T. H. Steinberg, E. Chernokalskaya, K. Berggren, M. F. Lopez, Z. Diwu, R. P. Haugland and W. F. Patton, *Electrophoresis*, 2000, **21**, 486–496.
13 O. Vagin, J. A. Kraut and G. Sachs, *Am. J. Physiol. Renal Physiol.*, 2009, **296**, F459–F469.
14 T. Tsukamoto and S. K. Nigam, *J. Biol. Chem.*, 1999, **274**, 24579–24584.
15 P. Dalhaimer, T. D. Pollard and B. J. Nolen, *J. Mol. Biol.*, 2008, **376**, 166–183.
16 A. Matsumoto, M. Naito, H. Itakura, S. Ikemoto, H. Asaoka, I. Hayakawa, H. Kanamori, H. Aburatani, F. Takaku and H. Suzuki, *Proc. Natl. Acad. Sci. U. S. A.*, 1990, **87**, 9133–9137.
17 M. S. Schepers, R. A. Duim, M. Asselman, J. C. Romijn, F. H. Schroder and C. F. Verkoelen, *Kidney Int.*, 2003, **64**, 493–500.
18 Y. O. Kim, H. J. Koh, S. H. Kim, S. H. Jo, J. W. Huh, K. S. Jeong, I. J. Lee, B. J. Song and T. L. Huh, *J. Biol. Chem.*, 1999, **274**, 36866–36875.
19 D. T. Hartong, M. Dange, T. L. McGee, E. L. Berson, T. P. Dryja and R. F. Colman, *Nat. Genet.*, 2008, **40**, 1230–1234.
20 X. Chen and I. G. Macara, *Nat. Cell Biol.*, 2005, **7**, 262–269.
21 T. Hirose, Y. Izumi, Y. Nagashima, Y. Tamai-Nagai, H. Kurihara, T. Sakai, Y. Suzuki, T. Yamanaka, A. Suzuki, K. Mizuno and S. Ohno, *J. Cell Sci.*, 2002, **115**, 2485–2495.
22 K. Bomsztyk, O. Denisenko and J. Ostrowski, *Bioessays*, 2004, **26**, 629–638.
23 G. Dreyfuss, V. N. Kim and N. Kataoka, *Nat. Rev. Mol. Cell Biol.*, 2002, **3**, 195–205.
24 T. Fukuda, T. Naiki, M. Saito and K. Irie, *Genes Cells*, 2009, **14**, 113–128.
25 L. R. Friend, S. P. Han, J. A. Rothnagel and R. Smith, *Biochim. Biophys. Acta*, 2008, **1783**, 1972–1980.
26 A. Mayeda, S. H. Munroe, J. F. Caceres and A. R. Krainer, *EMBO J.*, 1994, **13**, 5483–5495.
27 C. Patry, L. Bouchard, P. Labrecque, D. Gendron, B. Lemieux, J. Toutant, E. Lapointe, R. Wellinger and B. Chabot, *Cancer Res.*, 2003, **63**, 7679–7688.
28 M. H. Saier, Jr., *Am. J. Physiol.*, 1981, **240**, C106–C109.

Editorial

Renal and Urinary Proteomics

The study of the renal and urinary proteome with the goal to discover biomarkers of (renal) diseases is a promising and rapidly expanding area of research. The field has produced a wealth of data and information over the last few years and has reached a point where the initial discovery phase needs to be translated into clinically tangible results. The ultimate clinical utility of these approaches largely depends, as in many cases, on appropriate *study design*, which includes a clinically relevant question that can potentially be answered by studying the proteome, reproducible proteomic platforms, appropriate statistics and independent validation of potential biomarkers [1]. Despite the vast research efforts on biomarker discovery during the past decade, proteomic biomarkers have not yet achieved the desired clinical impact. We have therefore proposed ''Renal and Urinary Proteomics'' as a topic for a Special Issue of *Proteomics – Clinical Applications* to gather viewpoint and review articles to facilitate research on clinical proteomics. In addition, a number of original research contributions adhering to good practice for biomarker discovery are also included in this Special Issue.



Harald Mischak



Visith Thongboonkerd



Joost P. Schanstra



Antonia Vlahou

Two associations have been particularly active to promote this field of research and propose guidelines on clinical proteomics: The European Kidney and Urine Proteomics (EuroKUP, www.eurokup.org) COST Action and the Human Kidney and Urine Proteome Project (HKUPP, www.hkupp.org), one of the HUPO Initiatives. We are delighted to see that many contributions in this Special Issue originate from members of these two associations.

As aforementioned, transformation of basic proteomic research to clinically useful data and applications is a key issue and the evident main focus of clinical proteomics. An important issue, often overlooked, is the clinical question in the study. Working on human samples does not necessarily make a study clinically relevant. That is why we have invited a number of physicians to express their views and expectations on the use of clinical proteomics. Delles et al. lay out their ideal roadmap for biomarker discovery in vascular disease, and Spasovski et al. discuss the use of proteomics in chronic kidney disease (CKD) and list the needs and expected answers of clinical nephrologists. John Ioannidis proposes a roadmap for successful application of clinical proteomics, while Efthymios Manolis from the European Medicines Agency describes a new pathway for the qualification of novel methodologies. These contributions collectively should help to guide researchers of the field of clinical proteomics to focus their works towards the clinical applications and validation by the regulatory agencies.

© 2011 WILEY-VCH Verlag GmbH & Co. KGaA, Weinheim

Owing to its availability, ease of collection and correlation with pathophysiology of diseases, urine has been the sample source of choice in most of clinical proteomics studies, particularly on renal diseases. Zürbig and colleagues review published studies of urinary proteomics in kidney and urogenital diseases that have the high chance to end up as clinical tools. Sigdel et al. and Blanco-Colio et al. review these issues on two more focused topics: renal transplantation and vascular disease, respectively.

Determining the origin of urinary biomarkers is at this point a matter of educated guessing. For improved understanding of the underlying pathophysiology it is therefore important to determine the site of biomarker production in situ. Charonis et al. discuss in a viewpoint contribution at the beginning of the issue whether technology and renal tissue collection have advanced enough to perform parallel kidney tissue and urinary proteomic studies, and what would be the added value of this parallel analysis. This viewpoint paper is accompanied by a dataset brief contribution by Blutke and colleagues (placed at the end of this issue) that shows common pathological mechanisms in two mouse models of glomerular hypertrophy by analysis of the glomerular proteome, followed by validation on human biopsies of different CKD.

A number of original research manuscripts in this Special Issue describe the identification and initial validation of biomarkers of a variety of renal and non-renal diseases. Husi and colleagues identified, using SELDI-TOF MS, a number of potential biomarkers of gastrointestinal cancer that were subsequently validated in an independent cohort using immunoblotting. Chen et al. identified potential biomarkers of pre-eclampsia, a hypertensive disorder of pregnancy, using iTRAQ coupled to two-dimensional LC-MS/MS. Some of these potential biomarkers were subsequently validated using ELISA. Two original research contributions on the identification of urinary biomarkers of renal allograft rejection are also included in this Special Issue. Srivastava et al. identified several urinary biomarkers of long-term allograft loss using antibody arrays that were subsequently validated using reverse-capture protein microarrays. Urinary biomarkers of acute T-cell-mediated allograft rejection were identified using CE-MS by Metzger et al. and validated using the same technology on a blinded cohort. Some of the biomarkers suggested involvement of MMP8, which was subsequently validated on acute rejection biopsy material. Non-invasive detection/surveillance of (renal) diseases is particularly appreciated in the paediatric population. Piyaphanee and colleagues described the SELDI-TOF-based identification of a fragment of α-1B-glycoprotein as a marker to differentiate paediatric steroid resistant from steroid-sensitive nephrotic syndrome. Finally, an original study using a combination of SDS-PAGE, 2D-PAGE, Western blotting and protein identification by HPLC–MS/MS carried out by Castagna et al. identified changes in female urinary proteome along the menstrual cycle with and without contraception. Several potential biomarkers were found differentially expressed and the results were confirmed by immunoblotting. Pending further confirmation, some of these proteins may potentially represent new contraceptive targets.

Facing the ever increasing wealth of information produced by -omics studies, tools are under development to extract the data from multiple -omics sources. Mayer and colleagues present an example of the extraction of relevant pathophysiological information on diabetic nephropathy from public domain sources. Interestingly, while direct feature comparison showed little overlap, expansion of the features to pathways identified modification of complement and coagulation pathways, PPAR signalling and the renin angiotensin system in diabetic nephropathy. This mining example also highlights the importance of publicly accessible databases of (urinary) biomarkers of (renal) diseases. In this context, Siwy et al. present an update of the biomarkers identified by CE-MS for 47 pathophysiological conditions. All CE-MS data are now accessible in one database that will facilitate the comparison of biomarkers of different pathologies.

All these articles demonstrate the substantial potential of urinary proteomic biomarkers. At the same time, they also highlight a shortcoming that must be addressed now: numerous studies describe different potential biomarkers for a variety of diseases, but

© 2011 WILEY-VCH Verlag GmbH & Co. KGaA, Weinheim

their utility and performance in the actual clinical setting has generally not been addressed (with very few exceptions). It appears high time now to concentrate on qualifying/validating these biomarkers in large, multicentric efforts (best if done in a combined effort that allows assessment of several different biomarkers in the same setting). Only such an approach, best with advice from the regulatory agencies, will enable subsequent clinical utilization. If the vast number of potential biomarkers described by now cannot be translated into clinical practice or cannot even be properly validated, then the entire approach has failed in the end. As such, it is now urgent to combine efforts, seek funding for such multicentric, international validation studies of the described potential biomarkers, and then perform these studies. In parallel, biomarker discovery efforts should focus on addressing well-defined hypothesis-driven questions, which target a better understanding of tissue pathophysiology and as such have the potential to unravel new biology-driven biomarkers and therapeutic targets.

Altogether we hope that this Special Issue on Renal and Urinary Proteomics will be very useful for all the readers and researchers in this area, and that it helps to move forward this exciting field of research and catalyse the transformation of these data into concrete clinical tools.

Reference

[1] Mischak, H., Allmaier, G., Apweiler, R., Attwood, T. et al., Recommendations for biomarker identification and qualification in clinical proteomics. *Sci. Transl. Med.* 2010, *2*, 46ps42.



Harald Mischak
Mosaiques Diagnostics,
Hannover, Germany and
BHF Cardiovascular
Research Centre, University
of Glasgow, Glasgow, UK



Visith Thongboonkerd
Center for Research in Complex
Systems Science (CRCSS),
Siriraj Hospital,
Mahidol University,
Bangkok, Thailand



Joost P. Schanstra
Inserm U1040,
Toulouse, France



Antonia Vlahou
Biomedical Research
Foundation, Academy of
Athens, Athens, Greece

© 2011 WILEY-VCH Verlag GmbH & Co. KGaA, Weinheim

REVIEW

Urine proteomics in kidney and urogenital diseases: Moving towards clinical applications

Petra Zürbig[1], Hassan Dihazi[2]*, Jochen Metzger[1], Visith Thongboonkerd[3]* and Antonia Vlahou[4]**

[1] Mosaiques Diagnostics GmbH, Hannover, Germany
[2] Nephrology and Rheumatology UMG, Georg-August University, Goettingen, Germany
[3] Medical Proteomics Unit, Office for Research and Development, Faculty of Medicine Siriraj Hospital, Center for Research in Complex Systems Science, Mahidol University, Bangkok, Thailand
[4] Division of Biotechnology, Biomedical Research Foundation, Academy of Athens, Athens, Greece

To date, multiple biomarker discovery studies in urine have been conducted. Nevertheless, the rate of progression of these biomarkers to qualification and even more clinical application is extremely low. The scope of this article is to provide an overview of main clinically relevant proteomic findings from urine focusing on kidney diseases, bladder and prostate cancers. In addition, approaches for promoting the use of urine in clinical proteomics including potential means to facilitate the validation of existing promising findings (biomarker candidates identified from previous studies) and to increase the chances for success for the identification of new biomarkers are discussed.

Received: November 3, 2010
Revised: March 4, 2011
Accepted: March 9, 2011



Keywords:
Kidney / Urine

1 Urine proteome mining

The analysis of urine is an important task in clinical diagnostics. The proteome of human urine has been investigated comprehensively to analyze disease processes regarding the kidney and the urogenital tract [1, 2]. Alterations in the urinary proteome may reflect defects of tissues, whenever the function of them is affected. Urinary proteins/peptides are generated from glomerular filtration, as well as derive from shed epithelial cells, tubular secretion, semen, and secreted exosomes. Hence, urine is considered a goldmine for biomarkers for urogenital as well as systemic diseases [3, 4]. This is reflected by the fact that urine proteins have long been used as adjuncts to current diagnostic/prognostic means and clinical decision making, e.g. albuminuria, FDA approved bladder cancer (BCa) tests such as NMP22 Bladder-Check, BTA stat, etc. [5], just to name few examples. Nevertheless, it is clear that proteomics has not yet realized their full potential, as defined by providing biomarkers that will make clinical decision-making ''easier, better, faster, cheaper'' (quoted from [6]).

On the other hand, highly encouraging results have started becoming available (summarized below [7, 8]); these along with our accumulated knowledge by now on erroneous practices of the past along the clinical proteomics workflow (ranging from faulty study design to inappropriate data analysis and inadequate data reporting and design of verification studies [6, 9–11]) provide solid reasons to believe that urine proteomics will soon achieve their long anticipated clinical impact.

Regardless the clinical question, large-scale studies involving the qualitative and quantitative analysis of the human urine proteome are essential. Common proteomic technologies include a variety of methodological approaches,

Correspondence: Dr. Antonia Vlahou, Division of Biotechnology Biomedical Research Foundation, Academy of Athens, Soranou Efessiou 4, 11527 Athens Greece
E-mail: vlahoua@bioacademy.gr
Fax: +30-210-65-97-545

Abbreviations: AGE, advanced glycation end products; **BCa,** bladder cancer; **CAD,** coronary artery disease; **CKD,** chronic kidney disease; **DN,** diabetic nephropathy; **ECM,** extracellular matrix; **GFR,** glomerular filtration rate; **PCa,** prostate cancer

*Members of the European Kidney and Urine Proteomics COST Action (BM0702).

© 2011 WILEY-VCH Verlag GmbH & Co. KGaA, Weinheim

e.g. 2-DE MS, LC-MS, SELDI-MS, and CE-MS (reviewed in [12, 13]).

In brief, some of the main findings from the analysis of soluble urine proteins may be summarized in Table 1 (for exosomal proteins readers may check on Gonzales et al. [14] for a recent review). It should be noted that most proteome mining studies by now included the analysis of pooled urine samples; occasionally, results were confirmed on individual samples (e.g. [15]). Even though sample pooling diminishes individual variability, it is preferred during proteome mining for technical (protein enrichment) reasons.

Furthermore, urine contains many naturally occurring peptides deriving mainly from target-orientated digestion of specific proteins. These peptides can only be investigated using the so-called 'bottom-up' proteomic technologies (for more details, see [16]). One of these approaches is the CE-MS [17]. Currently, 953 urinary peptides have been identified at the sequence level (Siwy et al., accompanying paper).

Comparison of the published data in an effort to compile a comprehensive view of the urine proteome is very difficult and attempts are scarce [18], which is mainly due to differences in protein annotation, reporting systems described in different studies as well as lack of sufficient data on protein identifiers as defined by different platforms (e.g. experimental/observed mass, p*I* and other physicochemical characteristics), so as to enable inter-platform data comparison and distinction of protein isoforms.

In an effort to overcome this problem, Mischak et al. [19] reported the generation of urine samples (male and female pools), available in large quantities to support standardization purposes in urinary proteomic investigations. These 'standard' samples were characterized comprehensively by proteomic and peptidomic approaches (1-D gel-nano-LC MS/MS (GeLC-MS), 2-DE-MS, LC-MS/MS and CE-MS). For the urinary peptidome, the sequences of 361 peptides (including post-translational modifications), corresponding to 31 different protein precursors, are provided. Fifty-six percent of these peptides were identified by both LC-MS/MS and CE-MS/MS. In the case of proteome analysis, 329 different proteins are reported with most of them being identified by GeLC-MS. The combinatorial use of proteomic/peptidomic approaches allowed to cover a wide mass range and revealed their complementarities. These standard samples are available upon request to meet the needs for reliable data comparison during biomarker discovery and verification/validation as well as facilitate the detailed compilation of the urinary proteome.

Collectively, the existing proteome mining data clearly demonstrate that urine contains a wealth of information; known protein families are well represented in multiple forms (proteolytic products, modified isoforms, etc). Even though we lack the understanding of how exactly these urinary proteins and peptides relate to tissue physiology, the available data have been helpful for the design of clinical proteomic analyses targeting the identification of disease-specific proteins and peptides in urine.

A review of main clinically relevant proteomic findings from urine in the case of urogenital diseases, mainly kidney diseases, bladder and urogenital cancers, is provided below. An overview of the reported biomarkers is also provided in the Supporting Information Table.

2 Chronic kidney disease (CKD)/diabetic nephropathy (DN)

Renal damage and kidney diseases are often described by progressive loss of renal function over a period of months or years and can eventually lead to end-stage renal disease (ESRD). For survival, patients with ESRD require renal replacement therapy (dialysis and/or kidney transplantation). DN, glomerulonephritis, and hypertension are the most common causes of CKD in North America, Europe, and Japan [20]; notably, DN develops in up to 40% of all diabetic patients [21]. Currently, increased urinary albumin excretion in the range of 30–300 mg/day (microalbuminuria) is the best prognostic indicator of DN. Poor

Table 1. Summary of representative urine (soluble) proteome mining studies

Year of discovery	Authors	Number of proteins/ peptides identified	Method	References
2001	Spahr et al.	124	LC-MS/MS	[129]
2002	Pang et al.	103	1-DE and 2-DE-MS, LC-MS	[130]
2004	Pieper et al.	150	2-DE-MS	[131]
2004	Oh et al.	113	2-DE-MS	[132]
2002	Thongboonkerd et al.	47	2-DE-MS (acetone precipitation)	[133]
2006	Zerefos et al	141	2-DE-MS (preparative electrophoresis)	[134]
2005	Smith et al.	48	2-DE-MS	[135]
2005	Castagna et al.	383	2DE-MS (beads coated with hexameric peptide ligand libraries)	[136]
2006	Adachi et al.	1543	1-DE, LC-MS/MS	[137]
2009	Kentsis et al.	2362	Protein LC, 1-DE, LC-MS/MS (analysis of both exosomal and soluble factions)	[15]

© 2011 WILEY-VCH Verlag GmbH & Co. KGaA, Weinheim

glycemic control and increased arterial blood pressure are other well-known risk factors to develop DN. However, these clinical signs do not fully reflect the risk of developing DN. An indicator of elevated blood glucose levels similar to those observed in diabetic patients seems to be the increased non-enzymatic glycation of proteins. The levels of advanced glycation end products (AGE) reflect a balance between their formation and catabolism [22, 23] and a large body of evidence indicates that oxidative stress is the common denominator link for the major pathways involved in the development and progression of diabetic micro- as well as macro-vascular complications of diabetes.

Proteolysis of AGE results in the formation of AGE peptides excreted normally in urine. In diabetes patients regardless the co-existence of renal disease, AGE peptides additionally accrue in plasma. It has been suggested that these compounds may be involved in the onset and further development of late diabetic complications [24] due to their high reactivity. Uncertainty is increased by the fact that in some instances renal function is already reduced even at the very first signs of microalbuminuria and additionally not all microalbuminuric patients will progress to DN [25]. Glomerular filtration rate (GFR) is the current gold standard for the estimation of renal function; it requires infusion of external substances (e.g. inulin, iothalamat, Cr-EDTA), is expensive and time consuming, hence prohibiting regular use in clinical trials or extensive epidemiologic studies [26]. GFR may also be estimated using equations involving serum creatinine measurements (modification of diet in renal disease (GFRMDRD) equations or Cockcroft–Gault (GFRCG) equations) which have also imperfections [27, 28]. Therefore, the identification of reliable DN risk markers is a very important clinical need.

A detailed review on DN biomarkers was recently published by Ameur et al. [29]. Herein, we briefly summarize studies involving urine proteomics analysis and which we consider as meriting further attention based on either findings verification through follow-up studies and/or contribution to insight to disease pathophysiology. In general, a renal biopsy is the gold standard to identify renal diseases, but due to ethical objections a renal biopsy is nearly never taken from diabetic patients. Furthermore, several studies have indicated that the presence of retinopathy being present is a good alternative for discrimination between DN and non-diabetic glomerulopathy in type 2 diabetic patients with albuminuria [30–32]. Jain et al. [33] identified immunglobulin G, α-1-acid glycoprotein, α-1-microglobulin, and α-2-glycoprotein as biomarkers specific for microalbuminuric diabetes patients in a study involving 100 diabetic (type 2) patients. They also analyzed samples from non-diabetic patients, which were found to lack these biomarkers. These findings are in agreement with more recent results, as described below. To analyze the time of appearance of the biomarkers in correlation with albumin, the authors also tested diabetic patients over a longer period to monitor the microalbuminuria negative to positive alteration. The precedence of the biomarkers to albumin in the investigated cases signified their potential use as earlier markers of DN. Rao et al. [34] recently identified proteomic differences in the urine of diabetic subjects with and without macroalbuminuria (> 200 mg/g albumin/creatinine ratio) using 2-DE MS. The authors used immunodepletion of abundant proteins (e.g. IgG, IgA, albumin, antitrypsin, haptoglobin, transferrin), which facilitated the detection of increased levels of defense-response proteins, several glycoproteins, and vitamin D-binding protein in type 2 diabetic patients with macroalbuminuria. This result is in agreement with an earlier report by Thongboonkerd et al. [35], which similarly revealed an increase in vitamin-D-dependent calcium-binding protein (calbindin D28k) levels in animal models (transgenic mice model of type 1 diabetes). Collectively, these results suggest an involvement of Ca- and/or vitamin-D-binding proteins in the development of DN and, if further verified, may provide a stepping stone towards our improved understanding of the disease underlying pathophysiology. Using 2-DE MS, Varghese et al. [36] identified various plasma proteins in urine allowing differential diagnosis between DN and other types of chronic renal disease (e.g. membranous glomerulonephritis, focal segmental glomerulosclerosis, and lupus nephritis). These findings were in agreement with a large extent with earlier potential DN biomarkers identified by Rao et al. [34] (see also Supporting Information Table). Summarizing, it seems that most of the now described DN biomarkers correspond or originate from highly abundant blood proteins. Their detection in urine may be attributed to 'leakage' associated with the pathological state. However, if these changes can in fact also mark the onset of DN progression remains to be defined.

Various studies involving the analysis of the urine peptidome by CE-MS for the investigation of CKD and DN have been conducted [37–41]. Of special note are the work of Rossing et al. who analyzed urinary biomarker profiles in four groups of type 2 diabetic patients [40] as well as in diabetic type 1 patients with normoalbuminuria and macroalbuminuria [41]. Recently, a multi-center prospective blinded study by the PREDICTIONS network (http://www.rzuser.uni-heidelberg.de/~jb5/aboutus_index.htm) was performed to verify the pattern described in Rossing et al. [41]; In brief, using a set of 148 subjects, discrimination of diabetes mellitus type 2 patients with versus without DN was provided with an area under the curve (AUC) value of 0.957 after unblinding [42].

Additionally, Good et al. [37] established a CKD-specific biomarker pattern in a study involving the analysis of urine samples by CE-MS from 340 patients with biopsy-proven various types of CKD (DN, IgA nephropathy, focal segmental glomerulosclerosis, membranous glomerulonephritis, minimal change disease, vasculitis, and systemic lupus erythematosus) and 552 controls (healthy individuals

© 2011 WILEY-VCH Verlag GmbH & Co. KGaA, Weinheim

and patients with other diseases and no indication for CKD). This pattern consisted of 273 peptides and in a subsequent and independent heterogeneous cohort (34 controls and 110 cases) analyzed blindly, CKD was detected with sensitivity of 85.5% and specificity of 97.8%.

Many of the DN and all of the CKD biomarkers have been sequenced (Supporting Information Table); among the discriminatory peptides are albumin and uromodulin fragments, but there is also a disease-related marked and intriguing decline of specific collagen peptides. Collagen fragments, especially fragments of collagen α-1 (I) chain, appear to be the major constituents of urinary peptides [17]. These peptides likely reflect normal physiological turnover of the extracellular matrix (ECM) [43]. Specifically, urinary collagen fragments appear at reduced levels in diabetes, and even more, in DN or CKD. It is thereby plausible that decreased concentrations of collagen peptides in urine might be associated with a reduction in elastase activity [44, 45] with concomitant increase in ECM deposition. In addition to DN/CKD, collagen fragments are also the source of identified biomarkers for the diagnosis of coronary artery disease (CAD) [46, 47]. The main difference of the biomarkers for the diagnosis of CAD versus CKD is the direction of their regulation. Whereas most of the collagen-derived biomarkers for CAD showed increased urinary excretion, the collagen fragments indicated CKD by their relative paucity. The difference in their regulation may arise from different activity of collagenases. High levels of circulating collagenases have been identified in patients with stable angiographic coronary atherosclerosis [48] or peripheral arterial disease [49]. Elevated MMP-9 activity has been found in unstable plaques, suggesting a crucial role in plaque rupture [50]. In contrast, in CKD patients a decreased activity of collagenases was observed [51]. Regardless of the primary etiology, severe CKD is characterized by interstitial fibrosis, tubular atrophy, and glomerulosclerosis. Therefore, it has been assumed that the accumulation of proteins in the ECM and collagens that represent the fibrotic kidney may be the result of reduced activity of matrix metalloproteases [52]. Furthermore, accumulation of ECM was recently shown to be associated with decreased urinary excretion of several specific collagen fragments in patients with DN [41].

Several studies have also addressed the discovery of early diagnostic markers for CKD/DN. It should be noted that in these cases, the cross-sectional study design frequently used for discovery of diagnostic biomarkers is no longer applicable; a longitudinal study design is instead recommended. A first pilot study was performed by Otu et al. [53]. In this study urine samples of normalbuminuric type 2 diabetic Pima Indians were analyzed with SELDI-MS at baseline and after 10 years. In this study, patients who developed DN within this time (progressors) were compared with age-, gender-, and diabetes duration-matched controls, which had not developed DN (non-progressors). Several discriminatory peptides were found, providing a first hint that early predictive markers for the development of DN may exist in urine.

Along the same lines, Merchant et al. [54] performed a longitudinal study to investigate the urine profiles of microalbuminuric diabetic type 1 patients in relation to renal function. Specifically, the renal function of these patients was investigated over 10–12 years based on which patients were divided to non-progressors ($n = 40$) and progressors ($n = 21$), in a retrospective study. By the use of LC-MALDI-MS, peptides of tenascin-X, collagen α 1 (IV) and α 1 (V), zona occludens 3, FAT tumor suppressor 2, and inositol pentacisphosphate 2-kinase were detected as potential early biomarkers for renal function decline in microalbuminuric patients. The differential expression of inositol pentacisphosphate 2-kinase was further confirmed by immunohistochemical analysis of kidney biopsies. Both Otu et al. and Mechant et al. provided the proof of principle, e.g. showed the potential of urinary proteome/peptidome analysis for the prediction of DN. Along the same lines, in Rossing et al. [40] the validated DN biomarkers enabled pinpointing microalbuminuric diabetic type 1 patients that showed over a period of 3 years progression of disease, with a sensitivity of 100%. Further ongoing studies support that early diagnosis of DN development with high accuracy rates is possible for both normalbuminuric and microalbuminuric patients over a period of up to 6 years (Rossing et al., unpublished work).

Urine peptidomics has also been used for the evaluation of benefit of therapeutic intervention. Rossing et al. [40] analyzed urine samples from type 2 diabetes patients with CE-MS and generated a DN pattern of 113 biomarkers to distinguish between diabetes patients with and without DN. Macroalbuminuric patients were treated with different doses of candesartan (angiotensin II receptor blocker), which resulted in significant changes of 15 of the 113 urinary markers in the DN pattern to levels comparable with those of normoalbuminuric patients. These pattern changes were not strictly dose-dependent, nevertheless, changes of individual peptides (e.g. constituents of the pattern) correlated with alterations in urinary albumin concentrations at each candesartan dose. Furthermore, the CKD biomarkers described in Good et al. [37] were evaluated in a subgroup of hypertensive diabetic type 2 patients with microalbuminuria from a 2-year irbesartan versus placebo treatment trial (IRMA2 substudy) [55]. The group demonstrated that daily administration of 300 mg irbesartan over a period of 2 years induced specific changes at the expression levels of urinary peptides. The latter included the CKD biomarkers [37], as well as several additional urinary peptides which were not, however, altered in the placebo-treated individuals. Of high biological relevance are considered the changes of urinary collagen fragments associated with early diagnosis of DN. Thereby collectively these existing data support that urine proteomics has great potential in the development of novel diagnostic, but also prognostic as well as tools to assess the potential benefit of therapeutic intervention for DN/CKD [7].

© 2011 WILEY-VCH Verlag GmbH & Co. KGaA, Weinheim

3 Acute kidney injury

AKI is a common complication in hospitalized patients; a recent meta-analysis highlighted the increased mortality associated with AKI, independent of other factors. Over the last decade, the incidence of AKI has increased from 60 to 500 events/100 000 population [56].

Currently, no effective therapy of AKI is available. To improve the associated serious prognosis, efforts are focused on the primary and especially secondary prevention, rendering the early detection of AKI a clinical and research priority. Recent definitions of AKI, namely the Risk, Injury, Failure, Loss of renal function, and End-stage kidney disease (RIFLE) classification or the Acute Kidney Injury Network criteria, incorporate serum creatinine and urine output as the principal markers to define and detect AKI [57]. However, these and other clinically available and widely used markers (blood urea nitrogen, tubular enzymuria or proteinuria, elevated serum creatinine or oliguria) are less than optimal and have substantial further limitations [58]. Therefore, a fast, specific and reliable biomarker assay that enables monitoring of patients in a clinical setting is of great clinical interest.

In the last 5 years, numerous new markers such as neutrophil-gelatinase-associated lipocalin (NGAL), interleukin-18 (IL-18), cystatin C, and kidney injury molecule 1 in the urine and/or serum have been studied and proposed as early detection markers of AKI [59–62]. Persistently, these markers performed well in initial pilot trials. However, these promising results could often not be confirmed in later, larger multi-center trials and limitations of these biomarkers in the early diagnosis of renal injury were demonstrated [63–66].

A promising finding was described by Zhou et al. [67], who analyzed urinary exosomes from a rat model of cisplatin-induced AKI, by difference gel electrophoresis (2-D DIGE). Among the different regulated proteins, fetuin-A was found upregulated in the AKI animals, compared with animals with prerenal azotemia. Urinary fetuin-A was detected 2 days before the increase of creatinine in serum. This finding was further validated in animals with bilateral renal inschemia and reperfusion injury as well as in ICU patients with AKI.

Metzger et al. [68] applied CE-MS for the detection of urinary biomarkers – predictors for AKI. They used a training set of 87 urine samples, collected from ICU patients at different days grouped according to later development of AKI or maintenance of normal kidney function. Based on this analysis, an AKI-specific peptide profile (20 urinary polypeptides) was developed. The biomarkers were specific peptides derived from six different proteins. Fragments of α-1-antitrypsin, albumin, and β-2-microglobulin were upregulated; peptides derived from collagen type I and III and fibrinogen α were downregulated in AKI. Comparison of the peptides comprising the AKI and CKD biomarker profiles [37] demonstrated that two of five collagen 1 α (I) fragments of the former and one of three fibrinogen fragments in the latter (AKI) as well as, all albumin-derived fragments, one α 1-antitrypsin fragment, and one β-2-microglobulin fragment, overlapped. The AKI panel provided good diagnostic accuracy with an AUC value of 0.84 and 0.90, during validation in two blinded sets of prospectively, longitudinal collected samples from 20 ICU patients, and from 30 patients after hematopoietic stem cell transplantation, respectively. Additionally, 28 healthy controls all scored negative (100% specificity). Comparison of the AKI marker panel with levels of creatinine, cystatin C, KIM-1, IL-18, and NGAL supported that the proteomic profile could detect AKI, at least 4–5 days earlier than serum creatinine; further validation of these promising results is underway.

4 Acute renal allograft rejection

Acute rejection is an important factor that determines long-term function and survival of renal allografts. Approximately 15–30% of the transplanted patients suffer from one or multiple acute rejections which occur mainly in the first year of transplantation [69, 70].

Timely detection and sufficient anti-rejection therapy of acute rejection episodes is important to conserve allograft function. However, detection of acute rejection in an early stage is challenging [71]. Regular monitoring for increases in serum creatinine or decrease in creatinine clearance, with subsequent indicated biopsy, implies that the rejection is detected in an advanced stage where the graft is already impaired by the rejection process.

Protocol biopsies have been used to detect acute rejection in an earlier, subclinical stage, where functional impairment is not present yet [72]. An inherent limitation of this approach is that even with multiple biopsies it is impossible to capture every rejection episode. Therefore, many attempts have been made to develop non-invasive tests in blood or urine which are able to detect acute rejection [73–75]. Most of these approaches used single markers or combinations of a few markers. Mostly due to lacking specificity and sensitivity of these markers, none of these tests is established in the clinical routine and post-transplant care of the patients. Additionally, several groups have reported successful use of mass spectrometry of urinary samples to detect acute rejection using a panel of marker peptides [76–80]. Overall good performance was reported in theses studies with AUC values ranging from 0.85 to 0.97. Verification of these results on larger patient cohorts is pending.

Acute tubulointerstitial rejection is often associated with acute tubular injury (ATI) [81]. Therefore, an important clinical question is whether proteomic markers identified in acute rejection are indicative for the rejection process itself or if they are non-specifically reflect tubular injury. Schaub et al. described cleaved urinary β-2-microglobulin as a potential biomarker for acute tubular damage in renal allografts [82]. However, fragments of β-2-microglobulin corre-

© 2011 WILEY-VCH Verlag GmbH & Co. KGaA, Weinheim

late with ATI in samples with and without rejection, but not with rejection itself. In this line, β-2-microglobulin fragments were recently described as markers for acute kidney injury in non-transplanted patients [68].

Interestingly, various recent studies [79, 80, 83] (see Supporting Information Table) support that the levels of diverse collagen fragments are altered in samples with acute T-cell-mediated tubulointerstitial rejection. Aligning these fragments to other, commonly present urinary collagen α-1 (I) peptides, showed that those collagen fragments associated with rejection posses a characteristic sequence motif at their c-terminus which is indicative of increased ECM degradation by metalloproteinases. By immunohistological staining of biopsy sections, a significant number of MMP+ polymorphonuclear cells close to the endothelium were detected as early event of the rejection process. Therefore, metalloproteinase expression at peritubular capillaries may be an indicator for trans-endothelial migration of infiltrating cells into the interstitium and into the tubules [84, 85].

5 Urological malignancies

Several applications of proteomics technologies for cancer biomarker discovery have been reported. A brief summary of few representative studies on prostate and BCas involving follow-up validation of findings is provided below.

5.1 Prostate cancer

Prostate cancer (PCa) is third in incidence among other male malignancies [86]. Prostate-specific antigen (PSA) screening has largely facilitated PCa detection [87]; nevertheless, PSA has low specificity [88, 89] resulting in up to 700 000 unnecessary prostate biopsies per year in the USA. Additionally, currently it is not possible to differentiate between aggressive and more indolent prostate tumors; the latter have no major impact on mortality for 10–15 years [90], whereas in contrast the former may become metastatic within approximately 2–3 years [90], underscoring the need for novel prognostic makers.

Discovery of diagnostic markers for PCa has been extensively addressed [13, 91, 92]. It should be noted that even though there is ample literature evidence describing PCa biomarker discovery in plasma/serum and tissue, data on urine analysis are still scarce. First, urinary proteomic analyses were performed by Rehman et al. using 2-DE MS [93] and by M'Koma et al. using reverse phase chromatographic separation and MALDI-MS analysis [94], but verification of these findings and identification of the discriminatory peptides is lacking. Potential biomarkers revealed by these studies are listed in the Supporting Information Table.

Identification of CE-MS urinary profiles diagnostic for PCa was recently described [95]. In a prospective study, Theodorescu et al. described a panel of 12 peptide biomarkers (Supporting Information Table) which in a blinded test set detected PCa with a sensitivity of 83% and specificity of 97%. Of special note, the PCa-specific biomarkers were detectable solely in first void urine, indicating that these peptides may originate from prostatic fluids. There is by now increasing evidence in support of this hypothesis [96, 97] also emphasizing on the importance of urine sampling methodology in PCa biomarker discovery.

5.2 Bladder cancer

BCa is the second in incidence and mortality cancer of the genitourinary system accounting for an estimated 380 000 cases annually worldwide and 70 530 incidents and 14 680 deaths in US in 2010 (http://www.cancer.gov/cancertopics/types/bladder). BCa consists of a spectrum of malignancies categorized into three main groups of distinct clinical behavior, prognosis, and primary management: superficial (Ta-Tis-T1), locally invasive (T2-4), and metastatic cancer (N+/M+) [98, 99]. At initial diagnosis, most patients (70%) present superficial disease being restricted to the urothelium (Tis, Ta) and up to muscularis mucosa (T1); 20–30% have muscle-invasive tumor with approximately 5% exhibiting clinically evident distant metastases. Notably, BCa recurrence rate is about 20% with an associated 15% progression rate to higher grade and/or invasive lesions; this imposes frequent follow-up of patients by cystoscopy – an invasive and highly costly procedure – rendering BCa one of the most costly types of cancer in terms of management. Additionally, invasiveness results in very poor prognosis: more than 50% of cases succumb to their disease within 5 years [99]. Collectively, these facts define the clinical needs and research questions for BCa: these include development of early diagnostic markers for invasive cancers and definition of markers for recurrence and progression superior in accuracy to the current non-invasive golden standard test of urine cytology [100]; deciphering the molecular mechanisms associated with pathophysiology of the invasive phenotype to enable development of novel therapeutic approaches (reviewed in [6, 101]).

Multiple studies have been conducted towards discovering BCa protein biomarkers. Among the potential biomarkers that attracted a lot of interest are bladder tumor antigen, nuclear matrix protein 22, BLCA-4, hyaluronidase, cytokeratins (8, 18, 19), tissue polypeptide antigen, and tissue polypeptide-specific antigen, soluble Fas and survivin; nevertheless, their exact potential use in the clinic is still to be defined (reviewed in [6, 100, 102–103]). Some of these biomarkers were initially discovered following the application of classical proteomics technologies with the characteristic example of BCa antigen (BLCA-1,-4, -6). Using 2-DE analysis of urothelial tissue, the association of BLCA proteins with BCa was observed [104–107]. Detection of BLCA-4 in urine by the use of specific immunoassays

© 2011 WILEY-VCH Verlag GmbH & Co. KGaA, Weinheim

provided BCa detection with a specificity of 95% and a sensitivity of 89% [106]. Validation of these results in clinical trials is in progress. Multiple additional studies using 2-DE approaches have also been conducted through the years (reviewed in [108]; some additional representative findings [109, 110] are also shown in the Supporting Information Table, indicating various potential biomarkers; nevertheless, large-scale validation of the results and identification of specific use are still pending.

Recently, Orenes-Pinero et al. [111] identified differentially expressed proteins between patients with bladder tumors and controls using 2-D DIGE coupled to MS. These biomarkers (e.g. regenerating protein 1 (Reg-1; current name: Lithostathine-1-α), cytokeratin 10, T-cell surface glycoprotein CD5) were confirmed to be associated with BCa progression on BCa cell lines by immunoblotting and on bladder tumors by immunohistochemistry. Moreover, the association of Reg-1 with tumor staging and clinical outcome was confirmed by tissue microarrays. Notably, Reg-1 was validated using an independent test set ($n = 80$) resulting in an AUC of 0.88. These results suggest that the involvement of Reg1 in BCa progression merits further investigation, particularly in view of its association with progression of other types of tumors [112, 113].

SELDI technology has also been employed in the investigation of urine proteome for BCa detection by multiple investigators. The performance of SELDI profiles in detecting BCa ranges from 72 to 93% sensitivity and 63 to 87% specificity in blinded sets of samples from the different studies [114–119]. However, due to differences in chip surfaces and sample preparation methods employed in individual studies as well as lack of discriminatory peptide identifications, the data sets are not comparable.

Vlahou et al. [115] identified one of the transitional cell carcinoma (TCC) peptide markers detected by SELDI as α-defensins; this peptide was further found to induce BCa cell motility in vitro [120]. Along the same lines, Munro et al. [117] identified urinary α-defensins as a TCC biomarker in a study involving SELDI analysis of a total of 227 subjects. In a separate study, immunohistochemical analysis further confirmed the overexpression of α-defensins in invasive BCa [120]. Despite this evidence, the involvement of α-defensins in inflammatory processes raises concerns regarding the ultimate specificity of these proteins as urinary biomarkers for BCa detection; On the other hand, further investigation of the mechanism of α-defensin expression by bladder epithelial cells and its means of action (autocrine–paracrine) in relation to tumor cell motility and invasiveness may provide valuable insights for therapeutic intervention.

As reviewed in [13], Theodorescu et al. [121] analyzed urine samples with CE-MS of a total of 445 subjects including BCa patients and subjects with other malignant or benign urogenital diseases or no evidence of disease. Twenty-two BCa-specific markers were revealed and further validated in a blinded study involving a prospective cohort of 180 subjects (31 BCa patients, 138 patients with benign urological diseases, and 11 healthy individuals); the obtained sensitivity for BCa detection was 100% with specificity between 86 and 100% depending on the control type.

Recently, a CE-MS biomarker profile consisting of fragments of collagen α 1 (I) and (III), membrane-associated progesterone receptor component 1, and uromodulin was found to be predictive of muscle invasive BCa [13, 122], and as a component of nomogram also including tumor grade, it significantly improved sensitivity (92%) and specificity (68%) in detection of muscle invasive disease.

5.3 Outlook

There has been a remarkable expansion in the employment of urine in biomarker discovery the last few years. Characteristically, using the keywords 'urine' and 'protein biomarker' a PubMed search retrieves almost 5000 articles published in the last 10 years. If the keywords 'renal' or 'kidney' are further added to the search then >1300 articles are retrieved. The respective numbers for the previous two decades are significantly lower with ca. 2610 and 570 articles on urine protein biomarker (584 and 135 after adding the term 'renal') for the decades 1990–2000 and 1980–1990, respectively (Fig. 1). This significant increase in the last 10 years can be attributed in part to advancements in proteomics technologies which allowed for a better and more in depth exploration of the urine proteome; this fact along with the well-known advantages of urine (e.g. non-invasive collection, availability in large quantities, ability to reflect systemic diseases, etc.) established urine as a 'gold-mine' in biomarker research. Coverage of all available recent information on biomarker discovery for renal/urogenital diseases would be out of the realm of this review; we instead opted to emphasize on data from proteomic studies that have progressed to some extent in the 'biomarker validation' pipeline and which thereby may hold greater promise in achieving clinical impact in the near future.

Despite the existing promising findings, considering the extensive research efforts, resources, and ample literature on the subject, it would be expected that the impact of urinary proteomics on clinical practice would have already been

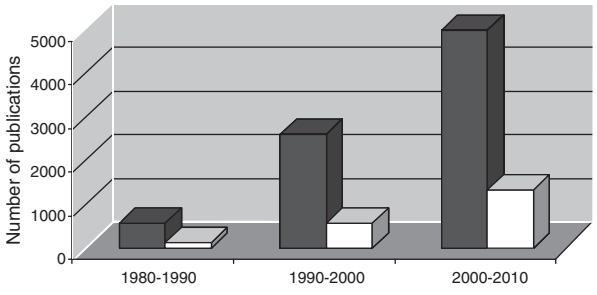


Figure 1. Number of publications on 'urine and protein biomarker' (gray bar) and 'urine and protein biomarker and kidney (or renal)' (white bar) in the last decades.

© 2011 WILEY-VCH Verlag GmbH & Co. KGaA, Weinheim

realized. The observed delay underscores the need for a thorough evaluation of steps involved in the biomarker pipeline – from initial discovery up to clinical assay development – targeting the identification of erroneous practices and bottlenecks and potential solutions to overcome them [9, 10, 123]. Along these lines, in the recent report by Mischak et al. [11] a group of ca. 50 investigators provide guidelines for identifying and qualifying proteomic biomarkers that could also be used as reporting requirements in biomarker discovery studies. Adherence to these recommendations is expected to result in a decrease in the number of false positives. e.g. pool of biomarkers entering the validation pipeline. This would mark a significant improvement in biomarker research, yet it is not sufficient to reach the ultimate goal of bringing proteomics findings to the clinical practice faster. Large-scale validation of biomarkers through rapid and inexpensive assays is an additional important bottleneck in the whole process. The technological needs (e.g. appropriate ELISA, high-throughput MS-based platforms) have been described [124, 125] and vigorous research efforts have been undertaken to optimize available platforms. An equally important factor that is frequently overlooked is the need for high numbers of high quality, clinically annotated urine samples to support such studies. As a first step, the EuroKUP (European Network for Kidney and Urine Proteomics) and HKUPP (Human Kidney and Urine Proteome Project) consortia have recently developed a standard protocol for urine collection (Tables 2 and 3) based on the accrued knowledge in the field and targeting a balance between perfection and feasibility at the clinical setting. This standard protocol may be seen as one little piece of a more extensive project addressing the development of common data elements (CDE) and a unified biobanking system for kidney (or other) diseases. At present, clinical samples for specific research questions even if available are disparate and of frequently questionable quality. Development and adoption of CDE will support the formation of a unified system for urine specimen collection and increase cross talk across institutes, clinical centers but also different studies and findings thereof. Such a task is not trivial and requires a coordinated effort from multiple disciplines. Experience from existing such initiatives [126, 127] can be recruited and aid significantly in this direction.

Collectively, urine proteomics has the potential to impact clinical decision-making in the diagnosis, prognosis as well as therapeutic intervention of kidney (and other) diseases. This statement can by now be supported by the existing experimental evidence. Undoubtedly, increase in understanding the disease pathophysiology and implementation of novel integrative (e.g. 'systems biology') approaches in biomarker research will gear up the discovery of successful biomarkers and therapeutic targets as supported in various recent reports [1, 128]. In parallel, however, to this effort, establishment of the needed infrastructure to ensure cross-talk between available and future resources, particularly of biospecimens, and importantly a more organized framework encompassing biomarker discovery and verification with a clear focus on clinical implementation and impact on specific clinical needs are urgently needed so as to prevent the loss of valuable biologic material and fulfill faster the

Table 2. Standard protocol for urine collection for proteome analysis developed by HKUPP and EuroKUP[a)]

(i) Type of urine sample Mid-stream of second morning urine (preferably) or morning random-catch urine
(ii) Container Sterile (preferably) or clean urine collectors
(iii) Pre-treatment Centrifuge at 1000 × *g* for 10 min to remove cell debris and casts
(iv) Storage Aliquot supernatant without disturbing the pellets and overfilling tubes Usual working volumes: 1.5, 10, or 50 mL Store at −80°C (preferably) or −20°C Record time until freezing (it should be no longer than 3 h; if longer, addition of preservatives is needed)
(v) Avoid freeze–thaw cycles. Always keep a record of this event

a) For detailed information and variations of standard protocol, please visit http://www.eurokup.org/node/137 and http://www.hkupp.org/Urine%20collectiion%20Documents.htm.

Table 3. Sample minimal identifiers recommended by HKUPP and EuroKUP

A. Storage information
1. Unique sample code
2. Storage temperature (−20/−80)
3. Institution
4. Date – time of collection
5. Time until freezing
6. Aliquot (volume) and number of aliquots
B. Case Information
7. Unique patient code
8. Clinical diagnosis
9. Age
10. Gender
11. Height
12. Weight
C. Recommended laboratory information
14. Urinary protein amount
15. Urine creatinine
16. Hematuria
17. Serum creatinine[a)]
18. Urine pH[a)]
19. Serum protein (serum albumin)[a)]
20. Serum cholesterol[a)]

a) Not absolutely needed (but usually helpful) information. In general, needed clinical information depends on the disease under investigation.

© 2011 WILEY-VCH Verlag GmbH & Co. KGaA, Weinheim

(well justified) high expectations from urine clinical proteomics.

The authors acknowledge funding supports as follows: EuroKUP COST Action (to P.Z., H.D., V.T., and A.V.), DECanBio FP7 (201333 to A.V.), and SysKID FP7 (241544 to P.Z.). The Thailand Research Fund RTA5380005, Office of the Higher Education Commission, and Mahidol University under the National Research Universities Initiative (to V.T.).

The authors have declared the following conflict of interest: Petra Zürbig and Jochen Metzger are employees of Mosaiques Diagnostics GmBH which developed CE-MS for clinical proteomics applications.

6 References

[1] Thongboonkerd, V., Current status of renal and urinary proteomics: ready for routine clinical application? *Nephrol. Dial. Transplant.* 2010, *25*, 11–16.

[2] Pisitkun, T., Johnstone, R., Knepper, M. A., Discovery of urinary biomarkers. *Mol. Cell. Proteomics* 2006, *5*, 1760–1771.

[3] Shihabi, Z. K., Konen, J. C., O'Connor, M. L., Albuminuria vs urinary total protein for detecting chronic renal disorders. *Clin. Sci.* 1991, *37*, 621–624.

[4] Yudkin, J. S., Forrest, R. D., Jackson, C. A., Microalbuminuria as predictor of vascular disease in non-diabetic subjects. Islington Diabetes Survey. *Lancet* 1988, *2*, 530–533.

[5] Shariat, S. F., Karam, J. A., Lotan, Y., Karakiewizc, P. I., Critical evaluation of urinary markers for bladder cancer detection and monitoring. *Rev. Urol.* 2008, *10*, 120–135.

[6] Lotan, Y., Shariat, S. F., Schmitz-Drager, B. J., Sanchez-Carbayo, M. et al., Considerations on implementing diagnostic markers into clinical decision making in bladder cancer. *Urol. Oncol.* 2010, *28*, 441–448.

[7] Mischak, H., Rossing, P., Proteomic biomarkers in diabetic nephropathy – reality or future promise? *Nephrol. Dial. Transplant.* 2010, *25*, 2843–2845.

[8] Nemirovskiy, O., Li, W. W., Szekely-Klepser, G., Design and validation of an immunoaffinity LC-MS/MS assay for the quantification of a collagen type II neoepitope peptide in human urine: application as a biomarker of osteoarthritis. *Methods Mol. Biol.* 2010, *641*, 253–270.

[9] Apweiler, R., Aslanidis, C., Deufel, T., Gerstner, A. et al., Approaching clinical proteomics: current state and future fields of application in cellular proteomics. *Cytometry A* 2009, *75*, 816–832.

[10] Knepper, M. A., Common sense approaches to urinary biomarker study design. *J. Am. Soc. Nephrol.* 2009, *20*, 1175–1178.

[11] Mischak, H., Allmaier, G., Apweiler, R., Attwood, T. et al., Recommendations for biomarker identification and qualification in clinical proteomics. *Sci. Transl. Med.* 2010, *2*, 46ps42.

[12] Thongboonkerd, V., Practical points in urinary proteomics. *J. Proteome Res.* 2007, *6*, 3881–3890.

[13] Siwy, J., Vlahou, A., Zimmerli, L. U., Zurbig, P., Schiffer, E., Clinical proteomics: current techniques and potential applications in the elderly. *Maturitas* 2011, *68*, 233–244.

[14] Gonzales, P. A., Pisitkun, T., Hoffert, J. D., Tchapyjnikov, D. et al., Large-scale proteomics and phosphoproteomics of urinary exosomes. *J. Am. Soc. Nephrol.* 2009, *20*, 363–379.

[15] Kentsis, A., Monigatti, F., Dorff, K., Campagne, F. et al., Urine proteomics for profiling of human disease using high accuracy mass spectrometry. *Proteomics Clin. Appl.* 2009, *3*, 1052–1061.

[16] Zürbig, P., Mischak, H., Peptidomics approach to proteomics. in: Soloviev, M., Shaw, C., Andren, P. E. (Eds.), *Peptidomics: Methods and Applications.* Wiley, Hoboken, NJ 2008, pp. 155–175.

[17] Coon, J. J., Zürbig, P., Dakna, M., Dominiczak, A. F. et al., CE-MS analysis of the human urinary proteome for biomarker discovery and disease diagnostics. *Proteomics Clin. Appl.* 2008, *2*, 964–973.

[18] Candiano, G., Santucci, L., Petretto, A., Bruschi, M. et al., 2D-electrophoresis and the urine proteome map: where do we stand? *J. Proteomics* 2010, *73*, 829–844.

[19] Mischak, H., Kolch, W., Aivalotis, M., Bouyssie, D. et al., Comprehensive human urine standards for comparability and standardization in clinical proteome analysis. *Proteomics Clin. Appl.* 2010, *4*, 464–478.

[20] Alebiosu, C. O., Ayodele, O. E., The global burden of chronic kidney disease and the way forward. *Ethn. Dis.* 2005, *15*, 418–423.

[21] Rossing, P., The changing epidemiology of diabetic microangiopathy in type 1 diabetes. *Diabetologia* 2005, *48*, 1439–1444.

[22] Thornalley, P. J., Battah, S., Ahmed, N., Karachalias, N. et al., Quantitative screening of advanced glycation endproducts in cellular and extracellular proteins by tandem mass spectrometry. *Biochem. J.* 2003, *375*, 581–592.

[23] Thornalley, P. J., Measurement of protein glycation, glycated peptides, and glycation free adducts. *Perit. Dial. Int.* 2005, *25*, 522–533.

[24] Witko-Sarsat, V., Friedlander, M., Nguyen, K. T., Capeillere-Blandin, C. et al., Advanced oxidation protein products as novel mediators of inflammation and monocyte activation in chronic renal failure. *J. Immunol.* 1998, *161*, 2524–2532.

[25] Perkins, B. A., Ficociello, L. H., Silva, K. H., Finkelstein, D. M. et al., Regression of microalbuminuria in type 1 diabetes. *N. Engl. J. Med.* 2003, *348*, 2285–2293.

[26] Stevens, L. A., Coresh, J., Schmid, C. H., Feldman, H. I. et al., Estimating GFR using serum cystatin C alone and in combination with serum creatinine: a pooled analysis of 3,418 individuals with CKD. *Am. J. Kidney Dis.* 2008, *51*, 395–406.

[27] Larsson, A., Flodin, M., Hansson, L. O., Carlsson, L., Patient selection has a strong impact on cystatin C and modifica-

© 2011 WILEY-VCH Verlag GmbH & Co. KGaA, Weinheim

tion of diet in renal disease (MDRD) estimated glomerular filtration rate. *Clin. Biochem.* 2008, *41*, 1355–1361.

[28] Prigent, A., Monitoring renal function and limitations of renal function tests. *Semin. Nucl. Med.* 2008, *38*, 32–46.

[29] Ameur, R. B., Molina, L., Bolvin, C., Kifagi, C. et al., Proteomic approaches for discovering biomarkers of diabetic nephropathy. *Nephrol. Dial. Transplant.* 2010, *25*, 2866–2875.

[30] Huang, F., Yang, Q., Chen, L., Tang, S. et al., Renal pathological change in patients with type 2 diabetes is not always diabetic nephropathy: a report of 52 cases. *Clin. Nephrol.*. 2007, *67*, 293–297.

[31] Parving, H. H., Gall, M. A., Skott, P., Jorgensen, H. E. et al., Prevalence and causes of albuminuria in non-insulin-dependent diabetic patients. *Kidney Int.* 1992, *41*, 758–762.

[32] Wong, T. Y., Choi, P. C., Szeto, C. C., To, K. F. et al., Renal outcome in type 2 diabetic patients with or without coexisting nondiabetic nephropathies. *Diabetes Care* 2002, *25*, 900–905.

[33] Jain, S., Rajput, A., Kumar, Y., Uppuluri, N. et al., Proteomic analysis of urinary protein markers for accurate prediction of diabetic kidney disorder. *J. Assoc. Physicians India* 2005, *53*, 513–520.

[34] Rao, P. V., Lu, X., Standley, M., Pattee, P. et al., Proteomic identification of urinary biomarkers of diabetic nephropathy. *Diabetes Care* 2007, *30*, 629–637.

[35] Thongboonkerd, V., Zheng, S., McLeish, K. R., Epstein, P. N., Klein, J. B., Proteomic identification and immunolocalization of increased renal calbindin-D28k expression in OVE26 diabetic mice. *Rev. Diabet. Stud.* 2005, *2*, 19–26.

[36] Varghese, S. A., Powell, T. B., Budisavljevic, M. N., Oates, J. C. et al., Urine biomarkers predict the cause of glomerular disease. *J. Am. Soc. Nephrol.* 2007, *18*, 913–922.

[37] Good, D. M., Zürbig, P., Argiles, A., Bauer, H. W. et al., Naturally occurring human urinary peptides for use in diagnosis of chronic kidney disease. *Mol. Cell. Proteomics* 2010, *9*, 2424–2437.

[38] Meier, M., Kaiser, T., Herrmann, A., Knueppel, S. et al., Identification of urinary protein pattern in type 1 diabetic adolescents with early diabetic nephropathy by a novel combined proteome analysis. *J. Diabetes Complications* 2005, *19*, 223–232.

[39] Mischak, H., Kaiser, T., Walden, M., Hillmann, M. et al., Proteomic analysis for the assessment of diabetic renal damage in humans. *Clin. Sci. (Lond)* 2004, *107*, 485–495.

[40] Rossing, K., Mischak, H., Parving, H. H., Christensen, P. K. et al., Impact of diabetic nephropathy and angiotensin II receptor blockade on urinary polypeptide patterns. *Kidney Int.* 2005, *68*, 193–205.

[41] Rossing, K., Mischak, H., Dakna, M., Zürbig, P. et al., Urinary proteomics in diabetes and CKD. *J. Am. Soc. Nephrol.* 2008, *19*, 1283–1290.

[42] Alkhalaf, A., Zurbig, P., Bakker, S. J., Bilo, H. J. et al., Multicentric validation of proteomic biomarkers in urine specific for diabetic nephropathy. *PLoS ONE* 2010, *5*, e13421.

[43] Rossing, K., Mischak, H., Rossing, P., Schanstra, J. P. et al., The urinary proteome in diabetes and diabetes-associated complications: new ways to assess disease progression and evaluate therapy. *Proteomics Clin. Appl.* 2008, *2*, 997–1007.

[44] Kafienah, W., Buttle, D. J., Burnett, D., Hollander, A. P., Cleavage of native type I collagen by human neutrophil elastase. *Biochem. J.* 1998, *330*, 897–902.

[45] Thongboonkerd, V., Barati, M. T., McLeish, K. R., Benarafa, C. et al., Alterations in the renal elastin-elastase system in type 1 diabetic nephropathy identified by proteomic analysis. *J. Am. Soc. Nephrol.* 2004, *15*, 650–662.

[46] Zimmerli, L. U., Schiffer, E., Zürbig, P., Kellmann, M. et al., Urinary proteomics biomarkers in coronary artery disease. *Mol. Cell. Proteomics* 2008, *7*, 290–298.

[47] von Zur Muhlen, C., Schiffer, E., Zuerbig, P., Kellmann, M. et al., Evaluation of urine proteome pattern analysis for its potential to reflect coronary artery atherosclerosis in symptomatic patients. *J. Proteome Res.* 2009, *8*, 335–345.

[48] Kalela, A., Koivu, T. A., Sisto, T., Kanervisto, J. et al., Serum matrix metalloproteinase-9 concentration in angiographically assessed coronary artery disease. *Scand. J. Clin. Lab. Invest.* 2002, *62*, 337–342.

[49] Tayebjee, M. H., Tan, K. T., MacFadyen, R. J., Lip, G. Y., Abnormal circulating levels of metalloprotease 9 and its tissue inhibitor 1 in angiographically proven peripheral arterial disease: relationship to disease severity. *J. Intern. Med.* 2005, *257*, 110–116.

[50] de Nooijer, R., Verkleij, C. J., von der Thusen, J. H., Jukema, J. W. et al., Lesional overexpression of matrix metalloproteinase-9 promotes intraplaque hemorrhage in advanced lesions but not at earlier stages of atherogenesis. *Arterioscler. Thromb. Vasc. Biol.* 2006, *26*, 340–346.

[51] Han, S. Y., Jee, Y. H., Han, K. H., Kang, Y. S. et al., An imbalance between matrix metalloproteinase-2 and tissue inhibitor of matrix metalloproteinase-2 contributes to the development of early diabetic nephropathy. *Nephrol. Dial. Transplant.* 2006, *21*, 2406–2416.

[52] Cheng, S., Pollock, A. S., Mahimkar, R., Olson, J. L., Lovett, D. H., Matrix metalloproteinase 2 and basement membrane integrity: a unifying mechanism for progressive renal injury. *FASEB J.* 2006, *20*, 1898–1900.

[53] Otu, H. H., Can, H., Spentzos, D., Nelson, R. G. et al., Prediction of diabetic nephropathy using urine proteomic profiling 10 years prior to development of nephropathy. *Diabetes Care* 2007, *30*, 638–643.

[54] Merchant, M. L., Perkins, B. A., Boratyn, G. M., Ficociello, L. H. et al., Urinary peptidome may predict renal function decline in type 1 diabetes and microalbuminuria. *J. Am. Soc. Nephrol.* 2009, *20*, 2065–2074.

[55] Andersen, S., Mischak, H., Zurbig, P., Parving, H. H., Rossing, P., Urinary proteome analysis enables assessment of renoprotective treatment in type 2 diabetic patients with microalbuminuria. *BMC Nephrol.* 2010, *11*, 29.

[56] Coca, S. G., Yusuf, B., Shlipak, M. G., Garg, A. X., Parikh, C. R., Long-term risk of mortality and other adverse

© 2011 WILEY-VCH Verlag GmbH & Co. KGaA, Weinheim

outcomes after acute kidney injury: a systematic review and meta-analysis. *Am. J. Kidney Dis.* 2009, *53*, 961–973.

[57] Choudhury, D., Acute kidney injury: current perspectives. *Postgrad. Med.* 2010, *122*, 29–40.

[58] Bellomo, R., Defining, quantifying, and classifying acute renal failure. *Crit. Care Clin.* 2005, *21*, 223–237.

[59] Han, W. K., Waikar, S. S., Johnson, A., Betensky, R. A. et al., Urinary biomarkers in the early diagnosis of acute kidney injury. *Kidney Int.* 2008, *73*, 863–869.

[60] Herget-Rosenthal, S., Marggraf, G., Husing, J., Goring, F. et al., Early detection of acute renal failure by serum cystatin C. *Kidney Int.* 2004, *66*, 1115–1122.

[61] Mishra, J., Dent, C., Tarabishi, R., Mitsnefes, M. M. et al., Neutrophil gelatinase-associated lipocalin (NGAL) as a biomarker for acute renal injury after cardiac surgery. *Lancet* 2005, *365*, 1231–1238.

[62] Parikh, C. R., Abraham, E., Ancukiewicz, M., Edelstein, C. L., Urine IL-18 is an early diagnostic marker for acute kidney injury and predicts mortality in the intensive care unit. *J. Am. Soc. Nephrol.* 2005, *16*, 3046–3052.

[63] Haase, M., Bellomo, R., Story, D., Davenport, P., Haase-Fielitz, A., Urinary interleukin-18 does not predict acute kidney injury after adult cardiac surgery: a prospective observational cohort study. *Crit. Care* 2008, *12*, R96.

[64] Han, W. K., Wagener, G., Zhu, Y., Wang, S., Lee, H. T., Urinary biomarkers in the early detection of acute kidney injury after cardiac surgery. *Clin. J. Am. Soc. Nephrol.* 2009, *4*, 873–882.

[65] Koyner, J. L., Bennett, M. R., Worcester, E. M., Ma, Q. et al., Urinary cystatin C as an early biomarker of acute kidney injury following adult cardiothoracic surgery. *Kidney Int.* 2008, *74*, 1059–1069.

[66] Wagener, G., Gubitosa, G., Wang, S., Borregaard, N. et al., Urinary neutrophil gelatinase-associated lipocalin and acute kidney injury after cardiac surgery. *Am. J. Kidney Dis.* 2008, *52*, 425–433.

[67] Zhou, H., Pisitkun, T., Aponte, A., Yuen, P. S. et al., Exosomal fetuin-A identified by proteomics: a novel urinary biomarker for detecting acute kidney injury. *Kidney Int.* 2006, *69*(*8*), 1471–1476.

[68] Metzger, J., Kirsch, T., Schiffer, E., Ulger, P. et al., Urinary excretion of twenty peptides forms an early and accurate diagnostic pattern of acute kidney injury. *Kidney Int.* 2010, *78*, 1252–1262.

[69] Paraskevas, S., Kandaswamy, R., Humar, A., Gillingham, K. J. et al., Risk factors for rising creatinine in renal allografts with 1 and 3 yr survival. *Clin. Transplant.* 2006, *20*, 667–672.

[70] Nankivell, B. J., Borrows, R. J., Fung, C. L., O'Connell, P. J. et al., Natural history, risk factors, and impact of subclinical rejection in kidney transplantation. *Transplantation* 2004, *78*, 242–249.

[71] Gwinner, W., Renal transplant rejection markers. *World J. Urol.* 2007, *25*, 445–455.

[72] Rush, D. N., Nickerson, P., Jeffery, J. R., McKenna, R. M. et al., Protocol biopsies in renal transplantation: research tool or clinically useful? *Curr. Opin. Nephrol. Hypertens.* 1998, *6*, 691–694.

[73] Platt, R. E., Wu, K. S., Poole, K., Newstead, C. G., Clark, B., Soluble CD30 as a prognostic factor for outcome following renal transplantation. *J. Clin. Pathol.* 2009, *62*, 662–663.

[74] Simon, R., Radmacher, M. D., Dobbin, K., McShane, L. M., Pitfalls in the use of DNA microarray data for diagnostic and prognostic classification. *J. Natl. Cancer Inst.* 2003, *95*, 14–18.

[75] Muthukumar, T., Dadhania, D., Ding, R., Snopkowski, C. et al., Messenger RNA for FOXP3 in the urine of renal-allograft recipients. *N. Engl. J. Med.* 2005, *353*, 2342–2351.

[76] Clarke, W., Silverman, B. C., Zhang, Z., Chan, D. W. et al., Characterization of renal allograft rejection by urinary proteomic analysis. *Ann. Surg.* 2003, *237*, 660–664.

[77] Schaub, S., Rush, D., Wilkins, J., Gibson, I. W. et al., Proteomic-based detection of urine proteins associated with acute renal allograft rejection. *J. Am. Soc. Nephrol.* 2004, *15*, 219–227.

[78] Wittke, S., Haubitz, M., Walden, M., Rohde, F. et al., Detection of acute tubulointerstitial rejection by proteomic analysis of urinary samples in renal transplant recipients. *Am. J. Transplant.* 2005, *5*, 2479–2488.

[79] Sigdel, T., Kaushal, A., Gritsenko, M., Norbeck, A. et al., Shotgun proteomics identifies proteins specific for acute renal transplant rejection. *Proteomics Clin. Appl.* 2010, *4*, 32–47.

[80] Ling, X. B., Sigdel, T. K., Lau, K., Ying, L. et al., Integrative urinary peptidomics in renal transplantation identifies biomarkers for acute rejection. *J. Am. Soc. Nephrol.* 2010, *21*, 646–653.

[81] Gwinner, W., Hinzmann, K., Erdbruegger, U., Scheffner, I. et al., Acute tubular injury in protocol biopsies of renal grafts: prevalence, associated factors and effect on long-term function. *Am. J. Transplant.* 2008, *8*, 1684–1693.

[82] Schaub, S., Wilkins, J. A., Antonovici, M., Krokhin, O. et al., Proteomic-based identification of cleaved urinary beta2-microglobulin as a potential marker for acute tubular injury in renal allografts. *Am. J. Transplant.* 2005, *5*, 729–738.

[83] Metzger, J., Chatzikyrkou, C., Broecker, V., Schiffer, E. et al., Diagnosis of subclinical and clinical acute T-cell mediated rejection in renal transplant patients by urinary proteome analysis. *Proteomics Clin. Appl.* 2011 (in press).

[84] Khatwa, U. A., Kleibrink, B. E., Shapiro, S. D., Subramaniam, M., MMP-8 promotes polymorphonuclear cell migration through collagen barriers in obliterative bronchiolitis. *J. Leukoc. Biol.* 2010, *87*, 69–77.

[85] Faveeuw, C., Preece, G., Ager, A., Transendothelial migration of lymphocytes across high endothelial venules into lymph nodes is affected by metalloproteinases. *Blood* 2001, *98*, 688–695.

[86] Gronberg, H., Prostate cancer epidemiology. *Lancet* 2003, *361*, 859–864.

© 2011 WILEY-VCH Verlag GmbH & Co. KGaA, Weinheim

[87] Stamey, T. A., Yang, N., Hay, A. R., McNeal, J. E. et al., Prostate-specific antigen as a serum marker for adenocarcinoma of the prostate. *N. Engl. J. Med.* 1987, *317*, 909–916.

[88] Schroder, F. H., Hugosson, J., Roobol, M. J., Tammela, T. L. et al., Screening and prostate-cancer mortality in a randomized European study. *N. Engl. J. Med.* 2009, *360*, 1320–1328.

[89] Presti, J. C., Jr., Prostate cancer: assessment of risk using digital rectal examination, tumor grade, prostate-specific antigen, and systematic biopsy. *Radiol. Clin. North Am.* 2000, *38*, 49–58.

[90] Siddiqui, E., Mumtaz, F. H., Gelister, J., Understanding prostate cancer. *J. R. Soc. Promot. Health* 2004, *124*, 219–221.

[91] Bickers, B., Aukim-Hastie, C., New molecular biomarkers for the prognosis and management of prostate cancer – the post PSA era. *Anticancer Res.* 2009, *29*, 3289–3298.

[92] You, J., Cozzi, P., Walsh, B., Willcox, M. et al., Innovative biomarkers for prostate cancer early diagnosis and progression. *Crit. Rev. Oncol. Hematol.* 2010, *73*, 10–22.

[93] Rehman, I., Azzouzi, A. R., Catto, J. W., Allen, S. et al., Proteomic analysis of voided urine after prostatic massage from patients with prostate cancer: a pilot study. *Urology* 2004, *64*, 1238–1243.

[94] M'koma, A. E., Blum, D. L., Norris, J. L., Koyama, T. et al., Detection of pre-neoplastic and neoplastic prostate disease by MALDI profiling of urine. *Biochem. Biophys. Res. Commun.* 2006, *353*, 829–834.

[95] Theodorescu, D. A, Schiffer, E., Bauer, H. W., Douwes, F. et al., Discovery and validation of urinary biomarkers for prostate cancer. *Proteomics Clin. Appl.* 2008, *2*, 556–570.

[96] Obiezu, C. V., Shan, S. J., Soosaipillai, A., Luo, L. Y. et al., Human kallikrein 4: quantitative study in tissues and evidence for its secretion into biological fluids. *Clin. Chem.* 2005, *51*, 1432–1442.

[97] Acevedo, B., Perera, Y., Torres, E., Penton, D. et al., Fast and novel purification method to obtain the prostate specific antigen (PSA) from human seminal plasma. *Prostate* 2006, *66*, 1029–1036.

[98] Dinney, C. P., McConkey, D. J., Millikan, R. E., Wu, X. et al., Focus on bladder cancer. *Cancer Cell* 2004, *6*, 111–116.

[99] Sylvester, R. J., Natural history, recurrence, and progression in superficial bladder cancer. *Scientific World J.* 2006, *6*, 2617–2625.

[100] Cajulis, R. S., Haines,G. K. III, Frias-Hidvegi, D., McVary, K., Bacus, J. W., Cytology, flow cytometry, image analysis, and interphase cytogenetics by fluorescence in situ hybridization in the diagnosis of transitional cell carcinoma in bladder washes: a comparative study. *Diagn. Cytopathol.* 1995, *13*, 214–223.

[101] Latini, D. M., Lerner, S. P., Wade, S. W., Lee, D. W., Quale, D. Z., Bladder cancer detection, treatment and outcomes: opportunities and challenges. *Urology* 2010, *75*, 334–339.

[102] Goodison, S., Rosser, C. J., Urquidi, V., Urinary proteomic profiling for diagnostic bladder cancer biomarkers. *Expert. Rev. Proteomics* 2009, *6*, 507–514.

[103] Herman, M. P., Svatek, R. S., Lotan, Y., Karakiewizc, P. I., Shariat, S. F., Urine-based biomarkers for the early detection and surveillance of non-muscle invasive bladder cancer. *Minerva Urol. Nefrol.* 2008, *60*, 217–235.

[104] Getzenberg, R. H., Konety, B. R., Oeler, T. A., Quigley, M. M. et al., Bladder cancer-associated nuclear matrix proteins. *Cancer Res.* 1996, *56*, 1690–1694.

[105] Konety, B. R., Nguyen, T. S., Brenes, G., Sholder, A. et al., Clinical usefulness of the novel marker BLCA-4 for the detection of bladder cancer. *J. Urol.* 2000, *164*, 634–639.

[106] Nielsen, M. E., Gonzalgo, M. L., Schoenberg, M. P., Getzenberg, R. H., Toward critical evaluation of the role(s) of molecular biomarkers in the management of bladder cancer. *World J. Urol.* 2006, *24*, 499–508.

[107] Van Le, T. S., Miller, R., Barder, T., Babjuk, M. et al., Highly specific urine-based marker of bladder cancer. *Urology* 2005, *66*, 1256–1260.

[108] Schiffer, E., Mischak, H., Theodorescu, D., Vlahou, A., Challenges of using mass spectrometry as a bladder cancer biomarker discovery platform. *World J. Urol.* 2008, *26*, 67–74.

[109] Celis, J. E., Ostergaard, M., Basse, B., Celis, A. et al., Loss of adipocyte-type fatty acid binding protein and other protein biomarkers is associated with progression of human bladder transitional cell carcinomas. *Cancer Res.* 1996, *56*, 4782–4790.

[110] Iwaki, H., Kageyama, S., Isono, T., Wakabayashi, Y. et al., Diagnostic potential in bladder cancer of a panel of tumor markers (calreticulin, gamma -synuclein, and catechol-o-methyltransferase) identified by proteomic analysis. *Cancer Sci.* 2004, *95*, 955–961.

[111] Orenes-Pinero, E., Corton, M., Gonzalez-Peramato, P., Algaba, F. et al., Searching urinary tumor markers for bladder cancer using a two-dimensional differential gel electrophoresis (2D-DIGE) approach. *J. Proteome Res.* 2007, *6*, 4440–4448.

[112] Astrosini, C., Roeefzaad, C., Dai, Y. Y., Dieckgraefe, B. K. et al., REG1A expression is a prognostic marker in colorectal cancer and associated with peritoneal carcinomatosis. *Int. J. Cancer* 2008, *123*, 409–413.

[113] Minamiya, Y., Kawai, H., Saito, H., Ito, M. et al., REG1A expression is an independent factor predictive of poor prognosis in patients with non-small cell lung cancer. *Lung Cancer* 2008, *60*, 98–104.

[114] Mueller, J., von Eggeling, F., Driesch, D., Schubert, J. et al., ProteinChip technology reveals distinctive protein expression profiles in the urine of bladder cancer patients. *Eur. Urol.* 2005, *47*, 885–893.

[115] Vlahou, A., Schellhammer, P. F., Mendrinos, S., Patel, K. et al., Development of a novel proteomic approach for the detection of transitional cell carcinoma of the bladder in urine. *Am. J. Pathol.* 2001, *158*, 1491–1502.

[116] Vlahou, A., Giannopoulos, A., Gregory, B. W., Manousakas, T. et al., Protein profiling in urine for the diagnosis of bladder cancer. *Clin. Chem.* 2004, *50*, 1438–1441.

© 2011 WILEY-VCH Verlag GmbH & Co. KGaA, Weinheim

[117] Munro, N. P., Cairns, D. A., Clarke, P., Rogers, M. et al., Urinary biomarker profiling in transitional cell carcinoma. *Int. J. Cancer* 2006, *119*, 2642–2650.

[118] Zhang, Y. F., Wu, D. L., Guan, M., Liu, W. W. et al., Tree analysis of mass spectral urine profiles discriminates transitional cell carcinoma of the bladder from noncancer patient. *Clin. Biochem.* 2004, *37*, 772–779.

[119] Liu, W., Guan, M., Wu, D., Zhang, Y. et al., Using tree analysis pattern and SELDI-TOF-MS to discriminate transitional cell carcinoma of the bladder cancer from noncancer patients. *Eur. Urol.* 2005, *47*, 456–462.

[120] Holterman, D. A., Diaz, J. I., Blackmore, P. F., Davis, J. W. et al., Overexpression of alpha-defensin is associated with bladder cancer invasiveness. *Urol. Oncol.* 2006, *24*, 97–108.

[121] Theodorescu, D., Wittke, S., Ross, M. M., Walden, M. et al., Discovery and validation of new protein biomarkers for urothelial cancer: a prospective analysis. *Lancet Oncol.* 2006, *7*, 230–240.

[122] Schiffer, E., Vlahou, A., Petrolekas, A., Stravodimos, K. et al., Prediction of muscle-invasive bladder cancer using urinary proteomics. *Clin. Cancer Res.* 2009, *15*, 4935–4943.

[123] Smith, M. P., Banks, R. E., Wood, S. L., Lewington, A. J., Selby, P. J., Application of proteomic analysis to the study of renal diseases. *Nat. Rev. Nephrol.* 2009, *5*, 701–712.

[124] Brennan, D. J., O'Connor, D. P., Rexhepaj, E., Ponten, F., Gallagher, W. M., Antibody-based proteomics: fast-tracking molecular diagnostics in oncology. *Nat. Rev. Cancer* 2010, *10*, 605–617.

[125] Makawita, S., Diamandis, E. P., The bottleneck in the cancer biomarker pipeline and protein quantification through mass spectrometry-based approaches: current strategies for candidate verification. *Clin. Chem.* 2010, *56*, 212–222.

[126] Amin, W., Parwani, A. V., Schmandt, L., Mohanty, S. K. et al., National Mesothelioma Virtual Bank: a standard based biospecimen and clinical data resource to enhance translational research. *BMC Cancer* 2008, *8*, 236.

[127] Langseth, H., Luostarinen, T., Bray, F., Dillner, J., Ensuring quality in studies linking cancer registries and biobanks. *Acta Oncol.* 2010, *49*, 368–377.

[128] Molina, F., Dehmer, M., Perco, P., Graber, A. et al., Systems biology: opening new avenues in clinical research. *Nephrol. Dial. Transplant.* 2010, *25*, 1015–1018.

[129] Spahr, C. S., Davis, M. T., McGinley, M. D., Robinson, J. H. et al., Towards defining the urinary proteome using liquid chromatography-tandem mass spectrometry. I. Profiling an unfractionated tryptic digest. *Proteomics* 2001, *1*, 93–107.

[130] Pang, J. X., Ginanni, N., Dongre, A. R., Hefta, S. A., Opitek, G. J., Biomarker discovery in urine by proteomics. *J. Proteome Res.* 2002, *1*, 161–169.

[131] Pieper, R., Gatlin, C. L., McGrath, A. M., Makusky, A. J. et al., Characterization of the human urinary proteome: a method for high-resolution display of urinary proteins on two-dimensional electrophoresis gels with a yield of nearly 1400 distinct protein spots. *Proteomics* 2004, *4*, 1159–1174.

[132] Oh, J., Pyo, J. H., Jo, E. H., Hwang, S. I. et al., Establishment of a near-standard two-dimensional human urine proteomic map. *Proteomics* 2004, *4*, 3485–3497.

[133] Thongboonkerd, V., McLeish, K. R., Arthur, J. M., Klein, J. B., Proteomic analysis of normal human urinary proteins isolated by acetone precipitation or ultracentrifugation. *Kidney Int.* 2002, *62*, 1461–1469.

[134] Zerefos, P. G., Vougas, K., Dimitraki, P., Kossida, S. et al., Characterization of the human urine proteome by preparative electrophoresis in combination with 2-DE. *Proteomics* 2006, *6*, 4346–4355.

[135] Smith, G., Barratt, D., Rowlinson, R., Nickson, J., Tonge, R., Development of a high-throughput method for preparing human urine for two-dimensional electrophoresis. *Proteomics* 2005, *5*, 2315–2318.

[136] Castagna, A., Cecconi, D., Sennels, L., Rappsilber, J. et al., Exploring the hidden human urinary proteome via ligand library beads. *J. Proteome Res.* 2005, *4*, 1917–1930.

[137] Adachi, J., Kumar, C., Zhang, Y., Olsen, J. V., Mann, M., The human urinary proteome contains more than 1500 proteins including a large proportion of membranes proteins. *Genome Biol.* 2006, *7*, R80.1–R80.16.

© 2011 WILEY-VCH Verlag GmbH & Co. KGaA, Weinheim

Biochemical and Biophysical Research Communications 424 (2012) 629–634

Contents lists available at SciVerse ScienceDirect

Biochemical and Biophysical Research Communications

journal homepage: www.elsevier.com/locate/ybbrc

Isolation and characterizations of oxalate-binding proteins in the kidney

Piyachat Roop-ngam, Sakdithep Chaiyarit, Nutkridta Pongsakul, Visith Thongboonkerd *

Medical Proteomics Unit, Office for Research and Development, Faculty of Medicine Siriraj Hospital, and Center for Research in Complex Systems Science, Mahidol University, Bangkok, Thailand

ARTICLE INFO

Article history:
Received 4 July 2012
Available online 14 July 2012

Keywords:
Kidney stone
Nephrolithiasis
Oxalate
Oxalate-binding
Proteins
Proteomics

ABSTRACT

Oxalate-binding proteins are thought to serve as potential modulators of kidney stone formation. However, only few oxalate-binding proteins have been identified from previous studies. Our present study, therefore, aimed for large-scale identification of oxalate-binding proteins in porcine kidney using an oxalate-affinity column containing oxalate-conjugated EAH Sepharose 4B beads for purification followed by two-dimensional gel electrophoresis (2-DE) to resolve the recovered proteins. Comparing with those obtained from the controlled column containing uncoupled EAH-Sepharose 4B (to subtract the background of non-specific bindings), a total of 38 protein spots were defined as oxalate-binding proteins. These protein spots were successfully identified by quadrupole time-of-flight mass spectrometry (MS) and/or tandem MS (MS/MS) as 26 unique proteins, including several nuclear proteins, mitochondrial proteins, oxidative stress regulatory proteins, metabolic enzymes and others. Identification of oxalate-binding domain using the PRATT tool revealed "*L-x(3,5)-R-x(2)-[AGILPV]*" as a functional domain responsible for oxalate-binding in 25 of 26 (96%) unique identified proteins. We report herein, for the first time, large-scale identification and characterizations of oxalate-binding proteins in the kidney. The presence of positively charged arginine residue in the middle of this functional domain suggested its significance for binding to the negatively charged oxalate. These data will enhance future stone research, particularly on stone modulators.

© 2012 Elsevier Inc. All rights reserved.

1. Introduction

Recently, kidney stone disease has been investigated extensively at the molecular level. Among all stone types, calcium oxalate (CaOx) is the most common inorganic matrix found in kidney stones [1]. In addition to inorganic matrix, organic compounds, particularly proteins, are also found in kidney stones [2]. Many previous studies have focused on identification of CaOx kidney stone modulators and proposed that some of the calcium- and oxalate-binding proteins may serve as the stone modulators [3–6]. From these efforts, some of calcium-binding proteins that have inhibitory activity against CaOx crystal growth and aggregation have been successfully identified [7–12]. On the other hand, a much fewer number of previous studies have attempted to characterize oxalate-binding proteins, which also have potential role in kidney stone disease [6]. A number of oxalate-binding proteins have been isolated from kidney homogenate and stone matrix [6]. Among these, only histone has been successfully identified and characterized [13]. This under-investigation is probably due to a lack of simple method for isolation of oxalate-binding proteins in the past.

We have recently developed an oxalate-affinity chromatographic column for highly efficient and simplified isolation/purification of oxalate-binding proteins [14]. In the present study, our oxalate-affinity chromatographic column containing oxalate-conjugated EAH Sepharose 4B beads was applied to purify oxalate-binding proteins from porcine kidney. The recovered proteins were resolved by 2-DE compared to those recovered from the controlled column containing unconjugated EAH-Sepharose 4B (to subtract the background of non-specific bindings). The oxalate-binding proteins were then identified by Q-TOF MS and/or MS/MS analyses. Finally, the identified proteins were subjected to identification of functional domain responsible for oxalate-binding.

2. Materials and methods

2.1. Preparation of oxalate-affinity chromatographic column

The oxalate-affinity chromatographic column was prepared as we described previously [14]. In principle, oxalic acid was conjugated (through carboxylic groups) to EAH Sepharose 4B (via primary amine groups). Coupling efficacy was determined quantitatively

* Corresponding author. Address: Head of Medical Proteomics Unit, Director of Center for Research in Complex Systems Science (CRCSS), Siriraj Hospital, Mahidol University, 10th Floor Srisawarinthira Building, 2 Prannok Road, Bangkoknoi, Bangkok 10700, Thailand. Fax: +66 2 4195503.
E-mail addresses: vthongbo@yahoo.com, thongboonkerd@dr.com (V. Thongboonkerd).

0006-291X/$ - see front matter © 2012 Elsevier Inc. All rights reserved.
http://dx.doi.org/10.1016/j.bbrc.2012.07.015

by measuring the remaining primary amine groups on EAH-Sepharose 4B beads using a competitive nindydrin assay [14]. For the controlled column, EAH Sepharose 4B beads were treated and processed with similar procedures as for the oxalate-affinity column, but without oxalic acid conjugation.

2.2. Isolation of oxalate-binding proteins from porcine kidney

A porcine kidney was bought from a local fresh poultry market. The tissue was then dissected into thin slices, washed with phosphate buffered saline (PBS), snap frozen in liquid nitrogen and ground into powder using pre-chilled mortar and pestle. Tissue powder was then resuspended in Tris–HCl buffer (pH 6.5). The kidney sample was then centrifuged at 12,000*g*, 4 °C for 5 min to remove the particulate matters. The supernatant was saved and protein concentration was measured by the Bradford method. To isolate oxalate-binding proteins, 3 mg of the recovered porcine kidney proteins was passed through the affinity column with a flow rate of 1 mL/min. Thereafter, the column was first eluted with 20 mL of a binding buffer containing 10 mM 2-morpholinoethanesulfonic acid (MES) in NaOH (pH 6.5), 150 mM NaCl, 2 mM $MgCl_2$, 2 mM $CaCl_2$, and 5 mM KCl to remove non-specific binding proteins. Oxalate-binding proteins were then eluted with 10 mL of an elution buffer containing 10 mM MES in NaOH (pH 6.5), 150 mM NaCl, 2 mM $MgCl_2$, 2 mM $CaCl_2$, 5 mM KCl, 1 M NaCl and 1 mM oxalic acid with 10 fractions (1 mL/fraction). In parallel, 3 mg of the recovered porcine kidney proteins was passed through the controlled column with a flow rate of 1 mL/min. The subsequent steps were exactly the same as for the oxalate-affinity column.

2.3. 2-DE

The eluted protein fractions obtained from the previous step were pooled, desalted by dialysis against 18 MΩ cm (dI) water, and concentrated by lyophilization. The concentrated proteins were then resuspended in 150 μl of rehydration buffer containing 7 M urea, 2 M thiourea, 2% 3-[(3-cholamidopropyl) dimethylammonio]-1-propanesulfonate (CHAPS), 120 mM dithiothreitol (DTT), 2% ampholytes (pH 3–10), 40 mM Tris–HCl, and a trace amount of bromophenol blue. The protein solution was then rehydrated overnight in an Immobiline™ DryStrip, non-linear pH 3–10 (GE Healthcare Bio-Sciences, Uppsala, Sweden). Thereafter, the isoelectric focusing (IEF) was run in Ettan IPGphor III IEF System (GE Healthcare Bio-Sciences) at 20 °C, using a stepwise mode to reach 9083 V h with a current limit of 50 μA/strip. After the IEF completion, proteins on the strip were equilibrated in a buffer containing 6 M urea, 130 mM DTT, 30% glycerol, 112 mM Tris-base, 4% SDS and 0.002% bromophenol blue for 15 min, and then with another buffer containing 6 M urea, 135 mM iodoacetamide, 30% glycerol, 112 mM Tris-base, 4% SDS and 0.002% bromophenol blue for 10 min. For the second dimension, the proteins on the IPG strip were resolved further in 12% polyacrylamide slab gel (8×9.5 cm) using the SE260 Mini-Vertical Electrophoresis Unit (GE Healthcare Bio-Sciences) with a constant voltage of 150 V for 2 h. The resolved protein spots were stained with SYPRO Ruby fluorescence dye (Invitrogen-Molecular Probes; Eugene, OR) and visualized with Typhoon laser scanner (GE Healthcare).

2.4. Spot matching and quantitative intensity analysis

Image Master 2D Platinum (GE Healthcare) software was used for matching and analysis of protein spots in 2-D gels. Parameters used for spot detection were (i) minimal area = 10 pixels; (ii) smooth factor = 2.0; and (iii) saliency = 2.0. A reference gel used for matching the corresponding protein spots among different gels was created from an artificial gel by combining all of the spots presenting in different gels into one image. Background subtraction was performed and the intensity volume of each spot was normalized with total intensity volume (summation of the intensity volumes obtained from all spots within the same 2-D gel). Differentially expressed protein spots were defined as those, which were present only in the sample derived from oxalate-affinity chromatographic column or had intensity levels > 3-fold as compared to those obtained from the controlled column. These differentially expressed protein spots were excised and subjected to in-gel tryptic digestion and identification by Q-TOF MS and MS/MS analyses.

2.5. In-gel tryptic digestion

The excised protein spots were washed twice with 200 μL of 50% acetonitrile (ACN)/25 mM NH_4HCO_3 buffer (pH 8.0) at room temperature for 15 min, and then washed once with 200 μL of 100% ACN. After washing, the solvent was removed, and the gel pieces were dried by a SpeedVac concentrator (Savant; Holbrook, NY) and rehydrated with 10 μL of 1% (w/v) trypsin (Promega; Madison, WI) in 25 mM NH_4HCO_3. After rehydration, the gel pieces were crushed and incubated at 37 °C for at least 16 h. Peptides were subsequently extracted twice with 50 μL of 50% ACN/5% trifluoroacetic acid (TFA); the extracted solutions were then combined and dried with the SpeedVac concentrator. The peptide pellets were resuspended with 10 μL of 0.1% TFA and purified using $ZipTip_{C18}$ (Millipore; Bedford, MA). The peptide solution was drawn up and down in the $ZipTip_{C18}$ 10 times and then washed with 10 μL of 0.1% formic acid by drawing up and expelling the washing solution three times. The peptides were finally eluted with 5 μL of 75% ACN/0.1% formic acid.

2.6. Protein identification by Q-TOF MS and MS/MS analyses

The trypsinized samples were premixed 1:1 with the matrix solution containing 5 mg/mL α-cyano-4-hydroxycinnamic acid (CHCA) in 50% ACN, 0.1% (v/v) TFA and 2% (w/v) ammonium citrate, and deposited onto the 96-well MALDI target plate. The samples were analyzed by Q-TOF Ultima™ mass spectrometer (Micromass; Manchester, UK), which was fully automated with predefined probe motion pattern and the peak intensity threshold for switching over from MS survey scanning to MS/MS, and from one MS/MS to another. Within each sample well, parent ions that met the predefined criteria (any peak within the *m/z* 800–3000 range with intensity above 10 count ± include/exclude list) were selected for CID MS/MS using argon as the collision gas and a mass dependent ± 5 V rolling collision energy until the end of the probe pattern was reached. The MS and MS/MS data were extracted and outputted as the searchable *.txt* and *.pkl* files, respectively, for independent searches using the MASCOT search engine (http://www.matrixscience.com) to query to the NCBI mammalian protein database, assuming that peptides were monoisotopic. Fixed modification was carbamidomethylation at cysteine residues, whereas variable modification was oxidation at methionine residues. Only one missed trypsin cleavage was allowed, and peptide mass tolerances of 100 and 50 ppm were allowed for peptide mass fingerprinting and MS/MS ions search, respectively.

2.7. Identification of oxalate-binding domain

The PRATT tool (http://www.ebi.ac.uk/Tools/pratt/) [15,16], provided by the European Bioinformatics Institute (EBI) was used for characterization of the functional domain in the identified oxalate-binding proteins. All the proteins identified by Q-TOF MS and/or MS/MS analyses (in FASTA format) were altogether aligned and

subjected to the unbiased opened search (without any restrictions or predefined pattern) to define the functional domain responsible for oxalate-binding. After obtaining oxalate-binding domain, sequences of some of the known kidney proteins, which are not the oxalate-binding proteins (see their identities in *Supplementary* Table S1), were submitted to search for such functional domain (to demonstrate the specificity of the identification of the oxalate-binding domain).

3. Results & discussion

The efficacy and specificity of the oxalate-affinity chromatographic column were confirmed in our previous study [14] using the known oxalate-binding protein p62 [17] as the positive control and carbonic anhydrase as the negative control. The extracted porcine kidney proteins were then passed through the oxalate-affinity column to isolate oxalate-binding proteins. In parallel, the proteins were passed through the controlled column to subtract the background of non-specific bindings. The eluate fractions from each column were pooled, and the recovered proteins were resolved by 2-DE and visualized by SYPRO Ruby staining. Using the Image Master 2D Platinum software to match and quantify protein spots across different gels, a total of 38 protein spots were defined as differentially expressed spots between the two groups (Fig. 1). All of these potential oxalate-binding proteins were successfully identified by Q-TOF MS and/or MS/MS analyses as 26 unique proteins. Note that some of them had many isoforms and were thus identified as one unique protein. Details of their identities, identification numbers, identification scores, percentage of sequence coverage (%Cov), numbers of matched peptides, isoelectric points (pI) and molecular weights (MW) are summarized in Table 1.

All the identified proteins were subjected to characterization of oxalate-binding domain using the PRATT tool (http://www.ebi.ac.uk/Tools/pratt/) [15,16], provided by the European Bioinformatics Institute (EBI). The data revealed a domain/pattern "L-x(3,5)-R-x(2)-[AGILPV]" in 25 of 26 (approximately 96%) unique proteins identified by Q-TOF MS and/or MS/MS analyses (Fig. 2). Among these 25 proteins with oxalate-binding domain, 15 proteins had more than one oxalate-binding domain in their sequences, and the greatest number of this domain in each protein was 19, which was found in the sequence of transformation/transcription domain-associated protein isoform 2 (spot #38). Interestingly, the presence of positively charged arginine residue in the middle of this functional domain suggested its significance for binding to the negatively charged oxalate. To demonstrate the specificity of this oxalate-binding domain, sequences of some of the known kidney proteins, which are not oxalate-binding proteins (see their identities in *Supplementary* Table S1), were also submitted to the PRATT tool to search for such functional domain. The data revealed that none of these non-oxalate-binding kidney proteins had the domain "*L-x(3,5)-R-x(2)-[AGILPV]*" in their sequences (*Supplementary* Table S1). These data implicate the specificity of this functional domain, which is responsible for oxalate-binding.

The present study identified histone H2A (spot #14) as one of the nuclear oxalate-binding proteins in porcine kidney, consistent to the data reported in a previous study demonstrating that histone serves as a known oxalate-binding protein in kidney homogenate and stone matrix [13]. These concordant results strengthened that our oxalate-affinity chromatographic column is reliable and effective for isolation and enrichment of oxalate-binding proteins. In previous studies, one third of oxalate-binding proteins have been found in mitochondria of renal cells [6]. There were a number of mitochondrial oxalate-binding proteins identified in this study, including mitochondrial precursor of ATP synthase subunit beta (spot #13), mitochondrial Aacyl-CoA dehydrogenase (spot #19), mitochondrial NADH:ubiquinone oxidoreductase 51 kDa subunit (spot #22), and mitochondrial malate dehydrogenase 2 NAD (spot #24).

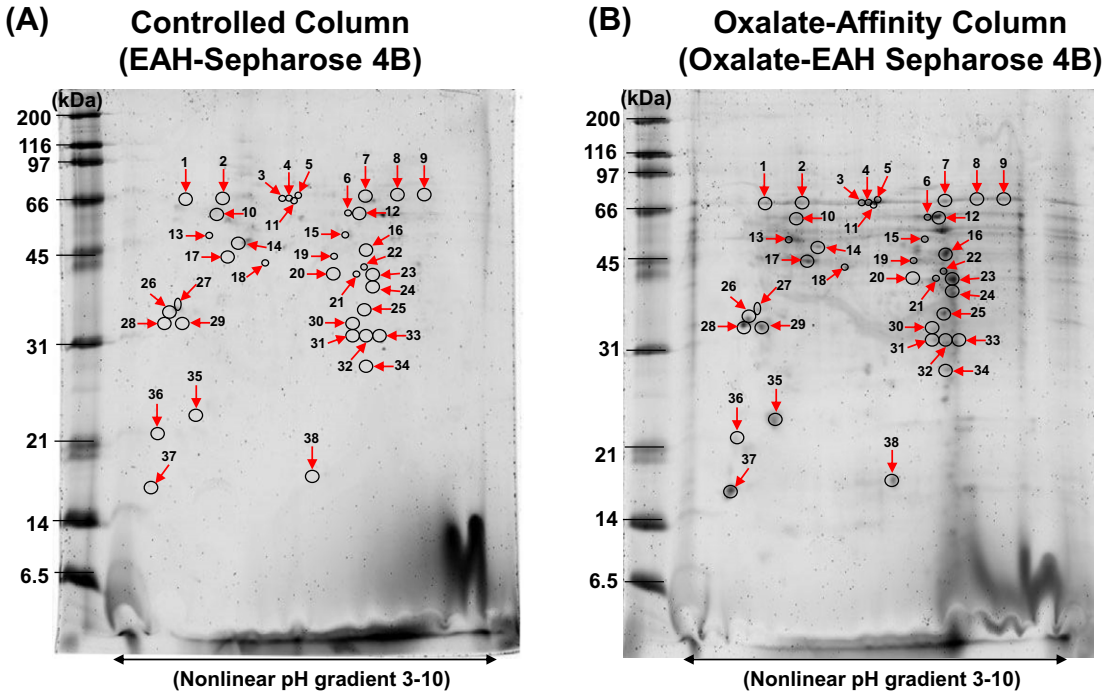


Fig. 1. 2-DE map of oxalate-binding proteins in porcine kidney. Porcine kidney proteins were passed through either controlled column containing EAH-Sepharose 4B beads (A) or oxalate-affinity column containing oxalate-conjugated EAH-Sepharose 4B beads (B). The eluate fractions from each column were pooled and the recovered proteins were resolved by 2-DE, and visualized by SYPRO Ruby staining. Protein spots that were present only in the sample derived from oxalate-affinity chromatographic column or had intensity levels > 3-fold as compared to those obtained from the controlled column were subjected to identification by Q-TOF MS and MS/MS analyses (see details in Table 1).

Table 1
Summary of oxalate-binding proteins in porcine kidney identified by Q-TOF MS and/or MS/MS analyses.

Spot No.	Protein name	NCBI ID	Identified by	Identification scores(MS, MS/MS)	%Cov (MS, MS/MS)	No. of matched peptides (MS, MS/MS)	p*I*	MW (kDa)
1	Albumin	gi|833798	MS, MS/MS	96, 24	20, 2	12, 1	5.92	71.36
2	Albumin	gi|833798	MS, MS/MS	92, 63	26, 6	13, 3	5.92	71.36
3	Albumin	gi|833798	MS, MS/MS	81, 77	22, 4	11, 2	5.92	71.36
4	Albumin	gi|833798	MS, MS/MS	123, 69	33, 4	15, 2	5.92	71.36
5	Albumin	gi|124257959	MS	105, NA	28, NA	14, NA	5.92	71.55
6	Catalase	gi|356460899	MS	114, NA	30, NA	12, NA	6.60	60.18
7	Heterogeneous nuclear ribonucleoprotein M	gi|158455026	MS	65, NA	32, NA	12, NA	9.18	58.37
8	Albumin	gi|833798	MS, MS/MS	103, 159	28, 4	14, 2	5.92	71.36
9	Albumin	gi|833798	MS	90, NA	24, NA	13, NA	5.92	71.36
10	Catalase	gi|356460899	MS	132, NA	36, NA	15, NA	6.60	60.18
11	Albumin	gi|833798	MS, MS/MS	141, 101	34, 6	16, 3	5.92	71.36
12	Catalase	gi|356460899	MS, MS/MS	125, 154	41, 13	14, 15	6.60	60.18
13	ATP synthase subunit beta, mitochondrial precursor	gi|54792127	MS	148, NA	43, NA	16, NA	5.19	56.32
14	Histone H2A.2	gi|31979	MS/MS	NA, 15	NA, 12	NA, 1	9.52	13.64
15	Adenylate kinase 7-like, partial	gi|149592814	MS	74, NA	15, NA	14, NA	7.09	136.97
16	60S ribosomal protein L32-like	gi|296188853	MS/MS	NA, 19	NA, 9	NA, 1	10.58	16.14
17	TNFAIP3-interacting protein 2 isoform 2	gi|239787094	MS	73, NA	34, NA	9, NA	6.12	37.17
18	Sp110 nuclear body protein isoform 6	gi|332815728	MS	78, NA	22, NA	12, NA	9.02	79.66
19	Aacyl-CoA dehydrogenase, mitochondrial	gi|113018	MS/MS	NA, 25	NA, 3	NA, 1	8.63	46.93
20	Fructose-1,6-bisphosphatase	gi|3288991	MS	103, NA	35, NA	11, NA	6.85	36.97
21	Coiled-coil domain-containing protein 40	gi|332263895	MS	74, NA	16, NA	14, NA	5.35	130.47
22	Mitochondrial NADH:ubiquinone oxidoreductase 51 kDa subunit	gi|263364	MS/MS	NA, 7	NA, 7	NA, 1	9.94	14.61
23	p21(CDKN1A)-activated kinase 7	gi|193787901	MS	81, NA	32, NA	11, NA	6.91	65.17
24	Mitochondrial malate dehydrogenase 2, NAD	gi|89574151	MS, MS/MS	109, 30	51, 4	10, 1	8.39	29.92
25	Fibrinogen betaB 1-118	gi|223130	MS/MS	NA, 70	NA, 11	NA, 1	6.17	12.89
26	Adenylosuccinate lyase, partial	gi|334347573	MS	74, NA	25, NA	9, NA	6.36	50.93
27	Transformation/transcription domain-associated protein	gi|344244337	MS	89, NA	11, NA	19, NA	8.30	228.20
28	Uncharacterized protein C3orf77-like	gi|332215705	MS	78, NA	13, NA	18, NA	8.17	192.59
29	Tissue-type plasminogen activator-like	gi|334312618	MS	95, NA	23, NA	11, NA	8.65	65.03
30	Tubulin polymerization-promoting protein family member 3-like isoform 1	gi|332227511	MS	81, NA	46, NA	8, NA	9.18	19.10
31	60S ribosomal protein L32-like	gi|296188853	MS/MS	NA, 19	NA, 9	NA, 1	10.58	16.14
32	CD164 antigen, sialomucin, isoform CRA_c	gi|119568736	MS/MS	NA, 21	NA, 22	NA, 1	12.00	7.27
33	60S ribosomal protein L32-like	gi|296188853	MS/MS	NA, 19	NA, 9	NA, 1	10.58	16.14
34	CD164 antigen, sialomucin, isoform CRA_c	gi|119568736	MS/MS	NA, 20	NA, 22	NA, 1	12.00	7.27
35	CD164 antigen, sialomucin, isoform CRA_c	gi|119568736	MS/MS	NA, 20	NA, 22	NA, 1	12.00	7.27
36	Retinitis pigmentosa GTPase regulator	gi|262050614	MS/MS	NA, 13	NA, 0	NA, 1	8.40	169.82
37	78 kDa glucose-regulated protein, partial	gi|829365	MS/MS	NA, 25	NA, 60	NA, 1	4.66	30.76
38	Transformation/transcription domain-associated protein isoform 2, partial	gi|380799023	MS	76, NA	9, NA	25, NA	8.60	380.25

NCBI = National Center for Biotechnology Information.
%Cov = %Sequence coverage [(number of the matched residues/total number of residues in the entire sequence) × 100%].
NA = Not applicable.

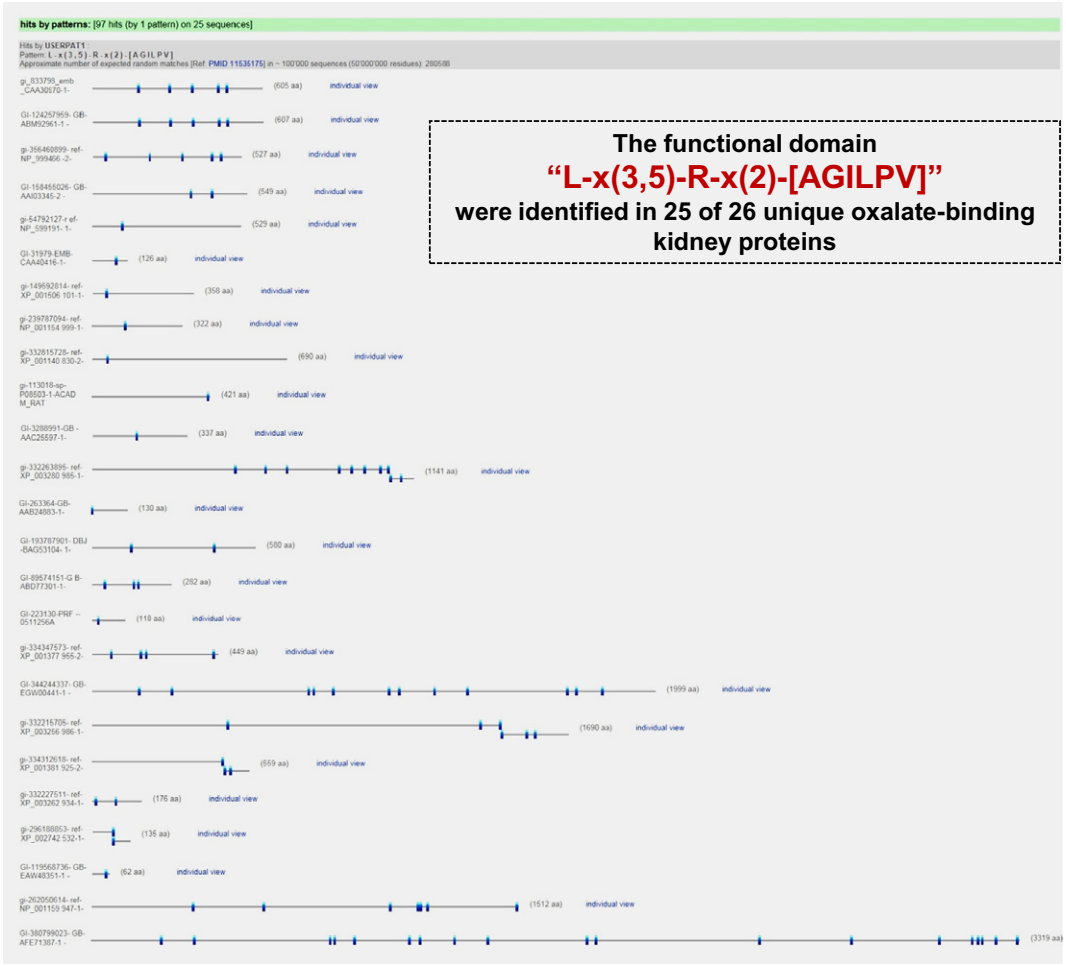


Fig. 2. Identification of oxalate-binding domain. The FASTA format of amino acid sequences of all the identified proteins listed in Table 1 were submitted to the PRATT search tool (http://www.ebi.ac.uk/Tools/pratt/) [15,16]. The data showed the domain "*L-x(3,5)-R-x(2)-[AGILPV]*" in the sequences of 25 of 26 unique proteins identified in Table 1. Among these, 15 had more than one oxalate-binding domain and the greatest number was found in transformation/transcription domain-associated protein isoform 2 (19 sites).

A number of oxidative stress regulatory proteins were identified as oxalate-binding proteins in our present study, including three isoforms of catalase (spots #6, 10, 12), mitochondrial NADH:ubiquinone oxidoreductase 51 kDa subunit (spot #22), and 78 kDa glucose-regulated protein (GRP78) (spot #37). Interestingly, catalase is responsible for catalyzing hydrogen peroxide (H_2O_2) to water (H_2O) and oxygen (O_2) [18]. There is evidence demonstrating that oxalate can induce renal cell injury by lipid peroxidation through reactive oxygen species such as superoxide anion, hydroxyl radicals and hydrogen peroxide. The accumulation of these free radicals is correlated with the decreased level of antioxidant enzymes including catalase, and catalase activity is decreased in rat kidney treated with oxalate [19]. Therefore, the decrease in level and activity of catalase might result to the reduced ability of this enzyme to bind to oxalate. *In vivo* binding of this enzyme to oxalate may be mediated by anti-oxidative processes to protect cell injury from oxidative stress.

Moreover, some metabolic enzymes were identified as oxalate-binding proteins in this study, e.g. malate dehydrogenase (spot #24). This enzyme has been proposed to bind with oxalate since its catalytic subunit binds with malate, which has a molecular structure similar to oxalate. Interestingly, malate dehydrogenase has been also identified in a previous study by Park, et al. [20] using an oxalate-affinity chromatography to purify malate synthase. These findings suggest that the ability of oxalate to bind with this enzyme may be due to the molecular mimicry of oxalate structure to the specific enzyme substrates.

Interestingly, we also identified many forms of albumin (spots #1–5, 8, 9, and 11) and three isoforms of CD164 (sialomucin) (spots #32, 34 and 35) as the oxalate-binding proteins in porcine kidney. Albumin is widely known as a sticky protein that can bind non-specifically to other proteins and various surfaces, whereas sialomucin has been reported as the secreted or membrane-associated mucin that can act as an adhesion receptor [21,22]. By their properties, it might be postulated that these two proteins could bind non-specifically to the oxalate-affinity column. However, the negative identification of the oxalate-binding domain in the non-oxalate-binding kidney proteins strengthened that albumin and sialomucin were really the oxalate-binding proteins based on the oxalate-binding domain found in their sequences.

In summary, several oxalate-binding proteins were identified from porcine kidney in our present study by a combination of oxalate-affinity purification and proteomics approach. Sequence analysis revealed that almost all of these identified proteins had the oxalate-binding domain "*L-x(3,5)-R-x(2)-[AGILPV]*". These data offer many opportunities for further investigations to address functional significance of these oxalate-binding proteins in renal physiology and pathogenic mechanisms of kidney stone disease.

Acknowledgments

This study was supported by Office of the Higher Education Commission and Mahidol University under the National Research Universities Initiative, and the Thailand Research Fund (RTA5380005 to VT). VT is also supported by "Chalermphrakiat" Grant, Faculty of Medicine Siriraj Hospital.

Appendix A. Supplementary data

Supplementary data associated with this article can be found, in the online version, at http://dx.doi.org/10.1016/j.bbrc.2012.07.015.

References

[1] G. Schubert, Stone analysis, Urol. Res. 34 (2006) 146–150.
[2] F.L. Coe, J.H. Parks, J.R. Asplin, The pathogenesis and treatment of kidney stones, N. Engl. J. Med. 327 (1992) 1141–1152.
[3] R.C. Walton, J.P. Kavanagh, B.R. Heywood, P.N. Rao, The association of different urinary proteins with calcium oxalate hydromorphs. Evidence for non-specific interactions, Biochim. Biophys. Acta 1723 (2005) 175–183.
[4] R. Selvam, P. Kalaiselvi, A novel basic protein from human kidney which inhibits calcium oxalate crystal growth, BJU. Int. 86 (2000) 7–13.
[5] B. Hess, Y. Nakagawa, F.L. Coe, Inhibition of calcium oxalate monohydrate crystal aggregation by urine proteins, Am. J. Physiol. 257 (1989) F99–106.
[6] R. Selvam, P. Kalaiselvi, Oxalate binding proteins in calcium oxalate nephrolithiasis, Urol. Res. 31 (2003) 242–256.
[7] J.C. Lieske, S. Deganello, Nucleation, adhesion, and internalization of calcium-containing urinary crystals by renal cells, J. Am. Soc. Nephrol. 10 (Suppl. 14) (1999) S422–S429.
[8] V. Kumar, G. Farell, J.C. Lieske, Whole urinary proteins coat calcium oxalate monohydrate crystals to greatly decrease their adhesion to renal cells, J. Urol. 170 (2003) 221–225.
[9] S. Chutipongtanate, Y. Nakagawa, S. Sritippayawan, J. Pittayamateekul, P. Parichatikanond, B.R. Westley, F.E. May, P. Malasit, V. Thongboonkerd, Identification of human urinary trefoil factor 1 as a novel calcium oxalate crystal growth inhibitor, J. Clin. Invest. 115 (2005) 3613–3622.
[10] P.K. Grover, L.A. Thurgood, R.L. Ryall, Effect of urine fractionation on attachment of calcium oxalate crystals to renal epithelial cells: implications for studying renal calculogenesis, Am. J. Physiol. Renal Physiol. 292 (2007) F1396–F1403.
[11] V. Thongboonkerd, S. Chutipongtanate, T. Semangoen, P. Malasit, Urinary trefoil factor 1 is a novel potent inhibitor of calcium oxalate crystal growth and aggregation, J. Urol. 179 (2008) 1615–1619.
[12] P.K. Grover, L.A. Thurgood, T. Wang, R.L. Ryall, The effects of intracrystalline and surface-bound proteins on the attachment of calcium oxalate monohydrate crystals to renal cells in undiluted human urine, BJU. Int. 105 (2010) 708–715.
[13] P. Latha, P. Kalaiselvi, P. Varalakshmi, G. Rameshkumar, Characterization of histone (H1B) oxalate binding protein in experimental urolithiasis and bioinformatics approach to study its oxalate interaction, Biochem. Biophys. Res. Commun. 345 (2006) 345–354.
[14] P. Roop-ngam, V. Thongboonkerd, Development of an oxalate-affinity chromatographic column to isolate oxalate-binding proteins, Anal. Methods 2 (2010) 1051–1055.
[15] I. Jonassen, Efficient discovery of conserved patterns using a pattern graph, Comput. Appl. Biosci. 13 (1997) 509–522.
[16] I. Jonassen, J.F. Collins, D.G. Higgins, Finding flexible patterns in unaligned protein sequences, Protein Sci. 4 (1995) 1587–1595.
[17] P. Sivakamasundari, P. Kalaiselvi, R. Sakthivel, R. Selvam, P. Varalakshmi, Nuclear pore complex oxalate binding protein p62: expression in different kidney disorders, Clin. Chim. Acta 347 (2004) 111–119.
[18] T. Henzler, E. Steudle, Transport and metabolic degradation of hydrogen peroxide in *Chara corallina*: model calculations and measurements with the pressure probe suggest transport of H(2)O(2) across water channels, J. Exp. Bot. 51 (2000) 2053–2066.
[19] S. Thamilselvan, K.J. Byer, R.L. Hackett, S.R. Khan, Free radical scavengers, catalase and superoxide dismutase provide protection from oxalate-associated injury to LLC-PK1 and MDCK cells, J. Urol. 164 (2000) 224–229.
[20] J.B. Park, H.Z. Chae, Y.S. Kim, Purification and characterization of malate synthase from *Acinetobacter calcoaceticus* grown on malonate, Korean Biochem. J. 19 (1986) 235–241.
[21] S.M. Watt, H.J. Buhring, I. Rappold, J.Y. Chan, J. Lee-Prudhoe, T. Jones, A.C. Zannettino, P.J. Simmons, R. Doyonnas, D. Sheer, L.H. Butler, CD164, a novel sialomucin on CD34(+) and erythroid subsets, is located on human chromosome 6q21, Blood 92 (1998) 849–866.
[22] S. Forde, B.J. Tye, S.E. Newey, M. Roubelakis, J. Smythe, C.P. McGuckin, R. Pettengell, S.M. Watt, Endolyn (CD164) modulates the CXCL12-mediated migration of umbilical cord blood CD133+ cells, Blood 109 (2007) 1825–1833.

Clin Chem Lab Med 2012;50(9):1697–1698 © 2012 by Walter de Gruyter • Berlin • Boston. DOI 10.1515/cclm-2012-0101

Letter to the Editor

Phosphate inhibits calcium oxalate crystal growth and crystallization through reducing free calcium ions: a morphological analysis and calcium consumption assay

Somchai Chutipongtanate and Visith Thongboonkerd*

Medical Proteomics Unit, Office for Research and Development, Faculty of Medicine Siriraj Hospital, and Center for Research in Complex Systems Science, Mahidol University, Thailand

Keywords: calcium oxalate; crystal growth; inhibitor; nephrolithiasis; phosphate.

There are several lines of evidence demonstrating that phosphate serves as a calcium oxalate (CaOx) stone inhibitor, yet also promotes epitaxial deposition (or heterogeneous nucleation) of CaOx through precipitated calcium phosphate (CaP) crystals (1, 2). However, these dual modulatory effects of phosphate on CaOx crystals had been previously examined by indirect methods (e.g., spectrophotometric turbidimetry, dual constant composition). In the present study, we re-evaluated the modulatory effects of phosphate on CaOx crystals using a direct method (i.e., morphological study) to directly measure size, number and total mass of CaOx crystals upon exposure to various dosages of phosphate. Moreover, mechanism of phosphate action on CaOx crystals was addressed using a calcium consumption assay.

CaOx monohydrate (COM) crystals were prepared in the absence (control) or presence of phosphate (NaH_2PO_4) at various concentrations (0.5, 2.5, 4.0, 5.5 and 7.0 mM) (see also Supplemental data, Methods, which accompanies the article at http://www.degruyter.com/view/j/cclm.2012.50.issue-9/issue-files/cclm.2012.50.issue-9.xml). Note that physiologic concentrations of phosphate in the normal urine were 2.5–5.5 mM. After 1-h incubation, COM crystal morphology was examined under phase-contrast microscopy (CKX41, Olympus Co. Ltd., Tokyo, Japan). Quantitative analyses of COM crystal size (reflecting crystal growth), number (reflecting crystallization rate) and total mass (reflecting the final product of crystallization and growth) were performed using ImageMaster™ 2-D Platinum Software (GE Healthcare, Uppsala, Sweden), as described previously (3).

The data showed that the size, number and total mass of COM crystals were significantly reduced by phosphate treatment in a dose-dependent manner (Figure 1; see also Supplemental data, Figure S1). The degrees of inhibition were up to 62.5±1.3, 55.4±3.9, and 83.3±1.2% for crystal size, number and total mass, respectively. Note that phosphate did not alter pH of the solution (data not shown); hence, its inhibitory effect did not involve pH-induced changes in CaOx solubility. Precipitation of amorphous CaP crystals was observed in the samples treated with 2.5–7.0 mM phosphate; however, epitaxial deposition of CaOx on these precipitates was not detected (Figure 1).

To address the mechanism of action of phosphate on CaOx crystals, we performed a recently established calcium consumption assay (4). Briefly, 3 µL of the solution from COM crystallization reaction was mixed with 200 µL of Arsenazo III reagent (BioSystems S.A., Barcelona, Spain) to measure free calcium ions remained in the solution (see details of this assay and calculation in the Supplemental data, Methods). The data showed that all dosages of phosphate caused significant reduction (consumption) of free calcium ions in the crystallization solution (Supplemental data, Figure S2). This result was consistent to many clinical datasets demonstrating that phosphate therapy could lower urinary calcium levels in hypercalciuric patients; thus, reducing CaOx saturation state and the stone risk.

Taken together, our data revealed that phosphate significantly inhibited crystallization and growth of COM crystals, while epitaxial deposition of CaOx crystals was not detected in our present study. This direct evidence underscores the beneficial role of phosphate as a CaOx stone inhibitor and supports its use in clinical practice.

*Corresponding author: Visith Thongboonkerd, MD, FRCPT
Professor and Head of Medical Proteomics Unit, Director of Center for Research in Complex Systems Science, Siriraj Hospital, Mahidol University, 12th Floor Adulyadej Vikrom Building, 2 Prannok Road, Bangkoknoi, Bangkok 10700, Thailand
Phone/Fax: +66 2 4184793,
E-mail: thongboonkerd@dr.com; vthongbo@yahoo.com
Received February 16, 2012; accepted February 29, 2012; previously published online March 24, 2012

Unauthenticated | 202.28.180.202
Download Date | 11/15/12 9:16 AM

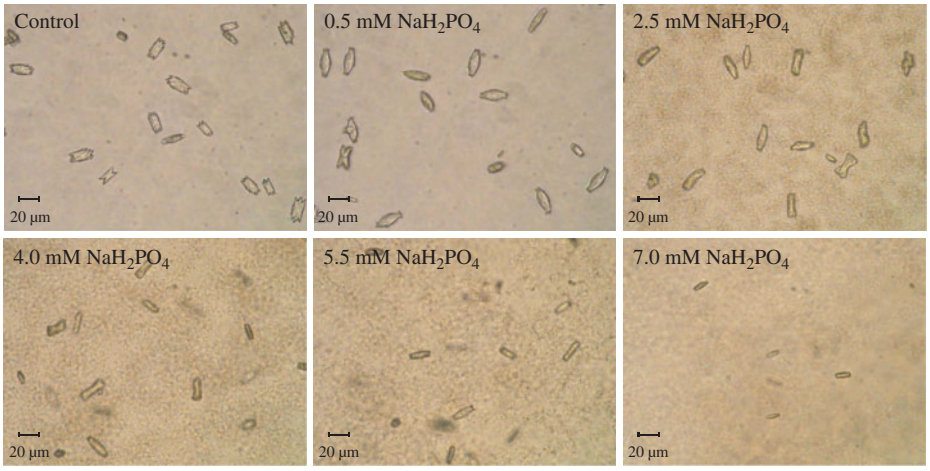


Figure 1 Morphological study of effects of phosphate on COM crystals.
COM crystallization was carried out using 5.0 mM $CaCl_2$ and 0.5 mM NaC_2O_4 in 10 mM Tris-HCl buffer containing 90 mM NaCl (pH 7.4), in the absence (control) or presence of phosphate (NaH_2PO_4) at various concentrations. Quantitative data and statistical analysis are presented in Supplementary Figure S1.

Acknowledgments

This study was supported by Office of the Higher Education Commission and Mahidol University under the National Research Universities Initiative, and The Thailand Research Fund (RTA5380005) to VT.

Conflict of interest statement

Authors' conflict of interest disclosure: The authors stated that there are no conflicts of interest regarding the publication of this article. Research funding played no role in the study design; in the collection, analysis, and interpretation of data; in the writing of the report; or in the decision to submit the report for publication.
Research funding: None declared.
Employment or leadership: None declared.
Honorarium: None declared.

References

1. Escribano J, Balaguer A, Pagone F, Feliu A, Roque IF. Pharmacological interventions for preventing complications in idiopathic hypercalciuria. Cochrane Database Syst Rev 2009;1:CD004754.
2. Tang R, Nancollas GH, Giocondi JL, Hoyer JR, Orme CA. Dual roles of brushite crystals in calcium oxalate crystallization provide physicochemical mechanisms underlying renal stone formation. Kidney Int 2006;70:71–8.
3. Thongboonkerd V, Chutipongtanate S, Semangoen T, Malasit P. Urinary trefoil factor 1 is a novel potent inhibitor of calcium oxalate crystal growth and aggregation. J Urol 2008;179:1615–9.
4. Chutipongtanate S, Thongboonkerd V. Establishment of a novel colorimetric assay for high-throughput analysis of calcium oxalate crystal growth modulation. Analyst 2010;135:1309–14.

Unauthenticated | 202.28.180.202
Download Date | 11/15/12 9:16 AM

DOI: 10.1111/j.1365-2362.2012.02674.x

PERSPECTIVE

Implementation of proteomic biomarkers: making it work

Harald Mischak[1,2,*,†,‡], John P.A. Ioannidis[3,4,5,6,*], Angel Argiles[7,‡], Teresa K. Attwood[8,†], Erik Bongcam-Rudloff[9,10,†], Mark Broenstrup[11], Aristidis Charonis[12,†], George P Chrousos[13], Christian Delles[1], Anna Dominiczak[1,†], Tomasz Dylag[14], Jochen Ehrich[15], Jesus Egido[16,†], Peter Findeisen[17], Joachim Jankowski[18,†,‡], Robert W. Johnson[19], Bruce A. Julien[20], Tim Lankisch[21], Hing Y. Leung[22], David Maahs[23], Fulvio Magni[24,†], Michael P. Manns[21], Efthymios Manolis[25], Gert Mayer[26], Gerjan Navis[27], Jan Novak[28], Alberto Ortiz[16,†,‡], Frederik Persson[29], Karlheinz Peter[30,†], Hans H. Riese[31], Peter Rossing[29,†], Naveed Sattar[1], Goce Spasovski[32,†,‡], Visith Thongboonkerd[33,†], Raymond Vanholder[34,†,‡], Joost P. Schanstra[35,†] and Antonia Vlahou[36,†]

[1]BHF Glasgow Cardiovascular Research Centre, Institute of Cardiovascular and Medical Sciences, College of Medical, Veterinary and Life Sciences, University of Glasgow, Glasgow, UK, [2]Mosaiques diagnostics, Hannover, Germany, [3]Clinical and Molecular Epidemiology Unit, Department of Hygiene and Epidemiology, University of Ioannina School of Medicine, Ioannina, Greece, [4]Stanford Prevention Research Center, Department of Medicine, Stanford University School of Medicine, Stanford, CA, USA, [5]Department of Health Research and Policy, Stanford University School of Medicine, Stanford, CA, USA, [6]Department of Statistics, Stanford University School of Humanities and Sciences, Stanford, CA, USA, [7]RD Néphrologie, Montpellier Cedex, France, [8]Faculty of Life Sciences and School of Computer Science, University of Manchester, Manchester, UK, [9]Department of Immunology, Genetics and Pathology, Uppsala University, Uppsala, Sweden, [10]Department of Animal Breeding and Genetics, Swedish University of Agricultural Sciences, Uppsala, Sweden, [11]Sanofi-Aventis Deutschland GmbH D-65926 Frankfurt am Main, Germany, [12]Divisions of Histology and Biotechnology, Biomedical Research Foundation, Academy of Athens, Athens, Greece, [13]First Department of Pediatrics, Athens University Medical School, Aghia Sophia Children's Hospital, Athens, Greece, [14]European Commission, Directorate-General for Research and Innovation, Unit F5: Personalised Medicine, 21 rue du Champ de Mars, Brussels, Belgium, [15]Hannover Medical School, Department of Pediatrics, Hannover, Germany, [16]IIS-Fundación Jiménez Díaz, Autonoma University, Madrid, Spain, [17]C Institute of Clinical Chemistry, Universitätsklinikum Mannheim, Mannheim, Germany, [18]Charité (CBF), Medizinische Klinik IV, Berlin, Germany, [19]Abbott Laboratories, Abbott Park, IL, USA, [20]Department of Medicine, University of Alabama at Birmingham, Birmingham, AL, USA, [21]Department of Gastroenterology, Hepatology and Endocrinology, Hannover Medical School, Hannover, Germany, [22]The Beatson Institute for Cancer Research, Garscube Estate, Glasgow, UK, [23]Barbara Davis Center for Childhood Diabetes, University of Colorado Denver, Aurora, CO, USA, [24]Department of Experimental Medicine, University of Milano-Bicocca, Monza, Italy, [25]European Medicines Agency, London, UK, [26]Department of Internal Medicine IV, Medical University of Innsbruck, Innsbruck, Austria, [27]Division of Nephrology, Department of Internal Medicine, University Medical Centre Groningen, University of Groningen, Groningen, The Netherlands, [28]Department of Microbiology, University of Alabama at Birmingham, Birmingham, AL, USA, [29]Steno Diabetes Center, Gentofte, Denmark, [30]Baker Heart Research Institute, Melbourne, Victoria, Australia, [31]European Projects Office, Institute of Health Carlos III, Madrid, Spain, [32]Department of Nephrology, Medical Faculty, University of Skopje, Skopje, Former Yugoslav Republic of Macedonia, [33]Faculty of Medicine at Siriraj Hospital, Mahidol University, Bangkok, Thailand, [34]Department of Nephrology, Ghent University Hospital, Ghent, Belgium, [35]Institut National de la Santé et de la Recherche Médicale (INSERM), U1048, Institut of Cardiovascular and Metabolic Disease and Université Toulouse III Paul-Sabatier,Toulouse, France, [36]Division of Biotechnology, Biomedical Research Foundation, Academy of Athens, 11527 Athens, Greece

*The first two authors contributed equally.

†Member of the European Kidney and Urine Proteomics COST Action (EuroKUP).

‡Member of the European Uremic Toxins (EUTox) Work Group.

Re-use of this article is permitted in accordance with the Terms and Conditions set out at http://wileyonlinelibrary.com/onlineopen#OnlineOpen_Terms

ABSTRACT

While large numbers of proteomic biomarkers have been described, they are generally not implemented in medical practice. We have investigated the reasons for this shortcoming, focusing on hurdles downstream of biomarker verification, and describe major obstacles and possible solutions to ease valid biomarker implementation. Some of the problems lie in suboptimal biomarker discovery and validation, especially lack of validated platforms with well-described performance characteristics to support biomarker qualification. These issues have been acknowledged and are being addressed, raising the hope that valid biomarkers may start accumulating in the foreseeable future. However, successful biomarker discovery and qualification alone does not suffice for successful implementation. Additional challenges include, among others, limited access to appropriate specimens and insufficient funding, the need to validate new biomarker utility in interventional trials, and large communication gaps between the parties involved in implementation. To address this problem, we propose an implementation roadmap. The implementation effort needs to involve a wide variety of stakeholders (clinicians, statisticians, health economists, and representatives of patient groups, health insurance, pharmaceutical companies, biobanks, and regulatory agencies). Knowledgeable panels with adequate representation of all these stakeholders may facilitate biomarker evaluation and guide implementation for the specific context of use. This approach may avoid unwarranted delays or failure to implement potentially useful biomarkers, and may expedite meaningful contributions of the biomarker community to healthcare.

Keywords Biomarker, biomarker implementation, clinical proteomics, clinical studies, expert panel, proteomics.

Eur J Clin Invest 2012; 42 (9): 1027–1036

Introduction

Clinical proteomics is defined as proteome analysis intended to improve the medical practice, for example, in relation to diagnosis, prevention, prognosis or therapy. Its success should be judged from the conferred clinical impact after implementation of its findings in everyday practice. The last decade has been marked by significant technological advancements in proteomics, especially with regard to mass spectrometry and bioinformatic solutions for data analysis. Over 4000 manuscripts including the words 'clinical' and 'proteomics' were indexed in MEDLINE in the last decade. Multiple proteomic biomarkers have been described for a variety of diseases, and several biomarkers have shown added value over current disease-management approaches, based on validation studies (e.g. in chronic kidney disease [1–3], reviewed in [4,5]). Nevertheless, implementation of the results in medical practice appears to be scarce [6]. Despite the promising findings, the impact of clinical proteomics (and biomarkers in general) on clinical decision-making, patient management and welfare appears insufficient.

Much of the problem may still lie in suboptimal discovery and validation processes for proteomic and other highly touted biomarkers. Analytical validation must be done prior to even starting a study, and the performance characteristics of the platform must be known [7–11]. Empirical evidence has shown that even in the best-studied and most studied biomarkers from diverse fields beyond proteomics, initial expectations may be inflated, and true effects may be much smaller than originally believed [12,13]. As others have pointed out, a plethora of factors can before, during and after sample analysis complicate biomarker discovery and validation and lead to false discoveries [14]. Nevertheless, it is to be expected that, as these factors are more clearly recognised, discovery and validation processes might be improved to a point where they are no longer the main bottleneck to progress. Enhanced attention is already given to clinical proteomics workflows, with special emphasis on experimental design of biomarker discovery, standardisation of procedures, data analysis and interpretation of results [11,15–17]. Mandatory requirements for contributors have, to some degree, been adopted by scientific journals (e.g. http://www.mcponline.org/site/cpmeeting/cguidelines.pdf). Technological bottlenecks associated with the transformation of discoveries into potential clinical assay are being identified and addressed [18–21]. Hopefully, if these efforts and insights become systematically exploited and implemented, valid biomarkers may start accumulating in the foreseeable future, perhaps even at a rapid pace. However, even then, successful biomarker discovery and qualification alone does not suffice for successful clinical implementation. The objective of this article is to highlight the critical hurdles downstream of biomarker discovery and verification, and to suggest potential ways to overcome them.

 © 2012 The Authors. European Journal of Clinical Investigation © 2012 Stichting European Society for Clinical Investigation Journal Foundation

Challenges in transforming biomarker discoveries into clinical application

Frequently, the discovery of biomarkers is considered a successful endpoint of clinical proteomics. Discovery and publication is a prerequisite for biomarker development, but it must be transformed into the ultimate goal of this particular translational proteomics research: clinical application. While highly ranked publications can have a prompt and major personal impact on the involved scientists (e.g. increased funding and advancement of academic career), the actual implementation requires substantially more time and is associated with diverse, unforeseeable challenges, which can bring the process to a standstill. Many scientists appear unwilling to venture down this tortuous and uncertain path.

In addition, different categories of biomarkers exist, depending on their intended use, as defined, for example, by Khleif *et al.* [22]: A biomarker is a characteristic that is objectively measured and evaluated as an indicator of normal biological processes, pathogenic processes or pharmacologic responses to a therapeutic intervention. At least, four different categories of biomarkers should be differentiated: (i) diagnostic biomarkers (early detection biomarkers, disease classification); (ii) predictive biomarkers (predict patients likely to respond to a specific agent, predict patients likely to have an adverse event to a specific agent); (iii) metabolism biomarkers (dose defining); and (iv) outcome biomarkers (forecast response, progression or recurrence).

Implementation requires demonstration of clinical validity and utility, and benefit for the patient [23,24]. This process is demanding in time, as well as clinical, scientific and financial resources, and generally requires large studies. These include the assessment of performance on introduction of the novel biomarker over and above routinely available information; randomised trials to test improvement in clinical outcomes by using the biomarker; and late implementation and dissemination studies to show that the biomarker was successfully applied in everyday practice, with improved outcomes in large populations and a concomitant decrease in the cost of care – or, at least, without a substantial increase [25]. Such implementation testing is likely to take years, often exceeding a decade, and continues even after the biomarker has been applied and used widely in the community.

Biomarkers are actively sought for the majority of diseases associated with major societal and economic burden in developed countries (e.g. dementia, renal and cardiovascular disease, and most malignancies). However, it may generally take many years to clearly demonstrate the value of incorporating these biomarkers in management decisions in randomised trials that are evaluated based on hard endpoints. Possible solutions with shorter time horizons include the use of surrogate endpoints and/or the analysis of biomarkers in already available collections of samples with known outcomes. Surrogate endpoints may sometimes be misleading [26]. Therefore, there is debate about whether clinical implementation should be based only on results from studies that assess hard endpoints, or whether lower-level evidence that can be assessed faster may suffice. An expedited approval and implementation process based on surrogate and/or retrospective evidence may carry the risk of introducing expensive, useless or even harmful tests [27]. On the other hand, withholding an apparently beneficial test may deny a benefit for patients. As a consequence, a decision needs to be made at an early point in time whether evidence based on surrogates will be acceptable: for example, whether there is the potential for major health gains by introducing a biomarker with only modest evidence to support its use, or whether a hard endpoint must be assessed before implementation.

Evaluation of biomarkers based on analysis of previously collected samples with known outcome can be useful for the preliminary assessment of predictive or diagnostic efficacy, and the efficient reclassification of participants into informative risk categories with different implications for preventive or therapeutic intervention. However, such studies may involve a selection bias and do not guarantee that the use of biomarkers would improve the clinical outcome.

Another major impediment to implementation is that scientists are generally not well informed about the required steps from initial discovery to translation into a clinically useful assay. In fact, a clear road map towards implementation does not exist and guidance is scarce. Furthermore, regulatory requirements, if existing and applicable, are generally unknown to most researchers. This uncertainty and lack of adequate knowledge, in combination with the aforementioned need for substantial efforts and funding to demonstrate clinical validity, utility and added value of biomarkers over current clinical standards through, in principle, large trials, generally bring the further development of discovery findings to a standstill.

Performance of biomarkers superior to that for current standards does not automatically result in actual clinical implementation for several additional reasons: (i) biomarkers, even if facilitating substantial improvements in patient assessment, may initially fall short in influencing patient management, owing to the lack of appropriate interventions; (ii) patients may not wish to know about their risk of disease, especially if there is no proven intervention available; (iii) beyond the value at the clinical level, a biomarker must prove its cost-effectiveness [17], and this may differ by country, healthcare system and study approach applied by health economists; and (iv) physicians may resist changing the *status quo* in daily clinical practice, especially if this change is associated with personal financial consequences (procedures profitable for the physicians are not likely to be replaced).

Substantial uncertainty exists about the road towards implementation of biomarkers. There are multiple, interrelated steps where a plethora of different parties are involved, including researchers, clinicians, healthcare providers, funding and regulatory agencies, legislative, educative, and health insurance bodies, industry and patient groups. Each of these groups views the implementation from a different and unique angle, and cross-communication is often challenging. This results in fragmentation and severe gaps in the flow of information that may impede the clinical translation of research advancements.

A real-life example

The following typical scenario exemplifies how various challenges may create interactive hurdles for implementation of properly qualified biomarkers. Early detection of diabetic nephropathy, followed by appropriate therapy, is expected to prevent progression to advanced renal disease [28,29], improve quality of life and life expectancy of patients, and reduce the societal economic burden. Considering that biomarkers have been discovered and that associations of specific proteins or protein patterns have been validated in blinded studies (e.g. [2]), the next step would be to further validate these markers in prospective clinical trials. Of paramount importance are the definition of the endpoint(s) (in this case, detection of progression of chronic kidney disease – for example, end-stage renal disease with need for renal replacement therapy) and proof of an at least incremental superiority to existing diagnostic standards (e.g. assessment of albuminuria). The ideal study for such a chronic, slowly progressive disease with a substantial proportion of diabetic patients not affected requires the prospective collection of samples over many years in a large population for the accumulation of sufficient data to evaluate a hard endpoint. This long time-frame is a major setback for everybody. To exemplify the challenge, several of the major trials in the area are listed in Table 1. In most trials, only surrogate endpoints based on albuminuria were assessed, and, for several of the trials, hard endpoints for chronic kidney disease (doubling of serum creatinine concentration or end-stage renal disease) were not reported. Unfortunately, collection of follow-up data to assess hard endpoints at a later point in time was generally not foreseen. Apparent benefit of intervention based on a surrogate parameter (reduction of albuminuria) has been demonstrated in currently manifested stages of disease [28,29], but one needs to extrapolate whether a benefit would apply also to earlier stages. Patients with diabetes may be reluctant to be informed

Table 1 Duration, demographic parameters and outcome of major trials testing early intervention in diabetic nephropathy

	DIRECT I	DIRECT II	HOPE	BENEDICT	ADVANCE	ROADMAP
Treated (*N*)	1662	951	1808	601	5569	2232
Placebo (*N*)	1664	954	1769	603	5571	2215
Age (years)	31	57	65	62	66	57·7
Diabetes type	Type I	Type II	Type II	Type II	Type II	Type II
Diabetes duration (years)	9·1	8·8	11	8	8	6
BP (Systol/diastol)	117/73	133/78	142/80	151/88	145/81	136/81
Active treatment	Candesartan	Candesartan	Ramipril	Trandolapril	Perindopril/Indapamide	Olmesartan
Duration of treatment (years)	4·7	4·7	4·5	3·6	4·3	3·2
Incidence of new microalbuminuria (%)	5·0/5·0	12·0/13·0	33/38	5·8/11	19·6/23·6	8·2/9·8
Doubling of Screa (*N*)	NA	NA	NA	NA	55/45	23/23
ESRD (*N*)	NA	NA	10/8	NA	25/21	0/0
Death (*N*)	14/13	37/35	196/248	12	408/471	26/15
Rate of death (%/year)	0·17	0·80	2·76	0·28	1·83	0·29
Rate of onset ESRD (%/year)	NA	NA	0·11	NA	0·10	0·00
Rate of doubling of Screa (%/year)	NA	NA	NA	NA	0·21	0·43

BP, blood pressure; Screa, serum creatinine; ESRD, end stage renal disease; NA, not accessible.
Data reported were extracted from DIRECT I [41], DIRECT II [42,43], HOPE [44], BENEDICT [28], ADVANCE [45] and ROADMAP [29]. While most trials demonstrated a positive effect of intervention when assessing a surrogate parameter, albuminuria, a benefit based on hard endpoints was generally not demonstrated and was frequently not even assessed. The events are shown as number of events or percentage, as appropriate, in the active treatment/control arm.

 © 2012 The Authors. European Journal of Clinical Investigation © 2012 Stichting European Society for Clinical Investigation Journal Foundation

about early signs of kidney disease (e.g. years before recurrent microalbuminuria), given that many current therapeutic options are not proven to be effective at that stage, while potentially more effective intervention measures are still under development. We are hence faced with a fundamental question: Shall we implement such biomarkers now and employ current intervention strategies based on the assumption they will bring a significant benefit at early stages of disease, or shall we, prior to implementation, investigate whether the intervention strategies bring a significant benefit, either based on surrogate endpoints (e.g. albuminuria) or on hard endpoints? Thus, while prevention of diabetic nephropathy (or any other disease) is a worthy goal, the implementation path is far less clear.

Given these considerations, one may reflect that perhaps research in these specific areas should not be even initiated, because it will not result in any tangible impact on the current situation; or that the current situation should be altered in a way that positive results from research have a realistic chance to be implemented to improve the current clinical status. The latter option is certainly preferable, but the goals need to be rigorously defined, and critical issues must be clearly identified to advance.

An agenda to facilitate implementation of valid biomarkers

The implementation problem is gaining increasing recognition, and actions towards improving the situation have been initiated: the substantial financial need to support biomarker validation and qualification studies has been acknowledged by funding agencies – prominent examples are the recent EU FP7 calls for proposals for collaborative projects (http://ec.europa.eu/research/participants/portal/page/fp7_calls [30]). Additional examples include the Joint Programming Initiative in Neurodegenerative Diseases, which is funding the first pilot call for research projects in 'Optimisation of biomarkers and harmonisation of their use between clinical centres'; and the new ERA-Net TRANSCAN, which has proposed the topic 'Validation of biomarkers for personalised cancer medicine'. In the aforementioned example of diabetic nephropathy, a clinical trial (PRIORITY; FP7 2012–2016) is being launched, exploring the potential benefit of intervention on early diabetic kidney injury, based on a panel of urinary protein biomarkers [31]; and the 'Early Prevention of Diabetes Complications in Europe' (e-PREDICE) was also funded to investigate changes in biomarkers for microvascular damage, endothelial function, oxidation and inflammation, conferred as a result of different drug treatments designed for the early prevention of diabetic complications. Similar efforts are also underway in many other fields and in other countries, for example, in the USA, the Early Detection Research Network of the National Cancer Institute (http://edrn.nci.nih.gov) [32]. These are certainly major advances, shifting the emphasis from biomarker discovery to clinical application. Nevertheless, the implementation process, as a whole, still appears to be substantially under-funded.

Aiming to facilitate successful implementation of research findings in medical practice, the European Medical Research Council (EMRC) recently published the ESF/EMRC 'forward look' (http://www.esf.org/emrc; May 2011), describing the different hurdles in the process. To spear-head an implementation road map and identify the special turns it must take in the case of proteomics findings, the European Kidney and Urine proteomics COST Action, during its regular meeting (Madrid 2011), organised a session on clinical implementation of research findings pertinent to kidney diseases. In this meeting, researchers, clinicians and representatives from biobanks, industry, funding and regulatory agencies were invited to present their views of the implementation process. Jointly, these initiatives showed that biomarker research should adhere to a much more organised format, taking into consideration the needs and perspectives of the whole spectrum of involved parties: from scientists in the discovery laboratory to end-users (patients, physicians), including regulatory bodies. We suggest the following steps to facilitate implementation of clinical proteomics findings (Fig. 1):

- Perform initial discovery and validation for the specific context of use. If positive;
- Approach a suitable multidisciplinary panel (described in detail below) to evaluate evidence, and if positive, to provide guidance for further study design;
- Apply for funding and, in parallel, request samples from biobanks, when available, or initiate new sample collection (considering the panel's recommendations);
- Perform biomarker evaluation;
- Approach the panel for evaluation of the additional data and, if positive, for guidance for clinical study design;
- Apply for funding and perform intervention study to evaluate expected benefit. Preferably, hard endpoints should be assessed, if they can be reached in a reasonable period of time. If this is not possible, and the biomarkers are considered to have potentially life-saving clinical potential, validated surrogate endpoints may be employed, mandating additional follow-up to assess the hard endpoints;
- Approach the panel for evaluation of the evidence from the intervention study. If positive;
- Implement in clinical practice – perhaps on a limited, conditional basis until information on hard endpoints is considered robust enough;

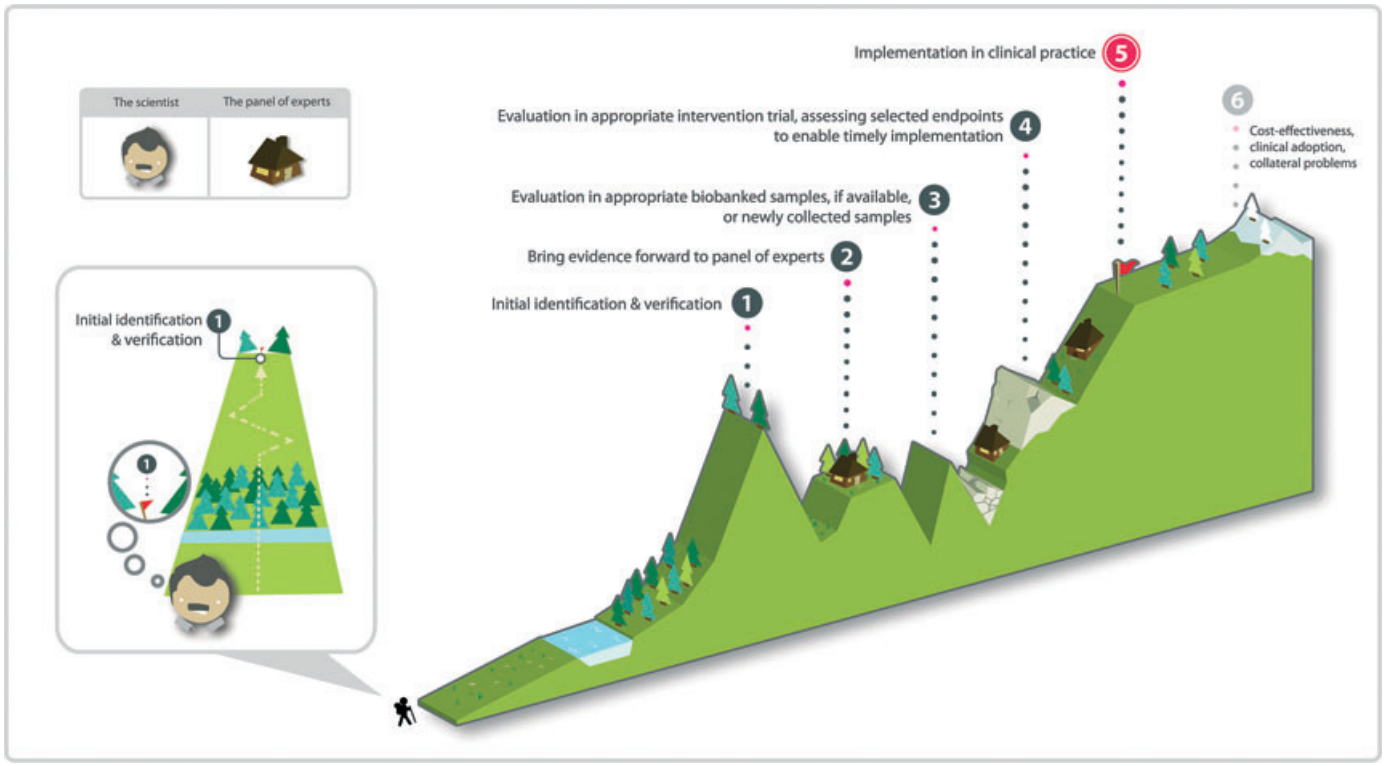


Figure 1 Implementation of novel biomarkers represents a substantially harder challenge than initially thought by scientists. As shown on the left-hand side of the cartoon, the current belief is that the major efforts are required during initial identification and verification of proteomics biomarkers. Implementation in the clinic is conceived as being simply a matter of continuing uphill, the 'last few steps' to the red flag. However, we argue that this is not true. While initial identification, verification and establishment of an appropriate analytical platform are without doubt major steps, even more substantial efforts are required on the road to actual implementation, which evidently is much longer than anticipated, and full of risks and additional obstacles. Among the major challenges are access to specific knowledge, sufficient funding, access to appropriate specimens, demonstration of reproducibility and performance of interventional trials. We propose support by a multidisciplinary panel immediately after initial verification, to accompany scientists on this road to implementation and to help avoid potentially useful biomarkers failing to reach the clinic. Once implementation in the clinic has been accomplished, the process does not stop, as cost-effectiveness, clinical adoption and collateral problems still must be monitored.

- Apply feedback mechanisms to evaluate cost-effectiveness, clinical adoption, problems in routine application, unanticipated collateral problems.

Key issues to settle in this process include the following:

- The definition of clinical needs and desired context of use for new biomarkers should be specifically emphasised [16]. Different approaches to establish research priorities may be considered: for example, expert committees, peer review, research-gap generation or value of information modelling. A key question is who should be involved in the process and how? Some countries have established organisations to define and implement clinical priorities in a multidisciplinary and multistakeholder process, such as the Centre for Biomedical Network Research (CIBER) in Spain and the organisation INVOLVE of the UK Department of Health. Whether this is the optimal way to proceed remains to be seen. Generation of Web-based platforms allowing description of research priorities per disease and stakeholder (patient groups, health insurance companies, clinical societies, law-making bodies, etc.) appears to be a good starting-point to record existing views and to allow a more informed initiation of biomarker discovery efforts.
- A knowledgeable independent body or panel is required to evaluate the results of initial biomarker verification and qualification efforts as well as the respective claims and clinical

 © 2012 The Authors. European Journal of Clinical Investigation © 2012 Stichting European Society for Clinical Investigation Journal Foundation

utility in a transparent and unbiased manner. Currently, claims made for biomarkers are usually made by the scientists involved in the original studies, fostering unwarranted optimism and allegiance bias. The European Medicines Agency (EMA) and the US Food and Drug Administration (FDA) aim to provide evidence-based advice on biomarker qualification. One example is the voluntary biomarker qualification programme [33]. Biomarker data evaluation and guidance can be enhanced by the active involvement of a multidisciplinary panel (clinicians, clinical chemists, statisticians, health economists, representatives from patient groups, health insurance, pharmaceutical and biotechnology companies, (publicly funded) biobanks and regulatory agencies) that would evaluate existing data and provide specific recommendations for a road map towards clinical implementation of the biomarker for the specific context of use (including use of biobanked samples, surrogate and hard endpoints etc.; Fig. 1). Demonstration of reproducibility for markers that move towards clinical experimentation is vital; hence, evaluation should include repeatability checks by experienced statisticians/bioinformaticians using the raw data.

- Availability of funding for biomarker implementation studies. As an example, a certain part of the EU FP7 funding for collaborative projects under the Health theme is directed to clinical research projects, including investigator-driven clinical trials, to bring basic health research closer to the clinic (the 2011 call details can be found at http://ec.europa.eu/research/participants/portal/page/cooperation?callIdentifier=FP7-HEALTH-2012-INNOVATION-1). Positive evaluation of biomarker data by the panel (II) could be regarded as a positive recommendation also for funding purposes. Such implementation-focused projects should involve representatives of all parties mentioned above, as partners or members of an advisory board, to ensure timely implementation.
- Increased accessibility to biobanks. Availability of appropriate and clinically well-documented samples is frequently a major bottleneck for biomarker studies, even if all other aforementioned gaps are filled. Biobanks can largely expedite the assessment of predictive or diagnostic ability of biomarkers. Use of samples from biobanks could rapidly provide answers regarding biomarker validity and guide (or spare) further qualification studies through prospective trials [34–38]. The EU-funded Biobanking and Biomolecular Resources Research Infrastructure (BBMRI) project (http://www.bbmri.eu/) aims to build a coordinated, large-scale pan-European biobanking infrastructure, initially based on existing sample collections, resources, technologies and expertise [39]; it is intended to work as an interconnected node structure including biobanks, biomolecular resources, harmonised standards, databases and bioinformatics, as well as a platform for assessing ethical, legal and societal issues. This approach is promising; however, it has not yet been fully realised, and substantial difficulties in accessing existing biobanks are encountered. In addition, harmonisation of quality control tools and sample collection protocols, both significantly influence the results obtained, has not been achieved yet, but is mandatory. These issues not only affect *in vitro* diagnostic tests [40] but also have a major impact on multiparametric '-omics' approaches and can override disease-related patterns or even abolish meaningful data interpretation.

Improvement efforts should be focused on transparency, creation of clear rules for sample accessibility and procedures for requests, including clear timelines; comprehensive listing of samples retrieved for all projects (outlining their type and the respective research project, so as to avoid duplication of efforts); streamlining of consent processes; and generation of the appropriate legislation that allows use of the stored samples. Stored samples should be associated with consent for the sample to be used in any scientific investigation. If analysing the sample is dependent on obtaining a new consent from the donor (who may well be deceased) individually for every experiment, then the value of such a biobank is minute, as its content can generally not be used because of this legal restriction.

Conclusion

Implementation of biomarkers is a complex process that would significantly benefit from the establishment of a general road map. While we have focused on proteomic biomarkers in this article, the considerations and suggestions extend well beyond the boundaries of the proteomics community and are relevant to all new biomarker technologies.

Potential consequences of implementation should be contemplated from the very beginning of the developmental process, even at the stage of biomarker discovery. We also suggest potential means to achieve these aims. Final success, the implementation of the biomarker to benefit patients, cannot be guaranteed upfront, even if the biomarker proves to be valuable, because there is a continuous evolution of the landscape, with all of its political, societal and clinical implications. The -omics revolution, and development of personalised medicine approaches, will add greater complexity and new challenges to the implementation process in the coming years. However, if mechanisms for efficient communication and guidance on a road map towards clinical implementation are apparent and disseminated, we will be much better equipped to react more promptly and make the required adjustments. The biomarker community will be better

positioned overall to make more meaningful contributions to clinical care, which after all should be the principal goal of all parties involved.

Acknowledgements

This study is supported in part by the EuroKUP COST Action (BM0702) and the and by the European Community's 7th Framework Programme, grant agreement number HEALTH-F2-2009-241544 (SysKID). We would like to thank Aurelien Despierris for designing the cartoon (Fig. 1). Several of the authors are employed in part or fully by industry, and/or receive funding from industry, as also evident from their affiliations, but the article does not show partiality towards specific industry products or otherwise.

Disclaimer

TD: The views expressed are purely those of the author and may not in any circumstances be regarded as stating an official position of the European Commission. EM: The views expressed in this paper are the personal views of the author and may not be understood or quoted as being made on behalf of or reflecting the position of the European Medicines Agency or one of its committees or working parties.

Address

BHF Glasgow Cardiovascular Research Centre, Institute of Cardiovascular and Medical Sciences, College of Medical, Veterinary and Life Sciences, University of Glasgow, Glasgow G12 8TA, UK (H. Mischak, C. Delles, A. Dominiczak, N. Sattar); Mosaiques diagnostics, 30625 Hannover, Germany (H. Mischak); Clinical and Molecular Epidemiology Unit, Department of Hygiene and Epidemiology, University of Ioannina School of Medicine, 45110 Ioannina, Greece (J. P. A. Ioannidis); Stanford Prevention Research Center, Department of Medicine, Stanford University School of Medicine, Stanford, CA 94305, USA (J. P. A. Ioannidis); Department of Health Research and Policy, Stanford University School of Medicine, Stanford, CA 94305, USA (J. P. A. Ioannidis); Department of Statistics, Stanford University School of Humanities and Sciences, Stanford, CA 94305, USA (J. P. A. Ioannidis); RD Néphrologie, 34090 Montpellier Cedex, France (A. Argiles); Faculty of Life Sciences and School of Computer Science, University of Manchester, Manchester M13 9PL, UK (T. K. Attwood); Department of Immunology, Genetics and Pathology, Uppsala University, SE-751 24 Uppsala, Sweden (E. Bongcam-Rudloff); Department of Animal Breeding and Genetics, Swedish University of Agricultural Sciences, SE-751 24 Uppsala, Sweden (E. Bongcam-Rudloff); Sanofi-Aventis Deutschland GmbH D-65926 Frankfurt am Main, Germany (M. Broenstrup); Divisions of Histology and Biotechnology, Biomedical Research Foundation, Academy of Athens, 11527 Athens, Greece (A. Charonis); First Department of Pediatrics, Athens University Medical School, Aghia Sophia Children's Hospital, 11527 Athens, Greece (G. P Chrousos); European Commission, Directorate-General for Research and Innovation, Unit F5: Personalised Medicine, 21 rue du Champ de Mars, Brussels, Belgium (T. Dylag); Department of Pediatrics, Hannover Medical School, 30625 Hannover, Germany (J. Ehrich); IIS-Fundación Jiménez Díaz, Autonoma University, Madrid, Spain (J. Egido, A. Ortiz); C Institute of Clinical Chemistry, Universitätsklinikum Mannheim, 68167 Mannheim, Germany (P. Findeisen); Charité (CBF), Medizinische Klinik IV, 12200 Berlin, Germany (J. Jankowski); Abbott Laboratories, Abbott Park, IL 60064, USA (R. W. Johnson); Department of Medicine, University of Alabama at Birmingham, Birmingham, AL 35294, USA (B. A. Julien); Department of Gastroenterology, Hepatology and Endocrinology, Hannover Medical School, 30625 Hannover, Germany (T. Lankisch, M. P. Manns); The Beatson Institute for Cancer Research, Garscube Estate, Glasgow G61 1BD, UK (H. Y. Leung); Barbara Davis Center for Childhood Diabetes, University of Colorado Denver, Aurora, CO, USA (D. Maahs); Department of Experimental Medicine, University of Milano-Bicocca, Monza, Italy (F. Magni); European Medicines Agency, London, UK (E. Manolis); Medical University of Innsbruck, Department of Internal Medicine IV, 6020 Innsbruck, Austria (G. Mayer); Division of Nephrology, Department of Internal Medicine, University Medical Centre Groningen, University of Groningen, Groningen, The Netherlands (G. Navis); Department of Microbiology, University of Alabama at Birmingham, Birmingham, AL 35294, USA (J. Novak); Steno Diabetes Center, DK-2820 Gentofte, Denmark (F. Persson, P. Rossing); Baker Heart Research Institute, Melbourne, Vic. 8008, Australia (K. Peter); European Projects Office, Institute of Health Carlos III, Madrid, Spain (H. H. Riese); Department of Nephrology, Medical Faculty, University of Skopje, 1000 Skopje, Former Yugoslav Republic of Macedonia (G. Spasovski); Faculty of Medicine at Siriraj Hospital, Mahidol University, Bangkok 10700, Thailand (V. Thongboonkerd); Department of Nephrology, Ghent University Hospital, B 9000 Ghent, Belgium (R. Vanholder); Institut National de la Santé et de la Recherche Médicale (INSERM), U1048, Institut of Cardiovascular and Metabolic Disease and Université Toulouse III Paul-Sabatier,Toulouse, France (J. P. Schanstra); Division of Biotechnology, Biomedical Research Foundation, Academy of Athens, 11527 Athens, Greece (A. Vlahou).

Correspondence to: Harald Mischak, BHF Glasgow Cardiovascular Research Centre, Institute of Cardiovascular and Medical Sciences, College of Medical, Veterinary and Life Sciences, University of Glasgow, Glasgow, UK. Tel.: +44 141 330 6210; fax: +44 141 330 1689; e-mail: Harald.Mischak@glasgow.ac.uk

Received 17 March 2012; accepted 18 March 2012

 © 2012 The Authors. European Journal of Clinical Investigation © 2012 Stichting European Society for Clinical Investigation Journal Foundation

References

1 Merchant ML, Perkins BA, Boratyn GM, Ficociello LH, Wilkey DW, Barati MT *et al*. Urinary peptidome may predict renal function decline in type 1 diabetes and microalbuminuria. *J Am Soc Nephrol* 2009;**20**:2065–74.

2 Good DM, Zürbig P, Argiles A, Bauer HW, Behrens G, Coon JJ *et al*. Naturally occurring human urinary peptides for use in diagnosis of chronic kidney disease. *Mol Cell Proteomics* 2010;**9**:2424–37.

3 Sethi S, Theis JD, Leung N, Dispenzieri A, Nasr SH, Fidler ME *et al*. Mass spectrometry-based proteomic diagnosis of renal immunoglobulin heavy chain amyloidosis. *Clin J Am Soc Nephrol* 2010;**5**:2180–7.

4 Spasovski G, Ortiz A, Vanholder R, El NM. Proteomics in chronic kidney disease: the issues clinical nephrologists need an answer for. *Proteomics Clin Appl* 2011;**5**:233–40.

5 Zurbig P, Dihazi H, Metzger J, Thongboonkerd V, Vlahou A. Urine proteomics in kidney and urogenital diseases: moving towards clinical applications. *Proteomics Clin Appl* 2011;**5**:256–68.

6 Anderson NL. The clinical plasma proteome: a survey of clinical assays for proteins in plasma and serum. *Clin Chem* 2010;**56**:177–85.

7 Semmes OJ, Feng Z, Adam BL, Banez LL, Bigbee WL, Campos D *et al*. Evaluation of serum protein profiling by surface-enhanced laser desorption/ionization time-of-flight mass spectrometry for the detection of prostate cancer: I. Assessment of platform reproducibility. *Clin Chem* 2005;**51**:102–12.

8 Haubitz M, Good DM, Woywodt A, Haller H, Rupprecht H, Theodorescu D *et al*. Identification and validation of urinary biomarkers for differential diagnosis and evaluation of therapeutic intervention in ANCA associated vasculitis. *Mol Cell Proteomics* 2009;**8**:2296–307.

9 Chau CH, Rixe O, McLeod H, Figg WD. Validation of analytic methods for biomarkers used in drug development. *Clin Cancer Res* 2008;**14**:5967–76.

10 Lee JW, Hall M. Method validation of protein biomarkers in support of drug development or clinical diagnosis/prognosis. *J Chromatogr B Analyt Technol Biomed Life Sci* 2009;**877**:1259–71.

11 Mischak H, Apweiler R, Banks RE, Conaway M, Coon JJ, Dominizak A *et al*. Clinical Proteomics: a need to define the field and to begin to set adequate standards. *Proteomics Clin Appl* 2007;**1**:148–56.

12 Ioannidis JP, Panagiotou OA. Comparison of effect sizes associated with biomarkers reported in highly cited individual articles and in subsequent meta-analyses. *JAMA* 2011;**305**:2200–10.

13 Biomarker bias. *Nat Med* 2012;**17**:763.

14 Diamandis EP. Cancer biomarkers: can we turn recent failures into success? *J Natl Cancer Inst* 2010;**102**:1462–7.

15 Knepper MA. Common sense approaches to urinary biomarker study design. *J Am Soc Nephrol* 2009;**20**:1175–8.

16 Mischak H, Allmaier G, Apweiler R, Attwood T, Baumann M, Benigni A *et al*. Recommendations for biomarker identification and qualification in clinical proteomics. *Sci Transl Med* 2010;**2**:46ps42.

17 Ioannidis JP. A roadmap for successful applications of clinical proteomics. *Proteomics Clin Appl* 2011;**5**:241–7.

18 Rifai N, Gillette MA, Carr SA. Protein biomarker discovery and validation: the long and uncertain path to clinical utility. *Nat Biotechnol* 2006;**24**:971–83.

19 Hood BL, Stewart NA, Conrads TP. Development of high-throughput mass spectrometry-based approaches for cancer biomarker discovery and implementation. *Clin Lab Med* 2009;**29**:115–38.

20 Boja ES, Jortani SA, Ritchie J, Hoofnagle AN, Tezak Z, Mansfield E *et al*. The journey to regulation of protein-based multiplex quantitative assays. *Clin Chem* 2011;**57**:560–7.

21 Remily-Wood ER, Liu RZ, Xiang Y, Chen Y, Thomas CE, Rajyaguru N *et al*. A database of reaction monitoring mass spectrometry assays for elucidating therapeutic response in cancer. *Proteomics Clin Appl* 2011;**5**:383–96.

22 Khleif SN, Doroshow JH, Hait WN. AACR-FDA-NCI Cancer Biomarkers Collaborative consensus report: advancing the use of biomarkers in cancer drug development. *Clin Cancer Res* 2010;**16**: 3299–318.

23 Sattar N. Biomarkers for diabetes prediction, pathogenesis or pharmacotherapy guidance? Past, present and future possibilities. *Diabet Med* 2012;**29**:5–13.

24 Ioannidis JP, Khoury MJ. Improving validation practices in ''omics'' research. *Science* 2011;**334**:1230–2.

25 Ioannidis JP, Tzoulaki I. What makes a good predictor?: the evidence applied to coronary artery calcium score. *JAMA* 2010;**303**:1646–7.

26 Fleming TR, DeMets DL. Surrogate end points in clinical trials: are we being misled? *Ann Intern Med* 1996;**125**:605–13.

27 Ransohoff DF, Khoury MJ. Personal genomics: information can be harmful. *Eur J Clin Invest* 2010;**40**:64–8.

28 Ruggenenti P, Fassi A, Ilieva AP, Bruno S, Iliev IP, Brusegan V *et al*. Preventing microalbuminuria in type 2 diabetes. *N Engl J Med* 2004;**351**:1941–51.

29 Haller H, Ito S, Izzo JL Jr, Januszewicz A, Katayama S, Menne J *et al*. Olmesartan for the delay or prevention of microalbuminuria in type 2 diabetes. *N Engl J Med* 2011;**364**:907–17.

30 Dylag T, Jehenson P, van de Loo JW, Sanne JL. Basic and clinical proteomics from the EU Health Research perspective. *Proteomics Clin Appl* 2010;**4**:888–91.

31 Mischak H, Rossing P. Proteomic biomarkers in diabetic nephropathy–reality or future promise? *Nephrol Dial Transplant* 2010;**25**:2843–5.

32 Verma M, Wright GL Jr, Hanash SM, Gopal-Srivastava R, Srivastava S. Proteomic approaches within the NCI early detection research network for the discovery and identification of cancer biomarkers. *Ann N Y Acad Sci* 2001;**945**:103–15.

33 Manolis E, Vamvakas S, Isaac M. New pathway for qualification of novel methodologies in the European medicines agency. *Proteomics Clin Appl* 2011;**5**:248–55.

34 Keogh B. European biobanks forge cross-border ties. *J Natl Cancer Inst* 2011;**103**:1429–31.

35 Murtagh MJ, Demir I, Harris JR, Burton PR. Realizing the promise of population biobanks: a new model for translation. *Hum Genet* 2011;**130**:333–45.

36 Mitchell R, Conley JM, Davis AM, Cadigan RJ, Dobson AW, Gladden RQ. Genomics. Genomics, biobanks, and the trade-secret model. *Science* 2011;**332**:309–10.

37 Budimir D, Polasek O, Marusic A, Kolcic I, Zemunik T, Boraska V *et al*. Ethical aspects of human biobanks: a systematic review. *Croat Med J* 2011;**52**:262–79.

38 Kaye J. From single biobanks to international networks: developing e-governance. *Hum Genet* 2011;**130**:377–82.

39 Wichmann HE, Kuhn KA, Waldenberger M, Schmelcher D, Schuffenhauer S, Meitinger T *et al*. Comprehensive catalog of European biobanks. *Nat Biotechnol* 2011;**29**:795–7.

40 Poste G. Bring on the biomarkers. *Nature* 2011;**469**:156–7.

41 Chaturvedi N, Porta M, Klein R, Orchard T, Fuller J, Parving HH *et al*. Effect of candesartan on prevention (DIRECT-Prevent 1) and progression (DIRECT-Protect 1) of retinopathy in type 1 diabetes: randomised, placebo-controlled trials. *Lancet* 2008;**372**:1394–402.

42 Sjolie AK, Klein R, Porta M, Orchard T, Fuller J, Parving HH *et al.* Effect of candesartan on progression and regression of retinopathy in type 2 diabetes (DIRECT-Protect 2): a randomised placebo-controlled trial. *Lancet* 2008;**372**:1385–93.
43 Bilous R, Chaturvedi N, Sjolie AK, Fuller J, Klein R, Orchard T *et al.* Effect of candesartan on microalbuminuria and albumin excretion rate in diabetes: three randomized trials. *Ann Intern Med* 2009;**151**:11–4.
44 Heart Outcomes Prevention Evaluation (HOPE) Study Investigators. Effects of ramipril on cardiovascular and microvascular outcomes in people with diabetes mellitus: results of the HOPE study and MICRO-HOPE substudy. Heart Outcomes Prevention Evaluation Study Investigators. *Lancet* 2000;**355**:253–9.
45 Patel A, MacMahon S, Chalmers J, Neal B, Woodward M, Billot L *et al.* Effects of a fixed combination of perindopril and indapamide on macrovascular and microvascular outcomes in patients with type 2 diabetes mellitus (the ADVANCE trial): a randomised controlled trial. *Lancet* 2007;**370**:829–40.

 © 2012 The Authors. European Journal of Clinical Investigation © 2012 Stichting European Society for Clinical Investigation Journal Foundation

European Journal of Pharmacology 689 (2012) 219–225

Contents lists available at SciVerse ScienceDirect

European Journal of Pharmacology

journal homepage: www.elsevier.com/locate/ejphar

Pulmonary, gastrointestinal and urogenital pharmacology

Citrate, not phosphate, can dissolve calcium oxalate monohydrate crystals and detach these crystals from renal tubular cells

Somchai Chutipongtanate [a,b,1], Sakdithep Chaiyarit [a,b,1], Visith Thongboonkerd [a,b,*]

[a] Medical Proteomics Unit, Office for Research and Development, Faculty of Medicine Siriraj Hospital, Mahidol University, Bangkok 10700, Thailand
[b] Center for Research in Complex Systems Science, Mahidol University, Bangkok 10700, Thailand

ARTICLE INFO

Article history:
Received 25 January 2012
Received in revised form
31 May 2012
Accepted 9 June 2012
Available online 17 June 2012

Keywords:
Calcium oxalate
Citrate
Crystal
Dissolution
Kidney stone
Phosphate

ABSTRACT

Dissolution therapy of calcium oxalate monohydrate (COM) kidney stone disease has not yet been implemented due to a lack of well characterized COM dissolution agents. The present study therefore aimed to identify potential COM crystal dissolution compounds. COM crystals were treated with deionized water (negative control), 5 mM EDTA (positive control), 5 mM sodium citrate, or 5 mM sodium phosphate. COM crystal dissolution activities of these compounds were evaluated by phase-contrast and video-assisted microscopic examinations, semi-quantitative analysis of crystal size, number and total mass, and spectrophotometric oxalate-dissolution assay. In addition, effects of these compounds on detachment of COM crystals, which adhered tightly onto renal tubular cell surface, were also investigated. The results showed that citrate, not phosphate, had a significant dissolution effect on COM crystals as demonstrated by significant reduction of crystal size (approximately 37% decrease), crystal number (approximately 53% decrease) and total crystal mass (approximately 72% decrease) compared to blank and negative controls. Spectrophotometric oxalate-dissolution assay successfully confirmed the COM crystal dissolution property of citrate. Moreover, citrate could detach up to 85% of the adherent COM crystals from renal tubular cell surface. These data indicate that citrate is better than phosphate for dissolution and detachment of COM crystals.

© 2012 Elsevier B.V. All rights reserved.

1. Introduction

A major problem in management of COM kidney stone disease is its high recurrence rate as approximately 50% of the stone formers have recurrent stones within 10 years after the stone removal (Worcester and Coe, 2008). Although this recurrence rate tends to decline by prevention with high fluid intake (Borghi et al., 1996), dietary modifications (Borghi et al., 2002), and medical treatments (e.g., thiazide and alkali) (Pak, 2008), the recurrent stones remain in approximately 15–40% of cases who have received these interventions (Borghi et al., 2002; Coe et al., 2005; Fink et al., 2009), suggesting that the prevention against recurrent COM kidney stone disease require additional and better strategies.

Dissolution therapy has been widely accepted as an effective treatment for uric acid stone (Ngo and Assimos, 2007). It has been also investigated for many stone types, including calcium phosphate (Xiang-bo et al., 2005), cystine (Tiselius, 2010), and struvite (Heimbach et al., 2000). Ideally, dissolution agents may be used as primary treatment to dissolve the whole calculi, adjuvant therapy to dissolve residual stone fragments after surgical removal, or prophylactic therapy to prevent recurrent stones (Ngo and Assimos, 2007). Unfortunately, this treatment modality has not been implemented for COM kidney stone disease due to the lack of strong evidence and characterizations of COM dissolution agents. EDTA, a well-known calcium-chelating agent, had been previously shown to have dissolution activity on COM stone in vitro (Burns and Cargill, 1987). However, the toxicity of this agent limits its applications in vivo (Kane et al., 1989; Oosterlinck et al., 1991). In contrast to uric acid stone, adjustment of urinary pH has minimal or no effect on the solubility of COM stone. Therefore, identification of COM stone dissolution agents, which are applicable in vivo, is needed for better management of COM kidney stone disease. Citrate and phosphate have been used for "prophylactic treatment" aiming to "prevent" recurrent COM kidney stone for a long time (Escribano et al., 2009; Tracy and Pearle, 2009). However, their "dissolution effects" on COM crystals, which are the major crystalline compositions of kidney stones, remained unclear and under-investigated.

The present study therefore aimed to evaluate COM crystal dissolution properties of citrate and phosphate using morphological evaluation and semi-quantitative measurement of COM

* Corresponding author. at: Professor and Head of Medical Proteomics Unit, Director of Center for Research in Complex Systems Science (CRCSS), Siriraj Hospital, Mahidol University, 12th Floor Adulyadej Vikrom Building, 2 Prannok Road, Bangkoknoi, Bangkok 10700, Thailand. Tel./fax .: +66 2 4184793.
E-mail addresses: thongboonkerd@dr.com, vthongbo@yahoo.com (V. Thongboonkerd).
[1] Both authors share equal contributions.

0014-2999/$ - see front matter © 2012 Elsevier B.V. All rights reserved.
http://dx.doi.org/10.1016/j.ejphar.2012.06.012

crystal size, number and total mass. Serial analysis was performed by video-assisted morphological study to monitor the dissolution activities of these compounds within 1-h of the treatment. Validation of their dissolution activities was performed by spectrophotometric oxalate-dissolution assay to measure the increased levels of free oxalate ions as the end products of COM crystal dissolution. Finally, effects of these compounds on detachment of COM crystals, which were adhered tightly on renal tubular cell surface, were also investigated.

2. Materials and methods

2.1. COM crystal preparation and treatment with citrate and phosphate

COM crystals were generated according to our protocols published previously (Thongboonkerd et al., 2006; 2008). Briefly, COM crystals were prepared in 24-well, polystyrene, disposable cell culture cluster (with lid) (Corning Inc.; Corning, NY) by mixing calcium chloride ($CaCl_2 \cdot 2H_2O$) and sodium oxalate ($Na_2C_2O_4$) at final concentrations of 5.0 and 0.5 mM, respectively, in a buffer containing 10 mM Tris–HCl (pH 7.4) and 90 mM NaCl. After 1-h of COM crystallization, the supernatant was discarded, whereas the crystals were gently washed with 100% methanol and dried at room temperature (25 °C). These crystals were then used as a "blank" control.

To examine the dissolution effect, COM crystals were prepared as aforementioned, followed by an addition with 1-ml of dI water ("negative" control), 5 mM sodium EDTA (Na_4EDTA; final pH=9.49) ("positive" control), 5 mM sodium citrate ($Na_3Citrate$; $Na_3C_6H_5O_7$; final pH=8.48) (the normal range of urinary citrate is 1.5–7.5 mM (Chutipongtanate and Thongboonkerd, 2010)), or 5 mM sodium phosphate (NaH_2PO_4; final pH=5.70) (the normal range of urinary phosphate is 2.5–5.5 mM (Chutipongtanate and Thongboonkerd, 2010)). After 1-h incubation at room temperature (25 °C), dissolution effect of each treatment was evaluated as follows (all these experiments were done in triplicate).

2.2. Semi-quantitative analyses of COM crystal size, number and total mass

COM crystal dissolution effect of each treatment was initially screened by phase-contrast microscopic examination using an Olympus CKX41 inverted light microscope (Olympus Co. Ltd.; Tokyo, Japan). Crystal size was semi-quantitatively analyzed by ImageMaster 2D Platinum software (GE Healthcare; Uppsala, Sweden), which can accurately measure crystal area (Thongboonkerd et al., 2008). The crystal size was measured and averaged from at least 100 crystals in individual samples. Crystal number was counted and averaged from 10 high-power fields (HPF). Crystal mass, which is the most important parameter to evaluate dissolution activity, was then calculated by the following equation:

$$\text{Crystal mass(pixels/HPF)} = \text{Averaged crystal area(pixels)} x \text{ Crystal number(No./HPF)} \quad (1)$$

2.3. Video-assisted monitoring of COM crystal dissolution

Video-assisted dissolution study was performed to monitor the dissolution activity of each compound on COM crystals. COM crystal preparation and interventions were performed as described above but with video recording of dissolution events using a digital camera connected with Olympus CKX41 inverted phase-contrast microscope (Olympus Co. Ltd). The video files were replayed and images were periodically extracted at various time-points, including 0, 1, 2, 5, 10, 30, and 60 min after the intervention. At each time-point, the crystal size was measured using ImageMaster 2D Platinum software (GE Healthcare) as aforementioned.

2.4. Spectrophotometric oxalate-dissolution assay

COM crystal dissolution would result to dissociation of CaOx molecules and increased levels of free calcium and oxalate ions in the solution. The increasing level of free oxalate ions was detectable by UV–visible spectrophotometry at λ214 nm (Nakagawa et al., 1985). Therefore, COM crystal dissolution activity could be measured using spectrophotometric oxalate-dissolution assay, which was modified from the oxalate-depletion assay used as the gold standard to quantitatively analyze COM crystal growth (Nakagawa et al., 1985). COM crystal seeds (160 μg) were added to a cuvette containing 1-ml of dI water in the absence or presence of 5 mM sodium EDTA, 5 mM sodium citrate, or 5 mM sodium phosphate. The mixture was continuously and gently stirred at room temperature (25 °C) using a mini-magnetic bar. Degree of oxalate resolution (which reflected degree of COM crystal dissolution) was then monitored for up to 60 min using a Shimadzu UV-160 A spectrophotometer (Shimadzu; Kyoto, Japan).

2.5. Investigation of COM crystal detachment

Detachment of COM crystals that tightly adhered on renal tubular cell surface was also investigated by video-assisted monitoring. Madin-Darby Canine Kidney (MDCK) cells (approximately 1×10^6 cells) were cultivated in complete Eagle's minimum essential medium (MEM) (GIBCO, Invitrogen Corporation; Grand Island, NY) supplemented with 10% fetal bovine serum, 1.2% penicillin G/streptomycin and 2 mM glutamine in 10-mm^2 dish inside a humidified incubator at 37 °C with 5% CO_2. The cells were maintained for approximately 24-h or until confluent monolayer was observed. Thereafter, the culture medium was removed and replace with the fresh medium containing COM crystals (100 μg COM crystals/ml MEM medium). The cells were further maintained for 1-h at 37 °C to allow COM crystals to adhere tightly onto MDCK renal tubular cell surface. Non-adherent crystals were then removed by three vigorous washes with PBS. To observe detachment of the adherent COM crystals, Na_4EDTA ("positive" control), $Na_3Citrate$ or NaH_2PO_4 was added to 1-ml MEM medium to make the final concentration of 5 mM for each. An equal volume of dI water was also added to 1-ml MEM medium and used as the "negative" control. Final pH levels of MEM medium with Na_4EDTA, $Na_3Citrate$ and NaH_2PO_4 were 7.69, 8.04 and 6.92, respectively. These media were added to the cells and the cells were further maintained for 1-h under video-assisted monitoring using a digital camera connected with Olympus CKX41 inverted phase-contrast microscope (Olympus Co. Ltd). The video images were periodically extracted at various time-points, including 0, 1, 2, 5, 10, 30, and 60 min after the intervention. At each time-point, the percentage of the remained adherent crystals was then calculated using the following equation:

$$\%\ \text{COM crystal detachment} = 100x[(\text{COM}t_0 - \text{COM}t_n)/\text{COM}t_0] \quad (2)$$

where $\text{COM}t_0$ was the average number of the adherent crystals at basal time-point (0 min) and $\text{COM}t_n$ was the average number of the adherent crystals remained at any specific time-point. This experiment was also performed in triplicate.

2.6. Statistical analysis

All the quantitative data are reported as mean ± S.E.M. Multiple comparisons were performed using ANOVA with Tukey's post-hoc

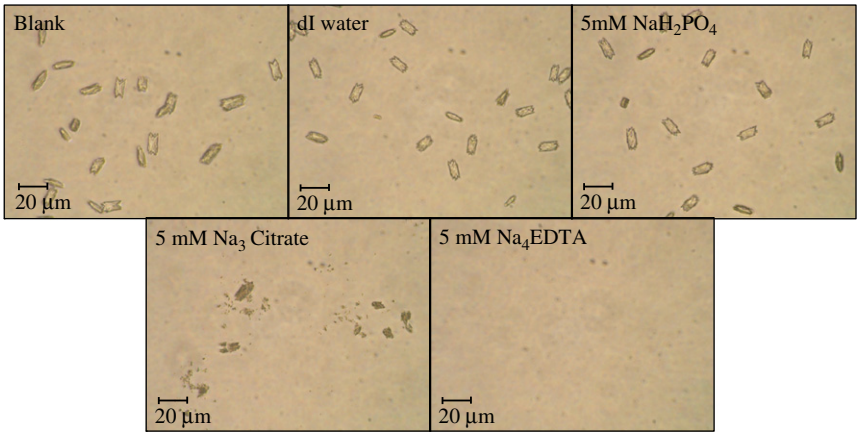


Fig. 1. Morphological evaluation of COM crystal dissolution effects. COM crystals were incubated for 1-h with dI water ("negative" control), 5 mM sodium EDTA (Na_4EDTA) ("positive" control), 5 mM sodium citrate ($Na_3Citrate$), or 5 mM sodium phosphate (NaH_2PO_4). COM crystals without any treatment served as the "blank" control. Images were taken from an Olympus CKX41 inverted light microscope (original magnification=400X for all panels). All experiments were done in triplicate.

test (SPSS, version 11.5). *P* values < 0.05 were considered statistically significant.

3. Results

After 1-h incubation, COM crystal dissolution activities of 5 mM sodium citrate and 5 mM sodium phosphate were initially screened by phase-contrast microscopic examination using 5 mM sodium EDTA as the "positive" control and dI water as the "negative" control, whereas plain COM crystals without any addition served as the "blank" control. As expected, dI water had no effects on COM crystals, whereas sodium EDTA had a potent COM dissolution activity as demonstrated by complete dissolution of all COM crystals at 1-h post-incubation (Fig. 1). Treatment with sodium citrate also showed a significant dissolution effect on COM crystals but with a lesser potency as compared to sodium EDTA. In contrast, sodium phosphate had no obvious effects on COM crystals as the resulting crystals looked similar to those of blank and negative controls (Fig. 1).

At the same incubation time-point (1-h), crystal size, number and total mass were semi-quantitatively analyzed using ImageMaster 2D Platinum software (GE Healthcare) to precisely evaluate the degree of dissolution effects of all compounds (Fig. 2). Consistent to the qualitative data as aforementioned, EDTA had a potent dissolution activity against COM crystals as all the crystals were completely dissolved after treatment with EDTA for 1-h. The dissolution effect of citrate was then compared to that of phosphate. For crystal size, phosphate slightly reduced COM crystal size (approximately 9% decrease), whereas citrate had much stronger effects (approximately 37% decrease) compared to negative and blank controls (Fig. 2A). This data suggested that semi-quantitative analysis using ImageMaster 2D Platinum software was more sensitive than qualitative analysis using phase-contrast microscopy to detect subtle changes in crystal size. For crystal number, only citrate was able to reduce COM crystal number (approximately 50% decrease) (Fig. 2B). This result implicated that some COM crystals (particularly the small ones) were completely dissolved within 1-h incubation with sodium citrate, whereas phosphate was not effective for COM crystal dissolution. Finally, the remaining COM crystal mass after dissolution was calculated (see Eq. (1) in the Materials and methods section). The data showed that citrate dramatically reduced COM total crystal mass (approximately 72% decrease), whereas phosphate reduced total crystal mass with a much lesser extent (approximately 16% decrease) (Fig. 2C). Taken together, these

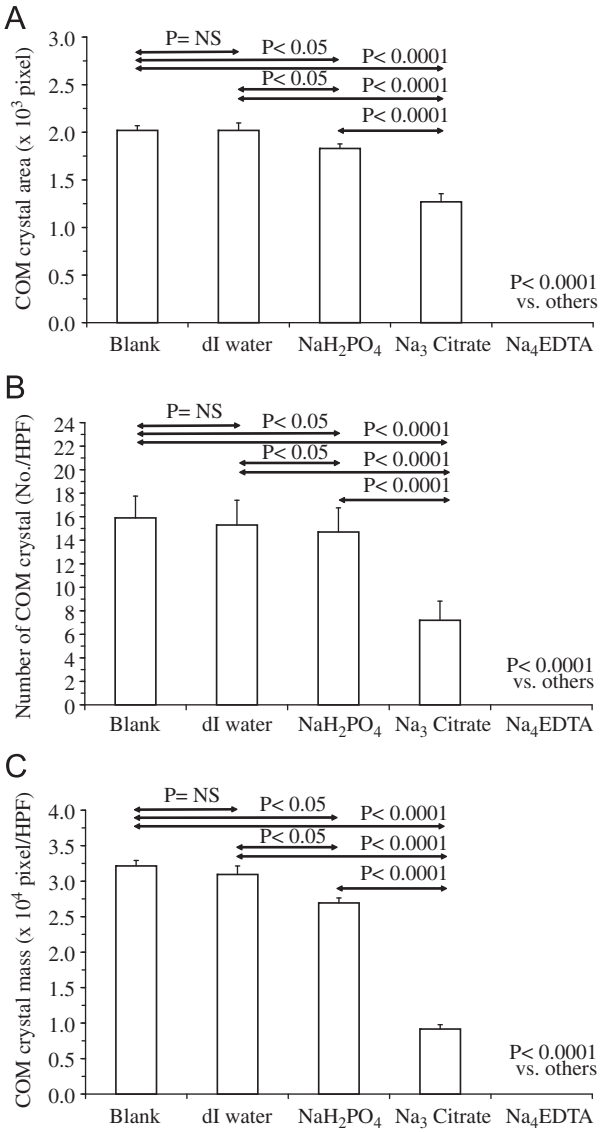


Fig. 2. Semi-quantitative analyses of COM crystal size (A), number (B) and total mass (C) after 1-h incubation of COM crystals with dI water ("negative" control), 5 mM sodium EDTA (Na_4EDTA) ("positive" control), 5 mM sodium citrate ($Na_3Citrate$), or 5 mM sodium phosphate (NaH_2PO_4). COM crystals without any treatment served as the "blank" control. Each bar was derived from 3 independent experiments and the data are reported as mean ± S.E.M. NS=not significant.

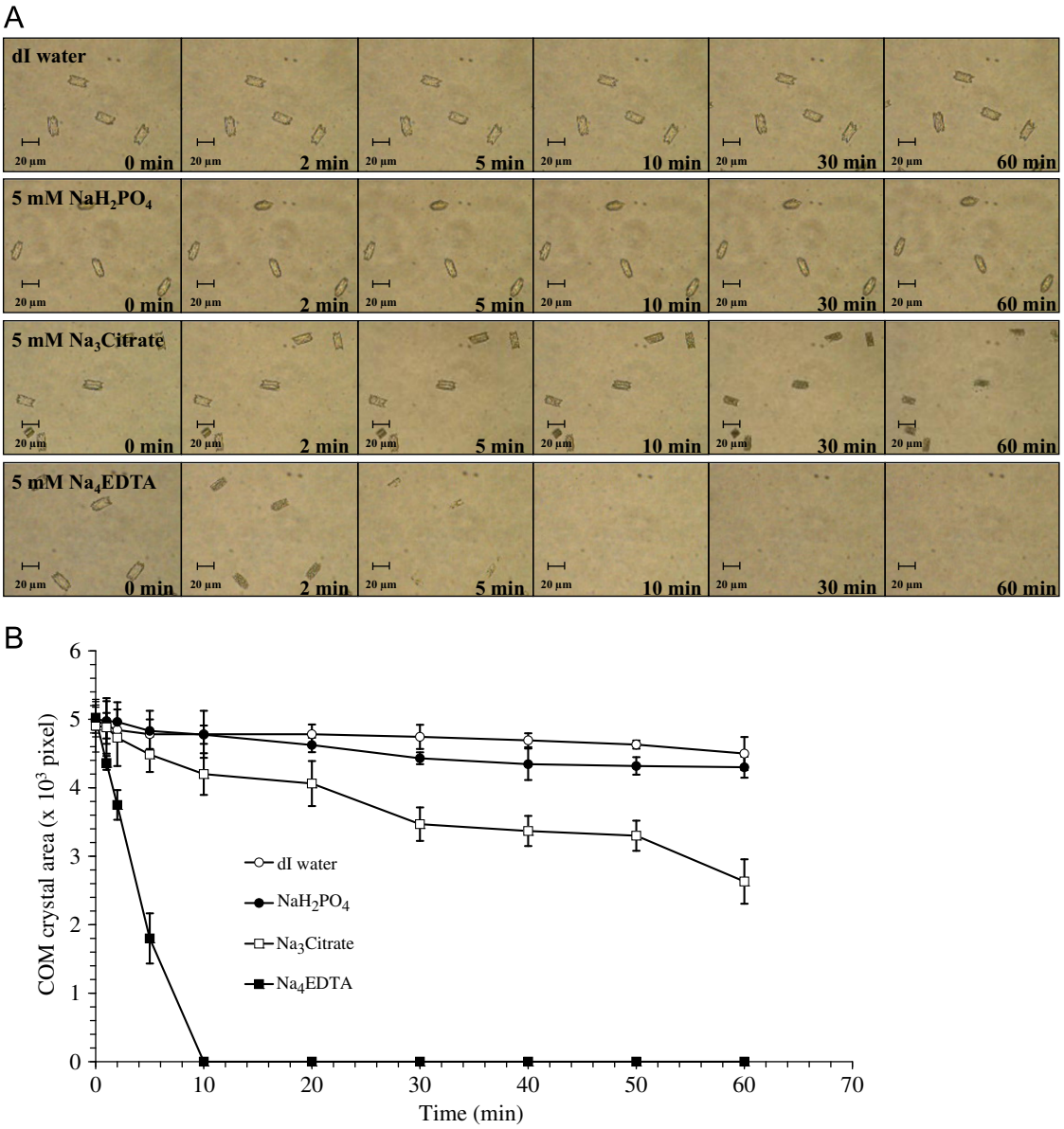


Fig. 3. Video-assisted COM crystal dissolution study. During 1-h incubation period of COM crystals with dI water, 5 mM sodium EDTA, 5 mM sodium citrate, or 5 mM sodium phosphate, the dissolution events were monitored and recorded using a digital camera (A). The video files were replayed and images were periodically extracted from various time-points. Thereafter, COM crystal size was serially measured at different time-points (B). The data are presented as mean ± S.E.M.

data indicated that citrate may be the better candidate to be used as a dissolution agent against COM crystals as compared to phosphate.

We initially examined effects of EDTA, citrate and phosphate at 1-h incubation period, at which the results were the final products of all spatial changes. We then monitored for serial changes of dissolution events within 1-h by video-assisted microscopic study (Fig. 3A). The results demonstrated that EDTA completely dissolved all COM crystals within 10-min, whereas citrate exhibited a gradual reduction of COM crystal size, starting from 20-min of incubation through the end of the assay (1-h). In contrast, phosphate did not show obvious dissolution activity (Fig. 3A and B).

The dissolution activities of these compounds were validated by spectrophotometric oxalate-dissolution assay (Fig. 4). Similar to the initial sets of data, EDTA had the strongest dissolution activity as demonstrated by a rapid increase in levels of free oxalate ions within only 10-min after incubation. Citrate also provided a potent dissolution activity, particularly at 1-h after incubation. It should be noted that, however, both dI water and sodium phosphate treatments were also associated with slightly increased levels of free oxalate ions. This phenomenon might be due to the physical interference in spectrophotometric oxalate-dissolution assay (in which the solution was continuously stirred), whereas this physical interference was absent in microscopic examinations (in which the solution was still, without stirring).

As pH of the solution might be the concern for evaluation of the dissolution activities of these compounds, we examined whether pH had an effect on COM crystal dissolution or not. As the final pH of the solution with 5 mM Na_4EDTA, 5 mM $Na_3Citrate$ and 5 mM NaH_2PO_4 was 9.49, 8.48 and 5.70, respectively, we examined effects of pH 5.0–10.0 on COM crystal size and free oxalate levels using the assays described in the Materials and methods section (Video-assisted monitoring of COM crystal dissolution and Spectrophotometric oxalate-dissolution assay

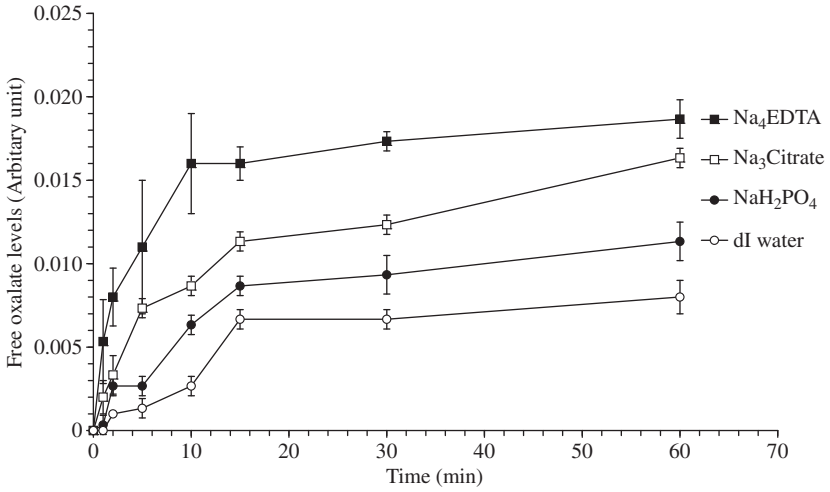


Fig. 4. Spectrophotometric oxalate-dissolution assay. COM crystal seeds (160 μg) were added to a cuvette containing 1-ml of dI water in the absence or presence of 5 mM sodium EDTA, 5 mM sodium citrate or 5 mM sodium phosphate. Levels of free oxalate ions (which reflected degree of COM crystal dissolution) was then serially monitored using absorbance at λ214 nm for up to 60 min. Each data point was derived from 3 independent experiments and the data are reported as mean ± S.E.M.

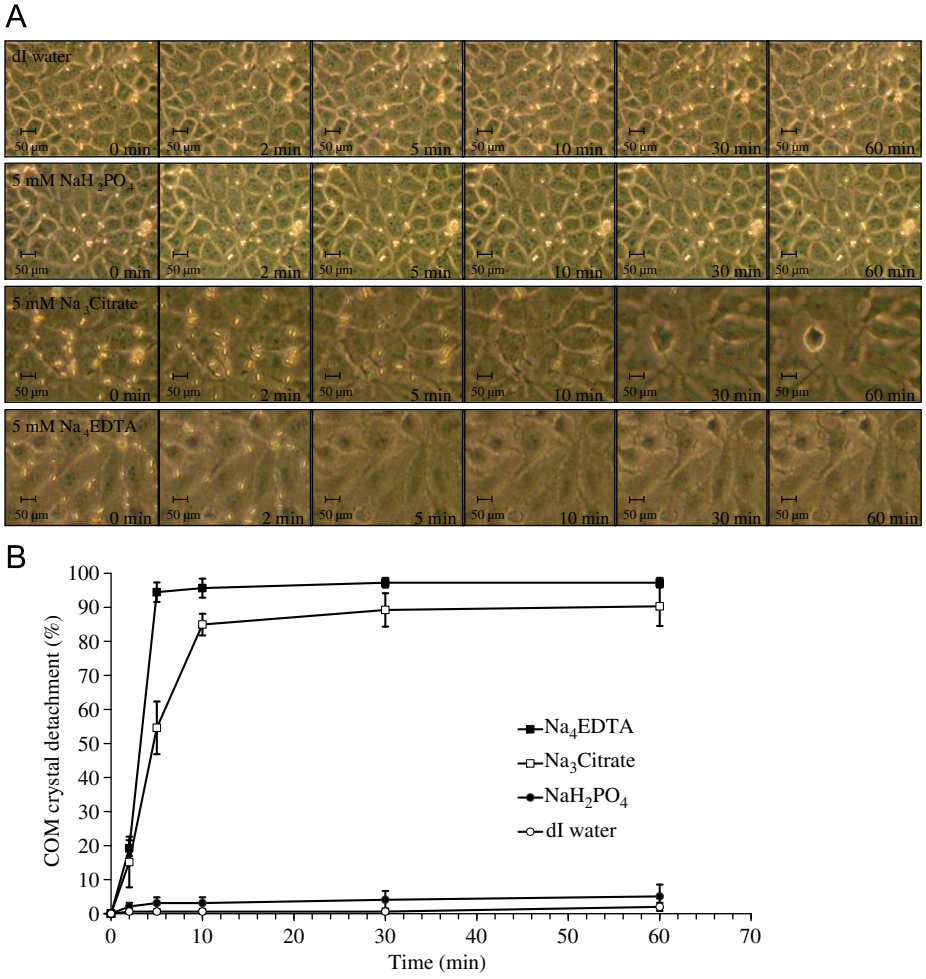


Fig. 5. Video-assisted COM crystal detachment study. After 1-h incubation of COM crystals with MDCK renal tubular cells, detachment of the adherent COM crystals by MEM medium containing dI water, 5 mM sodium EDTA, 5 mM sodium citrate, or 5 mM sodium phosphate were monitored and recorded using a digital camera (A). The video files were replayed and images were periodically extracted at various time-points. Thereafter, the number of remained adherent COM crystals was used for calculation of the degree of COM crystal detachment (B) (see Eq. (2) in the Materials and methods section). The data are presented as mean ± S.E.M. (n=3 independent experiments for each data point).

sections), but without EDTA, citrate and phosphate. The pH of dI water was adjusted to 5.0–10.0 by concentrated HCl or NaOH. The data revealed that pH had no significant effects on COM crystal dissolution (Supplementary Figs. S1 and S2). Thus, the effects of EDTA and citrate on COM crystal dissolution as aforementioned were not the results of their differential pH levels.

We extended our present study to also examine another mechanism of action of dissolution agent, i.e., crystal detachment activity (since dissociation of COM crystals at cell-crystal interface might disrupt adhesive force, particularly ionic interaction (Sheng et al., 2005), between the adherent COM crystals and apical surface of renal tubular epithelial cells. After allowing COM crystals to adhere tightly onto MDCK renal tubular cell surface for 1-h, the effects of all examined compounds on adherent COM crystals were monitored by video-assisted microscopic examination (Fig. 5A) and the degree of COM crystal detachment was calculated (see Eq. (2) in the Materials and methods section). Consistent with the other sets of data, EDTA rapidly dissolved and detached all COM crystals within 5-min. Citrate also showed the potent detachment activity (approximately 85% detachment) within 10-min after the treatment, whereas phosphate again showed no obvious detachment activities on the adherent COM crystals (Fig. 5A and Fig. 5B).

4. Discussion

Our present study successfully demonstrated COM crystal dissolution activity of citrate by direct measurements (i.e., morphological evaluation, semi-quantitative measurement of crystal size, number and total mass, as well as video-assisted study) and indirect measurement (i.e., spectrophotometric oxalate-dissolution assay). Note that we used sodium salts of all compounds (EDTA, citrate and phosphate) as to eliminate the effects of cations in our present study. Additionally, our preliminary data revealed that sodium chloride had no effects on COM dissolution (unpublished data). Therefore, any dissolution effects observed would be the results of EDTA, citrate or phosphate, not sodium.

Indeed, the dissolution effect of citrate against CaOx had been previously investigated by Saso et al. (1998) using an indirect assay of CaO_x dissolution based on weight reduction of CaOx tablets (artificial packing of CaOx particulates). However, the analysis based only on weight reduction was considered as a rough approximation method. Another limitation was that CaOx tablet was artificial packing of CaOx particulates, which did not present crystalline faces and edges correlated with clinical calculi. In contrast, our present study performed a direct measurement of dissolution activity using a much higher sensitive method against clinically relevant COM crystals (both monoclinic prismatic and twin forms of COM prepared in this study are usually presented in the urine of stone formers (Thongboonkerd et al., 2006; 2008)). In addition, COM crystal detachment activity of citrate is reported herein for the first time. We hypothesized that citrate, as a small anionic molecule, may be able to penetrate into cell-crystal interface, and disrupt adhesive force between cells and crystals by calcium chelation and/or charge neutralization, resulting to COM crystal detachment. Better understanding of this mechanism of action may lead to rationally drug design and new strategy for medical management of COM kidney stone disease.

In contrast to citrate, phosphate seemed to have no significant benefit on COM crystal dissolution and detachment (yielded only minimal or modest degree of dissolution activity without a significant effect on crystal number and no detachment activity presented). Thus, phosphate is considerably ineffective to apply for COM stone dissolution therapy, whereas citrate provides much more potential advantages in management of COM kidney stone disease. Although it is unclear whether citrate administration is able to serve as primary therapy of COM stone or not, it should provide some benefits as an adjuvant therapy for elimination of residual stone fragments after surgical removal. This adjuvant therapy may facilitate dissolution and detachment of the retained COM crystals and/or fragments, especially those adhered onto surface of urinary tract, thereby offers a better clearance of potential nuclei for recurrent stones. Moreover, dissolution and detachment activities of citrate provides a new insight into the prophylactic therapy of recurrent COM kidney stone disease as citrate not only prevents crystallization, growth and aggregation of COM crystals (Tracy and Pearle, 2009), but also dissolves the successfully formed COM crystals and detaches the adherent COM crystals from renal tubular cell surface.

5. Conclusions

In summary, our present study provided the direct evidence demonstrating that citrate at 5 mM concentration had COM crystal dissolution and detachment effects. Nevertheless, some concerns should be raised for citrate administration in routine clinical practice. It is still unknown what should be the appropriate dose that provides the optimal clinical outcome, which must balance between the dissolution efficacy and the adverse events, e.g., gastrointestinal complications (Fazil Marickar et al., 2010). This issue requires a prospective randomized clinical study to determine the optimal dose of citrate for dissolution and detachment therapy to reach the most favorable clinical outcome in COM kidney stone formers.

Acknowledgements

This study was supported by Office of the Higher Education Commission and Mahidol University under the National Research Universities Initiative, and The Thailand Research Fund (RTA5380005) to VT. VT is also supported by "Chalermphrakiat" Grant, Faculty of Medicine Siriraj Hospital.

Appendix A. Supporting information

Supplementary data associated with this article can be found in the online version at http://dx.doi.org/10.1016/j.ejphar.2012.06.012

References

Borghi, L., Meschi, T., Amato, F., Briganti, A., Novarini, A., Giannini, A., 1996. Urinary volume, water and recurrences in idiopathic calcium nephrolithiasis: a 5-year randomized prospective study. J. Urol. 155, 839–843.
Borghi, L., Schianchi, T., Meschi, T., Guerra, A., Allegri, F., Maggiore, U., Novarini, A., 2002. Comparison of two diets for the prevention of recurrent stones in idiopathic hypercalciuria. N. Engl. J. Med. 346, 77–84.
Burns, J.R., Cargill III, J.G., 1987. Kinetics of dissolution of calcium oxalate calculi with calcium-chelating irrigating solutions. J. Urol. 137, 530–533.
Chutipongtanate, S., Thongboonkerd, V., 2010. Systematic comparisons of artificial urine formulas for in vitro cellular study. Anal. Biochem. 402, 110–112.
Coe, F.L., Evan, A., Worcester, E., 2005. Kidney stone disease. J Clin. Invest. 115, 2598–2608.
Escribano, J., Balaguer, A., Pagone, F., Feliu, A., Roque, I.F., 2009. Pharmacological interventions for preventing complications in idiopathic hypercalciuria. Cochrane Database Syst. Rev. CD004754.
Fazil Marickar, Y.M., Salim, A., Vijay, A., 2010. Effect of blind treatment on stone disease. Urol. Res. 38, 205–209.
Fink, H.A., Akornor, J.W., Garimella, P.S., MacDonald, R., Cutting, A., Rutks, I.R., Monga, M., Wilt, T.J., 2009. Diet, fluid, or supplements for secondary prevention of nephrolithiasis: a systematic review and meta-analysis of randomized trials. Eur. Urol. 56, 72–80.
Heimbach, D., Jacobs, D., Muller, S.C., Hesse, A., 2000. Improving cystine stone therapy: an in vitro study of dissolution. Urology 55, 17–21.
Kane, M.H., Rodman, J.S., Horten, B., Reckler, J., Marion, D., Vaughan Jr., E.D., 1989. Urothelial injury from ethylenediaminetetraacetic acid used as an irrigant in the urinary tract. J. Urol. 142, 1359–1360.

Nakagawa, Y., Abram, V., Parks, J.H., Lau, H.S., Kawooya, J.K., Coe, F.L., 1985. Urine glycoprotein crystal growth inhibitors. Evidence for a molecular abnormality in calcium oxalate nephrolithiasis. J. Clin. Invest. 76, 1455–1462.
Ngo, T.C., Assimos, D.G., 2007. Uric acid nephrolithiasis: recent progress and future directions. Rev. Urol 9, 17–27.
Oosterlinck, W., Verbeeck, R., Cuvelier, C., Verplaetse, H., Verbaeys, A., 1991. Toxicity of litholytic ethylenediaminetetraacetic acid solutions to the urothelium of the rat and dog. Urol. Res. 19, 265–268.
Pak, C.Y., 2008. Pharmacotherapy of kidney stones. Expert Opin. Pharmacother. 9, 1509–1518.
Saso, L., Valentini, G., Leone, M.G., Grippa, E., Silvestrini, B., 1998. Development of an in vitro assay for the screening of substances capable of dissolving calcium oxalate crystals. Urol. Int. 61, 210–214.
Sheng, X., Jung, T., Wesson, J.A., Ward, M.D., 2005. Adhesion at calcium oxalate crystal surfaces and the effect of urinary constituents. Proc. Nat. Acad. Sci. U.S.A. 102, 267–272.
Thongboonkerd, V., Chutipongtanate, S., Semangoen, T., Malasit, P., 2008. Urinary trefoil factor 1 is a novel potent inhibitor of calcium oxalate crystal growth and aggregation. J. Urol. 179, 1615–1619.
Thongboonkerd, V., Semangoen, T., Chutipongtanate, S., 2006. Factors determining types and morphologies of calcium oxalate crystals: Molar concentrations, buffering, pH, stirring and temperature. Clin. Chim. Acta 367, 120–131.
Tiselius, H.G., 2010. New horizons in the management of patients with cystinuria. Curr. Opin. Urol. 20, 169–173.
Tracy, C.R., Pearle, M.S., 2009. Update on the medical management of stone disease. Curr. Opin. Urol. 19, 200–204.
Worcester, E.M., Coe, F.L., 2008. Nephrolithiasis. Prim. Care 35, 369–391.
Xiang-bo, Z., Zhi-ping, W., Jian-min, D., Jian-zhong, L., Bao-liang, M., 2005. New chemolysis for urological calcium phosphate calculi—a study in vitro. BMC. Urol. 5, 9.

Journal of proteome research

Article

pubs.acs.org/jpr

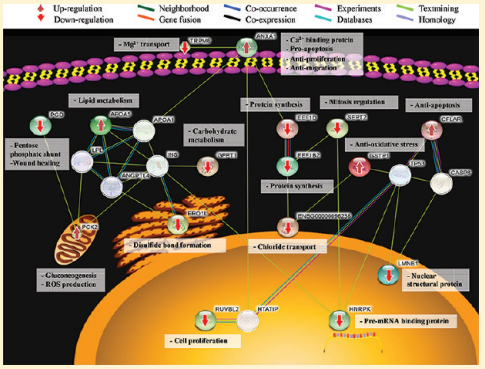
High Calcium Enhances Calcium Oxalate Crystal Binding Capacity of Renal Tubular Cells via Increased Surface Annexin A1 but Impairs Their Proliferation and Healing

Somchai Chutipongtanate, Kedsarin Fong-ngern, Paleerath Peerapen, and Visith Thongboonkerd*

†Medical Proteomics Unit, Office for Research and Development, Faculty of Medicine, Siriraj Hospital, and Center for Research in Complex Systems Science, Mahidol University, 10700 Bangkok, Thailand

Supporting Information

ABSTRACT: Hypercalciuria is associated with kidney stone formation and impaired renal function. However, responses of renal tubular cells upon exposure to high-calcium environment remain largely unknown. We thus performed a proteomic analysis of altered proteins in renal tubular cells induced by high-calcium and evaluated functional significance of these changes. MDCK cells were maintained with or without 20 mM $CaCl_2$ for 72 h. Cellular proteins were then analyzed by two-dimensional electrophoresis (2-DE) (n = 5 gels derived from 5 independent culture flasks per group). Spot matching and quantitative intensity analysis revealed 20 protein spots (from a total of 700) that were differentially expressed between the two groups. These altered proteins were then identified by Q-TOF-MS and MS/MS analyses, including those involved in calcium binding, protein synthesis, carbohydrate metabolism, lipid metabolism, cell proliferation, mitosis regulation, apoptosis, cell migration, oxidative stress, and ion transport. Protein network analysis and functional validation revealed that high-calcium-exposed cells had 36.5% increase in calcium oxalate monohydrate (COM) crystal-binding capacity. This functional change was consistent to the expression data in which annexin A1 (ANXA1), a membrane-associated calcium-binding protein, was markedly increased on the apical surface of high-calcium-exposed cells. Pretreatment with anti-ANXA1 antibody could neutralize this increasing crystal-binding capacity. Moreover, high-calcium exposure caused defects in cell proliferation and wound healing. These expression and functional data demonstrate the enhanced crystal-binding capacity but impaired cell proliferation and wound healing in renal tubular cells induced by high-calcium. Taken together, these phenomena may contribute, at least in part, to the pathogenic mechanisms of hypercalciuria-induced nephrolithiasis and impaired renal function. Our in vitro study offers several candidates for further targeted functional studies to confirm their relevance in hypercalciuria and kidney stone disease in vivo.



KEYWORDS: *calcium, hypercalciuria, kidney, nephrolithiasis, proteomics, stone, tubular cells*

INTRODUCTION

Hypercalciuria is defined as excessive urinary excretion of calcium (>200 mg/d in male; >150 mg/d in female) caused by several primary (or idiopathic) and secondary (i.e., genetic disorders, hormonal abnormalities, malignancies, and granulomatous diseases) etiologies.[1−4] Clinical significance of hypercalciuria is mostly resulted from its complications; i.e., impaired renal function and calcium oxalate monohydrate (COM) kidney stone disease (nephrolithiasis).[1,3,4] Vice versa, approximately 40% of COM stone formers have hypercalciuria.[4,5] It has been evidenced that high urinary calcium levels can enhance urinary COM supersaturation and thus facilitates COM crystallization, growth, and aggregation, leading to the development of COM nephrolithiasis.[4,6] Previous studies have demonstrated that high-calcium could enhance the adhesion of COM crystals onto renal tubular cell surface in a dose-dependent manner with still unknown mechanism(s).[7,8] The retained COM crystals can then grow further and/or aggregate with the nearby crystals, leading to the formation of stone nidus and COM nephrolithiasis. This hypothesis has been supported by the correlation between urine calcium levels and clinical stone incidence.[5,9] Despite some explanations for the lithogenic role of hypercalciuria (mostly chemical driven processes) in COM kidney stone formation, responses of renal tubular cells to this high-calcium environment (cellular driven processes) remain unclear. Whether these cellular driven processes play any significant roles, in return, to the development of COM nephrolithiasis remain unknown.

Another major complication of hypercalciuria is impaired renal function. Hypercalciuria due to some genetic disorders such as mutations of *PCLN-1* gene[10] or *CLCN5* gene[11] is associated with chronic kidney disease. Several lines of evidence have suggested that targeted intrarenal microstructure affected by hypercalciuria may be confined to renal tubules.[12−15] Electron microscopic

Received: January 23, 2012
Published: May 28, 2012

ACS Publications © 2012 American Chemical Society

evaluation of the kidney derived from an animal model of hypercalciuria has shown dramatic histopathological changes in proximal and distal renal tubular cells, i.e., loss of brush border, apical vacuolization, and low-grade cell swelling.[15] In addition, clinical investigations in hypercalciuric patients have also demonstrated renal tubular dysfunctions.[12−14] Therefore, it is likely that defects in renal tubules may be the major mechanism for hypercalciuria-induced impaired renal function.

The present study aimed to evaluate cellular responses of renal tubular cells after exposure to high-calcium environment. Among several tubular cell types, distal renal tubular cell is most suitable for this study because, first, it plays a crucial role in renal calcium handling[16,17] and, second, it has been hypothesized to be a locale for COM crystals to interact with renal cells.[8,18] Madin−Darby Canine Kidney (MDCK) cells, which were derived from distal nephron and are used widely as the representing cells of distal renal tubules,[19,20] were examined for altered protein expression after exposure to the high-calcium environment by a gel-based proteomics approach, followed by protein network analysis. Thereafter, functional significance of the expression data predicted by protein network modeling was validated by highly focused functional studies, including enhanced COM crystal-binding capacity, impaired cell proliferation, and impaired wound healing.

MATERIALS AND METHODS

Cell Cultivation and Intervention

For proteomic analysis, MDCK cells were inoculated in 75 cm^2 culture flask (approximately 3×10^6 cells/flask; $n = 5$ independent flasks per group). For functional studies of COM crystal-binding capacity, cell proliferation, cell death, and wound healing, MDCK cells were inoculated in a 6-well, polystyrene, cell culture cluster (with lid) (Corning Inc.; Corning, NY) (approximately 1×10^5 cells/well; $n = 3$ wells per group in each experiment). For all experiments, the cells were maintained in complete Eagle's minimum essential medium (MEM) (GIBCO, Invitrogen Corporation; Green Island, NY) supplemented with 10% fetal bovine serum (FBS), 1.2% penicillinG/streptomycin, and 2 mM glutamine, with or without the addition of 20 mM $CaCl_2$. Each culture medium was refreshed every day, and the cells were maintained in a humidified incubator at 37 °C with 5% CO_2 for 72 h before harvest.

For isolation of apical membranes, polarized MDCK cells were prepared by using Transwells (Costar; Cambridge, MA). Briefly, MDCK cells at a density of $5.0−7.5 \times 10^4$ cells/mL were plated and grown on a prewetted, collagen-coated, permeable polycarbonate membrane insert (0.4 μm pore size) for 4 days. The culture medium (with or without the addition of 20 mM $CaCl_2$) was refreshed every other day. The collagen was coated onto the permeable polycarbonate membrane by dissolving collagen type IV powder (Sigma; St. Louis, MO) in 0.25% acetic acid at 4 °C. The collagen solution was then added onto the membrane insert (6−10 $\mu g/cm^2$) to cover the whole surface area of the membrane and incubated at 4 °C overnight before experiments.

Protein Extraction

After 72 h maintenance with or without 20 mM $CaCl_2$, the cell monolayer was harvested by directly scraping into the tube containing PBS. The cells were then washed with PBS three times. After the final wash, the cell suspensions were centrifuged at 10 000 rpm for 2-min, and the cell pellets were resuspended in a buffer containing 7 M urea, 2 M thiourea, 4% 3-[(3-cholamidopropyl) dimethyl-ammonio]-1-propanesulfonate (CHAPS), 120 mM dithiothreitol (DTT), 2% ampholytes (pH 3−10), and 40 mM Tris-HCl, and further incubated at 4 °C for 30 min. Unsolubilized debris and particulate matters were removed by a centrifugation at 10 000 rpm for 2 min. Protein concentrations were determined using the Bradford method.

2-DE, Spot Matching, Quantitative Intensity Analysis, Q-TOF-MS, and MS/MS Analyses

For details of 2-DE, spot matching, quantitative intensity analysis, in-gel tryptic digestion, Q-TOF-MS, and MS/MS analyses, please see the Supporting Information.

Protein Network Analysis and Evaluation of Subcellular Localization

To obtain functional significance of the expression proteomics data, the Search Tool for the Retrieval of INteracting Genes/Proteins (STRING) software (http://string-db.org) was utilized.[21] This publicly available software weighs and integrates the data on protein−protein associations, both physical (direct) and functional (indirect) interactions, from numerous sources including experimental repositories, computational predictions, and public literatures, which cover 2.5 million proteins from 630 organisms.[21] By these extensive potential interactions, functional connectivity (or partnership) among the altered proteins derived from an expression proteomics study can then be assessed to generate a relevant protein association network.[21] All the altered proteins in high-calcium-exposed MDCK cells were inputted into STRING 8.3 to retrieve the data for (i) protein function; (ii) subcellular localization; and (iii) protein interaction/functional connectivity.

2-D Western Blot Analysis to Confirm the Increased Level of ANXA1 in Whole Cell Lysate

Some of the proteomic data were confirmed by 2-D Western blot analysis, which has an advantage over the conventional 1-D Western blotting to observe expression levels and locales of multiple isoforms of a particular protein. Cellular proteins (an equal amount of 100 μg total protein per sample) were resolved by 2-DE (as described above) and transferred onto nitrocellulose membranes (Whatman; Dassel, Germany) using a semidry transfer apparatus (Bio-Rad; Milano, Italy) at 75 mA for 1 h. Nonspecific bindings were blocked with 5% skim milk in PBS at room temperature for 1 h. The membranes were then incubated with mouse monoclonal anti-ANXA1 IgG1 (1:1000 in 5% skim milk/PBS) (Chemicon International, Inc.; Temecula, CA) at 4 °C overnight. After washing, the membranes were further incubated with rabbit antimouse IgG conjugated with horseradish peroxidase (1:2000 in 5% skim milk/PBS) (DakoCytomation; Glostrup, Denmark) at room temperature for 1 h. Immunoreactive protein spots were then visualized with SuperSignal West Pico chemiluminescence substrate (Pierce Biotechnology; Rockford, IL).

Isolation of Apical Membrane and Cytosolic Fractions and 1-D Western Blot Analysis to Confirm the Increased Surface Expression of ANXA1

Apical membranes of the polarized MDCK cells were isolated by a peeling method, of which principle is based on hydrous affinity and/or ionic interaction, as described previously.[22] After culture with or without $CaCl_2$ for 72 h, the culture medium was removed, and the polarized cells were rinsed twice with ice-cold membrane preserving buffer (1 mM $MgCl_2$ and 0.1 mM $CaCl_2$ in PBS). Thereafter, Whatman filter paper (0.18 mm thick, Whatman International Ltd.; Maidstone, UK) prewetted with deionized

dx.doi.org/10.1021/pr3000738 | J. Proteome Res. 2012, 11, 3650−3663

water was placed onto the polarized cell monolayer. After 5 min of incubation, the filter paper was peeled out, and the apical membranes retained at the paper surface were harvested by rehydration in deionized water and gentle scrapping. This apical membrane-enriched fraction was then lyophilized and subjected to protein extraction. The remaining cells were also harvested by scrapping and centrifuged at 10 000*g* for 10 min. The pellet was discarded, and the supernatant was collected as a cytosolic fraction. 1-D Western blot analysis was performed to evaluate the apical surface and cytosolic expression of ANXA1. All the procedures for 1-D Western blot analysis were similar to those for 2-D Western blot analysis, except only SDS-PAGE that was used to separate proteins (20 μg total protein per lane) instead of 2-DE.

Laser-Scanning Confocal Microscopic Examination to Confirm the Increased Surface Expression of ANXA1

Apical surface expression of annexin A1 was also examined by laser-scanning confocal microscopy. Briefly, MDCK cells (approximately 1×10^5 cells per sample) were cultivated on coverslips (cleaved mica disk diameter: 9.5 mm, V-1 grade, SPI supplier; Toronto, Canada). After the cells were maintained with or without 20 mM $CaCl_2$ for 72 h, they were rinsed with membrane preserving buffer (1 mM $MgCl_2$ and 0.1 mM $CaCl_2$ in PBS) and fixed with 3.7% formaldehyde in PBS at 25 °C for 15 min. After extensive washing with membrane preserving buffer, the cells were incubated with mouse monoclonal anti-ANXA1 (1:50 in 1% BSA/PBS) at 37 °C for 1 h. The cells were then rinsed with PBS three times and then incubated with AlexaFluor-488-conjugated goat antimouse IgG (Invitrogen/Molecular Probe; Burlington, Canada) (1:5000 in 1% BSA/PBS) containing 0.1 μg/mL Hoechst dye (DNA staining for nuclear localization) (Invitrogen/Molecular Probes) at 37 °C for 1 h. Thereafter, the coverslips were mounted with 50% glycerol/PBS for subsequent examination of the XY, XZ, and YZ planes using a laser-scanning confocal microscope equipped with an LSM5 Image Browser (LSM 510 Meta, Carl Zeiss; Jena, Germany).

COM Crystal-Binding Assay

COM crystals were generated according to our protocols published previously.[23] MDCK cells were cultivated in a 6-well, polystyrene, disposable cell culture cluster (with lid) with or without 20 mM $CaCl_2$ for 72 h as described above. Thereafter, the culture medium was removed, and the cells were washed with warm PBS twice and incubated with 1% BSA in membrane preserving buffer (1 mM $MgCl_2$ and 0.1 mM $CaCl_2$ in PBS) at 37 °C with 5% CO_2 for 15 min to block nonspecific bindings. Thereafter, the blocking solution was discarded, the cells were washed with warm PBS four times, and the cultured medium was replaced with 2 mL of 10% FBS-supplemented MEM with or without $CaCl_2$, anti-ANXA1 mAb (IgG1), or isotype IgG1 as to divide these cells into 4 groups, including (i) control (normal culture without $CaCl_2$); (ii) high-calcium (with 20 mM $CaCl_2$),; (iii) high-calcium + anti-ANXA1 mAb (with 20 mM $CaCl_2$ and neutralization with 0.5 μg/mL mouse monoclonal anti-ANXA1); and (iv) high-calcium + IgG1 (with 20 mM $CaCl_2$ and 0.5 μg/mL IgG1, which was used as the isotype control of anti-ANXA1 mAb) ($n = 3$ per group). After 30 min of incubation at 37 °C with 5% CO_2, the cells were extensively washed again with warm PBS four times. COM crystal-cell adhesion was initiated by the addition of 10% FBS-supplemented MEM containing 100 μg/mL COM crystals into each culture well. The cells were further incubated in a humidified incubator at 37 °C with 5% CO_2 for 30 min. Thereafter, the cells were vigorously washed by warm PBS five times to remove unbound COM crystals. Finally, numbers of the adhered COM crystals, total cell numbers, and numbers of COM crystal-adhered cells were quantitated in at least 15 randomized high power fields (HPF) per culture well. Numbers of the adhered COM crystals were then normalized by total cell numbers and are presented as numbers of COM crystals per 100 cells (No./100 cells). Percentage of COM crystal-adhered cells (%) = [(number of COM crystal-adhered cells/total cell number) × 100%]. All the experiments were performed in triplicate.

Cell Proliferation Assay

The degree of cell proliferation was determined by a conventional method using hemacytometer cell counting chamber. MDCK cells were prepared as for the above experiment to evaluate COM crystal-binding capacity. At the indicated time-points (24, 48, and 72 h after treatments), the cells were detached from the culture well using 0.1% trypsin in 2.5 mM EDTA and were immediately resuspended in 1 mL of FBS-containing MEM to terminate trypsin activity. Trypan blue staining was used to exclude dead cells and the numbers of viable cells were counted using hemacytometer. All the experiments were performed in triplicate.

Flow Cytometric Analysis of Cell Death (Annexin V/Propidium Iodide Costaining)

MDCK cells from the monolayer (including both adherent and floating cells) were trypsinized with 3 mL of 0.1% trypsin in 2.5 mM EDTA and resuspended in 10 mL of MEM. The harvested cells were centrifuged at 1500 rpm at 4 °C for 5 min and washed with PBS. Cell pellets were resuspended with annexin V buffer (10 mM HEPES, 140 mM NaCl ,and 2.5 mM $CaCl_2 \cdot 2H_2O$; pH 7.4) at a final concentration of 5×10^5 cells/mL and then incubated with FITC-labeled annexin V (BD Biosciences; San Jose, CA), on ice for 15 min in the dark. Propidium iodide (BD Biosciences) was added into the samples at a final concentration of 10 μL/mL prior to analysis. The cells were then analyzed by flow cytometry (FACScan, Becton Dickinson Immunocytometry System; San Jose, CA), and MDCK cells treated with 2 μg/mL camptothecin was used as a positive control. This experiment was performed in triplicate. Percentage of total cell death (% cell death) = [(number of both apoptotic and necrotic cells/number of all cells) × 100%].

Evaluation of Wound Healing by Scratch Assay

Wound healing study by scratch assay was performed as described previously.[24,25] Briefly, MDCK cells were inoculated in a 6-well, polystylene plate (with lid) and maintained in the controlled or high-calcium medium as aforementioned. After 72 h of incubation with controlled or high-calcium culture medium, the cell monolayers were horizontally scratched along the culture well diameter using a 200 μL plastic pipet tip to create a cell-free area. After gently washing with warm PBS to remove the debris and detached cells, the cultures were further maintained in the controlled or high-calcium medium at 37 °C with 5% CO_2. At the indicated time-points (0, 3, 6, 9, and 12 h after the scratch), each scratch wound was visualized for cellular morphological changes (from polygonal to spindle-shape with a loss of cell-to-cell contact) and multiple traveling waves (a well-known cellular behavior of wound healing) under a phase-contrast microscope and imaged by a digital camera. This image was submitted to Tarosoft Image framework v.0.9.6 (Nikon Corp.; Tokyo, Japan), which adopted to accurately measure the width of the wound (or cell-free width). All the experiments were performed in triplicate.

dx.doi.org/10.1021/pr3000738 | J. Proteome Res. 2012, 11, 3650−3663

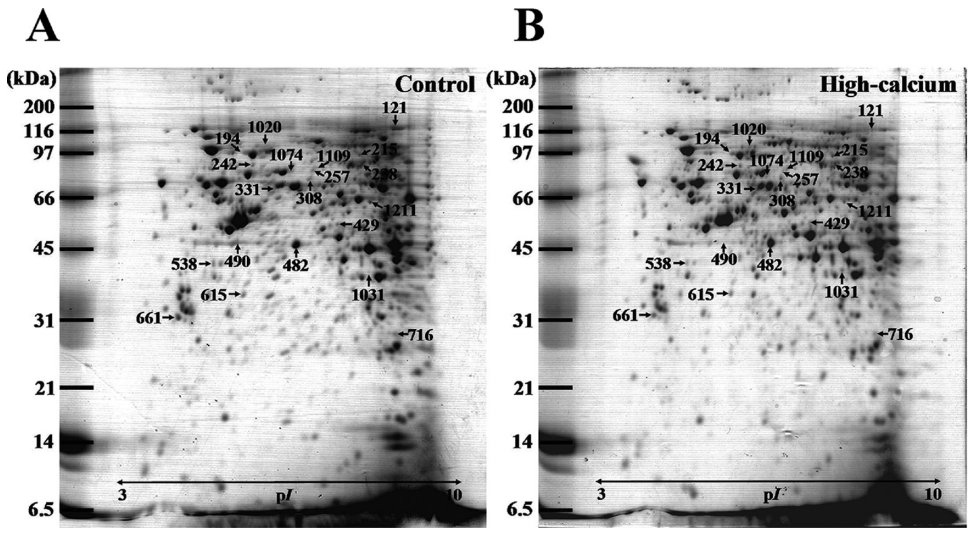


Figure 1. Representative 2-D gel images of proteins derived from controlled (A) and high-calcium-exposed MDCK cells (B). An equal amount of total protein (200 μg) derived from each sample was resolved by 2-DE using a pH gradient of 3−10 (nonlinear) for the IEF (first dimensional separation) and 12% SDS-PAGE for the second dimensional separation. The resolved protein spots were then visualized by SYPRO Ruby staining (n = 5 gels derived from 5 independent culture flasks for each group; a total of 10 gels were included for spot matching and quantitative intensity analysis). The differentially expressed protein spots with $p < 0.05$ were then identified by Q-TOF-MS and/or MS/MS analyses and are labeled with numbers (see also Table 1).

Statistical Analysis

The quantitative data are presented as mean ± SEM. All statistical analyses were performed using SPSS software version 13.0 (SPSS; Chicago, IL). Comparisons of the data obtained from two sets of samples (i.e., control vs high-calcium) in all experiments (except for COM crystal-binding assay) were performed by unpaired Student's t test, whereas multiple comparisons by ANOVA were performed for COM crystal-binding assay. P values less than 0.05 were considered statistically significant.

RESULTS

Proteome Analysis

MDCK cells were maintained in the absence (control) or presence of 20 mM $CaCl_2$ (high-calcium) for 72 h. Thereafter, the controlled and high-calcium-exposed MDCK cells were harvested for protein extraction and were subjected to 2-DE analysis (n = 5 gels derived from 5 independent culture flasks per group). Spot matching revealed approximately 700 protein spots visualized in each 2-D gel. From these, quantitative intensity analysis and statistics revealed only 20 protein spots whose expression levels were significantly altered in the high-calcium-exposed group (including 6 up-regulated proteins, 9 down-regulated proteins, 1 protein that was detectable only after high-calcium exposure, and 4 proteins that were undetectable after high-calcium exposure) (Figure 1). These altered protein spots were subsequently identified using Q-TOF-MS and MS/MS analyses. Table 1 summarizes identities, identification scores, spot intensities, and other related information of all the altered proteins.

Validation of Expression Proteomics Data by 2-D Western Blot Analysis

As summarized in Table 1, three forms of annexin A1 (ANXA1) (spot no. 482, 1031, and 1109) were up-regulated 1.39-, 20.60-, and 6.13-folds, respectively. The increase in these three forms of ANXA1 was validated by 2-D Western blot analysis using mouse monoclonal anti-ANXA1 as a primary antibody. In 2-D Western blot analysis, analytical procedures were similar to conventional (1-D) Western blot analysis but used 2-DE to resolve the proteins prior to immunoblotting, instead of SDS-PAGE. The result clearly showed the increased levels of three forms of ANXA1 in the high-calcium-exposed cells (Figure 2), confirming the proteome data and mass spectrometric protein identification.

Protein Network Analysis and Subcellular Localization

Global protein network analysis using STRING 8.3 software[21] was performed to gain functional significance of the altered proteins identified from expression proteomics study. All the altered proteins were submitted to STRING 8.3 to acquire three types of their expanded information, including functions, subcellular localizations, and interactions/associations with other identified proteins as well as noninputted proteins obtained from available databases and literatures. A successful map of protein association network with subcellular localization is shown in Figure 3, whereas Table 2 summarizes potential functions and subcellular localizations of individual proteins retrieved from UniProt (http://www.uniprot.org), EMBL-EBI (http://www.ebi.ac.uk), and/or PudMed (http://www.pubmed.org) databases.

From this protein network modeling, at least three potential functions were highlighted. First, up-regulation of calcium-binding protein (ANXA1) on apical surface of distal renal tubular cells may increase COM crystal-binding capability. Second, coordinated changes of up-regulation of antiproliferation protein (ANXA1) and down-regulation of proteins involved in protein synthesis (EEF1B2 and EEF1D), mitosis regulation (SEPT2), pre-mRNA processing (HNRPK), and cell proliferation (RUVBL1) suggested that the high-calcium-exposed MDCK cells had some defects in cell proliferation. Third, up-regulation of antimigration protein (ANXA1) and down-regulation of protein involved in wound healing (PGD) suggested that the high-calcium-exposed MDCK cells may have a defect in wound healing. All these hypotheses were subsequently addressed by several highly focused functional studies as follows.

dx.doi.org/10.1021/pr3000738 | J. Proteome Res. 2012, 11, 3650−3663

Table 1. Summary of the Altered Proteins in MDCK Cells after Exposure to High-Calcium (Identified by Q-TOF-MS and/or MS/MS Analyses)[a]

spot no.	protein name	NCBI entry	identified by	identification scores (MS, MS/MS)	%Cov[b] (MS, MS/MS)	no. of matched peptides (MS, MS/MS)	p*I*	MW (kDa)	intensity level (mean ± SEM) control	intensity level (mean ± SEM) high-calcium	ratio (high-calcium/control)	*P* value
Up-Regulated Proteins												
215	phosphoenolpyruvate carboxykinase 2, mitochondrial isoform 1	gil73962498	MS	112, NA	29, NA	18, NA	7.14	71.49	0.0905 ± 0.0110	0.1286 ± 0.0094	1.42	0.031
238	apolipoprotein A-V	gil 126326986	MS	68, NA	30, NA	10, NA	7.02	59.04	0.0829 ± 0.0049	0.1089 ± 0.0101	1.31	0.049
482	annexin A1	gil73946797	MS/MS	136, 199	57, 20	15, 4	5.84	38.89	0.8152 ± 0.0799	1.1349 ± 0.1069	1.39	0.044
716	glutathione *S*-transferase, pi	gil57099635	MS, MS/MS	78, 46	50, 5	8, 1	7.72	23.92	0.0633 ± 0.0265	0.1480 ± 0.0160	2.34	0.026
1031	annexin A1	gil73946797	MS, MS/MS	133, 84	56, 8	13, 2	6.97	39.14	0.0038 ± 0.0037	0.0779 ± 0.0136	20.60	0.001
1109	annexin A1	gil73946797	MS	142, NA	56, NA	12, NA	5.84	38.89	0.0050 ± 0.0035	0.0312 ± 0.0081	6.13	0.019
Down-Regulated Proteins												
242	heterogeneous nuclear ribonucleoprotein K	gil460789	MS, MS/MS	84, 33	26, 2	11, 1	5.13	51.33	0.1089 ± 0.0084	0.0787 ± 0.0068	0.72	0.024
257	ERO1-like protein alpha precursor	gil73963815	MS	90, NA	36, NA	14, NA	5.97	55.18	0.0609 ± 0.0045	0.0426 ± 0.0038	0.70	0.015
308	ERO1-like protein alpha precursor	gil73963815	MS	76, NA	30, NA	10, NA	5.97	55.18	0.0879 ± 0.0215	0.0270 ± 0.0138	0.31	0.045
331	RuvB-like 2	gil5730023	MS	91, NA	36, NA	12, NA	5.49	51.29	0.1304 ± 0.0105	0.0844 ± 0.0123	0.65	0.022
429	septin-2	gil73994331	MS, MS/MS	117, 87	35, 7	17, 3	8.24	60.43	0.0779 ± 0.0038	0.0617 ± 0.0056	0.79	0.045
538	elongation factor 1-delta isoform 3	gil73974686	MS/MS	NA, 77	NA, 17	NA, 2	4.94	30.33	0.0948 ± 0.0131	0.0559 ± 0.0046	0.59	0.024
615	chloride intracellular channel protein 1	gil57094359	MS, MS/MS	119, 44	54, 4	11, 2	5.18	27.35	0.1182 ± 0.0198	0.0354 ± 0.0161	0.30	0.012
661	elongation factor 1-beta [*Homo sapiens*]	gil4503477	MS/MS	NA, 114	NA, 10	NA, 1	4.50	24.92	0.2486 ± 0.0115	0.1518 ± 0.0299	0.61	0.017
1074	glutamine-fructose-6-phosphate aminotransferase	gil 126304009	MS	71, NA	23, NA	10, NA	6.09	77.93	0.0819 ± 0.0132	0.0395 ± 0.0067	0.48	0.021
Protein That Was Detectable Only after High-Calcium Exposure												
1020	CASP8 and FADD-like apoptosis regulator precursor	gil 148283492	MS	69, NA	32, NA	9, NA	6.38	55.98	0.0000 ± 0.0000	0.0436 ± 0.0120	Divided by 0	0.007
Proteins That Were Undetectable after High-Calcium Exposure												
121	transient receptor potential cation channel, subfamily M, member 6	gil 119582957	MS	75, NA	19, NA	10, NA	8.67	92.59	0.1076 ± 0.0297	0.0000 ± 0.0000	0.00	0.007
194	lamin B1	gil 296485609	MS	78, NA	12, NA	25, NA	5.35	62.22	0.0355 ± 0.0149	0.0000 ± 0.0000	0.00	0.044
490	unidentified	NA	NA	NA, NA	NA, NA	NA, NA	NA	NA	0.0375 ± 0.0109	0.0000 ± 0.0000	0.00	0.009
1211	6-phosphogluconate dehydrogenase, decarboxylating isoform 1	gil73950940	MS	69, NA	29, NA	10, NA	6.65	53.58	0.0578 ± 0.0218	0.0000 ± 0.0000	0.00	0.029

[a]NA = not applicable. [b]%Cov = % sequence coverage [(number of matched residues)/(total number of residues in the entire sequence) × 100%].

dx.doi.org/10.1021/pr3000738 | J. Proteome Res. 2012, 11, 3650−3663

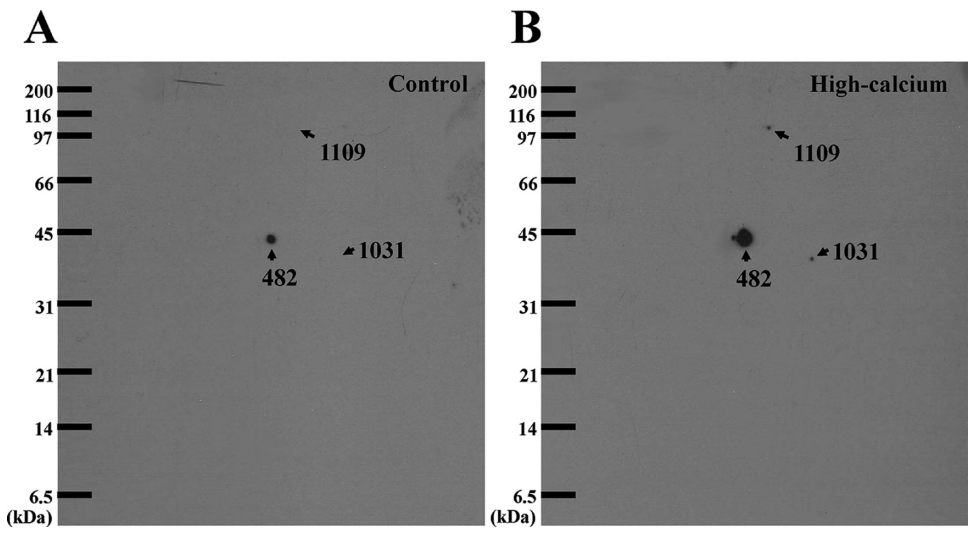


Figure 2. 2-D Western blot analysis of ANXA1. Proteins derived from the controlled and high-calcium-exposed MDCK cells (with an equal amount of 100 μg total protein) were resolved with 2-DE and transferred onto nitrocellulose membranes. Proteins on the membranes were then examined by Western blot analysis using mouse monoclonal anti-ANXA1 as a primary antibody and rabbit antimouse IgG conjugated with HRP as a secondary antibody. Immunoreactive spots were then visualized by chemiluminescence and autoradiography. Spot no. 482, 1031, and 1109 corresponded to the three forms of ANXA1 that were markedly increased in the high-calcium-expose cells (see also Figure 1 and Table 1).

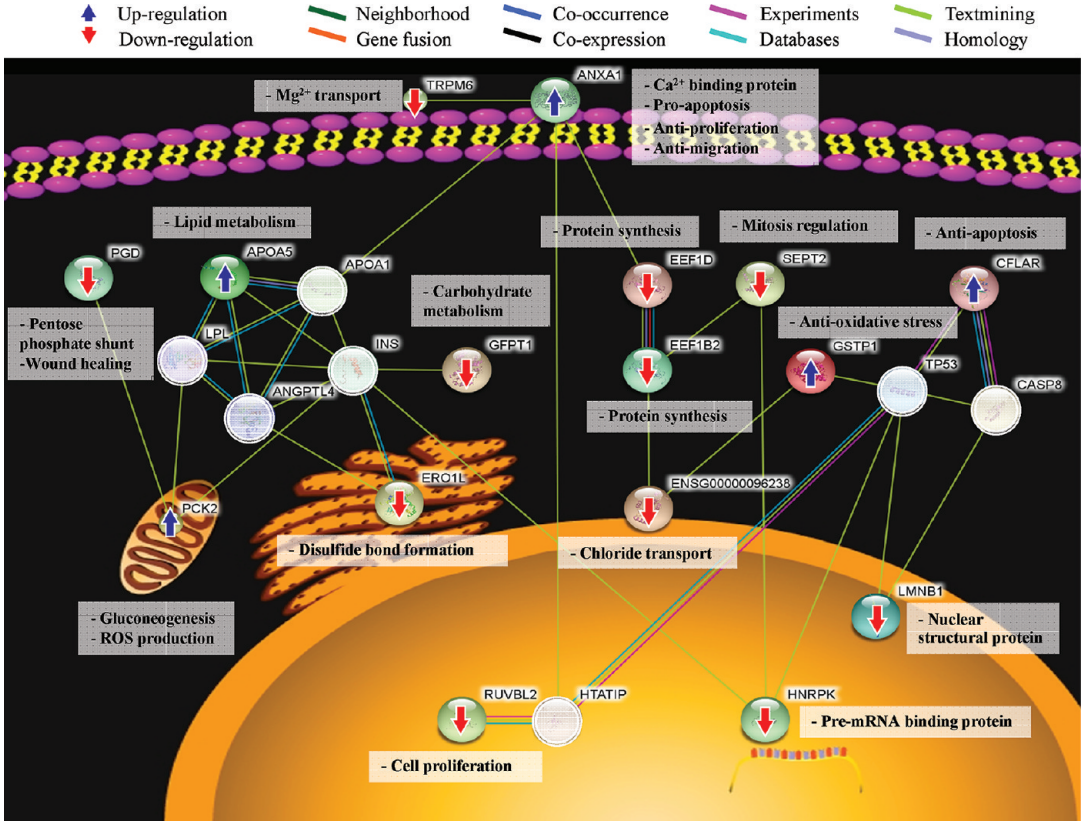


Figure 3. Protein network analysis and prediction of subcellular localization. All the altered proteins identified by expression proteomics approach were submitted to STRING 8.3. The inputted proteins, which were identified as the significantly altered proteins, are demonstrated as the colored nodes, whereas those curated from protein database and literatures are designated as the white nodes. Each line represents a specific type of association between protein nodes. Up-regulation and down-regulation of each protein is labeled with upward and downward arrows, respectively.

Validation of the Increased Surface Expression of ANXA1 at Apical Membranes

From protein network analysis and prediction of subcellular localization, the increase in ANXA1, which is a calcium-binding protein, might be localized at apical membranes of renal tubular cells and related to the increased COM crystal-binding capacity. Although 2-D Western blot analysis successfully confirmed the increase of ANXA1 in the high-calcium-exposed cells (Figure 2), this data did not address subcellular localization of such increase (because whole cell lysate was used). To address this issue, apical

dx.doi.org/10.1021/pr3000738 | J. Proteome Res. 2012, 11, 3650−3663

Table 2. Functional Roles and Subcellular Localizations of the Identified Altered Proteins and the Interacting Proteins Predicted by the Protein Association Network Modeling

gene name	protein name	function(s)	subcellular localization
Up-Regulated Proteins			
ANXA1	annexin A1	calcium binding; Antiproliferation; pro-apoptosis; Antimigration	plasma membrane; cytoplasm; nucleus
APOA5	apolipoprotein A-V	lipid metabolism	cytoplasm
CFLAR	CASP8 and FADD-like apoptosis regulator precursor	antiapoptosis	cytoplasm
GSTP1	glutathione *S*-transferase P	antioxidant enzyme	cytoplasm
PCK2	phosphoenolpyruvate carboxykinase, mitochondrial isoform	gluconeogenesis; involved in oxidative stress	mitochondria
Down-Regulated Proteins			
ENSG00000096238	chloride intracellular channel protein 1	pH-dependent chloride ion channel	nuclear membrane
EEF1D	elongation factor 1-delta	protein biosynthesis	cytoplasm
EEF1B2	elongation factor 1-beta	protein biosynthesis	cytoplasm
ERO1L	endoplasmic oxidoreductin-1-like protein	disulfide bond formation	endoplasmic reticulum
GFPT1	glucosamine-fructose-6-phosphate aminotransferase 1	carbohydrate metabolism	cytoplasm
HNRPK	heterogeneous nuclear ribonucleoprotein K	major pre-mRNA binding protein	nucleus
LMNB1	lamin B-1	nuclear structural protein	nuclear membrane
PGD	6-phosphogluconate dehydrogenase, decarboxylating	pentose phosphate shunt; Involved with wound healing	cytoplasm
RUVBL2	RuvB-like protein 2	cell proliferation	nucleus
SEPT2	septin-2	mitosis regulation	cytoplasm
TRPM6	transient receptor potential melastatin 6	magnesium (and calcium) transport	plasma membrane
Predicted Interacted Proteins Whose Abundance Levels Were Unknown			
ANGPTL4	angiopoietin-related protein 4	antiproliferation; Antimigration	cytoplasm
APOA1	apolipoprotein A-I	lipid metabolism	cytoplasm
CASP8	Caspase 8	Pro-apoptosis	cytoplasm
HTATIP	histone acetyltransferase HIV-1 Tat interactive protein	gene transcription	nucleus
LPL	lipoprotein lipase	lipid degradation	secreted protein
INS	insulin	glucose metabolism	secreted protein
TP53	tumor suppressor p53	antiproliferation; pro-apoptosis	cytoplasm

membranes were isolated from the cells using a peeling method described recently.[22] The purity of this isolation was confirmed by evaluations of markers for apical (gp135) and basolateral (Na+/K+-ATPase-α1) membranes.[22] Thereafter, the apical membrane fraction was subjected to 1-D Western blot analysis for ANXA1 comparing between controlled and high-calcium conditions. The data confirmed that, first, ANXA1 was present in apical membranes and that, second, apical membrane ANXA1 was significantly increased in the high-calcium-exposed cells as compared to the controls (Figure 4A). Additionally, the cytosolic fraction was also collected and subjected to 1-D Western blot analysis for ANXA1. The data demonstrated that, first, two ANXA1 isoforms in cytosolic fraction had lower molecular masses as compared to the one found in apical membrane fraction and that, second, these two ANXA1 isoforms found in cytosolic fraction were also increased in the high-calcium-exposed cells as compared to the controls (Figure 4A). Taken together, the increases in all three isoforms of ANXA1 found in both apical and cytosolic fractions by 1-D Western blot analysis were consistent to the findings observed by proteomic analysis (Figure 1 and Table 1) and 2-D Western blot analysis (Figure 2).

The increase in apical membrane expression of ANXA1 in the high-calcium-exposed cells was also confirmed by laser-scanning confocal microscopy. The cells were labeled with primary antibody (anti-ANXA1 mAb) without permeabilization to avoid interfering staining of the intracellular compartment (another localization of ANXA1). The immunofluorescence data nicely confirmed that the apical membrane expression of ANXA1 was markedly increased in the high-calcium-exposed cells (Figure 4B).

COM Crystal-Binding Capacity and the Effect of Neutralization by Anti-ANXA1 mAb

The increase of ANXA1 levels on apical surface of distal renal tubular cells may exert some important roles in the pathogenic mechanisms of COM nephrolithiasis, particularly COM crystal-binding capacity. Our hypothesis that the increased expression of ANXA1 on apical surface could enhance COM crystal-binding capacity was then addressed. After 72 h of incubation with or without 20 mM $CaCl_2$, the culture medium was replaced with 10% FBS-supplemented MEM with or without $CaCl_2$, anti-ANXA1 mAb, or IgG1 as described in the materials and methods section. After 30 min of incubation, the cells were then treated with 100 μg/mL COM crystals for 30 min. Thereafter, the cells were vigorously washed using PBS five times to remove unbound COM crystals. Finally, numbers of the adhered COM crystals were quantitatively analyzed in triplicate. The data showed a significantly greater number of the adhered COM crystals on the surface of the high-calcium-exposed cells as compared to the controls (Figure 5). Neutralization with anti-ANXA1, not IgG1 isotype control, could reduce the number of adhered crystals to the basal levels (Figure 5).

Cell Proliferation Assay and Quantitative Analysis of Cell Death

Morphological examination during the cell maintenance and the proposed functional changes by protein network modeling

dx.doi.org/10.1021/pr3000738 | *J. Proteome Res.* 2012, 11, 3650−3663

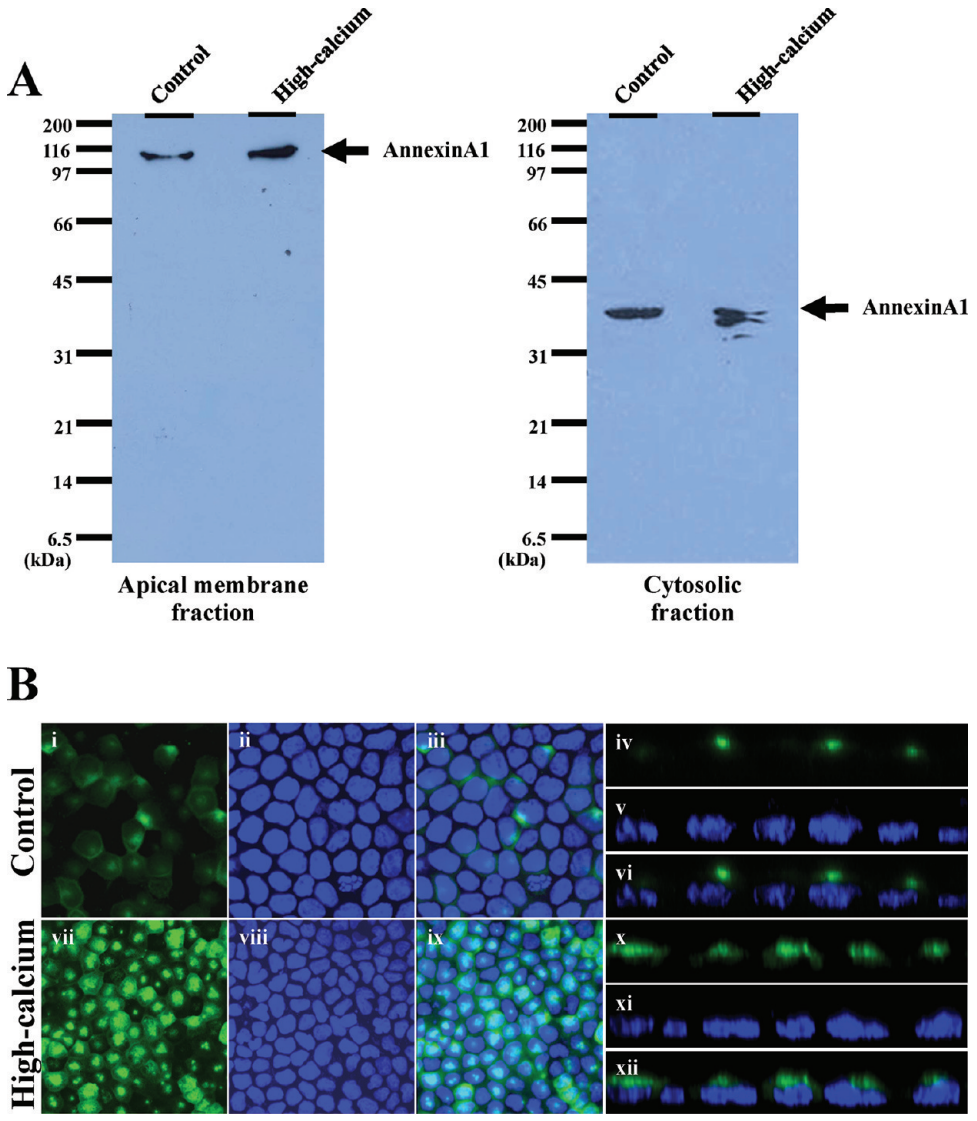


Figure 4. Validation of the increased surface expression of ANXA1 at apical membranes of the high-calcium-exposed cells. (A) 1-D Western blot analysis of apical membrane and cytosolic fractions was performed using mouse monoclonal anti-ANXA1 as a primary antibody and rabbit antimouse IgG conjugated with HRP as a secondary antibody. Immunoreactive bands were then visualized by chemiluminescence and autoradiography. (B) Surface expression of ANAXA1 on apical membranes was also evaluated by immunofluorescence staining and laser-scanning confocal microscopy. ANXA1 is presented in green, whereas nuclei are presented in blue (Hoechst dye). Panels (i–iii) and (vii–ix) show the top view, whereas panels (iv–vi) and (x–xii) illustrate the sagittal sections. Original magnification power was 630× in all panels.

(Figure 3) suggested that the high-calcium-exposed cells might have a defect in cell proliferation. To address this hypothesis, the total numbers of MDCK cells (which reflected the degree of cell proliferation) in the controlled and high-calcium-exposed conditions were serially evaluated at 24, 48, and 72 h after the treatment. The data showed that the high-calcium-exposed cells had significant decreases in the total cell numbers (approximately 50.9 ± 12.7, 42.9 ± 11.5, and 42.0 ± 4.5% decreases compared to those of controls at 24, 48 and 72 h post-treatment, respectively) (Figure 6A). However, one might argue that the reduction of total cell numbers might be from cytotoxicity of high-calcium as there were changes in some proteins involved in cytotoxicity. We thus performed quantitative analysis of cell death using flow cytometry and annexin V/propidium iodide co-staining to measure both cell apoptosis and necrosis. The cell death assay revealed comparable percentages of apoptotic and necrotic cells as well as total cell death (5.05 ± 0.31 vs 5.07 ± 0.85% for control vs high-calcium; P = 0.971) in both conditions (Figure 6B), implicating that the reduction of total cell numbers was from impaired cell proliferation, not from the cytotoxicity of high-calcium.

Evaluation of Wound Healing by Scratch Assay

Another functional abnormality of the high-calcium-exposed cells highlighted from the protein network modeling was the defect in wound healing. To address this functional abnormality, the artificial wounds were created on the confluent monolayer of the controlled and high-calcium-exposed cells. These scratched wounds had sharp-edge and the width of the wound (or cell-free width) (measured immediately after the scratch) was highly consistent (approximately 649.1 ± 8.9 μm from 18 independent experiments; coefficient of variation or CV = 1.37%). Wound healing capability of the controlled and high-calcium treated cells were then evaluated at various time-points by morphological examination and quantitative measurement of cell-free width. In the controlled condition, the cells localized at the scratched edges

dx.doi.org/10.1021/pr3000738 | J. Proteome Res. 2012, 11, 3650–3663

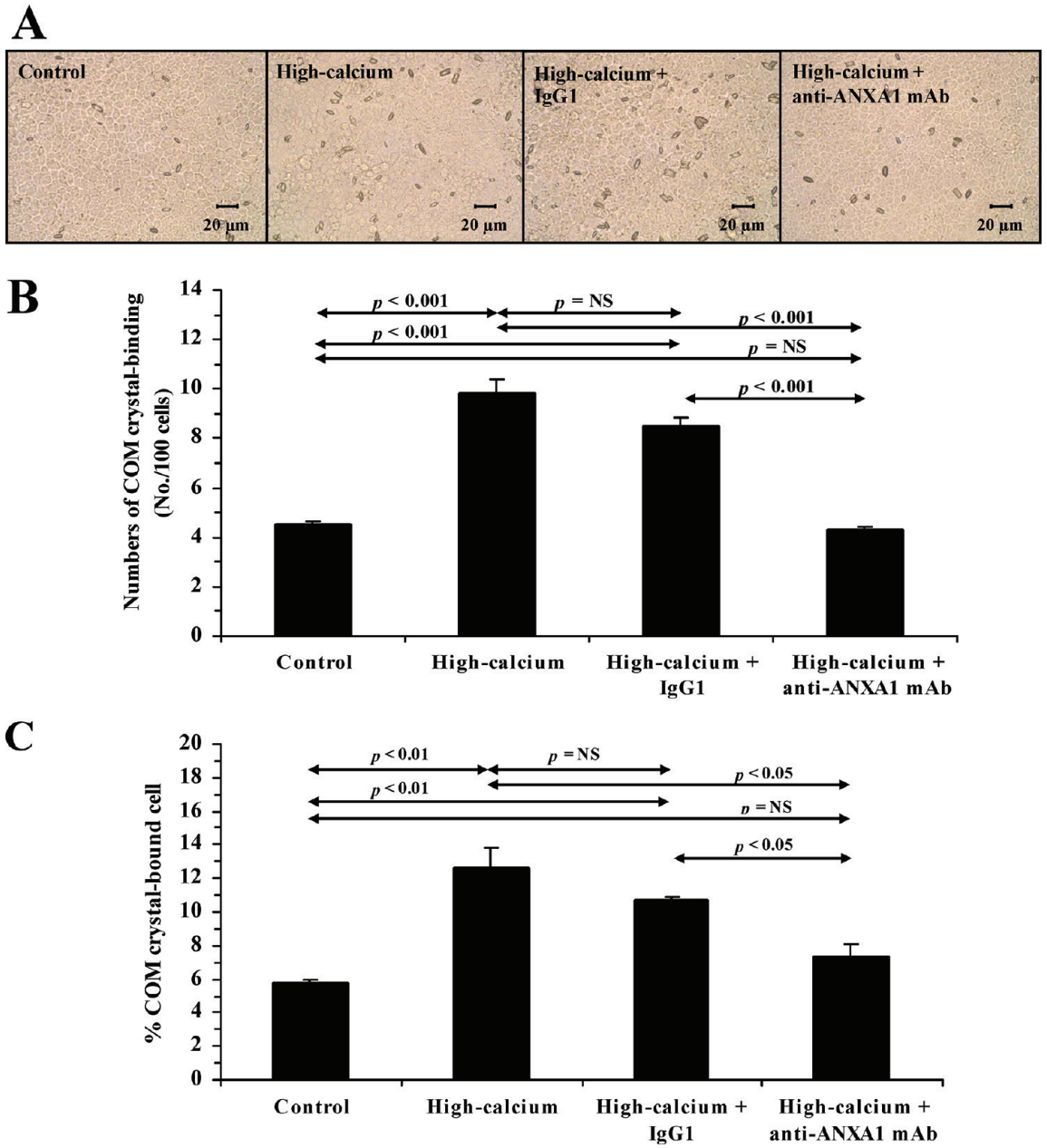


Figure 5. COM crystal-binding capacity and the effect of neutralization by anti-ANXA1 mAb. (A) Phase-contrast microscopic examination of 4 groups of cells, including (i) control (normal culture without $CaCl_2$); (ii) high-calcium (with 20 mM $CaCl_2$); (iii) high-calcium + anti-ANXA1 mAb (with 20 mM $CaCl_2$ and neutralization with 0.5 μg/mL mouse monoclonal anti-ANXA1); and (iv) high-calcium + IgG1 (with 20 mM $CaCl_2$ and 0.5 μg/mL IgG1, which was used as the isotype control of anti-ANXA1 mAb) (n = 3 per group). Original magnification power was 400× for all panels. (B) Quantitative analysis of the adhered COM crystals in individual groups per 100 cells (no./100 cells). (C) Percentage of COM crystal-adhered cells (%). The data of each bar is presented as mean ± SEM of three independent experiments. * = $P < 0.0001$ versus the control condition. NS = not statistically significant.

had morphological changes and gradually migrated to the cell-free area, starting at 3 h postscratching (Figure 7A). In the high-calcium condition, these morphological changes and cell migration required a longer time to develop (starting at 6 h postscratching). At 12 h postscratching, the wounds in the controlled condition were successfully closed by the migratory cells, whereas the wounds in the high-calcium-exposed condition remained unclosed (Figure 7A). Quantitative measurement of the cell-free widths also confirmed the delay or impairment of wound healing in the high-calcium-exposed cells as demonstrated by significantly greater cell-free widths in the high-calcium-exposed cells compared to the controls at all time-points (Figure 7B).

DISCUSSION

Hypercalciuria is the most common metabolic cause of COM nephrolithiasis[1,3−5] and can also lead to impaired renal tubular function.[12−14,26] However, cellular responses of distal renal tubular cells to the hypercalciuric state remained largely unknown. We therefore performed a gel-based proteomics study to identify altered proteins in distal renal tubular cells in response to high-calcium exposure (Figure 1 and Table 1). These altered proteins were involved in several cellular functions,

dx.doi.org/10.1021/pr3000738 | J. Proteome Res. 2012, 11, 3650−3663

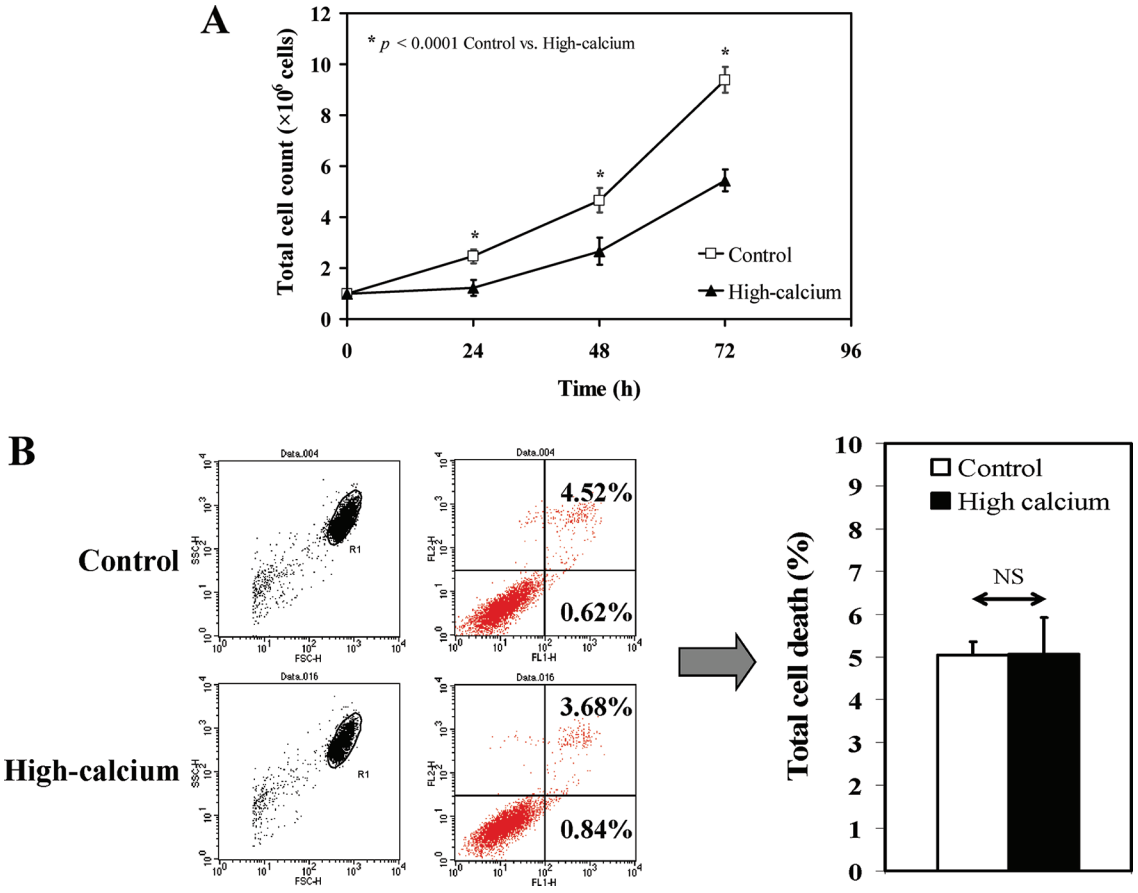


Figure 6. Cell proliferation assay (A) and quantitative analysis of cell death (B). (A) At 24, 48, and 72 h post-treatment, the cells were detached from the culture well using 0.1% trypsin in 2.5 mM EDTA and were immediately resuspended in 1 mL of FBS-containing MEM to terminate trypsin activity. Trypan blue staining was used to exclude dead cells, and the numbers of viable cells were counted using hemacytometer. (B) After 72 h of incubation, both controlled and high-calcium-treated cells were examined for percentage of the total cell death using flow cytometry with annexin V and propidium iodide co-staining. All the quantitative data are presented as mean ± SEM of three independent experiments. * = $P < 0.0001$ versus the control condition. NS = not statistically significant.

including calcium binding, protein synthesis, carbohydrate metabolism, lipid metabolism, cell proliferation, mitosis regulation, apoptosis, cell migration, oxidative stress, and ion transport (Table 2). After identification of these altered proteins, protein network analysis (Figure 3) and several highly focused functional studies (Figures 4–7) were sequentially performed to address functional significance of the expression proteomics data.

Protein network analysis using STRING 8.3 was very useful as this bioinformatic tool provided several important aspects to further design highly focused functional studies. These included potential functions of the altered proteins, their subcellular localizations, protein–protein interactions, and the involved biological processes/pathways to create new hypotheses. In our present study, several hypotheses were guided from protein association network analysis including:

Hypothesis I: The expression proteomics data and prediction of subcellular localization and cellular function suggested that ANXA1 was up-regulated on apical surface of renal tubular cells upon exposure to high-calcium and might promote COM crystal-cell adhesion.

Hypothesis II: The coordinated changes of up-regulation of antiproliferative protein (ANXA1) and down-regulation of proteins involved in cell proliferation (RUVBL2), mitosis regulation (SEPT2), mRNA processing (HNRPK), and protein biosynthesis (EEF1B2 and EEF1D) strongly suggested that renal tubular cells under the high-calcium condition had a defect in cell proliferation.

Hypothesis III: The coordinated changes of up-regulation of antimigration protein (ANXA1) and down-regulation of protein involved in wound healing (PGD) suggested that the high-calcium-exposed cells had a defect in epithelial wound healing.

It seemed that ANXA1 played pivotal roles in high-calcium-induced changes in renal tubular cells as this protein was involved in all of these hypotheses. This was probably due to its multiple biological functions, including calcium- and phospholipid-binding activity, inhibition of cell proliferation and migration, anti-inflammation, and immunological regulation.[27] Therefore, we first confirmed the expression proteomics data by 2-D Western blot analysis (Figure 2), which demonstrated up-regulation of three forms of ANXA1, consistent to the proteomic data. Finally, all of the aforementioned hypotheses were addressed and indeed confirmed by several highly focused functional studies as follows.

Validation of Hypothesis I resulted in the identification of ANXA1, a calcium-binding protein, as a novel COM crystal-binding molecule on apical surface of renal tubular cells (Figure 5). From expression proteomics data, up-regulation of ANXA1 in high-calcium-exposed MDCK cells implicated that this protein is

dx.doi.org/10.1021/pr3000738 | J. Proteome Res. 2012, 11, 3650–3663

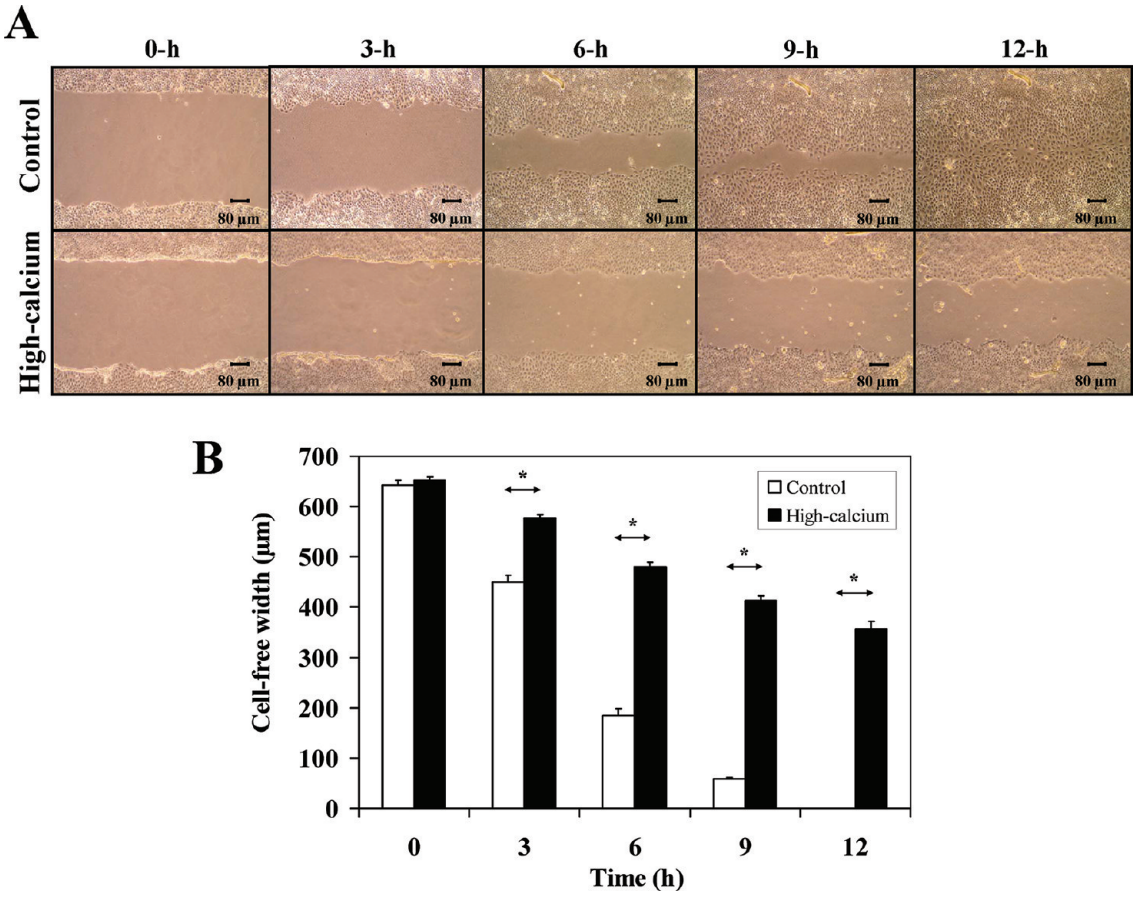


Figure 7. Evaluation of wound healing by scratch assay. After 72 h of incubation, artificial wounds were created on the confluent monolayers of the controlled and high-calcium-exposed cells. At the indicated time-points, these wounds were imaged by phase contrast microscopy (A) and the cell-free widths were measured and analyzed by Tarosoft Image framework v.0.9.6 software (B). All the quantitative data are presented as mean ± SEM of three independent experiments. * = $P < 0.0001$ versus the control condition. In all panels of part A, original magnification power was 100×.

involved in COM kidney stone formation. This proposed role of ANXA1, however, would be reasonable only if this protein was expressed on the apical membranes of renal tubular cells (in addition to its well-known locale in cytoplasm). Although 2-D Western blot analysis confirmed the expression proteomics data, it did not provide subcellular localization of the change. We therefore isolated apical membranes and confirmed that ANXA1 was also expressed at apical membranes of renal tubular cells and was up-regulated when the cells were exposed to high-calcium (Figure 4). This solid data led to a further hypothesis that the up-regulation of this calcium-binding protein (ANXA1) on the cell surface would result to the enhanced COM crystal-binding capacity of the high-calcium-exposed cells. The latter was nicely confirmed by COM crystal-binding assay, which demonstrated that the high-calcium-exposed cells had increased COM crystal-binding capacity and neutralization by anti-ANXA1, not its isotype control (IgG1), successfully prevented this enhancement (Figure 5). ANXA1 has been extensively studied for its clinical applications in several malignancies,[28−30] inflammation,[31,32] neuroendocrine,[33] and antinociception.[34] A recent study by Thurgood et al.[35] has demonstrated that ANXA1 was a common constituent of calcium oxalate dihydrate (COD) crystals, which were crystallized in the human urine. However, its functional significance in COM kidney stone disease remained unclear. Our present study provided functional evidence demonstrating that ANXA1 on apical surface of distal renal tubular cells could serve as the COM crystal receptor and may play a crucial role in COM stone formation.

Validation of Hypothesis II revealed that proliferation of renal tubular cells was suppressed by the high-calcium environment (Figure 6A), whereas the effect of cell death on the reduced numbers of the cells was excluded by quantitative analysis of cell death using flow cytometry with annexin V/propidium iodide co-staining, which demonstrated that both apoptotic and necrotic cell death were not increased by high-calcium (Figure 6B). This functional defect in cell proliferation was confidently proposed from the strong interactions/associations of ANXA1, RUVBL2, SEPT2, HNRPK, EEF1B2, and EEF1D (Figure 3). ANXA1 seemed to play a major role in this subset of protein network. ANXA1 is well characterized as a regulator of the antiproliferative process by blocking epidermal growth factor (EGF)-mediated cell proliferation, activating extracellular signal-regulated kinase (ERK)-mediated disruption of actin cytoskeleton, and inhibiting cyclin D1.[27,36] Antiproliferative activity of ANXA1 is localized at its N-terminus since this part of the peptide fragment significantly inhibits growth and proliferation of A549 lung cancer cells in vitro.[37] The antiproliferative activity of ANXA1 has been demonstrated also in clinical cancer tissues,[27] and down-regulation of ANXA1 has been observed in several cancer types; e.g., esophageal squamous cell carcinoma,[38] prostatic adenocarcinoma,[39] and bladder cancer,[40] as cancer cells attempt to suppress antiproliferative proteins to exhibit their tumorigenic properties.[27] The coordinated down-regulation of proteins

dx.doi.org/10.1021/pr3000738 | J. Proteome Res. 2012, 11, 3650−3663

involved in cell proliferation (RUVBL2), mitosis regulation (SEPT2), mRNA processing (HNRPK), and protein biosynthesis (EEF1D and EEF1B2) were then considered as the downstream effectors of antiproliferative effect of ANXA1 because most of these proteins are involved in the common pathway of cell proliferation machinery.

Validation of Hypothesis III revealed that renal tubular cells under high-calcium environment had a significant defect in wound healing (Figure 7). This hypothesis was confidently proposed from the coordinated changes of ANXA1 and PGD in the high-calcium-exposed cells. ANXA1 was presumably contributed to the defective wound healing process by its antimigration activity. Several previous studies have demonstrated that ANXA1 could inhibit migration of several cell types in vitro and in vivo[41−43] via the activation of formyl peptide receptor (FPR).[44] Another player in this functional defect was PGD, which plays an important role in the pentose phosphate shunt and has been reported to be associated with wound healing capability.[45,46] An argument might be raised that the impaired cell proliferation might be responsible for (or contribute to) the defective wound healing. It is known that wound healing is the result of overlapping processes of cell proliferation and migration. Nevertheless, it seems that the impaired cell migration plays more dominant role during the acute phase response of wound healing.[24,25] This concept has been strongly supported by the study of Storesund et al.,[25] which demonstrated that wound healing capacity of normal oral keratinocytes in the presence of trefoil factor 3 was not affected by mitomycin C, a potent inhibitor of cell proliferation, but was markedly affected by cytochalasin B, a potent inhibitor of cell migration. Hence, we believe that the impaired migration was the major cause of the defective wound healing although the impaired cell proliferation could not be entirely excluded. The defect in wound healing of the high-calcium-exposed cells may implicate some aspects of renal tubular impairment caused by hypercalciuria.[10−15] As the cells lose their regeneration capacity, renal tubules may be unable to fully restore their structures and/or functions after exposure to the noxious stimuli.

It should be noted that, first, although MDCK cells represent mainly distal renal tubular cells, several lines of evidence have suggested that these cells also represent some features of collecting duct cells.[47,48] Buchholz et al.[47] used MDCK cells as the model for principal and alpha-intercalated cells of collecting duct to demonstrate cystogenesis and cyst growth in response to cAMP and ATP signaling, whereas Dos Santos, et al.[48] showed that MDCK cells could respond to aldosterone (a hormone that stimulated H^+ secretion by intercalated cells of collecting duct) through a genomic pathway in order to enhance vacuolar H^+-ATPase activity. Therefore, effects of high-calcium on MDCK cells observed in the present study reflected not only pathophysiologic changes in distal renal tubular cells but also (although partially) some phenomena in renal collecting duct.

Second, an addition of 20 mM $CaCl_2$ to the culture medium could increase the osmolarity up to approximately 15% of the basal level (data not shown). Thus, effects of increased osmolarity should be taken into account. Further studies are required to differentiate effects of high-calcium from those of increased osmolarity. Finally, our data may be applicable to kidney stones that are originated from the intratubular luminal site but not applicable to kidney stones that are originated from the interstitial site (Randall's plaque)[49,50] of which pathogenic mechanisms differ.

In summary, our present study revealed pathophysiological responses of MDCK cells upon 72 h of exposure to the high-calcium environment. These changes may, at least in part, explain the common complications occurred in hypercalciuric patients, including COM kidney stone formation and renal tubular impairment. Our in vitro study offers several candidates for further targeted studies to confirm their relevance in hypercalciuria and kidney stone disease in vivo. According to the involvements of ANXA1 observed in vitro, it is speculated that this multifunctional protein may serve as a central regulator in hypercalciuric complications by enhanced COM crystal-binding capacity, impaired cell proliferation, and impaired wound healing. Therefore, ANXA1 may be considered as a novel drug target for preventing kidney stone formation complicated by hypercalciuria. Finally, our present study also demonstrated that a classical proteomics approach (starting from expression proteomics followed by bioinformatic analysis) can be used to obtain additional and very important data to generate new hypotheses, which can then be addressed by highly focused functional studies. This is thus the ideal approach for unraveling the pathogenic mechanisms and pathophysiology of diseases as well as for defining novel therapeutic targets.

■ ASSOCIATED CONTENT

Supporting Information

Supplementary methods. This material is available free of charge via the Internet at http://pubs.acs.org.

■ AUTHOR INFORMATION

Corresponding Author

*Phone/Fax: +66-2-4184793. E-mail: thongboonkerd@dr.com or vthongbo@yahoo.com.

Notes

The authors declare no competing financial interest.

■ ACKNOWLEDGMENTS

We are grateful to Professor Shui-Tein Chen and Dr. Supachok Sinchaikul for their technical support on mass spectrometric analyses. This study was supported by the Office of the Higher Education Commission and Mahidol University under the National Research Universities Initiative, and The Thailand Research Fund (RTA5380005) to V.T. K.F. and P.P. are supported by the Royal Golden Jubilee Ph.D. Program of The Thailand Research Fund, whereas V.T. is also supported by the "Chalermphrakiat" Grant, Faculty of Medicine, Siriraj Hospital.

■ ABBREVIATIONS USED

ANGPTL4, angiopoietin-related protein 4; ANXA1, annexin A1; APOA1, apolipoprotein A-I; APOA5, apolipoprotein A-V; CASP8, caspase 8; CFLAR, CASP8 and FADD-like apoptosis regulator; ENSG00000096238, chloride intracellular channel protein 1; EEF1B2, elongation factor 1-beta; EEF1D, elongation factor 1-delta; ERO1L, endoplasmic oxidoreductin-1-like protein; GFPT1, glucosamine-fructose-6-phosphate aminotransferase 1; GSTP1, glutathione *S*-transferase Pi; HNRPK, heterogeneous nuclear ribonucleoprotein K; HTATIP, histone acetyltransferase; INS, insulin; LMNB1, lamin B-1; LPL, lipoprotein lipase; PCK2, phosphoenolpyruvate carboxykinase, mitochondrial isoform; PGD, 6-phosphogluconate dehydrogenase, decarboxylating; RUVBL2, RuvB-like protein 2; SEPT2,

septin-2; TP53, tumor suppressor p53; TRPM6, transient receptor potential melastatin 6

REFERENCES

(1) Liebman, S. E.; Taylor, J. G.; Bushinsky, D. A. Idiopathic hypercalciuria. *Curr. Rheumatol. Rep.* **2006**, *8*, 70−75.

(2) Vezzoli, G.; Soldati, L.; Gambaro, G. Update on primary hypercalciuria from a genetic perspective. *J. Urol.* **2008**, *179*, 1676−1682.

(3) Worcester, E. M.; Coe, F. L. New insights into the pathogenesis of idiopathic hypercalciuria. *Semin. Nephrol.* **2008**, *28*, 120−132.

(4) Worcester, E. M.; Coe, F. L. Nephrolithiasis. *Prim. Care* **2008**, *35* (vii), 369−391.

(5) Lerolle, N.; Lantz, B.; Paillard, F.; Gattegno, B.; Flahault, A.; Ronco, P.; Houillier, P.; Rondeau, E. Risk factors for nephrolithiasis in patients with familial idiopathic hypercalciuria. *Am. J. Med.* **2002**, *113*, 99−103.

(6) Asplin, J. R.; Parks, J. H.; Coe, F. L. Dependence of upper limit of metastability on supersaturation in nephrolithiasis. *Kidney Int.* **1997**, *52*, 1602−1608.

(7) Lieske, J. C.; Farell, G.; Deganello, S. The effect of ions at the surface of calcium oxalate monohydrate crystals on cell-crystal interactions. *Urol. Res.* **2004**, *32*, 117−123.

(8) Rabinovich, Y. I.; Daosukho, S.; Byer, K. J.; El Shall, H. E.; Khan, S. R. Direct AFM measurements of adhesion forces between calcium oxalate monohydrate and kidney epithelial cells in the presence of Ca^{2+} and Mg^{2+} ions. *J. Colloid Interface Sci.* **2008**, *325*, 594−601.

(9) Curhan, G. C.; Willett, W. C.; Speizer, F. E.; Stampfer, M. J. Twenty-four-hour urine chemistries and the risk of kidney stones among women and men. *Kidney Int.* **2001**, *59*, 2290−2298.

(10) Weber, S.; Schneider, L.; Peters, M.; Misselwitz, J.; Ronnefarth, G.; Boswald, M.; Bonzel, K. E.; Seeman, T.; Sulakova, T.; Kuwertz-Broking, E.; Gregoric, A.; Palcoux, J. B.; Tasic, V.; Manz, F.; Scharer, K.; Seyberth, H. W.; Konrad, M. Novel paracellin-1 mutations in 25 families with familial hypomagnesemia with hypercalciuria and nephrocalcinosis. *J. Am. Soc. Nephrol.* **2001**, *12*, 1872−1881.

(11) Ludwig, M.; Utsch, B.; Balluch, B.; Frund, S.; Kuwertz-Broking, E.; Bokenkamp, A. Hypercalciuria in patients with CLCN5 mutations. *Pediatr. Nephrol.* **2006**, *21*, 1241−1250.

(12) Stapleton, F. B.; Miller, L. A. Renal function in children with idiopathic hypercalciuria. *Pediatr. Nephrol.* **1988**, *2*, 229−235.

(13) Bonilla-Felix, M.; Villegas-Medina, O.; Vehaskari, V. M. Renal acidification in children with idiopathic hypercalciuria. *J. Pediatr.* **1994**, *124*, 529−534.

(14) Worcester, E. M.; Gillen, D. L.; Evan, A. P.; Parks, J. H.; Wright, K.; Trumbore, L.; Nakagawa, Y.; Coe, F. L. Evidence that postprandial reduction of renal calcium reabsorption mediates hypercalciuria of patients with calcium nephrolithiasis. *Am. J. Physiol Renal Physiol.* **2007**, *292*, F66−F75.

(15) Akil, I.; Kavukcu, S.; Inan, S.; Yilmaz, O.; Atilla, P.; Islekel, H.; Nese, N.; Muftuoglu, S. Evaluation of histologic changes in the urinary tract of hypercalciuric rats. *Pediatr. Nephrol.* **2006**, *21*, 1681−1689.

(16) Unwin, R. J.; Capasso, G.; Shirley, D. G. An overview of divalent cation and citrate handling by the kidney. *Nephron Physiol.* **2004**, *98*, 15−20.

(17) Boros, S.; Bindels, R. J.; Hoenderop, J. G. Active Ca(2+) reabsorption in the connecting tubule. *Pfluegers Arch.* **2009**, *458*, 99−109.

(18) Lieske, J. C.; Deganello, S. Nucleation, adhesion, and internalization of calcium-containing urinary crystals by renal cells. *J Am. Soc. Nephrol.* **1999**, *10* (Suppl14), S422−S429.

(19) Rindler, M. J.; Chuman, L. M.; Shaffer, L.; Saier, M. H., Jr. Retention of differentiated properties in an established dog kidney epithelial cell line (MDCK). *J. Cell Biol.* **1979**, *81*, 635−648.

(20) Saier, M. H., Jr. Growth and differentiated properties of a kidney epithelial cell line (MDCK). *Am. J. Physiol.* **1981**, *240*, C106−C109.

(21) Jensen, L. J.; Kuhn, M.; Stark, M.; Chaffron, S.; Creevey, C.; Muller, J.; Doerks, T.; Julien, P.; Roth, A.; Simonovic, M.; Bork, P.; von Mering, C. STRING 8--a global view on proteins and their functional interactions in 630 organisms. *Nucleic Acids Res.* **2009**, *37*, D412−D416.

(22) Fong-ngern, K.; Chiangjong, W.; Thongboonkerd, V. Peeling as a novel, simple, and effective method for isolation of apical membrane from intact polarized epithelial cells. *Anal. Biochem.* **2009**, *395*, 25−32.

(23) Thongboonkerd, V.; Semangoen, T.; Chutipongtanate, S. Factors determining types and morphologies of calcium oxalate crystals: Molar concentrations, buffering, pH, stirring and temperature. *Clin. Chim. Acta* **2006**, *367*, 120−131.

(24) Rodriguez, L. G.; Wu, X.; Guan, J. L. Wound-healing assay. *Methods Mol. Biol.* **2005**, *294*, 23−29.

(25) Storesund, T.; Hayashi, K.; Kolltveit, K. M.; Bryne, M.; Schenck, K. Salivary trefoil factor 3 enhances migration of oral keratinocytes. *Eur. J. Oral Sci.* **2008**, *116*, 135−140.

(26) Megevand, M.; Favre, H. Distal renal tubular dysfunction: a common feature in calcium stone formers. *Eur. J. Clin. Invest.* **1984**, *14*, 456−461.

(27) Lim, L. H.; Pervaiz, S. Annexin 1: the new face of an old molecule. *FASEB J.* **2007**, *21*, 968−975.

(28) Wang, L. P.; Bi, J.; Yao, C.; Xu, X. D.; Li, X. X.; Wang, S. M.; Li, Z. L.; Zhang, D. Y.; Wang, M.; Chang, G. Q. Annexin A1 expression and its prognostic significance in human breast cancer. *Neoplasma* **2010**, *57*, 253−259.

(29) Yu, G.; Wang, J.; Chen, Y.; Wang, X.; Pan, J.; Li, Q.; Xie, K. Tissue microarray analysis reveals strong clinical evidence for a close association between loss of annexin A1 expression and nodal metastasis in gastric cancer. *Clin. Exp. Metastasis* **2008**, *25*, 695−702.

(30) Wang, K. L.; Wu, T. T.; Resetkova, E.; Wang, H.; Correa, A. M.; Hofstetter, W. L.; Swisher, S. G.; Ajani, J. A.; Rashid, A.; Hamilton, S. R.; Albarracin, C. T. Expression of annexin A1 in esophageal and esophagogastric junction adenocarcinomas: association with poor outcome. *Clin. Cancer Res.* **2006**, *12*, 4598−4604.

(31) Perretti, M.; Dalli, J. Exploiting the Annexin A1 pathway for the development of novel anti-inflammatory therapeutics. *Br. J. Pharmacol.* **2009**, *158*, 936−946.

(32) McArthur, S.; Cristante, E.; Paterno, M.; Christian, H.; Roncaroli, F.; Gillies, G. E.; Solito, E. Annexin A1: a central player in the anti-inflammatory and neuroprotective role of microglia. *J. Immunol.* **2010**, *185*, 6317−6328.

(33) John, C. D.; Gavins, F. N.; Buss, N. A.; Cover, P. O.; Buckingham, J. C. Annexin A1 and the formyl peptide receptor family: neuro-endocrine and metabolic aspects. *Curr. Opin. Pharmacol.* **2008**, *8*, 765−776.

(34) Pieretti, S.; Di Giannuario, A.; De Felice, M.; Perretti, M.; Cirino, G. Stimulus-dependent specificity for annexin 1 inhibition of the inflammatory nociceptive response: the involvement of the receptor for formylated peptides. *Pain* **2004**, *109*, 52−63.

(35) Thurgood, L. A.; Wang, T.; Chataway, T. K.; Ryall, R. L. Comparison of the specific incorporation of intracrystalline proteins into urinary calcium oxalate monohydrate and dihydrate crystals. *J. Proteome. Res.* **2010**, *9*, 4745−4757.

(36) Alldridge, L. C.; Bryant, C. E. Annexin 1 regulates cell proliferation by disruption of cell morphology and inhibition of cyclin D1 expression through sustained activation of the ERK1/2 MAPK signal. *Exp. Cell Res.* **2003**, *290*, 93−107.

(37) Croxtall, J. D.; Choudhury, Q.; Flower, R. J. Inhibitory effect of peptides derived from the N-terminus of lipocortin 1 on arachidonic acid release and proliferation in the A549 cell line: identification of E-Q-E-Y-V as a crucial component. *Br. J. Pharmacol.* **1998**, *123*, 975−983.

(38) Xia, S. H.; Hu, L. P.; Hu, H.; Ying, W. T.; Xu, X.; Cai, Y.; Han, Y. L.; Chen, B. S.; Wei, F.; Qian, X. H.; Cai, Y. Y.; Shen, Y.; Wu, M.; Wang, M. R. Three isoforms of annexin I are preferentially expressed in normal esophageal epithelia but down-regulated in esophageal squamous cell carcinomas. *Oncogene* **2002**, *21*, 6641−6648.

(39) Kang, J. S.; Calvo, B. F.; Maygarden, S. J.; Caskey, L. S.; Mohler, J. L.; Ornstein, D. K. Dysregulation of annexin I protein expression in high-grade prostatic intraepithelial neoplasia and prostate cancer. *Clin. Cancer Res.* **2002**, *8*, 117−123.

(40) Xiao, G. S.; Jin, Y. S.; Lu, Q. Y.; Zhang, Z. F.; Belldegrun, A.; Figlin, R.; Pantuck, A.; Yen, Y.; Li, F.; Rao, J. Annexin-I as a potential target for

green tea extract induced actin remodeling. *Int. J. Cancer* **2007**, *120*, 111−120.
(41) Perretti, M.; Croxtall, J. D.; Wheller, S. K.; Goulding, N. J.; Hannon, R.; Flower, R. J. Mobilizing lipocortin 1 in adherent human leukocytes downregulates their transmigration. *Nat. Med.* **1996**, *2*, 1259−1262.
(42) Getting, S. J.; Flower, R. J.; Perretti, M. Inhibition of neutrophil and monocyte recruitment by endogenous and exogenous lipocortin 1. *Br. J. Pharmacol.* **1997**, *120*, 1075−1082.
(43) Perretti, M.; Ingegnoli, F.; Wheller, S. K.; Blades, M. C.; Solito, E.; Pitzalis, C. Annexin 1 modulates monocyte-endothelial cell interaction in vitro and cell migration in vivo in the human SCID mouse transplantation model. *J. Immunol.* **2002**, *169*, 2085−2092.
(44) Rescher, U.; Danielczyk, A.; Markoff, A.; Gerke, V. Functional activation of the formyl peptide receptor by a new endogenous ligand in human lung A549 cells. *J. Immunol.* **2002**, *169*, 1500−1504.
(45) Im, M. J.; Hoopes, J. E. Enzyme activities in regenerating epithelium during wound healing. IV. Aminotransferases and NADP-dependent enzymes. *J. Surg. Res.* **1973**, *15*, 262−270.
(46) Dunham, J.; Shedden, R. G.; Catterall, A.; Bitensky, L.; Chayen, J. Pentose-shunt oxidation in the periosteal cells in healing fractures. *Calcif. Tissue Res.* **1977**, *23*, 77−81.
(47) Buchholz, B.; Teschemacher, B.; Schley, G.; Schillers, H.; Eckardt, K. U. Formation of cysts by principal-like MDCK cells depends on the synergy of cAMP- and ATP-mediated fluid secretion. *J Mol. Med.* **2011**, *89*, 251−261.
(48) Dos Santos, P. M.; Freitas, F. P.; Mendes, J.; Tararthuch, A. L.; Fernandez, R. Differential regulation of H+-ATPases in MDCK-C11 cells by aldosterone and vasopressin. *Can. J. Physiol. Pharmacol.* **2009**, *87*, 653−665.
(49) Evan, A. P.; Lingeman, J. E.; Coe, F. L.; Parks, J. H.; Bledsoe, S. B.; Shao, Y.; Sommer, A. J.; Paterson, R. F.; Kuo, R. L.; Grynpas, M. Randall's plaque of patients with nephrolithiasis begins in basement membranes of thin loops of Henle. *J. Clin. Invest.* **2003**, *111*, 607−616.
(50) Bushinsky, D. A. Nephrolithiasis: site of the initial solid phase. *J. Clin. Invest.* **2003**, *111*, 602−605.

Journal of proteome research

Article

pubs.acs.org/jpr

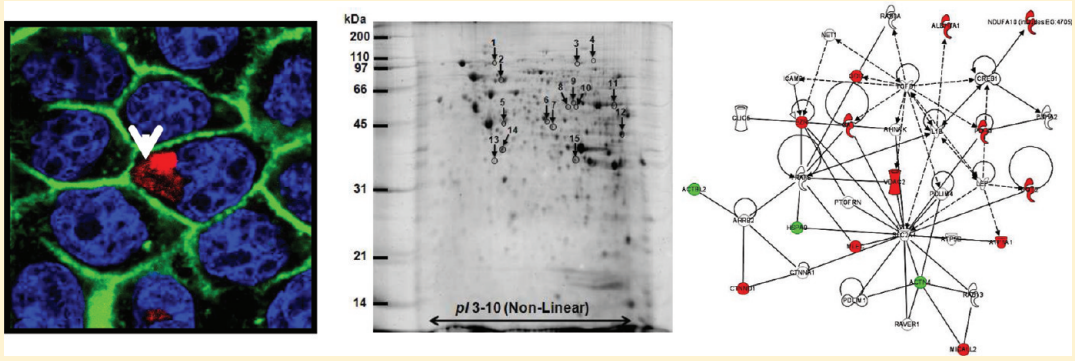
Changes in Mitochondrial Proteome of Renal Tubular Cells Induced by Calcium Oxalate Monohydrate Crystal Adhesion and Internalization Are Related to Mitochondrial Dysfunction

Sakdithep Chaiyarit[†,‡] and Visith Thongboonkerd*[,†,‡]

[†]Medical Proteomics Unit, Office for Research and Development, Faculty of Medicine Siriraj Hospital, Mahidol University, Bangkok, Thailand

[‡]Center for Research in Complex Systems Science, Mahidol University, Bangkok, Thailand

Supporting Information



ABSTRACT: Calcium oxalate monohydrate (COM) crystals, the major crystalline compound in kidney stones, have been suggested to induce oxidative stress by overproduction of reactive oxygen species (ROS) and renal tubular cell injury. Our present study aimed to examine changes in mitochondrial proteome in distal renal tubular cells induced by COM crystals (100 μg of crystals/mL of culture medium). Adhesion and internalization of COM crystals by MDCK cells were examined by fluorescent and laser-scanning confocal microscopy. Moreover, the internalized COM crystals were quantified by flow cytometry. Thereafter, mitochondria were isolated from controlled and COM-treated cells, and mitochondrial proteins were subjected to 2-DE-based comparative proteomic analysis, which revealed 15 differentially expressed proteins. These significantly altered proteins were identified by Q-TOF MS and MS/MS analyses, including those involved in several biological processes, e.g., cellular structure, carbohydrate metabolism, and energy metabolism. 2-D Western blot analysis confirmed the increase of ezrin and decrease of β-actin. Global protein network analysis was then performed to obtain additional functional significance of the identified proteins and to guide for subsequent functional analysis. The results implicated that the altered proteins were involved in energy production and might contribute to mitochondrial dysfunction. The loss of ROS regulation by mitochondria was finally confirmed by OxyBlot assay, which demonstrated markedly increased levels of the oxidatively modified mitochondrial proteins in the COM-treated cells in a dose-dependent manner. Our data may lead to a better understanding of molecular mechanisms of mitochondrial dysfunction underlying the overt oxidative stress induced by COM crystals in kidney stone disease.

KEYWORDS: *calcium oxalate, crystal adhesion, internalization, mitochondria, oxidation, proteomics*

INTRODUCTION

Calcium oxalate monohydrate (COM) is the most common type of crystalline compound found in stone matrices and urine of patients with kidney stone disease.[1] COM crystals are able to interact with several eukaryotic cells, including endothelial cells, fibroblasts, leukocytes, erythrocytes, pulmonary cells, and renal tubular cells, leading to inflammation and cell death. Several studies have suggested that retention of COM crystals in the kidney is an important step to trigger a cascade of mechanisms for the development of kidney stones.[1−3] Additionally, kidney stone disease is associated with oxidative stress that can induce renal tubular cell damage. Many reports have shown that COM crystals can induce overproduction of reactive oxygen species (ROS) in renal tubular epithelial cells followed by tubular injury and inflammation.[4] The increased ROS level then activates p38 mitogen-activated protein kinase (MAPK) and c-Jun N-terminal kinase (JNK) that subsequently induce transcription factors such as nuclear factor-κB (NF-κB) and activator protein-1 (AP-1).[4] These transcription factors can then activate the inflammatory cascade and increase the expression of stone modulator proteins (i.e., osteopontin, bikunin, and α-1-microglobulin),

Received: January 9, 2012
Published: April 18, 2012

 © 2012 American Chemical Society

chemokine (i.e., monocyte chemotactic protein-1; MCP1), cytokine (e.g., interleukin-6; IL-6), and growth factors (i.e., platelet-derived growth factor; PDGF, and transforming growth factor- β; TGF-β).[5,6] Generally, mitochondria play a significant role in controlling the production of superoxide and H_2O_2 in all cells and tissues.[7] However, the response of mitochondria to COM crystals remained poorly understood.

In pathogenic mechanisms of kidney stone disease, COM crystal adhesion onto the surface of renal tubular cells followed by crystal internalization into the cells is an important step for kidney stone formation.[1−3] Our present study, therefore, aimed to explore alterations in mitochondrial proteins in distal renal tubular cells in response to COM crystal adhesion and internalization using a proteomics approach. Madin−Darby canine kidney (MDCK) cell was used as a model in this study. Crystal adhesion and internalization were carefully examined using florescence-labeled COM crystals to justify our study model. Two-dimensional gel electrophoresis (2-DE) followed by tandem mass spectrometry (MS/MS) was performed to identify differentially expressed mitochondrial proteins in the COM-treated cells compared to the controlled cells. Global protein network analysis was then employed to obtain additional functional significance of the identified proteins and to guide for subsequent functional analysis, which was then performed to confirm the important role of mitochondria in regulation of oxidative stress response in renal tubular cells upon exposure to COM crystals.

MATERIALS AND METHODS

COM Crystal Preparation and Labeling

Plain (nonlabeled or nonfluorescent) COM crystals were prepared as described previously.[8,9] Briefly, 5 mM $CaCl_2 \cdot 2H_2O$ was mixed with 0.5 mM $Na_2C_2O_4$ in a buffer containing 90 mM Tris-HCl and 10 mM NaCl (pH 7.4). The solution was incubated at 25 °C overnight, and COM crystals were harvested by a centrifugation at 2000*g* for 5 min. The supernatant was discarded, and COM crystals were resuspended in methanol. After another centrifugation at 2000*g* for 5 min, methanol was discarded, and the crystals were air-dried overnight at room temperature.

Fluorescence-labeled COM crystals were prepared as described in detail in our previous study.[10] Briefly, the COM crystals were crystallized as aforementioned but in the presence of 0.58 μg/mL of rabbit antimouse IgG conjugated with FITC (DAKO; Glostrup, Denmark). COM crystals were imaged by light microscope, Olympus CKX41 phased-contrast microscope (Olympus Co. Ltd.; Tokyo, Japan), and Nikon ECLIPSE 80i fluorescence microscope (Nikon Corp.; Tokyo, Japan).

After COM crystals were prepared as aforementioned, the dried pellets of COM crystals were decontaminated by UV light radiation for 30 min.

Cell Culture

Madin−Darby canine kidney (MDCK) cells were grown in complete Eagle's minimum essential medium (MEM) (GIBCO, Invitrogen Corporation; Grand Island, NY) supplemented with 10% fetal bovine serum, 1.2% penicillin G/streptomycin, and 2 mM glutamine in 75 cm^2 tissue culture flasks. The cultured cells were maintained in a humidified incubator at 37 °C with 5% CO_2.

Evaluation of Crystal−Cell Interaction (Adhesion and Internalization)

Crystal Adhesion. MDCK cells (approximately 7.5×10^4 cells) in MEM were subcultured on a coverslip (cleaved mica disk diameter: 9.5 mm, V-1 grade, SPI Supplies; Toronto, Canada). The cells were maintained at 37 °C with 5% CO_2 for 24 h in a humidified incubator. Thereafter, the cells were washed with phosphate buffered saline (PBS) to eliminate detached cells and incubated with plain (nonlabeled) or fluorescence-labeled COM crystals in MEM (100 μg of crystals/mL of culture medium). The cells were grown further for 48 h. The nonadherent crystals were then removed by three washes with PBS. The coverslip was then mounted with 50% glycerol, and crystal adhesion was then examined under light, phase-contrast, and fluorescent microscopes with differential interference contrast (DIC) mode.

Crystal Internalization. MDCK cells were maintained and treated with COM crystals for 48 h as aforementioned for crystal adhesion assay. Thereafter, the cells were fixed with 3.8% formaldehyde in PBS at room temperature for 10 min and permeabilized with 1% Triton X-100 in PBS at room temperature for 10 min. The cells were then stained with Oreagon Green-conjugated phalloidin (Invitrogen − Molecular Probes; Eugene, OR) and Hoechst-dye 33342 (Invitrogen − Molecular Probes) in the dark at 37 °C for 1 h. The coverslip was then mounted with antifade solution (Invitrogen − Molecular Probes) on a glass slide. The images were then taken under LSM 510 META laser-scanning confocal microscope (Carl Zeiss, Inc.; Oberkochen, Germany). The extracellularly adhered crystals and intracellularly internalized crystals were visualized by their property to reflect the light at λ 633 nm of Kr-laser in red as previously described elsewhere.[11]

Flow Cytometric Quantitation of the Internalized COM Crystals

For quantitative analysis of the internalized crystals by flow cytometry, approximately 3×10^6 MDCK cells were grown in 75 cm^2 tissue culture flasks. The cells were maintained in a humidified incubator at 37 °C with 5% CO_2 for 24 h and then treated with plain (nonlabeled) crystals or fluorescence-labeled COM crystals (100 μg of crystals/mL of culture medium). After 48-h incubation, the cells were washed with PBS and incubated with trypsin−EDTA solution to eliminate non-internalized (both adherent and nonadherent) crystals. The internalized fluorescent COM crystals were then quantitated by a flow cytometer (FACScan, Becton Dickinson Immunocytometry System; San Jose, CA) using the blank control (MDCK cells without crystals) and the cells with nonfluorescent crystals to subtract the background.

Mitochondrial Isolation

Mitochondria were isolated from MDCK cells without or with COM treatment (100 μg of crystals/mL of culture medium) for 48 h to induce crystal adhesion/internalization as aforementioned using the protocol described previously.[12] Briefly, the cells were sonicated in an isolation buffer containing 0.25 M sucrose and 10 mM HEPES (pH 7.5) using a Bandelin Sonopuls HD 200 probe sonicator (Bandelin Electronic; Berlin, Germany) at MS 72/D (50 cycles) for 10 s in an icebox. The samples were then centrifuged at 1000*g* for 10 min to remove intact cells and debris. The supernatants were collected and then centrifuged at 20000*g* for 25 min. The pellets were saved, washed once with fresh isolation buffer (0.25 M sucrose and 10 mM HEPES; pH 7.5), and then centrifuged again at 20000*g* for 25 min. The mitochondrial pellets were then saved for subsequent experiments.

dx.doi.org/10.1021/pr300018c | J. Proteome Res. 2012, 11, 3269−3280

Their purity was examined by Janus green B staining, transmission electron microscopic (TEM) examination, and Western blot analyses of markers for individual subcellular organelles, as previously described.[12]

Two-Dimensional Gel Electrophoresis (2-DE)

Mitochondrial pellets were resuspended in a buffer containing 7 M urea, 2 M thiourea, 4% 3-[(3-cholamidopropyl) dimethylammonio]-1-propanesulfonate (CHAPS), 120 mM dithiothreitol (DTT), 2% ampholytes (pH 3−10) and 40 mM Tris-HCl, and further incubated at 4 °C for 30 min. Protein concentrations in individual samples were measured by the Bradford method using Bio-Rad protein assay (Bio-Rad Laboratories; Hercules, CA).

Mitochondrial proteins derived from individual samples were resolved in individual 2-D gels (n = 5 gels were derived from 5 individual culture flasks for each condition; a total of 10 gels were analyzed in this study). The proteins (100 μg for each sample) were premixed with a rehydration buffer containing 7 M urea, 2 M thiourea, 2% CHAPS, 120 mM DTT, 40 mM Tris-base, 2% ampholytes (pH 3−10), and bromophenol blue to make the final volume of 150 μL/sample. The mixtures were rehydrated onto immobilized pH gradient (IPG) strips (pI 3−10, nonlinear) (GE Healthcare; Uppsala, Sweden) at room temperature for 10−15 h. The first dimensional separation or isoelectric focusing (IEF) was performed in Ettan IPGphor III IEF System (GE Healthcare) at 20 °C using a stepwise mode to reach 9,083 V·hours. After the IEF, the IPG strips were equilibrated in an equilibration buffer containing 6 M urea, 130 mM DTT, 112 mM Tris-base, 4% SDS, 30% glycerol, and 0.002% bromophenol blue for 15 min. The strips were then equilibrated for an additional 15 min in another equilibration buffer, in which DTT was replaced with 135 mM iodoacetamide. The second dimensional separation was performed in 12.5% polyacrylamide slab gel using SE260 mini-vertical electrophoresis unit (GE Healthcare) at 150 V for approximately 2 h. The resolved protein spots were visualized with deep purple fluorescence protein stain (GE Healthcare).

Matching and Intensity Analysis of Protein Spots

Image Master 2D Platinum (GE Healthcare) software was used for matching and analysis of protein spots in 2-D gels. Parameters used for spot detection were (i) minimal area = 10 pixels; (ii) smooth factor = 2.0; and (iii) saliency = 2.0. A reference gel was created from an artificial gel combining all of the spots presenting in different gels into one image. The reference gel was then used for matching the corresponding protein spots among different gels. Background subtraction was performed and the intensity volume of each spot was normalized with total intensity volume (summation of the intensity volumes obtained from all spots within the same 2-DE gel).

In-Gel Tryptic Digestion

Only protein spots whose intensity levels significantly differed between the two groups (controlled vs COM-treated) were excised from 2-DE gels, washed twice with 200 μL of 50% acetonitrile (ACN)/25 mM NH_4HCO_3 buffer (pH 8.0) at room temperature for 15 min, and then washed once with 200 μL of 100% ACN. After washing, the solvent was removed, and the gel pieces were dried by a SpeedVac concentrator (Savant; Holbrook, NY) and rehydrated with 10 μL of 1% (w/v) trypsin (Promega; Madison, WI) in 25 mM NH_4HCO_3. After rehydration, the gel pieces were crushed with siliconized blue stick and incubated at 37 °C for at least 16 h. Peptides were subsequently extracted twice with 50 μL of 50% ACN/5% trifluoroacetic acid (TFA); the extracted solutions were then combined and dried with the SpeedVac concentrator. The peptide pellets were resuspended with 10 μL of 0.1% TFA and purified using $ZipTip_{C18}$ (Millipore; Bedford, MA). The peptide solution was drawn up and down in the $ZipTip_{C18}$ for ten times and then washed with 10 μL of 0.1% formic acid by drawing up and expelling the washing solution for three times. The peptides were finally eluted with 5 μL of 75% ACN/0.1% formic acid.

Protein Identification by Q-TOF MS and MS/MS Analyses

The trypsinized samples were premixed 1:1 with the matrix solution containing 5 mg/mL of α-cyano-4-hydroxycinnamic acid (CHCA) in 50% ACN, 0.1% (v/v) TFA, and 2% (w/v) ammonium citrate and deposited onto the 96-well MALDI target plate. The samples were analyzed by Q-TOF Ultima mass spectrometer (Micromass; Manchester, U.K.), which was fully automated with predefined probe motion pattern and the peak intensity threshold for switching over from MS survey scanning to MS/MS and from one MS/MS to another. Within each sample well, parent ions that met the predefined criteria (any peak within the m/z 800−3000 range with intensity above 10 count ± include/exclude list) were selected for CID MS/MS using argon as the collision gas and a mass dependent ±5 V rolling collision energy until the end of the probe pattern was reached. The MS and MS/MS data were extracted and outputted as the searchable *.txt* and *.pkl* files, respectively, for independent searches using the MASCOT search engine (http://www.matrixscience.com) to query to the NCBI mammalian protein database, assuming that peptides were monoisotopic. Fixed modification was carbamidomethylation at cysteine residues, whereas variable modification was oxidation at methionine residues. Only one missed trypsin cleavage was allowed, and mass tolerances of 100 and 50 ppm were allowed for peptide mass fingerprinting (PMF) and MS/MS ions search, respectively. Proteins with probability-based MOWSE (MS) scores ≥72 or MS/MS ions scores ≥36 were considered significant hits.

Global Protein Network Analysis

All of the altered mitochondrial proteins were subjected to global protein network analysis using Ingenuity pathways analysis (IPA) tool by Ingenuity Systems (http://www.ingenuity.com)[13] to query each identified protein to all other identified proteins as well as scientific findings curated from the literature relating to genes, cells, diseases, drugs, and other biological entities. Moreover, the altered mitochondrial proteins were also examined by the Human Mitochondrial Protein Database (HMPDb) (http://bioinfo.nist.gov), which provides inclusive information on mitochondrial and human nuclear encoded proteins involved in mitochondrial biogenesis and function. This database combines the information from SwissProt, LocusLink, Protein Data Bank (PDB), GenBank, Genome Database (GDB), Online Mendelian Inheritance in Man (OMIM), Human Mitochondrial Genome Database (mtDB), MITOMAP, Neuromuscular Disease Center, and Human 2-D PAGE databases that are integrated for the study of mitochondria and the associated diseases.

Confirmation of the Proteomic Data by 2-D Western Blot Analysis

To verify the changes in mitochondrial proteins induced by COM crystals as identified by proteomic analysis, 2-D Western blot analysis was performed. 2-DE was performed as aforementioned in

dx.doi.org/10.1021/pr300018c | J. Proteome Res. 2012, 11, 3269−3280

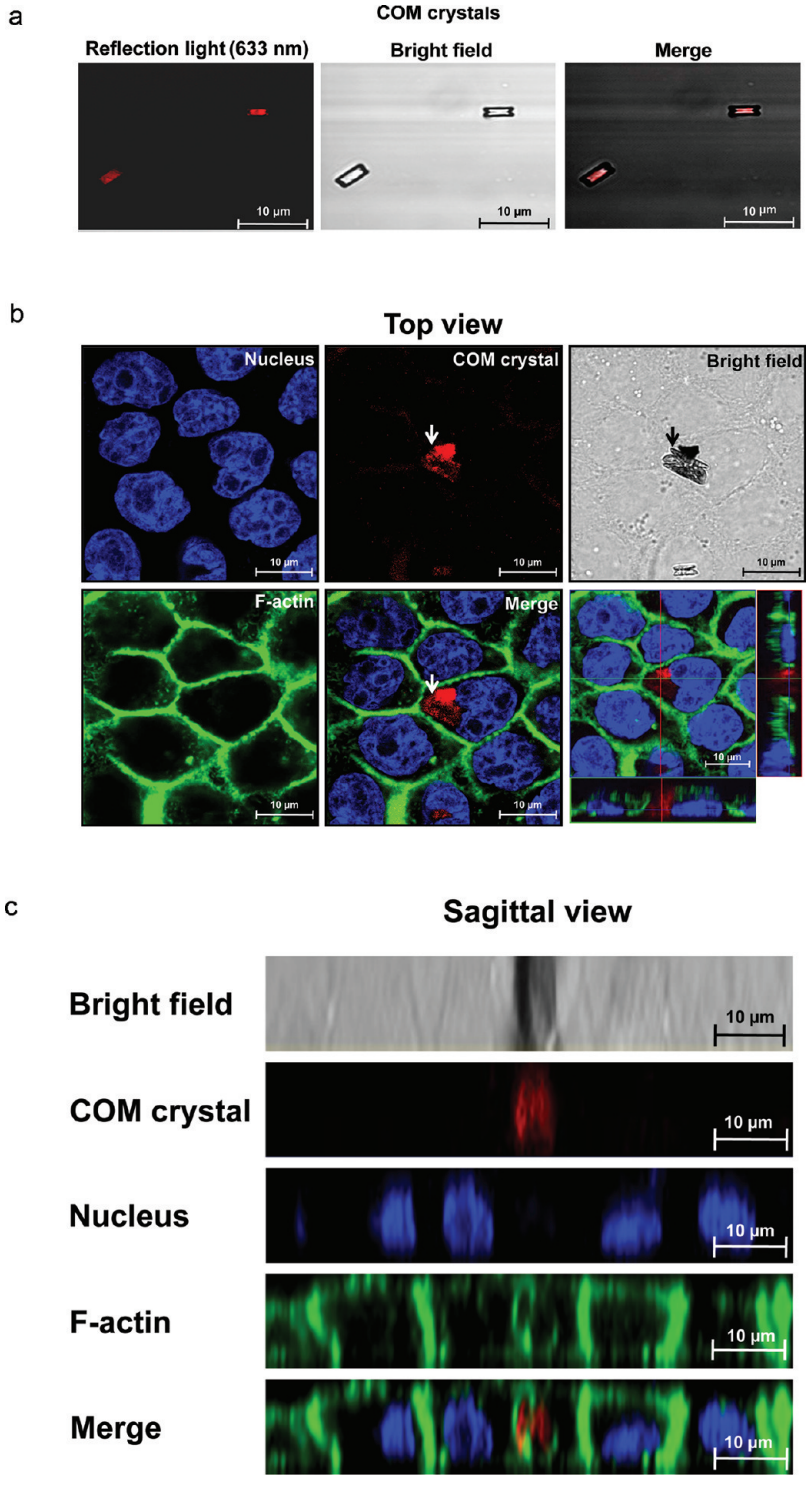


Figure 1. Internalization of COM crystals into MDCK cells. Panel (A) shows light reflection of plain COM crystals in red at λ 633 nm, whereas (B) and (C) show top and sagittal views, respectively, of the confocal micrographs of the internalized COM crystals in MDCK cells. After MDCK cells were incubated with COM crystals for 48 h, the nonadherent crystals were removed by vigorous washes with PBS three times, whereas the adherent crystals were detached and/or dissolved by trypsin/EDTA solution. Arrows indicate COM crystals that were reflected and visualized in red. Cell nuclei (blue) and boundaries (as represented by F-actin) (green) were stained with Hoechst-dye 33342 and Oreagon Green-conjugated phalloidin, respectively. The images in all panels were taken from a laser-scanning confocal microscope equipped with LSM5 Image Browser (LSM 510 META, Carl Zeiss; Oberkochen, Germany).

the section "2-DE". The resolved proteins were then transferred onto a nitrocellulose membrane using a semidry transfer apparatus at 75 mA for 1 h. Nonspecific bindings were blocked with 5% skim milk in PBS at room temperature for 1 h. The membrane was then incubated with mouse monoclonal antiezrin (villin-2) or anti-β-actin (both were from Santa Cruz Biotechnology; Santa Cruz, CA; with a dilution of 1:1,000 in 1% skim milk/PBS) at 4 °C overnight. The membrane was

dx.doi.org/10.1021/pr300018c | J. Proteome Res. 2012, 11, 3269−3280

then further incubated with rabbit antimouse IgG conjugated with horseradish peroxidase (HRP) (DAKO; Glostrup, Denmark) (1:2000 in 1% skim milk/PBS) at room temperature for 1 h. Reactive protein spots were then visualized with SuperSignal West Pico chemiluminescence substrate (Pierce Biotechnology, Inc.; Rockford, IL).

OxyBlot Assay

To verify the loss of mitochondrial ROS regulation, immunoblot detection of oxidatively modified proteins was performed according to the protocol of OxyBlot protein oxidation detection kit (S7150) (Chemicon; Temecula, CA). Briefly, MDCK cells were incubated without or with 100 μg (subtoxic dose) or 500 μg (toxic dose) of COM crystals/mL of culture medium for 48 h. Subsequently, mitochondria were isolated as aforementioned in the section "Mitochondrial Isolation", and mitochondrial proteins were derivatized with or without 2,4-dinitrophenylhydrazine (DNPH). The derivatized and nonderivatized mitochondrial proteins were resolved by SDS-PAGE and then transferred onto a nitrocellulose membrane. Thereafter, the membrane was incubated with primary antibody against DNP moiety of the oxidatively modified proteins at room temperature for 1 h and then with respective secondary antibody conjugated with HRP at room temperature for 1 h. Finally, the oxidatively modified proteins were detected by SuperSignal West Pico chemiluminescence substrate (Pierce Biotechnology, Inc.).

Statistical Analysis

All quantitative data are reported as Mean ± SEM, unless stated otherwise. Statistical analyses were performed using SPSS software version 13.0 (SPSS; Chicago, IL). Comparisons between two sets of data (i.e., controlled vs COM-treated) were performed by unpaired Student's *t* test, whereas multiple comparisons among more than two sets of data were performed by ANOVA with Tukey's posthoc test. *P*-values less than 0.05 were considered statistically significant.

RESULTS

Justification of the Study Model: COM Crystal Adhesion and Internalization

The goal of this study was to identify a set of altered mitochondrial proteins in distal renal tubular cells induced by COM crystal adhesion and internalization. Therefore, the most crucial issue was the confirmation of COM crystal adhesion and internalization to justify the model of this study. To investigate crystal−cell interaction, 100 μg of COM crystals/mL of culture medium were incubated with MDCK cells. Our previous study has reported that this dosage of COM crystals was not too toxic to the MDCK cells, as the total cell death (including early/late apoptosis and necrosis) was not significantly increased.[14] Therefore, changes in mitochondrial proteins to be identified would represent responses of mitochondria to COM crystal stimuli, not the changes reflected by severe cellular injury or cell death. After incubation of MDCK cells with this dosage of COM crystals for 48 h, both crystal adhesion and internalization were clearly demonstrated by phase-contrast microscopy (Supporting Information Figure S1). With this condition, approximately 80% of MDCK cells were adhered by COM crystals.

Laser-Scanning Confocal Microscopic Examination of the Internalized COM Crystals

However, it should be noted that phase-contrast microscopic examination could not precisely discriminate extracellular (adherent) from intracellular (internalized) crystals. Fortunately,

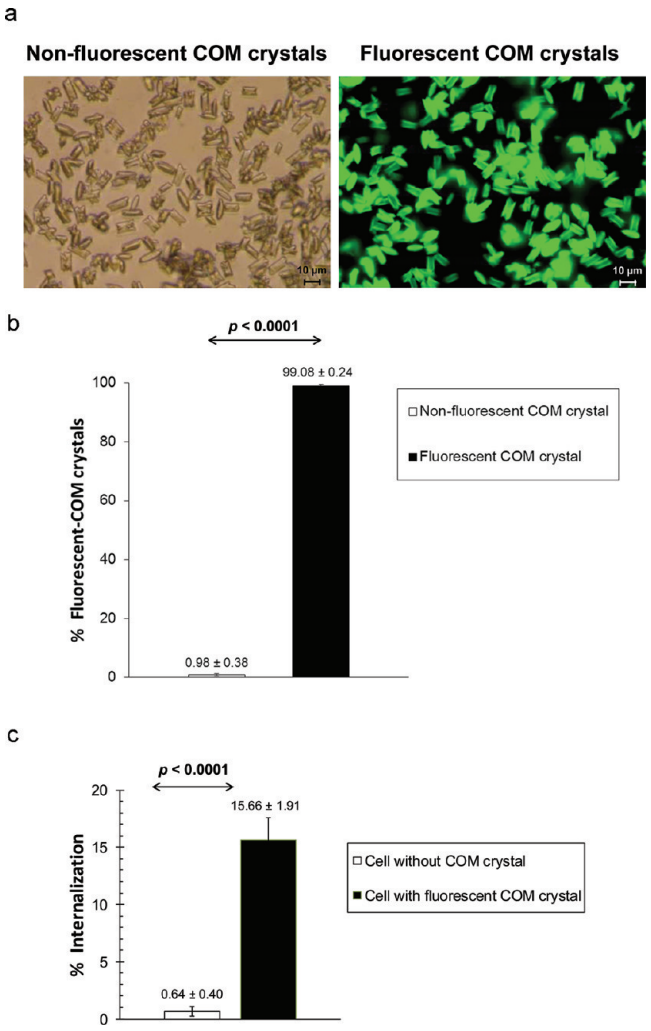


Figure 2. Quantitative analysis of the internalized fluorescent COM crystals using flow cytometry. (A) Side-by-side comparison of nonlabeled (nonfluorescent) and FITC-conjugated (fluorescent) COM crystals (in green) without cells. (B) Percentages of crystals, which were detectable as fluorescent COM crystals by flow cytometry. More than 99% of FITC-conjugated crystals were detectable as the fluorescent COM crystals, and the background of the nonfluorescent COM crystals was negligible (n = 5 independent experiments). (C) The flow cytometric analysis of fluorescent COM crystals was applied to quantitative analysis of the internalized COM crystals in MDCK cells (n = 5 independent experiments). After MDCK cells were incubated with COM crystals for 48 h, the nonadherent crystals were removed by vigorous washes with PBS three times, whereas the adherent crystals were detached and/or dissolved by trypsin/EDTA solution.

COM crystals could reflect the light at λ 633 nm to be visualized in red.[11] We therefore employed a laser-scanning confocal microscope to precisely analyze the internalized crystals. The results confirmed that plain COM crystals could be visualized in red at λ 633 nm (Figure 1A). Additionally, with MDCK cells, the internalized plain COM crystals could be precisely localized and demonstrated by top (Figure 1B) and sagittal (Figure 1C) views.

Flow Cytometric Quantitation of the Internalized COM Crystals

Although laser-scanning confocal microscopic examination could provide the precise information of intracellular locales

dx.doi.org/10.1021/pr300018c | J. Proteome Res. 2012, 11, 3269−3280

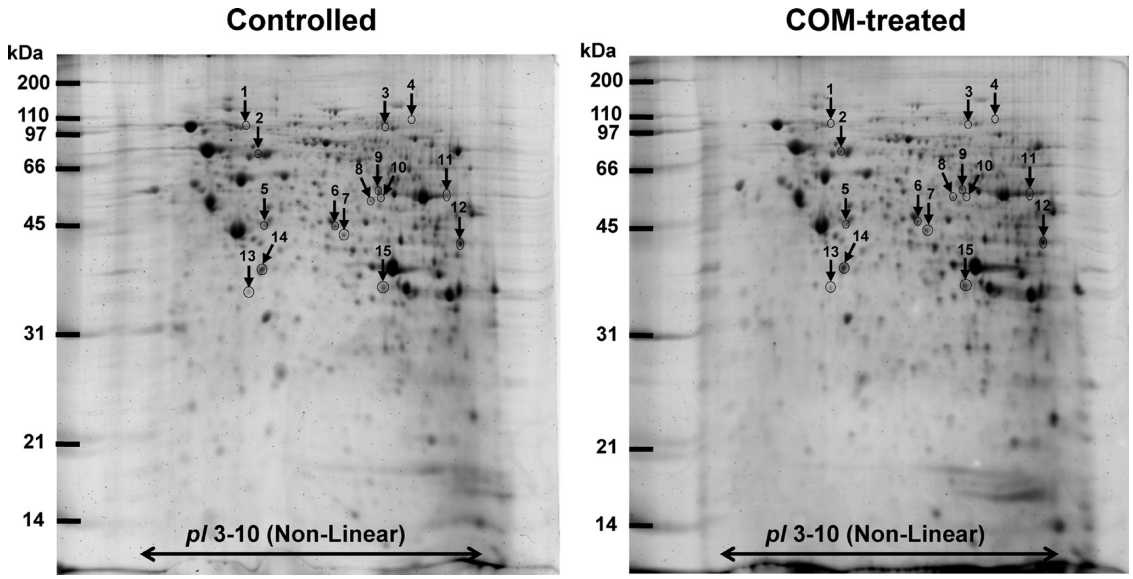


Figure 3. The 2-D proteome map of differentially expressed mitochondrial proteins in controlled versus COM-treated MDCK cells. Spot matching and quantitative intensity analysis were performed for 10 gels derived from 10 independent mitochondrial samples (5 per group). The map was created from a representative 2-DE gel image from 5 individuals in each group. The differentially expressed spots are labeled with numbers, which correspond to those reported in Table 1.

of COM crystals, this qualitative data did not yield the precise quantitative result (i.e., numbers and percentage of the internalized crystals). Therefore, we generated fluorescence-labeled COM crystals (Figure 2A) and used flow cytometry to quantitate the fluorescent signals of FITC-positive crystals. As >99% FITC-conjugated crystals were detectable as the fluorescent COM crystals together with negligible background of the nonfluorescent COM crystals, this data indicated that quantitative analysis of fluorescent COM crystals by flow cytometry is feasible (Figure 2B). Using this flow cytometric quantitative method, the data revealed that 15.66 ± 1.91% of COM crystals were internalized after incubation with MDCK cells for 48 h (Figure 2C).

Altered Mitochondrial Proteome in MDCK Cells Induced by COM Crystal Adhesion and Internalization

After carefully justifying the study model, mitochondria were isolated from the controlled and COM-treated cells. The purity of mitochondrial isolation was confirmed by Janus green B staining, TEM, and Western blot analyses of markers for mitochondria (cytochrome C oxidase-IV; COX-4), nucleus (c-Jun), cytoplasm (calpain-1), endoplasmic reticulum (glucose-regulated protein 94 kDa; GRP-94), and lysosome (lysosomal-associated membrane protein-2; LAMP-2), as described in our previous study[12] (data not shown).

The mitochondrial proteome profiles of controlled vs COM-treated cells were then compared using 2-DE (n = 5 gels derived from 5 individual culture flasks for each condition; a total of 10 gels were analyzed in this study). Using deep purple fluorescence dye, 897 ± 9 and 892 ± 12 protein spots were visualized in individual gels derived from controlled and COM-treated cells, respectively. Coefficient of variation (CV) of these protein spots was 2.23−2.91%. Spot matching, intensity analysis, and statistics revealed 15 differentially expressed protein spots (12 were increased, whereas other 3 spots were decreased) in the COM-treated samples as compared to the controls (Figure 3). All of these 15 significantly altered proteins were excised from 2-D gel and successfully identified by Q-TOF MS and MS/MS analyses. Details of these identified proteins (including identities, identification numbers, methods of identification, percentages of sequence coverage, numbers of matched peptides, isoelectric points or pI, molecular weights or MW, quantitative intensity data, fold changes, and p-values) are provided in Table 1. These identified proteins were functionally classified based on the Human Mitochondrial Protein Database (HMPDb) (http://bioinfo.nist.gov), including cell cycle regulation, cellular structure, carbohydrate metabolism, protein/amino acid metabolism, energy metabolism, ion transport, and signal transduction (Table 1).

Validation of the Proteomic Data by 2-D Western Blot Analysis

Two of the significantly altered proteins identified by proteomic analysis were randomly selected for subsequent validation by conventional method. 2-D Western blot analysis nicely confirmed the increased level of villin-2 (ezrin) (spot #8) (Figure 4A) and decreased level of β-actin (spot #5) (Figure 4B) in the COM-treated MDCK cells. Note that 2-D Western blot analysis captured the increased levels of two forms of villin-2 (ezrin), whereas 2-DE-based proteomic analysis identified only one significantly increased form of this protein. This might be simply explained by the higher sensitivity of immunoblot method as compared to 2-DE to identify changes in levels of low abundant proteins.

Global Protein Network Analysis of Significantly Altered Mitochondrial Proteins

Using Ingenuity pathway analysis (IPA) tool (http://www.ingenuity.com), each identified protein was queried to all 15 identified proteins and scientific findings curated from the literature relating to genes, cells, diseases, drugs, and other biological entities.[13] The data demonstrated that significantly altered mitochondrial proteins participated mainly in the network of gene expression, organismal functions, and carbohydrate metabolism, which determined energy production and might contribute to mitochondrial dysfunction (Figure 5).

dx.doi.org/10.1021/pr300018c | J. Proteome Res. 2012, 11, 3269−3280

Table 1. Summary of Differentially Expressed Mitochondrial Proteins Whose Levels Were Significantly Altered by COM Crystal Adhesion and Internalization[a]

spot no.	protein name	NCBI ID	identified by	identification scores (MS, MS/MS)	% cov	no. of matched peptides (MS, MS/MS)	pI	MW (kDa)	intensity levels (arbitrary unit) (mean ± SEM)		ratio (COM-treated/ Controlled)	p-values
									controlled	COM-treated		
	Cell cycle regulation											
4	Stress-70 protein, mitochondrial precursor (75 kDa glucose regulated protein) (GRP 75) (Peptide-binding protein 74) (PBP74) (Mortalin) (MOT) isoform 15	gil73970906	MS	98, NA	23, NA	15, NA	5.83	73.70	0.2476 ± 0.0179	0.1702 ± 0.0198	0.69	0.020
8	Villin-2 isoform 9	gil73945744	MS, MS/MS	120, 49	34, 3	17, 1	5.8	67.32	0.0925 ± 0.0128	0.1606 ± 0.0036	1.74	0.001
	Cellular structure											
1	MICAL-like 2	gil109495311	MS	75, NA	20, NA	13, NA	9.64	111.47	0.0298 ± 0.0029	0.0564 ± 0.0105	1.90	0.040
2	Actinin, alpha 4 isoform 2	gil73947718	MS	93, NA	26, NA	16, NA	5.27	105.31	0.0711 ± 0.0088	0.0387 ± 0.0090	0.54	0.033
3	Catenin delta-1 (p120 catenin) (p120(ctn)) (Cadherin-associated Src substrate) (CAS) (p120(cas)) isoform 3	gil73982226	MS, MS/MS	100, 78	24, 1	13, 1	6.71	93.03	0.0137 ± 0.0015	0.0313 ± 0.0043	2.28	0.010
5	Actin, cytoplasmic 1 (Beta-actin 1)	gil57043600	MS/MS	NA, 36	NA, 4	NA, 1	5.29	42.23	0.2059 ± 0.0166	0.1443 ± 0.0123	0.70	0.017
	Carbohydrate metabolism											
7	Antiquitin	gil73971017	MS/MS	NA, 81	NA, 5	NA, 2	8.22	59.12	0.0438 ± 0.0062	0.0714 ± 0.0038	1.63	0.005
13	Pyruvate dehydrogenase E1 component beta subunit, mitochondrial precursor (PDHE1-B) isoform 4	gil73985155	MS, MS/MS	94, 52	42, 9	12, 2	5.51	37.54	0.4739 ± 0.0361	0.5964 ± 0.0263	1.26	0.025
15	Protein KIAA0152 precursor isoform 1	gil73994752	MS, MS/MS	59, 127	28, 10	8, 2	5.27	32.22	0.0709 ± 0.0082	0.1056 ± 0.0055	1.49	0.008
	Protein or amino acid metabolism											
10	Ornithine aminotransferase, mitochondrial precursor (Ornithine—oxo-acid aminotransferase) isoform 1	gil73998800	MS, MS/MS	163, 124	51, 9	17, 3	6.44	48.75	0.1397 ± 0.0051	0.1714 ± 0.0094	1.23	0.031
12	Aspartate aminotransferase, mitochondrial precursor (Transaminase A) (Glutamate oxaloacetate transaminase-2) isoform 3	gil73975238	MS, MS/MS	106, 167	37, 13	12, 3	9.2	43.67	0.3111 ± 0.0373	0.4407 ± 0.0364	1.42	0.038
	Energy metabolism											
6	ATP synthase alpha chain, mitochondrial precursor isoform 1	gil73961223	MS, MS/MS	120, 25	39, 2	15, 1	6.22	47.31	0.1503 ± 0.0280	0.3815 ± 0.0655	2.54	0.012
11	NADH dehydrogenase (ubiquinone) 1 alpha subcomplex, 10, 42 kDa precursor	gil73994237	MS, MS/MS	113, 31	47, 3	12, 1	6.61	41.09	0.0974 ± 0.0080	0.1701 ± 0.0178	1.75	0.006
	Ion transport											
14	Voltage-dependent anion channel 2 isoform 2	gil73953093	MS	101, NA	45, NA	10, NA	7.48	32.07	0.1660 ± 0.0310	0.3160 ± 0.0156	1.90	0.003
	Signal transduction											
9	GDP dissociation inhibitor 2	gil50978926	MS	102, NA	37, NA	12, NA	6.11	50.80	0.0415 ± 0.0067	0.0772 ± 0.0062	1.86	0.005

[a]All these proteins were successfully identified by Q-TOF MS and MS/MS analyses. NA = not applicable; NCBI = National Center for Biotechnology Information; % cov = % sequence coverage [(number of the matched residues/total number of residues in the entire sequence) × 100%].

dx.doi.org/10.1021/pr300018c | J. Proteome Res. 2012, 11, 3269−3280

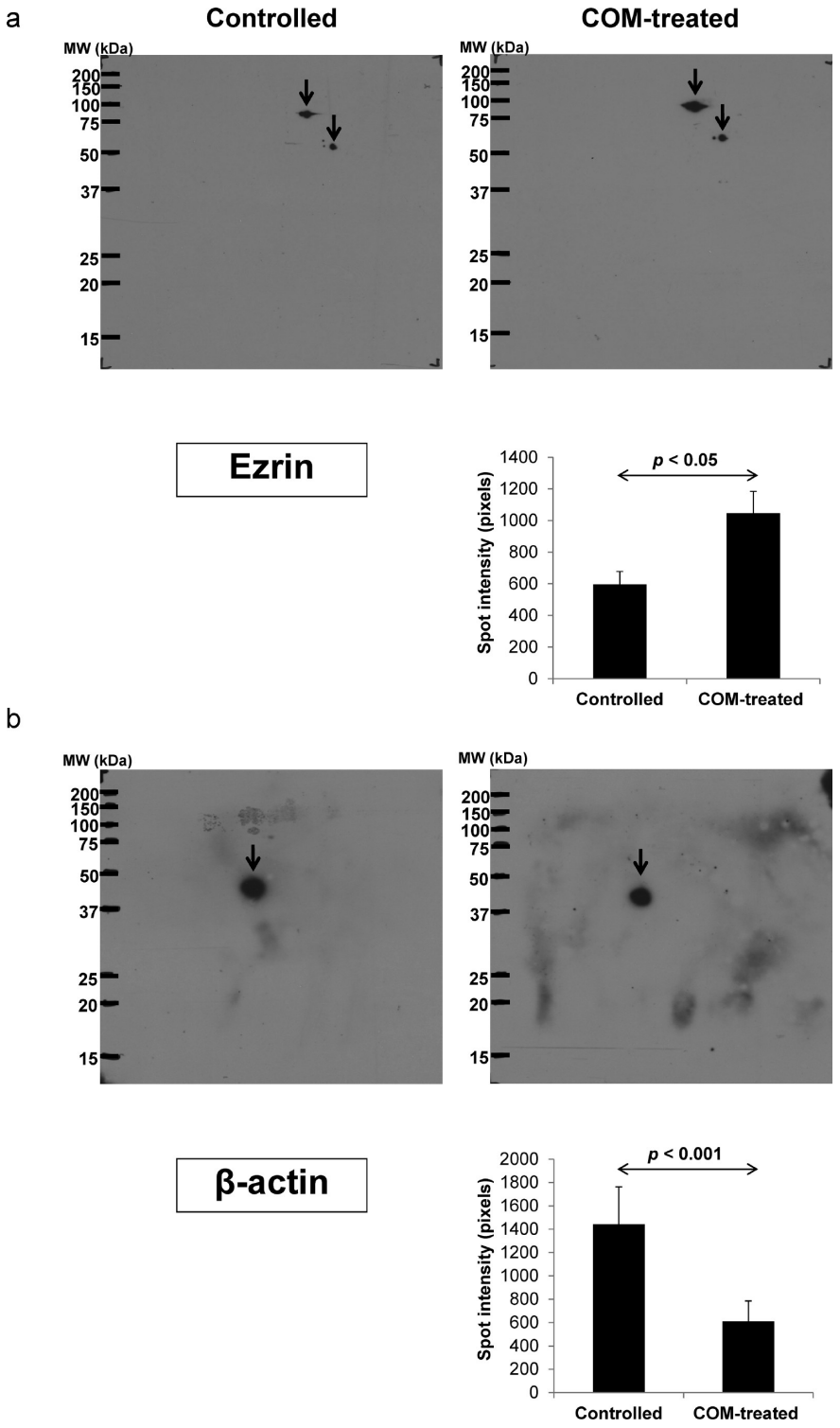


Figure 4. Validation of the proteomic data by 2-D Western blot analysis. Mitochondrial proteins (100 μg/each sample) from controlled and COM-treated MDCK cells were resolved in 2-DE and transferred onto nitrocellulose membranes. After blocking nonspecific bindings, the membranes were incubated with mouse monoclonal antiezrin (A) or mouse monoclonal anti-β-actin antibody (B). After incubation with rabbit antimouse IgG conjugated with horseradish peroxidase (HRP), the immunoreactive protein spots were visualized with a chemiluminescence substrate. Spot intensity levels of immunoreactive proteins were quantitated using Image Master 2D Platinum (GE Healthcare) software. N = 3 independent experiments for each protein.

Markedly Increased Levels of Oxidatively Modified Mitochondrial Proteins in the Com-Treated Cells

To verify functional significance of the significantly altered proteins as predicted by global protein network analysis, OxyBlot assay was performed to quantitate oxidatively modified mitochondrial proteins in the COM-treated cells compared to the controls. The data revealed that the oxidatively modified mitochondrial proteins were markedly increased in the COM-treated cells in a dose-dependent manner (100 vs 500 μg of COM crystals/mL of culture medium) (Figure 6).

dx.doi.org/10.1021/pr300018c | J. Proteome Res. 2012, 11, 3269−3280

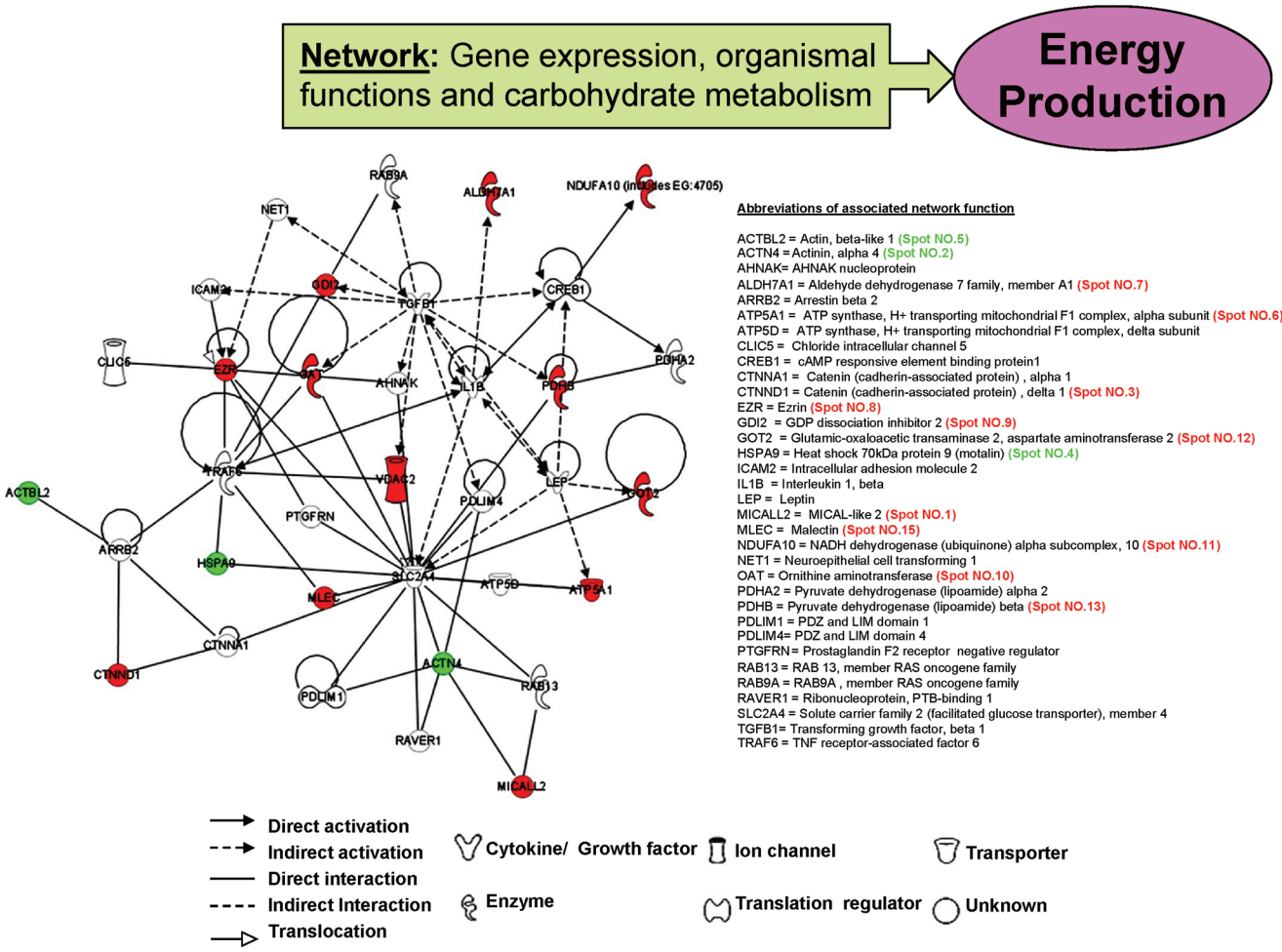


Figure 5. Global protein network analysis of the altered mitochondrial proteins. Using Ingenuity pathways analysis (IPA) tool (http://www.ingenuity.com),[13] the altered mitochondrial proteins formed a network involved in gene expression, organismal functions, and carbohydrate metabolism. Red and green nodes show mitochondrial proteins, which were up-regulated and down-regulated in COM-treated MDCK cells, respectively.

This functional data strengthened the hypothesis that COM crystals induce mitochondrial dysfunction and oxidative stress in renal tubular cells.

DISCUSSION

Adhesion and internalization of COM crystals into renal tubular epithelial cells has been proposed to induce mitochondrial dysfunction, leading to oxidative stress, tubular cell injury, and ultimately, kidney stone formation.[15,16] To clarify the important role of mitochondria in response to COM exposure, we applied proteomics to define changes in mitochondrial proteome induced by COM crystal adhesion and internalization. In the present study, MDCK cells were treated with subtoxic dose of COM crystals (100 μg of crystals/mL of culture medium) for 48 h. The data obtained from our previous study[14] have shown that this dosage and incubation period were not toxic to the MDCK cells, as early/late apoptotic and necrotic cell death did not significantly increase after such exposure. In addition, COM crystal adhesion and internalization were clearly confirmed by light, phase-contrast, and laser-scanning confocal microscopies (Supporting Information Figure S1 and Figure 1) and quantitated by flow cytometry (Figure 2). Approximately 80% of MDCK cells were adhered by COM crystals, whereas about 16% of these cells had internalized COM crystals. Therefore, our study model was justified to define response of mitochondria to COM crystal adhesion and internalization, as changes in the mitochondrial proteome were not due to changes affected by severe cytotoxicity or cell death, which is an end-point of the disease process, not the pathophysiological changes during the disease development.

2-DE-based proteomic analysis revealed 15 differentially expressed mitochondrial proteins in the COM-treated cells compared to the controlled cells (Table 1 and Figure 3). Some of these significantly altered proteins with potential roles in mitochondrial dysfunction induced by COM crystal adhesion and internalization are highlighted as follows. Pyruvate dehydrogenase E1 component beta subunit is a member of the mitochondrial PDH complex, which is crucial for sugar metabolism.[17] This enzyme is involved in glycolysis, oxidoreductase, and tricarboxylic acid cycle, which are confined in mitochondria. Our present study observed the increased level of this mitochondrial enzyme in the COM-treated cells. Together with previous evidence reporting the increased activities of other mitochondrial enzymes, i.e., succinate dehydrogenase, isocitrate dehydrogenase, malate dehydrogenase, and respiratory complex enzymes,[16,18] the increased level of pyruvate dehydrogenase E1 component beta subunit was proposed as a response to reserve energy production during stress induced by crystal exposure.

dx.doi.org/10.1021/pr300018c | J. Proteome Res. 2012, 11, 3269−3280

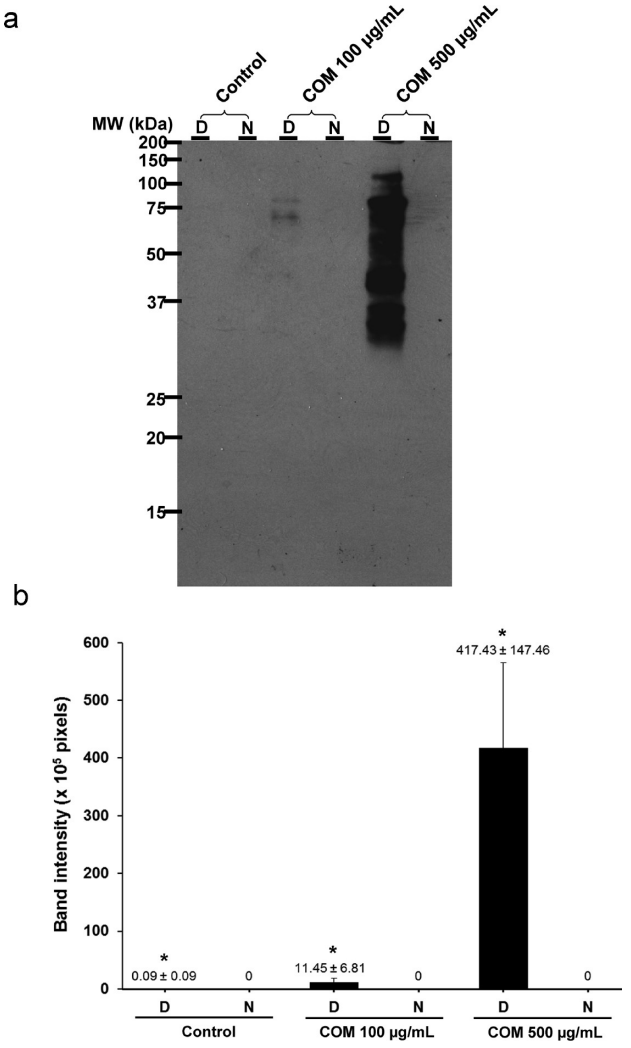


Figure 6. Increased levels of oxidatively modified mitochondrial proteins in the COM-treated MDCK cells. Immunoblot detection of proteins modified by ROS was performed using OxyBlot protein oxidation detection kit (S7150) (Chemicon; Temecula, CA). MDCK cells were treated without or with 100 or 500 μg of COM crystals/mL of MEM for 48 h. Subsequently, mitochondrial proteins were isolated and then derivatized with 2,4-dinitrophenylhydrazine (DNPH). The derivatized and nonderivatized mitochondrial proteins were resolved by SDS-PAGE followed by Western blotting using anti-DNP moiety of the oxidatively modified proteins as the primary antibody (A). Densitometric analysis was performed to quantitate the oxidatively modified proteins in the COM-treated cells compared to the controls (n = 3 independent experiments) (B). D = derivatized samples; N = nonderivatized samples; * = $p < 0.001$ vs nonderivatized samples and negative controls.

Nicotinamide adenine dinucleotide (NADH) dehydrogenase (ubiquinone) 1 alpha subcomplex is a subunit of Complex I of oxidative phosphorylation (OXPHOS) system.[19] Complex I is crucial for electron transport to the respiratory chain, and reduction of oxygen to $O_2^{\cdot -}$ mainly occurs at Complex I prior to the transfer into mitochondrial matrix.[20] Subsequently, $O_2^{\cdot -}$ generated from Complex I can be changed to H_2O_2 by Cu/Zn-superoxide dismutase (SOD) or Mn-SOD in mitochondria.[21] In this study, ubiquinone subunit of Complex I was increased in response to COM crystal interaction. Hence, this might be the core mechanism underlying the increase of cellular ROS in renal tubular cells in response to COM crystals.

ATP synthase alpha chain, mitochondrial precursor isoform 1 is a subunit of mitochondrial membrane ATP synthase (F_1F_0 ATP synthase).[19,22] This complex generates ATP from ADP in the respiratory chain. In the present study, ATP synthase alpha chain mitochondrial precursor was increased in the COM-treated cells. In addition, this enzyme participates in Complex V of the OXPHOS system.[19,22] Therefore, its increase was thought to be related to energy homeostasis and oxidative stress mechanisms.

Mitochondrial chaperone heat shock protein 70 (also known as mortalin) is a member of HSP70 family. Although mortalin distributes in multiple subcellular organelles, its main locale is in mitochondria. Previous studies have demonstrated that overexpression of mortalin reduced ROS production,[23,24] and vice versa, increased ROS generation was associated with the declined level of this protein.[25] Thus, the decreased level of mortalin in the COM-treated cells might be a result of the increase of cellular ROS in renal tubular cells in response to COM crystals, leading to mitochondrial dysfunction.

Voltage-dependent anion channel (VDAC) 2, also known as a small mitochondrial pore forming protein, serves as the channel for metabolite and ion flux throughout the outer mitochondrial membrane.[26] In addition, VDAC can also bind with metabolic enzymes and thus links cytoplasmic metabolism to mitochondrial respiration and the OXPHOS system.[27] In this study, VDAC2 was increased in the COM-treated cells and might lead to the release of ROS and cytochrome c to cytoplasm. In contrast, its increase might facilitate the transportation of nuclear encoded proteins to mitochondria to activate energy production.[28] Additionally, influx and efflux of calcium ion to and from mitochondria via this channel might involve the regulation of ATP and ROS production.[7]

Villin-2, also known as ezrin or cytovillin, is a member of ezrin/radixin/moesin (ERM) family that plays a key role as the linker between plasma membrane and actin cytoskeletal assembly.[29] Recently, Western blot analysis was performed to confirm the mitochondrial locale of ezrin.[30] The TEM analysis together with immuno-gold labeling has also confirmed that ezrin binds to mitochondria[31] Thus, ezrin should be considered as one of the mitochondria-associated proteins. Ezrin is involved in signal transduction, cell growth and morphogenesis,[32] as well as adhesion.[33] Recent evidence has demonstrated that overexpression of ezrin has protective effects on mitochondrial function in renal tubular cells.[30] The increased level of ezrin in the COM-treated cells might serve as a protective effect against mitochondrial dysfunction induced by COM crystals. On the other hand, our previous study using a cytotoxic dose of COM crystals (1000 μg of crystals/mL of culture medium) found the decreased level of ezrin in the COM-treated cells,[34] which was opposite to the data reported in the present study using a much lower dose of COM crystals (100 μg of crystals/mL of culture medium). These disparate results might be due to different doses of COM crystals used and/or differential cellular compartments that were examined (whole cell in the previous study vs mitochondria in this study). On the basis of these findings, ezrin might serve as a "switch protein" for protecting mitochondrial dysfunction during an early stage and involving in cytotoxicity and cell death during the late stage of crystal-cell interactions.

β-Actin belongs to actin cytoskeletal assembly that plays a pivotal role in maintaining cellular structure and integrity,[35] and regulation of cellular motility, cell division, and intracellular trafficking.[36] Although β-actin mainly localizes in the cytoplasm, especially in the endoplasmic reticulum, recent studies have highlighted the role of β-actin in mitochondrial function.[37,38]

dx.doi.org/10.1021/pr300018c | J. Proteome Res. 2012, 11, 3269−3280

Thus, β-actin should be considered as another mitochondria-associated protein. Previous studies have reported that the accumulation β-actin in mitochondria is associated with mitochondrial fission and release of apoptotic factors into the cytoplasm.[37,38] The decreased level of mitochondria-associated β-actin found in our present study might be the defense mechanism to prevent the cells from fatality. However, the precise role of the decreased level of mitochondria-associated β-actin in the COM-treated cells deserved further investigations.

As these significantly altered proteins seemed to involve ROS overproduction and mitochondrial dysfunction, as the aggravating or compensatory mechanisms, their functional significance should be further elucidated. We used the IPA tool (http://www.ingenuity.com)[13] for global protein network analysis as to obtain additional information of the functional network of these significantly altered proteins. The results strengthened that these proteins participated mainly in the network of gene expression, organismal functions, and carbohydrate metabolism, which determined energy production and might contribute to mitochondrial dysfunction (Figure 5). We then employed OxyBlot assay to address functional significance of these altered mitochondrial proteins identified in our present study. The data obtained from OxyBlot analysis confirmed that there were increased levels and accumulation of the oxidatively modified mitochondrial proteins as a result of COM crystal adhesion and internalization in a dose-dependent manner (Figure 6), indicating ROS overproduction and mitochondrial dysfunction in the COM-treated cells.

In summary, we present herein, for the first time, alterations in mitochondrial proteome in renal tubular cells in response to COM crystal adhesion and internalization. Both expression and functional data have pointed out that these significantly altered proteins were involved, as the aggravating factors or compensatory mechanisms, mainly in mitochondrial dysfunction and oxidative stress that are important for the kidney stone pathogenesis.

■ ASSOCIATED CONTENT

Supporting Information

Figure S1: Interaction of CaOx crystals with renal tubular (MDCK) cells. This information is available free of charge via the Internet at http://pubs.acs.org.

■ AUTHOR INFORMATION

Corresponding Author

*Phone/Fax: +66-2-4184793. E-mail: thongboonkerd@dr.com, vthongbo@yahoo.com.

Notes

The authors declare no competing financial interest.

■ ACKNOWLEDGMENTS

We are grateful to Prof. Shui-Tein Chen and Dr. Supachok Sinchaikul for their assistance on mass spectrometric analyses. This study was supported by the Thailand Research Fund (TRF) (RTA5380005) and Office of the Higher Education Commission and Mahidol University under the National Research Universities Initiative. S.C. was supported by Siriraj Graduate Thesis Scholarship. V.T. is also supported by "Chalermphrakiat" Grant, Faculty of Medicine Siriraj Hospital.

■ REFERENCES

(1) Coe, F. L.; Evan, A.; Worcester, E. Kidney stone disease. *J. Clin. Invest.* **2005**, *115*, 2598−2608.
(2) Verkoelen, C. F.; Verhulst, A. Proposed mechanisms in renal tubular crystal retention. *Kidney Int.* **2007**, *72*, 13−18.
(3) Khan, S. R.; Cockrell, C. A.; Finlayson, B.; Hackett, R. L. Crystal retention by injured urothelium of the rat urinary bladder. *J. Urol.* **1984**, *132*, 153−157.
(4) Habibzadegah-Tari, P.; Byer, K.; Khan, S. R. Oxalate induced expression of monocyte chemoattractant protein-1 (MCP-1) in HK-2 cells involves reactive oxygen species. *Urol. Res.* **2005**, *33*, 440−447.
(5) Hansel, D. E.; Dhara, S.; Huang, R. C.; Ashfaq, R.; Deasel, M.; Shimada, Y.; Bernstein, H. S.; Harmon, J.; Brock, M.; Forastiere, A.; Washington, M. K.; Maitra, A.; Montgomery, E. CDC2/CDK1 expression in esophageal adenocarcinoma and precursor lesions serves as a diagnostic and cancer progression marker and potential novel drug target. *Am. J. Surg. Pathol.* **2005**, *29*, 390−399.
(6) Khan, S. R. Role of renal epithelial cells in the initiation of calcium oxalate stones. *Nephron Exp. Nephrol.* **2004**, *98*, e55−e60.
(7) Brookes, P. S.; Yoon, Y.; Robotham, J. L.; Anders, M. W.; Sheu, S. S. Calcium, ATP, and ROS: a mitochondrial love-hate triangle. *Am. J. Physiol.: Cell Physiol.* **2004**, *287*, C817−C833.
(8) Thongboonkerd, V.; Semangoen, T.; Chutipongtanate, S. Factors determining types and morphologies of calcium oxalate crystals: Molar concentrations, buffering, pH, stirring and temperature. *Clin. Chim. Acta* **2006**, *367*, 120−131.
(9) Thongboonkerd, V.; Chutipongtanate, S.; Semangoen, T.; Malasit, P. Urinary trefoil factor 1 is a novel potent inhibitor of calcium oxalate crystal growth and aggregation. *J. Urol.* **2008**, *179*, 1615−1619.
(10) Chaiyarit, S.; Mungdee, S.; Thongboonkerd, V. Non-radioactive labelling of calcium oxalate crystals for investigations of crystal-cell interaction and internalization. *Anal. Methods* **2010**, *2*, 1536−1541.
(11) Verkoelen, C. F.; van der Boom, B. G.; Houtsmuller, A. B.; Schroder, F. H.; Romijn, J. C. Increased calcium oxalate monohydrate crystal binding to injured renal tubular epithelial cells in culture. *Am. J. Physiol.* **1998**, *274*, F958−F965.
(12) Chaiyarit, S.; Thongboonkerd, V. Comparative analyses of cell disruption methods for mitochondrial isolation in high-throughput proteomics study. *Anal. Biochem.* **2009**, *394*, 249−258.
(13) Rajagopalan, D.; Agarwal, P. Inferring pathways from gene lists using a literature-derived network of biological relationships. *Bioinformatics* **2005**, *21*, 788−793.
(14) Semangoen, T.; Sinchaikul, S.; Chen, S. T.; Thongboonkerd, V. Proteomic analysis of altered proteins in distal renal tubular cells in response to calcium oxalate monohydrate crystal adhesion: Implications for kidney stone disease. *Proteomics Clin. Appl.* **2008**, *2*, 1099−1109.
(15) McMartin, K. E.; Wallace, K. B. Calcium oxalate monohydrate, a metabolite of ethylene glycol, is toxic for rat renal mitochondrial function. *Toxicol. Sci.* **2005**, *84*, 195−200.
(16) Meimaridou, E.; Lobos, E.; Hothersall, J. S. Renal oxidative vulnerability due to changes in mitochondrial-glutathione and energy homeostasis in a rat model of calcium oxalate urolithiasis. *Am. J. Physiol.: Renal Physiol.* **2006**, *291*, F731−F740.
(17) Arjunan, P.; Nemeria, N.; Brunskill, A.; Chandrasekhar, K.; Sax, M.; Yan, Y.; Jordan, F.; Guest, J. R.; Furey, W. Structure of the pyruvate dehydrogenase multienzyme complex E1 component from *Escherichia coli* at 1.85 Å resolution. *Biochemistry* **2002**, *41*, 5213−5221.
(18) Veena, C. K.; Josephine, A.; Preetha, S. P.; Rajesh, N. G.; Varalakshmi, P. Mitochondrial dysfunction in an animal model of hyperoxaluria: a prophylactic approach with fucoidan. *Eur. J. Pharmacol.* **2008**, *579*, 330−336.
(19) Coenen, M. J.; van den Heuvel, L. P.; Smeitink, J. A. Mitochondrial oxidative phosphorylation system assembly in man: recent achievements. *Curr. Opin. Neurol.* **2001**, *14*, 777−781.
(20) St Pierre, J.; Buckingham, J. A.; Roebuck, S. J.; Brand, M. D. Topology of superoxide production from different sites in the

mitochondrial electron transport chain. *J. Biol. Chem.* **2002**, *277*, 44784−44790.
(21) O'Brien, K. M.; Dirmeier, R.; Engle, M.; Poyton, R. O. Mitochondrial protein oxidation in yeast mutants lacking manganese- (MnSOD) or copper- and zinc-containing superoxide dismutase (CuZnSOD): evidence that MnSOD and CuZnSOD have both unique and overlapping functions in protecting mitochondrial proteins from oxidative damage. *J. Biol. Chem.* **2004**, *279*, 51817−51827.
(22) Leary, S. C.; Sasarman, F. Oxidative phosphorylation: synthesis of mitochondrially encoded proteins and assembly of individual structural subunits into functional holoenzyme complexes. *Methods Mol. Biol.* **2009**, *554*, 143−162.
(23) Voloboueva, L. A.; Duan, M.; Ouyang, Y.; Emery, J. F.; Stoy, C.; Giffard, R. G. Overexpression of mitochondrial Hsp70/Hsp75 protects astrocytes against ischemic injury in vitro. *J. Cereb. Blood Flow Metab.* **2008**, *28*, 1009−1016.
(24) Liu, Y.; Liu, W.; Song, X. D.; Zuo, J. Effect of GRP75/mthsp70/PBP74/mortalin overexpression on intracellular ATP level, mitochondrial membrane potential and ROS accumulation following glucose deprivation in PC12 cells. *Mol. Cell. Biochem.* **2005**, *268*, 45−51.
(25) Hua, G.; Zhang, Q.; Fan, Z. Heat shock protein 75 (TRAP1) antagonizes reactive oxygen species generation and protects cells from granzyme M-mediated apoptosis. *J. Biol. Chem.* **2007**, *282*, 20553−20560.
(26) Roy, S. S.; Ehrlich, A. M.; Craigen, W. J.; Hajnoczky, G. VDAC2 is required for truncated BID-induced mitochondrial apoptosis by recruiting BAK to the mitochondria. *EMBO Rep.* **2009**, *10*, 1341−1347.
(27) Rahmani, Z.; Maunoury, C.; Siddiqui, A. Isolation of a novel human voltage-dependent anion channel gene. *Eur. J. Hum. Genet.* **1998**, *6*, 337−340.
(28) Wallace, D. C.; Fan, W. Energetics, epigenetics, mitochondrial genetics. *Mitochondrion* **2010**, *10*, 12−31.
(29) Algrain, M.; Turunen, O.; Vaheri, A.; Louvard, D.; Arpin, M. Ezrin contains cytoskeleton and membrane binding domains accounting for its proposed role as a membrane-cytoskeletal linker. *J. Cell Biol.* **1993**, *120*, 129−139.
(30) Tian, T.; Lindell, S. L.; Henderson, S. C.; Mangino, M. J. Protective effects of ezrin on cold storage preservation injury in the pig kidney proximal tubular epithelial cell line (LLC-PK1). *Transplantation* **2009**, *87*, 1488−1496.
(31) Lakshman, M.; Subramaniam, V.; Jothy, S. CD44 negatively regulates apoptosis in murine colonic epithelium via the mitochondrial pathway. *Exp. Mol. Pathol.* **2004**, *76*, 196−204.
(32) Berryman, M.; Gary, R.; Bretscher, A. Ezrin oligomers are major cytoskeletal components of placental microvilli: a proposal for their involvement in cortical morphogenesis. *J. Cell Biol.* **1995**, *131*, 1231−1242.
(33) Helander, T. S.; Carpen, O.; Turunen, O.; Kovanen, P. E.; Vaheri, A.; Timonen, T. ICAM-2 redistributed by ezrin as a target for killer cells. *Nature* **1996**, *382*, 265−268.
(34) Thongboonkerd, V.; Semangoen, T.; Sinchaikul, S.; Chen, S. T. Proteomic analysis of calcium oxalate monohydrate crystal-induced cytotoxicity in distal renal tubular cells. *J. Proteome Res.* **2008**, *7*, 4689−4700.
(35) Vicente-Manzanares, M.; Viton, M.; Sanchez-Madrid, F. Measurement of the levels of polymerized actin (F-actin) in chemokine-stimulated lymphocytes and GFP-coupled cDNA transfected lymphoid cells by flow cytometry. *Methods Mol. Biol.* **2004**, *239*, 53−68.
(36) Revenu, C.; Athman, R.; Robine, S.; Louvard, D. The co-workers of actin filaments: from cell structures to signals. *Nat. Rev. Mol. Cell Biol.* **2004**, *5*, 635−646.
(37) Tang, H. L.; Le, A. H.; Lung, H. L. The increase in mitochondrial association with actin precedes Bax translocation in apoptosis. *Biochem. J.* **2006**, *396*, 1−5.
(38) Boldogh, I. R.; Pon, L. A. Interactions of mitochondria with the actin cytoskeleton. *Biochim. Biophys. Acta* **2006**, *1763*, 450−462.

JOURNAL OF PROTEOMICS 75 (2012) 3240–3247



Available online at www.sciencedirect.com

SciVerse ScienceDirect

www.elsevier.com/locate/jprot



Urinary proteomics revealed prostaglandin H_2D-isomerase, not Zn-α2-glycoprotein, as a biomarker for active lupus nephritis

Poorichaya Somparn[a], *Nattiya Hirankarn*[b,c,*], *Asada Leelahavanichkul*[c], *Weerapan Khovidhunkit*[d], *Visith Thongboonkerd*[e,f], *Yingyos Avihingsanon*[g,**]

[a]*Biomedical Science, Interdisciplinary Program, Graduate School Chulalongkorn University, Bangkok 10330, Thailand*
[b]*Lupus Research Unit, Faculty of Medicine, Chulalongkorn University, Bangkok 10330, Thailand*
[c]*Department of Microbiology, Faculty of Medicine, Chulalongkorn University, Bangkok 10330, Thailand*
[d]*Hormonal and Metabolic Disorders Research Unit, Department of Medicine, Faculty of Medicine Chulalongkorn University, Bangkok 10330, Thailand*
[e]*Medical Proteomics Unit, Office for Research and Development, Faculty of Medicine Siriraj Hospital, Mahidol University, Bangkok 10700, Thailand*
[f]*Center for Research in Complex Systems Science, Mahidol University, Bangkok 10700, Thailand*
[g]*Lupus Research Unit, Department of Medicine, Faculty of Medicine, Chulalongkorn University, Bangkok 10330, Thailand*

ARTICLE INFO

Article history:
Received 19 January 2012
Accepted 21 March 2012
Available online 30 March 2012

Keywords:
Biomarker
Lupus nephritis
Prostaglandin H_2D-isomerase
Proteomics
Urine
Zn-α2-glycoprotein

ABSTRACT

Although renal histopathology is the gold standard for the diagnosis and prognosis of lupus nephritis (LN), the invasiveness of renal biopsy warrants the discovery of novel non-invasive diagnostic and prognostic biomarkers. In the present study, urine samples from 10 LN patients (5 active and 5 inactive) were analyzed by two-dimensional gel electrophoresis (2-DE) to screen for potential biomarkers of active LN. Quantitative analysis and statistics revealed 16 protein spots whose levels significantly differed between groups. These proteins were successfully identified by electrospray ionization quadrupole time-of-flight tandem mass spectrometry (ESI-Q-TOF MS/MS). Among these potential candidates, differential levels of urinary Zn-α2-glycoprotein (ZA2G) and prostaglandin H_2D-isomerase (PGDS) were further validated by enzyme-linked immunosorbent assay (ELISA) in another independent group of 78 subjects, including 30 active LN, 26 inactive LN, 14 non-LN glomerular diseases, and 8 healthy normal individuals. Whereas ZA2G levels were elevated in urine of patients with active LN and non-LN glomerular diseases, PGDS was elevated only in the urine of the active LN group. Urinary PGDS, not ZA2G, may serve as a biomarker for active LN and upon validation in larger studies, may become the non-invasive test to evaluate the disease activity in future management of LN.

© 2012 Elsevier B.V. All rights reserved.

Abbreviations: LN, lupus nephritis; ZA2G, Zn-alpha2-glycoprotein; PGDS, prostaglandin H_2D-isomerase; 2-DE, two-dimensional gel electrophoresis; SLE, systemic lupus erythematosus; SLEDAI-2K, SLE Disease Activity Index 2000; ROC, receiver operating characteristic curve.

* *Correspondence to:* N. Hirankarn, Lupus Research Unit, Faculty of Medicine, Chulalongkorn University, Bangkok 10330, Thailand. Tel./fax: +66 2 2564132x624, +66 2 2525952.
** *Corresponding author*. Tel./fax: +66 2 2564251x204, +66 2 2529200.
E-mail addresses: Nattiyap@gmail.com (N. Hirankarn), Yingyos.a@gmail.com (Y. Avihingsanon).

1874-3919/$ – see front matter © 2012 Elsevier B.V. All rights reserved.
doi:10.1016/j.jprot.2012.03.034

1. Introduction

Lupus nephritis (LN) is the disease of kidney involvement in systemic lupus erythematosus (generally known as SLE) that affects many patients around the globe, particularly in Asian countries [1]. The diagnosis of LN is challenging because the clinical course, manifestations and disease severity vary largely in individual patients. Currently, the gold standard for the diagnosis and prognosis of LN is renal biopsy and histopathology. Serum levels of auto-antibodies and complements, as well as the degree of proteinuria, may assist in the diagnosis of LN and monitoring of the disease activity [2]. Other parameters, such as serum creatinine, urinary protein level, and urinary sediments, can also be utilized to assess response of the LN patients to immunosuppressive therapy [2]. However, these tests have certain limitations and cannot distinguish the different classes of LN. Furthermore, it has been shown that there are inconsistencies between these parameters and renal histopathology. As a result, renal biopsy and histopathology remains the most reliable method to evaluate the disease activity of LN. The procedure is, however, invasive and may result in several complications, such as bleeding, arterio-venous fistula and infection [3]. In addition, this invasive procedure is not practical when repeated or serial evaluations are required to monitor the disease activity.

Without an appropriate and practical tool to diagnose and monitor patients with active LN, which is frequently relapsed and unresponsive to immunosuppressive therapy, LN frequently leads to end-stage renal disease (ESRD) [1]. Therefore, discovery of novel non-invasive biomarkers for the diagnosis and prognosis of LN and for monitoring its relapse is urgently required [4]. Recent advanced technologies such as urinary proteomics offer opportunities for unbiased discovery of novel non-invasive (urinary) biomarkers and, hence, are expected to serve such goal [5]. Our present study therefore applied urinary proteomics to identify novel urinary biomarkers that may be used as alternative diagnostic and prognostic tools to detect and monitor LN.

2. Materials and methods

2.1. Study design and human subjects

2.1.1. Initial screening set

According to LN classification criteria of the American College of Rheumatology [6], 10 patients with LN (5 active and 5 inactive) were included in this study for initial screening of potential candidates by proteomic analysis. All these LN patients had documented biopsy-proven class III or IV according to the 2003 International Society of Nephrology/Renal Pathology Society Classification (ISN/RPS) [7]. The inclusion criteria for active LN were: 1) urine protein creatinine index>1 g/day; and 2) active urine sediments (red blood cells>5 cells/high-power field (HPF) or white blood cells>5 cells/HPF). The inclusion criteria for inactive LN were: 1) urine protein creatinine index<0.5 g/day; and 2) inactive urine sediments (red blood cells<5 cells/HPF and white blood cells<5 cells/HPF). At the time of visit, the disease activity of each patient was calculated using SLE Disease Activity Index 2000 (SLEDAI-2K) scoring system [8].

2.1.2. Validation set

Another independent group of 78 subjects, including 30 active LN, 26 inactive LN, 14 non-LN glomerular diseases (6 with focal segmental glomerulosclerosis, 6 with minimal change disease, 1 with nephrotic disease and 1 with membranous glomerulopathy), and 8 healthy normal individuals, were recruited for subsequent validation of proteomic data by ELISA to define the so called "disease-specific biomarkers" for active LN. The study was approved by and conducted according to the regulations stipulated by the Ethics Committee for Human Research, Faculty of Medicine, Chulalongkorn University, Bangkok, Thailand.

2.2. Urine collection and sample preparation for proteomic analysis

Random midstream urine samples were collected and centrifuged at 1000 *g*, 4 °C for 5 min to remove cellular debris and particulate matter. Urinary proteins were then precipitated with 75% ethanol on ice for 10 min followed by centrifugation at 12,000 *g* for 5 min. Protein pellets were resuspended in a buffer containing 7 M urea, 2 M thiourea, 4% 3-[(3-cholamidopropyl) dimethyl-ammonio]-1-propanesulfonate (CHAPS), 120 mM dithiothreitol (DTT), 2% ampholytes (pH 3–10) and 40 mM Tris–HCl, and further incubated at 4 °C for 30 min. Protein solutions were dialyzed against 18 MΩ·cm (dI) water at 4 °C overnight and concentrated using a filtrating column (Amicon-15; Millipore; Billerica, MA). Protein concentrations were measured by the Bradford method using Bio-Rad protein assay (Bio-Rad; Hercules, CA).

2.3. Two-dimensional gel electrophoresis (2-DE) and image analysis

Proteins were resolved by 2-DE as previously described [9]. Briefly, the first dimensional separation was performed in Ettan IPGphor II Isoelectric Focusing Unit with Immobilized pH gradient (IPG) strips (Amersham Biosciences; Piscataway, NJ) at 20 °C to reach a total of 28,400 V·h. Then, the IPG strips (with pH gradients of 3–10) were equilibrated with an equilibration buffer containing 50% glycerol, 50 mM Tris base, 2% SDS, 130 mM DTT and 0.002% bromophenol blue for 15 min. The strips were further incubated for 15 min in another similar equilibration buffer, which replaced 130 mM DTT with 135 mM iodoacetamide. The second dimensional separation was performed using SE 600 Ruby system (Amersham Biosciences) with the current of 30 μA/gel. The resolved protein spots were visualized by Coomassie Brilliant Blue R-250 stain (Bio-Rad; Hercules, CA) and imaged by ImageMaster scanner (GE Healthcare; Piscataway, NJ). Spot matching across gels and intensity analysis were performed using Image Master 2D Platinum software (GE Healthcare; Piscataway, NJ).

2.4. Protein identification by electrospray ionization quadrupole time-of-flight tandem mass spectrometry (ESI-Q-TOF MS/MS)

Differentially expressed protein spots were excised from the 2-DE gels and subjected to in-gel tryptic digestion as

previously described [10]. Briefly, the excised protein spots were washed three times with 200 μl of 25 mM NH_4HCO_3/50% acetonitrile (ACN). The gel pieces were dehydrated with 200 μl of 100% ACN, rehydrated with 12.5 μg/ml of sequencing grade trypsin (Promega; Madison, WI), and incubated at 37 °C for approximately 16 h. The supernatants were then transferred to a new tube and 100 μl of 50% ACN/0.5% formic acid was added. The mixtures were finally dried with a speedvac and resulting peptides were suspended in 10 μl of 50% ACN/0.1% formic acid. The peptides were then analyzed by MS/MS using micrOTOF-Q II™ ESI-Qq-TOF mass spectrometer (Bruker; Berman, Germany) equipped with an online nanoESI source. Protein identification was performed using the MASCOT search engine (http://www.matrixscience.com) queried against the SWISSPROT database with only one missed cleavage allowed, carbamidomethylation at cysteine residues as fixed modification, and oxidation at methionine residues as variable modifications. Mass tolerance of parent and fragmented ions were 1.0 Da and 0.6 Da, respectively. MS/MS ions scores ≥38 were considered significant hits.

2.5. *Validation of the proteomic data by ELISA*

Validation of the proteomic data was performed in another independent group of 78 subjects, as mentioned previously. ELISA was performed according to manufacturers' instructions using the commercially available ELISA kits for ZA2G (Biovendor; Brno, Czech Republic) and PGDS (Cayman Chemical; Ann Arbor, MI) to confirm differential levels of the corresponding urinary proteins among groups.

2.6. *Statistical analysis*

Statistical analysis was performed using SPSS software version 11.5 (SPSS Inc.; Chicogo, IL). Student's *t*-test was utilized to compare the intensity data of each matched protein spot between active and inactive LN groups, whereas Tukey's post-hoc multiple comparisons were performed to compare differential levels of ZA2G and PGDS, as well as clinical parameters among groups. Linear regression analysis was performed to define correlations between two parameters using Pearson's correlation test. p Values <0.05 were considered statistically significant.

3. Results

For the initial screening to identify potential candidates of urinary biomarkers to differentiate active from inactive LN, we performed 2-DE analysis of 5 urine samples derived from active LN patients compared to 5 urine samples obtained from inactive LN patients. Among these 10 patients, their gender, age and serum creatinine levels did not significantly differ, whereas there were significant differences in other parameters indicating the disease activity of LN (Table 1). Spot matching and statistical analysis of intensity data revealed 16 protein spots, which displayed significant differences in their levels between the two clinical groups of LN (Fig. 1). All of these differentially expressed protein spots were successfully identified by ESI-Q-TOF MS/MS (Table 2). Among these, two proteins including α2-HS glycoprotein (spot #5) and prostaglandin H_2D-isomerase (PGDS) (spot #38) were detectable only in the urine of active LN. In addition, three forms of

Table 1 – Demographic data and laboratory parameters of active and inactive LN patients in the initial screening set.

Patient characteristics	Active LN	Inactive LN
Gender (female:male)	5:0	5:0
Age (year)	38.60±2.24	31.60±3.28
Serum creatinine (mg/dl)	1.01±0.07	0.74±0.08
eGFR (ml/min) [11]	63.49±5.66	110.80±15.20 *
Urine protein creatinine index	3.07±0.64	0.24±0.06 *
White blood cell (cell/mm^3)	103.20±61.99	3.00±0.84 *
Red blood cell (cell/mm^3)	28.00±8.03	11.60±7.38 *
SLEDAI-2K	15.00±2.33	4.00±1.76 *
Renal SLEDAI-2K	11.20±0.80	4.00±1.76 *
Steroid dosage (mg/day)	11.86±1.92	2.30±0.51 *

Data are expressed as mean±SEM.
eGFR = estimated glomerular filtration rate.
SLEDAI-2K = SLE Disease Activity Index 2000.
* $p<0.05$ active *versus* inactive LN.

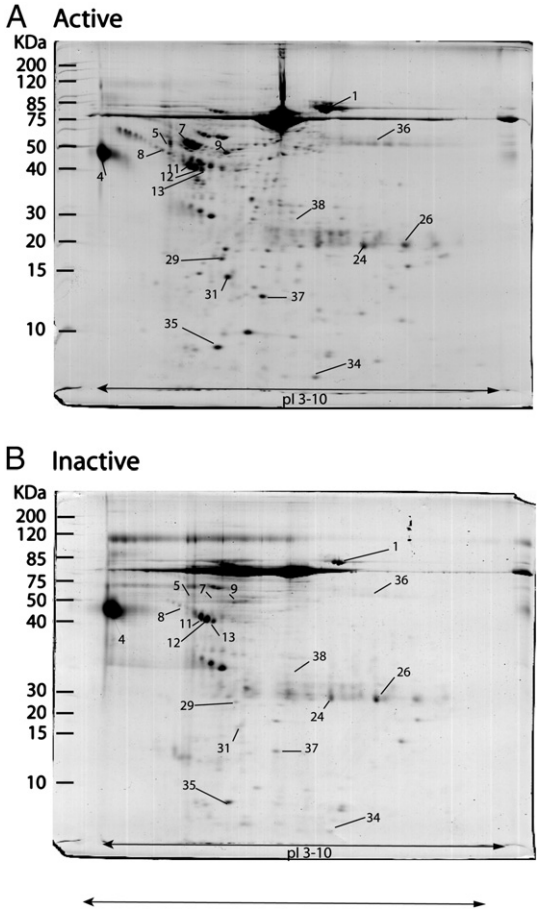


Fig. 1 – 2-D gel map of urinary proteins with differential levels in active (A) *versus* inactive (B) LN patients. A total of 10 gels (5 in each group) were subjected to spot matching and intensity analysis. The proteins with significantly differential levels are labeled with numbers, which correspond to those reported in Table 2.

Table 2 – Summary of proteins with differential levels in active *versus* inactive LN.

Spot no.	Protein name	Accession number	Intensity(arbitrary unit)		Ratio (active/inactive)	p-value	MS/MS score	%Cov	No. of matched peptide
			Active LN (Mean ± SEM)	Inactive LN (Mean ± SEM)					
1	Serotransferrin	P02787	5.688 ± 0.566	1.990 ± 0.731	2.86	0.004	1877	66	93
4	Alpha-1-glycoprotein	P02763	18.330 ± 1.928	11.105 ± 1.389	1.65	0.018	980	57	45
5	Alpha-2-HS glycoprotein	P02765	0.801 ± 0.031	0.000 ± 0.000	DIV/0	<0.0001	592	65	15
8	Haptoglobin	P00738	0.011 ± 0.005	0.004 ± 0.001	2.75	0.046	347	30	31
7	Alpha-1-antitrypsin	P01009	2.529 ± 0.359	0.899 ± 0.361	2.81	0.013	1548	69	47
9	Albumin	P02768	0.021 ± 0.003	0.006 ± 0.001	3.50	0.003	577	46	49
11	Zn-alpha2-glycoprotein	P25311	0.767 ± 0.071	0.232 ± 0.034	3.31	0.001	430	52	20
12	Zn-alpha2-glycoprotein	P25311	2.039 ± 0.376	0.304 ± 0.112	6.71	0.002	1028	55	37
13	Zn-alpha2-glycoprotein	P25311	0.225 ± 0.022	0.041 ± 0.009	5.49	<0.0001	941	61	30
24	Ig kappa chain V-III SLE region	P18135	1.385 ± 0.453	0.319 ± 0.071	4.34	0.048	175	36	5
26	Ig kappa chain V-III HAH region	P01620	0.754 ± 0.159	0.154 ± 0.059	4.90	0.077	215	39	17
29	Ig kappa chain C region	P01834	0.021 ± 0.009	0.009 ± 0.005	2.33	0.045	108	61	6
31	Retinol-binding protein 4	P02753	0.367 ± 0.102	0.050 ± 0.011	7.34	0.014	620	70	36
35	Beta-2-microglobulin	P61769	0.031 ± 0.007	0.005 ± 0.001	6.20	0.022	38	26	2
37	Transthyretin	P02766	0.101 ± 0.026	0.022 ± 0.005	4.59	0.019	332	69	13
38	Prostaglndin-H2-D isomerase	P41222	0.016 ± 0.006	0.000 ± 0.000	DIV/0	<0.0001	156	32	4

%Cov = % sequence coverage [(number of matched residues)/(total number of residues in the entire sequence) × 100%];
DIV/0 = divided by zero.

immunoglobulin kappa chain (spots #24, 26 and 29) and three isoforms of Zn-α2-glycoprotein (ZA2G) (spots #11–13) were all increased in the urine of active LN.

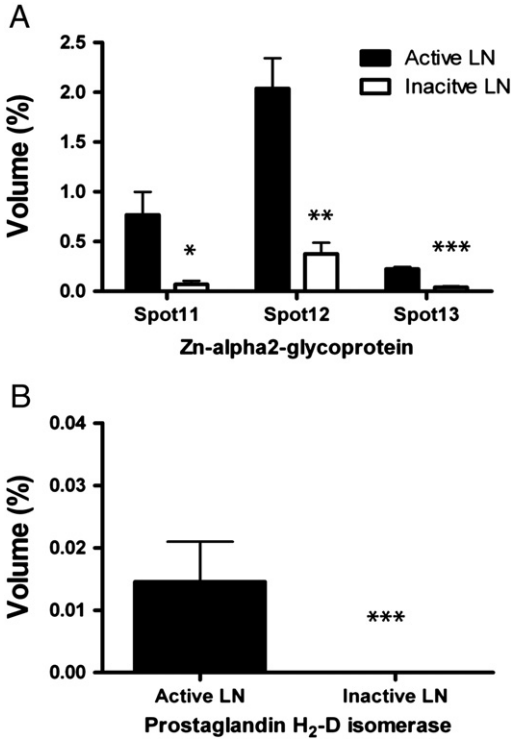


Fig. 2 – Histogram demonstrating differential levels of ZA2G (A) and PGDS (B) in active *versus* inactive LN obtained from proteomic analysis. The intensity data are presented as mean ± SEM (n = 5 gels derived from 5 individual subjects in each group). * p = 0.001; ** p = 0.002; *** p < 0.0001.

To confirm the initial screening results, the proteomic data were validated by ELISA in another independent set of 78 subjects, including 30 active LN, 26 inactive LN, 14 non-LN glomerular diseases (6 with focal segmental glomerulosclerosis, 6 with minimal change disease, 1 with nephrotic disease and 1 with membranous glomerulopathy, and 8 healthy normal individuals). In this validation set, there were no significant differences in gender, age or serum creatinine among groups (Table 3). Two differentially excreted proteins were selected for the validation (Fig. 2). These included ZA2G (because of the high magnitude of its change; 3.31–6.71 fold increases in the three isoforms in active LN) and PGDS (because of its presence only in active LN). In addition, a pathophysiological role of PGDS during an inflammatory response and its chemoattractant property make this protein an attractive biomarker.

ELISA was performed to validate differential levels of urinary ZA2G and PGDS among groups. The ELISA results showed that urinary ZA2G levels in active LN were significantly higher than those in inactive LN and healthy controls (Fig. 3A), which confirmed the proteomic data (Table 2 and Fig. 2A). However, ZA2G could not serve as a "biomarker for active LN" because its level in non-LN glomerular diseases was comparable to that of active LN. This result suggested that ZA2G was merely a marker for "glomerular leakage" or "glomerular injury".

We also found that urinary levels of PGDS measured by ELISA were significantly increased in active LN as compared to those of the other three groups (Fig. 3B), which confirmed the result from the proteomic experiment (Table 2 and Fig. 2B). More importantly, the result indicated that PGDS might serve as a biomarker for active LN because its levels in the other three groups were significantly lower than those in active LN.

Table 3 – Demographic data and laboratory parameters of all subjects in the validation set.

Patient characteristics	Active LN	Inactive LN	Non-LN glomerular diseases	Healthy controls
Gender (female:male)	28:2	26:0	9:5	8:0
Age (year)	32.77±1.42	34.52±1.46	40.38±2.76	26.66±1.66
Serum Creatinine (mg/dl)	0.92±0.05	0.80±0.06	0.97±0.09	0.64±0.05
eGFR ([11]) (ml/min)	78.27±4.82	98.84±6.67 *	77.65±9.02	113.33±11.14 §
Urine protein creatinine index	3.37±0.42	0.21±0.06 *	4.83±0.57	0.09±0.01 §
White blood cell (cell/mm^3)	25.50±2.64	2.31±0.59 *	1.62±0.18 #	0
Red blood cell (cell/mm^3)	24.55±4.47	6.92±3.97 *	7.96±3.71 #	0
SLEDAI-2K	15.36±1.88	2.17±0.76 *	NA	NA
Renal SLEDAI-2K	11.60±0.62	2.24±0.57 *	NA	NA
Steroid dosage (mg/day)	11.86±1.92	2.30±0.51 *	NA	NA

eGFR = estimated glomerular filtration rate.
NA = not applicable.
SLEDAI-2K = SLE Disease Activity Index 2000.
* $p<0.05$ active LN *versus* inactive LN.
# $p<0.05$ active LN *versus* non-LN glomerular diseases.
§ $p<0.05$ active LN *versus* healthy controls.

To strengthen the notion that PGDS might serve as a disease-specific biomarker for active LN, whereas ZA2G was merely a marker for glomerular leakage or injury, we evaluated the correlation of urinary levels of ZA2G and PGDS with the degree of proteinuria (using urine protein creatinine index) and with estimated glomerular filtration rate (eGFR) [11]. We found that urinary ZA2G levels were significantly and positively correlated with urine protein creatinine index, whereas they were inversely correlated with eGFR (Fig. 4A and C). In contrast, PGDS was significantly correlated only with urine protein creatinine index (which reflected both disease activity and glomerular leakage/injury) (Fig. 4B), but not with eGFR (which reflected glomerular leakage/injury, not the disease activity) (Fig. 4D).

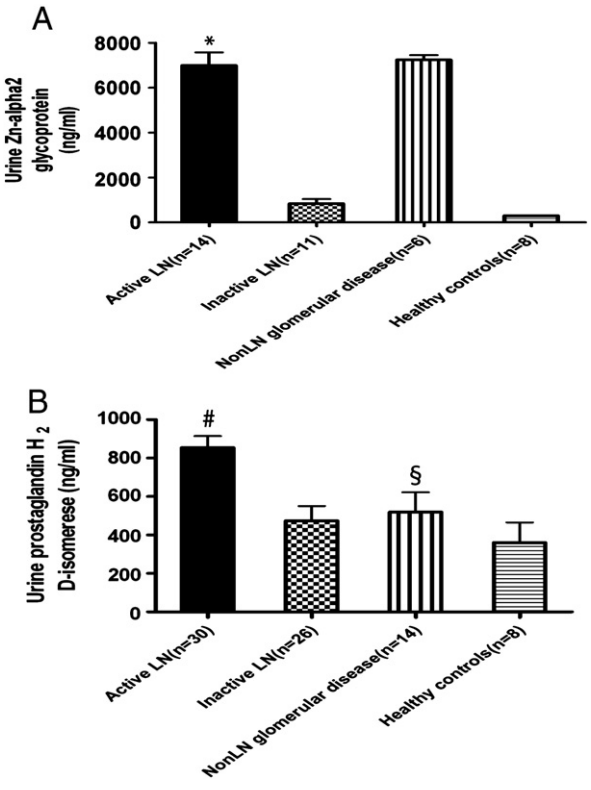


Fig. 3 – Validation of the increased levels of ZA2G (A) and PGDS (B) in active LN by ELISA. The data are presented as mean±SEM (n=30 for active LN, 26 for inactive LN, 14 for non-LN glomerular diseases, and 8 for healthy normal controls). Multiple comparisons were performed by Tukey's post-hoc test. For ZA2G; * $p<0.0004$ *versus* inactive LN and healthy controls, but not statistically significant *versus* non-LN glomerular diseases. For PGDS; # $p<0.002$ *versus* inactive LN, healthy controls and § $p<0.025$ *versus* non-LN glomerular diseases.

Finally, the receiver operating characteristic curve (ROC) of urinary excretion of PGDS was plotted in order to predict whether the patients had active LN or not (Fig. 5). The area under the ROC curve for urinary excretion of PGDS in active LN *versus* inactive LN was 0.794 (95% confidence interval=0.674–0.914). Using this confidence interval, the sensitivity and specificity to discriminate active LN from inactive LN were 78% and 73%, respectively (Fig. 5A). The area under the ROC curve for urinary excretion of PGDS in active LN *versus* inactive LN and non-LN glomerular diseases was 0.730 (95% confidence interval=0.554–0.906). Using this confidence interval, the sensitivity and specificity to discriminate active LN from inactive LN and other glomerular diseases were 92% and 50%, respectively (Fig. 5B).

4. Discussion

LN, one of the major manifestations and the leading cause of death of SLE patients, remains common around the world with heterogeneous clinical presentations. Our present study, using a proteomics approach, was aimed to define novel urinary biomarkers, which can be used as alternatives to renal histopathology obtained from a renal biopsy for the diagnosis and prognosis of LN. Currently, there are several methodologies for urinary proteomics [5,12]. Among these, surface-enhanced laser desorption/ionization time-of-flight mass spectrometry (SELDI-TOF MS) has recently been employed to identify potential candidates of biomarkers for LN. Those candidates have been identified as hepcidin, prostaglandin D

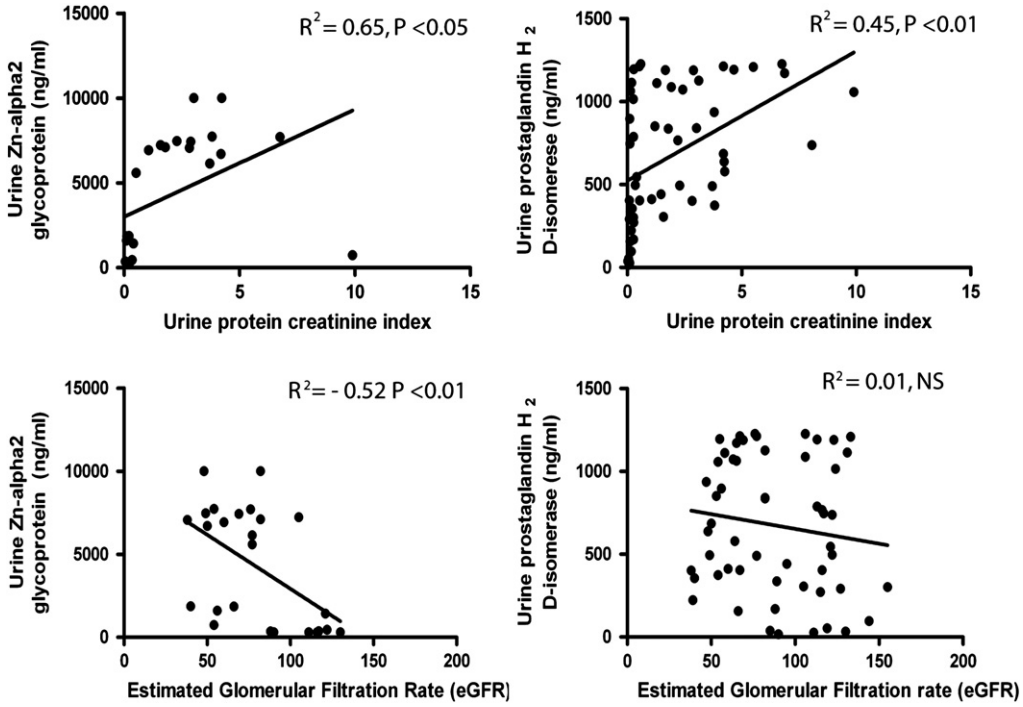


Fig. 4 – Correlations of ZA2G (A and C) and PGDS (B and D) levels with urine protein creatinine index (A and B) and estimated glomerular filtration rate (eGFR) (C and D). These correlations were evaluated by linear regression analysis using Pearson's correlation test. N = 56. NS: not significant.

synthase, alpha-1-acid-glycoprotein, transferrin and ceruloplasmin using SELDI-TOF MS [13,14]. However, regardless of the proteomic techniques used, the discovered proteins need further validation in a larger sample size.

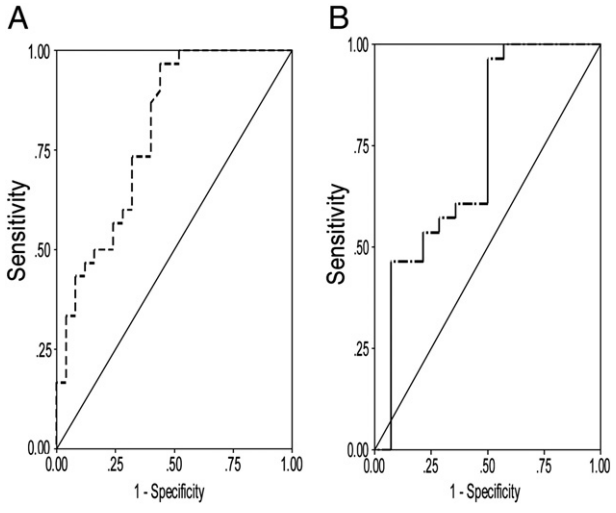


Fig. 5 – The receiver–operator characteristic curve (ROC) curves of PGDS to predict active LN. The fraction of true-positive (sensitivity) and that of false-positive results (1-specificity) for (A) discriminate active LN from inactive LN and (B) discriminate lupus nephritis from other glomerular diseases. The areas under the curves were 0.794 and 0.730 for panels A and B, respectively.

In our present study, a 2-DE approach was chosen to screen for biomarker candidates in the urine to differentiate active from inactive LN. Our reason of using a 2-DE approach was that 2-DE permits a precise validation of the initially screened data [15]. Using 2-DE followed by precise protein identification by ESI-Q-TOF MS/MS, we identified a number of urinary proteins whose levels significantly differed between active and inactive LN groups. As expected, urinary levels of several inflammatory mediators were greater in patients with active LN. However, we focused our attention to ZA2G and PGDS in active LN (Fig. 2) and subsequently validated the result in a larger independent set of urine samples. Among these candidate proteins, PGDS was an interesting marker because it was previously discovered as urine biomarker of active LN in children [13].

ZA2G is a single chain polypeptide found in body fluids such as urine, serum, cerebrospinal fluid, and saliva [16–19]. It is associated with several functions including lipid mobilization, fertilization, repair process and, possibly, immune response. Both *in vivo* and *in vitro* studies have reported that ZA2G can inhibit tubular proliferative response and delay recovery of the kidney from damage [20]. However, ZA2G has a similar structure with Class I major histocompatibility complex (MHC) and may activate an auto-immune response [21]. Interestingly, we found that urinary levels of three isoforms of ZA2G were all increased (3.31–6.71 folds; Table 2 and Fig. 2A) in active LN as compared to inactive LN, consistent with the data reported previously [22]. Our subsequent ELISA experiments confirmed its difference between active and inactive LN (Fig. 3A), however, we also found that the increased level of urinary ZA2G was not specific for active LN as its level was

increased in non-LN glomerular diseases as well (Fig. 3A), most likely due to glomerular leakage or injury. A significant correlation between urinary ZA2G level and urine protein creatinine index (Fig. 4A) and its inverse correlation with eGFR (Fig. 4C) strengthen this hypothesis.

PGDS is a homodimer of which each subunit has a size of 21–31 kDa [23]. PGDS catalyzes the isomerization of prostaglandin H_2 (PGH_2) to produce prostaglandin D_2 (PGD_2), which is involved in sleep regulation, platelet aggregation, allergy, inflammatory response, and chemoattractant activity [23–27]. In the kidney, PGDS is constitutively expressed in podocytes, mesangial cells, and tubular epithelial cells of outer medulla and cortex [28]. Interestingly, PGDS has been reported to have a strong correlation level with the severity of lupus nephritis in mice [29]. It is also associated with glomerular inflammation in diabetic mice [30]. In the study of childhood SLE, PGDS was discovered as a urinary biomarker of active LN. However, it was unclear whether PGDS was specific for LN because there was no comparison with non-LN glomerular diseases [13]. In our present study, the proteomic data revealed absence of this protein in inactive LN but its presence in active LN (Table 2 and Fig. 2B). With this clear difference and its potential role, this protein could be a more relevant biomarker for active LN. Our ELISA results confirmed that the increased level of urinary PGDS was specific for active LN as compared to inactive LN, non-LN glomerular diseases, and healthy controls (Fig. 3B). The lack of correlation between urinary PGDS level and eGFR (Fig. 4D) also suggested that the increased level of urinary PGDS did not reflect the glomerular leakage/injury. With the satisfactory levels of sensitivity and specificity of this protein to discriminate active LN from inactive LN and other glomerular diseases (Fig. 5), PGDS could serve as a suitable biomarker for active LN.

5. Summary

We used a 2-DE approach to identify a number of candidates of urinary biomarkers for active LN. Among these, the increased levels of ZA2G and PGDS were subsequently validated by ELISA in an independent validation set with a larger sample size. The results obtained from ELISA confirmed the proteomic data. The data also indicated that urinary PGDS, but not ZA2G, may serve as a "disease-specific" biomarker for active LN. However, further studies are required to validate the findings and define specific context of use for PDGS in lupus nephritis.

6. Conflict of interest

All authors declare no conflicts of interest in the present study.

Acknowledgments

This study was supported by the National Research University Project of CHE and the Ratchadaphiseksomphot Endowment Fund (HR1163A), Cluster and Program Management Office (CPMO) of National Science and Technology Development Agency (P-10-10221), and the Thailand Research Fund (TRF) Senior Research Scholarship (RTA5380005). P. Somparn was supported by the Royal Golden Jubilee Ph.D. Program and Chulalongkorn University. V. Thongboonkerd was also supported by Office of the Higher Education Commission and Mahidol University under the National Research Universities Initiative.

REFERENCES

[1] Avihingsanon Y, Hirankarn N. Major lupus organ involvement: severe lupus nephritis. Lupus 2010;19:1391–8.
[2] Balow JE. Clinical presentation and monitoring of lupus nephritis. Lupus 2005;14:25–30.
[3] Whittier WL, Korbet SM. UpToDate: indications for and complications of renal biopsy. http://www.uptodate.com/contents/indications-for-and-complications-of-renal-biopsy/ (accessed Jan 4, 2012).
[4] Mosley K, Tam FW, Edwards RJ, Crozier J, Pusey CD, Lightstone L. Urinary proteomic profiles distinguish between active and inactive lupus nephritis. Rheumatology (Oxford) 2006;45:1497–504.
[5] Thongboonkerd V. Urinary proteomics: towards biomarker discovery, diagnostics and prognostics. Mol Biosyst 2008;4:810–5.
[6] Tan EM, Cohen AS, Fries JF, Masi AT, McShane DJ, Rothfield NF, et al. The 1982 revised criteria for the classification of systemic lupus erythematosus. Arthritis Rheum 1982;25:1271–7.
[7] Weening JJ, D'Agati VD, Schwartz MM, Seshan SV, Alpers CE, Appel GB, et al. The classification of glomerulonephritis in systemic lupus erythematosus revisited. Kidney Int 2004;65:521–30.
[8] Gladman DD, Ibanez D, Urowitz MB. Systemic lupus erythematosus disease activity index 2000. J Rheumatol 2002;29:288–91.
[9] Thongboonkerd V, Chutipongtanate S, Kanlaya R. Systematic evaluation of sample preparation methods for gel-based human urinary proteomics: quantity, quality, and variability. J Proteome Res 2006;5:183–91.
[10] Li G, Waltham M, Anderson NL, Unsworth E, Treston A, Weinstein JN. Rapid mass spectrometric identification of proteins from two-dimensional polyacrylamide gels after in gel proteolytic digestion. Electrophoresis 1997;18:391–402.
[11] Praditpornsilpa K, Townamchai N, Chaiwatanarat T, Tiranathanagul K, Katawatin P, Susantitaphong P, et al. The need for robust validation for MDRD-based glomerular filtration rate estimation in various CKD populations. Nephrol Dial Transplant 2011;26:2780–5.
[12] Thongboonkerd V. Current status of renal and urinary proteomics: ready for routine clinical application? Nephrol Dial Transplant 2010;25:11–6.
[13] Suzuki M, Wiers K, Brooks EB, Greis KD, Haines K, Klein-Gitelman MS, et al. Initial validation of a novel protein biomarker panel for active pediatric lupus nephritis. Pediatr Res 2009;65:530–6.
[14] Zhang X, Jin M, Wu H, Nadasdy T, Nadasdy G, Harris N, et al. Biomarkers of lupus nephritis determined by serial urine proteomics. Kidney Int 2008;74:799–807.
[15] Thongboonkerd V. Practical points in urinary proteomics. J Proteome Res 2007;6:3881–90.
[16] Irmak S, Tilki D, Heukeshoven J, Oliveira-Ferrer L, Friedrich M, Huland H, et al. Stage-dependent increase of orosomucoid and zinc-alpha2-glycoprotein in urinary bladder cancer. Proteomics 2005;5:4296–304.

[17] Yeung DC, Lam KS, Wang Y, Tso AW, Xu A. Serum zinc-alpha2-glycoprotein correlates with adiposity, triglycerides, and the key components of the metabolic syndrome in Chinese subjects. J Clin Endocrinol Metab 2009;94:2531–6.
[18] Roher AE, Maarouf CL, Sue LI, Hu Y, Wilson J, Beach TG. Proteomics-derived cerebrospinal fluid markers of autopsy-confirmed Alzheimer's disease. Biomarkers 2009;14: 493–501.
[19] Ramachandran P, Boontheung P, Xie Y, Sondej M, Wong DT, Loo JA. Identification of N-linked glycoproteins in human saliva by glycoprotein capture and mass spectrometry. J Proteome Res 2006;5:1493–503.
[20] Schmitt R, Marlier A, Cantley LG. Zag expression during aging suppresses proliferation after kidney injury. J Am Soc Nephrol 2008;19:2375–83.
[21] Sanchez LM, Chirino AJ, Bjorkman P. Crystal structure of human ZAG, a fat-depleting factor related to MHC molecules. Science 1999;283:1914–9.
[22] Oates JC, Varghese S, Bland AM, Taylor TP, Self SE, Stanislaus R, et al. Prediction of urinary protein markers in lupus nephritis. Kidney Int 2005;68:2588–92.
[23] Urade Y, Hayaishi O. Prostaglandin D synthase: structure and function. Vitam Horm 2000;58:89–120.
[24] Grill M, Peskar BA, Schuligoi R, Amann R. Systemic inflammation induces COX-2 mediated prostaglandin D2 biosynthesis in mice spinal cord. Neuropharmacology 2006;50:165–73.
[25] Smith JB. Prostaglandins and platelet aggregation. Acta Med Scand Suppl 1981;651:91–9.
[26] Satoh T, Moroi R, Aritake K, Urade Y, Kanai Y, Sumi K, et al. Prostaglandin D2 plays an essential role in chronic allergic inflammation of the skin via CRTH2 receptor. J Immunol 2006;177:2621–9.
[27] Monneret G, Gravel S, Diamond M, Rokach J, Powell WS. Prostaglandin D2 is a potent chemoattractant for human eosinophils that acts via a novel DP receptor. Blood 2001;98: 1942–8.
[28] Nagata N, Fujimori K, Okazaki I, Oda H, Eguchi N, Uehara Y, et al. De novo synthesis, uptake and proteolytic processing of lipocalin-type prostaglandin D synthase, beta-trace, in the kidneys. FEBS J 2009;276:7146–58.
[29] Wu T, Fu Y, Brekken D, Yan M, Zhou XJ, Vanarsa K, et al. Urine proteome scans uncover total urinary protease, prostaglandin D synthase, serum amyloid P, and superoxide dismutase as potential markers of lupus nephritis. J Immunol 2010;184:2183–93.
[30] Ogawa M, Hirawa N, Tsuchida T, Eguchi N, Kawabata Y, Numabe A, et al. Urinary excretions of lipocalin-type prostaglandin D2 synthase predict the development of proteinuria and renal injury in OLETF rats. Nephrol Dial Transplant 2006;21:924–34.

JOURNAL OF PROTEOMICS 76 (2012) 239–250



Available online at www.sciencedirect.com

SciVerse ScienceDirect

www.elsevier.com/locate/jprot



Characterizations and proteome analysis of platelet-free plasma-derived microparticles in β-thalassemia/hemoglobin E patients☆

Porntip Chaichompoo[a,b,1], *Panida Kumya*[a,1], *Ladawan Khowawisetsut*[a], *Wararat Chiangjong*[c,d], *Sakdithep Chaiyarit*[c,d], *Nutkridta Pongsakul*[c,d], *Noppadol Sirithanaratanakul*[e], *Suthat Fucharoen*[b], *Visith Thongboonkerd*[c,d,*], *Kovit Pattanapanyasat*[a,f,**]

[a]*Department of Immunology and Office for Research and Development, Faculty of Medicine Siriraj Hospital, Mahidol University, Bangkok, Thailand*
[b]*Thalassemia Research Center, Institute of Molecular Biosciences, Mahidol University, Nakhon Pathom, Thailand*
[c]*Medical Proteomics Unit, Office for Research and Development, Faculty of Medicine Siriraj Hospital, Mahidol University, Bangkok, Thailand*
[d]*Center for Research in Complex Systems Science, Mahidol University, Bangkok, Thailand*
[e]*Department of Medicine, Faculty of Medicine Siriraj Hospital, Mahidol University, Bangkok, Thailand*
[f]*Center for Emerging and Neglected Infectious Diseases, Mahidol University, Nakhon Pathom, Thailand*

ARTICLE INFO

Available online 15 June 2012

Keywords:
Microparticle
Oxidative stress
Platelet
Procoagulant
Proteome
Thalassemia

ABSTRACT

Aggregatability and oxidative damage of red blood cells (RBCs), platelet activation and increased amount of blood cells-derived microparticles (MPs) are thought to be the etiologies for the thrombotic risk in thalassemia, but with unclear mechanisms. Here we report cellular origins and increases in number, oxidative stress status, and procoagulant activity, as well as altered proteome of MPs isolated from β-thal/HbE patients. Flow cytometric analysis revealed that β-thal/HbE patients had significantly higher levels of phosphatidylserine (PS)-bearing MPs in platelet-free plasma (PFP) as compared to normal subjects. The high levels of MPs correlated with not only the increased procoagulant activity but also the increased platelet counts. Additionally, these PS-bearing MPs were originated mostly from platelets and RBCs, both of which had increased levels of reactive oxygen species. Proteome analysis of MPs by 2-DE followed by Q-TOF MS and MS/MS analyses identified 29 proteins with significantly altered levels in MPs derived from β-thal/HbE patients (e.g. the increased levels of peroxiredoxin 6, apolipoprotein E, cyclophilin A and heat shock protein 90). These findings suggest that the oxidative damage in platelets and RBCs potentially induces production of MPs with altered proteome that may, in turn, facilitate thromboembolic complications, which are commonly found in thalassemic patients. This article is part of a Special Issue entitled: Integrated omics.

© 2012 Elsevier B.V. All rights reserved.

☆ This article is part of a Special Issue entitled: Integrated omics.

* *Correspondence to:* V. Thongboonkerd, Medical Proteomics Unit, Office for Research and Development, 10th Fl-Srisawarinthira Bldg., Siriraj Hospital, 2 Prannok Rd., Bangkoknoi, Bangkok 10700, Thailand. Tel.: +66 2 4195500; fax: +66 2 4195503.
** *Correspondence to:* K. Pattanapanyasat, Center of Excellence for Flow Cytometry, Office for Research and Development, 12th Fl-Adulyadejvikrom Bldg., Siriraj Hospital, 2 Prannok Rd., Bangkoknoi, Bangkok 10700, Thailand.
E-mail addresses: thongboonkerd@dr.com, vthongbo@yahoo.com (V. Thongboonkerd), grkpy@mahidol.ac.th (K. Pattanapanyasat).
[1] These authors contributed equally to this work.

1874-3919/$ – see front matter © 2012 Elsevier B.V. All rights reserved.
doi:10.1016/j.jprot.2012.06.004

1. Introduction

Thalassemia is a group of the inherited disorders with hemolytic anemia caused by partial or complete deficiency in synthesis of α- or β-globin chains of hemoglobin (Hb) [1–3]. Excessive unmatched α-globin chains in β-thalassemia (β-thal) in the form of irreversible hemichromes bound to the cytoplasmic surface of thalassemic red blood cells (RBCs) plasma membranes produce oxidative damage to membrane lipids and protein components, leading to various membrane defects, including lipid peroxidation, clustering of spectrin-band 3, cation imbalance, complement fixation, and loss of membrane phospholipid asymmetry [4,5]. Disruption of the asymmetric organization of phospholipids in thalassemic RBCs membrane bilayers results to the formation of RBCs "senescence" antigens such as phosphatidylserine (PS) to be exposed on the outer surface. It is widely accepted that PS is one of the key membrane phospholipids that cause thalassemic RBCs to be rigid and aggregatable, leading to premature cell removal by erythrophagocytosis [6–8]. Several studies have also shown that the negatively charged PS can induce procoagulant activity of RBCs in patients with β-thal and sickle cell disease [8,9], whereas annexin V, which has a high affinity to anionic phospholipids, can block the procoagulant activity of thalassemic RBCs [9,10].

The presence of PS on outer leaflet of cells facilitates membrane blebbing and release of microparticles (MPs) with a diameter of <1 μm [11]. MPs display surface proteins of multiple originating cells, including platelets, RBCs, endothelial cells, monocytes, and granulocytes [12]. Among these, platelets-derived MPs are the most abundant MPs found in the blood circulation, constituting 70%–90% of the total number of MPs [13]. Although physiological roles of MPs vary, they have been implicated in thrombosis as the high levels of circulating MPs derived from blood cells have been found in patients with an increased risk for thromboembolic events, including myocardial infarction, idiopathic thrombocytopenic purpura, disseminated intravascular coagulation, and thalassemia [14–16]. In addition, our previous studies have shown that β-thal/HbE patients, particularly those who underwent splenectomy, had significantly increased amounts of PS-bearing MPs originated from activated platelets, one of the confounding factors responsible for the dissemination of prothrombotic manifestation in these patients [17].

Apart from the phospholipid moieties that are essential for the initiation of blood coagulation, MPs also contain many important proteins (both membrane and cytoplasmic proteins) derived from the cells of origin [11,18,19]. Since MPs in β-thal/HbE patients are mainly derived from activated platelets, it is reasonable that some of the protein constituents may contribute to cohesiveness and aggregatability, so called "hypercoagulable state" in these patients by amplifying thrombin generation and initiating platelet activation. It has been shown that the number of platelet-derived MPs is elevated following platelet activation, but the changes in amount and protein profiles depend on types of stimuli [20]. However, the mechanism of MPs shed from platelets and other blood cells in thalassemia remains unclear. We have postulated that the high levels of MPs originated from activated platelets and RBCs are partly due to the increased oxidative stress in these cells, and that the increased amounts of circulating platelets- and RBCs-derived MPs are responsible for the membrane-associated procoagulant activities. The present study thus aimed to address this hypothesis by evaluation of oxidative stress status in thalassemic platelets and RBCs. We then performed proteome analysis of MPs derived from platelets and RBCs of β-thal/HbE patients compared to those obtained from healthy individuals.

2. Materials and methods

2.1. Patients and sample collection

A total of 30 subjects were recruited from Division of Hematology, Department of Medicine, Siriraj Hospital, Mahidol University, Bangkok, Thailand. These included 15 β-thal/HbE patients who were splenectomized and 15 age-matched healthy controls. The diagnosis of β-thal/HbE was made by standard hematological techniques and Hb typing. All patients had normal glucose-6-phosphate dehydrogenase levels, no evidence of concurrent infection, no hospitalization, and no blood transfusion for at least 12 weeks. There was no history of thromboembolic events and atherosclerosis prior to the initiation of the study and during the sampling period. After obtaining informed consent, 15 ml of venous blood was collected by venepuncture and aliquoted into vacuum tubes containing K_3EDTA, trisodium heparin, and 3.2% trisodium citrate (Becton Dickinson Biosciences, BDB; San Jose, CA). All blood samples were collected at room temperature (RT) and processed within 6 h. This study was approved by the Institutional Review Board of the Faculty of Medicine, Siriraj Hospital, Mahidol University (approval number 74/2547).

2.2. Reagents and monoclonal antibodies

Annexin V conjugated with fluorescein isothiocyanate (FITC), mouse anti-human CD45 (clone 2D1) conjugated with peridinin chlorophyll protein (PerCP), and mouse anti-human glycophorin A (GPA) (clone GA-R2(HIR2)) conjugated with allophycocyanin (APC) were purchased from BDB-Pharmingen™ (San Diego, CA). Mouse monoclonal anti-human CD105 (endoglin) (clone SN6) conjugated with phycoerythrin (PE) was purchased from e-Bioscience (San Diego, CA), whereas mouse anti-human CD41a (clone VIPL3) conjugated with phycoerythrin-Cy5 (PE.Cy5) was obtained from Caltag Laboratories (Burlingame, CA). FITC-F(ab')$_2$ or PE-F(ab')$_2$ goat anti-mouse IgG were purchased from BDB and used as the isotype IgG control. All the monoclonal antibodies (mAbs) were utilized at the concentrations recommended by the manufacturers.

2.3. Isolation of MPs

MPs were isolated using methods previously described by several groups [18–21] with some modifications. Briefly, cell-free plasma was prepared by a centrifugation of each freshly drawn trisodium citrate blood sample at 1500 ×g for 15 min at 20 °C. Each cell-free plasma sample was collected and then centrifuged at 14,000 ×g for 2 min at 20 °C to obtain platelet-free-plasma (PFP). Afterward, the upper 90% of the PFP was gently removed by pipetting and re-centrifuged at 14,000 ×g for another 45 min. The upper 90% of the supernatant was

then again removed. The remaining material containing MPs was resuspended in a known volume of Hank's balanced salt solution (HBSS)–HEPES buffer (BDB) and kept at −80 °C for subsequent experiments.

2.4. Evaluation for cellular origins of MPs

To evaluate their cellular origins, isolated MPs were simultaneously examined for multiple known cellular markers using various mAbs as described in our previous study [17]. Briefly, 5 μL of pelleted MPs was mixed with a variety of fluorochrome-conjugated annexin V or mAbs specific for CD41a, GPA, CD45, or CD105 in Hank's balanced salt solution (HBSS)–HEPES buffer (BDB) containing 2.5 mM $CaCl_2$ or 2.5 mM EDTA to make a final volume of 100 μL. These mixtures were incubated at RT for 15 min in the dark. After incubation, the stained sample was diluted with 400 μL HBSS–HEPES buffer and acquired using FACSCalibur™ flow cytometer (BDB). For each stained MPs sample, at least 50,000 events were analyzed for their percentage of positive antigen and mean fluorescent channel (MFC) using CellQuest™ software (BDB).

2.5. Reactive oxygen species (ROS) and glutathione (GSH) assays

Because oxidative stress in peripheral blood components represents the imbalance between enhanced generation of ROS and decreased levels of cellular antioxidants, e.g. reduced glutathione (GSH), the levels of ROS and GSH in peripheral RBCs, platelets and isolated MPs were therefore used as the indicators for cellular oxidative stress in the blood components. Assessment was done using the method described by Amer, et al. [22] with minor modification. Briefly, 10 μL of K_3EDTA blood samples and isolated MPs from β-thalassemic patients and normal subjects were incubated either with 2', 7' dichlorofluorescein diacetate (DCFH-DA) dye (Sigma; St Louis, MO) dissolved in methanol (Sigma) at a final concentration of 0.4 mM for 15 min at 37 °C in a humidified incubator with 5% CO_2 or with 1-4-chloromercury phenyl-azo-2-naphthol (Mercury orange or MO) (Sigma) at a final concentration of 40 μM for 3 min at RT in the dark. The stained samples were washed twice and resuspended in phosphate buffered saline (PBS). Finally, the samples were further incubated with freshly prepared H_2O_2 (Sigma) at a final concentration of 2 mM (stimulation) or with PBS (unstimulation) for 30 min at RT in the dark. The stained samples were immediately acquired using FACSCalibur flow cytometer at approximately 1000 events/s and analyzed using CellQuest software.

2.6. Flow cytometric analysis

Measurements of ROS and GSH production in RBCs, platelets, and isolated MPs were determined by using a FACSCalibur with excitation by 488 nm light from a 15 mW argon ion laser. The size of each blood component was assessed by logarithmic amplification of the forward light scatter (FSC-H) and the side light scatter (SSC-H) signals. Logarithmic green, orange, red and long red fluorescence intensities of FITC, DCF, MO, PE, PE.Cy5, PerCP were measured through 530/30 band pass, 585/42 band pass, 661/16 band pass and 670 long pass filters, respectively. Instrument fluorescence calibration and sensitivity were performed by using Calibrite™ beads (BDB).

2.7. Prothrombinase assay

The Zymuphen MP-activity kit was purchased from Hyphen BioMed (France) as an enzyme immunoassay for *in vitro* measurement of MPs' procoagulant activity in human plasma. Fresh PFP samples or those kept at −80 °C were gently thawed at 37 °C for 15 min prior to the assay. Protocol for measuring the procoagulant activity was performed as detailed in the manufacturer's instruction. The level of MPs (in nM) was measured based on the standard control solutions provided in the kit. The developed color of the thrombin generation in each sample was measured at 405 nm using an ELISA Reader (Elx 808 IU, Biotex; Winooski, VT).

2.8. Protein extraction and 2-dimensional electrophoresis (2-DE)

Freshly isolated MPs were washed twice with PBS containing 0.32% citrate and the washing buffer was removed by centrifugation at 14,000 ×g for 10 min at 20 °C. Proteins from the isolated MPs pellets were then extracted using a lysis buffer containing 7 M urea, 2 M thiourea, 4% 3-[(3-cholamidopropyl) dimethylammonio]-1-propanesulfonate (CHAPS), 120 mM dithiothreitol (DTT), 40 mM Tris-base buffer, and 2% ampholytes (pH 3–10). Protein concentrations were determined using Bradford method. A total of 100 μg total protein pooled from two samples was run in each 2-D gel (overall, 5 gels derived from 10 individual samples were analyzed in each group). These sampling proteins obtained from patients or controls were premixed with a rehydration buffer containing 7 M urea, 2 M thiourea, 2% CHAPS, 120 mM DTT, 40 mM Tris-base, 2% ampholytes (pH 3–10), and bromophenol blue to make the final volume of 150 μl. The mixtures were rehydrated onto immobilized pH gradient (IPG) strips (pI 3–10, nonlinear) (GE Healthcare, Uppsala, Sweden) at RT for 10–15 h. The first-dimensional separation or isoelectric focusing (IEF) was performed in Ettan IPGphor III IEF System (GE Healthcare) at 20 °C using a step-wise mode to reach 9083 Vh with a limited current of 15 mA/strip. After IEF, the IPG strips were equilibrated in an equilibration buffer containing 6 M urea, 130 mM DTT, 112 mM Tris-base, 4% SDS, 30% glycerol, and 0.002% bromophenol blue. The strips were then equilibrated for additional 15 min in another similar equilibration buffer, in which DTT was replaced with 135 mM iodoacetamide. The second-dimensional separation was performed in 12.5% polyacrylamide slab gel using SE260 Mini-Vertical Electrophoresis Unit (GE Healthcare) at 150 V for approximately 2 h. The resolved protein spots were visualized by EMBL silver staining.

2.9. Protein spot matching and intensity analysis

Image Master 2D Platinum software (GE Healthcare) was used for matching and analysis of protein spots in 2-D gels. Parameters used for spot detection were (i) minimal area = 10 pixels; (ii) smooth factor = 2.0; and (iii) saliency = 2.0. A reference gel was created from an artificial gel combining all of the spots presenting in different gels into one image. The reference gel was then used for determination of existence and difference of

protein expression between gels. Background subtraction was performed and the intensity volume of each spot was normalized with total intensity volume (summation of the intensity volumes obtained from all spots within the same 2-D gel). Differentially expressed protein spots that were present consistently in at least 4 of 5 gels in each group and reached statistically significant threshold ($p<0.05$) in comparison between the two groups were subjected to in-gel tryptic digestion and identification by Q-TOF MS and MS/MS analyses.

2.10. *In-gel tryptic digestion*

The protein spots that were significantly different between the two groups (as defined above) were excised from 2-D gels, washed twice with 200 μl of 50% acetonitrile (ACN)/25 mM NH_4HCO_3 buffer (pH 8.0) at RT for 15 min, and then washed once with 200 μl of 100% ACN. After washing, the solvent was removed, and the gel pieces were dried by a SpeedVac concentrator (Savant; Holbrook, NY) and rehydrated with 10 μl of 1% (w/v) trypsin (Promega; Madison, WI) in 25 mM NH_4HCO_3. After rehydration, the gel pieces were crushed and incubated at 37 °C for at least 16 h. Peptides were subsequently extracted twice with 50 μl of 50% ACN/5% trifluoroacetic acid (TFA); the extracted solutions were then combined and dried with the SpeedVac concentrator. The peptide pellets were resuspended with 10 μl of 0.1% TFA and purified using $ZipTip_{C18}$ (Millipore; Bedford, MA). The peptide solution was drawn up and down in the $ZipTip_{C18}$ ten times and then washed with 10 μl of 0.1% formic acid by drawing up and expelling the washing solution three times. The peptides were finally eluted with 5 μl of 75% ACN/0.1% formic acid.

2.11. *Protein identification by Q-TOF MS and MS/MS analyses*

The trypsinized samples were premixed 1:1 with the matrix solution containing 5 mg/ml α-cyano-4-hydroxycinnamic acid (CHCA) in 50% ACN, 0.1% (v/v) TFA and 2% (w/v) ammonium citrate, and deposited onto the 96-well MALDI target plate. The samples were analyzed by Q-TOF Ultima™ mass spectrometer (Micromass; Manchester, UK), which was fully automated with predefined probe motion pattern and the peak intensity threshold for switching over from MS survey scanning to MS/MS, and from one MS/MS to another. Within each sample well, parent ions that met the predefined criteria (any peak within the *m/z* 800–3000 range with intensity above 10 counts ± include/exclude list) were selected for CID MS/MS using argon as the collision gas and a mass dependent ± 5 V rolling collision energy until the end of the probe pattern was reached. The MS and MS/MS data were extracted and outputted as the searchable *.txt* and *.pkl* files, respectively, for independent searches using the MASCOT search engine publicly available at *http://www.matrixscience.com*. The MS and MS/MS searches were performed against the mammalian NBCI protein database (accessed on February 12, 2012 with a total of 17,172,511 sequences) assuming that peptides were monoisotopic. Fixed modification was carbamidomethylation at cysteine residues, whereas variable modification was oxidation at methionine residues. Only one missed trypsin cleavage was allowed, and peptide mass tolerances of 100 and 50 ppm were allowed for peptide mass fingerprinting and MS/MS ions search, respectively. The thresholds for significant hits were 73 for MS probability-based MS scores and 40 for MS/MS ions scores. However, proteins that had lower MS or MS/MS scores but have been already reported in the proteomes of blood cells, platelets, or MPs were also included.

2.12. *Western blot analysis*

MPs samples were prepared as for 2-DE. An equal amount of 20 μg total protein derived from each sample was loaded into each lane of 12% SDS-PAGE gel. After SDS-PAGE, the separated proteins were transferred onto a nitrocellulose membrane (Whatman; Dassel, Germany) using Amersham ECL semidry blotter (GE Healthcare). Non-specific bindings were blocked with 1% skim milk in PBS at RT for 1 h. Thereafter, the membrane was washed three times with PBS and then incubated with mouse monoclonal anti-HSP90 or anti-fibrinogen (both were from Santa Cruz biotechnology; Santa Cruz, CA) at a dilution of 1:1000 in 1% skim milk/PBS at 4 °C overnight. After other three washes with PBS, the membrane was incubated with rabbit anti-mouse IgG conjugated with horseradish peroxidase (Dako; Glostrup, Denmark) with a dilution of 1:2000 in 1% skim milk/PBS at RT for 1 h. The immunoreactive protein bands were

Table 1 – Clinical and hematologic indices in β-thal/HbE patients and healthy individuals included in this study.

Parameters	β-thal/HbE patients	Healthy individuals with normal Hb typing	Normal range
No. of patients	15	15	-
Age (years)	30.93 ± 8.86	25.33 ± 1.80	-
Hemoglobin (g/l)	62.00 ± 11.00*	129.00 ± 14.00	120–180
Hematocrit (l/l)	0.223 ± 0.030*	0.393 ± 0.035	0.370–0.520
RBC count ($x10^{12}$/l)	3.00 ± 0.40*	4.50 ± 0.50	4.2–5.4
MCV (fl)	3.90 ± 8.30*	86.80 ± 7.40	80–99
MCH (pg)	20.60 ± 2.70*	28.50 ± 3.10	27–31
MCHC (g/l)	281.00 ± 25.01	321.00 ± 13.00	310–350
WBC count ($x10^9$/l)	17.05 ± 6.03*	6.29 ± 1.33	4–11
Platelet count (($x10^9$/l)	674.33 ± 161.49*	209.20 ± 60.78	150–440
Nucleated RBC/100 WBCs	515.07 ± 165.68*	0.00 ± 0.00	0

Hb = hemoglobin, RBC = red blood cell, MCV = mean corpuscular volume, MCH = mean corpuscular hemoglobin, MCHC = mean corpuscular hemoglobin concentration, WBC = white blood cell, * = $p<0.05$ compared to healthy individuals.

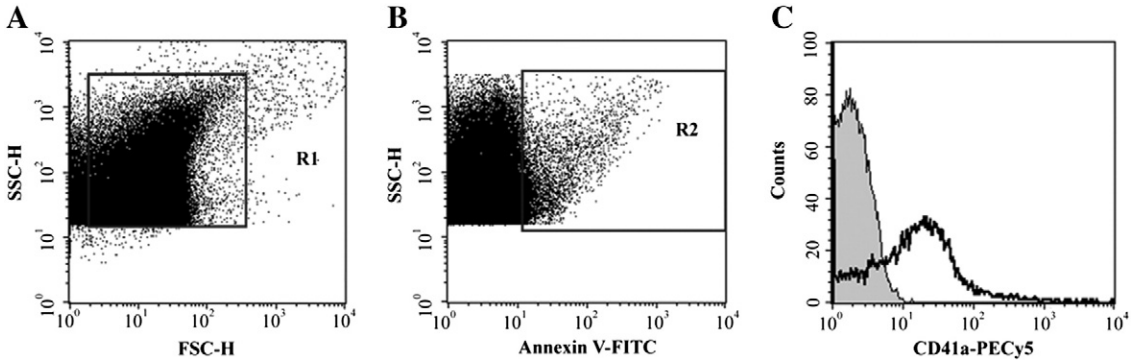


Fig. 1 – Representative flow cytometric dot-plots of PS-bearing microparticles (MPs) and their cellular origins in β-thal/HbE patients. These MPs were stained with FITC-conjugated annexin V and fluorochrome-conjugated anti-specific surface antigen (i.e. CD41a-PE.Cy5). Region R1 represented FSC-H/SSC-H light scatter gate of MPs (A). The percentage of annexin V+MPs was determined by SSC-H/annexin V+FITC in region R2 (B). The annexin V+MPs were further analyzed to determine the percentage of PE.Cy5 positive for CD41a (C). The percentage of platelets-derived annexin V+MPs was obtained by subtraction from the isotype IgG control.

visualized by SuperSignal West Pico chemiluminescence substrate (Pierce Biotechnology Inc.; Rockford, IL) and autoradiography. Band intensities were quantitated by Image Master densitometer (GE Healthcare).

2.13. *Statistical analyses*

Quantitative data are reported as mean±SD unless stated otherwise. Statistical analyses were performed using SPSS

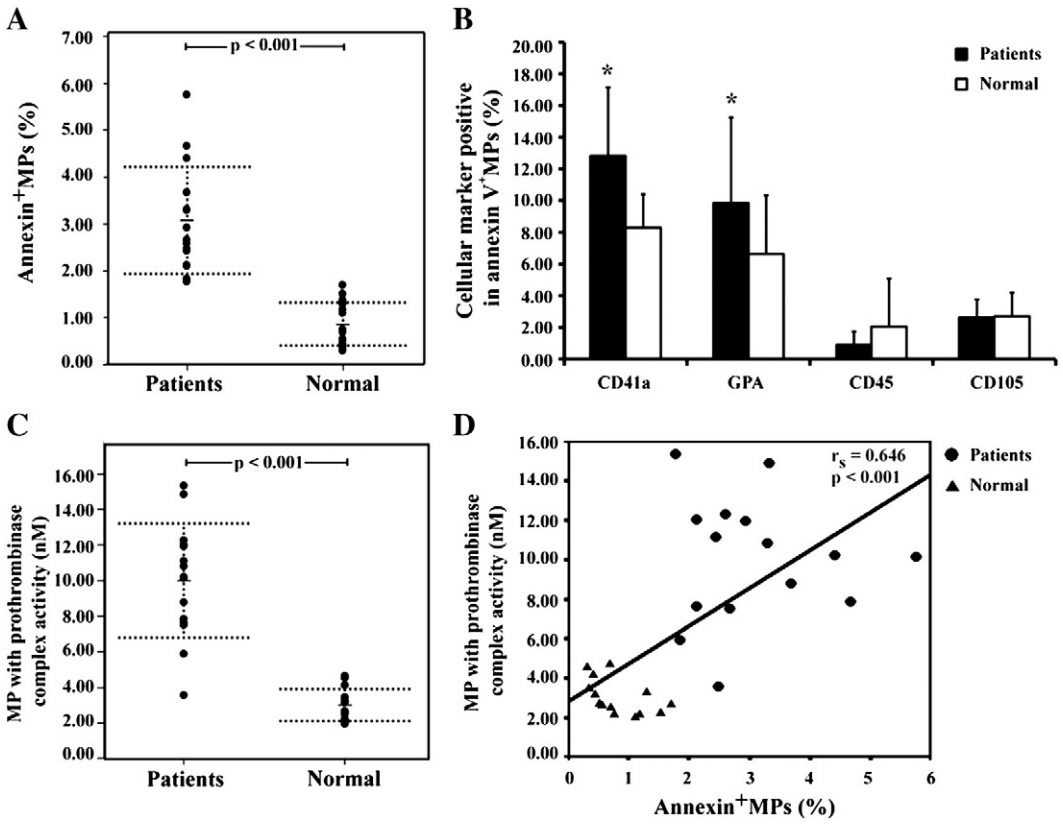


Fig. 2 – Percentage of annexin V+MPs (A), their cellular origins using known cellular markers, i.e. CD41a, GPA, CD45 and CD105 (B), and their procoagulant activity (prothrombinase complex activity) as assessed by using Zymuphen MP-activity kit (C). The relationship between the percentage of annexin V+MPs and the level of prothombinase complex activity is shown in (D). r_s=Spearman's correlation coefficient; *=p<0.05 as compared to the normal controls.

software, version 10.0 (SPSS Inc.; Chicago, IL). Comparisons of the clinical and laboratory parameters between groups were performed by non-parametric Mann–Whitney *U*-test. The correlation between two parameters was examined by simple linear regression analysis and Spearman's correlation test. Unpaired Student's *t*-test was used for comparing the spot intensity data between groups. The threshold for statistical significance for all comparisons was p-value<0.05.

3. Results

Basic hematologic characteristics for β-thal/HbE patients and healthy individuals are summarized in Table 1. Although with comparable age, the β-thal/HbE patients had marked decreases in Hb, hematocrit, RBC count, mean corpuscular volume (MCV) and mean corpuscular hemoglobin (MCH), and marked increases in numbers of white blood cells, platelets, and nucleated RBCs as compared to the normal controls.

Flow cytometric gating of isolated MPs using their FSC-H and SSC-H signals is shown in Fig. 1**A**. The percentage of annexin V+MPs in region R1 was determined from the two-parameter dot-plots of SSC-H/annexin V+FITC indicated as region R2 (Fig. 1**B**). The percentage of annexin V+MPs expressing a specific surface antigen (e.g. CD41a) in region R2 was determined by their antigen positive fluorescent histogram (Fig. 1**C**). The data showed a significantly higher percentage of annexin V+MPs in β-thal/HbE patients when compared with PFP from normal subjects (3.08%±1.14% vs. 0.87%±0.46%; p<0.001) (Fig. 2**A**). Evaluation of cellular origins of annexin V+MPs from both β-thal/HbE patients and healthy individuals by 3-color flow cytometric technique demonstrated the presence of distinct populations of these annexin V+MPs with the majority that expressed platelets (CD41a) and RBCs (GPA) antigens (Fig. 2**B**). The percentages of platelets-derived MPs (CD41a+/annexin V+) and RBCs-derived MPs (GPA+/annexin V+) were significantly higher in β-thal/HbE patients as compared to the normal subjects (12.82%±4.34% vs. 9.84%±5.41%, for platelets-derived MPs and 8.30%±2.10% vs. 6.64%±3.68%, p<0.05, for RBCs-derived MPs) (Fig. 2**B**). However, there were no significant differences in the percentages of leukocytes-derived MPs (CD45+/annexin V+) and endothelial cells-derived MPs (CD105+/annexin V+) observed between the thalassemic patients and normal subjects.

To investigate whether the annexin V+MPs from thalassemic patients promoted coagulation or not, we examined activation of the coagulation system by assessing the level of MPs with prothrombinase complex activity in PFP. The

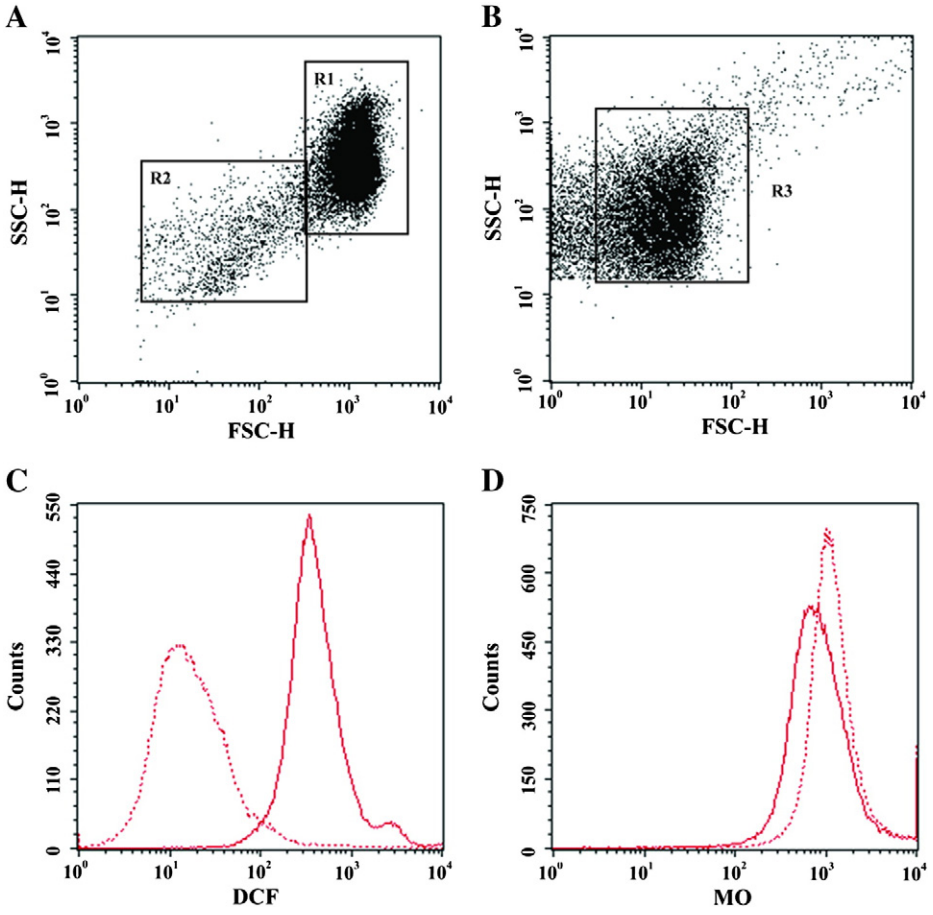


Fig. 3 – Representative flow cytometric dot-plots representing FSC-H/SSC-H light scatter gate of RBCs (R1 in A), **platelets** (R2 in A) **and MPs** (R3 in B). **Their ROS and GSH levels with (solid lines) and without (dotted lines) H_2O_2 treatment for 30 min are shown in** (C) **and** (D), **respectively. The ROS and GSH levels of each blood component (e.g. RBCs) are determined by the mean fluorescent channel (MFC) of the distribution histograms for DCF and MO, respectively.**

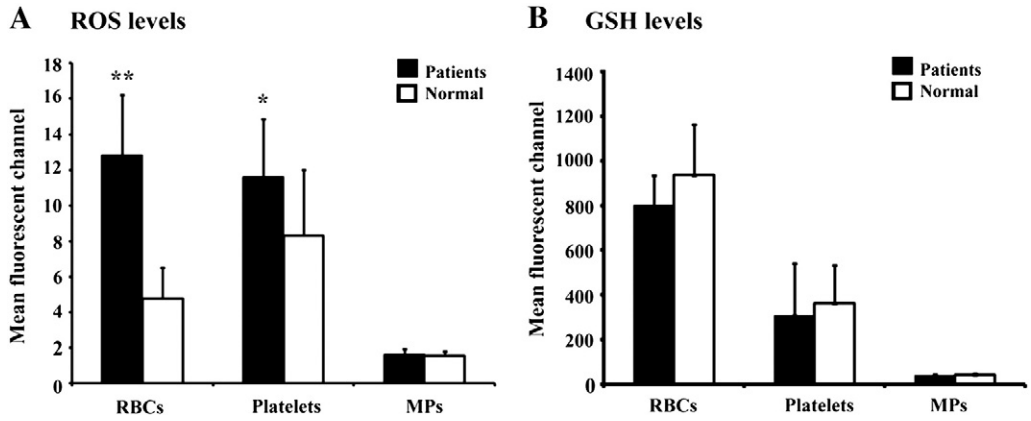


Fig. 4 – The oxidative status as measured by ROS (A) and GSH (B) levels in RBCs, platelets and MPs from β-thalassemia/HbE patients compared to normal subjects. $^{**}=p<0.001$ and $^{*}=p<0.05$ as compared to the normal controls.

prothrombinase assay revealed that PFP from β-thal/HbE patients had a significantly higher level of MPs with prothrombinase complex activity as compared to those from normal subjects (10.01±3.20 vs. 3.03±0.90 nM, $p<0.001$) (Fig. 2C). There was a significant correlation between the percentage of annexin V+MPs and the level of MPs with prothrombinase activity ($r_s=0.646$, $p<0.001$) (Fig. 2D). In addition, the level of MPs with prothrombinase activity was also correlated with platelet number ($r_s=0.729$, $p<0.001$) but was inversely correlated with RBC number ($r_s=0.752$, $p<0.001$) (data not shown).

Flow cytometric analysis of ROS and GSH in RBCs, platelets and MPs was achieved firstly by gating on the sizes of these blood components (Fig. 3). As demonstrated by the FSC-H/SSC-H dot-plots, RBC population (**R1** region in Fig. 3A) was easily distinguished from those of platelets (**R2** region in Fig. 3A) and MPs (**R3** region in Fig. 3B). Then, the ROS levels were determined by the MFC of DCF-derived green fluorescence (Fig. 3C), whereas GSH levels were determined by the MFC of MO-derived fluorescence histograms (Fig. 3D) of gated RBCs, platelets and MPs untreated and treated with H_2O_2. Results of oxidative stress assays revealed that β-thal/HbE patients had higher levels of ROS in RBCs and platelets as compared to the normal subjects ((12.82±3.41 vs. 4.77±1.76 MFC, $p<0.001$) and (11.59±3.28 vs. 8.33±3.67 MFC, $p<0.05$), respectively) (Fig. 4A). Although there was a trend showing that the levels of GSH in RBCs and platelets obtained from thalassemic patients were lower than those from normal subjects, these differences were not statistically significant (Fig. 4B). Interestingly, there were no significant differences in levels of ROS and GSH in the MPs isolated from thalassemia patients vs. normal subjects (Fig. 4A and B).

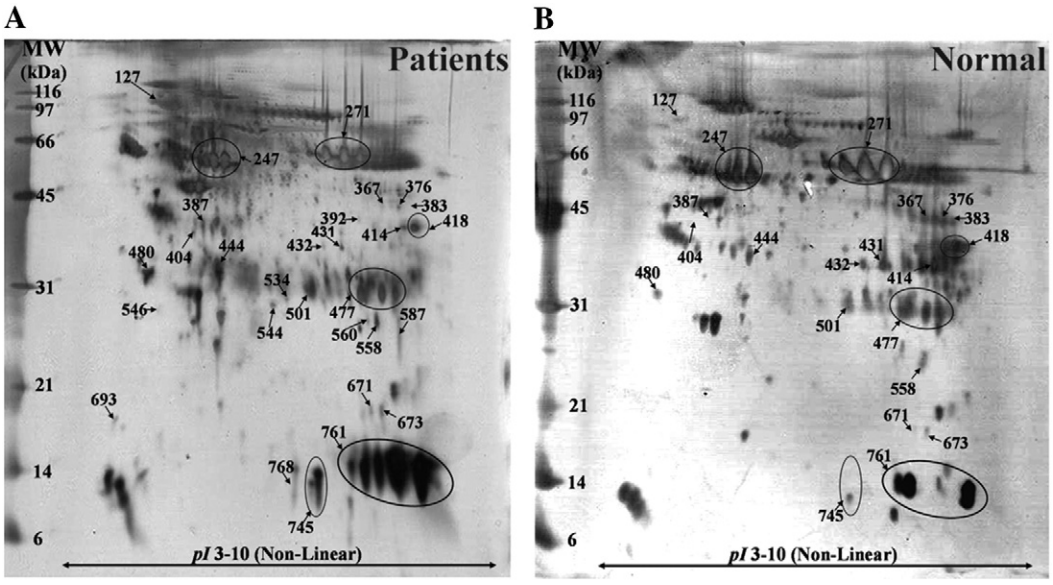


Fig. 5 – Representative 2-D proteome map of differentially expressed proteins in MPs derived from platelet-free plasma of 10 β-thal/HbE patients (A) versus 10 normal subjects (B). Within the same group, two samples were pooled and run in each 2-D gel (a total 10 gels, 5 from each group, were analyzed). Protein spot numbers correspond to those reported in Table 2.

Table 2 – Summary of differentially expressed proteins in platelet-free plasma-derived MPs of β-thal/HbE patients compared to those of normal subjects. These proteins were successfully identified by Q-TOF MS and MS/MS analyses.

Protein name	Spot no.	NCBI ID	Identified by	Identification scores (MS, MS/MS)	% Cov (MS, MS/MS)	No. of matched peptides (MS, MS/MS)	pI	MW (kDa)	Intensity levels (Mean ± SEM)		Ratio (Patients/ Normal)	p values
									β-thal/HbE Patients	Normal Subjects		
Proteins that were decreased in microparticles of β-thal/HbE patients												
Apo-B100 precursor	**418**	gi|28780	MS	71, NA	7, NA	24, NA	6.67	516.36	0.2092 ± 0.0803	6.1180 ± 1.7350	0.03	0.009
ASCC3 protein	**367**	gi|71052205	MS	80, NA	25, NA	13, NA	6.05	84.35	0.0411 ± 0.0170	0.6143 ± 0.1923	0.07	0.018
Chain A, heat shock 70kd protein, 42kd Atpase N-terminal domain	**247**	gi|6729803	MS, MS/MS	121, 203	29, 16	11, 5	6.69	41.97	2.3818 ± 0.4444	5.3669 ± 1.0249	0.44	0.028
Chain A, three-dimensional structure of dimeric human recombinant macrophage colony stimulating factor	**414**	gi|515141	MS	73, NA	59, NA	7, NA	5.19	17.66	0.4095 ± 0.0619	0.9247 ± 0.1027	0.44	0.003
Fibrin beta	**271**	gi|223002	MS	129, NA	39, NA	18, NA	7.95	51.36	6.4221 ± 0.5916	10.9028 ± 0.6408	0.59	0.001
Guanine nucleotide-binding protein G(q) subunit alpha	**432**	gi|2494885	MS	66, NA	30, NA	8, NA	5.58	41.73	0.0890 ± 0.0262	0.1996 ± 0.0081	0.45	0.004
Immunoglobulin heavy chain variable region	**383**	gi|22000154	MS	67, NA	100, NA	5, NA	4.46	7.81	0.0712 ± 0.0279	0.4323 ± 0.0369	0.16	<0.001
Pantothenate kinase 3, isoform CRA_b	**376**	gi|119581908	MS	62, NA	30, NA	7, NA	8.15	35.20	0.0201 ± 0.0105	0.5868 ± 0.1213	0.03	0.002
RNA polymerase II 140 kDa subunit	**431**	gi|3005758	MS	61, NA	24, NA	9, NA	8.76	54.80	0.2271 ± 0.0379	0.8897 ± 0.1552	0.26	0.003
Proteins that were increased in microparticles of β-thal/HbE patients												
Apolipoprotein E	**387**	gi|178853	MS	77, NA	38, NA	12, NA	5.81	36.24	0.1778 ± 0.0182	0.0069 ± 0.0070	25.42	<0.001
Chain A, cyclophilin A complexed with dipeptide Gly-Pro	**673**	gi|1633054	MS	75, NA	50, NA	7, NA	7.82	18.10	0.3366 ± 0.0649	0.0768 ± 0.0428	4.38	0.010
Chain A, molecular basis for the recognition of phosphorylated and phosphoacetylated histone H3 by 14-3-3	**480**	gi|83754467	MS	111, NA	44, NA	13, NA	4.97	29.41	1.0773 ± 0.0996	0.2632 ± 0.0390	4.09	<0.001
Chain A, X-Ray structure of the complex between carbonic anhydrase I and the phosphonate antiviral drug foscarnet	**477**	gi|158428858	MS, MS/MS	144, 215	58, 28	11, 4	6.9	28.41	6.5656 ± 0.3807	3.8214 ± 0.4189	1.72	0.001

Chain B, oxygen affinity modulation by the N-termini of the beta chains in human and bovine hemoglobin	**761**	gi|999565	MS, MS/MS	125, 114	75, 33	10, 3	6.70	15.87	22.5265 ± 1.8654	12.2316 ± 1.0639	1.84	0.001
Cytochrome P450, family 20, subfamily A, polypeptide 1, isoform CRA_c	**444**	gi|119590740	MS	70, NA	24, NA	10, NA	5.84	52.77	0.8158 ± 0.1383	0.2845 ± 0.0436	2.87	0.006
Hemoglobin mu chain	**745**	gi|51510893	MS/MS	NA, 55	NA, 21	NA, 2	6.12	15.72	2.1449 ± 0.2453	0.1903 ± 0.0456	11.27	<0.001
HSP90AA1 protein	**127**	gi|12654329	MS, MS/MS	83, 145	23, 10	13, 4	5.10	64.75	1.2091 ± 0.1116	0.3729 ± 0.0723	3.24	<0.001
Immunoglobulin light chain	**501**	gi|149673887	MS, MS/MS	71, 124	40, 23	6, 3	6.97	23.67	1.0677 ± 0.1017	0.6142 ± 0.0826	1.74	0.009
N-ethylmaleimide-sensitive factor attachment protein, alpha	**404**	gi|47933379	MS	79, NA	39, NA	9, NA	5.23	33.67	0.0756 ± 0.0123	0.0092 ± 0.0092	8.24	0.003
Trabeculin-alpha	**671**	gi|6273778	MS	75, NA	8, NA	29, NA	5.26	61.71	0.1440 ± 0.0284	0.0358 ± 0.0276	4.01	0.026
WWOX delta5-8	**558**	gi|15028465	MS	66, NA	38, NA	7, NA	9.22	35.59	0.5150 ± 0.0936	0.0912 ± 0.0561	5.64	0.005
Proteins that were detectable only in microparticles of β-thal/HbE patients												
Biliverdin-IX beta reductase isozyme I	**560**	gi|544759	MS	87, NA	47, NA	9, NA	7.31	21.96	0.1370 ± 0.0268	0.0000 ± 0.0000	#DIV/0!	0.001
hCG2005366, isoform CRA_a	**546**	gi|119619755	MS	74, NA	32, NA	6, NA	5.42	19.50	0.0451 ± 0.0145	0.0000 ± 0.0000	#DIV/0!	0.015
Hemoglobin mu chain	**768**	gi|51510893	MS/MS	NA, 42	NA, 10	NA, 1	6.12	15.72	0.7262 ± 0.1291	0.0000 ± 0.0000	#DIV/0!	<0.001
Matrilin 1, cartilage matrix protein, isoform CRA_b	**392**	gi|119628048	MS	69, NA	28, NA	10, NA	8.49	56.98	0.0323 ± 0.0102	0.0000 ± 0.0000	#DIV/0!	0.013
Myosin VIIB	**587**	gi|122937512	MS	69, NA	12, NA	18, NA	8.82	243.61	0.7366 ± 0.1947	0.0000 ± 0.0000	#DIV/0!	0.005
Peroxiredoxin 6	**544**	gi|4758638	MS	106, NA	57, NA	10, NA	6.00	25.13	0.0704 ± 0.0196	0.0000 ± 0.0000	#DIV/0!	0.007
Protein Rei, Bence-Jones	**534**	gi|229526	MS/MS	NA, 57	NA, 7	NA, 1	8.75	23.78	0.0712 ± 0.0270	0.0000 ± 0.0000	#DIV/0!	0.030
Zinc finger protein 233	**693**	gi|187953327	MS	73, NA	20, NA	11, NA	8.61	78.81	0.0495 ± 0.0175	0.0000 ± 0.0000	#DIV/0!	0.022

NCBI = National Center for Biotechnology Information.
%Cov = %Sequence coverage [(number of the matched residues/total number of residues in the entire sequence) × 100%].
NA = Not applicable.
#DIV/0! = Divided by zero.

Gel-based differential proteomics was performed to compare the proteome profile of MPs obtained from β-thal/HbE patients to that of MPs obtained from healthy individuals. The recovered MPs proteins from two individual samples within the same group were pooled and run in each 2-D gel (overall, 5 gels derived from 10 individual samples per group were analyzed). Using EMBL silver staining, approximately 1000–1200 protein spots were visualized in each 2-D gel (Fig. 5). Spot matching and statistical analysis revealed that levels of 29 protein spots significantly differed between the two groups (patients vs. controls). Among these, 9 were decreased, whereas other 12 proteins were increased and 8 were detectable only in MPs of β-thal/HbE patients. These significantly differed proteins were then identified by Q-TOF MS and MS/MS analyses (Table 2). Validation of the proteomic data was done on a randomly selected differentially expressed protein. The increased level of heat shock protein 90 (HSP90) was confirmed by Western blot analysis using fibrinogen as a loading control (Fig. 6).

4. Discussion

MPs are cell-derived membrane vesicles released from various blood cells. Among these, platelet-derived MPs are the majority of circulating MPs in normal subjects and thalassemic patients. A thorough proteomic characterization of MPs from normal healthy individuals showed a total of 203 unique proteins were assigned to plasma MPs, while 229 proteins were assigned to platelet-derived MPs [23]. The platelets-derived MPs express their procoagulant activity through an exposure of the negatively charged PS on the exofacial membrane [8–10,13,17,24]. Apart from platelets-derived MPs, MPs shed from RBCs have also been found in thalassemic patients [17,25]. The RBCs membranes undergo vesiculation under a variety of conditions, including disruption of the asymmetric organization of phospholipids, reduced ATP, elevated cytoplasmic calcium concentration and increased ROS, all of which eventually lead to the loss of RBCs

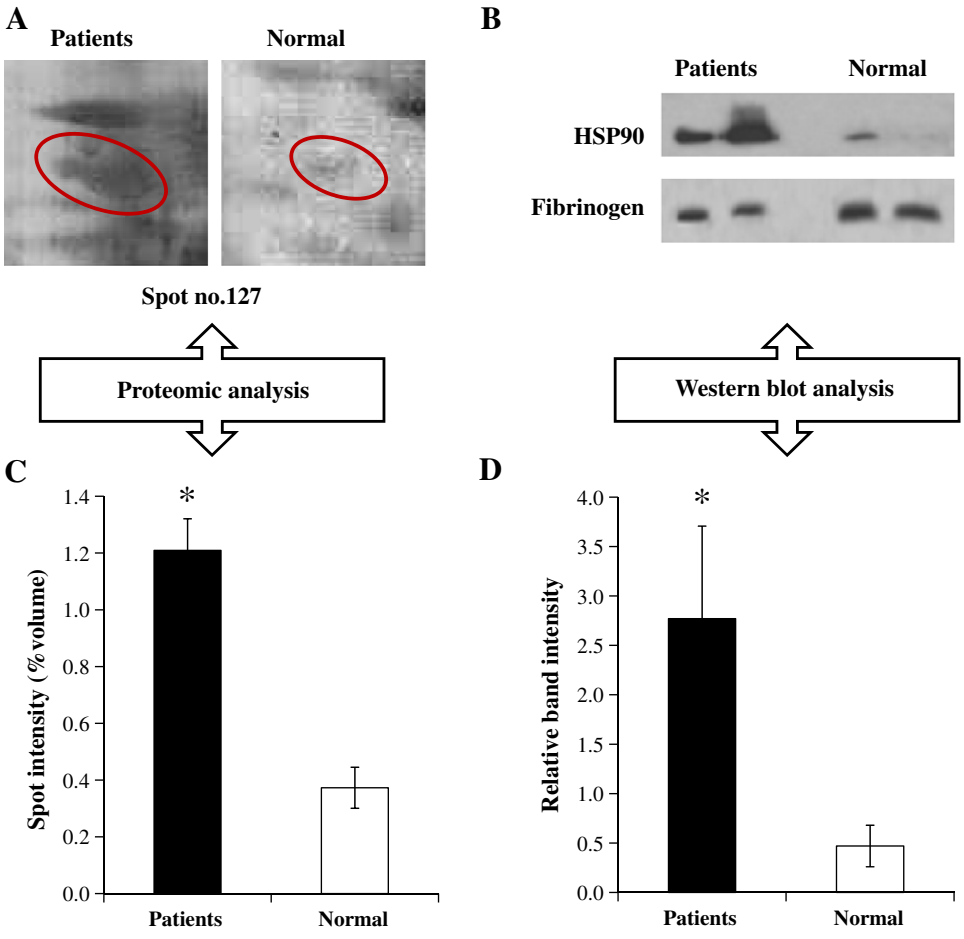


Fig. 6 – The increased level of HSP in β-thal/HbE patients was confirmed by Western blot analysis. (A) shows the cropped and zoom-in images of protein spot no. 127, which was identified as HSP90 by 2-DE-based proteomic analysis. (B) shows HSP90 band examined by Western blotting, whereas fibrinogen served as the loading control. (C) and (D) illustrate the intensity data of spot no. 127 and HSP90 band obtained from proteomic study and Western blot analysis, respectively. Each bar was derived from 5 samples, each of which was pooled from 2 subjects (a total of 10 subjects/group were analyzed). * = $p < 0.001$ as compared to the normal controls.

membranes in the form of MPs that are the characteristic features of thalassemic RBCs [4,8,15].

To confirm that there is oxidative damage in thalassemic platelets and RBCs, the levels of markers for oxidative stress in circulating MPs, platelets and RBCs from β-thal/HbE patients and normal subjects were measured in our present study using DCFH-DA dye and flow cytometer. The data confirmed that there were significantly higher levels of oxidative stress markers in thalassemic platelets and RBCs, but no significant differences in these markers were found in circulating MPs derived from the two groups (Fig. 4). The increased level of ROS in thalassemic platelets might be explained by their increasing tendency to undergo activation and aggregation as there is evidence showing that platelets in thalassemic patients are in a chronic activation state [17] expressing the activation markers such as CD62P and CD36 [15,17].

The data showing that the antigenic characteristics of shedding MPs were mostly originated from activated platelets (Fig. 2**B**) with proadhesive phenotype (CD41a/CD62P/CD36) [17] have suggested that the circulating MPs are thrombogenic and are involved in coagulation. For thalassemic RBCs, the increased levels of oxidative stress markers were most likely resulted from excessive accumulation of oxidized products. The unmatched α-globin chains in severely affected thalassemic RBCs are unstable and tend to be oxidized and precipitated within the RBCs. These unmatched α-globin chains then transform to hemichromes, which eventually disintegrate the release of iron toxic species and the formation of ROS that in turn oxidizes membrane lipids and results to altered membrane lipid organization and function [4–8]. In addition, the high percentage of PS+MPs (Fig. 2**A**) with high procoagulant activity (Fig. 2**C**) in thalassemic patients, and the relationship between the ROS levels and the MP procoagulant activity (Fig. 2**D**) suggested that the higher incidence of thromboembolic events and the existence of prothrombotic hemostatic anomalies commonly seen in β-thal/HbE patients are the consequence of chronic activation of platelets and defects in membrane phospholipid asymmetry of abnormal RBCs. The ROS levels of circulating MPs were significantly lower than those of platelets and RBCs in both thalassemic patients and healthy individuals. This was probably because MPs are the by-products derived from the common physiological processes of vesiculation and aging of platelets and RBCs.

Proteome analysis of MPs revealed differential levels of many proteins in MPs derived from β-thal/HbE patients as compared to the normal subjects. Most of these significantly altered proteins were involved mainly in regulation of the reduction–oxidation (redox) reaction, phospholipid turnover, and coagulation system. Our findings were in line with recent studies on the RBC proteome of β-thal/HbE patients, which evidenced high levels of redox regulators, i.e. peroxiredoxin, Cu-Zn super oxide dismutase, catalase and thioredoxin, in RBCs when compared to the healthy controls [26,27]. The increased levels of peroxiredoxin 6 and its binding protein, cyclophilin A, in patients' MPs might be for counterbalancing the oxidative stress frequently found in thalassemic and defective blood cells [22,28]. Peroxiredoxin 6 is a member of the thiol-specific antioxidant protein family that plays significant role in the redox regulatory pathways in cells to reduce free radicals and short chain organic, fatty acid and phospholipid hydroperoxides. This protein might play an important role in regulation of phospholipid turnover and protection against oxidative injury via enzymatic detoxification of hydroxyradicals using reducing equivalents from thiol-containing molecules such as GSH. Also, it has been shown that peroxiredoxin 6 protects RBCs from ROS-induced damage by binding to Hb, thus preventing RBCs from induction of spontaneous oxidation and methemoglobin formation [29].

Another antioxidant protein, apolipoprotein E (ApoE), is a well-known lipid-transporting protein, which acts as a scavenger of free radicals [30]. Soluble *N*-ethylmaleimide-sensitive factor attachment protein (α-SNAP) is another transporting protein that plays critical role in platelet exocytosis [31]. This protein interacts with G protein subunit ($G_{\alpha 12}$) that can induce vascular endothelial cadherin, which is responsible for maintaining functional stability in endothelial cells [32]. It is also important to note that there was a lower level of guanine nucleotide-binding protein G (q) subunit alpha (Gαq) in patients' MPs when compared to MPs from normal subjects. This protein is coupled to G protein complex that regulates platelet activation [33]. Thus, the decreased level of Gαq may lead to platelet dysfunction as previously reported in homozygous β-thalassemic patients [15,34]. Interestingly, there was a significant increase in level of HSP90 in patients' MPs. Up-regulation of other chaperones, namely HSP70 and α-hemoglobin stabilizing protein, has also been found in RBC proteome derived from β-thal/HbE patients [27]. This cytosolic chaperone accounts for 1%–2% of total cellular proteins and might reach to μM level under oxidative stress. It regulates diverse signaling pathways and, when associated with iNOS, facilitates NO synthesis [35].

Immunoglobulin (Ig) subunits were also found in isolated MPs. The protein Ig light chain was significantly increased, whereas Ig heavy chain variable region was significantly decreased in MPs derived from β-thal/HbE patients. We speculated that MPs-bound Ig may provide important mechanisms for clearance of MPs from the blood circulation via reticuloendothelial (RE) system and for maintaining MPs homeostasis. Because the abnormal asymmetry of phospholipids and the altered levels of several cytoskeletal proteins (e.g. trabeculin-alpha and myosin VIIB found in our present study) are important for MPs formation, further studies are required to address whether these proteins are involved in MPs clearance by macrophages in thalassemic patients.

In summary, our present study demonstrated that β-thal/HbE patients had significantly higher levels of PS-bearing MPs as compared to normal subjects, and that these MPs were originated mostly from oxidatively damaged platelets and RBCs. Moreover, the high levels of these PS-bearing MPs were correlated not only with the increased platelet counts in β-thal/HbE patients, but also with the increased procoagulant activity as measured by prothrombinase complex assay. In addition, the MPs isolated from β-thal/HbE patients also showed differential proteome profile as compared to those isolated from healthy individuals. The significantly altered proteins identified by mass spectrometry were involved mainly in regulation of cell stress. These findings suggest that the increased oxidative stress in platelets and RBCs in β-thal/HbE patients potentially induces MPs formation. Finally, the study of altered MPs proteome may lead to better understanding of the MPs biology

and their pathophysiological risk for thrombotic events commonly found in β-thal/HbE patients.

Acknowledgements

We are grateful to Prof. Shui-Tein Chen and Dr. Supachok Sinchaikul for their technical support on mass spectrometric analyses. This work was supported by Office of the Higher Education Commission and Mahidol University under the National Research Universities Initiative, the Thailand Research Fund (TRF) Senior Research Scholarship (to SF, VT, and KP), Chalermphrakiat Foundation of the Faculty of Medicine Siriraj Hospital (to VT and KP), Post-Doctoral Fellowship Program of Mahidol University (to PC), and the Royal Golden Jubilee PhD Program of TRF (to WC).

REFERENCES

[1] Weatherall DJ. Pathophysiology of thalassaemia. Baillieres Clin Haematol 1998;11:127–46.
[2] Schrier SL. Pathophysiology of thalassemia. Curr Opin Hematol 2002;9:123–6.
[3] Fucharoen S, Winichagoon P. Thalassemia and abnormal hemoglobin. Int J Hematol 2002;76(Suppl. 2):83–9.
[4] Wagner GM, Chiu DT, Yee MC, Lubin BH. Red cell vesiculation—a common membrane physiologic event. J Lab Clin Med 1986;108:315–24.
[5] Olivieri NF. The beta-thalassemias. N Engl J Med 1999;341:99–109.
[6] Zwaal RF, Schroit AJ. Pathophysiologic implications of membrane phospholipid asymmetry in blood cells. Blood 1997;89:1121–32.
[7] Kuypers FA, de Jong K. The role of phosphatidylserine in recognition and removal of erythrocytes. Cell Mol Biol (Noisy-le-Grand) 2004;50:147–58.
[8] Rund D, Rachmilewitz E. Beta-thalassemia. N Engl J Med 2005;353:1135–46.
[9] Helley D, Eldor A, Girot R, Ducrocq R, Guillin MC, Bezeaud A. Increased procoagulant activity of red blood cells from patients with homozygous sickle cell disease and beta-thalassemia. Thromb Haemost 1996;76:322–7.
[10] Chen S, Eldor A, Barshtein G, Zhang S, Goldfarb A, Rachmilewitz E, et al. Enhanced aggregability of red blood cells of beta-thalassemia major patients. Am J Physiol 1996;270:H1951–6.
[11] Hugel B, Martinez MC, Kunzelmann C, Freyssinet JM. Membrane microparticles: two sides of the coin. Physiology (Bethesda) 2005;20:22–7.
[12] Morel O, Toti F, Hugel B, Freyssinet JM. Cellular microparticles: a disseminated storage pool of bioactive vascular effectors. Curr Opin Hematol 2004;11:156–64.
[13] Flaumenhaft R. Formation and fate of platelet microparticles. Blood Cells Mol Dis 2006;36:182–7.
[14] Combes V, Simon AC, Grau GE, Arnoux D, Camoin L, Sabatier F, et al. In vitro generation of endothelial microparticles and possible prothrombotic activity in patients with lupus anticoagulant. J Clin Invest 1999;104:93–102.
[15] Eldor A, Rachmilewitz EA. The hypercoagulable state in thalassemia. Blood 2002;99:36–43.
[16] VanWijk MJ, VanBavel E, Sturk A, Nieuwland R. Microparticles in cardiovascular diseases. Cardiovasc Res 2003;59:277–87.
[17] Pattanapanyasat K, Gonwong S, Chaichompoo P, Noulsri E, Lerdwana S, Sukapirom K, et al. Activated platelet-derived microparticles in thalassaemia. Br J Haematol 2007;136:462–71.
[18] Freyssinet JM, Toti F. Formation of procoagulant microparticles and properties. Thromb Res 2010;125(Suppl. 1):S46–8.
[19] Rank A, Nieuwland R, Delker R, Kohler A, Toth B, Pihusch V, et al. Cellular origin of platelet-derived microparticles in vivo. Thromb Res 2010;126:e255–9.
[20] Shai E, Rosa I, Parguina AF, Motahedeh S, Varon D, Garcia A. Comparative analysis of platelet-derived microparticles reveals differences in their amount and proteome depending on the platelet stimulus. J Proteomics in press.
[21] Jy W, Horstman LL, Jimenez JJ, Ahn YS, Biro E, Nieuwland R, et al. Measuring circulating cell-derived microparticles. J Thromb Haemost 2004;2:1842–51.
[22] Amer J, Ghoti H, Rachmilewitz E, Koren A, Levin C, Fibach E. Red blood cells, platelets and polymorphonuclear neutrophils of patients with sickle cell disease exhibit oxidative stress that can be ameliorated by antioxidants. Br J Haematol 2006;132:108–13.
[23] Ostergaard O, Nielsen CT, Iversen LV, Jacobsen S, Tanassi JT, Heegaard NH. Quantitative proteome profiling of normal human circulating microparticles. J Proteome Res 2012;11:2154–63.
[24] Ahn YS, Jy W, Jimenez JJ, Horstman LL. More on: cellular microparticles: what are they bad or good for? J Thromb Haemost 2004;2:1215–6.
[25] Pattanapanyasat K, Noulsri E, Fucharoen S, Lerdwana S, Lamchiagdhase P, Siritanaratkul N, et al. Flow cytometric quantitation of red blood cell vesicles in thalassemia. Cytometry B Clin Cytom 2004;57:23–31.
[26] Bhattacharya D, Saha S, Basu S, Chakravarty S, Chakravarty A, Banerjee D, et al. Differential regulation of redox proteins and chaperones in HbEbeta-thalassemia erythrocyte proteome. Proteomics Clin Appl 2010;4:480–8.
[27] Chakrabarti A, Bhattacharya D, Basu A, Basu S, Saha S, Halder S. Differential expression of red cell proteins in hemoglobinopathy. Proteomics Clin Appl 2011;5:98–108.
[28] Jin M, Drwal G, Bourgeois T, Saltz J, Wu HM. Distinct proteome features of plasma microparticles. Proteomics 2005;5:1940–52.
[29] Stuhlmeier KM, Kao JJ, Wallbrandt P, Lindberg M, Hammarstrom B, Broell H, et al. Antioxidant protein 2 prevents methemoglobin formation in erythrocyte hemolysates. Eur J Biochem 2003;270:334–41.
[30] Economou-Petersen E, Aessopos A, Kladi A, Flevari P, Karabatsos F, Fragodimitri C, et al. Apolipoprotein E epsilon4 allele as a genetic risk factor for left ventricular failure in homozygous beta-thalassemia. Blood 1998;92:3455–9.
[31] Lemons PP, Chen D, Bernstein AM, Bennett MK, Whiteheart SW. Regulated secretion in platelets: identification of elements of the platelet exocytosis machinery. Blood 1997;90:1490–500.
[32] Andreeva AV, Kutuzov MA, Vaiskunaite R, Profirovic J, Meigs TE, Predescu S, et al. G alpha12 interaction with alphaSNAP induces VE-cadherin localization at endothelial junctions and regulates barrier function. J Biol Chem 2005;280:30376–83.
[33] Brass LF, Hoxie JA, Manning DR. Signaling through G proteins and G protein-coupled receptors during platelet activation. Thromb Haemost 1993;70:217–23.
[34] Stuart MJ. Platelet dysfunction in homozygous beta-thalassemia. Pediatr Res 1979;13:1345–9.
[35] Yoshida M, Xia Y. Heat shock protein 90 as an endogenous protein enhancer of inducible nitric-oxide synthase. J Biol Chem 2003;278:36953–8.

View Online / Journal Homepage / Table of Contents for this issue
Dynamic Article Links

Molecular BioSystems

Cite this: *Mol. BioSyst.*, 2012, **8**, 2312–2322

www.rsc.org/molecularbiosystems

PAPER

Marked changes in red cell membrane proteins in hereditary spherocytosis: a proteomics approach

Chantana Polprasert,†[a] Wararat Chiangjong†[b] and Visith Thongboonkerd*[bc]

Received 9th January 2012, Accepted 18th May 2012
DOI: 10.1039/c2mb25009h

Published on 18 May 2012 on http://pubs.rsc.org | doi:10.1039/C2MB25009H
Downloaded by Mahidol University on 07 August 2012

Hereditary spherocytosis (HS) is the most common red cell membrane defect resulting from protein abnormalities. However, changes in red cell membrane proteins in HS remain under-investigated. We therefore evaluated red cell membrane proteome in non-splenectomized, mild-degree HS patients ($n = 9$) compared to healthy individuals ($n = 5$). Proteins derived from the red cell membranes of each subject were resolved in each two-dimensional gel and visualized by Deep Purple fluorescence staining. Spot matching and quantitative intensity analysis revealed 56 differentially expressed protein spots (41 increased and 15 decreased), which were then successfully identified by quadrupole time-of-flight mass spectrometry. Among these, seven isoforms/subunits of spectrin were markedly increased (up to 10.51 folds), whereas two isoforms/subunits of band-3 protein were decreased approximately 50% as compared to normal red cells. However, two isoforms/subunits of protein 4.1 were increased, while another isoform/subunit was decreased. All these significantly altered proteins were subjected to global protein network analysis using Ingenuity Pathways Analysis tool, which revealed three important networks related to HS, including *Network I*: Cell death, genetic and hematological disorders; *Network II*: Cell cycle, carbohydrate metabolism and molecular transport; and *Network III*: Genetic and hematological disorders, cell-to-cell signaling and interactions. These data offer many opportunities and new roadmaps for further functional studies to better understand the biology and pathogenic mechanisms of HS.

Introduction

Hereditary spherocytosis (HS) is the most common inherited chronic hemolytic anemia and the most common red cell membrane defect worldwide, particularly in northern Europe and the United States of America, where it affects approximately 1 : 2000 of the general population in these areas.[1] HS is also highly prevalent in Asia, including Thailand. Clinical and laboratory features of HS include chronic hemolytic anemia, mild splenomegaly, jaundice, presence of spherocytes in peripheral blood smear, and a positive osmotic fragility test.[1] Alterations in red cell membrane proteins, most likely due to genetic abnormalities, lead to abnormal red cell morphology and osmotic fragility, which causes hemolysis in HS patients.[1–3] Previous reports have indicated that HS is associated with deficiencies of red cell membrane band-3 protein, spectrin, ankyrin, protein 4.2, and Rh complex, as a single defect or combined effects.[1–3] In a series of 300 HS patients, band-3 and spectrin deficiencies were the two most common protein defects, accounting for 54% and 31% of cases, respectively.[4] However, several other defects remained undefined and have been thought to also play roles in the pathogenesis of HS.

The defects or deficiencies of red cell membrane proteins in HS have been previously examined based entirely on SDS-PAGE protein separation.[5] However, this one-dimensional (1-D) separation of proteins based only on their molecular masses may provide erroneous results, as a single band of proteins resolved in SDS-PAGE (1-D PAGE) gel frequently has numerous proteins with similar molecular masses. In 1975, O'Farrell[6] and Klose[7] introduced two-dimensional polyacrylamide gel electrophoresis (2-D PAGE) to separate a large complement of proteins, based on differential isoelectric points and molecular masses. This technique permits separation of proteins in a complex mixture into hundreds to thousands of components (or spots in a 2-D gel). In the present study, we thus applied 2-D PAGE to globally examine alterations in red cell membrane proteins in HS patients compared to the normal controls. The significantly altered proteins were subsequently identified by Q-TOF mass spectrometry (MS) and

[a] *Division of Hematology, Department of Internal Medicine, Faculty of Medicine, Srinakarinwirot University, Bangkok, Thailand*
[b] *Medical Proteomics Unit, Office for Research and Development, Faculty of Medicine, Siriraj Hospital, Mahidol University, 12th Floor Adulyadej Vikrom Building, 2 Prannok Road, Bangkoknoi, Bangkok 10700, Thailand. E-mail: thongboonkerd@dr.com, vthongbo@yahoo.com; Fax: +66-2-4184793; Tel: +66-2-4184793*
[c] *Center for Research in Complex Systems Science, Mahidol University, Bangkoknoi, Bangkok, Thailand*
† Equal contributions as first authors.

This journal is © The Royal Society of Chemistry 2012

Published on 18 May 2012 on http://pubs.rsc.org | doi:10.1039/C2MB25009H
Downloaded by Mahidol University on 07 August 2012

tandem MS (MS/MS), and then subjected to global protein network analysis.

Results and discussion

In the present study, 9 HS patients (7 females and 2 males), who were mildly anemic and did not require a splenectomy, were included and their demographic as well as laboratory data are detailed in Table 1. These HS patients did not have a history of frequent blood transfusion and had no transfusion within four months prior to this study. The normal controls included 5 healthy individuals (4 females and 1 male), who were donors at the blood bank and passed all routine laboratory screenings. CBC showed that hemoglobin (Hb), hematocrit (Hct), mean corpuscular volume (MCV), mean corpuscular hemoglobin (MCH), mean corpuscular hemoglobin concentration (MCHC), red cell distribution width (RDW), total bilirubin (TB) and indirect bilirubin (IB) were within the normal ranges in the normal controls. In HS patients, Hb and Hct showed mild anemia and both total and indirect bilirubin levels were increased. Peripheral blood smears demonstrated numerous spherocytes in HS patients (Fig. 1). Moreover, osmotic fragility test showed positive result in all HS patients. Other tests were also performed to exclude other causes of hemolytic anemia, hemoglobinopathies, glucose-6-phosphate dehydrogenase (G6PD) deficiency, and paroxysmal nocturnal hemoglobinuria. These data confirmed the diagnosis of HS in all 9 patients.

Plasma membranes were isolated from the red blood cells of each subject and the recovered membrane proteins were resolved in each 2-D gel. Using Deep Purple fluorescence dye (GE healthcare), the total numbers of protein spots detected in individual 2-D gels were 603 ± 20 and 654 ± 37 spots/gel in HS and normal red cells, respectively. Spot matching and quantitative intensity analysis revealed a total of 56 differentially expressed protein spots, of which 41 were significantly increased, whereas another 15 were significantly decreased in HS. These differentially expressed protein spots are labeled with numbers in the 2-D proteome map (Fig. 2) and were successfully identified by Q-TOF MS and MS/MS analyses. Their mass spectrometric data (identities, identification scores, sequence coverage, number of matched peptides, isoelectric point or pI, molecular weight or MW, *etc.*),

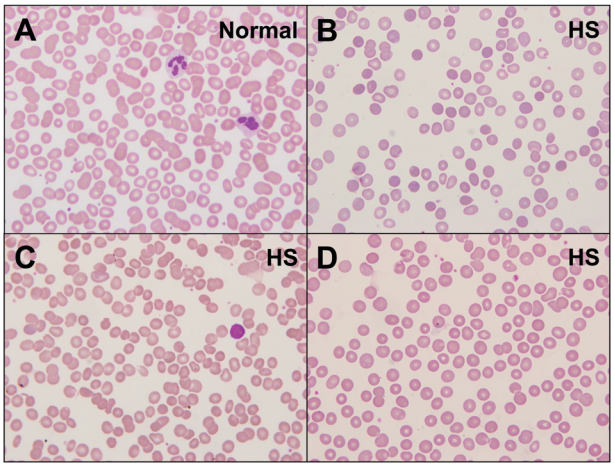


Fig. 1 Peripheral blood smears. Numerous spherocytes were detected in peripheral blood smears of HS patients (B–C), whereas red blood cell morphology was normal in healthy individuals (A). Original magnification power was 400× in all panels.

quantitative data (intensity levels) and *p* values are summarized in Table 2.

All the identified proteins were classified based on their main cellular functions, including those involved in cellular component organization, transport, cellular process, metabolic process, developmental process, cell communication, cell cycle, immune system process, response to stimulus, system process, cell adhesion, apoptosis and reproduction (in an order from highest to lowest numbers of the identified proteins in each group) (Fig. 3). All these significantly altered proteins were also subjected to global protein network analysis using Ingenuity Pathways Analysis (IPA) tool (http://www.ingenuity.com).[8] Accession numbers of all the identified proteins together with degrees of changes were uploaded to the IPA software and interaction networks were generated. The results showed three important functional networks of the identified proteins that were significantly altered in HS, including *Network I*: Cell death, genetic and hematological disorders (Fig. 4A); *Network II*: Cell cycle, carbohydrate metabolism and molecular transport (Fig. 4B); and *Network III*: Genetic and hematological disorders, cell-to-cell signaling and interactions (Fig. 4C).

Table 1 Patient information and blood tests

Patient No.	Gender	Age (year)	Hb (g/dL)	Hct (%)	MCV (fL)	MCH (pg)	MCHC (%)	RDW (%)	TB (mg%)	IB (mg%)
1	Female	31	9.4	26.9	82.3	28.8	34.9	18.7	4.78	3.23
2	Female	35	11.0	31.0	88.0	31.0	35.0	20.0	4.86	4.48
3	Female	27	11.6	32.0	88.0	32.0	36.0	16.0	4.50	4.30
4	Female	28	9.8	26.3	75.0	30.0	34.8	20.2	1.47	1.22
5	Male	43	13.6	37.0	81.5	30.0	36.8	18.8	4.96	4.76
6	Female	15	9.9	27.4	79.9	28.7	36.0	24.3	1.10	0.80
7	Female	22	12.0	35.0	83.0	29.0	35.0	17.0	3.00	2.65
8	Female	38	9.2	27.4	85.9	28.8	33.6	16.6	0.62	0.42
9	Male	65	12.8	37.2	95.0	32.7	34.4	20.0	4.90	4.40
Mean ± SD	—	33.8 ± 14.4	11.0 ± 1.6	31.1 ± 4.4	84.3 ± 5.7	30.1 ± 1.5	35.2 ± 1.0	19.1 ± 2.5	3.35 ± 1.83	2.92 ± 1.72
Min–Max	—	15–65	9.2–13.6	26.3–37.2	75.0–95.0	28.7–32.7	33.6–36.8	16.0–24.3	0.62–4.96	0.42–4.76
Normal range	—	—	12–16	37–47	80–95	27–32	32–36	12–14	0–1	0–1

Abbreviations used: Hb = hemoglobin; Hct = hematocrit; MCV = mean corpuscular volume; MCH = mean corpuscular hemoglobin; MCHC = mean corpuscular hemoglobin concentration; RDW = red cell distribution width; TB = total bilirubin; IB = indirect bilirubin.

Published on 18 May 2012 on http://pubs.rsc.org | doi:10.1039/C2MB25009H
Downloaded by Mahidol University on 07 August 2012

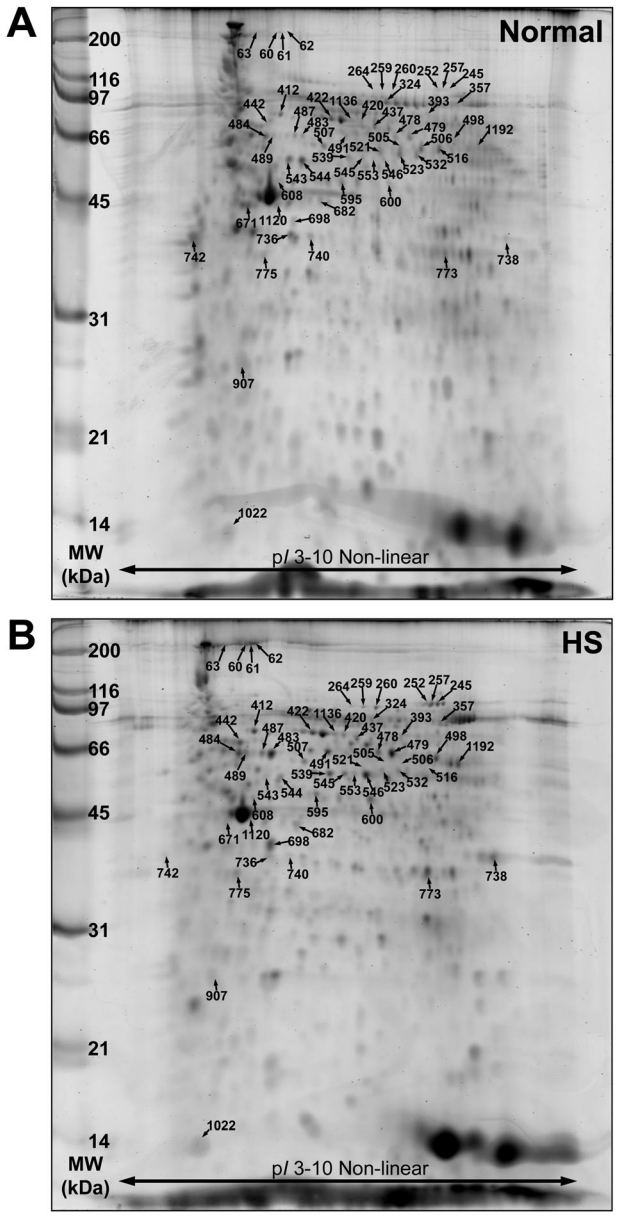


Fig. 2 2-D proteome map of differentially expressed membrane proteins in red cells. A total of 9 gels derived from red cell membranes of 9 HS patients (**A**) were compared to 5 gels derived from healthy controls (**B**). Spot matching and quantitative intensity analysis revealed 56 differentially expressed protein spots (labeled with numbers) that were successfully identified by Q-TOF MS and MS/MS analyses (see Table 2).

Interestingly, even with unbiased entries of the list of altered proteins identified and related information without any clue on the disease model, genetic and hematological disorders were found in both *Network I* and *Network III*, underlying the relevance of this global protein network analysis to shed light onto biological phenomena. In *Network I*, many altered proteins in HS were red cell membrane proteins such as spectrin, and cytoskeletal proteins such as myosin and tubulin, which play crucial roles in cellular morphology. In addition, HS was also associated with altered oxidative stress regulatory proteins such as catalase and chaperonin, which are related to cell death response. Many previous studies have demonstrated the association between oxidative stress and erythrocytic cell death and hemolysis.[9–12] In *Network II*, some altered proteins were involved in cell cycle including kinesin family member 20B (Kif20B) and tubulin gamma complex associated protein 2. In addition, many altered proteins were involved in carbohydrate metabolism such as phosphoribosyl pyrophosphate synthetase 1, proteasome 26S ATPase subunit 2 and thyroid hormone receptor interactor 11, and in molecular transport including epidermal growth factor receptor pathway substrate 15 like 1, golgin B1 and selenium binding protein 1. Our data were consistent with the findings reported in many previous studies, indicating that HS is associated with an abnormal cell cycle, carbohydrate metabolism and molecular transport.[13,14] In *Network III*, the altered proteins in HS were associated with cell–cell signaling and interactions, including fibrinogen, dystonin, MHC class II and myosin, consistent with the findings reported in a previous study.[15]

Note that most of the identified proteins reported in Table 2 had probabilistic MS scores >73 or MS/MS scores >40 with $p < 0.05$ (which were considered as significant hits).[16–18] However, some of the proteins had lower scores as they were either identified in previous proteome studies of red cell membranes[11,19,20] or had the same identity as the adjacent protein spot with multiple forms (most likely due to post-translational modifications).[21] In addition, the aim of this study was to screen for proteome changes in HS without any specific assumption of what would be changed. We therefore did not calculate for statistical power and sample size in this preliminary study, of which the initial screening of proteome changes in HS was done in a relatively small sample size. Thus, validation of the proteomic data is crucially required. To confirm these proteomic data, we performed Western blot analyses of α-tubulin (spot #698) and TCP-1(spots #483 and 491 with the same molecular mass), which are the common nodes of the interactions found in *Network I* (Fig. 4A). Carbonic anhydrase II served as the loading control (Fig. 5A). The band intensities of α-tubulin and TCP-1 were normalized with that of carbonic anhydrase II. Quantitative band intensity analysis with such normalization revealed significantly increased levels of both α-tubulin and TCP-1 (Fig. 5B), consistent with the proteomic data shown in Fig. 2 and Table 2.

Most of the significantly altered proteins in HS were involved in organization of cytoskeleton and membrane of erythrocytes as approximately 16% of changes fell into this group (Fig. 3). Among these, some proteins had multiple subunits or isoforms. Differential isoforms of one subunit of a protein might occur due to post-translational modifications or cleavage (such as the case of band-3 protein, spot #907, which was most likely the cleavage product of the main isoform present at spot #742; see Fig. 2). Three types of changes in these multiple isoforms/subunits of the same protein were observed including: (i) all isoforms/subunits were consistently increased in HS; (ii) all isoforms/subunits were consistently decreased in HS; and (iii) some isoforms/subunits were increased, whereas other isoforms/subunits were decreased. For example, all seven identified isoforms/subunits of spectrin (spots #60–62, 420, 442, 489, and 738) were markedly

 This journal is © The Royal Society of Chemistry 2012

View Online

Table 2 Red cell membrane proteins whose levels were significantly altered in HS patients compared to healthy controls

Spot no.	Protein name	NCBI ID	Identified by	Identification scores (MS, MS/MS)	%Cov (MS, MS/MS)	No. of matched peptides (MS, MS/MS)	p*I*	MW (kDa)	Intensity (Mean ± SEM) Normal	HS	Ratio (HS/ Normal)	*p* value
Red cell membrane proteins whose levels were significantly increased in HS patients												
422	Albumin	gi|158258947	MS, MS/MS	96, 26	26, 1	14, 1	5.91	71.22	0.1164 ± 0.0055	0.2165 ± 0.0410	1.86	0.041
698	Alpha-tubulin	gi|37492	MS/MS	NA, 36	NA, 3	NA, 1	5.02	50.81	0.1178 ± 0.0098	0.2880 ± 0.0380	2.44	0.002
437	Beta myosin heavy chain	gi|94397543	MS	92, NA	16, NA	23, NA	5.77	213.16	0.0535 ± 0.0132	0.1055 ± 0.0086	1.97	0.012
682	Bromodomain containing protein 1 isoform 2	gi|109094587	MS	71, NA	18, NA	15, NA	8.82	121.50	0.0298 ± 0.0139	0.1082 ± 0.0206	3.64	0.008
498	Catalase	gi|189067487	MS, MS/MS	86, 46	22, 3	11, 2	6.75	59.90	0.0665 ± 0.0192	0.1591 ± 0.0208	2.39	0.007
357	Chain A, crystal structure of the Protein 4.1r membrane binding domain	gi|13096731	MS	89, NA	36, NA	10, NA	7.59	32.69	0.0423 ± 0.0099	0.1019 ± 0.0185	2.41	0.016
546	Chaperonin containing TCP1, subunit 2	gi|5453603	MS	99, NA	30, NA	12, NA	6.01	57.79	0.0514 ± 0.0087	0.1975 ± 0.0284	3.84	0.001
479	Chaperonin subunit 6A	gi|121490543	MS	141, NA	46, NA	17, NA	5.79	54.10	0.1103 ± 0.0175	0.2104 ± 0.0140	1.91	0.002
478	Coronin, actin binding protein, 1C	gi|126306437	MS	80, NA	18, NA	15, NA	5.18	133.40	0.0628 ± 0.0063	0.1088 ± 0.0091	1.73	0.001
608	Dynamin 1-like, isoform CRA_c	gi|149019703	MS	70, NA	24, NA	6, NA	6.34	46.67	0.0465 ± 0.0127	0.0996 ± 0.0079	2.14	0.009
507	Elongation factor-2 kinase isoform 1	gi|114661517	MS	65, NA	21, NA	11, NA	5.02	77.74	0.0673 ± 0.0062	0.0918 ± 0.0070	1.37	0.022
60	Erythroid alpha spectrin	gi|338438	MS	92, NA	13, NA	21, NA	4.98	282.02	0.0390 ± 0.0274	0.2224 ± 0.0505	5.70	0.008
1192	Erythroid Protein 4.1 isoform A	gi|182073	MS/MS	NA, 34	NA, 1	NA, 1	5.31	87.06	0.0573 ± 0.0192	0.1537 ± 0.0198	2.68	0.005
553	Gprin1 protein	gi|149264149	MS	72, NA	19, NA	13, NA	8.70	80.45	0.0203 ± 0.0012	0.0562 ± 0.0062	2.77	<0.001
412	Heat shock 70 kDa protein 8 isoform 2 variant	gi|62896815	MS, MS/MS	99, 36	36, 2	12, 1	5.62	53.58	0.0740 ± 0.0111	0.1354 ± 0.0083	1.83	0.002
245	Heterogeneous nuclear ribonucleoprotein M isoform b	gi|157412270	MS	72, NA	31, NA	14, NA	8.94	73.86	0.0084 ± 0.0052	0.0538 ± 0.0119	6.42	0.005
1136	IP3 3-kinase	gi|396429	MS	79, NA	27, NA	10, NA	5.77	74.98	0.0321 ± 0.0072	0.0747 ± 0.0082	2.33	0.002
393	Keratin 1	gi|7331218	MS	71, NA	23, NA	11, NA	8.16	66.15	0.0232 ± 0.0084	0.0527 ± 0.0074	2.27	0.026
1022	Keratin, type II microfibrillar; Low-sulfur keratin	gi|125115	MS	74, NA	29, NA	5, NA	4.56	12.90	0.4626 ± 0.0599	0.6402 ± 0.0356	1.38	0.039
484	Kif20b protein	gi|219521773	MS	83, NA	13, NA	20, NA	5.69	200.45	0.1031 ± 0.0248	0.2428 ± 0.0570	2.36	0.047
252	MHC class II antigen	gi|111379998	MS	93, NA	80, NA	7, NA	5.38	10.94	0.0149 ± 0.0065	0.0714 ± 0.0167	4.80	0.010
259	MHC class II antigen	gi|186703093	MS	73, NA	79, NA	6, NA	5.80	10.02	0.0210 ± 0.0060	0.0398 ± 0.0032	1.90	0.031
600	MIC2 like 1	gi|109503337	MS	71, NA	22, NA	5, NA	7.67	32.14	0.0724 ± 0.0182	0.1355 ± 0.0172	1.87	0.030
63	Myosin, heavy chain 4, skeletal muscle	gi|119911910	MS	89, NA	14, NA	23, NA	5.61	223.93	0.0379 ± 0.0315	0.1886 ± 0.0420	4.98	0.014
260	Myosin, heavy polypeptide 7B, cardiac muscle, beta, isoform CRA_a	gi|119596642	MS	78, NA	16, NA	19, NA	5.78	225.57	0.0251 ± 0.0067	0.0703 ± 0.0090	2.80	0.002

Published on 18 May 2012 on http://pubs.rsc.org | doi:10.1039/C2MB25009H
Downloaded by Mahidol University on 07 August 2012

View Online

Table 2 (*continued*)

Spot no.	Protein name	NCBI ID	Identified by	Identification scores (MS, MS/MS)	%Cov (MS, MS/MS)	No. of matched peptides (MS, MS/MS)	p*I*	MW (kDa)	Intensity (Mean ± SEM) Normal	Intensity (Mean ± SEM) HS	Ratio (HS/Normal)	*p* value
775	*N*-ethylmaleimide-sensitive factor attachment protein, alpha, isoform CRA_g	gi|119577902	MS	81, NA	44, NA	9, NA	5.68	22.20	0.1218 ± 0.0168	0.2306 ± 0.0186	1.89	0.001
773	Phosphoribosyl pyrophosphate synthetase 1	gi|4506127	MS, MS/MS	80, 28	39, 3	10, 1	6.51	35.33	0.1536 ± 0.0262	0.2842 ± 0.0333	1.85	0.010
595	Proteasome 26S ATPase subunit 2	gi|4506209	MS	106, NA	29, NA	14, NA	5.71	49.00	0.0449 ± 0.0070	0.0828 ± 0.0073	1.84	0.003
257	PTK2 protein tyrosine kinase 2 beta, isoform CRA_b	gi|148704055	MS	74, NA	20, NA	14, NA	5.77	112.90	0.0052 ± 0.0034	0.0501 ± 0.0141	9.69	0.013
487	Scavenger receptor class A, member 5	gi|156523110	MS	81, NA	29, NA	12, NA	6.87	53.99	0.0470 ± 0.0086	0.1099 ± 0.0088	2.34	<0.001
539	Selenium binding protein 1	gi|16306550	MS	100, NA	23, NA	11, NA	5.93	52.93	0.0910 ± 0.0074	0.1222 ± 0.0062	1.34	0.010
442	Spectrin beta isoform 4	gi|114653508	MS	97, NA	12, NA	24, NA	5.23	268.51	0.0918 ± 0.0169	0.2026 ± 0.0349	2.21	0.016
62	Spectrin, alpha, erythrocytic 1 (elliptocytosis 2) isoform 1	gi|109017475	MS	105, NA	13, NA	25, NA	4.88	282.74	0.0126 ± 0.0068	0.1142 ± 0.0247	9.08	0.003
420	Spectrin, alpha, erythrocytic 1 (elliptocytosis 2) isoform 1	gi|109017475	MS	64, NA	9, NA	19, NA	4.88	282.74	0.0504 ± 0.0114	0.0831 ± 0.0061	1.65	0.043
61	Spectrin, alpha, erythrocytic 1 (elliptocytosis 2) isoform 2	gi|109017473	MS	89, NA	13, NA	25, NA	4.87	280.70	0.0155 ± 0.0074	0.1624 ± 0.0449	10.51	0.011
738	Spectrin, beta, non-erythrocytic 1 isoform 1	gi|109102943	MS	61, NA	10, NA	21, NA	5.35	265.74	0.1148 ± 0.0391	0.4371 ± 0.0741	3.81	0.003
489	Spectrin, beta, non-erythrocytic 2	gi|9507135	MS	76, NA	13, NA	21, NA	5.61	272.02	0.0523 ± 0.0165	0.1227 ± 0.0195	2.35	0.018
491	T-complex poly-peptide 1	gi|149641164	MS	108, NA	33, NA	14, NA	5.85	58.55	0.0515 ± 0.0086	0.1241 ± 0.0145	2.41	0.001
483	T-complex protein 1, theta subunit (TCP-1-theta) (CCT-theta) isoform 3	gi|74001082	MS	72, NA	23, NA	9, NA	5.46	53.52	0.0727 ± 0.0168	0.2647 ± 0.0217	3.64	<0.001
545	Thyroid hormone receptor interactor 11	gi|194038274	MS	65, NA	9, NA	15, NA	5.24	224.00	0.0495 ± 0.0036	0.0971 ± 0.0066	1.96	<0.001
264	Tubulin, gamma complex associated protein 2 variant	gi|62898904	MS	64, NA	20, NA	11, NA	6.38	103.01	0.0049 ± 0.0031	0.0329 ± 0.0075	6.67	0.006
Red cell membrane proteins whose levels were significantly decreased in HS patients												
742	Chain P, crystal structure of the cytoplasmic domain of human erythro-cyte Band-3 protein	gi|14277739	MS, MS/MS	67, 68	28, 8	8, 2	4.49	42.62	0.6655 ± 0.1214	0.3288 ± 0.0620	0.49	0.048
907	Chain P, crystal structure of the cytoplasmic domain of human erythrocyte Band-3 protein	gi|14277739	MS, MS/MS	83, 127	31, 8	9, 2	4.49	42.62	0.5509 ± 0.0899	0.2665 ± 0.0425	0.48	0.030
523	Chaperonin containing Tcp1, subunit 4 (delta)	gi|6753322	MS	76, NA	21, NA	12, NA	8.24	58.54	0.1276 ± 0.0198	0.0636 ± 0.0174	0.50	0.036

Published on 18 May 2012 on http://pubs.rsc.org | doi:10.1039/C2MB25009H
Downloaded by Mahidol University on 07 August 2012

This journal is © The Royal Society of Chemistry 2012

Table 2 (*continued*)

Spot no.	Protein name	NCBI ID	Identified by	Identification scores (MS, MS/MS)	%Cov (MS, MS/MS)	No. of matched peptides (MS, MS/MS)	p*I*	MW (kDa)	Intensity (Mean ± SEM) Normal	HS	Ratio (HS/ Normal)	*p* value
532	Chaperonin containing Tcp1, subunit 4 (delta)	gi|6753322	MS	75, NA	17, NA	10, NA	8.24	58.54	0.1309 ± 0.0143	0.0722 ± 0.0124	0.55	0.012
671	Dystonin, isoform CRA_b	gi|119624862	MS	72, NA	12, NA	20, NA	5.97	316.44	0.3117 ± 0.0326	0.1049 ± 0.0205	0.34	0.001
506	Epidermal growth factor receptor pathway substrate 15-like 1	gi|156120391	MS	72, NA	18, NA	11, NA	4.89	88.06	0.1470 ± 0.0152	0.0621 ± 0.0093	0.42	0.002
324	Erythrocyte membrane protein Band 4.1 isoform 4	gi|42716291	MS, MS/MS	76, 71	23, 4	11, 2	6.19	72.31	0.1889 ± 0.0170	0.1073 ± 0.0115	0.57	0.004
516	Fibrinogen, beta chain isoform 3	gi|55623354	MS	80, NA	32, NA	11, NA	8.63	56.56	0.1779 ± 0.0223	0.0886 ± 0.0216	0.50	0.016
521	Golgi autoantigen, golgin subfamily b, macrogolgin 1	gi|20302065	MS	85, NA	10, NA	25, NA	5.01	365.62	0.1136 ± 0.0061	0.0480 ± 0.0139	0.42	0.001
505	NEDD4-binding protein 1 (N4BP1)	gi|109462432	MS	74, NA	33, NA	7, NA	7.82	34.13	0.0525 ± 0.0085	0.0095 ± 0.0043	0.18	0.004
1120	Putative calcium binding transporter	gi|28551967	MS	76, NA	28, NA	11, NA	6.82	49.55	0.0966 ± 0.0213	0.0251 ± 0.0085	0.26	0.024
543	Renal tumor antigen, isoform CRA_c	gi|149044116	MS	79, NA	35, NA	11, NA	9.86	49.05	0.2015 ± 0.0234	0.1209 ± 0.0183	0.60	0.024
544	Selenium binding protein 1	gi|16306550	MS	77, NA	34, NA	10, NA	5.93	53.93	0.3245 ± 0.0287	0.2293 ± 0.0117	0.71	0.025
740	Tubulin, gamma complex associated protein 2 variant	gi|62898904	MS	68, NA	20, NA	12, NA	6.38	103.01	0.0961 ± 0.0042	0.0708 ± 0.0088	0.74	0.025
736	Zinc finger protein 268 (Zinc finger protein HZF3) isoform 3	gi|73947821	MS	67, NA	14, NA	9, NA	9.18	96.87	0.2023 ± 0.0102	0.1171 ± 0.0096	0.58	<0.001

NCBI = National Center for Biotechnology Information; %Cov = %Sequence coverage [(number of the matched residues/total number of residues in the entire sequence) × 100%]; NA = Not applicable.

Published on 18 May 2012 on http://pubs.rsc.org | doi:10.1039/C2MB25009H
Downloaded by Mahidol University on 07 August 2012

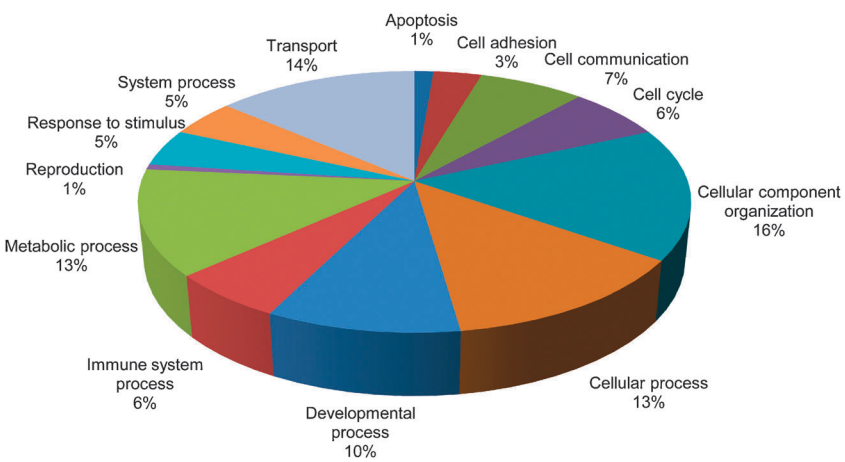


Fig. 3 Functional classifications of all 56 significantly altered membrane proteins in red cells of HS patients compared to normal red cells.

increased (up to 10.51 folds), whereas two forms of band-3 protein (spots #742 and 907) were both decreased (approximately 50%) as compared to normal red cells. However, two isoforms/subunits of protein 4.1 (band-4.1 protein) (spots #357 and 1192) were increased, while another isoform/subunit (spot #324) was decreased (Table 2). The important roles of these three proteins in the pathogenesis of HS are highlighted as follows.

Spectrin, a cytoskeletal protein, consists of α and β subunits encoded by *SPTA1* and *SPTB* genes, respectively.[22]

Published on 18 May 2012 on http://pubs.rsc.org | doi:10.1039/C2MB25009H
Downloaded by Mahidol University on 07 August 2012

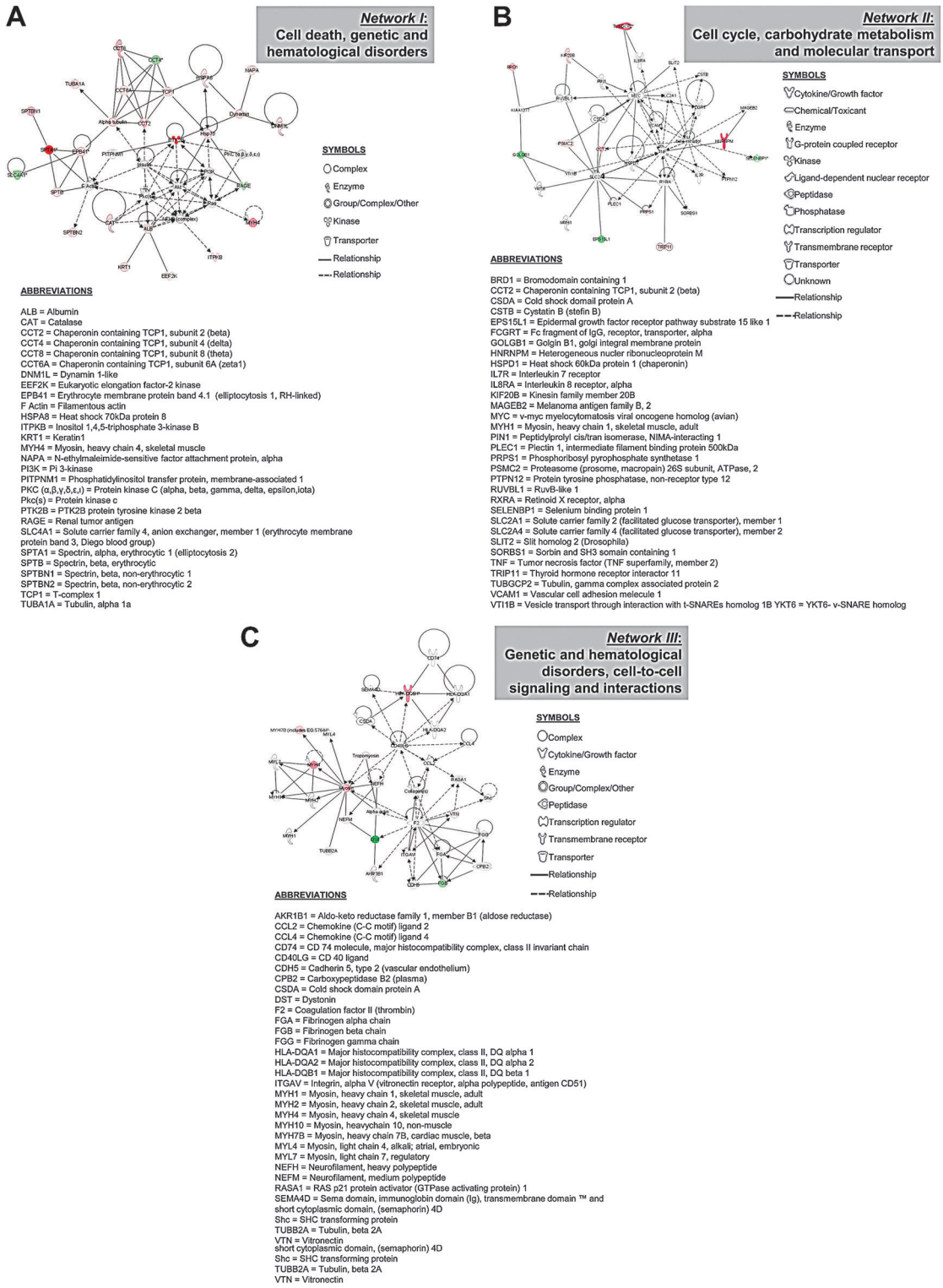


Fig. 4 Ingenuity pathway analysis (IPA) revealed three important functional networks of the identified proteins that were significantly altered in HS, including *Network I*: Cell death, genetic and hematological disorders (A); *Network II*: Cell cycle, carbohydrate metabolism and molecular transport (B); and *Network III*: Genetic and hematological disorders, cell-to-cell signaling and interactions (C). The proteins marked with red are those identified in the present study as up-regulated proteins, whereas those marked with green are the down-regulated ones. The intensities of color shades indicate degrees of changes (*i.e.* the most intense shade indicates the highest degree of changes identified in this study). The ones without color were those curated from the literature.

 This journal is © The Royal Society of Chemistry 2012

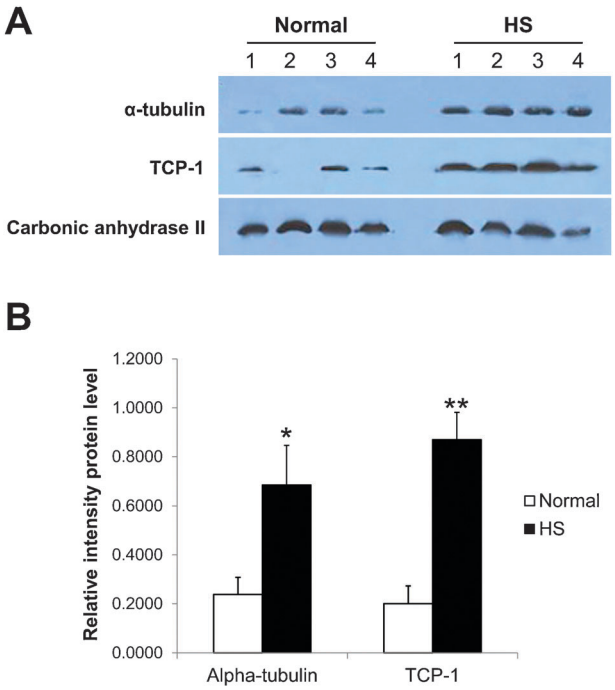


Fig. 5 Validation of the proteomic data by Western blot analysis of α-tubulin (spot #698 in Table 2) and TCP-1 (spots #483 and 491 in Table 2 with the same molecular mass) (A). Carbonic anhydrase II served as the loading control. The band intensities of α-tubulin and TCP-1 were normalized with that of carbonic anhydrase II (B). * = $p < 0.05$ and ** = $p < 0.01$.

Spectrin serves as the membrane-associated cytoskeletal compartment to support the erythrocyte membrane and has been found not only in erythrocytes but also in non-erythrocytic cells.[23] In HS, spectrin deficiency has been detected more frequently in childhood than in adulthood.[4] However, in our present study, various isoforms of both α and β spectrin were markedly increased in HS adult patients with 1.65–10.51 (5.04 ± 1.34) folds of the increase. Our data were contradictory to those of previous reports,[1,24] most likely due to the following. First, we employed a more sensitive technique (namely proteomic analysis using 2-D PAGE) with much better resolution[6,7] as compared to the commonly used SDS-PAGE in previous studies. This was reflected by multiple isoforms/subunits of spectrin that could be identified in our present study and thus would provide the more precise data. Second, our HS patients had a mild degree of anemia without any need for frequent blood transfusion and splenectomy, and had no transfusion within four months prior to this study. Differential clinical entities might reflect different underlying molecular mechanisms of the pathogenesis of HS, which is highly heterogeneous.[1,4]

Transmembrane band-3 protein, the red cell anion exchanger (AE1/SLC4A1), plays an important role in assembling and stabilizing erythrocyte membrane.[25] Band-3 proteins can form dimers and tetramers, as well as a complex with ankyrin 1.[1] Band-3 deficiency has been identified in 54% of HS adult patients.[4,26] In homozygous HS, band-3 defect can cause extreme fragility of the red cells and loss of anion transport activity, resulting to hemolytic anemia.[27] In the present study, two isoforms of band-3 protein were significantly decreased in the red cells of HS patients, consistent with the previous data.

Protein 4.1, a member of the mammalian 4.1 family, plays a crucial role in maintaining erythrocyte shape and to control membrane properties based on temporal sequence of synthesis, assembly, and turnover of membrane and cytoskeletal proteins.[28–30] Protein 4.1 commonly interacts with glycophorin C, band-3 protein, spectrin, protein p55 and actin for deformability and stability functions.[31–33] Recent studies have reported that different isoforms of protein 4.1 have marked differences in binding properties and partners.[31,34] Moreover, different regions in its sequence are responsible for such differential properties and functions.[31,34] In previous studies, the data have shown that deficiency of protein 4.1 is a main cause of hereditary elliptocytosis due to *EBP41* gene disruption.[25,35,36] In the present study, we identified three isoforms of protein 4.1, including isoform 4 (spot #324; 72.31 kDa) that was decreased, whereas isoform A (spot #1192; 87.06 kDa) and its membrane binding domain (spot #357; 32.69 kDa) were increased in HS. Unlike elliptocytosis in which protein 4.1 is down-regulated, HS has up-regulation in some isoforms or regions, whereas another isoform was down-regulated. These disparate results indicate that various forms of protein 4.1 are very important to control red cell morphology and patterns of their alterations determine types of the red cell membrane defect.

In addition to spectrin, band-3 protein and protein 4.1, other typical cytoskeletal proteins were also significantly altered in HS, including actin, myosin and tubulin. Moreover, many proteins with other molecular functions were also identified as the significantly altered proteins (Table 2). Roles of all of these proteins in the pathogenesis of HS are very interesting and deserve further investigation. However, alterations in the two well-known proteins, ankyrin and protein 4.2, were not identified in our HS patients. This might be simply explained because changes in these proteins were under the threshold for significant differences defined in our present study or defects in these two proteins might not be the case for HS in Thailand. The latter reflects the high heterogeneity of HS.

In summary, we report herein alterations in many red cell membrane proteins in HS using a proteomics approach. Some of these findings were consistent to the data reported previously, whereas some other findings were novel. However, further functional studies of proteins involved in HS are required to better understand the biology and pathogenic mechanisms of HS.

Materials and methods

Patients, routine labs, and osmotic fragility test

This study was approved by the Institutional Ethical Committee (approval no. SWUEC 19/2552). A total of 9 HS patients and 5 normal healthy individuals, who were the donors at blood bank and passed all the routine laboratory screenings, were included in this study. HS was diagnosed by a history of chronic anemia with intermittent jaundice, splenomegaly, and laboratory tests. All the patients and normal individuals were

Published on 18 May 2012 on http://pubs.rsc.org | doi:10.1039/C2MB25009H
Downloaded by Mahidol University on 07 August 2012

Published on 18 May 2012 on http://pubs.rsc.org | doi:10.1039/C2MB25009H
Downloaded by Mahidol University on 07 August 2012

subjected to complete blood count (CBC), peripheral blood smear, measurement of blood bilirubin levels, and osmotic fragility test. Other tests were also performed to exclude other causes of hemolytic anemia, hemoglobinopathies, glucose-6-phosphate dehydrogenase (G6PD) deficiency, and paroxysmal nocturnal hemoglobinuria.

Isolation of red cell membranes and protein extraction

Red cells in whole blood preserved in ethylenediaminetetraacetic acid were isolated by a centrifugation to discard buffy coat and plasma. The packed red cells were washed with PBS three times and the cells were disrupted by hypoosmotic technique using deionized water (dI). After complete cell disruption, membrane fragments, which were unsolubilized in dI, were washed with PBS six times to remove cytoplasmic and hemoglobin, which is the major abundant protein in red cells and might interfere with membrane proteome analysis. The membrane fragments were then washed 3 times with dI to remove excess salts in PBS. In all washing steps, membrane fragments were collected by centrifugation at 10 000 × *g* at 4 °C for 5 min. After the final wash with dI, the membrane fragments were harvested by a centrifugation at 20 000 × *g* at 4 °C for 45 min and dI was discarded. Proteins in the membrane pellet were extracted using a 2-D lysis buffer containing 7 M urea, 2 M thiourea, 4% 3-[(3-cholamidopropyl) dimethylammonio]-1-propanesulfonate (CHAPS), 2% ampholytes pH 3–10, 120 mM dithiothreitol (DTT) and 40 mM Tris-HCl. Protein concentrations in individual samples were measured by the Bradford method using Bio-Rad protein assay (Bio-Rad Laboratories; Hercules, CA).

2-D PAGE and visualization of protein spots

For each 2-D gel, a total of 100 μg proteins derived from red cell membrane fragments of each sample were premixed with a rehydration buffer containing 7 M urea, 2 M thiourea, 2% CHAPS, 120 mM DTT, 40 mM Tris-base, 2% ampholytes (pH 3–10) and a trace amount of bromophenol blue to make the final volume of 150 μL per sample. The mixture was then rehydrated into Immobiline DryStrip (non-linear pH gradient of 3.0–10.0) (GE Healthcare; Uppsala, Sweden) at room temperature for 15 h. The first dimensional separation or isoelectric focusing (IEF) was performed in Ettan IPGphor II IEF System (GE Healthcare) at 20 °C, using a stepwise mode to reach 9083 Vh. Thereafter, the strip was first equilibrated for 15 min in an equilibration buffer containing 6 M urea, 130 mM DTT, 112 mM Tris-base, 4% SDS, 30% glycerol, and 0.002% bromophenol blue, and then in another similar buffer, where DTT was replaced with 135 mM iodoacetamide, for 15 min. The second dimensional separation was performed in 12% polyacrylamide gel using SE260 mini-Vertical Electrophoresis Unit (GE Healthcare) at 150 V for approximately 2 h. The resolved protein spots were then visualized with Deep Purple fluorescence staining (GE Healthcare) and the gel images were taken using Typhoon laser scanner (GE Healthcare). Gel images were captured with an excitation of 532 nm and emission of 610-nm band-pass filter. The photomultiplier tube (PMT) was tuned to 600 V to obtain the resolution at 100 μm pixel size.

Spot matching and quantitative intensity analysis

Image Master 2D Platinum (GE Healthcare) software was used for matching and analysis of protein spots in 2-D gels. Parameters used for spot detection were (i) minimal area = 10 pixels; (ii) smooth factor = 2.0; and (iii) saliency = 2.0. A reference gel used for matching the corresponding protein spots among different gels was created from an artificial gel by combining all of the spots presenting in different gels into one image. Background subtraction was performed and the intensity volume of each spot was normalized with total intensity volume (summation of the intensity volumes obtained from all spots within the same 2-D gel). Significant differences in intensity levels of protein spots were determined by statistical analysis.

In-gel tryptic digestion

All the protein spots whose intensity levels significantly differed between groups were excised from 2-D gels, washed twice with 200 μL of 50% acetonitrile (ACN)/25 mM NH_4HCO_3 buffer (pH 8.0) at room temperature for 15 min, and then washed once with 200 μL of 100% ACN. After washing, the solvent was removed, and the gel pieces were dried by a SpeedVac concentrator (Savant; Holbrook, NY) and rehydrated with 10 μL of 1% (w/v) trypsin (Promega; Madison, WI) in 25 mM NH_4HCO_3. After rehydration, the gel pieces were crushed and incubated at 37 °C for at least 16 h. Peptides were subsequently extracted twice with 50 μL of 50% ACN/5% trifluoroacetic acid (TFA); the extracted solutions were then combined and dried with the SpeedVac concentrator. The peptide pellets were resuspended with 10 μL of 0.1% TFA and purified using $ZipTip_{C18}$ (Millipore; Bedford, MA). The peptide solution was drawn up and down in the $ZipTip_{C18}$ ten times and then washed with 10 μL of 0.1% formic acid by drawing up and expelling the washing solution three times. The peptides were finally eluted with 5 μL of 75% ACN/0.1% formic acid.

Protein identification by Q-TOF MS and MS/MS analyses

The trypsinized samples were premixed 1 : 1 with the matrix solution containing 5 mg mL^{-1} α-cyano-4-hydroxycinnamic acid (CHCA) in 50% ACN, 0.1% (v/v) TFA and 2% (w/v) ammonium citrate, and deposited onto the 96-well MALDI target plate. The samples were analyzed by Q-TOF Ultima™ mass spectrometer (Micromass; Manchester, UK), which was fully automated with a predefined probe motion pattern and the peak intensity threshold for switching over from MS survey scanning to MS/MS, and from one MS/MS to another. Within each sample well, parent ions that met the predefined criteria (any peak within the *m*/*z* 800–3000 range with an intensity above 10 count ± include/exclude list) were selected for CID MS/MS using argon as the collision gas and a mass dependent ±5 V rolling collision energy until the end of the probe pattern was reached. The MS and MS/MS data were extracted and outputted as the searchable *.txt* and *.pkl* files, respectively, for independent searches using the MASCOT search engine (http://www.matrixscience.com) to query the NCBI mammalian protein database, assuming that peptides were monoisotopic. Fixed modification was carbamidomethylation at cysteine residues, whereas variable modification was oxidation

 This journal is © The Royal Society of Chemistry 2012

at methionine residues. Only one missed trypsin cleavage was allowed, and peptide mass tolerances of 100 and 50 ppm were allowed for peptide mass fingerprinting and MS/MS ions search, respectively.

Global protein network analysis

All of the altered proteins were subjected to global protein network analysis using Ingenuity Pathways Analysis (IPA) tool by Ingenuity® Systems (http://www.ingenuity.com) to query each identified protein against other identified proteins and scientific findings curated from the literature relating to genes, cells, diseases, drugs and other biological entities.[8] Finally, relevant network(s) or pathway(s) of interacting proteins are reported.

Western blot analysis

Western blot analysis was performed with 4 HS and 4 normal samples. Red cell membranes were isolated (as aforementioned) and membrane proteins were extracted by 1 × Leammli's buffer. Protein concentrations in individual samples were measured by Bradford's assay. Equal amounts of total proteins were loaded in each lane of 12% SDS-PAGE gel (20 μg/lane). The resolved proteins were then transferred onto a nitrocellulose membrane (Whatman; Dassel, Germany) using Amersham ECL semidry blotter (GE Healthcare) at 85 mA for 1.5 h. Non-specific bindings were blocked with 1% skim milk in PBS at room temperature for 1 h. Thereafter, the membrane was washed three times with PBS before incubating with mouse monoclonal anti-α-tubulin (Santa Cruz biotechnology; Santa Cruz, CA), goat polyclonal anti-TCP-1 (Santa Cruz biotechnology), or rabbit polyclonal anti-carbonic anhydrase II (Chemicon international; Billerica, MA) at a dilution of 1 : 1000 in 1% skimmed milk/PBS at 4 °C overnight. The other three washes were carried out with PBS and the membrane was incubated with corresponding secondary antibodies conjugated with horseradish peroxidase (Dako; Glostrup, Denmark) with a dilution of 1 : 2000 in 1% skimmed milk/PBS at room temperature for 1 h. The immunoreactive protein bands were visualized by SuperSignal West Pico chemiluminescence substrate (Pierce Biotechnology Inc.; Rockford, IL) and autoradiography. Band intensities were quantitated by Image Master densitometer (GE Healthcare).

Statistical analyses

All statistical analyses were performed using SPSS software version 13.0 (SPSS; Chicago, IL). Normal distribution of the intensity data of corresponding protein spots matched across different gels and those of protein bands were examined by Kolmogorov-Smirnov test. Comparisons of these data between the two groups were performed by unpaired Student's *t*-test when the data distributed normally or otherwise by Mann-Whitney non-parametric test. *P* values less than 0.05 were considered statistically significant.

Abbreviations

2-D PAGE	two-dimensional polyacrylamide gel electrophoresis
ACN	acetonitrile
CHAPS	3-[(3-cholamidopropyl) dimethyl-ammonio]-1-propanesulfonate
dI	deionized water
DTT	dithiothreitol
G6PD	glucose-6-phosphate dehydrogenase
HS	hereditary spherocytosis
IEF	isoelectric focusing
IPA	Ingenuity Pathways Analysis
MS	mass spectrometry
MS/MS	tandem mass spectrometry
Q-TOF	quadrupole time-of-flight
TFA	trifluoroacetic acid

Acknowledgements

We are grateful to Prof. Shui-Tein Chen and Dr Supachok Sinchaikul for their technical support on mass spectrometric analyses. This study was financially supported by Research Division, Faculty of Medicine, Srinakarinwirot University (to CP), Office of the Higher Education Commission and Mahidol University under the National Research Universities Initiative, and The Thailand Research Fund (RTA5380005) (to VT). WC is supported by the Royal Golden Jubilee PhD Program of The Thailand Research Fund, whereas VT is also supported by "Chalermphrakiat" Grant, Faculty of Medicine Siriraj Hospital.

References

1 S. Perrotta, P. G. Gallagher and N. Mohandas, *Lancet*, 2008, **372**, 1411–1426.
2 D. E. Discher and P. Carl, *Cell Mol. Biol. Lett.*, 2001, **6**, 593–606.
3 H. M. Van Dort, D. W. Knowles, J. A. Chasis, G. Lee, N. Mohandas and P. S. Low, *J. Biol. Chem.*, 2001, **276**, 46968–46974.
4 M. Mariani, W. Barcellini, C. Vercellati, A. P. Marcello, E. Fermo, P. Pedotti, C. Boschetti and A. Zanella, *Haematologica*, 2008, **93**, 1310–1317.
5 G. Fairbanks, T. L. Steck and D. F. Wallach, *Biochemistry*, 1971, **10**, 2606–2617.
6 P. H. O'Farrell, *J. Biol. Chem.*, 1975, **250**, 4007–4021.
7 J. Klose, *Humangenetik.*, 1975, **26**, 231–243.
8 D. Rajagopalan and P. Agarwal, *Bioinformatics*, 2005, **21**, 788–793.
9 T. H. Lee, S. U. Kim, S. L. Yu, S. H. Kim, D. S. Park, H. B. Moon, S. H. Dho, K. S. Kwon, H. J. Kwon, Y. H. Han, S. Jeong, S. W. Kang, H. S. Shin, K. K. Lee, S. G. Rhee and D. Y. Yu, *Blood*, 2003, **101**, 5033–5038.
10 Y. Iuchi, F. Okada, K. Onuma, T. Onoda, H. Asao, M. Kobayashi and J. Fujii, *Biochem. J.*, 2007, **402**, 219–227.
11 E. M. Pasini, H. U. Lutz, M. Mann and A. W. Thomas, *J. Proteomics*, 2010, **73**, 421–435.
12 H. Ghoti, E. Fibach, M. Dana, S. M. Abu, H. Jeadi, A. Braester, Z. Matas and E. Rachmilewitz, *Ann. Hematol.*, 2011, **90**, 509–513.
13 A. Chesney, D. Good and M. Reis, *Methods Cell Biol.*, 2011, **103**, 311–332.
14 J. Delaunay, *Blood Rev.*, 2007, **21**, 1–20.
15 A. Strunecka, L. Krpejsova, E. Kmonickova, H. Hrusova, H. Jakoubkova, T. Marik and V. Brabec, *Biomed. Biochim. Acta*, 1991, **50**, 93–100.
16 M. Hirosawa, M. Hoshida, M. Ishikawa and T. Toya, *Comput. Appl. Biosci.*, 1993, **9**, 161–167.
17 D. N. Perkins, D. J. Pappin, D. M. Creasy and J. S. Cottrell, *Electrophoresis*, 1999, **20**, 3551–3567.
18 D. B. Weatherly, J. A. Atwood, III, T. A. Minning, C. Cavola, R. L. Tarleton and R. Orlando, *Mol. Cell. Proteomics*, 2005, **4**, 762–772.
19 E. M. Pasini, M. Kirkegaard, P. Mortensen, H. U. Lutz, A. W. Thomas and M. Mann, *Blood*, 2006, **108**, 791–801.
20 E. M. Pasini, H. U. Lutz, M. Mann and A. W. Thomas, *J. Proteomics*, 2010, **73**, 403–420.

Published on 18 May 2012 on http://pubs.rsc.org | doi:10.1039/C2MB25009H
Downloaded by Mahidol University on 07 August 2012

View Online

21 U. Zimny-Arndt, M. Schmid, R. Ackermann and P. R. Jungblut, *Methods Mol. Biol.*, 2009, **492**, 65–91.
22 J. Delaunay, *Acta Haematol.*, 2002, **108**, 210–218.
23 D. G. Kakhniashvili and S. R. Goodman, *Protein Expression Purif.*, 2001, **23**, 249–251.
24 J. S. Hill, W. H. Sawyer, G. J. Howlett and J. S. Wiley, *Biochem. J*, 1982, **201**, 259–266.
25 C. S. Birkenmeier and J. E. Barker, *J. Pathol.*, 2004, **204**, 450–459.
26 S. Rocha, I. Rebelo, E. Costa, C. Catarino, L. Belo, E. M. Castro, J. M. Cabeda, J. Barbot, A. Quintanilha and A. Santos-Silva, *Eur. J. Haematol.*, 2005, **74**, 374–380.
27 L. J. Bruce, *Curr. Opin. Hematol.*, 2008, **15**, 184–190.
28 W. Nunomura and Y. Takakuwa, *Front. Biosci.*, 2006, **11**, 1522–1539.
29 M. Hanspal, J. S. Hanspal, R. Kalraiya, S. C. Liu, K. E. Sahr, D. Howard and J. Palek, *Blood*, 1992, **80**, 530–539.
30 A. J. Baines, P. M. Bennett, E. W. Carter and C. Terracciano, *Blood Cells, Mol., Dis.*, 2009, **42**, 211–215.
31 W. Nunomura, M. Parra, M. Hebiguchi, K. Sawada, N. Mohandas and Y. Takakuwa, *Biochem. J.*, 2009, **417**, 141–148.
32 P. Boivin, *Pathol. Biol. (Paris)*, 1984, **32**, 717–735.
33 W. Diakowski, M. Grzybek and A. F. Sikorski, *Folia Histochem. Cytobiol.*, 2006, **44**, 231–248.
34 W. Nunomura, K. Kinoshita, M. Parra, P. Gascard, X. An, N. Mohandas and Y. Takakuwa, *Biochem. J.*, 2010, **432**, 407–416.
35 L. D. Walensky, Z. T. Shi, S. Blackshaw, A. C. DeVries, G. E. Demas, P. Gascard, R. J. Nelson, J. G. Conboy, E. M. Rubin, S. H. Snyder and N. Mohandas, *Curr. Biol.*, 1998, **8**, 1269–1272.
36 P. G. Gallagher, *Semin. Hematol.*, 2004, **41**, 142–164.

Published on 18 May 2012 on http://pubs.rsc.org | doi:10.1039/C2MB25009H
Downloaded by Mahidol University on 07 August 2012

This journal is © The Royal Society of Chemistry 2012

Nephrol Dial Transplant (2012) 27: 4125–4130
doi: 10.1093/ndt/gfs057
Advance Access publication 29 March 2012

Extensive characterizations of bacteria isolated from catheterized urine and stone matrices in patients with nephrolithiasis

Ratree Tavichakorntrakool[1,2], Vitoon Prasongwattana[3], Seksit Sungkeeree[1,2], Phitsamai Saisud[1,2], Pipat Sribenjalux[1,2], Chaowat Pimratana[4], Sombat Bovornpadungkitti[4,†], Pote Sriboonlue[3] and Visith Thongboonkerd[5,6]

[1]Centre for Research and Development of Medical Diagnostic Laboratories, Faculty of Associated Medical Science, Khon Kaen University, Khon Kaen, Thailand, [2]Department of Clinical Microbiology, Faculty of Associated Medical Science, Khon Kaen University, Khon Kaen, Thailand, [3]Department of Biochemistry, Faculty of Medicine, Khon Kaen University, Khon Kaen, Thailand, [4]Division of Urological Surgery, Khon Kaen Hospital, Khon Kaen, Thailand, [5]Medical Proteomics Unit, Office for Research and Development, Faculty of Medicine Siriraj Hospital, Mahidol University, Bangkok, Thailand and [6]Center for Research in Complex Systems Science, Mahidol University, Bangkok, Thailand

Correspondence and offprint requests to: Visith Thongboonkerd; E-mail: thongboonkerd@dr.com
[†]Posthumous.

Abstract

Background. Urinary tract infections are generally known to be associated with nephrolithiasis, particularly struvite stone, in which the most common microbe found is urea-splitting bacterium, i.e. *Proteus mirabilis*. However, our observation indicated that it might not be the case of stone formers in Thailand. We therefore extensively characterized microorganisms associated with all types of kidney stones.

Methods. A total of 100 kidney stone formers (59 males and 41 females) admitted for elective percutaneous nephrolithotomy were recruited and microorganisms isolated from catheterized urine and cortex and nidus of their stones were analyzed.

Results. From 100 stone formers recruited, 36 cases had a total of 45 bacterial isolates cultivated from their catheterized urine and/or stone matrices. Among these 36 cases, chemical analysis by Fourier-transformed infrared spectroscopy revealed that 8 had the previously classified 'infection-induced stones', whereas the other 28 cases had the previously classified 'metabolic stones'. Calcium oxalate (in either pure or mixed form) was the most common and found in 64 and 75% of the stone formers with and without bacterial isolates, respectively. *Escherichia coli* was the most common bacterium (approximately one-third of all bacterial isolates) found in urine and stone matrices (both nidus and periphery). Linear regression analysis showed significant correlation ($r = 0.860$, $P < 0.001$) between bacterial types in urine and stone matrices. Multidrug resistance was frequently found in these isolated bacteria. Moreover, urea test revealed that only 31% were urea-splitting bacteria, whereas the majority (69%) had negative urea test.

Conclusions. Our data indicate that microorganisms are associated with almost all chemical types of kidney stones and urea-splitting bacteria are not the major causative microorganisms found in urine and stone matrices of the stone formers in Thailand. These data may lead to rethinking and a new roadmap for future research regarding the role of microorganisms in kidney stone formation.

Keywords: antibiotic susceptibility; prevalence; stone matrix; urine; uropathogenic bacteria

Introduction

Kidney stone disease (nephrolithiasis) remains a common public health problem worldwide and is highly prevalent in the northeastern region of Thailand [1–3]. Urinary tract infections (UTIs) are well known to be associated with kidney stone formation [4]. Moreover, antimicrobial resistance has been frequently observed in bacteria isolated from stone formers with UTIs [5]. Although the association between nephrolithiasis and UTIs is generally known and frequently detected, its prevalence, causative microorganisms and their antimicrobial susceptibility patterns remain under-investigated. Previous studies have reported that the most common type of kidney stones caused by UTIs is struvite stone containing magnesium ammonium phosphate and the most common microbe found in struvite stone is urea-splitting bacterium, i.e. *Proteus mirabilis* [6–8]. However, our observation indicated that it might not be the case of stone formers in Thailand. We therefore re-evaluated and extensively characterized microorganisms isolated from urine and stone matrices of patients with all types of kidney stones, chemically analyzed by Fourier-transformed infrared (FTIR) spectroscopy and also examined antimicrobial susceptibility patterns of the isolated bacteria. Moreover, urea and citrate tests were performed to classify these bacteria

© The Author 2012. Published by Oxford University Press on behalf of ERA-EDTA. All rights reserved.
For Permissions, please e-mail: journals.permissions@oup.com

Downloaded from http://ndt.oxfordjournals.org/ at Mahidol University / Library & Information Center on November 14, 2012

into urea-splitting, non-urea-splitting, citrate-utilizing or non-citrate-utilizing group.

Materials and methods

Ethics statement

All the experiments involved human subjects and clinical samples were conducted according to the principles expressed in the Declaration of Helsinki, and written informed consent was provided by the study participants. This study was reviewed and approved by the Institutional Ethical Committee at Khon Kaen University.

Subjects and sample collection

A total of 100 kidney stone formers (59 males and 41 females) with idiopathic etiology admitted to Khon Kaen Hospital for elective kidney stone removal by percutaneous nephrolithotomy because of large stone and/or obstruction were consecutively recruited during 2009–10. All these subjects had no symptoms and signs of UTIs. The exclusion criteria included (i) underlying systemic diseases and secondary causes of nephrolithiasis (e.g. primary hyperparathyroidism, vitamin D excess, hyperthyroidism, renal tubular acidosis, etc.), (ii) active UTIs or other infections within 1 year prior to admission, (iii) history of antibiotic treatment of UTIs within 1 year prior to admission and (iv) no permission from the subjects. In addition, 30 healthy individuals who had no stones (15 males and 15 females) served as the negative controls for urine culture.

Sample preparation, isolation and identification of bacteria

Catheterized urine samples and stones were collected from all subjects. For the catheterized urine, the samples were collected before prophylactic antibiotic treatment routinely used for surgical stone removal. Stone samples were washed several times with deionized water and each stone was then divided into two parts, as symmetrical as possible, by horizontal or sagittal plane. For the first part, stone matrices were taken from 'periphery' (cortex) and 'nidus' (nucleus) portions by scraping. For the second part, the stone was crushed into powder by sterilized mortar and pestle and was then used for bacterial culture and chemical analysis of the 'whole stone'. The catheterized urine samples and all samples derived from three locales of individual stones (including periphery, nidus and whole stone) were then cultivated in blood and MacConkey agar (Oxoid, Hampshire, UK) at 37°C for 24 and 48 h, respectively. Positive bacterial cultures were considered when there were $>1 \times 10^3$ colony forming units/mL urine. Thereafter, all bacterial isolates in urine and stone matrices were identified by standard biochemical tests [9].

Antimicrobial susceptibility test

All bacterial isolates were tested for antimicrobial susceptibility by the disc diffusion assay on Mueller-Hinton agar (Oxoid) and incubated at 37°C for 24 h. The antibiotics used in individual 6-mm discs (Oxoid) included: amikacin (AK, 30 μg); ampicillin (AMP, 10 μg); cephalothin (CF, 30 μg); sulfamethoxazole/trimethoprim (SXT, 1.25/23.75 μg); gentamicin (GM, 10 μg); norfloxacin (NOR, 10 μg); ofloxacin (OFX, 5 μg); cefotaxime (CTX, 30 μg); ceftazidime (CAZ, 30 μg); netilmicin (NET, 30 μg), oxacillin (OX, 1 μg); cefoxitin (FOX, 30 μg); fosfomycin (FOS, 50 μg); fusidic acid (FA, 10 μg), vancomycin (VA, 30 μg); penicillin (P, 10 U); tetracycline (TE, 30 μg); ciprofloxacin (CIP, 5 μg) and tazocin (TZP, 110 μg). Extended-spectrum β-lactamase-producing bacteria (indicating resistance to third-generation cephalosporins) were also determined by double-disc diffusion test, following the standards of Clinical and Laboratory Standards Institute.

Analysis of chemical compositions of stones

The analysis of chemical compositions of each stone was done using stone powder derived from the second part of stone sections (as aforementioned) that was left after bacterial culture. Chemical analysis was performed using FTIR spectroscopy as described previously [10].

Statistical analysis

All the quantitative data are reported as mean ± SEM, unless stated otherwise. Comparisons between the two groups of samples were performed by unpaired *t*-test, whereas correlation between two variables was determined by linear regression analysis using SPSS software (version 11.0; SPSS Corporation, Chicago, IL). P-values <0.05 were considered statistically significant.

Results and discussion

From a total of 100 stone formers, 36 (19 males and 17 females) had bacteria isolated from catheterized urine samples and/or stone matrices, whereas other 64 subjects (40 males and 24 females) had no microorganisms detected. Their demographic and clinical chemistry data are shown in Table 1. Statistical analysis showed no significant differences between stone formers with and without bacterial isolates in their gender, age, urine pH, white blood cell count, blood urea nitrogen, serum creatinine, K^+, Na^+, Cl^- and HCO_3^- levels. Their stone sizes were also comparable (1.15 ± 0.07 versus 1.21± 0.06 in width and 3.56 ± 0.29 versus 3.12 ± 0.20 in length) (Table 1). Urine culture was also performed in 30 healthy normal individuals who had no stones (15 males and 15 females). The results showed negative bacterial culture in the urine of this negative control group.

From 36 stone formers, a total of 45 bacterial isolates were found. Among these, 6 isolates were detected only in urine samples (of 4 stone formers), 18 were found only in stone matrices (of 12 stone formers) and 21 were observed in both urine and stone matrices (of 20 stone formers) (Table 2). The top three most common bacteria

Table 1. Demographic and clinical chemistry data of all stone formers with and without bacterial isolates[a]

Parameters	Stone formers (total $n = 100$)		
	With bacterial isolates ($n = 36$)	Without bacterial isolates ($n = 64$)	P-value
Gender (male:female)	19:17	40:24	NS
Age (years)	50.69 ± 2.20	54.14 ± 1.61	NS
Urine pH	6.22 ± 0.12	6.01 ± 0.10	NS
Blood tests			
WBC (10^3/mm^3)	7.96 ± 0.50	7.63 ± 0.31	NS
BUN (mg/dL)	16.56 ± 1.92	15.96 ± 2.10	NS
Creatinine (mg/dL)	1.38 ± 0.12	1.20 ± 0.07	NS
K (mEq/L)	3.98 ± 0.07	3.94 ± 0.06	NS
Na (mEq/L)	138.85 ± 0.93	139.98 ± 0.43	NS
Cl^- (mEq/L)	106.34 ± 1.33	106.81 ± 1.23	NS
HCO_3^- (mEq/L)	27.10 ± 0.61	26.20 ± 0.37	NS
Stone size			
Width	1.15 ± 0.07	1.21 ± 0.06	NS
Length	3.56 ± 0.29	3.12 ± 0.20	NS

[a]NS, not significant.

Table 2. Source and number of bacterial isolates detected in 36 stone formers

Number \ Source	Detected only in urine	Detected only in stone matrix	Detected in both urine and stone matrix	Total number
Number of cases with bacterial isolates	4	12	20	36
Number of bacterial isolates	6	18	21	45

Downloaded from http://ndt.oxfordjournals.org/ at Mahidol University / Library & Information Center on November 14, 2012

found in urine samples were *Escherichia coli*, *Enterococcus* spp. and *Klebsiella/Enterobacter* spp., respectively, and those found in stone matrices were *E. coli*, *P. mirabilis* and *Klebsiella* spp., respectively (Table 3). Overall, *E. coli* was the most common bacterium found in both urine and stone matrices (approximately one-third of all bacterial isolates). Other bacteria found included *Klebsiellapneumonia*, *Pseudomonas aeruginosa*, *Staphylococcus* coagulase negative, *Citrobacter freundii*, *Acinetobacter baumannii*, *Acinetobacterlwoffii*, *Citrobacter diversus*, *Salmonella* spp. and *Staphylococcus* coagulase positive (Table 3).

Table 3. Types of bacteria isolated from urine and stone matrices

Bacteria	Number of bacterial isolates in urine (%)	Number of bacterial isolates in stone matrices		
		Periphery	Nidus	Whole stone (%)
E. coli	9 (33.33)	13	13	14 (35.90)
Enterococcus spp.	5 (18.52)	2	2	2 (5.13)
Klebsiella spp.	3 (11.11)	2	4	4 (10.26)
Enterobacter spp.	3 (11.11)	1	2	2 (5.13)
Proteus mirabilis	2 (7.41)	5	5	5 (12.82)
Klebsiella pneumoniae	1 (3.70)	2	1	3 (7.69)
Pseudomonas aeruginosa	1 (3.70)	2	2	2 (5.13)
Staphylococcus coagulase negative	1 (3.70)	1	1	1 (2.56)
Citrobacter freundii	1 (3.70)	1	1	1 (2.56)
Acinetobacter baumannii	1 (3.70)	1	1	1 (2.56)
Acinetobacter lwoffii	0 (0.00)	1	1	1 (2.56)
Citrobacter diversus	0 (0.00)	1	1	1 (2.56)
Salmonella spp.	0 (0.00)	1	1	1 (2.56)
Staphylococcus coagulase positive	0 (0.00)	0	1	1 (2.56)
Total	27 (100)	33	36	39 (100)

The association between nephrolithiasis and UTIs can be either (i) kidney stone formation developed following UTIs (the so-called 'infection-induced stones') or (ii) nephrolithiasis with subsequent UTIs as its complications (the so-called 'stones with subsequent infections') [6, 7]. Whether they are infection-induced stones or stones with subsequent infections, the stones themselves are the important source of secondary infection [4]. Therefore, complete eradication of the associated UTIs is possible after the stones have been removed [6, 11]. It has been thought that types of bacteria in the stone nidus implicate the causative microorganisms involved in stone formation and the pathogenesis of 'infection-induced stones', whereas those found in the stone periphery implicate microorganisms entrapped into the stones during secondary UTIs (stones with subsequent infections). The latter should have microorganisms found only in the periphery of stone matrices, not in the stone nidus. Moreover, types of bacteria found in the stone nidus of infection-induced stones should be different from those entrapped recently into the periphery of stones with subsequent infections. In our present study, it is very interesting that types of bacteria found in the stone nidus were almost identical to those found in the stone periphery, as well as the whole stone (Table 3). Moreover, linear regression analysis showed significant correlation ($r = 0.860$, $P < 0.001$) between types of bacteria found in catheterized urine samples and those of stone matrices (Figure 1). Among 20 stone formers who had bacterial isolates in both urine and stone matrices, 19 had exactly the same organisms found in both samples, whereas 1 had different strains of *E. coli* found in urine and stone matrices. These data led to a hypothesis that the microorganisms found in both urine and stone matrices were not the entrapped bacteria from secondary UTIs but were indeed the causative

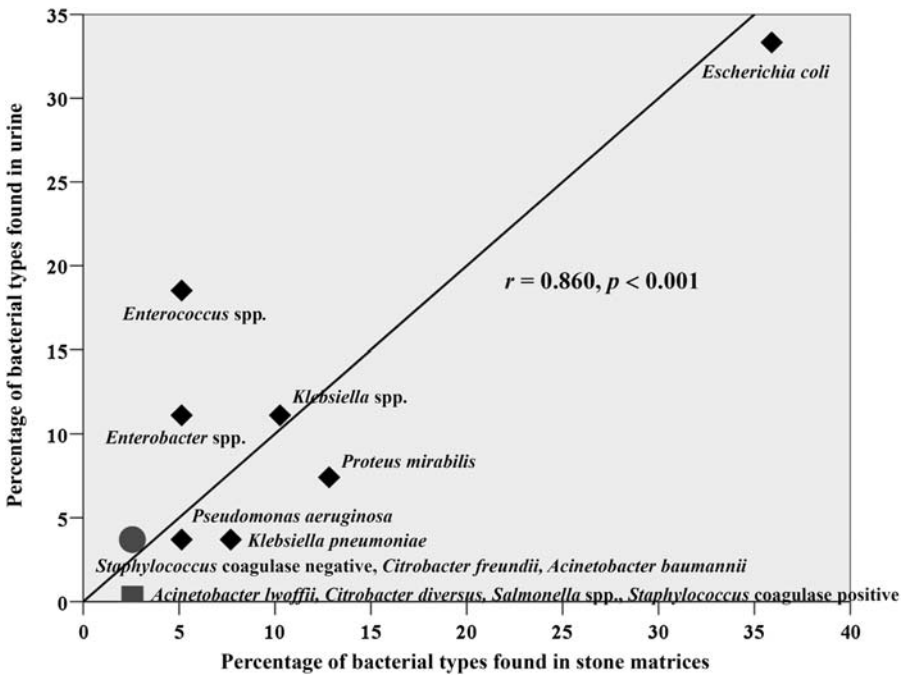


Fig. 1. Linear regression analysis of types of bacteria found in urine and stone matrices.

Downloaded from http://ndt.oxfordjournals.org/ at Mahidol University / Library & Information Center on November 14, 2012

bacteria involved in the stone formation and pathogenesis. The data also implicate that they remained in these samples most likely due to resistance to antibiotics, thus hardly to be eradicated and easily to be further entrapped in the stone periphery.

To address this, antimicrobial susceptibility assay was performed. The data revealed that the bacteria isolated from urine and stone matrices had multidrug resistance, and their antimicrobial resistance patterns are shown in Tables 4 and 5, respectively. From a total of 27 bacterial isolates detected in catheterized urine samples, 19 (~70%) had antimicrobial resistance (mostly to multiple drugs) (Table 4). Similarly, from 39 bacterial isolates detected in stone matrices, 24 (~62%) had antimicrobial resistance (mostly to multiple drugs) (Table 5). This is the first dataset demonstrating the high proportion and patterns of antimicrobial resistance in bacteria isolated from urine and stone matrices of the stone formers.

FTIR spectroscopic analysis revealed that of all 100 stone formers, 15 showed chemical compositions fitted

Table 4. Antimicrobial resistance of 27 bacterial isolates obtained from urine[a]

Bacteria	Antimicrobial resistance										
Enterobacteriaceae	Number	AK (%)	AMP (%)	CF (%)	SXT (%)	GM (%)	NOR (%)	OFX (%)	CTX (%)	CAZ (%)	ESBL producer (%)
E. coli	9	0	67	44	56	22	33	44	22	22	22
Klebsiella spp.	3	33	100	100	67	100	100	100	67	67	0
Enterobacter spp.	3	67	100	100	67	67	67	67	67	67	0
Proteus mirabilis	2	0	0	0	0	0	0	0	0	0	0
Klebsiella pneumoniae	1	0	100	100	0	0	100	100	100	100	100
Citrobacter freundii	1	0	100	100	0	0	0	0	0	0	0
Non-fermentative Gram-negative bacilli	Number	AK (%)	SXT (%)	GM (%)	OFX (%)	CTX (%)	CAZ (%)	NET (%)	TZP (%)		
Pseudomonas aeruginosa	1	100	0	100	100	100	0	100	100		
Acinetobacter baumannii	1	ND	ND	ND	ND	ND	ND	ND	ND		
Enterococcus	Number	AMP (%)	GM (%)	VA (%)	P (%)	TE (%)	CIP (%)				
Enterococcus spp.	5	0	20	0	0	80	40				
Staphylococcus	Number	CF (%)	SXT (%)	GM (%)	OFX (%)	OX (%)	FOX (%)	FOS (%)	FA (%)	VA (%)	
Staphylococcus coagulase negative	1	0	0	0	0	0	0	0	0	0	
Total bacterial isolates in urine	27										

[a]ND, not determined; number, number of bacterial isolates.

Table 5. Antimicrobial resistance of 39 bacterial isolates obtained from stone matrices[a]

Bacteria	Antimicrobial resistance										
Enterobacteriaceae	Number	AK (%)	AMP (%)	CF (%)	SXT (%)	GM (%)	NOR (%)	OFX (%)	CTX (%)	CAZ (%)	ESBL producer (%)
E. coli	14	0	57	36	57	14	21	29	14	14	14
Proteus mirabilis	5	0	20	0	20	0	0	0	0	0	0
Klebsiella spp.	4	0	100	75	50	75	75	75	50	50	0
Klebsiella pneumoniae	3	0	100	67	0	0	33	33	33	33	33
Enterobacter spp.	2	0	100	100	0	0	0	0	50	50	0
Citrobacter freundii	1	0	100	100	0	0	0	0	0	0	0
Citrobacter diversus	1	0	0	100	0	0	0	0	0	0	0
Salmonella spp.	1	0	0	0	0	0	0	0	0	0	0
Non-fermentative Gram-negative bacilli	Number	AK (%)	SXT (%)	GM (%)	OFX (%)	CTX (%)	CAZ (%)	NET (%)	TZP (%)		
Pseudomonas aeruginosa	2	50	50	50	100	50	0	50	50		
Acinetobacter baumannii	1	ND	ND	ND	ND	ND	ND	ND	ND		
Acinetobacter lwoffii	1	0	0	100	100	100	0	100	0		
Enterococcus	Number	AMP (%)	GM (%)	VA (%)	P (%)	TE (%)	CIP (%)				
Enterococcus spp.	2	0	0	0	0	50	0				
Staphylococcus	Number	CF (%)	SXT (%)	GM (%)	OFX (%)	OX (%)	FOX (%)	FOS (%)	FA (%)	VA (%)	
Staphylococcus coagulase negative	1	0	0	0	0	0	0	0	0	0	
Staphylococcus coagulase positive	1	0	0	0	0	0	0	0	0	0	
Total bacterial isolates in stone	39										

[a]ND, not determined; number, number of bacterial isolates.

Downloaded from http://ndt.oxfordjournals.org/ at Mahidol University / Library & Information Center on November 14, 2012

into the previously classified or so-called 'infection-induced stones', whereas the majority (85 cases) had chemical compositions fitted into those previously classified as 'metabolic stones' (Table 6). This proportion remained when compared these two stone groups among the 36 stone formers with positive bacterial isolates. Only eight had chemical compositions fitted into the so-called 'infection-induced stones' and only five were struvite (magnesium ammonium phosphate). Among all chemical compositions, calcium oxalate (in either pure or mixed form) was the most common and found in 64 and 75% of the stone formers with and without bacterial isolates, respectively. Comparing stone formers with versus without bacterial isolates, the three most common chemical compositions found in those with bacterial isolates included calcium oxalate mixed with phosphate, magnesium ammonium phosphate (struvite) and uric acid, whereas the three most common chemical compositions for those without bacterial isolates were calcium oxalate mixed with phosphate, pure calcium oxalate and uric acid (Table 6).

In addition, urea test on the bacteria isolated from 36 stone formers revealed that the majority (25 of 36, ~69%) of microorganisms were non-urea-splitting bacteria, whereas only 31% (11 of 36) were urea-splitting (urease-producing) bacteria (Table 7). For citrate test, the majority (22 of 36, ~61%) of microorganisms were non-citrate-utilizing bacteria, whereas only 39% (14 of 36) were citrate-utilizing bacteria (Table 7).

Our present study indicates that the prevalence of UTIs associated with nephrolithiasis is still high (36%) in the northeastern region of Thailand (Table 1). This prevalence is even higher than that of a recent study done in Baghdad demonstrating that 24.4% of cases had bacterial isolates [5]. There were some contradictory results comparing our present study to the previous Baghdad study [5]. We found that the majority of stone formers who had positive bacterial isolates were males (Table 1), whereas they reported that females had a higher chance to have positive bacterial isolates [5]. Moreover, we also found that urea-splitting bacteria were not the major microorganisms found in our case series (Table 7), whereas they reported 74% of the isolated microorganisms were urea-splitting bacteria [5]. These contradictory results might be due to geographical differences and, more importantly, different pathogenic mechanisms of nephrolithiasis and its association with UTIs.

Table 6. Chemical compositions of all kidney stones ($n = 100$)

	Stone formers with bacterial isolates (from a total of 36)		Stone formers without bacterial isolates (from a total of 64)		Total number (from a total of 100)		
Chemical composition of stone	*N*	%	*N*	%	*N*	%	Stone size (width × length) (cm)
Previously classified as 'infection-induced stones'	8	22.22	7	10.94	15	15	1.55 ± 0.18 × 4.17 ± 0.39
Magnesium ammonium phosphate (Struvite)	5	13.89	4	6.25	9	9	1.24 ± 0.13 × 4.51 ± 0.48
Calcium phosphate/carbapatite	3	8.33	2	3.13	5	5	1.90 ± 0.40 × 3.80 ± 0.80
Calcium phosphate/oxalate/carbapatite	0	0	1	1.56	1	1	2.50 × 3.00
Previously classified as 'metabolic stones'	28	77.78	57	89.06	85	85	1.12 ± 0.04 × 3.12 ± 0.17
Calcium oxalate/phosphate	18	50.00	33	51.56	51	51	1.10 ± 0.06 × 2.88 ± 0.23
Calcium oxalate	2	5.56	13	20.32	15	15	1.12 ± 0.09 × 2.93 ± 0.43
Uric acid	5	13.89	9	14.06	14	14	1.27 ± 0.14 × 4.00 ± 0.40
Calcium oxalate/uric acid	3	8.33	1	1.56	4	4	1.05 ± 0.05 × 3.90 ± 0.49
Calcium phosphate	0	0	1	1.56	1	1	0.70 × 2.80

Table 7. Urea and citrate tests in 36 stone formers with bacterial isolates

	Stone formers with bacterial isolates (total $n = 36$)			
	Urea test		Citrate test	
Chemical composition of stone	Number of urea-splitting bacteria ($n = 11$)	Number of non-urea-splitting bacteria ($n = 25$)	Number of citrate-utilizing bacteria ($n = 14$)	Number of non-citrate-utilizing bacteria ($n = 22$)
Previously classified as 'infection-induced stones' ($n = 8$)	5	3	3	5
Magnesium ammonium phosphate (Struvite) ($n = 5$)	4	1	1	4
Calcium phosphate/carbapatite ($n = 3$)	1	2	2	1
Calcium phosphate/oxalate/carbapatite ($n = 0$)	0	0	0	0
Previously classified as 'metabolic stones' ($n = 28$)	6	22	11	17
Calcium oxalate/phosphate ($n = 18$)	4	14	7	11
Calcium oxalate ($n = 2$)	0	2	0	2
Uric acid ($n = 5$)	1	4	3	2
Calcium oxalate/uric acid ($n = 3$)	1	2	1	2
Calcium phosphate ($n = 0$)	0	0	0	0

Downloaded from http://ndt.oxfordjournals.org/ at Mahidol University / Library & Information Center on November 14, 2012

In the present study, among the 45 bacterial isolates found in 36 stone formers, the most common was *E.coli* found in approximately one-third of all bacterial isolates. *P. mirabilis* was found only in 7.41 and 12.82% of bacteria isolated from urine samples and stone matrices, respectively (Table 3). This data were contradictory to that of the case series in Baghdad [5]. However, the data in our present study were consistent to that previously reported on the case series in southern part of Thailand, in which the two most common agents found in staghorn calculi were *Corynebacterium* spp. and *E.coli*, whereas urease-producing bacteria were found only in 25% [12]. Interestingly, among urease-producing bacteria found in the latter study, only *Klebsiella* spp. and *Pseudomonas* spp. were isolated, whereas *P. mirabilis* was not detected [12].

In addition, hypocitraturia is a major metabolic abnormality found in stone formers in the northeastern part of Thailand [13, 14]. The information on citrate-utilizing bacteria in urine and stone matrices may be another important factor for kidney stone formation in this area. However, the majority of bacterial isolates found in our present study were non-citrate-utilizing bacteria (Table 7). These conflicting results on the citrate assay might implicate that hypocitraturia found in this population is likely due to metabolic causes, not due to citrate-utilizing bacteria.

Nevertheless, limitations of our present study should be noted. First, sizes of all stones obtained in our present study were relatively large (Table 1) (as the patients were recruited from those who were admitted to the hospital for elective kidney stone removal by percutaneous nephrolithotomy). Bacteria found in urine and stone matrices might promote formation and growth of these relatively large stones. On the other hand, these large stones are more susceptible for bacterial colonization. Therefore, extensive investigations of smaller stones are required to address this concern. Second, although all the subjects recruited into this study had no active UTIs or antibiotic treatment of UTIs within 12 months prior to the admission, their precise information and details of infections (particularly UTIs) and antibiotic treatments in the past (>12 months before the admission) are not available. Thus, it is inconclusive in our present study that when and how antibiotic resistance occurred.

In summary, our data indicate that the prevalence of UTIs associated with nephrolithiasis is still high (36%) in the northeastern region of Thailand. In addition, UTIs are frequently associated with almost all chemical types of kidney stones, not only struvite, and *E. coli*, not urea-splitting bacteria, is the most common causative microorganism found in urine and stone matrices of the stone formers in Thailand. Based on their locales in the stone nidus, we hypothesized that the microorganisms found in both urine and stone matrices were not the entrapped bacteria from secondary UTIs but were indeed the causative bacteria involved in the stone formation and pathogenesis. These bacteria remained in the urine most likely due to multidrug resistance, thus hardly to be eradicated and easily to be further entrapped in the stone periphery. However, further extensive investigations of smaller stones and elucidations of the effects of microbes on stone formation and growth are crucial. These data may lead to rethinking and a new roadmap for future research regarding the causative role of microorganisms in kidney stone formation.

Acknowledgements. We wish to express our deep appreciation to all the subjects for providing the invaluable clinical specimens. We also thank Drs Mitree Pakarasung and Titima Srilunchang for their suggestions and are grateful to Sunthon Suwanatrai, Piyanat Pitakwong and Thanaporn Keawsing for their technical assistance. This study was supported by The Thailand Research Fund (R.T. is a New TRF-CHE Research Scholar #MRG5380061, whereas V.T. is a Senior TRF Research Scholar #RTA5380005), Office of the Higher Education Commission and Mahidol University under the National Research Universities Initiative (to V.T.). V. T. is also supported by 'Chalermphrakiat' Grant, Faculty of Medicine Siriraj Hospital. The funders had no role in study design, data collection and analysis, decision to publish or preparation of the manuscript.

Conflict of interest statement. None declared.

(See related article by Borghi *et al*. Nephrolithiasis and urinary tract infections: 'the chicken or the egg' dilemma? *Nephrol Dial Transplant* 2012; 27: 3982–3985.)

References

1. Nimmannit S, Malasit P, Susaengrat W *et al*. Prevalence of endemic distal renal tubular acidosis and renal stone in the northeast of Thailand *Nephron* 1996; 72: 604–610
2. Tungsanga K, Sriboonlue P, Borwornpadungkitti S *et al*. Urinary acidification in renal stone patients from northeastern Thailand *J Urol* 1992; 147: 325–328
3. Sriboonlue P, Prasongwatana V, Chata K *et al*. Prevalence of upper urinary tract stone disease in a rural community of north-eastern Thailand *Br J Urol* 1992; 69: 240–244
4. Zanetti G, Paparella S, Trinchieri A *et al*. Infections and urolithiasis: current clinical evidence in prophylaxis and antibiotic therapy *Arch Ital Urol Androl* 2008; 80: 5–12
5. Qaader DS, Yousif SY, Mahdi LK. Prevalence and etiology of urinary stones in hospitalized patients in Baghdad *East Mediterr Health J* 2006; 12: 853–861
6. Miano R, Germani S, Vespasiani G. Stones and urinary tract infections *Urol Int* 2007; 79 Suppl 132–36
7. Griffith DP. Infection-induced renal calculi *Kidney Int* 1982; 21: 422–430
8. McLean RJ, Nickel JC, Noakes VC *et al*. An in vitro ultrastructural study of infectious kidney stone genesis *Infect Immun* 1985; 49: 805–811
9. Garrity GM, Brenner DJ, Krieg NR *et al.Bergey's Manual of Systematic Bacteriology* 2005New York, NYSpringer1–1108
10. Sriboonlue P, Chaichitwanichakul W, Pariyawongsakul P. Types and composition of urinary stones in 4 community hospitals *J Natl Res Council Thailand* 1993; 25: 1–8
11. Dogan HS, Guliyev F, Cetinkaya YS *et al*. Importance of microbiological evaluation in management of infectious complications following percutaneous nephrolithotomy *Int Urol Nephrol* 2007; 39: 737–742
12. Tanthanuch M. Staghorn calculi in southern Thailand *J Med Assoc Thai* 2006; 89: 2086–2090
13. Sriboonlue P, Prasongwattana V, Tungsanga K *et al*. Blood and urinary aggregator and inhibitor composition in controls and renal-stone patients from northeastern Thailand *Nephron* 1991; 59: 591–596
14. Reungjui S, Prasongwatana V, Premgamone A *et al*. Magnesium status of patients with renal stones and its effect on urinary citrate excretion *BJU Int* 2002; 90: 635–639

Received for publication: 10.5.2011; Accepted in revised form: 5.2.2012

Downloaded from http://ndt.oxfordjournals.org/ at Mahidol University / Library & Information Center on November 14, 2012

DOI 10.1002/prca.201270035 *Proteomics Clin. Appl.* 2012, *6*, 340–342

Commentary

The variability in tissue proteomics

Visith Thongboonkerd

Medical Proteomics Unit, Office for Research and Development, Faculty of Medicine Siriraj Hospital, and Center for Research in Complex Systems Science, Mahidol University, Bangkok, Thailand

Variability is one of the most critical issues of concern in clinical proteomics. In this issue of *Proteomics Clinical Applications*, Yoshida et al. [*Proteomics Clin. Appl.* 2012, *6*, 412–417] describe the effects of blood and number of washes on the human glomerular proteome isolated from the kidney by laser microdissection. The blood-derived proteins occupied almost 50% of all the identified proteins in the unwashed samples, whereas varying the number of washes (from 1–5) with PBS yielded only 43–80% of the proteins identified in each sample that were common in all samples. This urges caution to all proteomists to carefully consider sample preservation and preparation for tissue proteome analysis.

Keywords:
EuroKUP / Glomerulus / HKUPP / Kidney / Urine / Variability

Issues of biological and technical variabilities have been discussed in the proteomics community for quite some time [1, 2]. In addition, pre-analytical variability (from collection, initial sample treatment, preservation, fixation, storage, etc.) in clinical proteomics studies has been communicated more widely in recent years [3–5]. However, there are several aspects that still require further elucidation. Moreover, some causes of these variabilities are difficult to manage and it remains unclear whether they should be prevented or clarified at the initial collection phase, in the middle, or at the final analytical phase of proteomic analysis. A Technical Brief article published in this issue of *Proteomics Clinical Applications* by Yoshida et al. [6] from Niigata University, a key group of the Human Kidney and Urine Proteome Project (HKUPP) [7, 8], is a great example for discussion on this as yet unsolved issue of variability.

The kidney is one of the vital organs that regulate normal homeostasis and is considered as one of the most sophisticated tissues. There are several intrarenal macro- and microstructures, including cortex, medulla, vessels, pelvis, nephrons, etc. The nephron is the most crucial intrarenal functional unit responsible for both excretory and secretory functions of the kidney. A nephron and related microstructures include glomerulus, afferent/efferent arterioles, Bowman's capsule, proximal convoluted tubule, cortical collecting duct, distal convoluted tubule, Henle's loop, Bellini's duct, peritubular capillaries, arcuate artery/vein, and Juxtaglomerular apparatus. Each glomerulus comprises glomerular capillary tufts, Bowman's capsule/space, afferent/efferent arterioles, endothelial cells, mesangial cells, podocytes and glomerular basement membranes, as well as the related Juxtaglomerular cells. The end product of the excretory function of the nephron is urine, which is a valuable biological sample for clinical proteomics, particularly for biomarker discovery. Based on my own experience and personal communications with colleagues from HKUPP [7, 8], European Network for Kidney and Urine Proteomics (EuroKUP) [9, 10] and other kidney/urine proteomics labs, the biological variability of kidney-derived samples is ranged in the following order (cell lines < isolated primary cells < isolated intrarenal microstructures < whole kidney < urine). In addition to inter-individual variability, the urine also has a high degree of intra-individual variability due to diurnal variation of urinary protein excretion within a day [2, 11]. Moreover, physiological changes and dietary/water intake dramatically affect the urinary proteome [2, 11]. The kidney-derived cell and tissue proteomes have less problems with intra-individual variability, while contamination of blood-derived proteins (from

Correspondence: Professor Visith Thongboonkerd, Head of Medical Proteomics Unit and Director of Center for Research in Complex Systems Science (CRCSS), Siriraj Hospital, Mahidol University, 6th Floor – SiMR Building, 2 Prannok Road, Bangkoknoi, Bangkok 10700, Thailand
E-mail: thongboonkerd@dr.com
Fax: +66-2-4195503

© 2012 WILEY-VCH Verlag GmbH & Co. KGaA, Weinheim

plasma/serum, red blood cells, leukocytes, platelets, and microparticles) is of greater concern.

It is advisable to discriminate the source of blood-derived proteins (e.g. albumin, hemoglobin subunits, globulins, etc.) that can easily interfere with cell/tissue proteome analyses. The blood-derived proteins can originate from bleeding during surgical procedures and also from intraorgan vessels and capillaries. The latter is not a problem for proteomic analysis of organs without sophisticated microstructures enriched with capillaries, and simple washing of the tissue can completely eliminate the blood contamination from bleeding during surgical procedures. However, this is not the case for the kidney, particular glomerulus, of which glomerular tufts enriched with capillary loops can harbor a considerable amount of blood. Simple washing is not as effective as for other organs. Sectioning the kidney into thin slices is usually required to eliminate blood from the tissue.

In this issue of *Proteomics Clinical Applications*, Yoshida et al. [6] describe the effects of blood as well as number of washes on the human glomerular proteome isolated from the kidney by laser microdissection. The data were obtained from four replicates of each sample using an information-based-acquisition (IBA) technique to reduce redundant identifications by high-throughput mass spectrometry [12]. Although technical variability could not be entirely excluded, the variability found was most likely from blood-derived proteins and varying the number of washes. Without washing, albumin and hemoglobin subunits occupied almost 50% of all the identified proteins (Fig. 1 in [6]). Washing the microdissected glomeruli with PBS 1–5 times resulted in a marked reduction in the abundance of blood-derived proteins. Nevertheless, blood-derived proteins could not be completely eliminated even after 5 washes with PBS (Fig. 2C and Supporting Information in [6]).

While most of the blood-derived proteins could be eliminated, increasing the number of washes was associated with an increase in abundance of integral membrane, cytoskeletal and extracellular matrix proteins. Interestingly, a degree of depletion of some hydrophilic proteins was observed. As a result, only 43–80% of the proteins identified in each sample were found common in all individual samples with different numbers of washes (Fig. 2B in [6]). Theoretically, washing with isotonic and neutral solutions such as PBS should not affect much on the cellular and tissue proteomes. However, in practice, this really can affect protein compositions in cells and tissues. My laboratory has also observed the same phenomenon as seen in the study by Yoshida and colleagues [6], indicating that the washing step, even with an isotonic and neutral solution such as PBS, is really a matter to concern. This could be simply explained that multiple washing steps might eliminate (dissolve) some of the hydrophilic proteins (most likely the extracellular proteins or those presented in the interstitial space), while the highly hydrophobic proteins remained.

The critical issues that should be further elucidated are "what?" "when?" and "how?" to eliminate both the contaminated blood from bleeding and the blood harboring inside capillary loops within the tissue. Definitely, a simple wash should be done immediately after surgical procedures to eliminate blood contamination originating from bleeding. However, it is still inconclusive as to what would be the most appropriate method (e.g. extensive intravascular flushing vs. washing the tissue slices) and when would be the most suitable time (e.g. before vs. after tissue storage) to eliminate blood harboring inside capillary loops within the tissue. A systematic analysis is required to address these issues of concern to define the most effective and practical method that can maximally eliminate blood-derived proteins but can, on the other hand, efficiently preserve the cell and tissue proteomes. This issue should be further elucidated not only by proteomists in HKUPP and EuroKUP networks, but also by all proteomists who deal with tissue proteomics of other organs.

The author is supported by Office of the Higher Education Commission and Mahidol University under the National Research Universities Initiative, The Thailand Research Fund (RTA5380005), and the "Chalermphrakiat" Grant, Faculty of Medicine Siriraj Hospital.

The author has declared no conflict of interest.

References

[1] Zech, H., Echtermeyer, C., Wohlbrand, L., Blasius, B. et al., Biological versus technical variability in 2-D DIGE experiments with environmental bacteria. *Proteomics* 2011, *11*, 3380–3389.

[2] Nagaraj, N., Mann, M., Quantitative analysis of the intra- and inter-individual variability of the normal urinary proteome. *J Proteome. Res.* 2011, *10*, 637–645.

[3] Espina, V., Mueller, C., Edmiston, K., Sciro, M. et al., Tissue is alive: New technologies are needed to address the problems of protein biomarker pre-analytical variability. *Proteomics Clin. Appl.* 2009, *3*, 874–882.

[4] Jackson, D. H., Banks, R. E., Banking of clinical samples for proteomic biomarker studies: a consideration of logistical issues with a focus on pre-analytical variation. *Proteomics Clin. Appl.* 2010, *4*, 250–270.

[5] Espina, V., Mueller, C., Reduction of preanalytical variability in specimen procurement for molecular profiling. *Methods Mol. Biol.* 2012, *823*, 49–57.

[6] Yoshida, Y., Nameta, M., Kuwano, M., Zhang, Y. et al., Proteomic approach to human kidney glomerulus prepared by laser microdissection from frozen biopsy specimens: Exploration of proteome after removal of blood-derived proteins. *Proteomics Clin. Appl.* 2012, *6*, 412–417.

[7] Yamamoto, T., Langham, R. G., Ronco, P., Knepper, M. A. et al., Towards standard protocols and guidelines for urine proteomics: A report on the Human Kidney and Urine Proteome Project (HKUPP) Symposium and Workshop 6 October 2007, Seoul, Korea and 1 November 2007, San Francisco, CA, USA. *Proteomics* 2008, *8*, 2156–2159.

© 2012 WILEY-VCH Verlag GmbH & Co. KGaA, Weinheim

[8] Yamamoto, T., The 4th Human Kidney and Urine Proteome Project (HKUPP) workshop. 26 September 2009, Toronto, Canada. *Proteomics* 2010, *10*, 2069–2070.

[9] Vlahou, A., Charonis, A., Benigni, A., Report on the first combined working group and management committee meeting of EuroKUP (Urine and Kidney Proteomics cost action). *J. Proteomics* 2009, *71*, 682–684.

[10] Vlahou, A., Allmaier, G., Attwood, T., Bongcam-Rudloff, E. et al., 2nd Combined Working Group and Management Committee Meeting of Urine and Kidney Proteomics COST Action 29–30 March 2009, Nafplio, Greece. *Proteomics Clin. Appl.* 2009, *3*, 1017–1022.

[11] Thongboonkerd, V., Chutipongtanate, S., Kanlaya, R., Systematic evaluation of sample preparation methods for gel-based human urinary proteomics: quantity, quality, and variability. *J. Proteome. Res.* 2006, *5*, 183–191.

[12] Yokosuka, T., Yoshinari, K., Kobayashi, K., Ohtake, A. et al., 'Information-Based-Acquisition' (IBA) technique with an ion-trap/time-of-flight mass spectrometer for high-throughput and reliable protein profiling. *Rapid Commun. Mass Spectrom.* 2006, *20*, 2589–2595.

© 2012 WILEY-VCH Verlag GmbH & Co. KGaA, Weinheim

Talanta 101 (2012) 240–245

Contents lists available at SciVerse ScienceDirect

Talanta

journal homepage: www.elsevier.com/locate/talanta

A novel assay to evaluate promoting effects of proteins on calcium oxalate crystal invasion through extracellular matrix based on plasminogen/plasmin activity

Wararat Chiangjong, Visith Thongboonkerd *

Medical Proteomics Unit, Office for Research and Development, Faculty of Medicine Siriraj Hospital, and Center for Research in Complex Systems Science, Mahidol University, Bangkok, Thailand

ARTICLE INFO

Article history:
Received 9 August 2012
Received in revised form
12 September 2012
Accepted 13 September 2012
Available online 19 September 2012

Keywords:
Calcium oxalate
Crystal invasion
Kidney stone
Matrix gel
Plasmin
Plasminogen

ABSTRACT

One of the important processes in kidney stone development is crystal invasion through extracellular matrix (ECM). Some proteins in renal tissue or urine have been thought to aggravate crystal invasion. However, this pathogenic mechanism has been previously under-investigated due to a lack of crystal invasion assay. In the present study, we have developed a novel assay for the investigations of calcium oxalate monohydrate (COM) crystal invasion. Matrix gel was loaded into an in-house migration chamber made on a glass slide to simulate the ECM environment. COM crystals were coated with the tested protein, which was then bound with plasminogen. The crystal-protein-(plasminogen) complex and urokinase plasminogen activator (uPA) were placed on-top of the matrix gel. If the tested protein had plasminogen-binding capability, the remaining plasminogen would be activated by uPA to plasmin, which caused crystal migration through the matrix gel. We then applied this novel assay to evaluate effects of some abundant kidney/urine proteins (including purified albumin, carbonic anhydrase, lysozyme and Tamm–Horsfall protein) on COM crystal invasion. The data revealed that albumin, which is the known plasminogen-binding protein, dramatically induced plasmin activity and crystal invasion, whereas other proteins had no significant effects as compared to the control. In summary, we have successfully developed a novel assay for the investigations of crystal invasion based on the plasminogen/plasmin system. This assay is applicable to examine proteins that may serve as potential aggravators of crystal invasion and thus will be very useful for further studies on kidney stone development.

© 2012 Elsevier B.V. All rights reserved.

1. Introduction

Calcium oxalate monohydrate (COM) is a major crystalline compound to form kidney stones [1]. Important mechanisms of COM kidney stone formation include crystal growth, adhesion, aggregation and invasion [2,3]. Recent lines of evidence have demonstrated that the deposited crystals can migrate between intracellular and intercellular compartments, and finally translocate into renal interstitium, leading to activation of immune response and accumulation of inflammatory cells (i.e., monocytes and macrophages) [4]. However, the detailed process of crystal invasion through extracellular matrix (ECM) into the renal interstitium remained unclear, while recruitment of the inflammatory cells into this locale has been extensively studied in many disease models [5–7]. This pathogenic mechanism has been previously under-investigated due to a lack of crystal invasion assay.

Plasminogen/plasmin is a well-known system that regulates innate and adaptive immune responses, coagulation/thrombolysis by fibrin and fibrin degradation products, and extracellular proteolysis [8,9]. Plasminogen is primarily synthesized and secreted by hepatocytes and other cells in kidney, adrenal glands, brain, testis, heart, lungs, uterus, spleen, thymus, and intestines [10,11]. Urokinase plasminogen activator (uPA) was initially found in human urine and can convert plasminogen to plasmin, which can degrade fibrin and ECM components [12,13]. Activation of plasminogen on the cell surface can promote fibrinolysis, cell migration and prohormone processing on various cells [13–16]. The cells, which bind to plasminogen, also express cell-surface plasminogen activator receptor. The co-localization of plasminogen and its activator receptor can promote plasminogen activation [17]. For example, monocyte/macrophage cell surface that presents plasminogen receptor can bind to plasminogen, which is then converted to plasmin by plasminogen activation cascade [14,15].

* Corresponding author. Tel.: +66 2 4195500; fax: +66 2 4195503.
E-mail addresses: thongboonkerd@dr.com, vthongbo@yahoo.com (V. Thongboonkerd).

0039-9140/$ - see front matter © 2012 Elsevier B.V. All rights reserved.
http://dx.doi.org/10.1016/j.talanta.2012.09.019

Unlike monocytes/macrophages and other cells, COM crystals have no plasminogen receptor on their surfaces. However, the crystals are able to invade into ECM. Actually, COM crystals can bind to a number of various kidney/urine proteins [18,19]. We thus hypothesized that these proteins, on the other hand, are able to bind to plasminogen that is also present in kidney/urine. Plasminogen is then converted by uPA to plasmin, which subsequently degrades ECM component, thereby crystal invasion. In the present study, we have developed a novel assay for the investigations of proteins that might be involved in COM crystal invasion based on the reaction of uPA to activate plasminogen to plasmin. We then applied this novel assay to evaluate effects of some abundant kidney/urine proteins (including purified albumin, carbonic anhydrase, lysozyme and Tamm–Horsfall protein) on COM crystal invasion.

2. Materials and methods

2.1. COM crystal preparation

The stock solutions of 10 mM calcium chloride and 1 mM sodium oxalate were prepared in a buffer containing 90 mM Tris–HCl (pH 7.4) and 10 mM NaCl. The two solutions were gently mixed (1:1) and then incubated at room temperature (RT) overnight. The mixture was centrifuged at 12,000 rpm at 25 °C for 5 min and then COM crystal pellet was collected. The harvested COM crystals were washed with absolute methanol three times and were then dried at 37 °C overnight. Typical COM crystal morphology was observed under a light microscope before use.

2.2. Preparation of a migration chamber containing matrix gel

Materials for making a migration chamber included glass slide (Sail Boat Lab Co., Ltd.; Zhejiang, China), Menzel–Glaser cover slip (Glasbearbeitungswerk GmbH; Braunschweig, Germany), used X-ray film (Kodak, Carestream Health, Inc.; Rochester, NY), two-sided adhesive tape (Siam Armstrong Co., Ltd.; Bangkok, Thailand) and sealing material used for slide mounting (e.g., nail polish) (Fig. 1A). The methods for making a migration chamber are detailed in Fig. 1B. First, the used X-ray film was cut into U-shape (approximately to a size of the cover slip) and then cleaned with 70% alcohol. Three pieces of the U-shape X-ray film were adhered together by two-sided adhesive tape strips. Actually, the number of the U-shape X-ray film, which was used as a spacer, could be modified based on the desired thickness of the matrix gel inside the migration chamber. This spacer was then adhered to a glass slide and, on the other side, to a cover slip using two-sided adhesive tape strips. This chamber was then sealed with nail polish and was decontaminated by UV irradiation for 30 min before use. BD Matrigel™ Basement Membrane Matrix (BD Bioscience; Franklin Lakes, NJ) (containing collagen types I–VI, laminin, fibronectin, osteopontin, and vitronectin) was dissolved in a pre-chilled Eagle's minimum essential medium (MEM) (Gibco; Grand Island, NY) on ice to make 4.5–6 mg/ml final working solution of the matrix gel. Approximately 200 μl of the matrix gel was added into the migration chamber and left at 37 °C for at least 4 h (Fig. 1B).

2.3. COM crystal-protein binding assay and SDS-PAGE

COM crystals (5 mg) were incubated with 1 μg of each of the proteins to be tested in 1 ml of PBS. These tested proteins included purified bovine serum albumin (BSA), carbonic anhydrase (Sigma), lysozyme (Sigma), and Tamm–Horsfall protein (all were from Sigma; St. Louis, MO). The crystal–protein mixture was gently and continuously rotated at 4 °C overnight. The mixture was then centrifuged at 15,000 rpm and 4 °C for 5 min, and the supernatant was discarded. The pellet was extensively washed with PBS three times, 4 mM EDTA three times, and again with PBS three times using high-speed vortex (to make sure that weak or non-specific bindings were completely eliminated). The bound protein was eluted by 1 X Laemmli's buffer, resolved in 12% SDS-PAGE gel using SE260 mini-Vertical Electrophoresis Unit (GE Healthcare; Uppsala, Sweden) at 150 V for approximately 2 h, and then stained with Deep Purple fluorescence dye (GE Healthcare). The gel image was captured by a Typhoon laser

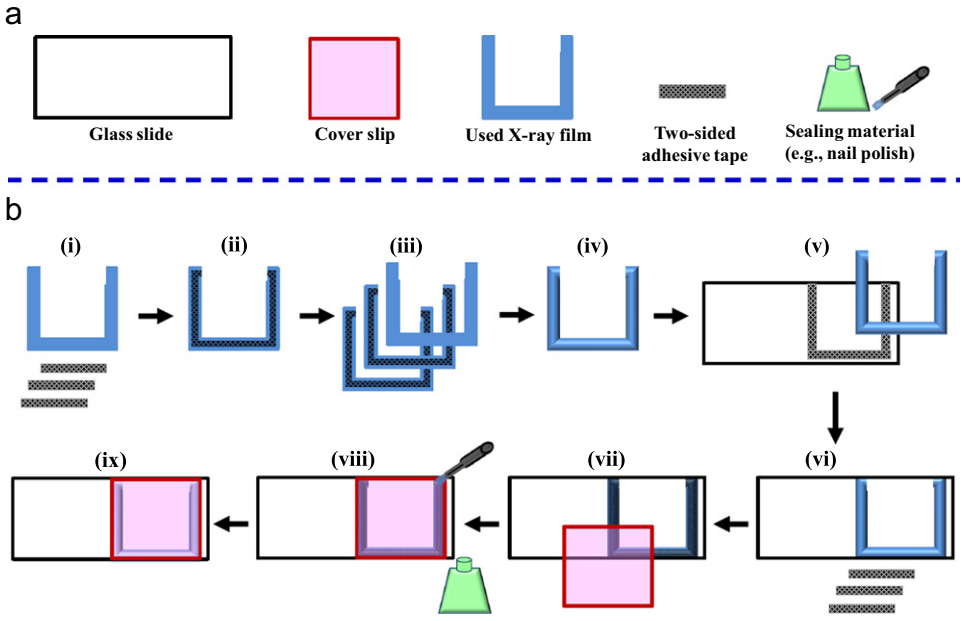


Fig. 1. Preparation of a migration chamber containing matrix gel. All the materials used for making the migration chamber are indicated in panel (A), whereas stepwise methods are detailed in panel (B). (i) The used X-ray film was cut into U-shape (approximately to a size of a cover slip), whereas two-sided adhesive tape was cut into strips. (ii) U-shape X-ray film was adhered with two-sided adhesive tape strips. (iii)–(iv) Three pieces of the U-shape X-ray film were adhered together by two-sided adhesive tape strips to make a spacer. (v) The U-shape spacer was then adhered to a glass slide. (vi)–(vii) A cover slip was adhered on the U-shape spacer using two-sided adhesive tape strips. (viii) This chamber was then sealed with a sealing material (e.g., nail polish). (ix) The migration chamber was then dried and decontaminated by UV irradiation before use.

scanner (GE Healthcare). Intensity of bands appeared in each whole lane was quantitated by Image Master densitometer (GE Healthcare).

2.4. Plasmin activity assay

One microgram of a protein (BSA, carbonic anhydrase, lysozyme, or Tamm–Horsfall protein) in 100 μl of 50 mM $NaHCO_3$ was coated onto each of 96-well plate at 4 °C overnight. Thereafter, the uncoated protein was removed and the well was washed with PBS three times. Thereafter, 200 μl of 6 nM Lys-plasminogen (Fitzgerald Industries International; Acton, MA) in PBS was added into the well and was further incubated at 37 °C for 4 h. The unbound plasminogen was discarded and the well was washed with PBS five times. Thereafter, 200 μl of 1 nM uPA (Fitzgerald Industries International) in PBS and 0.15 mM chromogenic substrate S-2251 (Chromogenix, Instrumentation Laboratory Company; Lexington, MA) were added and incubated with the samples at 37 °C for 24 h. The control was decided using only 100 μl of 50 mM $NaHCO_3$ to coat the well without protein, but with the presence of plasminogen, uPA and chromogenic substrate at later steps. The absorbance of each sample at 0 h and 24-h post-incubation with uPA was measured at λ405 nm using Anthos HTII Microplate Reader (Anthos Labtec Instruments; Salzburg, Austria). The plasmin activity was obtained by subtracting the 24 h absorbance with that of 0 h absorbance of each individual sample.

2.5. COM crystal invasion assay

A total of 20 μg COM crystals was added into 200 μl of MEM. Then, 1 μg of the tested protein (BSA, carbonic anhydrase, lysozyme, or Tamm–Horsfall protein) was added and the mixture was incubated at 4 °C overnight with gently continuous agitation (Fig. 2A). The unbound protein was discarded by a centrifugation at 15,000 rpm and 4 °C for 5 min, and the crystal-protein complex was washed with PBS. Thereafter, 200 μl of 0.3 pM Lys-plasminogen in PBS was mixed and incubated with the crystal-protein complex at 37 °C for 1 h (Fig. 2B). The unbound plasminogen was discarded by a centrifugation at 15,000 rpm for 5 min and the pellet was washed with PBS once. Then, 100 μl of 0.15 pM uPA in PBS was mixed with the crystal-protein-(plasminogen) complex (Fig. 2C) (Note: If the tested protein had plasminogen-binding capability, the remaining plasminogen would be activated by uPA to plasmin, which caused crystal migration. In contrast, if the tested protein did not bind to plasminogen, there would not be plasmin as the final product.). The mixture was then added on-top of the matrix gel inside the migration chamber and incubated at 37 °C for 24 h (Fig. 2D). After 24 h incubation, the solution remained on the upper part of the migration chamber was removed by absorption using a gauze or tissue paper. The invaded COM crystals inside the matrix gel were then imaged using a light microscope with differential interference contrast (DIC) mode (Nikon H600L, Nikon Corp.; Tokyo, Japan) (Fig. 2D). The crystal invasion distance was measured and averaged from at least 50 crystals/field in 15 different fields within the same chamber using Image Frame Work software version 0.9.6 (Tarosoft®; Nonthaburi, Thailand). For the control, COM crystals were processed as aforementioned without binding protein, but with the presence of plasminogen and uPA at later steps.

2.6. Statistical analysis

All the experiments were performed in triplicate independently. The quantitative data are reported as mean ± SEM. Statistical analysis was performed using unpaired Student's *t*-test to compare plasmin activity and COM crystal invasion to the controls. P values less than 0.05 were considered statistically significant.

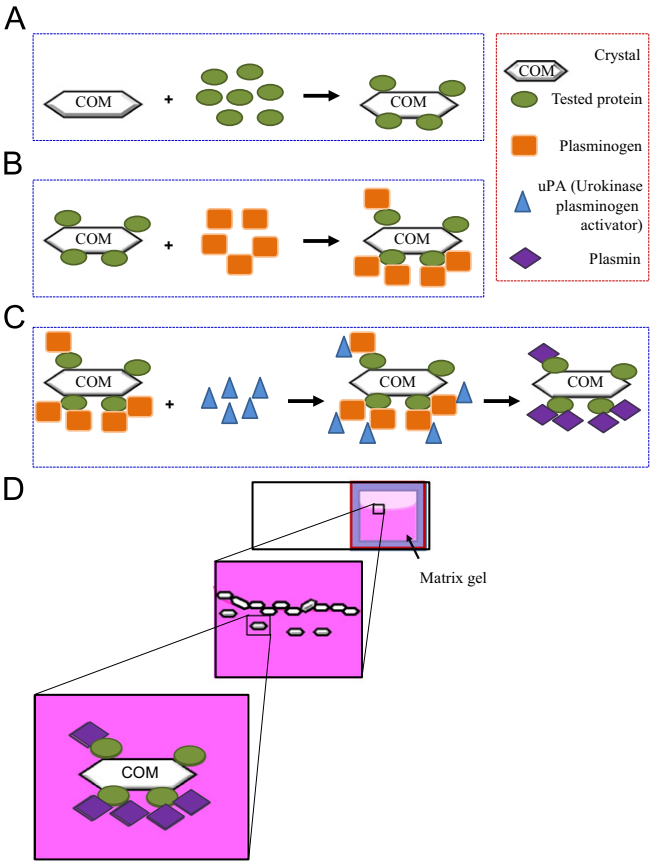


Fig. 2. Methodology of COM crystal invasion assay. (A) *Step 1* COM crystals were incubated with a tested protein at 4 °C overnight. (B) *Step 2* Lys-plasminogen was incubated with the crystal-protein complex at 37 °C for 1 h. (C) *Step 3* uPA in PBS was mixed with the crystal-protein-(plasminogen) complex. If the tested protein had plasminogen-binding capability, the remaining plasminogen would be activated by uPA to plasmin, which caused crystal migration. In contrast, if the tested protein did not bind to plasminogen, there would not be plasmin as the final product. (D) *Step 4* The mixture of crystal-protein-(plasminogen) complex and uPA was added on-top of the matrix gel inside the migration chamber and incubated at 37 °C for 24 h. The invaded COM crystals inside the matrix gel were then imaged using a light microscope with differential interference contrast (DIC) mode.

3. Results and discussion

Multi-step process of intratubular kidney stone formation is initiated with supersaturation of calcium and oxalate ions, followed by crystal nucleation, crystal growth and aggregation [20]. Additionally, the crystals can be internalized into the cells by endocytosis and then migrate through basement membrane and ECM [21,22]. In another theory of kidney stone development, the stone is initiated primarily in the tubulointerstitial compartment with the well-known Randall's plaque formation [23]. The plague is essential to develop the stone, particularly at the basement membrane of the thin Henle's loop [24]. Both intratubular and interstitial pathogenic mechanisms of kidney stone disease have the common crucial processes required for the stone development, including crystal retention, crystal invasion, and tissue inflammation [25]. While crystal retention and tissue inflammation have been extensively investigated in association with kidney stone disease, crystal invasion has been previously under-investigated because there was no available tool or assay to address such important pathogenic mechanism.

In the present study, we aimed to (i) develop a novel assay to investigate COM crystal invasion; and (ii) apply such novel assay to evaluate effects of some abundant kidney/urine proteins on COM crystal invasion. We first made an in-house migration chamber by using common materials and reagents available in almost all life-science laboratories (Fig. 1A). These included common glass slide for microscopy, cover slip, used X-ray film, two-sided adhesive tape, and sealing material used for slide mounting (e.g., nail polish). Stepwise methodology for making the migration chamber is detailed in Section 2 (Fig. 1**B**). Thereafter, the matrix gel (containing collagen types I–VI, laminin, fibronectin, osteopontin, and vitronectin) was added into this chamber. Crystal-protein-(plasminogen) complex was prepared as detailed step-by-step in Section 2 (see also Fig. 2). It should be noted that this crystal invasion assay is based on plasminogen/plasmin system. If the tested protein had plasminogen-binding capability, the remaining plasminogen would be activated by uPA to plasmin, which caused crystal migration. In contrast, if the tested protein did not bind to plasminogen, there would not be plasmin as the final product and the crystals could not migrate (Fig. 2).

We then confirmed that all the tested proteins, which are abundant kidney/urine proteins, could bind to COM crystals (in *Step 1* of the COM crystal invasion assay described in Fig. 2A) for reasonable application in subsequent COM crystal invasion assay. The data obtained from COM crystal-protein binding assay and SDS-PAGE using equal amount of each purified protein confirmed that all the tested proteins, including purified albumin, carbonic anhydrase, lysozyme, and Tamm–Horsfall protein were bound to the crystals, as demonstrated by their bands at respective sizes (Fig. 3A). To determine relative amounts of all proteins bound to COM crystals, intensity of protein bands appeared in each whole lane was measured. The data showed that albumin, carbonic anhydrase, and lysozyme had comparable relative amount of the bound fraction, whereas Tamm–Horsfall protein had the greatest amount of the bound fraction (Fig. 3B).

To also confirm that *Steps 2 and 3* of the COM crystal invasion assay (as described in Fig. 2B,C) worked well, plasmin activity was measured in individual samples. This experiment was also to prove that once the protein was bound to the crystals, if it had a plasminogen-binding capability, plasminogen would remain in the crystal-protein-(plasminogen) complex and thus could be activated by uPA to plasmin. Plasmin could then cut the chromogenic substrate (H-D-Val-Leu-Lys-pNA) to amino acid residues (H-D-Val-Leu-Lys) and chromophore (pNA), which presented the yellow color that was measurable at λ405 nm. The data confirmed that some the COM crystal-binding proteins (i.e., albumin) could retain plasminogen in the crystal-protein-(plasminogen) complex and thus could activate the plasmin activity, whereas other COM crystal-binding proteins had no effects on plasmin activity (Fig. 4). This data was in agreement with the findings reported previously that albumin serves as a carrier protein for plasminogen and thus could bind to plasminogen for subsequent activation to plasmin [26,27]. It should be noted that the plasmin activity was obtained by subtracting the absorbance of the sample at 24 h post-incubation with uPA to that of 0 h. Unlike other conventional enzymatic assays, e.g. ELISA, in which non-specific bindings (or another word, bindings of proteins onto the plate surface) are

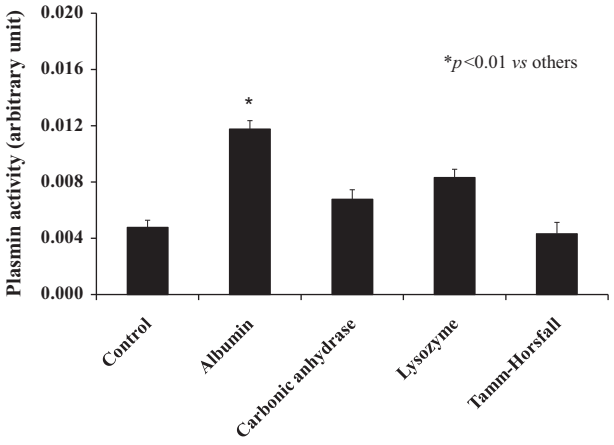


Fig. 4. An assay to confirm that plasminogen could bind to a specific plasminogen-binding protein. The tested protein (purified albumin, carbonic anhydrase, lysozyme, or Tamm–Horsfall protein) was coated onto each of 96-well plate at 4 °C overnight, whereas the controlled well was incubated with 100 μl of 50 mM $NaHCO_3$ without protein. After washing, Lys-plasminogen was added into the well and was further incubated at 37 °C for 4 h. After the final wash, uPA and chromogenic substrate S-2251 were then incubated with the samples at 37 °C for 24 h. The plasmin activity was measured at λ405 nm using a microplate reader. Each bar was derived from three independent experiments and the data are reported as mean ± SEM. $^*p < 0.01$ compared to other groups.

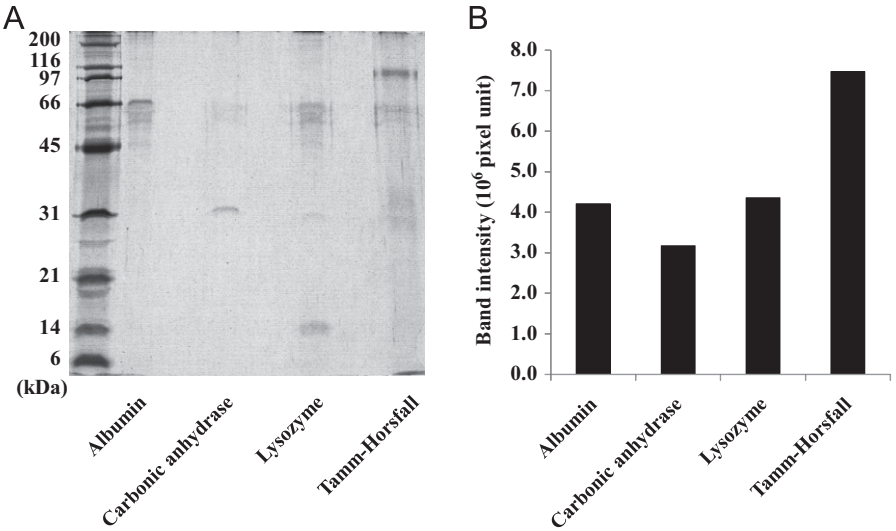


Fig. 3. SDS-PAGE to confirm that the tested protein was bound to COM crystals. COM crystals were incubated with purified albumin (BSA), carbonic anhydrase, lysozyme, or Tamm–Horsfall protein at 4 °C overnight. The bound protein was then eluted by 1 X Laemmli's buffer, resolved in 12% SDS-PAGE gel, and stained with Deep Purple fluorescence dye (A). Intensity of bands appeared in each whole lane was then quantitated using a densitometer (B).

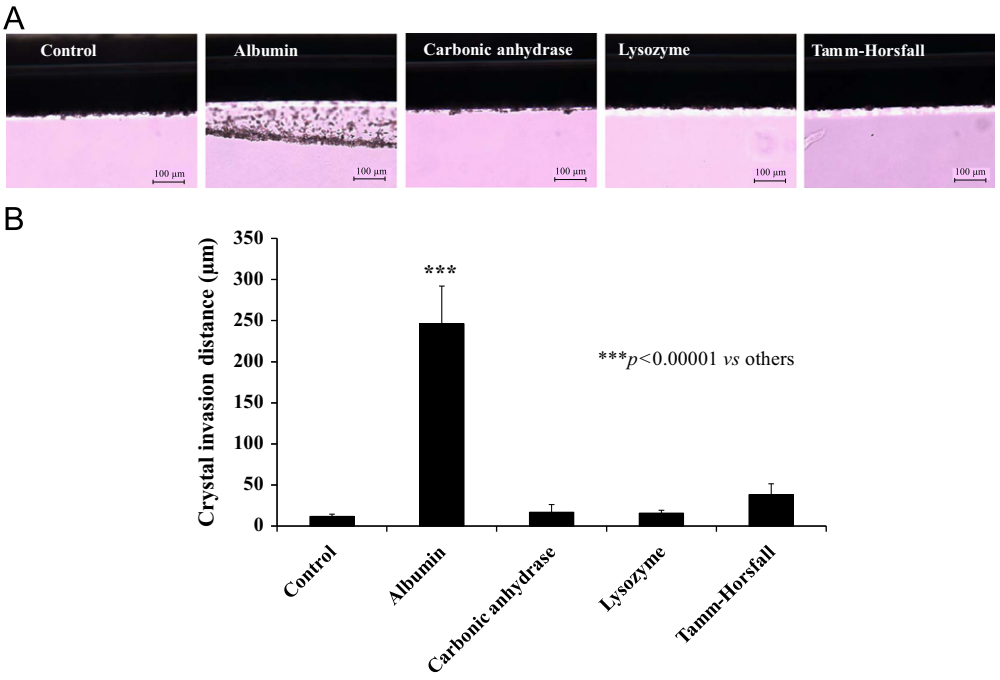


Fig. 5. COM crystal invasion assay to evaluate effects of proteins on crystal invasion. The assay was performed as detailed in Figs. 1 and 2 (A) At the end, the micrographs of the invaded crystals were obtained from individual assays to examine the tested proteins. The bar indicates 100 μm scale. (B) The crystal invasion distance was measured and averaged from at least 50 crystals/field in 15 different fields within the same chamber. For the control, COM crystals were processed as aforementioned in the presence of plasminogen and uPA, but without a binding protein on the crystal surface. Each bar was derived from three independent experiments and the data are reported as mean ± SEM. $^{***}p < 0.00001$ compared to other groups.

normally blocked by BSA in the blocking step, the present study omitted such blocking step to avoid the interference from the blocking protein (BSA) to the plasmin activity. Without any blocking, plasminogen could also bind to the plate surface non-specifically. Therefore, the control sample without any tested protein (but with plasminogen, uPA, and chromogenic substrate) revealed a background of plasminogen activity. In contrast to the other proteins that had comparable background plasmin activity as compared to the control, albumin provided significantly greater plasmin activity (Fig. 4).

The crystal-protein-(plasminogen) complex together with uPA (which was originally found in the urine and also ECM of the kidney) was then used for subsequent COM crystal invasion assay. The crystal invasion data (Fig. 5) were consistent to those of plasmin activity shown in Fig. 4. The findings demonstrated that only the crystals bound with albumin, which was the only protein that could induce plasmin activity, caused the crystal invasion, whereas other proteins had no significant effects as compared to the control (Fig. 5). Considering the relative amounts of individual proteins bound to the crystals (Fig. 3), the selectivity of albumin for induction of COM crystal invasion could be highlighted. Whereas Tamm–Horsfall protein had the greatest amount of the bound fraction and carbonic anhydrase and lysozyme had comparable relative amount of the bound fraction as compared to albumin, none of them showed significant induction of COM crystal invasion.

In summary, we have successfully developed an in vitro assay for the investigations of COM crystal invasion, based on the reaction of plasminogen and uPA, which can activate plasminogen to plasmin that causes crystal invasion through ECM. This novel assay is also applicable to examine the proteins of interest to search for the potential protein modulators that serve as the activators of COM crystal invasion. Thus, it will be very useful for further studies on kidney stone development.

Acknowledgments

We are grateful to Dr. Sakdithep Chaiyarit for his technical assistance. This study was supported by Office of the Higher Education Commission and Mahidol University under the National Research Universities Initiative, The Thailand Research Fund (RTA5380005), and Faculty of Medicine Siriraj Hospital. WC is supported by the Royal Golden Jubilee PhD Program, whereas VT is also supported by the "Chalermphrakiat" Grant, Faculty of Medicine Siriraj Hospital.

References

[1] G. Schubert, Urol. Res. 34 (2006) 146–150.
[2] S.R. Khan, K.J. Byer, S. Thamilselvan, R.L. Hackett, W.T. McCormack, N.A. Benson, K.L. Vaughn, G.W. Erdos, J. Am. Soc. Nephrol. 10 (Suppl 14) (1999) S457–S463.
[3] C.F. Verkoelen, A. Verhulst, Kidney Int. 72 (2007) 13–18.
[4] R. de Water, C. Noordermeer, T.H. van der Kwast, H. Nizze, E.R. Boeve, D.J. Kok, F.H. Schroder, Am. J. Kidney Dis. 33 (1999) 761–771.
[5] M.D. Boyle, R. Lottenberg, Methods 21 (2000) 99–102.
[6] G. Al Atrash, R.P. Kitson, Y. Xue, A.P. Mazar, M.H. Kim, R.H. Goldfarb, Anticancer Res. 21 (2001) 1697–1704.
[7] K. Lahteenmaki, P. Kuusela, T.K. Korhonen, FEMS Microbiol. Rev. 25 (2001) 531–552.
[8] M. Del Rosso, F. Margheri, S. Serrati, A. Chilla, A. Laurenzana, G. Fibbi, Curr. Pharm. Des. 17 (2011) 1924–1943.
[9] C.P. Ponting, J.M. Marshall, S.A. Cederholm-Williams, Blood Coagul. Fibrinolysis 3 (1992) 605–614.
[10] F.J. Castellino, V.A. Ploplis, Thromb. Haemost. 93 (2005) 647–654.
[11] L. Zhang, D. Seiffert, B.J. Fowler, G.R. Jenkins, T.C. Thinnes, D.J. Loskutoff, R.J. Parmer, L.A. Miles, Thromb. Haemost. 87 (2002) 493–501.
[12] M.V. Carriero, M.P. Stoppelli, Curr. Pharm. Des. 17 (2011) 1944–1961.
[13] B. Fuhrman, Atherosclerosis 222 (2012) 8–14.
[14] K.D. Phipps, A.P. Surette, P.A. O'Connell, D.M. Waisman, Cancer Res. 71 (2011) 6676–6683.
[15] E.F. Plow, R. Das, Blood 113 (2009) 5371–5372.
[16] L.A. Miles, F.J. Castellino, Y. Gong, Trends Cardiovasc. Med. 13 (2003) 21–30.
[17] J. Felez, L.A. Miles, P. Fabregas, M. Jardi, E.F. Plow, R.H. Lijnen, Thromb. Haemost. 76 (1996) 577–584.
[18] R. Selvam, P. Kalaiselvi, Urol. Res. 31 (2003) 242–256.

[19] K. Fong-ngern, P. Peerapen, S. Sinchaikul, S.T. Chen, V. Thongboonkerd, J. Proteome. Res. 10 (2011) 4463–4477.
[20] S. Hamamoto, K. Taguchi, Y. Fujii, Clin. Calcium 21 (2011) 1481–1487.
[21] J.C. Lieske, H. Swift, T. Martin, B. Patterson, F.G. Toback, Proc. Natl. Acad. Sci. U. S. A. 91 (1994) 6987–6991.
[22] M.S. Schepers, R.A. Duim, M. Asselman, J.C. Romijn, F.H. Schroder, C.F. Verkoelen, Kidney Int. 64 (2003) 493–500.
[23] A.P. Evan, J.E. Lingeman, F.L. Coe, J.H. Parks, S.B. Bledsoe, Y. Shao, A.J. Sommer, R.F. Paterson, R.L. Kuo, M. Grynpas, J. Clin. Invest. 111 (2003) 607–616.
[24] A.P. Evan, J.E. Lingeman, F.L. Coe, E.M. Worcester, Semin. Nephrol. 28 (2008) 111–119.
[25] M. Asselman, C.F. Verkoelen, Curr. Opin. Urol. 12 (2002) 271–276.
[26] N. Behrendt, K. Dano, FEBS Lett. 393 (1996) 31–36.
[27] N. Behrendt, M. Ploug, E. Ronne, G. Hoyer-Hansen, K. Dano, Methods Enzymol. 223 (1993) 207–222.

Author's personal copy

Talanta 98 (2012) 123–129

Contents lists available at SciVerse ScienceDirect

Talanta

journal homepage: www.elsevier.com/locate/talanta

Systematic comparisons of various spectrophotometric and colorimetric methods to measure concentrations of protein, peptide and amino acid: Detectable limits, linear dynamic ranges, interferences, practicality and unit costs

Somchai Chutipongtanate [a,b,1], Kamolwan Watcharatanyatip [a,b,1], Teerada Homvises [a,b], Kewalee Jaturongkakul [a,b], Visith Thongboonkerd [a,b,*]

[a] Medical Proteomics Unit, Office for Research and Development, Faculty of Medicine Siriraj Hospital, Mahidol University, Bangkok, Thailand
[b] Center for Research in Complex Systems Science, Mahidol University, Bangkok, Thailand

ARTICLE INFO

Article history:
Received 4 April 2012
Received in revised form
20 June 2012
Accepted 21 June 2012
Available online 30 June 2012

Keywords:
BCA
Biuret
Bradford
Lowry
Ninhydrin
Protein assay

ABSTRACT

There is limited and inconclusive information regarding detectable limits and linear dynamic ranges of various quantitative protein assays. We thus performed systematic comparisons of seven commonly used methods, including direct spectrophotometric quantitation at λ205 and λ280 nm (A205 and A280, respectively), bicinchoninic acid (BCA), Biuret, Bradford, Lowry and Ninhydrin methods. Purified BSA, porcine kidney extract, tryptic digested peptides derived from purified BSA, and glycine, were used as representative purified protein, complex protein mixture, peptide and amino acid, respectively. Bradford method was the most sensitive assay (LOD=0.006 mg/ml) and had the widest range of detectability (LOD–UOD=0.006–100 mg/ml) for purified protein and complex protein mixture. For peptide, A205, A280, Lowry and Ninhydrin methods had a comparable LOD (0.006 mg/ml), but Ninhydrin method had the widest detectability range (LOD–UOD=0.006–100 mg/ml). For amino acid, A205 and Ninhydrin methods had a comparable LOD (0.006 mg/ml), but A205 had a wider detectability range (LOD–UOD=0.006–6.250 mg/ml). Biuret method offered the widest linear dynamic range for purified protein and complex protein mixture (0.391–100 mg/ml), A280 offered the widest linear dynamic range for peptide (0.024–6.250 mg/ml), and Ninhydrin method offered the widest linear dynamic range for amino acid (0.024–0.195 mg/ml). Both Laemmli's and 2-D lysis buffers had dramatic interfering effects on all assays. Concerning the practicality and unit costs, A205 and A280 were the most favorable. Among the colorimetric methods, Bradford method consumed the least amount of samples and shortest analytical time with the lowest unit cost. These are the most extensive comparative data of commonly used quantitative protein assays that will be useful for selecting the most suitable method for each study.

© 2012 Elsevier B.V. All rights reserved.

1. Introduction

Quantitative protein assay is one of the essential methodologies in protein research and life sciences [1]. It is used in a prerequisite step prior to subsequent protein analysis, e.g. gel electrophoresis, proteomic analysis, Western blot analysis, ELISA, enzyme kinetic study, etc. Many assays have been established and are widely used in protein research and life sciences. Commonly used assays to measure protein concentrations in the samples include direct spectrophotometric quantitation at λ205 and λ280 nm (A205 and A280, respectively), bicinchoninic acid (BCA), Biuret, Bradford, Lowry and Ninhydrin methods [2–4]. Selection of these quantitative protein assays is usually based on compatibility of these methods with the samples to be analyzed [1,3]. One of the most important factors for such selection is the estimated range of concentrations and interfering substances contained in the samples. As such, Biuret assay is the method of choice for the samples with high protein concentrations (5–160 mg/ml), while BCA, Bradford and Lowry methods are more suitable for the samples with low protein concentrations (1–2000 μg/ml) [3]. The samples containing reducing agents or copper chelating reagents are frequently measured by Bradford method, whereas those containing detergents are better measured by BCA assay [3]. Occasionally, additional steps

* Correspondence to: Siriraj Hospital, Mahidol University, 12th Floor Adulyadej Vikrom Building, 2 Prannok Road, Bangkoknoi, Bangkok 10700, Thailand. Tel./fax: +66 2 4184793.
E-mail addresses: thongboonkerd@dr.com, vthongbo@yahoo.com (V. Thongboonkerd).
[1] Equal contributions by these authors.

0039-9140/$ - see front matter © 2012 Elsevier B.V. All rights reserved.
http://dx.doi.org/10.1016/j.talanta.2012.06.058

Author's personal copy

to dilute or pretreat the samples (e.g. dialysis, precipitation) to reduce effects of interfering substances prior to measuring protein concentrations may be required [5].

Previously, there were some attempts to compare various quantitative protein assays aiming to define the most suitable one for various applications [6–13]. Due to the disparate results among these previous studies [6–13], it is inconclusive that which one is the most suitable quantitative protein assay for general applications. It seems that each assay has some advantages for certain applications but, on the other hand, exhibits some disadvantages for other applications [6–13]. Moreover, there is limited information on the detectable limits and linear dynamic ranges of the individual methods. Therefore, extensive comparisons of the commonly used quantitative protein assays in a systematic manner are crucially required to address this issue.

The present study aimed to systematically compare detectable limits and linear dynamic ranges of seven commonly used quantitative protein assays, including A205, A280, BCA, Biuret, Bradford, Lowry and Ninhydrin methods. Purified bovine serum albumin (BSA), porcine kidney extract, tryptic digested peptides derived from purified BSA, and glycine with 2-fold serial concentrations (ranging from 0.006 to 100 mg/ml) were used as representative purified protein, complex protein mixture, peptide, and amino acid, respectively. The examined parameters included lower limit of detection (LOD), upper limit of detection (UOD), range of linearity and % interference by Laemmli's and 2-D lysis buffers, which are the most commonly used lysis buffers in biochemical and proteomic studies, respectively. In addition, practicality (concerning the sample consumption or the amount of sample that must be discarded and could not be recovered after the assay, number of pipetting/reaction, and estimated time consumed) and approximated unit costs were also compared.

2. Materials and methods

2.1. Sample preparation

BSA (Sigma-Aldrich Corp.; St. Louis, MO), porcine kidney protein extract, tryptic digested peptides derived from purified BSA, and purified L-glycine (Sigma-Aldrich Corp.) were used as the representatives of purified protein, complex protein mixture, peptide, and amino acid, respectively.

For complex protein mixture, dry powder of porcine kidney extract was prepared from a porcine kidney bought from a local fresh poultry market. Briefly, a cube of porcine kidney tissue (approximately 1 g) was chopped to several small pieces and washed several times with ice-cold phosphate buffered saline (PBS). The sample was then brisky frozen by liquid nitrogen and ground into powder using pre-chilled mortar and pestle. Proteins were extracted from the tissue powder using a lysis buffer containing 7 M urea, 2 M thiourea, 4% CHAPS (3[(3cholamidopropyl) dimethyl-ammonio]-1-propanesulfonate), 120 mM DTT, and 40 mM Tris-base. The extracted protein solution was dialyzed against deionized (dI) (18.2 MΩ cm) water (1000 ml × 4 changes for 24 h) through cellulose dialysis tubing membranes with a molecular weight cut off of 6000–8000 Da (Spectrum Laboratories; Rancho Dominguez, CA) to remove compositions of the lysis buffer and to retain only porcine kidney proteins in the solution. Kidney proteins were then dried using a lyophilizer (ModulyoD-230, Thermo Fisher Scientific; Waltham, MA).

For peptide, 1 g purified BSA (Sigma-Aldrich Corp.) was dissolved in 100 ml Tris–HCl buffer (pH 8.0) and incubated with 5 ml of 200 mM DTT at room temperature (RT) for 1 h. The sample was subsequently incubated with 20 ml of 200 mM iodoacetamide at RT for 1 h and then with 20 mg trypsin (Invitrogen; Grand Island, NY) at 37 °C for 16 h. The tryptic digested peptides were then dried using the ModulyoD-230 lyophilizer (Thermo Fisher Scientific).

For all samples, dry weight, one of the gold standard methods for measuring protein amount [14], was used for preparing the sample solutions at a concentration of 100 mg/ml in dI water. These samples were then serially (2-fold) diluted in dI water, resulting to 15 sample concentrations ranging from 0.006 to 100 mg/ml.

3. Quantitative protein assays

All following measurements were performed in triplicate and dI water was used as the blank control.

3.1. Direct spectrophotometric quantitation at λ205 and λ280 nm (A205 and A280)

A205 and A280 methods were the simple direct spectrophotometric measurements of absorbance of peptide bonds at λ205 nm and aromatic amino acids, cystine and disulfide bonds of cysteine residues at λ280 nm, respectively [2]. Briefly, 1 ml of each sample was added into a 1 ml quartz cuvette, which was then placed into a UV–visible spectrophotometer (Shimadzu; Kyoto, Japan). Absorbance of the sample was then read at λ205 and λ280 nm, respectively.

3.2. BCA method

BCA assay combines the reduction of Cu^{2+} to Cu^{1+} by peptide bonds of the protein in an alkaline solution with the selective colorimetric reaction of BCA–Cu^{1+} to form purple complex, which is strongly absorbed at λ562 nm [15]. BCA assay was performed according to the manufacturer's protocol. Briefly, 100 µl of samples was added into 2 ml of BCA working reagent (catalog #PI23227, Pierce Biotechnology; Rockford, IL), which contains BCA reagents A and B (50:1). The reaction mixture was incubated at 37 °C for 30 min in a water bath. Subsequently, the reaction mixture was cooled at RT and the absorbance was measured at λ562 nm using a UV–visible spectrophotometer (Shimadzu).

3.3. Biuret method

Biuret assay is based on the reaction of cupric ions to peptide bonds of protein under alkaline condition. This reaction changes blue color of the solution to purple [16]. Biuret assay was performed according to the manufacturer's protocol. Briefly, 20 µl of each sample was mixed with 1 ml of Biuret reagent (catalog #T1949, Sigma-Aldrich Corp.) and further incubated at RT for 10 min. The absorbance of the mixture was measured at λ540 nm using a UV–visible spectrophotometer (Shimadzu).

3.4. Bradford method

Bradford assay measures proteins by their binding capacities to Coomassie Brilliant Blue (CBB) to form a protein-dye complex. This interaction shifts the peak absorbance of the dye from λ465 nm to λ595 nm, resulting to change of the solution color from red-brown to blue [17]. The procedure was performed as described previously [17] using Bio-Rad protein microassay (catalog #500-0006, Bio-Rad Laboratories; Hercules, CA). Briefly, 2 µl of each sample was mixed with 798 µl of dI water. The solution was then incubated with 200 µl of Bradford reagent at RT for 5 min. The absorbance of the mixture was measured at λ595 nm using a UV–visible spectrophotometer (Shimadzu).

Author's personal copy

3.5. Lowry method

The principle of Lowry assay is similar to that of Biuret assay, but Lowry assay includes folin-phenol reagent into the reaction to enhance the sensitivity of the Biuret reaction [18]. Modified Lowry assay (catalog #TP0200, Sigma-Aldrich Corp.) was employed in this study. The procedure was performed according to the manufacturer's protocol. Briefly, 200 μl of each sample was added into 2.2 ml of reagent A (Biuret reagent) and further incubated for 10 min at RT. Thereafter, 100 μl of reagent B (folin and Ciocalteau's phenol reagent) was added into the reaction mixture and further incubated at RT for 30 min. The absorbance of the mixture was measured at λ550 nm using a UV–visible spectrophotometer (Shimadzu).

3.6. Ninhydrin method

Ninhydrin assay measures protein concentration based on the amount of amino acid residues. This principle involves the reaction between free amino group with 1,2,3-indantoin monohydrate (ninhydrin), resulting to a complex product with Ruhemann's purple color, which has the peak absorbance at λ570 nm. Briefly, the samples were hydrolyzed at 100 °C overnight using 6 N HCl to completely breakdown the intact proteins into amino acid residues. Thereafter, 2 ml of each hydrolyzed sample was mixed with 2 ml of ninhydrin working reagent containing 0.5 g of ninhydrin (ACS grade) (catalog #151173-10G, Sigma-Aldrich Corp.) in 30 ml of isopropanol and 20 ml of 0.1 M acetate buffer (pH 5.5). The reaction solution was incubated in boiling water bath for 15 min, cooled at RT and then added with 3 ml of 50% ethanol. The absorbance of the mixture was measured at λ570 nm using a UV–visible spectrophotometer (Shimadzu).

4. Lower limit of detection (LOD) and upper limit of detection (UOD)

The absorbance values obtained from each method were plotted against the concentrations (0.006–100 mg/ml) of each sample to determine LOD and UOD of each method for individual samples. LOD was defined as the lowest concentration of which absorbance could be distinguished from that of the blank control (dI water) with significant p value (<0.05), whereas UOD was defined as the highest concentration that still had significant difference in its absorbance as compared to the adjacent lower concentration. As such, UOD was the first concentration that formed the plateau phase of the dose-response curve. All LOD and UOD values reported in the "Results" section were derived from average values of triplicate sets of data obtained from three independent sets of experiments.

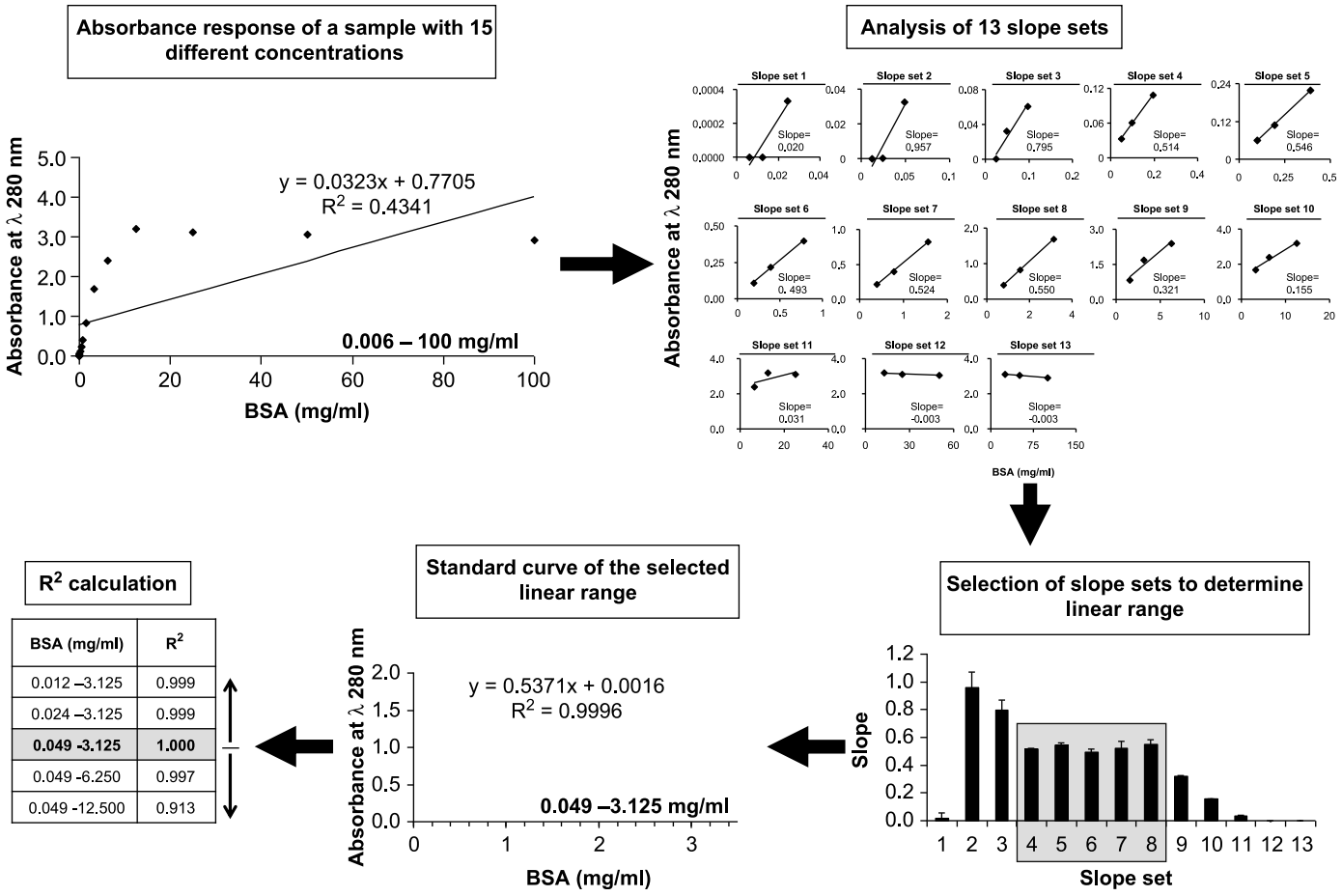


Fig. 1. Schematic diagram to summarize workflow to determine the linear dynamic ranges of quantitative assays used for measurement of protein, peptide and amino acid concentrations in the samples (BSA was used as an example). Initially, screening of the linear dynamic range of each assay for individual samples was performed using 15 of 2-fold concentrations (from 0.006 to 100 mg/ml) of individual samples. A total of 13 slope sets were generated using 3-consecutive concentrations for each slope set. Multiple comparisons among all these 13 slope sets were performed and the two or more consecutive slope sets, which had no statistically significant differences, were highlighted and selected. All the concentrations within the selected consecutive slope sets were then used to establish a standard curve. To validate the linearity of the selected consecutive slope sets, coefficient of determination (R^2) of this range was compared to those of the other extended ranges of concentrations (which extended to include 2 higher or 2 lower concentrations from the selected linear range). It would be expected that R^2 of the selected linear range was greatest (and closed to 1.000).

Author's personal copy

5. Linear dynamic range

Initially, screening of the linear dynamic range of each assay for individual samples was performed using all 15 (2-fold) concentrations (from 0.006 to 100 mg/ml) of individual samples. Three consecutive concentrations were used for determining a slope of linear curve. This resulted to a total of 13 slope sets generated from all 15 concentrations (Fig. 1). Multiple comparisons among all these 13 slope sets were performed (as detailed in "Statistical Analysis") and the two or more consecutive slope sets, which had no statistically significant differences, were highlighted and selected. All concentrations within the selected consecutive slope sets were then used to establish a standard curve. To validate the linearity of the selected consecutive slope sets, coefficient of determination (R^2) of this range was compared to those of the other extended ranges of concentrations (which extended to include 2 higher or 2 lower concentrations from the selected linear range) (Fig. 1). It would be expected that R^2 of the selected linear range was greatest (and closed to 1.000).

6. Interference by Laemmli's and 2-D lysis buffers

Interfering effects of Laemmli's and 2-D lysis buffers on each quantitative protein assay for individual samples were determined using the average concentrations of these samples within the linear dynamic range of each assay (as detailed above). In this set of experiments, dry BSA, porcine kidney protein extract (prepared as aforementioned), tryptic digested peptides derived from purified BSA (prepared as aforementioned), and purified L-glycine were resuspended in Laemmli's buffer (2% SDS, 10% glycerol, 5% β-mercaptoethanol, 0.01% bromophenol blue, 60 mM Tris–HCl; pH 6.8) or 2-D lysis buffer (7 M urea, 2 M thiourea, 4% CHAPS, 2% (v/v) ampholytes (pH 3–10), 120 mM DTT, and 40 mM Tris-base). The samples dissolved in dI water served as the controls. The interfering effects of Laemmli's and 2-D lysis buffers were quantitated and are reported as %Interference, which was calculated using the following formula:

$$\%\text{Interference} = \frac{(\boldsymbol{C}_{\text{Buffer}} - \boldsymbol{C}_{\text{dI}}) \times 100}{\boldsymbol{C}_{\text{dI}}}$$

where $\boldsymbol{C}_{\textbf{Buffer}}$ was the concentration measured from the sample in Laemmli's or 2-D lysis buffer, whereas $\boldsymbol{C}_{\textbf{dI}}$ was the concentration measured from the same sample in dI water. The positive value of %Interference reflected over-estimation (the obtained concentration was significantly greater than that obtained from the sample in dI water), whereas the negative value of %Interference reflected under-estimation (the obtained concentration was significantly lower than that obtained from the sample in dI water). All data of %Interference reported in the "Results" section were derived from average values of triplicate sets of data obtained from three independent sets of experiments.

7. Practicality and unit cost

Assay-related parameters including practicality (concerning the sample consumption or the amount of sample that must be discarded and could not be recovered after the assay, number of pipetting/reaction, and estimated time consumed) and approximated unit costs were also compared among different quantitative protein assays. The details for amount of samples used, number of pipetting/reaction, and estimated time consumed were noted. Unit cost was calculated using the following formula:

$$\text{Unit cost (US\$/reaction)} = \frac{\text{Total price of an assay kit}}{\text{Total number of reaction by an assay kit}}$$

Note that only consumables (not including instrumentations and accessories, which are hard to compare) were used for this calculation.

8. Statistical analysis

Multiple comparisons were performed using ANOVA with Tukey's post-hoc test (SPSS, version 13.0). Linear regression analysis was performed to define the correlation between the two parameters. P values < 0.05 were considered statistically significant.

9. Results and discussion

Previously, evaluation of quantitative protein assays was based mainly on analysis of the purified proteins (particularly BSA), because the complex protein mixture was more difficult to interpret due to protein-to-protein variability [3]. In our present study, purified BSA, porcine kidney extract, tryptic digested peptides derived from purified BSA, and purified glycine were used as the representative samples for purified protein, complex protein mixture, peptide, and amino acid, respectively. The main reasons to employ these four samples in this study are: (1) They are common types of samples submitted to quantitative protein assays; (2) While there are several methods available for measurements of purified proteins and complex protein mixtures, fewer are available for measurements of peptides and amino acids of which the demands have been increasing, particularly in the proteomics/peptidomics era [19]; and (3) This study intended to evaluate effects of different sample types on each quantitative protein assay, i.e., limits of detection, ranges of linearity, and interferences by sample buffers. To compare individual assays in a systematic manner, we used a wide range of concentrations of these samples (from 0.006 to 100 mg/ml) prepared from their dried weights with serial 2-fold dilutions. Thereafter, a total of 15 concentrations of purified BSA, porcine kidney extract, tryptic digested peptides derived from purified BSA, and purified glycine were measured by seven commonly used quantitative protein assays.

We first evaluated the detectable limits of individual quantitative protein assays for each sample type (Table 1). The data showed that Bradford method was the most sensitive assay (LOD = 0.006 mg/ml) and had the widest detectable limits (LOD to UOD = 0.006–100 mg/ml) for purified protein (purified BSA) and complex protein mixture (porcine kidney extract). These data were consistent to those reported in previous studies indicating that Bradford assay was very sensitive and suitable for the sample with low protein concentrations such as the urine [6]. Ninhydrin assay and A205 had a comparable sensitivity (LOD = 0.006 mg/ml) as of Bradford method for detection of purified BSA and porcine kidney extract, respectively. Nevertheless, UOD of Ninhydrin assay and A205 (UOD = 0.781 mg/ml for both) for detection of purified BSA and porcine kidney extract, respectively, was much lower than that of Bradford method (UOD = 100 mg/ml). This result strengthened that Bradford method provided the widest detectable range for purified proteins and complex protein mixtures. On the other hand, the least sensitive method for detection of purified BSA and porcine kidney extract was Biuret assay (LOD = 0.391 mg/ml), consistent to the results obtained from previous studies demonstrating that Biuret was insensitive and was not appropriate for detecting proteins in the sample with low protein concentrations [3,6].

For peptide, A205, A280, Lowry and Ninhydrin methods had a comparable LOD (0.006 mg/ml), but Ninhydrin method had the

Author's personal copy

Table 1
Comparative analysis of detectable limits and linear dynamic ranges of various quantitative protein assays.

Parameters	Direct spectrophotometric assay		Colorimetric assay				
	A205	A280	BCA	Biuret	Bradford	Lowry	Ninhydrin
Lower limit of detection (LOD)							
Purified BSA (mg/ml)	0.012	0.049	0.024	0.391	0.006	0.012	0.006
Porcine kidney extract (mg/ml)	0.006	0.049	0.024	0.391	0.006	0.012	0.049
Peptide (mg/ml)	0.006	0.006	0.012	NA	NA	0.006	0.006
Purified glycine (mg/ml)	0.006	NA	NA	NA	NA	NA	0.006
Upper limit of detection (UOD)							
Purified BSA (mg/ml)	0.195	12.500	3.125	100	100	3.125	0.781
Porcine kidney extract (mg/ml)	0.781	3.125	6.250	100	100	6.250	1.563
Peptide (mg/ml)	25.000	25.000	6.250	NA	NA	12.500	100
Purified glycine (mg/ml)	6.250	NA	NA	NA	NA	NA	0.195
Range of linearity							
Purified BSA (mg/ml)	0.012–0.195	0.049–3.125	0.024–1.563	0.391–100	0.781–12.500	0.012–1.563	0.024–0.391
R^2	0.999	1.000	1.000	1.000	0.999	0.998	0.995
Porcine kidney extract (mg/ml)	0.024–0.195	0.098–1.563	0.049–1.563	0.391–100	0.781–6.250	0.098–1.563	0.195–1.563
R^2	0.998	0.999	0.998	0.998	0.998	1.000	0.997
Peptide (mg/ml)	0.006–0.098	0.024–6.250	0.024–1.563	NA	NA	0.024–0.391	0.012–0.098
R^2	1.000	1.000	0.996	NA	NA	0.999	0.999
Purified glycine (mg/ml)	0.006–0.098	NA	NA	NA	NA	NA	0.024–0.195
R^2	1.000	NA	NA	NA	NA	NA	0.999

Abbreviations used: A205, absorbance at λ205 nm; A280, absorbance at λ280 nm; BCA, bicinchoninic acid; BSA, bovine serum albumin; NA, not applicable; R^2, coefficient of determination.

widest detectability range (LOD to UOD=0.006–100 mg/ml) (Table 1). The data also showed that Biuret and Bradford methods are not applicable for peptide measurement. For amino acid, both A205 and Ninhydrin method had a comparable LOD of 0.006 mg/ml, but A205 had a wider range of the detectability (LOD to UOD=0.006–6.250 mg/ml) (Table 1). It should be noted that only these two methods are theoretically and practically applicable for detection and measurement of amino acid residues. Our data confirmed that glycine is not detectable or measurable by other five methods (Table 1).

The accuracy of a quantitative protein assay relies on precise correlation between actual concentrations and measured values (mostly absorbance derived from UV–visible spectrophotometry). Linear dynamic ranges of individual protein assays for each sample were screened systematically using 15 of 2-fold concentrations (from 0.006 to 100 mg/ml) of individual samples (Fig. 1). Briefly, each slope set was derived from 3-consecutive concentrations and a total of 13 slope sets were obtained. Multiple comparisons were performed among all these 13 slope sets and the two or more consecutive slope sets, which had no statistical differences, were highlighted and selected. All the concentrations within the selected consecutive slope sets were then used to establish a standard curve (Supplementary Figs. S1–S7). To validate the linearity of the selected consecutive slope sets, coefficient of determination (R^2) of this range was compared to those of the other extended ranges of concentrations (which extended to include 2 higher or 2 lower concentrations from the selected linear range). Our data demonstrated that R^2 values of the selected linear ranges of individual protein assays for each sample were greatest (and closed to 1.000) as compared to the extended ranges of concentrations (Supplementary Figs. S1–S7).

For purified BSA and porcine kidney extract, the broadest range of linearity was obtained from Biuret assay (linear dynamic range=0.391–100 mg/ml, R^2=1.000 and 0.998 for purified BSA and porcine kidney extract, respectively) (Table 1; Supplementary Figs. S4A and B). This result was consistent to previous reports [3,6], in which the major advantage of Biuret assay over the others was its wide linear range. On the other hand, A205 had the narrowest range of linearity for purified BSA and porcine kidney extract (0.012–0.195 and 0.024–0.195 mg/ml, respectively) (Table 1; Supplementary Figs. S1A and B). Thus, A205 is useful to quantitate samples with diluted protein concentrations ($<$200 μg/ml) [2]. For peptide, the widest range of linearity was obtained from A280 (linear dynamic range=0.024–6.250 mg/ml; R^2=0.999) (Table 1; Supplementary Fig. S2C), whereas Ninhydrin method offered the narrowest linear dynamic range (0.012–0.098 mg/ml) (Table 1; Supplementary Fig. S7C). For glycine, which was detectable only by A205 and Ninhydrin methods, Ninhydrin assay offered a slightly wider linear dynamic range (Table 1; Supplementary Fig. S7C).

The precision of quantitation is also determined by effects of interfering substances, if any, in the samples. Unfortunately, most of chemicals in sample buffers (lysis/extraction buffers) have some degrees of such interference [3], which may lead to over- or under-estimation of protein, peptide, and amino acid concentrations. However, effects of these commonly used sample buffers on protein, peptide, and amino acid quantitation were not thoroughly examined in the past. Among these sample buffers, Laemmli's and 2-D lysis buffers are most widely used in current protein research and life sciences. We therefore evaluated the interfering effects of these two commonly used sample buffers on protein, peptide, and amino acid quantitation in our present study.

To evaluate such effects in a systematic way, we used the average concentrations of proteins, peptide, and amino acid within their linear dynamic ranges of each assay as described with details above to ensure that the samples were in the measurable ranges and errors of quantitation was affected by interfering compositions in the sample buffers, not from the limited ranges of detectability of each assay. Dry purified BSA, porcine kidney extract, tryptic digested peptide, and purified glycine were dissolved in dI water, Laemmli's buffer or 2-D lysis buffer. Concentrations of proteins, peptide or glycine derived from the samples in Laemmli's or 2-D lysis buffer were compared to those obtained from the samples dissolved in dI water (Supplementary Figs. S8–S14). The results illustrated that both Laemmli's and 2-D lysis buffers had dramatic effects on all seven commonly used assays (Table 2). For measuring purified BSA and porcine kidney extract, Biuret assay had the greatest interfering effects from both Laemmli's (418% and 1049% over-estimation, respectively) and 2-D lysis buffers (768% and 1499% over-estimation, respectively) (Table 2; Supplementary Fig. S11). In contrast, Bradford

Author's personal copy

Table 2
Comparative analysis of %Interference by Laemmli's and 2-D lysis buffers in various quantitative protein assays.

Interference by	Direct spectrophotometric assay		Colorimetric assay				
	A205	A280	BCA	Biuret	Bradford	Lowry	Ninhydrin
Laemmli's buffer							
Purified BSA (%)	37	176	−86	418	−56	203	259
Porcine kidney extract (%)	932	147	−79	1049	3	470	96
Peptide (%)	259	140	−123	NA	NA	1663	27,825
Purified glycine (%)	3687	NA	NA	NA	NA	NA	259
2-D lysis buffer							
Purified BSA (%)	35	176	110	768	32	203	−66
Porcine kidney extract (%)	896	146	61	1499	139	470	−40
Peptide (%)	264	404	327	NA	NA	1665	2782
Purified glycine (%)	3607	NA	NA	NA	NA	NA	−77

Abbreviations used: A205, absorbance at λ205 nm; A280, absorbance at λ280 nm, BCA, bicinchoninic acid; BSA, bovine serum albumin; NA, not applicable.

Table 3
Comparative analysis of practicality and unit costs of various quantitative protein assays.

Parameters	Direct spectrophotometric assay		Colorimetric assay				
	A205	A280	BCA	Biuret	Bradford	Lowry	Ninhydrin
Sample consumption or the amount of sample that must be discarded after the assay (µl/reaction)	0	0	100	20	2	200	2000
Number of pipetting/reaction	1	1	4	3	4	4	4
Estimated time consumed (min/reaction)	5	5	50	15	10	35	1465
Approximated unit cost (US$/reaction)	0	0	0.392	0.144	0.045	0.320	0.059

Abbreviations used: A205, absorbance at λ205 nm; A280, absorbance at λ280 nm; BCA, bicinchoninic acid.

assay had the least interfering effects from Laemmli's and 2-D lysis buffers for measuring purified BSA and porcine kidney extract (Table 2; Supplementary Fig. S12). For measuring peptide, Ninhydrin method had the greatest interfering effects from both Laemmli's (27,825% over-estimation) and 2-D lysis buffers (2782% over-estimation) (Table 2; Supplementary Fig. S14C). However, BCA method had the least interfering effects from Laemmli's buffer, whereas A205 had the least interfering effects from 2-D lysis buffer for measuring peptide (Table 2**;** Supplementary Figs. S10C and S8C, respectively). For measuring purified glycine, A205 had greater interfering effects from both Laemmli's (3687%) and 2-D lysis buffers (3607%) (Table 2; Supplementary Fig. S8D), as compared to Ninhydrin assay.

The marked interferences from Laemmli's and 2-D lysis buffers alerted us for attention before submitting protein, peptide and amino acid samples recovered in these sample buffers for quantitation. It is advisable to strictly use protein, peptide and amino acid standards dissolved in the same buffer as of the samples, not dI water, to create a standard curve. Moreover, the same sample buffer should be used as the blank control for any quantitative protein assays. This is the simplest and probably the best way to avoid interfering effects from sample buffers. However, the investigators have to create several protein, peptide, or amino acid standards for individual sample buffers to ensure the precise quantitation in each type of samples.

In addition to detectable limits, linear dynamic ranges and interferences by sample buffers, selection of quantitative protein assay may also rely on the practicality of each assay and its unit cost. In our present study, the sample consumption (or the amount of sample that could not be recovered after the assay), number of pipetting/reaction, estimated time consumed, and unit cost were compared among individual assays (Table 3). The data demonstrated that both direct spectrophotometric methods (A205 and A280) were the simplest (required only one pipetting step) and consumed least amount of the samples. A205 and A280 determined protein/peptide concentrations based on light absorbance, which did not require any chemical reagents, additional manipulations and colorimetric reactions. Therefore, proteins and peptides could be fully recovered for subsequent analyses [2]. Moreover, both A205 and A280 consumed the shortest analytical time and had the lowest unit cost (indeed, there were no consumables used in these methods thereby the unit cost was zero) (Table 3). There is no doubt that A205 and A280 methods can be performed in any laboratory with an available UV–visible spectrophotometer. Comparing among five colorimetric assays, Bradford method consumed only a minimal amount of sample (2 µl/reaction), which was 50-fold, 10-fold, 100-fold and 1000-fold less than those consumed in BCA, Biuret, Lowry and Ninhydrin assays, respectively. In addition, Bradford method required the shortest analytical time (10 min/reaction) and had the lowest unit cost (0.045 US$/reaction) as compared to the other colorimetric assays (Table 3).

In summary, we present herein the most comprehensive data obtained from systematic comparative analyses of commonly used quantitative protein assays in term of their detectable limits, linear dynamic ranges, interferences, practicality and unit costs. Each method has both advantages and disadvantages that must be considered when ones select an appropriate method for measuring concentrations of proteins, peptides or amino acids in the samples. Our data will be useful for selecting the most suitable quantitative assay for each study.

Acknowledgments

We are grateful to Siriwan Mungdee and Paleerath Peerapen for their assistance. This study was supported by Office of the Higher Education Commission and Mahidol University under the National Research Universities Initiative, and The Thailand

Author's personal copy

Research Fund (RTA5380005) to VT. Both SC and VT are also supported by "Chalermphrakiat" Grant, Faculty of Medicine Siriraj Hospital.

Appendix A. Supporting information

Supplementary data associated with this article can be found in the online version at http://dx.doi.org/10.1016/j.talanta.2012.06.058.

References

[1] J.E. Noble, M.J. Bailey, Methods Enzymol. 463 (2009) 73–95.
[2] M.H. Simonian, Curr. Protoc. Cell Biol. (2002), Appendix 3 A.3B.1–A.3B.7.
[3] R.I. Krohn, Curr. Protoc. Cell Biol. (2002), Appendix 3 A.3H.1–A.3H.28.
[4] M. Friedman, J. Agric. Food Chem. 52 (2004) 385–406.
[5] T. Berkelman, Methods Mol. Biol. 424 (2008) 43–49.
[6] L.A. McElderry, I.F. Tarbit, A.J. Cassells-Smith, Clin. Chem. 28 (1982) 356–360.
[7] B. Okutucu, A. Dincer, O. Habib, F. Zihnioglu, J. Biochem. Biophys. Methods 70 (2007) 709–711.
[8] R. Seevaratnam, B.P. Patel, M.J. Hamadeh, J. Biochem. 145 (2009) 791–797.
[9] H.H. Nishi, J. Kestner, R.J. Elin, Clin. Chem. 31 (1985) 95–98.
[10] L.P. Kirazov, L.G. Venkov, E.P. Kirazov, Anal. Biochem. 208 (1993) 44–48.
[11] R.P. Keller, M.C. Neville, Clin. Chem. 32 (1986) 120–123.
[12] M. Fountoulakis, J.F. Juranville, M. Manneberg, J. Biochem. Biophys. Methods 24 (1992) 265–274.
[13] S.H. Kao, H.K. Wong, C.Y. Chiang, H.M. Chen, Proteomics 8 (2008) 2178–2184.
[14] R. Lovrien, D. Matulis, Curr. Protoc. Microbiol. (2005), Appendix 3 A.3A.1–A.3A.14.
[15] P.K. Smith, R.I. Krohn, G.T. Hermanson, A.K. Mallia, F.H. Gartner, M.D. Provenzano, E.K. Fujimoto, N.M. Goeke, B.J. Olson, D.C. Klenk, Anal. Biochem. 150 (1985) 76–85.
[16] A.G. Gornall, C.J. Bardawill, M.M. David, J. Biol. Chem. 177 (1949) 751–766.
[17] M.M. Bradford, Anal. Biochem. 72 (1976) 248–254.
[18] O.H. Lowry, N.J. Rosebrough, A.L. Farr, R.J. Randall, J. Biol. Chem. 193 (1951) 265–275.
[19] K.N. Kapoor, D.T. Barry, R.C. Rees, I.A. Dodi, S.E. McArdle, C.S. Creaser, P.L. Bonner, Anal. Biochem. 393 (2009) 138–140.

Ann Hematol (2013) 92:365–377
DOI 10.1007/s00277-012-1629-5

ORIGINAL ARTICLE

Differential plasma proteome profiles of mild versus severe β-thalassemia/Hb E

Suneerat Hatairaktham · Chatchawan Srisawat · Noppadol Siritanaratkul · Wararat Chiangjong · Suthat Fucharoen · Visith Thongboonkerd · Ruchaneekorn W. Kalpravidh

Received: 5 June 2012 / Accepted: 5 November 2012 / Published online: 17 November 2012
© Springer-Verlag Berlin Heidelberg 2012

Abstract The severity of thalassemia is currently classified based on clinical manifestations and multiple tests. In the present study, we performed a plasma proteome analysis to identify differentially expressed proteins compared between normal subjects and patients with mild and severe forms of β-thalassemia/hemoglobin E (Hb E). Plasma samples were collected from patients with mild (n=8) and severe (n=12) forms as well as healthy normal individuals (n=12). Clinical chemistry revealed that several parameters, i.e., hematological indices, oxidative stress markers, antioxidant enzymes, and erythropoietic activity, had significant differences among these three groups. After removal of seven major abundant proteins, the plasma proteome profiles were compared using two-dimensional gel electrophoresis. Spot matching, quantitative intensity analysis, and statistics revealed differential levels of 32 and 9 proteins when comparing normal vs. patients and mild vs. severe forms, respectively. These proteins were successfully identified by quadrupole time-of-flight mass spectrometry and/or tandem mass spectrometry. The decreased level of ADP-ribosylation factor guanine nucleotide-exchange factor 2 in β-thalassemia/Hb E patients compared to healthy individuals and the decreased level of endothelin-converting enzyme 2 in severe form compared to the mild form of the disease were validated by Western blot analysis. Our data provide a number of proteins that may lead to better understanding of the pathophysiology of thalassemia or for novel biomarkers which can be used to simply differentiate mild and severe forms of β-thalassemia/Hb E without any need for multiple tests.

Keywords Anemia · β-thalassemia/Hb E · Biomarkers · Pathogenesis · Plasma proteome · Thalassemia

Electronic supplementary material The online version of this article (doi:10.1007/s00277-012-1629-5) contains supplementary material, which is available to authorized users.

S. Hatairaktham · C. Srisawat · R. W. Kalpravidh (✉)
Department of Biochemistry, Faculty of Medicine Siriraj Hospital, Mahidol University, Bangkok, Thailand
e-mail: ruchaneekorn.kal@mahidol.ac.th

N. Siritanaratkul
Department of Medicine, Faculty of Medicine Siriraj Hospital, Mahidol University, Bangkok, Thailand

W. Chiangjong · V. Thongboonkerd
Medical Proteomics Unit, Office for Research and Development, Faculty of Medicine Siriraj Hospital, Mahidol University, Bangkok, Thailand

S. Fucharoen
Thalassemia Research Center, Institute of Molecular Biosciences, Mahidol University, Salaya Campus, Nakhonpathom, Thailand

V. Thongboonkerd
Center for Research in Complex Systems Science, Mahidol University, Bangkok, Thailand

Introduction

Thalassemia is a group of inherited anemia characterized by quantitative defect of the functional globins in erythroid cells; its classification is primarily based on the impaired globin gene. Beta-thalassemia is caused by a mutation of the β-globin gene leading to an imbalanced α/β-globin ratio within mature red cells and their progenitors [1]. The excess α-globins liberate reactive iron, which potentially causes oxidative damage to red cell membrane lipids and proteins and also increases intracellular calcium, resulting in the significantly

increased exposure of phosphatidylserine (PS) to the outer leaflet, a feature of apoptosis. Subsequent pathological conditions include ineffective erythropoiesis, peripheral hemolysis, and, eventually, anemia [1]. Chronic anemia in thalassemic patients is a life-threatening condition caused by exacerbating iron overload, leading to secondary complications, i.e., osteopenia/osteoporosis, hepatosplenomegaly, iron-induced dysfunctions of various organs, thrombosis, diabetes, severe infection, and growth retardation [2].

Among the diverse β-thalassemia genotypes, β-thalassemia/Hb E compound heterozygote is much more prevalent in Southeast Asia. It inherits a β-thalassemia allele from one parent and an Hb E ($\beta^{26\ Glu\rightarrow Lys}$) allele from the other. Patients with β-thalassemia/Hb E show phenotypic diversity, with Hb levels ranging from 2 to 14 g/dL [3], and this diversity makes clinical stratification complicated. Currently, the classification of disease severity is based on clinical manifestations and multiple tests, without any simple marker available for such classification. In addition, the mechanisms underlying the phenotypic heterogeneity of β-thalassemia are still poorly understood. Moreover, current standard treatment of thalassemia (i.e., blood transfusion, iron chelation, splenectomy, and treatment of complications) is supportive based on symptoms of each patient whose clinical signs of many complications are obviously shown at the late stage of the disease. To identify novel biomarkers for disease severity and to understand these unclear pathophysiological mechanisms of thalassemia, proteomics may be a potential technique for such purposes, as has been proven in many other various diseases.

In the present study, we performed proteomics analysis to compare the plasma proteome profiles of patients with mild vs. severe forms of β-thalassemia/Hb E as well as patients vs. normal individuals. Plasma was used as the sample of choice because of its accessibility and noninvasiveness. Moreover, a large number of proteins in the plasma are originated from normal and abnormal cells/tissues [4]. However, the major limitation of plasma proteomics is the wide range of plasma protein concentrations which vary from milligrams per milliliter to picograms per milliliter for high and low abundant proteins, respectively [5]. Therefore, depletion of high-abundant proteins was performed to unmask low abundant proteins prior to proteome analysis in our study.

Material and methods

Patients and normal subjects

A total of 20 β-thalassemia/Hb E patients were recruited from the Division of Hematology, Department of Medicine, Siriraj Hospital (Bangkok, Thailand). These patients met all the inclusion criteria, which included: (1) age=18–45 years; (2) Hb typing=$\beta^0\beta^E$; (3) non-splenectomized; (4) no blood transfusion within 3 months prior to enrollment; and (5) stop intervention drugs (including iron chelator, vitamin E, and hydroxyurea) at least 2 weeks before blood sampling. Among the 20 recruited patients, eight had mild anemia (Hb concentration≥8 g/dL), whereas the other 12 had severe anemia (Hb concentration≤6 g/dL).

In addition, 12 healthy normal volunteers were recruited as the control group. These normal controls were sex- and age-matched with those patients, but had normal hemoglobin typing (Hb A_2A). None of the subjects were pregnant or lactating, smoking, alcohol drinking, had positive tests for hepatitis B and C viruses, and had administered unregistered drugs within 30 days before blood collection. All the subjects had signed the informed consent, and the protocol used in this study was approved by SIRIRAJ Institutional Review Board, Faculty of Medicine Siriraj Hospital, Mahidol University.

Blood collection, Hb typing, and hematological indices

Fasting blood drawn from normal subjects and β-thalassemia/Hb E patients were collected in K_3EDTA, sodium heparin, and clotted tubes. EDTA-preserved blood was analyzed for complete blood count and Hb typing using the Sysmex NE-1500 hematology analyzer (Sysmex, Japan) and HPLC (Variant Hemoglobin Testing System, Bio-Rad, Hercules, CA), respectively. The reticulocyte production index (RPI), also known as corrected reticulocyte count, was calculated using the following formula [6]:

$$\mathrm{RPI} = \frac{[\%\text{reticulocyte} \times (\text{actual \%Hct}/\text{normal \%Hct})]}{\text{reticulocyte maturation time}}$$

Platelet (Plt)-poor plasma for proteomics study was prepared from the remaining EDTA blood by double centrifugation at 1,500×*g* and 3,000×*g* for 10 min at 4 °C and kept at −80 °C until used. The packed red cells were washed three times and diluted to 50 % hematocrit with cold phosphate-buffered saline (PBS, pH 7.4) for the determination of red blood cell (RBC) oxidative stress or antioxidant parameters.

Serum was prepared from the clotted blood by double centrifugation at 1,500×*g* for 10 min at 4 °C and kept at −80 °C until used for the analysis of iron parameters or erythropoietic activities. Heparinized blood was stored at room temperature and analyzed for RBC vesiculation and PS exposure within the same day of blood collection.

Measurements of oxidative stress and antioxidant parameters

Malondialdehyde (MDA) is generally accepted and widely used as a marker of oxidative stress. In this study, the quantitation of plasma MDA was performed using a commercial HPLC kit (Immundiagnostik AG, Bensheim, Germany), whereas MDA in red blood cells was measured according to the method of Stocks and Dormandy [7]. The reaction between hydrogen peroxide-induced MDA and thiobarbituric acid forms a complex which can be measured by a spectrophotometer at 532 and 600 nm (for eliminating interference).

Antioxidant parameters in red blood cells were also analyzed. Superoxide dismutase (SOD) activity was determined based on its ability to inhibit the reaction between nitroblue tetrazolium (NBT) and superoxide anions [8]. The activity of SOD is expressed as units per gram of hemoglobin. One unit of SOD activity is defined as the amount of enzymes that inhibit the rate of NBT reduction by 50 %. Glutathione peroxidase (GPx) activity was determined in red blood cells by the method of Beutler [9] using the oxidation of NADPH in a coupled reaction containing *t*-butyl hydroperoxide and oxidized glutathione. Reduced glutathione (GSH) assay is based on the reaction between sulfhydryl group (−SH) and 5,5′-dithiobis-(2-nitrobenzoic acid) (DTNB) to give a stable yellow color [10]. The concentration of GSH is calculated from the difference of absorbance before and after adding DTNB.

Measurements of RBC vesiculation and phosphatidylserine exposure

Heparinized blood was analyzed for RBC vesiculation and PS exposure by a fluorescence-activated cell sorter (FACScalibur, Becton Dickinson, San Jose, CA) according to the method modified from Pattanapanyasat et al. [11]. Briefly, the blood was stained with annexin V-FITC, anti-human CD41a-TC (both from Becton Dickinson Biosciences), and anti-human glycophorin A-PE (Dako, Glostrup, Denmark). The samples were excited at 488-nm wavelength with 530/30- and 585/42-nm bandpass filters. The percentages of RBC vesicles and PS exposure from 100,000 events of recruited cells/vesicles were analyzed using the CellQuest software.

Measurements of iron parameters and erythropoietic activities

Serum ferritin was measured using Integra 700 (Roche, Basel, Switzerland). Serum transferrin receptor (sTfR), erythropoietin (EPO), and growth differentiation factor 15 (GDF-15) were determined using an ELISA kit (R&D Systems, Minneapolis, MN). The normal ranges of sTfR, EPO, and GDF-15 were 8.7–28.1 nmol/L, 3.3–16.6 mIU/mL, and 337–1060 pg/mL, respectively. Serum non-transferrin bound iron (NTBI) was assayed using reversed-phase HPLC with CP22 on-column derivatization followed by measurement of the complex at 450 nm using an online LCD detector [12].

Sample preparation for proteomics study

Platelet-poor plasma samples were individually depleted for seven major abundant proteins (including albumin, IgG, antitrypsin, IgA, transferrin, haptoglobin, and fibrinogen) using Multiple Affinity Removal System (MARS-7 spin-column, Agilent Technologies, Wilmington, DE). Briefly, 12 μL of each plasma sample was diluted 20-fold in buffer A, filtered through a 0.22-μm spin filter, and loaded onto the antibody spin column. The column was centrifuged at a slow rate (100×*g* for 1 min, 4 °C) and washed twice with buffer A by centrifugation at 200×*g* for 2 min according to the manufacturer's instructions. The flow-through and washed fractions were pooled, dialyzed, lyophilized, and resuspended with deionized water (18.2 MΩcm). Protein concentrations were determined with a spectrophotometer using the Bradford method [13].

Two-dimensional gel electrophoresis

Depleted plasma samples were mixed with rehydration buffer containing 7 M urea, 2 M thiourea, 2 % 3-[(3-cholamidopropyl) dimethyl-ammonio]-1-propanesulfonate, 2 % ampholytes (pH 3–10), 120 mM dithiothreitol (DTT), and 0.002 % bromophenol blue to yield 150 μg total protein in 150 μL total volume. The mixtures were absorbed overnight with immobilized pH gradient (IPG) strips (linear pH 4–7; GE Healthcare, Uppsala, Sweden) followed by the first dimensional separation using Ettan IPGphor 3 IEF System (GE Healthcare) with stepwise mode to reach 9,083 Vh. The strips were then incubated with equilibration buffer (6 M urea, 130 mM DTT, 30 % glycerol, 112 mM Tris base, 4 % SDS, and 0.002 % bromophenol blue) for 15 min and with another buffer (6 M urea, 135 mM iodoacetamide, 30 % glycerol, 112 mM Tris base, 4 % SDS, and 0.002 % bromophenol blue) for 15 min. The equilibrated strips were transferred onto 13 % polyacrylamide gel and the proteins further resolved in the second dimension using SE260 Mini-Vertical Electrophoresis Unit (GE Healthcare) at 150 V for approximately 2 h. The gels were stained with Deep Purple fluorescence dye (GE Healthcare) and scanned with a Typhoon 9200 laser scanner (GE Healthcare).

Quantitative intensity analysis

Protein spots in the scanned images were matched and analyzed with the Image Master 2D Platinum software

(GE Healthcare). Spots on all images were automatically detected using parameters adjusted as follows: (1) minimal area=10 pixels; (2) smooth factor=2.0; and (3) saliency=2.0. Subsequently, a reference gel was created by combining all spots representing on different gels into one image and used for matching process. After background subtraction, the quantity of individual spots was reported as the relative intensity volume (%vol) defined as the intensity volume normalized with the total intensity volume of the protein spots indicated in the same gel.

A series of gels were grouped in order to proceed with statistical analysis. Student's *t* test was used to determine the differences in the means of individual spots between two groups when comparing normal (n=12) vs. patients (n=20) and mild (n=8) vs. severe forms (n=12). Differentially expressed spots were defined as those with p values less than the threshold of 0.05.

In-gel tryptic digestion

Statistically differential expressed spots were manually excised from the gels and washed twice with 50 % acetonitrile (ACN)/25 mM ammonium bicarbonate (NH_4HCO_3) buffer (pH 8.0) and once with 100 % ACN. The liquid was discarded and the gel pieces were dried in a Speed Vac concentrator (Savant, Holbrook, NY). The particles were then soaked with 1 % (*w*/*v*) trypsin in 25 mM NH_4HCO_3 and incubated at 37 °C for at least 16 h. Subsequently, peptides were extracted twice with 50 % ACN/5 % trifluoroacetic acid (TFA), combined, dried, resuspended with 0.1 % TFA, and purified using $ZipTip_{C18}$. After washing three times with 0.1 % formic acid, the peptides were finally eluted with 75 % ACN/0.1 % formic acid for mass spectrometric analysis.

Protein identification

Tryptic samples premixed with the matrix solution (5 mg/mL α-cyano-4-hydroxycinnamic acid) were spotted onto the 96-well MALDI sample stage and analyzed using the Q-TOF Ultima™ MALDI mass spectrometer (Micromass, Manchester, UK). The parent ions with peaks within the *m*/*z* 800–3000 range and intensities>10 count±include/exclude list were selected for tandem mass spectrometry (MS/MS). The instrument was run with mass-dependent±5-V rolling collision energy until the end of the probe pattern was reached. Proteins were identified by searching the MS and MS/MS data with the MASCOT search engine (http://www.matrixscience.com). All searches were performed with the following settings: mammalian NCBI protein database; monoisotopic; fixed modification was carbamidomethylation at cysteine residues; variable modification was oxidation at methionine residues; one missed trypsin cleavage; mass tolerances of 100 and 50 ppm for peptide mass fingerprinting (PMF) and MS/MS ions search, respectively. Significant hits were considered when probability-based MOWSE scores were >69 or MS/MS ions scores were>37 for PMF and MS/MS analyses, respectively.

Western blotting

Western blot analysis of two randomly selected proteins, ADP-ribosylation factor guanine nucleotide exchange factor 2 (ARFGEF2) and endothelin-converting enzyme 2 (ECE2), was performed to validate the proteomic data. An equal amount of 30 μg of plasma proteins from each sample was loaded in each lane of 12 % SDS-PAGE and the resolved proteins were transferred onto nitrocellulose membranes (Whatman, Dassel, Germany) using a semi-dry electrophoretic transfer cell (Bio-Rad, Milan, Italy) at 85 mA for 1 h. The membranes were blocked for nonspecific bindings with 5 % skim milk in PBS at room temperature for 1 h, washed, and incubated with rabbit polyclonal anti-ARFGEF2 antibody (1:250 in 1 % BSA/PBS, Abcam Inc., Cambridge, UK) or rat monoclonal anti-human ECE2 antibody (1:250 in 1 % BSA/PBS, R&D Systems Inc., Minneapolis, MN) at 4 °C for three nights. The membranes were then washed and incubated with respective secondary antibodies conjugated with horseradish peroxidase (1:2,000, Dako) at room temperature for 1 h, followed by washing and incubating for 5 min with SuperSignal West Pico Chemiluminescence Substrate (Pierce Biotechnology Inc., Rockford, IL). The immunoreactive bands were detected by a high-performance film.

Statistical analysis

All quantitative data are reported as the mean±SEM unless stated otherwise. The comparisons of individual data between two sample sets were performed using unpaired Student's *t* test with SPSS software. Values of $p<0.05$ were considered statistically significant.

Results

A total of 20 β-thalassemia/Hb E subjects (8 mild and 12 severe cases) and 12 healthy normal individuals were recruited. Their age, gender, and hematological indices are shown in Table 1. There were no significant differences in age and gender among groups. β-thalassemia/Hb E patients had significantly lower levels of all hematological parameters, except for white blood cells (WBC) and reticulocyte

Table 1 Age, gender, and hematological indices of healthy normal subjects and β-thalassemia/Hb E patients

	Normal subjects (n=12)	β-thalassemia/Hb E patients		
		All patients (n=20)	Mild form (n=8)	Severe form (n=12)
Age (years)	29±2	26±2	26±2	26±2
Gender (M/F)	5/7	11/9	6/2	5/7
Hb (g/dL)	13.9±0.5	6.8±0.4[a]	8.3±0.5[a]	5.8±0.1[a,b]
Hct (%)	43.0±1.3	22.6±1.1[a]	27.1±1.6[a]	19.6±0.4[a,b]
RBC ($\times 10^6$/mL)	4.9±0.1	3.9±0.2[c]	4.6±0.4	3.4±0.1[a,b]
MCV (fL)	88.4±1.0	59.1±1.1[a]	59.9±2.3[a]	58.5±1.1[a]
MCH (pg)	28.7±0.4	17.8±0.4[a]	18.4±0.8[a]	17.3±0.4[a]
MCHC (g/dL)	32.3±0.2	29.9±0.3[a]	30.6±0.5[c]	29.3±0.3[a]
Plt ($\times 10^3$/mL)	264±10	174±15[a]	206±25[c]	153±17[a,d]
WBC ($\times 10^3$/mL)	6.1±0.4	8.6±0.7[c]	9.9±1.4[c]	7.8±0.8
Reticulocyte (%)	0.8±0.1	1.9±0.1[a]	1.9±0.1[a]	1.9±0.2[a]
RPI	0.8±0.1	0.6±0.1[c]	0.7±0.1	0.5±0.1[c,d]

Hb hemoglobin, *Hct* hematocrit, *MCH* mean corpuscular Hb, *MCHC* mean corpuscular Hb concentration, *MCV* mean corpuscular volume, *M*/*F* male/female, *Plt* platelets, *RBC* red blood cells, *RPI* reticulocyte production index, *WBC* white blood cells

[a] $p<0.001$ compared to normal

[b] $p<0.001$ compared to the mild form

[c] $p<0.05$ compared to normal

[d] $p<0.05$ compared to the mild form

count as compared with the normal controls. Patients with severe anemia had significantly lower Hb concentration, hematocrit (Hct), RBC count, Plt count, and RPI than those of the mild anemic group.

Patients with β-thalassemia/Hb E had strikingly increased levels of oxidative stress parameters (plasma and RBC MDA); RBC antioxidant parameters (SOD and GPx); circulating RBC vesicles and their PS exposure; erythropoietic activities (serum EPO and sTfR); and iron parameters (serum NTBI, GDF-15, and ferritin) as compared with normal controls (Table 2). Moreover, plasma MDA, RBC SOD, % PS-positive RBC vesicles, serum EPO, and serum sTfR were significantly greater in severe than in mild cases.

Plasma proteome profiles were analyzed using two-dimensional gel electrophoresis-based proteomics approach. A total of 402±18, 392±17, and 408±25 spots were detected on the plasma maps of healthy, mild, and severe anemia groups, respectively (for the statistics of gel comparison between these groups, see Electronic supplementary material Table S1). Spot matching and quantitative intensity analysis as well as statistics revealed 32 protein spots whose levels significantly differed in thalassemic patients compared to the normal controls (Fig. 1a). These included eight upregulated (1.44- to 13.32-fold increase) and 24 downregulated (absent to 0.72-fold decrease) protein spots (Table 3). All of these protein spots were excised and subjected to in-gel tryptic digestion and quadrupole time-of-flight mass spectrometry (Q-TOF MS) and/or MS/MS analyses. Details of these proteins (including identities, identification scores, sequence coverage, number of matched peptides, and quantitative intensity data) are provided in Table 3. After getting protein identities, we further gathered additional information from online databases including NCBI (http://www.ncbi.nlm.nih.gov/) and UniProtKB (http://expasy.org/). According to the protein function, these identified proteins can be categorized into 12 functional groups, including transcriptional regulation, signal transduction, immunity, ion channel, metabolic enzyme, protein metabolism, cytoskeletal protein, coagulation cascade, transporter protein, acute phase response, protein trafficking, and unknown function (Table 3).

Comparing between mild and severe forms of the disease, the analysis revealed nine differentially expressed protein spots (Fig. 1b), which met statistically significant levels. These included two upregulated (1.53- to 1.69-fold increase) and seven downregulated (0.19- to 0.70-fold decrease) protein spots (Table 4). All of these proteins were successfully identified by Q-TOF MS and/or MS/MS analyses, including those involved in ion channel, metabolic enzyme, stress response, protein metabolism, acute phase response, cell proliferation, regulation of vascular tone, and transcriptional regulation. Details of these proteins (including identities, identification scores, sequence coverage, number of matched peptides, and quantitative intensity data) are provided in Table 4.

Western blot analysis of randomly selected proteins was performed to confirm the proteomic results. The data showed the decreased level of ARFGEF2 in β-thalassemia/Hb E patients compared to healthy individuals and the decreased level of ECE2 in severe form compared to the mild form of the disease, as identified from proteomic analysis (Fig. 2).

Discussion

The comparison of hematological and biochemical parameters between β-thalassemia/Hb E patients and normal subjects revealed obvious alterations of these parameters in the disease group, including prolonged anemia (decreased Hb concentration at steady state); extra hemolysis (increased RBC vesicles and PS-positive RBC); ineffective erythropoiesis (decreased RBC count and increased levels of EPO, sTfR, and RPI); oxidative stress (increased plasma MDA, RBC MDA, and antioxidant enzymes' activities); and iron overload (increased serum NTBI, ferritin, and GDF-15

Table 2 Levels of oxidative stress parameters, antioxidant parameters, red cell vesiculation, erythropoietic activities, and iron parameters in healthy normal subjects and β-thalassemia/Hb E patients

	Normal subjects (n=12)	β-thalassemia/Hb E patients		
		All patients (n=20)	Mild form (n=8)	Severe form (n=12)
Oxidative stress parameters				
Plasma MDA (μM)	0.49±0.04	1.78±0.13[a]	1.26±0.10[a]	2.12±0.13[a,b]
RBC MDA (nmol/g Hb)	809±19	1,311±146[c]	1,314±256[c]	1,310±183[c]
Antioxidant parameters				
RBC SOD (U/g Hb)	2,327±81	5,869±417[a]	4,685±252[a]	6,793±519[a,b]
RBC GPx (U/g Hb)	29.9±1.7	68.9±3.0[a]	70.5±5.0[a]	68.3±3.9[a]
RBC GSH (mmol/L)	2.22±0.06	1.89±0.05[c]	1.93±0.07[c]	1.87±0.08[a]
RBC vesiculation and PS exposure				
% RBC vesicles	0.12±0.02	1.66±0.27[a]	1.34±0.44[a]	1.87±0.35[a]
% PS^+ RBC vesicles	0.05±0.01	0.08±0.02	0.05±0.01	0.10±0.03[c,d]
% PS^+ RBC	0.10±0.01	0.78±0.22[c]	0.79±0.40[c]	0.78±0.27[c]
Erythropoietic activities				
Serum EPO (IU/L)	7.3±0.8	127.7±16.9[a]	71.9±9.7[a]	164.9±21.6[a,d]
Serum sTfR (nmol/L)	19.7±2.0	168.3±12.8[a]	136.7±15.8[a]	189.4±16.4[a,d]
Iron parameters				
Serum GDF-15 (mg/dL)	375±28	11,091±725[a]	10,511±984[a]	11,477±1,034[a]
Serum NTBI (μM)	−0.92±0.21	4.05±0.43[a]	3.56±0.74[a]	4.38±0.52[a]
Serum ferritin (ng/mL)	82±21	929±150[a]	1037±271[a]	857±181[c]

EPO erythropoietin, *GDF-15* growth differentiation factor 15, *GPx* glutathione peroxidase, *GSH* reduced glutathione, *MDA* malondialdehyde, *NTBI* non-transferrin-bound iron, PS^+ phosphatidylserine-positive, *SOD* superoxide dismutase, *sTfR* soluble transferrin receptor

[a] $p<0.001$ compared to normal

[b] $p<0.001$ compared to the mild form

[c] $p<0.05$ compared to normal

[d] $p<0.05$ compared to the mild form

levels; Tables 1 and 2). In the present study, Hb concentration was used to indicate the disease severity because of its strong correlation with the degree of imbalanced α/β-globin ratio in various genetically modified thalassemic mice [14]. Less Hb concentration implies more amount of excess α-globin accumulated in erythroid precursors and mature RBC. Comparing the severe form with the mild form, patients with severe anemia had increased degree of ineffective erythropoiesis (lower RBC count with concurrently increasing erythropoietic activity, as shown by lower RPI and greater serum EPO and sTfR levels), increased oxidative stress (greater plasma MDA and RBC SOD activities), and enhanced PS exposure (greater level of PS-positive RBC vesicles; Tables 1 and 2).

We previously applied a proteomics study using plasma depleted of two high-abundant proteins (albumin and IgG), in which all of the differentially expressed proteins belong to coagulation factors and proteins involved in iron homeostasis, when compared between β-thalassemia/Hb E patients and normal subjects [15]. In this study, we prepared platelet-poor plasma from fasting blood to minimize the effect of dietary and platelet degranulation/activation on plasma proteome. Seven high-abundant proteins (albumin, IgG, antitrypsin, IgA, transferrin, haptoglobin, and fibrinogen) were removed from the plasma using the immunoaffinity MARS-7 depletion column, with expectation to identify more low-abundant ones. However, we found that the column cannot completely remove these, as shown by the presence of serum albumin (spots 490 and 580). This may be explained by thalassemia being regarded as an oxidative stress disease induced by iron overload within erythroid progenitors or circulating RBC [1], as could be seen by the significant increase of oxidative stress biomarkers including plasma and RBC MDA [16, 17], protein carbonyl [15, 18], or 8-oxo-7,8-dihydro-2′-deoxyguanosine [19]. Under the oxidative state, high-abundant proteins, especially albumin, are oxidatively modified, followed by conformation changes and, hence, altered binding properties [20]. However, the results showed a greater number of identified proteins (32 spots, 22 proteins) than our previous study (25 spots, 4 proteins). Moreover, we also further detected nine differentially expressed plasma proteins under different degrees of anemia.

To validate MS-based protein identities, the spots were mapped to the reference set of human plasma proteome presented in the Swiss-2DPAGE database (http://expasy.hcuge.ch/). We confirmed the following proteins' identities by matching both the isofocusing points (p*I*) and molecular weight values. These included complement factor C3 (spot 639), prothrombin (spots 361 and 366), antithrombin III (spots 471, 476, and 479), and alpha-1-antichymotrypsin (spots 472, 481, 487, and 498). Western blot analysis was also performed on randomly selected proteins to verify the accuracy of MS-based protein identification. The decreased level of ADP-ribosylation factor guanine nucleotide-exchange factor 2 (ARFGEF2) in β-thalassemia/Hb E patients compared to healthy individuals and the decreased level of endothelin-converting enzyme 2

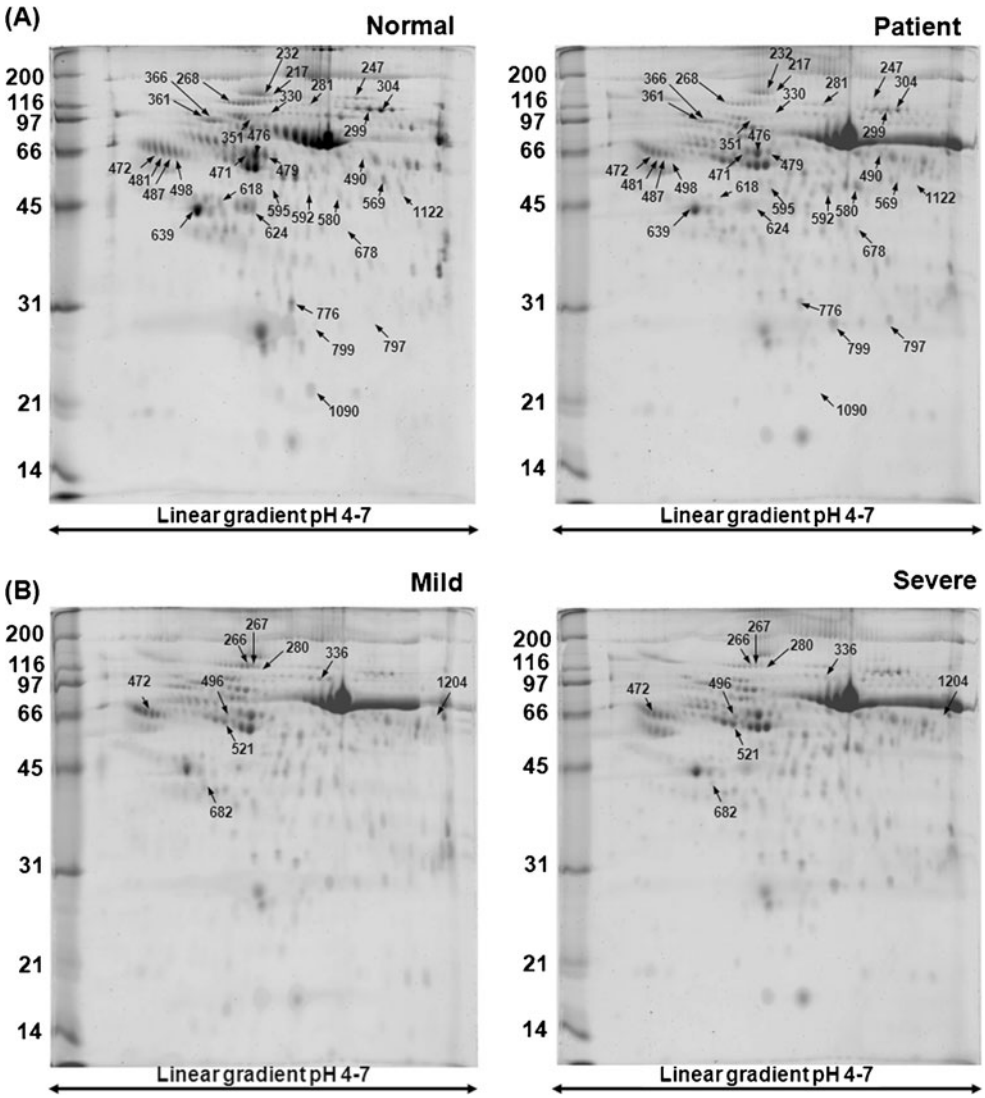


Fig. 1 Two-dimensional maps of differentially expressed protein spots in representative 2D gels of healthy normal subjects vs. β-thalassemia/Hb E patients (**A**) and mild vs. severe forms of β-thalassemia/Hb E (**B**). Details of these proteins (including identities, identification scores, sequence coverage, number of matched peptides, and quantitative intensity data) can be found in Tables 3 and 4

(ECE2) in severe form compared to the mild form of the disease were reported, which was consistent with the MS-based protein identification and proteomic results.

For data analysis, we accessed the UniProt and Pubmed databases for information about protein function, protein abundance, tissue specificity, disease association, etc. However, one of the main limitations is the poor specificity of the identified proteins. Many of these are intracellular proteins in many types of cells, and it is very difficult to elucidate their originated source in plasma. Therefore, we associated their functions to the key pathological conditions implicated in thalassemia, including oxidative stress, hypoxia, iron overload, ineffective erythropoiesis, and excess hemolysis [2], which may imply their possible role in pathogenesis. For example, ADP-ribosylation factor (Arf) guanine nucleotide exchange factor 2 (ARFGEF2; spot 1122) is a Golgi protein found in most cell types since it plays an important role in intracellular vesicle trafficking, exocytosis, and regulation of the Arf signal pathway by activating Arf through replacement of ADP-bound (inactive form) with ATP-bound (active form). Up to this date, there has been no study correlating ARFGEF2 and thalassemia. To further investigate, we related this protein's functions to thalassemic conditions, and previous studies implied its indirect role in ineffective erythropoiesis by regulating tumor necrosis factor alpha (TNF-α) bioavailability. In normal conditions, ARFGEF2 regulates the exocytosis of soluble tumor necrosis factor receptor-1, which competitively binds to circulating TNF-α, resulting in less amount of TNF-α influx [21]. Surplus TNF-α has been shown to cause apoptosis of β-thalassemia/Hb E erythroid progenitor cells [22] and also the direct inhibition of BFU-E colony formation by $CD34^+$ progenitor cells [23], of which "premature destruction" or "impaired differentiation" of erythroid progenitor cells are the characteristics of ineffective erythropoiesis in thalassemia [1]. However, further studies are required to assess the role of ARFGEF2 in ineffective erythropoiesis (at least to investigate whether this protein is secreted from apoptotic

Table 3 Summary of plasma proteins with differential levels in healthy normal subjects vs. β-thalassemia/Hb E patients

Spot no.	Protein name	NCBI ID	Identification scores (MS, MS/MS)	%Cov (MS, MS/MS)	No. of matched peptides (MS, MS/MS)	p*I*	MW (kDa)	Intensity (mean±SEM)		Intensity ratio (patient/ normal)	*p* values
								Normal	Patient		
Transcriptional regulation											
217	DNA topoisomerase 2-beta	gi|19913408	69, NA	13, NA	9, NA	8.83	135.02	0.0813±0.0065	0.0321±0.0092	0.39	0.0002
678	T-box 3 (ulnar mammary syndrome), isoform CRA_b	gi|119618476	83, NA	22, NA	8, NA	8.07	55.53	0.0515±0.0189	0.1563±0.0444	3.04	0.0410
776	Sodium channel modifier 1	gi|55960952	66, NA	32, NA	5, NA	9.25	22.10	0.8434±0.0964	0.5165±0.1043	0.61	0.0312
799	T-box 3 (ulnar mammary syndrome), isoform CRA_b	gi|119618476	79, NA	19, NA	8, NA	8.07	55.53	0.0612±0.0305	0.4312±0.1384	7.04	0.0160
Signal transduction											
232	Rho/rac guanine nucleotide exchange factor (GEF) 2, isoform CRA_b	gi|74198391	68, NA	17, NA	10, NA	6.44	109.59	0.1754±0.0180	0.1104±0.0223	0.63	0.0332
247	Adenomatous polyposis coli protein isoform a	gi|221040078	67, NA	19, NA	13, NA	6.27	127.35	0.0732±0.0117	0.0282±0.0082	0.39	0.0047
330	Adenomatous polyposis coli protein isoform b	gi|158260157	64, NA	16, NA	12, NA	6.05	147.15	0.0509±0.0103	0.0212±0.0095	0.42	0.0454
Immunity											
299	Chain A, human complement factor B	gi|134105218	68, 62	20, 3	10, 1	6.81	85.58	0.4663±0.0400	0.2591±0.0264	0.56	0.0003
304	Chain A, human complement factor B	gi|134105218	89, NA	23, NA	10, NA	6.81	85.58	0.5779±0.0461	0.2911±0.0389	0.50	0.0001
639	Complement component C3	gi|179665	NA, 117	NA, 1	NA, 2	6.02	188.59	2.7698±0.3733	1.6093±0.2131	0.58	0.0131
Ion channel											
592	Calcium-activated potassium channel subunit beta-2-like	gi|296224611	70, NA	44, NA	4, NA	8.65	15.04	0.1038±0.0288	0.3860±0.0952	3.72	0.0096
Metabolic enzyme											
351	Acetyl-CoA carboxylase 1	gi|11559962	66, NA	10, NA	17, NA	5.97	266.69	0.0701±0.0125	0.0281±0.0101	0.40	0.0161
797	Mitochondrial phosphoenolpyruvate carboxykinase 2 isoform 1 precursor isoform 2	gi|73962500	76, NA	23, NA	11, NA	8.34	72.20	0.0160±0.0090	0.2128±0.0773	13.32	0.0192
Protein metabolism											
268	E3 ubiquitin-protein ligase HERC6-like	gi|301755558	72, NA	15, NA	11, NA	8.71	134.42	0.0956±0.0120	0.0568±0.0067	0.59	0.0097
281	Truncated tumor necrosis factor alpha-induced protein 3	gi|225348450	72, NA	19, NA	10, NA	8.49	86.97	0.0582±0.0068	0.0838±0.0092	1.44	0.0361
Cytoskeletal protein											
595	Protein phosphatase Slingshot homolog 3, isoform CRA_c	gi|119594995	70, NA	39, NA	4, NA	11.01	16.84	0.0660±0.0150	0.1339±0.0272	2.03	0.0398
1090	Microtubule-actin cross-linking factor 1-like isoform 3	gi|291399212	92, NA	8, NA	26, NA	5.20	672.42	0.2681±0.0743	0.0499±0.0499	0.19	0.0016

Table 3 (continued)

Spot no.	Protein name	NCBI ID	Identification scores (MS, MS/MS)	%Cov (MS, MS/MS)	No. of matched peptides (MS, MS/MS)	p*I*	MW (kDa)	Intensity (mean±SEM)		Intensity ratio (patient/ normal)	*p* values
								Normal	Patient		
Coagulation cascade											
361	Prothrombin	gi|67624831	89, NA	24, NA	10, NA	5.70	71.40	0.1457±0.0308	0.0365±0.0137	0.25	0.0038
366	Prothrombin	gi|67624831	139, 75	34, 5	16, 2	5.70	71.40	0.2971±0.0341	0.1244±0.0278	0.42	0.0007
471	Chain A, the intact and cleaved human antithrombin III complex as a model for serpin–proteinase interactions	gi|999513	150, NA	53, NA	17, NA	5.95	49.35	0.5747±0.0439	0.4135±0.0393	0.72	0.0121
476	Chain A, the intact and cleaved human antithrombin III complex as a model for serpin–proteinase interactions	gi|999513	114, NA	45, NA	15, NA	5.95	49.35	1.4614±0.1020	0.9287±0.1032	0.64	0.0013
479	Chain I, crystal structure of antithrombin III	gi|118137309	135, NA	49, NA	16, NA	5.72	48.75	0.4793±0.0494	0.3220±0.0325	0.67	0.0142
Transporter protein											
490	Serum albumin	gi|11493459	86, NA	24, NA	9, NA	5.96	58.51	0.1107±0.0361	0.2269±0.0296	2.05	0.0209
580	Albumin	gi|7770217	76, NA	45, NA	8, NA	6.14	33.47	0.1373±0.0271	0.5028±0.1167	3.66	0.0059
Acute phase response											
472	Alpha-1-antichymotrypsin precursor	gi|177933	103, NA	34, NA	10, NA	5.32	45.57	0.7189±0.0843	0.3736±0.0546	0.52	0.0024
481	Alpha-1-antichymotrypsin precursor	gi|177933	92, NA	34, NA	8, NA	5.32	45.57	0.6173±0.0452	0.4193±0.0500	0.68	0.0061
487	Alpha-1-antichymotrypsin precursor	gi|177933	72, NA	34, NA	9, NA	5.32	45.57	0.4901±0.0485	0.3368±0.0457	0.69	0.0312
498	Alpha-1-antichymotrypsin precursor	gi|177933	84, NA	34, NA	10, NA	5.32	45.57	0.3447±0.0550	0.2030±0.0376	0.59	0.0448
Protein trafficking											
1122	ADP-ribosylation factor guanine nucleotide-exchange factor 2 (brefeldin A-inhibited), isoform CRA_a	gi|119596086	69, NA	15, NA	15, NA	5.96	203.19	0.1168±0.0240	0.0000±0.0000	0.00	0.0000
Unknown function											
569	hCG2040105	gi|119569386	71, NA	28, NA	10, NA	6.20	63.92	0.2452±0.0304	0.1282±0.0242	0.52	0.0065
618	Hypothetical protein	gi|113422578	80, NA	80, NA	6, NA	9.82	6.81	0.2730±0.0729	0.0199±0.0097	0.07	0.0023
624	Novel KRAB box containing protein	gi|149255350	70, NA	32, NA	10, NA	5.82	61.31	0.5185±0.0817	0.0888±0.0287	0.17	0.0001

NA not applicable

Table 4 Summary of plasma proteins with differential levels in mild vs. severe forms of β-thalassemia/Hb E patients

Spot no.	Protein name	NCBI ID	Identification scores (MS, MS/MS)	% Cov (MS, MS/MS)	No. of matched peptides (MS, MS/MS)	p*I*	MW (kDa)	Intensity (mean±SEM)		Intensity ratio (severe/mild)	*p* values
								Mild	Severe		
Ion channel											
266	Ryanodine receptor 2, cardiac	gi|124430578	85, NA	10, NA	27, NA	5.74	569.65	0.1959±0.0248	0.1301±0.0134	0.66	0.0391
Metabolic enzyme											
267	Aflatoxin B1 aldehyde reductase member 3-like	gi|296206881	72, NA	32, NA	9, NA	8.14	47.09	0.1828±0.0229	0.1181±0.0143	0.65	0.0334
Stress response											
280	Uncoupling protein 3	gi|4928052	68, NA	36, NA	7, NA	9.44	34.42	0.0876±0.0194	0.0362±0.0106	0.41	0.0396
Protein metabolism											
336	Catalytic phosphatidylinositol 3-kinase 3	gi|291394303	74, NA	20, NA	12, NA	6.03	106.56	0.1085±0.0096	0.0717±0.0119	0.66	0.0273
Acute phase response											
472	Alpha-1-antichymotrypsin precursor	gi|177933	103, NA	34, NA	10, NA	5.32	45.57	0.6575±0.0873	0.3736±0.0546	0.57	0.0170
521	Chain A, alpha1-antitrypsin	gi|157831596	114, NA	39, NA	11, NA	5.37	44.28	0.3268±0.0531	0.5509±0.0737	1.69	0.0241
Cell proliferation											
496	Antigen KI-67-like	gi|301772768	84, NA	13, NA	15, NA	9.82	223.69	0.1059±0.0178	0.1623±0.0184	1.53	0.0414
Regulation of vascular tone											
682	Endothelin-converting enzyme 2 isoform 4	gi|291400337	76, NA	24, NA	12, NA	5.29	92.31	0.2894±0.0184	0.2016±0.0262	0.70	0.0135
Transcriptional regulation											
1204	Zinc finger protein 734-like	gi|297713209	72, NA	23, NA	10, NA	8.89	80.98	0.1360±0.0339	0.0264±0.0169	0.19	0.0152

NA not applicable

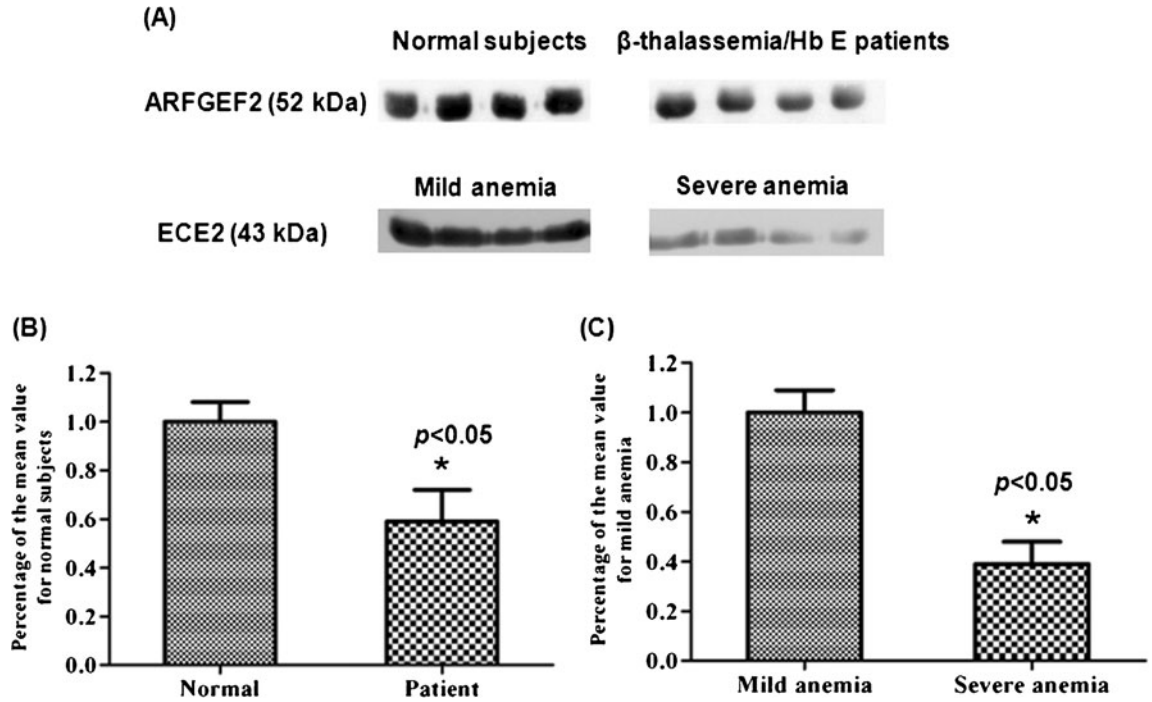


Fig. 2 Validation of proteomics data by Western blot analysis of ADP-ribosylation factor guanine nucleotide exchange factor 2 (*ARFGEF2*) and endothelin-converting enzyme 2 (*ECE2*) (**A**). The quantitative data shown in (**B**) and (**C**) confirmed the decrease of ARFGEF2 in β-thalassemia/Hb E patients compared to healthy individuals and the decrease of ECE2 in severe form compared to the mild form of the disease, respectively. *N*=4 for each group

hematopoietic progenitors and to determine the expression profiles compared between thalassemic and normal condition). Endothelin-converting enzyme 2 (ECE2; spot 682), another protein randomly selected for validation, is the enzyme that generates a powerful vasoconstrictor endothelin-1 (ET-1), which plays an important role in the pathogenesis of pulmonary hypertension, an early sign of heart disease [24, 25]. A few previous studies have reported elevated levels of serum ET-1 in patients with thalassemia [26, 27]. Further studies on the role of ET-1 and ECE in thalassemic pulmonary hypertension are interesting since heart failure is the leading cause of thalassemic death with unclear pathogenic mechanisms.

Several proteins have been reported in research papers related to thalassemia. The first two proteins belong to the complement factor group. Oxidation of protein band 3 on RBC membrane is thought to form a "neo-antigen" and activates complement-mediated phagocytosis by macrophages, leading to the premature destruction of thalassemic red cells [28]. In this study, the levels of complement factors B (spot 299) and C3 (spots 304 and 639) in β-thalassemia/Hb E patients decreased to 44, 50, and 59 % of normal subjects, respectively. This is consistent with the data reported by deCiutiis et al. [29], showing that factors B and C3 relatively decreased to 29 and 59 % of normal subjects, respectively. This might be due to their overutilization since such proteins play a major role in the activation of complement pathways.

Prothrombin (spots 361 and 366) and antithrombin III (spots 471, 476, and 479) are involved in hypercoagulation in thalassemia. Oxidative stress-induced Ca^{2+} influx into RBC disturbs the activities of scramblase and translocase, resulting in increased PS exposure to the outer leaflet of thalassemic erythrocytes [30]. PS exposure exerts a procoagulant effect by activating thrombin generation and platelet aggregation followed by converting fibrinogen to insoluble fibrin [31, 32]. This may explain the increased consumption of prothrombin as a consequence of PS exposure. In this study, the expression of two prothrombin spots (spots 361 and 366) in patients' plasma decreased 75 and 58 % compared to normal plasma, respectively, supported by Weeraphan et al. [15] with a decrease of 58 % by volume. Excess thrombin is inactivated by antithrombin III to keep hemostatic balance. Three spots of antithrombin III (spots 471, 476, and 479) in thalassemia plasma showed decreases of 28, 36, and 33 % spot volume compared to the normal plasma. This is consistent with data showing 21 % significantly decreased levels of serum antithrombin when compared between thalassemic patients' and controls' plasma [33].

In addition to the proteins mentioned above, we also identified other proteins with differential plasma proteome profiles, as shown in Tables 3 and 4, but their association with thalassemia is yet not clear. Most of them, e.g., sodium channel modifier 1, E3 ubiquitin protein ligase, DNA

topoisomerase, appear to be tissue leakage products which normally function within cells but are released into the plasma due to cell death or damage [34]. Thus, their plasma levels do not necessarily reflect their actual cellular levels because they also depend on the release rate from aging or diseased cells. Moreover, their cellular sources of origin responsible for the differential plasma levels is not yet certain since they can be found in various cell types. Their sources are also not necessarily limited to RBCs, but could be the heart, liver, spleen, multiple endocrine glands, bone, or any organs involved in thalassemia severity and complications [1]. Therefore, further investigation is needed to determine whether they have any role in the pathogenesis of thalassemia and its complications, and not just a mere association with thalassemia severity.

In summary, our present study provides a list of differentially expressed plasma proteins between healthy individuals vs. β-thalassemia/Hb E patients and mild vs. severe forms of β-thalassemia/Hb E. However, the proteins mentioned above may serve as good candidates for further studies on the pathophysiology of β-thalassemia/Hb E or for biomarkers to define the severity of β-thalassemia/Hb E.

Acknowledgments We are grateful to Prof. Shui-Tein Chen and Dr. Supachok Sinchaikul for their technical support on mass spectrometric analyses. This study was supported by Office of the Higher Education Commission and Mahidol University under the National Research Universities Initiative (to Thalassemia Research Center and Center for Research in Complex Systems Science); The Thailand Research Fund (RTA5380005); The Siriraj Graduate Thesis Scholarship (to S. Hatairaktham); and "Chalermphrakiat" grant, Faculty of Medicine Siriraj Hospital (to R.W. Kalpravidh, C. Srisawat, and V. Thongboonkerd).

Conflict of interest The authors declare that they have no conflict of interest.

References

1. Rund D, Rachmilewitz E (2005) Beta-thalassemia. N Engl J Med 353:1135–1146
2. Fucharoen S, Wasi P (2005) Thalassemia: clinical manifestation and pathophysiology. In: Fucharoen P, Fucharoen S (eds) Thalassemia: from molecular biology to clinical medicine. Department of Health, Ministry of Public Health, Bangkok, Thailand, pp 5–18
3. Fucharoen S, Winichagoon P, Pootrakul P, Piankijagum A, Wasi P (1987) Variable severity of Southeast Asian beta 0-thalassemia/HB E disease. Birth Defects Orig Artic Ser 23:241–248
4. Good DM, Thongboonkerd V, Novak J, Bascands JL, Schanstra JP, Coon JJ, Dominiczak A, Mischak H (2007) Body fluid proteomics for biomarker discovery: lessons from the past hold the key to success in the future. J Proteome Res 6:4549–4555
5. Fang X, Zhang WW (2008) Affinity separation and enrichment methods in proteomic analysis. J Proteomics 71:284–303
6. Pierre RV (2002) Reticulocytes. Their usefulness and measurement in peripheral blood. Clin Lab Med 22:63–79
7. Stocks J, Dormandy TL (1971) The autoxidation of human red cell lipids induced by hydrogen peroxide. Br J Haematol 20:95–111
8. Winterbourn CC, Hawkins RE, Brian M, Carrell RW (1975) The estimation of red cell superoxide dismutase activity. J Lab Clin Med 85:337–341
9. Beutler E (1984) Red cell metabolism: a manual of biochemical methods. Grune & Stratton, London
10. Griffith OW (1980) Determination of glutathione and glutathione disulfide using glutathione reductase and 2-vinylpyridine. Anal Biochem 106:207–212
11. Pattanapanyasat K, Noulsri E, Fucharoen S, Lerdwana S, Lamchiagdhase P, Siritanaratkul N, Webster HK (2004) Flow cytometric quantitation of red blood cell vesicles in thalassemia. Cytometry B Clin Cytom 57:23–31
12. Gosriwatana I, Loreal O, Lu S, Brissot P, Porter J, Hider RC (1999) Quantification of non-transferrin-bound iron in the presence of unsaturated transferrin. Anal Biochem 273:212–220
13. Bradford MM (1976) A rapid and sensitive method for the quantitation of microgram quantities of protein utilizing the principle of protein-dye binding. Anal Biochem 72:248–254
14. Srinoun K, Svasti S, Chumworathayee W, Vadolas J, Vattanaviboon P, Fucharoen S, Winichagoon P (2009) Imbalanced globin chain synthesis determines erythroid cell pathology in thalassemic mice. Haematologica 94:1211–1219
15. Weeraphan C, Srisomsap C, Chokchaichamnankit D, Subhasitanont P, Hatairaktham S, Charoensakdi R, Panichkul N, Siritanaratkul N, Fucharoen S, Svasti J, Kalpravidh RW (2012) Role of curcuminoids in ameliorating oxidative modification in beta-thalassemia/Hb E plasma proteome. J Nutr Biochem. doi:10.1016/j.jnutbio.2012.02.008
16. Walter PB, Fung EB, Killilea DW, Jiang Q, Hudes M, Madden J, Porter J, Evans P, Vichinsky E, Harmatz P (2006) Oxidative stress and inflammation in iron-overloaded patients with beta-thalassaemia or sickle cell disease. Br J Haematol 135:254–263
17. Kalpravidh RW, Siritanaratkul N, Insain P, Charoensakdi R, Panichkul N, Hatairaktham S, Srichairatanakool S, Phisalaphong C, Rachmilewitz E, Fucharoen S (2010) Improvement in oxidative stress and antioxidant parameters in beta-thalassemia/Hb E patients treated with curcuminoids. Clin Biochem 43:424–429
18. Trombetta D, Gangemi S, Saija A, Minciullo PL, Cimino F, Cristani M, Briuglia S, Piraino B, Isola S, Salpietro CD (2006) Increased protein carbonyl groups in the serum of patients affected by thalassemia major. Ann Hematol 85:520–522
19. Ferro E, Visalli G, Civa R, Rosa MA, Randazzo Papa G, Baluce B, D'Ascola DG, Piraino B, Salpietro C, Di Pietro A (2012) Oxidative damage and genotoxicity biomarkers in transfused and untransfused thalassemic subjects. Free Radic Biol Med 53:1829–1837. doi:10.1016/j.freeradbiomed.2012.08.592
20. Oettl K, Stauber RE (2007) Physiological and pathological changes in the redox state of human serum albumin critically influence its binding properties. Br J Pharmacol 151:580–590
21. Islam A, Shen X, Hiroi T, Moss J, Vaughan M, Levine SJ (2007) The brefeldin A-inhibited guanine nucleotide-exchange protein, BIG2, regulates the constitutive release of TNFR1 exosome-like vesicles. J Biol Chem 282:9591–9599
22. Kheansaard W, Panichob P, Fucharoen S, Tanyong DI (2011) Cytokine-induced apoptosis of beta-thalassemia/hemoglobin E erythroid progenitor cells via nitric oxide-mediated process in vitro. Acta Haematol 126:224–230
23. Rusten LS, Jacobsen SE (1995) Tumor necrosis factor (TNF)-alpha directly inhibits human erythropoiesis in vitro: role of p55 and p75 TNF receptors. Blood 85:989–996
24. Shao D, Park JE, Wort SJ (2011) The role of endothelin-1 in the pathogenesis of pulmonary arterial hypertension. Pharmacol Res 63:504–511
25. Mayyas F, Niebauer M, Zurick A, Barnard J, Gillinov AM, Chung MK, Van Wagoner DR (2010) Association of left atrial endothelin-

1 with atrial rhythm, size, and fibrosis in patients with structural heart disease. Circ Arrhythm Electrophysiol 3:369–379
26. Chaliasos N, Challa A, Hatzimichael E, Koutsouka F, Bourantas DK, Vlahos AP, Siamopoulou A, Bourantas KL, Makis A (2010) Serum adipocytokine and vascular inflammation marker levels in beta-thalassaemia major patients. Acta Haematol 124:191–196
27. Viprakasit V, Kankirawatana S, Akarasereenont P, Durongpisitkul K, Chotewuttakorn S, Tanphaichitr VS (2002) Baseline levels of plasma endothelin-1 (ET-1) and changes during transfusion in thalassemic patients. Am J Hematol 70:260–262
28. Pantaleo A, Giribaldi G, Mannu F, Arese P, Turrini F (2008) Naturally occurring anti-band 3 antibodies and red blood cell removal under physiological and pathological conditions. Autoimmun Rev 7:457–462
29. deCiutiis AC, Peterson CM, Polley MJ, Metakis LJ (1978) Alternative pathway activation in sickle cell disease and beta-thalassemia major. J Natl Med Assoc 70:503–506
30. Zwaal RF, Schroit AJ (1997) Pathophysiologic implications of membrane phospholipid asymmetry in blood cells. Blood 89:1121–1132
31. Atichartakarn V, Angchaisuksiri P, Aryurachai K, Onpun S, Chuncharunee S, Thakkinstian A, Atamasirikul K (2002) Relationship between hypercoagulable state and erythrocyte phosphatidylserine exposure in splenectomized haemoglobin E/beta-thalassaemic patients. Br J Haematol 118:893–898
32. Ruf A, Pick M, Deutsch V, Patscheke H, Goldfarb A, Rachmilewitz EA, Guillin MC, Eldor A (1997) In-vivo platelet activation correlates with red cell anionic phospholipid exposure in patients with beta-thalassaemia major. Br J Haematol 98:51–56
33. Angchaisuksiri P, Atichartakarn V, Aryurachai K, Archararit N, Chuncharunee S, Tiraganjana A, Rattanasiri S (2007) Hemostatic and thrombotic markers in patients with hemoglobin E/beta-thalassemia disease. Am J Hematol 82:1001–1004
34. Anderson NL, Anderson NG (2002) The human plasma proteome: history, character, and diagnostic prospects. Mol Cell Proteomics 1:845–867

Clinical Science (2013) **124**, 389–390 (Printed in Great Britain) doi: 10.1042/CS20120565

The promise and challenge of systems biology in translational medicine

Visith THONGBOONKERD

Medical Proteomics Unit, Office for Research and Development, Faculty of Medicine Siriraj Hospital, and Center for Research in Complex Systems Science, Mahidol University, Bangkok 10700, Thailand

Clinical Science www.clinsci.org

Abstract

Abnormalities in clinical parameters and routine laboratory tests are frequently detected at late stages of many diseases (too late to cure or to prevent life-threatening complications). Hence earlier diagnostic and prognostic markers are needed for decision making and improving therapeutic outcome. In the present issue of *Clinical Science*, Rudiger and co-workers report findings from a transcriptomic study, which revealed that changes in transcripts involved in amino-sugar metabolism, p53-dependent cell-cycle arrest, β-adrenergic signalling and intracellular calcium cycling in cardiac tissue of rats with early sepsis could discriminate survivors from non-survivors. These findings underscore the great potential of systems biology in translational medicine. However, further investigations should be done to make the benchside results more feasible for routine clinical practice.

Key words: body fluid, biomarker, diagnostics, prognostics, sepsis, systems biology, translational medicine

Clinical manifestations and abnormal laboratory tests are frequently present at late stages of many diseases. Moreover, such abnormalities are usually unable to predict disease outcome and therapeutic response. Even with appropriate treatment with standard regimens, mortality rates of some severe diseases remain high and life-threatening complications remain common. This urges clinicians and scientists to search for earlier diagnostic and prognostic markers, which will be helpful in decision making and improving therapeutic outcome. Between diagnostic and prognostic markers, defining the latter seems to be more difficult to achieve [1].

Over the last decade, systems biology has been widely applied to search for prognostic markers in many diseases [2–4]. A huge number of candidates for prognostic markers have been identified recently in various studies using clinical samples or animal models. However, the major shortcoming of these recent investigations is that most of them have reported only changes or differences between groups, whereas a much smaller number of studies have demonstrated the practicality of those findings in clinical practice [5,6]. In the present issue of *Clinical Science*, Rudiger and co-workers [7] report the data obtained from systems biology of early sepsis using a rat model. This is a well-performed study to demonstrate that a reduction in myocardial function and transcriptomic changes at an early phase of sepsis could predict clinical outcome in rats with sepsis.

The investigators first showed that, at 6 h after the induction of sepsis, cardiac stroke volume <0.17 ml could predict the mortality of rats with sepsis with 93 and 80% positive and negative predictive values respectively [7]. Transcriptomic analysis was subsequently performed to define altered transcripts and their pathways that were related with poor clinical outcome. The findings showed significant alterations in the expression of 527 transcripts in cardiac tissue of rats with sepsis. Some of these changes were related to anaesthesia and instrumentation, not to sepsis itself, whereas only 120 out of the 527 altered transcripts could discriminate survivors from non-survivors. Interestingly, network analysis revealed that the altered transcripts induced by sepsis were involved mainly in inflammatory process, organ injury, musculoskeletal disorder and cardiovascular disease, whereas those related to the poor clinical outcome were involved in amino-sugar metabolism, p53-dependent cell-cycle arrest, β-adrenergic signalling and intracellular calcium cycling [7]. This reflects a benefit from including more than one control group (i.e. naïve and sham groups in the present study) in a training set of transcriptomic screening to increase the 'specificity' of the findings [5,6]. In addition, it is advisable for any biomarker discovery studies to also include the disease controls (other diseases that mimic clinical and laboratory features of the disease of interest) to increase the feasibility for defining so-called 'disease-specific' markers.

Overall, the present study by Rudiger et al. [7] serves as a good example of systems biology aiming for clinical applications. However, these findings derived from an animal model should be validated in a large cohort of patients with sepsis to

Correspondence: Professor Visith Thongboonkerd (e-mail thongboonkerd@dr.com or vthongbo@yahoo.com)

determine their sensitivity and specificity to predict the poor clinical outcome in humans [8]. Moreover, elucidation of functional roles that these altered transcripts play in the mechanistic pathways of severe sepsis should be also performed to search for new therapeutic targets and for a more effective treatment of sepsis (with the ultimate goal to reduce life-threatening complications and mortality rate). It should be noted that selection of the samples for such investigations is a crucial issue. The present study by Rudiger et al. [7] focused on transcriptomic changes only in the cardiac tissue, because they aimed to correlate these changes with cardiac physiological data. As pathophysiological processes in various cells and tissues differ, it is expected that there are 'tissue-specific' alterations in transcriptomic, proteomic and other signatures [9]. This is also true for the present study, in which the investigators have indicated that transcriptomic analysis of concurrently taken liver samples revealed different signalling pathways [7]. Therefore 'tissue-specific' markers should be elucidated, particularly for the diseases in which mechanisms of injury of multiple organs are different. Otherwise, the 'disease-specific' markers that can be detected in all or most of the tissues must be defined.

Further investigations should be also directed to translating the benchside results to routine clinical practice. Although 'tissue-specific' markers are suitable for determining the specific organ injury, the practicality and their use in routine clinical practice may be limited. In addition, it may be illegal to obtain tissues or cells from the affected organs for monitoring a therapeutic response. Therefore biomarkers in easily accessible body fluids (whole blood, plasma/serum, urine etc.) may be more attractive. However, such markers should have a predictive value and represent the pathophysiology that can be detected at the tissue/organ level. Taking these into account, Taurino et al. [10] have reported previously in *Clinical Science* another promising transcriptomics study. In that study, mRNA and microRNA expression profiles were examined in whole blood to discover genes that could determine cardiovascular phenotypes in patients with coronary artery disease. Those genes were likely to play pivotal roles in the pathogenic mechanisms and progression of chronic coronary artery disease [10].

Finally, the selection of the type of body fluid for biomarker discovery needs attention. Changes observed in body fluids are most reliable to the diseases of organs that are closely related to such biofluids (e.g. urine for kidney diseases, pleural fluid for lung diseases, cerebrospinal fluid for brain and spinal cord diseases etc.), because abnormalities in these organs can directly affect secretion/excretion of those markers into the corresponding body fluids. Unlike others, plasma/serum is related to almost all of the organs. However, changes that can be observed in the plasma/serum must reach a threshold of the detectability of an assay to be used. As there is a wide dynamic range of levels of marker molecules in plasma/serum, the low abundant markers may be undetectable. Moreover, the changes observed in plasma/serum are the results of averaged effects from all of the affected organs, thereby reducing the organ specificity. Therefore selection of the samples to be investigated is not simple, but is indeed one of the most sophisticated issues in the study design for biomarker discovery.

In summary, the systems biology approach holds a great promise in translational medicine. However, there are several challenges that need further investigations to make the benchside results more feasible for routine clinical practice.

FUNDING

My own work is supported by The Thailand Research Fund [grant number RTA5380005], the Office of the Higher Education Commission and Mahidol University under the National Research Universities Initiative, a 'Chalermphrakiat" Grant, and the Faculty of Medicine Siriraj Hospital.

REFERENCES

1 Steyerberg, E. W., Pencina, M. J., Lingsma, H. F., Kattan, M. W., Vickers, A. J. and Van Calster, B. (2012) Assessing the incremental value of diagnostic and prognostic markers: a review and illustration. Eur. J. Clin. Invest. **42**, 216–228
2 Liotta, L. A. and Petricoin, III, E. F. (2012) -Omics and cancer biomarkers: link to the biological truth or bear the consequences. Cancer Epidemiol. Biomarkers Prev. **21**, 1229–1235
3 Lopez, E., Madero, L., Lopez-Pascual, J. and Latterich, M. (2012) Clinical proteomics and OMICS clues useful in translational medicine research. Proteome Sci. **10**, 35
4 Tang, W. H. (2012) Biomarkers in cardiovascular diseases: how can the "-omics" revolution be applicable at the bedside. Introduction. Prog. Cardiovasc. Dis. **55**, 1–2
5 Mischak, H., Allmaier, G., Apweiler, R., Attwood, T., Baumann, M., Benigni, A., Bennett, S. E., Bischoff, R., Bongcam-Rudloff, E., Capasso, G. et al. (2010) Recommendations for biomarker identification and qualification in clinical proteomics. Sci. Transl. Med. **2**, 46ps42
6 Mischak, H., Ioannidis, J. P., Argiles, A., Attwood, T. K., Bongcam-Rudloff, E., Broenstrup, M., Charonis, A., Chrousos, G. P., Delles, C., Dominiczak, A. et al. (2012) Implementation of proteomic biomarkers: making it work. Eur. J. Clin. Invest. **42**, 1027–1036
7 Rudiger, A., Dyson, A., Felsmann, K., Carre, J. E., Taylor, V., Hughes, S., Clatworthy, I., Protti, A., Pellerin, D., Lemm, J. et al. (2013) Early functional and transcriptomic changes in the myocardium predict outcome in a long-term rat model of sepsis. Clin. Sci. **124**, 391–401
8 Ioannidis, J. P. and Khoury, M. J. (2011) Improving validation practices in "omics" research. Science **334**, 1230–1232
9 Kampf, C., Bergman, J., Oksvold, P., Asplund, A., Navani, S., Wiking, M., Lundberg, E., Uhlen, M. and Ponten, F. (2012) A tool to facilitate clinical biomarker studies – a tissue dictionary based on the Human Protein Atlas. BMC Med. **10**, 103
10 Taurino, C., Miller, W. H., McBride, M. W., McClure, J. D., Khanin, R., Moreno, M. U., Dymott, J. A., Delles, C. and Dominiczak, A. F. (2010) Gene expression profiling in whole blood of patients with coronary artery disease. Clin. Sci. **119**, 335–343

Received 16 October 2012/19 October 2012; accepted 22 October 2012
Published as Immediate Publication 22 October 2012, doi: 10.1042/CS20120565

 © The Authors Journal compilation © 2013 Biochemical Society

J Biol Inorg Chem (2013) 18:299–308
DOI 10.1007/s00775-012-0974-0

ORIGINAL PAPER

Bacteria can promote calcium oxalate crystal growth and aggregation

Somchai Chutipongtanate · Suchitra Sutthimethakorn · Wararat Chiangjong · Visith Thongboonkerd

Received: 11 August 2012 / Accepted: 20 December 2012 / Published online: 20 January 2013
© SBIC 2013

Abstract Our previous report showed that uropathogenic bacteria, e.g., *Escherichia coli*, are commonly found inside the nidus of calcium oxalate (CaOx) kidney stones and may play pivotal roles in stone genesis. The present study aimed to prove this new hypothesis by direct examining CaOx lithogenic activities of both Gram-negative and Gram-positive bacteria. CaOx was crystallized in the absence (blank control) or presence of 10^5 CFU/ml *E. coli*, *Klebsiella pneumoniae*, *Staphylococcus aureus*, or *Streptococcus pneumoniae*. Fragmented red blood cell membranes and intact red blood cells were used as positive and negative controls, respectively. The crystal area and the number of aggregates were measured to initially screen for effects of bacteria on CaOx crystal growth and aggregation. The data revealed that all the bacteria tested dramatically increased the crystal area and number of crystal aggregates. Validation assays (spectrophotometric oxalate-depletion assay and an aggregation–sedimentation study) confirmed their promoting effects on both growth (20.17 ± 3.42, 17.55 ± 2.27, 16.37 ± 1.38, and 21.87 ± 0.85 % increase, respectively) and aggregation (57.45 ± 2.08, 51.06 ± 5.51, 55.32 ± 2.08, and 46.81 ± 3.61 % increase, respectively) of CaOx crystals. Also, these bacteria significantly enlarged CaOx aggregates, with the diameter greater than the luminal size of distal tubules, implying that tubular occlusion might occur. Moreover, these bacterial effects were dose-dependent and specific to intact viable bacteria, not intact dead or fragmented bacteria. In summary, intact viable *E. coli*, *K. pneumoniae*, *S. aureus*, and *S. pneumoniae* had significant promoting effects on CaOx crystal growth and aggregation. This functional evidence supported the hypothesis that various types of bacteria can induce or aggravate metabolic stone disease, particularly the CaOx type.

Keywords Bacteria · Calcium oxalate · Crystal growth · Crystal aggregation · Stone

Introduction

Infection-induced kidney stone disease was previously related to struvite [1–4], not metabolic stones. Struvite stone is mostly composed of magnesium ammonium phosphate. Since normal urine is usually undersaturated with ammonium phosphate, struvite stone occurs only when patients have a urinary tract infection (UTI) with a urease-producing organism such as *Proteus* [1–3]. Urease breaks down urinary urea into ammonia, which subsequently combines with water, resulting in the production of ammonium and hydroxide ions. Supersaturation of ammonia due to urease-producing bacteria and decreased solubility of phosphate due to elevated urine pH following hydroxide ion overproduction finally drive struvite stone formation [1–3].

On the other hand, metabolic stones have been characterized as the outcome of metabolic disturbances, e.g., hypercalciuria, hyperoxaluria, and hypocitraturia [4, 5], but not UTI. Alterations in urinary stone modulating factors, including metabolic substrates (i.e., calcium and oxalate)

Electronic supplementary material The online version of this article (doi:10.1007/s00775-012-0974-0) contains supplementary material, which is available to authorized users.

S. Chutipongtanate · S. Sutthimethakorn · W. Chiangjong · V. Thongboonkerd (✉)
Medical Proteomics Unit, Office for Research and Development, Faculty of Medicine Siriraj Hospital,
Center for Research in Complex Systems Science, Mahidol University, 6th Floor-SiMR Building,
2 Prannok Road, Bangkoknoi,
Bangkok 10700, Thailand
e-mail: thongboonkerd@dr.com; vthongbo@yahoo.com

[4, 5], stone inhibitors (i.e., citrate and some urinary anionic proteins) [4–8], and promoting factors (i.e., cell membranes and lipid vesicles) [9–11], contribute more to metabolic stone development. Once formed, metabolic stones might incidentally entrap some bacteria, which become the source of recurrent UTI [3]. Accordingly, UTI has only been understood as a complication, but not a cause, of metabolic stones.

Although almost all previous evidences have indicated that bacteria do not induce the formation of metabolic stones, a few recent reports have suggested that some metabolic stones, particularly calcium oxalate (CaOx), might originate from infections [12–15]. This speculation was based entirely on bacteriology and chemical compositional analysis of the internal parts of metabolic stones [12–15]. Among these studies, Sohshang et al. [14] reported that about 47 % of 100 calculi obtained from 100 stone formers had positive bacterial culture in the urine and stone nidus. *Escherichia coli* was the commonest organism isolated from the urine and stone nidus, and CaOx was the major component of the stone nidus [14]. These data were consistent with the findings reported in our recent study [15], in which bacteria were isolated from catheterized urine as well as stone cortex and nidus obtained from 100 kidney stone formers. Our study showed that 36 stone formers had 45 bacterial isolates from their catheterized urine and/or stone nidi [15]. Stone analysis revealed that most of these individuals with bacterial isolates had metabolic stones (CaOx was found in 64 % of cases). Moreover, *E. coli* was the commonest bacterium (about one third of all bacteria) found in the urine and stone matrices (both nidus and periphery), and urea-splitting bacteria were not the major causative microorganisms [15].

The findings that non-urea-splitting bacteria, particularly *E. coli*, predominate in the nidus of metabolic stones in our study [15] and other previous studies [12–15] have suggested a new hypothesis that various bacteria may induce or aggravate the genesis of metabolic stones [15, 16]. Unlike the pathogenic mechanisms of struvite stone, which is associated with urease-producing bacteria, the mechanisms of non-urea-splitting bacteria for the formation/promotion of metabolic stones remained largely unknown. The present study was thus conducted to prove this new hypothesis by evaluation of lithogenic activities of various bacteria with regard to CaOx crystals. Four common Gram-negative and Gram-positive bacterial species—*E. coli*, *Klebsiella pneumoniae*, *Staphylococcus aureus*, and *Streptococcus pneumoniae*—were analyzed in this study as representatives of uropathogenic and nonuropathogenic organisms, respectively. Direct morphological evaluation and image analysis of CaOx crystals [17] were performed to initially screen for the effects of these bacteria on crystal growth and aggregation. Lithogenic activities of bacteria were then validated by spectrophotometric oxalate-depletion assay [6] and a CaOx crystal aggregation–sedimentation study [7] (the gold-standard methods for analyzing CaOx crystal growth and aggregation, respectively). The size and morphology of bacteria-induced CaOx aggregates were also observed by phase-contrast microscopy to evaluate potential clinical relevance. Finally, the effects of differential doses and viability of bacteria on CaOx crystal growth and aggregation were addressed.

Materials and methods

CaOx crystallization without or with bacterial intervention

CaOx crystals were generated according to our previously published protocols [17]. To examine the effects of bacteria on CaOx crystallization, the crystals were prepared as mentioned before, but in the presence of 10^5 CFU/ml intact viable *E. coli*, *K. pneumoniae*, *S. aureus*, or *S. pneumoniae*. Details of the bacterial cultivation, growth, measurement of bacterial concentration/number, and preparation can be found in the electronic supplementary material.

Fragmented red blood cell (RBC) membranes (previously reported as the promoter of CaOx crystal growth and aggregation) [10] and intact RBCs (which had no effects on CaOx crystals) [10] at 10^5 cells per milliliter were used as positive and negative controls, respectively. After 1 h incubation at room temperature (25 °C), the supernatant was discarded, and the crystals were gently washed and then dried. The effects of bacteria on CaOx crystals were then evaluated as follows.

Initial screening for the effects of bacteria on CaOx crystal growth and aggregation

The effects of bacteria on CaOx crystal growth and aggregation were initially screened by crystal image analysis. After crystallization without or with bacteria at 25 °C, crystal images were taken by a phase-contrast inverted light microscope (CKX41; Olympus, Tokyo, Japan) connected to a digital camera. The crystal images were then analyzed by the ImageMaster 2D Platinum software program (GE Healthcare, Uppsala, Sweden) to quantitatively measure the crystal size and number of CaOx aggregates [17]. The crystal size was measured from 100 randomized individual crystals and then averaged for each sample. The number of crystal aggregates, which were defined as an assembly of two or more individual crystals tightly joined together [10, 11, 18], was counted and averaged from ten high-power fields. These experiments were done in triplicate.

Spectrophotometric oxalate-depletion assay

Modulating or promoting activities of bacteria with regard to CaOx crystal growth were confirmed by spectrophotometric oxalate-depletion assay at 25 °C, as described previously by Nakagawa et al. [6].

For the blank control, CaOx crystal seeds (160 μg) were added to 1-ml equilibrated solution containing 1 mM $CaCl_2 \cdot 2H_2O$, 1 mM $Na_2C_2O_4$, 10 mM tris(hydroxymethyl)aminomethane–HCl (pH 7.4), and 90 mM NaCl in a cuvette. Basically, the seeded crystals would grow further using excess calcium (from $CaCl_2$) and oxalate (from $Na_2C_2O_4$) ions, leading to depletion of free oxalate, which was detectable and monitored at 214 nm by a UV–visible spectrophotometer (UV-160A; Shimadzu, Kyoto, Japan).

For positive control, negative control, and the bacteria to be tested, each of them was added to the equilibrated solution to a final concentration of 10^5 cells per milliliter (for RBCs) or 10^5 CFU/ml (for bacteria) before the crystal seeds were added. Depletion of free oxalate would be accelerated if the bacteria promoted CaOx crystal growth. The rate of free oxalate depletion was calculated using the baseline value and the value after 60 s incubation with or without cells/bacteria. The relative crystal growth promoting activity was calculated using the following equation:

$$\% \text{ CaOx crystal growth promotion} = [(C - T)/C] \times 100$$

where C is the rate of free oxalate depletion without bacteria, and T is the rate of free oxalate depletion with the cells/bacteria to be tested

These experiments were done in triplicate.

CaOx crystal aggregation–sedimentation study

Modulating or promoting activities of bacteria with regard to CaOx crystal aggregation were confirmed by a CaOx crystal aggregation–sedimentation study at 25 °C, as described previously by Atmani and Khan [7] with a slight modification.

For the blank control, individual CaOx crystals (100 μg) were added to 1 ml solution containing 1 mM $CaCl_2 \cdot 2H_2O$, 0.1 mM $Na_2C_2O_4$, 10 mM tris(hydroxymethyl) aminomethane–HCl (pH 7.4), and 90 mM NaCl in a cuvette. The mixture was stirred at 800 rpm using a magnetic minibar. The crystal aggregation process consumed a number of individual CaOx crystals to form larger particulates. Sedimentation of these aggregates then resulted in a reduction of the solution turbidity, which could be monitored by a UV–visible spectrophotometer (Shimadzu UV-160A) at 620 nm for 60 min.

For positive control, negative control, and the bacteria to be tested, each of them was added to the equilibrated solution to a final concentration of 10^5 cells per milliliter (for RBCs) or 10^5 CFU/ml (for bacteria) before the crystals were added. Modulating or promoting activities of bacteria with regard to CaOx crystal aggregation were evaluated by comparing the turbidity slope in the presence and absence of bacteria at the end of the assay (60 min). In addition, the morphology of the aggregates generated by this reaction was observed under a phase-contrast microscope to reconfirm the crystal aggregation potency of bacteria. The maximal diameter of the largest CaOx aggregate in each high-power field was measured by Tarosoft Image Frame Work version 0.9.6 (Nikon, Tokyo, Japan). Each data point was derived from five individual samples.

Effects of differential doses and viability of bacteria on CaOx crystal growth and aggregation

The effects of differential doses of bacteria on CaOx crystal growth and aggregation were evaluated using 10–10^5 CFU/ml intact viable *E. coli* as the representative bacterium. To prepare intact dead bacteria, 10^5 CFU/ml viable *E. coli* was incubated with 4 % formaldehyde in phosphate-buffered saline at 25 °C for 30 min. The absence of viable bacteria after such treatment was confirmed by routine culture and microscopic examination. To prepare bacterial fragments, the intact dead *E. coli* bacteria at an identical concentration (10^5 CFU/ml) were sonicated in isotonic saline using a probe sonicator (Vibra-Cell 130-W ultrasonic processor with a VCX 130 FSJ footswitch; Sonics & Materials, Newtown, CT, USA) in an icebox for 30 min. Fragmented bacterial morphology was confirmed by microscopic examination. After crystallization without or with differential doses (10–10^5 CFU/ml) and various forms (intact viable, intact dead, and fragmented) of *E. coli* at 25 °C for 1 h, CaOx crystal growth and aggregation were evaluated as mentioned earlier. The crystal size was measured from 100 randomized individual crystals and then averaged for each sample. The number of crystal aggregates, which were defined as an assembly of two or more individual crystals tightly joined together [10, 11, 18], was counted and averaged from ten high-power fields. These experiments were done in triplicate.

Statistical analysis

All the quantitative data are reported as the mean ± the standard error of the mean. Multiple comparisons were performed using analysis of variance with Tukey's post hoc test (SPSS, version 11.5). $P < 0.05$ was considered statistically significant.

Results

Four common Gram-negative and Gram-positive bacterial species—*E. coli*, *K. pneumoniae*, *S. aureus*, and *S. pneumoniae*—were propagated in LB broth before estimation of bacterial numbers and concentrations by plate colony counting and turbidimetry at 600 nm (optical density at 600 nm) as detailed in the electronic supplementary material. Correlations of bacterial concentrations from plate colony counting and the optical density at 600 nm were analyzed by linear regression analysis (see Fig. S1). By this method, a concentration of 10^5 CFU/ml *E. coli*, *K. pneumoniae*, *S. aureus*, and *S. pneumoniae* was accurately prepared for subsequent analyses.

Crystal image analysis was initially performed to screen for CaOx lithogenic activities of *E. coli*, *K. pneumoniae*, *S. aureus*, and *S. pneumoniae*. Fragmented RBC membranes (which were previously reported as the stone-promoting factor) [10] and intact RBCs (which had no modulating effect) [10] were adopted as the positive and negative controls, respectively. Consistent with our previous report [10], morphological data showed that fragmented RBC membranes could promote CaOx crystal growth (as indicated by the increase in crystal size) and aggregation (as indicated by the increase in the number of crystal aggregates) as compared with the blank controls, whereas intact RBCs had no promoting activity (Fig. 1). Interestingly, all four bacteria (*E. coli*, *K. pneumoniae*, *S. aureus*, *S. pneumoniae*) promoted dramatic CaOx crystal growth and aggregation (Fig. 1). These initial results suggested that *E. coli*, *K. pneumoniae*, *S. aureus*, and *S. pneumoniae* had potential lithogenic effects on CaOx growth and aggregation.

To confirm the promoting effects of these bacteria on CaOx crystal growth, spectrophotometric oxalate-depletion assay was performed. At 60 s of monitoring, fragmented RBC membranes (the positive control) significantly promoted crystal growth (crystal growth promotion of 23.67 ± 3.36 %), whereas intact RBCs (the negative control) and the blank control had no effect on crystal growth (Fig. 2). *E. coli*, *K. pneumoniae*, *S. aureus*, and *S. pneumoniae* showed significant crystal-growth-promoting activity (crystal growth promotion of 20.17 ± 3.42, 17.55 ± 2.27, 16.37 ± 1.38 and 21.87 ± 0.85 %, respectively) (Fig. 2). This result obtained from spectrophotometric oxalate-depletion assay was consistent with that obtained from the initial screening experiment (Fig. 1), confirming that *E. coli*, *K. pneumoniae*, *S. aureus*, and *S. pneumoniae* had a direct lithogenic effect on CaOx crystal growth.

A CaOx crystal aggregation–sedimentation study was performed to validate the promoting effects of bacteria on CaOx crystal aggregation. Reduction of the solution turbidity at 620 nm resulted from sedimentation of the large particles or crystal aggregates, and thus could be used to reflect the degree of crystal aggregation. At 60 min, fragmented RBC membranes (the positive control) significantly aggravated crystal aggregation (53.19 ± 3.61 % increase), whereas intact RBCs (the negative control) and the blank control had no significant effect on crystal aggregation (Fig. 3a). *E. coli*, *k. pneumoniae*, *S. aureus*, and *S. pneumoniae* exhibited dramatic promoting activity with regard to crystal aggregation (with increases of 57.45 ± 2.08, 51.06 ± 5.51, 55.32 ± 2.08 and 46.81 ± 3.61 %, respectively) (Fig. 3a). This result confirmed that *E. coli*, *K. pneumoniae*, *S. aureus*, and *S. pneumoniae* had a direct lithogenic effect on CaOx crystal aggregation, consistent with the hypothesis proposed by Hirano et al. [19], in which the bacteria have been proposed to aggravate stone genesis by acting as adhesive molecules.

The aggregated products from the aggregation–sedimentation study were collected to observe their size and morphology under a phase-contrast light microscope. As shown in Fig. 3b, the CaOx aggregates induced by *E. coli*, *K. pneumoniae*, *S. aureus*, *S. pneumoniae*, and fragmented RBC membranes (positive control) were obviously larger than those induced by the blank control and intact RBCs (negative control). Some bacteria-induced CaOx aggregates formed as huge, tightly packed masses, which probably served as the stone core nidus. The maximal diameters of the CaOx aggregates induced by *E. coli*, *K. pneumoniae*, *S. aureus*, *S. pneumoniae*, and fragmented RBC membranes were 69.74 ± 4.79, 62.99 ± 2.88, 58.53 ± 5.64, 57.33 ± 7.57, and 63.49 ± 4.39 μm, respectively, which were obviously larger than those of the CaOx aggregates induced by the blank control and intact RBCs (26.14 ± 2.15 and 28.28 ± 0.93 μm, respectively) (Fig. 3c). Moreover, the size of these bacteria-induced huge CaOx aggregates exceeded the intraluminal diameter of distal renal tubule (approximately 20–30 μm) [20], suggesting that tubular occlusion by these bacteria-induced huge CaOx aggregates was possible.

Finally, the effects of differential doses and viability of bacteria were also evaluated. The data revealed that both growth and aggregation of CaOx crystals were affected by bacteria in a dose-dependent manner (Fig. 4). Interestingly, only the intact viable bacteria, not the intact dead or fragmented bacteria, had dramatic promoting effects on CaOx crystal growth and aggregation (Fig. 5).

Discussion

Previously, UTI was not recognized as a cause of metabolic stone disease. This might be due to the discordant correlation between UTI episodes and metabolic stone

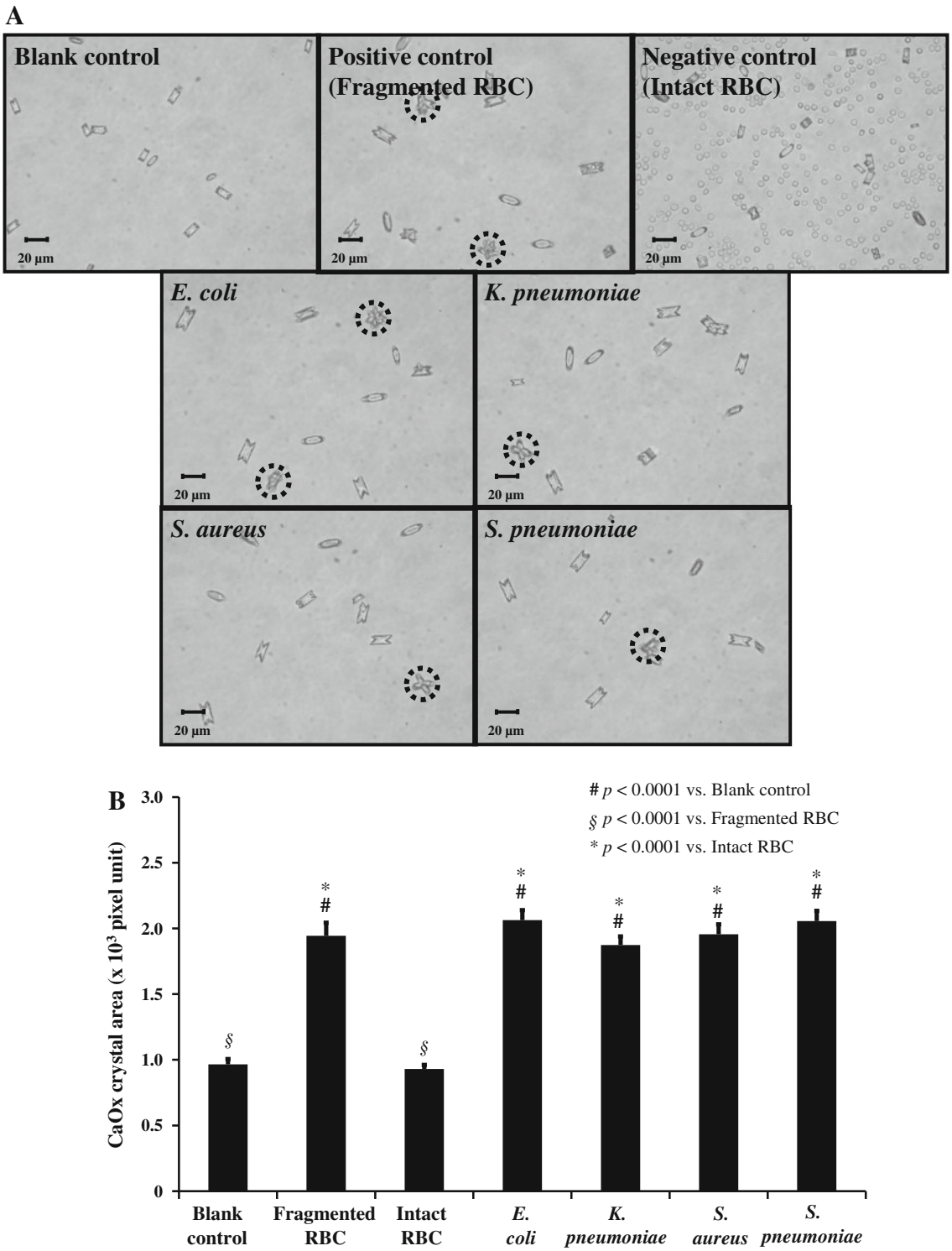


Fig. 1 Crystal image analysis. Calcium oxalate (*CaOx*) lithogenic effects of bacteria were initially screened by morphological evaluation (**a**). CaOx crystals were generated in the absence (blank control) or presence of 10^5 CFU/ml *Escherichia coli*, *Klebsiella pneumoniae*, *Staphylococcus aureus*, and *Streptococcus pneumoniae*. Fragmented red blood cell (*RBC*) membranes and intact RBCs (equivalent to 10^5 cells per assay) were used as positive and negative controls, respectively. *Dashed circles* indicate crystal aggregates (which were defined as groups of two or more crystals tightly joined together). Original magnification ×400 for all *panels*. Crystal images were captured by a digital camera and submitted to ImageMaster 2D Platinum for quantitative analysis of the CaOx crystal area (**b**) and the number of CaOx aggregates (**c**). Each *bar* was derived from three independent experiments and the data are reported as the mean ± the standard error of the mean (SEM). *HPF* high-power field

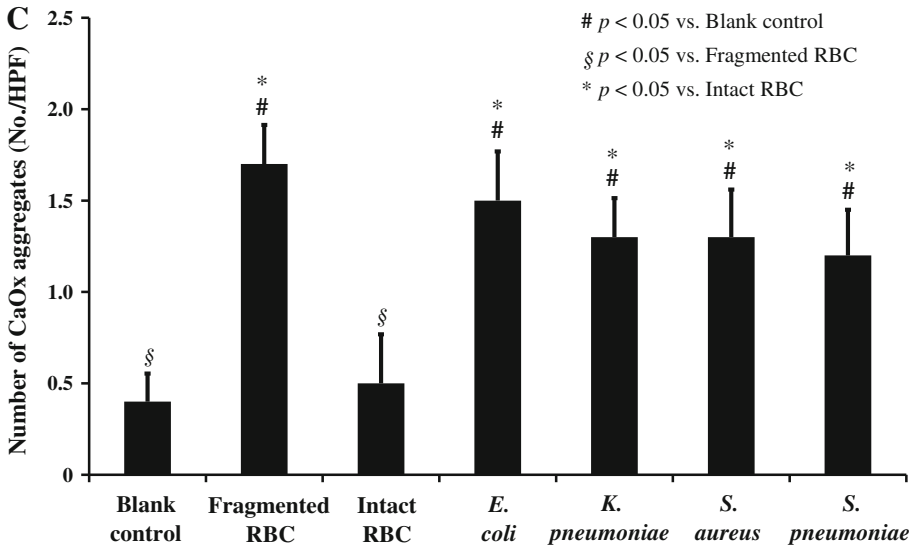


Fig. 1 continued

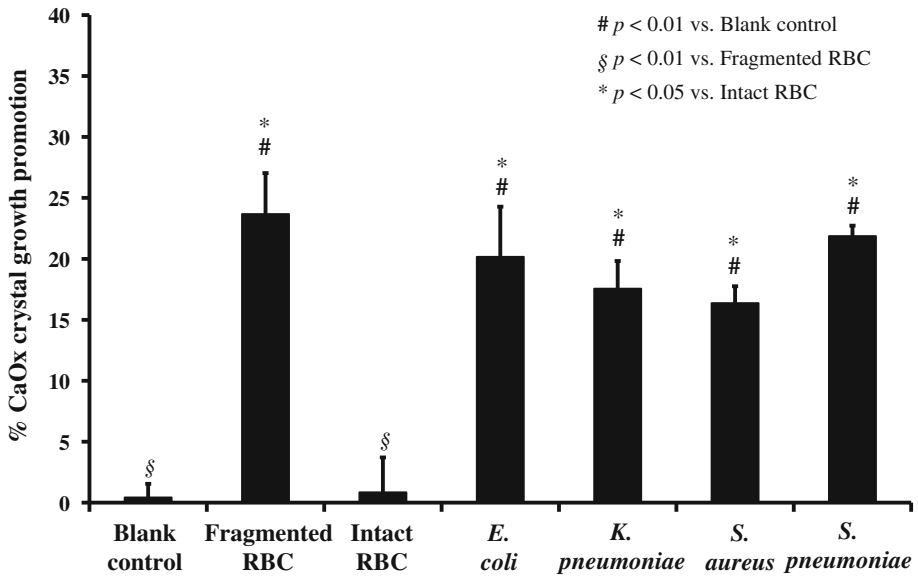


Fig. 2 Spectrophotometric oxalate-depletion assay. CaOx crystal seeds (160 μg) were added to 1 ml solution containing 1 mM $CaCl_2{\cdot}2H_2O$ and 1 mM $Na_2C_2O_4$ in a cuvette. Depletion of free oxalate (which indicated crystal growth) was detectable by measuring the absorbance at 214 nm for up to 60 s in the absence (blank control) or presence of 10^5 CFU/ml *E. coli*, *K. pneumoniae*, *S. aureus*, and *S. pneumoniae*. Fragmented RBC membranes and intact RBCs (equivalent to 10^5 cells per assay) were used as positive and negative controls, respectively. Each data point was derived from three independent experiments and the data are reported as the mean ± SEM

formation (unlike UTI with urease-producing bacteria and struvite stone formation). However, CaOx stone development is relatively slow (when compared with that of struvite), so it may require several months or many years after an UTI episode for a stone to grow to a clinically relevant size (which may be out of the range of the observational period). Moreover, direct CaOx lithogenic activities of bacteria had never been examined.

The nidus is defined as the innermost part of each stone that acts as an initiator of stone formation [21]. It is generally accepted that organic components in the stone nidus play a significant role in stone genesis [21]. Several organic substances deposited inside the CaOx stone nidus (such as anionic proteins, lipids and RBC membranes) [9, 10, 21, 22] have been reported to have lithogenic effects. Several lines of evidence of bacterial deposition inside the CaOx

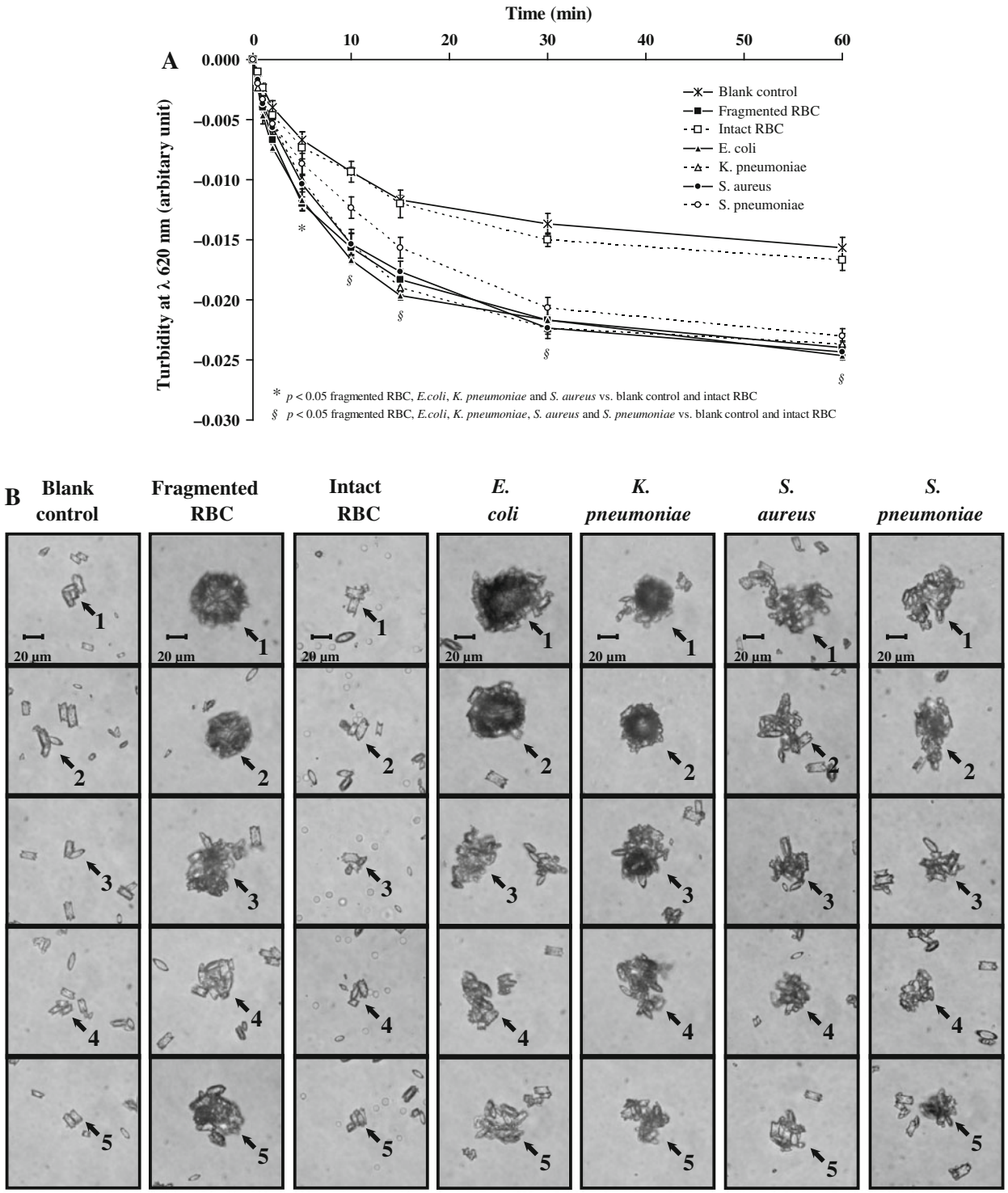


Fig. 3 CaOx crystal aggregation–sedimentation study. **a** Individual CaOx crystals (100 μg) were added to 1 ml solution containing 1 mM $CaCl_2{\cdot}2H_2O$ and 0.1 mM $Na_2C_2O_4$ in a cuvette. The mixture was stirred at 800 rpm using a magnetic minibar. Sedimentation of CaOx crystal aggregates reduced the solution turbidity, which was monitored at 620 nm for 60 min in the absence (blank control) or presence of 10^5 CFU/ml *E. coli*, *K. pneumoniae*, *S. aureus*, and *S. pneumoniae*. Fragmented RBC membranes and intact RBCs (equivalent to 10^5 cells per assay) were used as positive and negative controls, respectively. **b** Aggregated products of this reaction were morphologically observed under a phase-contrast microscope. The numbers *1–5* indicate individual samples that were used for subsequent measurement. **c** The maximal diameter of the largest CaOx aggregate in each high-power field was measured using Tarosoft Image Frame Work. The *dashed line* indicates the intraluminal diameter of distal renal tubules (approximately 30 μm). Each data point was derived from five individual samples and the data are reported as the mean ± SEM

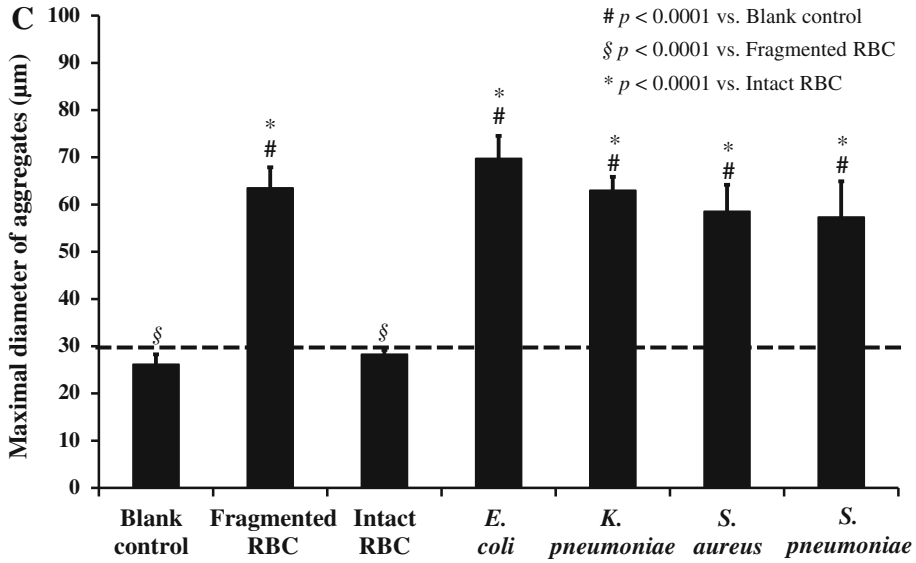


Fig. 3 continued

stone nidus have led to the question of whether uropathogenic bacteria (particularly *E. coli*) also have direct lithogenic activities or not. To the best of our knowledge, at least two publications have demonstrated lithogenic effects of bacteria indirectly [19, 23]. Hirano et al. [19] reported that bacteria tended to cause crystalline and organic matter to aggregate in the urine of stone formers and have suggested that bacteria may participate actively in stone genesis as adhesive molecules. Venkatesan et al. [23] showed that *E. coli* and *Proteus mirabilis* aggravated CaOx encrustation on the surface of polyurethane film, the same material as used in urinary stents. They also suggested that biofilm created by these bacteria might be responsible for CaOx encrustation. Nevertheless, direct lithogenic activities of those bacteria had not been investigated.

The present study demonstrated, for the first time, by a novel screening method [17] and gold-standard assays [6, 7] that bacteria can directly promote CaOx crystal growth and aggregation. The CaOx stone promoting activities of bacteria were comparable to those of fragmented RBC membranes, the most recently proposed CaOx stone promoter [10]. The findings in this study have also supported the new hypothesis regarding the lithogenic role of bacteria in the formation of metabolic stones proposed by our group [15] and in several other reports [12–14, 19, 23]. These lines of evidence have suggested reconsidering UTI as a possible cause of metabolic stone disease [16].

An unexpected finding was that all bacterial species used in this study showed CaOx lithogenic activities. We initially anticipated that only uropathogenic bacteria, i.e., *E. coli* and *K. pneumoniae*, would promote CaOx crystal growth and aggregation on the basis of clinical microbiology and previous results obtained from stone nidus culture [14, 15]. However, the data showed that nonuropathogenic bacteria, i.e., *S. aureus* and *S. pneumoniae*, also exhibit CaOx lithogenic effects. This might explain why the promoting activities of bacteria with regard to CaOx crystal growth and aggregation did not require a unique biological activity of bacteria (unlike struvite stone, which needs urease activity) [1–3], and that they might depend on a common property among bacteria.

Most bacteria have an overall negative charge at physiologic pH [24]. Ionic interaction between anions on the bacterial surface and cations (i.e., Ca^{2+}) on CaOx crystals should suspected, since this interaction has been reported as the adhesive force between stone-modulating factors (such as anionic urinary molecules or epithelial cell surfaces) and CaOx crystals by use of atomic force microscopy [25, 26]. However, the specific molecules on the bacterial surface responsible for this interaction remain unknown. Teichoic acid [27] and lipopolysaccharide [28], two abundant anionic molecules on bacterial cell walls which provide an overall negative charge to Gram-positive and Gram-negative bacteria, respectively, may be the key players in this setting. Interestingly, the promoting effects of bacteria on CaOx crystal growth and aggregation were dose-dependent (Fig. 4) and specific to the intact viable bacteria, not the intact dead or the fragmented bacteria (Fig. 5). Therefore, the role of activity and interactions of the intact viable bacteria with CaOx crystals must be taken into account for such promoting effects. Moreover, secretory products of these intact viable bacteria and their potential roles in CaOx crystal growth and aggregation should be further elucidated.

From these bases, we hypothesized that once bacteria interact with CaOx crystals, the anionic nature of bacteria

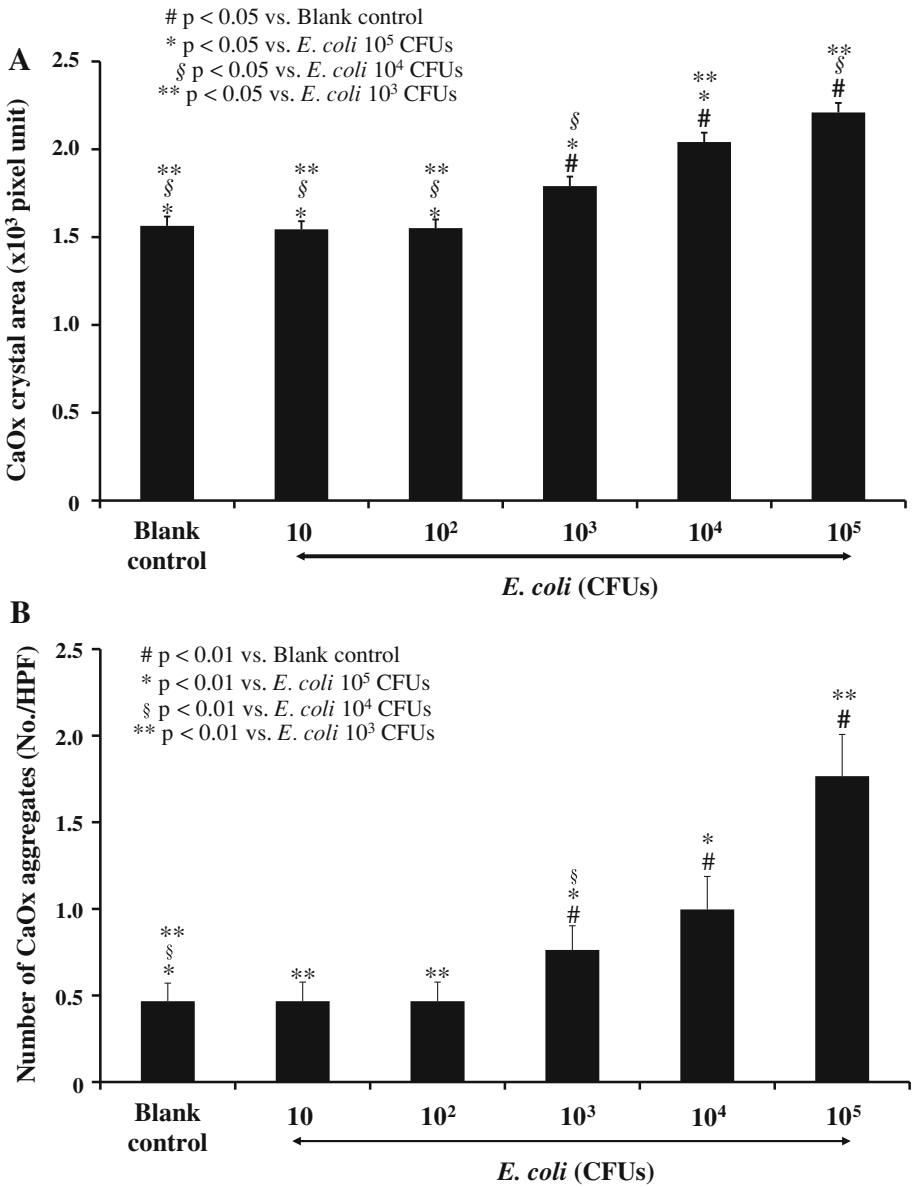


Fig. 4 Effects of differential doses of bacteria on CaOx crystal growth and aggregation. CaOx crystals were generated in the absence (blank control) or presence of 10–10^5 CFU/ml *E. coli*. The crystal area (**a**) and the number of crystal aggregates (**b**) were then analyzed. Each *bar* was derived from three independent experiments and the data are reported as the mean ± SEM

or their secretory products might attract free Ca^{2+} from renal tubular fluid, resulting in promotion of CaOx crystal growth. In addition, the intact viable bacteria interacting on the CaOx surface might act as linkers or adhesive molecules [19] among individual CaOx crystals, leading to the promotion of CaOx crystal aggregation. The huge, tightly impacted, round CaOx aggregates (as shown in Fig. 3b) seemed to be a subsequent result of lithogenic effects of bacteria. Since the size of the bacteria-induced CaOx aggregates was greater than the size of the lumen of distal renal tubules and collecting ducts [20] (as shown in Fig. 3c), these aggregates might be retained inside the kidney owing to tubular occlusion and may potentially act as the core nidus for stone development. Indeed, this proposed mechanism is similar to the mechanisms for cell membrane fragments and lipid vesicles reported previously [9–11], implying that abnormal presentation of anionic charged particulates within the urinary tract might lead to CaOx stone formation through a common pathway.

Definitely, an in vivo study using animal models is required to confirm the CaOx lithogenic roles of these bacteria. However, UTI induction in animal models may generate a number of interfering factors, e.g., altered stone inhibitors [4–8], inflammatory reaction [29], renal cell injury [30], cell debris and membrane fragments [10, 11], and the presence of antibiotics for UTI treatment (if used), such as ceftriaxone [31]. These factors can modulate CaOx stone genesis [4–8, 10, 11, 29–31] and thus may make the interpretation more complicated. Therefore, all these factors need to be considered during the experimental design in order to adjust the risk and to evaluate the outcome of UTI with regard to metabolic stone formation.

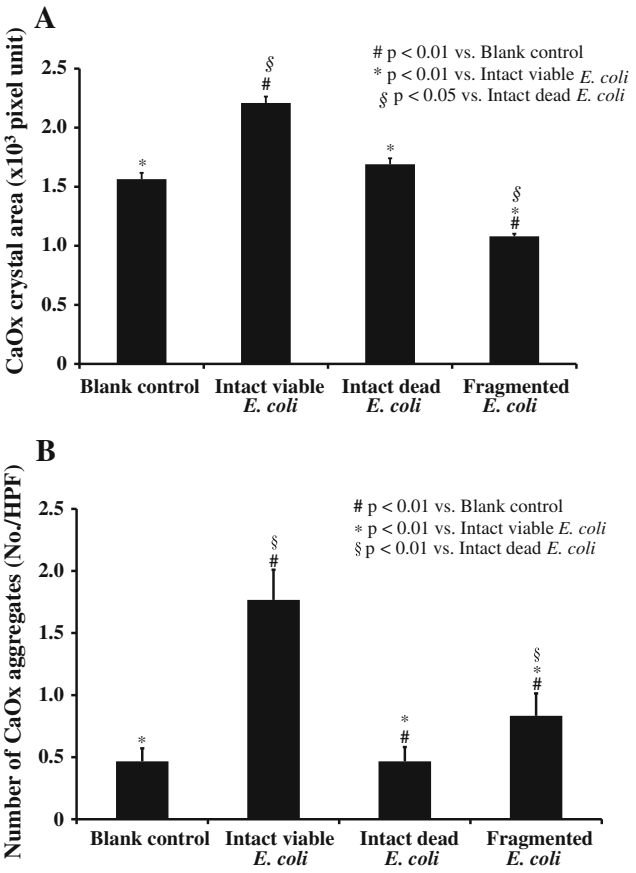


Fig. 5 Effects of viability of bacteria on CaOx crystal growth and aggregation. CaOx crystals were generated in the absence (blank control) or presence of 10^5 CFU/ml intact viable, intact dead, or fragmented *E. coli*. The crystal area (**a**) and the number of crystal aggregates (**b**) were then analyzed. Each *bar* was derived from three independent experiments and the data are reported as the mean ± SEM

In conclusion, we have reported, for the first time, that intact viable *E. coli*, *K. pneumoniae*, *S. aureus*, and *S. pneumoniae* can significantly promote CaOx crystal growth and aggregation in vitro. This functional evidence strongly supports the new hypothesis of bacteria-induced metabolic kidney stone disease. Nevertheless, further studies are required to confirm this new hypothesis and to elucidate the detailed mechanisms of the lithogenic activities of these intact viable bacteria.

Acknowledgments We are grateful to Somporn Srifuengfung and Chanwit Tribuddharat for their advice on microbiological techniques, and to Sakdithep Chaiyarit and Teerada Homvises for their technical support. This study was supported by the Office of the Higher Education Commission and Mahidol University under the National Research Universities Initiative (to V.T.), the Thailand Research Fund (MRG5380018 to S.C. and RTA5380005 to V.T.), and the Faculty of Medicine Siriraj Hospital. W.C. is supported by the Royal Golden Jubilee PhD Program, and V.T. is also supported by the Chalermphrakiat grant and the Faculty of Medicine Siriraj Hospital.

References

1. Bichler KH, Eipper E, Naber K, Braun V, Zimmermann R, Lahme S (2002) Int J Antimicrob Agents 19:488–498
2. Bichler KH, Eipper E, Naber K (2003) Urologe A 42:47–55
3. Miano R, Germani S, Vespasiani G (2007) Urol Int 79(Suppl 1):32–36
4. Coe FL, Evan A, Worcester E (2005) J Clin Invest 115:2598–2608
5. Pak CY (1998) Lancet 351:1797–1801
6. Nakagawa Y, Abram V, Parks JH, Lau HS, Kawooya JK, Coe FL (1985) J Clin Invest 76:1455–1462
7. Atmani F, Khan SR (1999) J Am Soc Nephrol 10(Suppl 14): S385–S388
8. Chutipongtanate S, Nakagawa Y, Sritippayawan S, Pittayamateekul J, Parichatikanond P, Westley BR, May FE, Malasit P, Thongboonkerd V (2005) J Clin Invest 115:3613–3622
9. Khan SR, Glenton PA, Backov R, Talham DR (2002) Kidney Int 62:2062–2072
10. Chutipongtanate S, Thongboonkerd V (2010) J Urol 184:743–749
11. Chutipongtanate S, Thongboonkerd V (2010) Chem Biol Interact 188:421–426
12. Yoshida O, Kiriyama T, Okada K, Okada Y, Watanabe H, Mishina T, Uchida M, Watanabe K, Tomoyoshi T, Takayama H (1984) Hinyokika Kiyo 30:191–198
13. Takeuchi H, Okada Y, Yoshida O, Arai Y, Tomoyoshi T (1989) Hinyokika Kiyo 35:749–754
14. Sohshang HL, Singh MA, Singh NG, Singh SR (2000) J Commun Dis 32:216–221
15. Tavichakorntrakool R, Prasongwattana V, Sungkeeree S, Saisud P, Sribenjalux P, Pimratana C, Bovornpadungkitti S, Sriboonlue P, Thongboonkerd V (2012) Nephrol Dial Transplant 27:4125–4130
16. Borghi L, Nouvenne A, Meschi T (2012) Nephrol Dial Transplant 27:3982–3984
17. Thongboonkerd V, Chutipongtanate S, Semangoen T, Malasit P (2008) J Urol 179:1615–1619
18. Nichols G, Byard S, Bloxham MJ, Botterill J, Dawson NJ, Dennis A, Diart V, North NC, Sherwood JD (2002) J Pharm Sci 91:2103–2109
19. Hirano S, Ohkawa M, Nakajima T, Orito M, Sugata T, Hisazumi H (1985) Hinyokika Kiyo 31:1387–1391
20. Freeman W, Bracegirdle B (1976) An advanced atlas of histology. Heinemann, London
21. Khan SR, Kok DJ (2012) In: Stoller ML, Meng MV (eds) Urinary stone disease. Humana, Totowa
22. Kim KM (1983) J Urol 129:855–857
23. Venkatesan N, Shroff S, Jeyachandran K, Doble M (2011) Urol Res 39:29–37
24. Bayer ME, Sloyer JL Jr (1990) J Gen Microbiol 136:867–874
25. Sheng X, Jung T, Wesson JA, Ward MD (2005) Proc Natl Acad Sci USA 102:267–272
26. Rabinovich YI, Esayanur M, Daosukho S, Byer KJ, El Shall HE, Khan SR (2006) J Colloid Interface Sci 300:131–140
27. Gross M, Cramton SE, Gotz F, Peschel A (2001) Infect Immun 69:3423–3426
28. Prokhorenko IR, Zubova SV, Ivanov AY, Grachev SV (2009) Int J Gen Med 2:33–38
29. Okada A, Yasui T, Fujii Y, Niimi K, Hamamoto S, Hirose M, Kojima Y, Itoh Y, Tozawa K, Hayashi Y, Kohri K (2010) J Bone Miner Res 25:2701–2711
30. Bigelow MW, Wiessner JH, Kleinman JG, Mandel NS (1997) Am J Physiol 272:F55–F62
31. Chutipongtanate S, Thongboonkerd V (2011) Biochem Biophys Res Commun 406:396–402

Journal of proteome research

Article

pubs.acs.org/jpr

Alterations in Macrophage Cellular Proteome Induced by Calcium Oxalate Crystals: The Association of HSP90 and F-Actin Is Important for Phagosome Formation

Nilubon Singhto,[†,‡] Kitisak Sintiprungrat,[†,‡] and Visith Thongboonkerd*[,†,§]

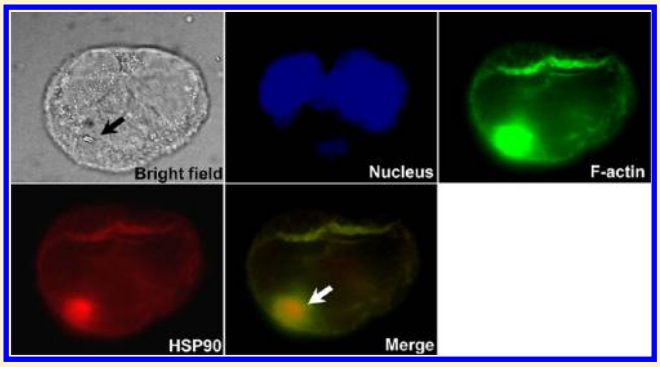
[†]Medical Proteomics Unit, Office for Research and Development, Faculty of Medicine Siriraj Hospital, Mahidol University, Bangkok, Thailand

[‡]Department of Immunology and Immunology Graduate Program, Faculty of Medicine Siriraj Hospital, Mahidol University, Bangkok, Thailand

[§]Center for Research in Complex Systems Science, Mahidol University, Bangkok, Thailand

Supporting Information

ABSTRACT: The presence of macrophages in renal interstitium is the key feature of progressive renal inflammation in kidney stone disease. However, response of macrophages to calcium oxalate monohydrate (COM) crystals, the major crystalline composition of kidney stone, remained unclear. This study aimed to investigate alterations in the cellular proteome of macrophages induced by COM crystals using a proteomics approach. U937-derived macrophages (by phorbol-12-myristate-13-acetate activation) were incubated without or with 100 μg/mL COM crystals for 24 h. Their cellular proteins were resolved by 2-DE (n = 10 gels; 5 were derived from 5 independent cultures in each group) and visualized with Deep Purple fluorescent dye. Spot matching, quantitative intensity analysis, and statistics revealed 18 differentially expressed protein spots, which were successfully identified by Q-TOF MS and MS/MS analyses. The altered levels of α-tubulin, β-actin and ezrin were validated by Western blot analysis. Protein interaction network analysis using STRING software showed that 90 kDa heat shock protein (HSP90) was associated with β-actin and α-tubulin (all these three proteins were increased in the COM-treated macrophages). Multiple immunofluorescence stainings confirmed the associations of HSP90 with filamentous form of actin (F-actin) and α-tubulin. However, only the association between HSP90 and F-actin was found on the phagosome membrane surrounding COM crystal, indicating that the association of HSP90 with F-actin, but not with α-tubulin, is important for phagosome formation. Silencing of HSP90 (siHSP90) reduced expression of cytoskeletal proteins and phagosome marker (Rab5) and successfully diminished COM crystal-induced phagocytosis and migration of macrophages. Our findings enlightened the significant role of these altered proteins, especially HSP90, in enhanced phagocytic activity of the COM-exposed macrophages.



KEYWORDS: *calcium oxalate, CaOx, COM, macrophage, phagocytosis, proteome, proteomics*

INTRODUCTION

Macrophage is the phagocytic cell that responds to both organic and inorganic compounds. When macrophages engulf foreign materials, the vesicular structure namely "phagosome" will be formed to surround the ingested particles.[1,2] Phagosome then undergoes maturation processes, including sequential fusion with lysosome (transforming to "phagolysosome") or other secretory vesicles.[1,3] The foreign materials will then be eliminated by enzymes or peroxide within the phagolysosome. For immune response, macrophages produce a wide range of inflammatory mediators, including proteolytic enzymes, reactive oxygen species (ROS) and chemokines, which are the prominent factors for subsequent tissue inflammation and damage.[3,4]

Response of macrophages to calcium oxalate monohydrate (COM) crystals, the major crystalline compound found in kidney stone matrices, has been thought to be one of the crucial mechanisms of kidney stone disease.[5] *In vivo* studies have suggested that the locales of COM crystals deposited in renal interstitium are surrounded by macrophages, each of which contains crystal(s) or crystalline particles inside the cell.[6] This evidence has suggested that macrophages play critical roles for removing crystal particles from the renal interstitial tissue. Moreover, exposure of COM crystals to cultivated macrophages can enhance production of tumor necrosis factor-α (TNF-α) and interleukin-6 (IL-6), as well as dissolution of COM crystals.[7] These cytokines produced from macrophages have important roles to exacerbate inflammatory reaction because they can further

Received: March 4, 2012
Published: July 6, 2013

ACS Publications © 2013 American Chemical Society

dx.doi.org/10.1021/pr4004097 | *J. Proteome Res.* 2013, 12, 3561−3572

activate the cascade of other cytokines.[8−10] The recruitment of macrophages into the site of COM crystal deposition and their amplification of inflammatory response can result to progressive renal inflammation and subsequently tissue injury.

Previously, response of macrophages to COM crystals was not well clarified and under-investigated. In the present study, we thus examined changes in cellular proteome of macrophages in response to COM crystals, which are the main pathogenic crystals leading to kidney stone formation. Identification of changes in the macrophage cellular proteome was performed by two-dimensional electrophoresis (2-DE) followed by quadrupole time-of-flight (Q-TOF) MS and MS/MS analyses. The proteomic data were then validated by Western blot analysis. Moreover, all the identified proteins were subjected to protein interaction network analysis to obtain functional significance of the identified proteins and to guide for subsequent functional studies and validation, which revealed insights into important roles of the significantly altered proteins in phagosome formation and phagocytosis, during COM crystal exposure.

MATERIALS AND METHODS

Cell Cultivation and Macrophage Differentiation

Macrophages were derived from U937 human monocytic cell line using phorbol myristate acetate (PMA) for differentiation.[11] Briefly, U937 cells were maintained in a humidified incubator with 5% CO_2 at 37 °C using RPMI 1640 (Gibco; Grand Island, NY) supplemented with 10% (v/v) heat-inactivated fetal bovine serum (FBS), 100 U/mL penicillin and 100 μg/mL streptomycin (Sigma; St. Louis, MO) in 75 cm^2 tissue culture flask (n = 5 individual culture flasks for each condition). The cell suspensions at a density of 1 × 10^6 cells/mL were treated with 100 ng/mL PMA (Fluka; Singapore) for 48 h (induction phase) as previously described.[11] After 2 days of the induction phase, the PMA-treated cells were vigorously washed twice with ice-cold PBS to remove PMA and nonadherent cells, whereas the adherent cells were further maintained as aforementioned for 48 h (recovery phase).

Intervention of Macrophages with COM Crystals

COM crystals were prepared as described with details in Supplementary Methods in the Supporting Information. Thereafter, the dried pellets of COM crystals were decontaminated by UV light exposure for 30 min. Culture medium was removed from semiconfluent monolayer of macrophages (approximately 15 × 10^6 cells) and replaced with the same plain medium without COM crystals (controlled group) or with COM-containing medium (100 μg COM crystals/mL culture medium) (COM-treated group) (n = 5 individual culture flasks for each condition). The controlled and COM-treated cells were further maintained in a humidified incubator with 5% CO_2 at 37 °C for 24 h. Morphological changes of the COM-treated macrophages were examined under an inverted phase-contrast microscope (Olympus Co. Ltd.; Tokyo, Japan).

Laser-scanning Confocal Microscopic Examination of Phagocytosis

To confirm the phagocytic activity of macrophages, the cells (macrophages) were grown on coverslip during recovery phase followed by incubation with 100 μg/mL COM crystals for 24 h. The parallel untreated cells (without COM crystals) served as the negative control. The cells were then washed with ice-cold PBS, fixed with 1% (v/v) formaldehyde in PBS at RT for 10 min, and permeabilized with 0.1% (v/v) tritonX-100 in PBS at room temperature (RT) (25 °C) for a further 10 min. After another wash with PBS, nonspecific bindings were blocked with 1% (w/v) BSA/PBS at RT for 1 h. F-actin was stained by Oreagon Green-conjugated phalloidin (Invitrogen − Molecular Probes; Eugene, Oregon) at a dilution of 1:40 for 1 h at 37 °C. Nucleus was stained by Hoechst dye (Invitrogen − Molecular Probes) at a dilution of 1:2000 for 5 min at RT. Note that COM crystals were detectable in red by a light reflection at λ633 nm. Finally, coverslips were mounted with 50% glycerol/PBS. Images were taken under LSM 510 Meta laser scanning microscope (Carl Zeiss; Jena, Germany).

Protein Extraction for Proteomic and Western Blot Analyses

Details are provided in Supplementary Methods in the Supporting Information.

2-DE and Visualization of Protein Spots

Details are provided in Supplementary Methods in the Supporting Information.

Spot Matching and Quantitative Intensity Analysis

Details are provided in Supplementary Methods in the Supporting Information.

In-gel Tryptic Digestion

Details are provided in Supplementary Methods in the Supporting Information.

Protein Identification by Quadrupole Time-of-flight (Q-TOF) MS and MS/MS Analyses

The trypsinized samples were premixed 1:1 with the matrix solution containing 5 mg/mL α-cyano-4-hydroxycinnamic acid (CHCA) in 50% ACN, 0.1% (v/v) TFA and 2% (w/v) ammonium citrate, and deposited onto the 96-well MALDI target plate. The samples were analyzed by Q-TOF Ultima mass spectrometer (Micromass; Manchester, UK), which was fully automated with predefined probe motion pattern and the peak intensity threshold for switching over from MS survey scanning to MS/MS, and from one MS/MS to another. Within each sample well, parent ions that met the predefined criteria (any peak within the m/z 800−3000 range with intensity above 10 count ± include/exclude list) were selected for CID MS/MS using argon as the collision gas and a mass dependent ±5 V rolling collision energy until the end of the probe pattern was reached. The MS and MS/MS data were extracted and outputted as the searchable *.txt* and *.pkl* files, respectively, for independent searches using the MASCOT search engine (http://www.matrixscience.com) to query against the NCBI mammalian protein database (with 1 057 487 mammalian entries; accessed on 07 April 2012), assuming that peptides were monoisotopic. Fixed modification was carbamidomethylation at cysteine residues, whereas variable modification was oxidation at methionine residues. Only one missed trypsin cleavage was allowed, and peptide mass tolerances of 1.2 and 0.6 Da were allowed for peptide mass fingerprinting (PMF) and MS/MS ions search, respectively. Proteins with probability-based MOWSE (MS) scores ≥73 or MS/MS ions scores ≥48 were considered significant hits.

Confirmation of the Proteomic Data by Western Blot Analysis

A total of 30 μg of proteins extracted from each sample were resolved by 12% SDS-PAGE at 150 V for approximately 2 h using SE260 mini-Vertical Electrophoresis Unit (GE Healthcare). After the completion of SDS-PAGE, the resolved proteins were transferred onto a nitrocellulose membrane and nonspecific bindings were blocked with 5% (w/v) skim milk in PBS at RT for 1 h. The membrane was then incubated with

dx.doi.org/10.1021/pr4004097 | J. Proteome Res. 2013, 12, 3561−3572

mouse monoclonal anti-ezrin (1:1000), anti-α-tubulin (1:1000), anti-β-actin (1:1000), or anti-GAPDH (1:2000) as primary antibody. All of these antibodies were purchased from Santa Cruz Biotechnology (Santa Cruz; CA) and diluted in 1% (w/v) skim milk/PBS. After an overnight incubation at 4 °C, the membrane was washed and then further incubated with rabbit anti-mouse IgG conjugated with horseradish peroxidase (1:2000−1:4000 in 1% (w/v) skim milk/PBS) (Dako; Glostrup, Denmark) at RT for 1 h. Reactive protein bands were then visualized with SuperSignal West Pico chemiluminescence substrate (Pierce Biotechnology, Inc.; Rockford, IL) using an autoradiogram.

Protein Interaction Network Analysis

All of the significantly altered proteins in the COM-treated macrophages were subjected to protein interaction network analysis using STRING tool (version 8.3) (http://string.embl.de/).[12] The predicted protein−protein associations were queried through experimentally derived physical protein interactions from literatures combining with the databases of curated biological pathway knowledge.[12]

Multiple Immunofluorescence Stainings to Demonstrate Colocalizations of Proteins

To investigate the colocalized proteins related to phagosome, macrophages were grown on coverslip during recovery phase prior to treatment with 100 μg/mL COM crystals for 24 h. The untreated cells (without COM crystals) served as the negative control. The cells were then washed three times with PBS, fixed with 1% (v/v) formaldehyde in PBS at RT for 10 min, and permeabilized with 0.1% (v/v) tritonX-100 in PBS at RT for further 10 min. After another wash with PBS, nonspecific bindings were blocked with 1% (w/v) BSA/PBS at RT for 1 h. F-actin was stained by Oreagon Green-conjugated phalloidin (Invitrogen − Molecular Probes) at a dilution of 1:40 for 1 h at 37 °C. HSP90 and α-tubulin were probed with mouse monoclonal anti-HSP90α/β (Santa Cruz Biotechnology) and mouse monoclonal anti-α-tubulin antibodies (Santa Cruz Biotechnology), respectively, at a dilution of 1:50 in 1% (w/v) BSA/PBS. The cells were then washed with PBS three times and further incubated with goat anti-mouse IgG conjugated with Cy3 (Dako) or goat anti-mouse IgG conjugated with Alexa Flour 488 (Invitrogen − Molecular Probes), at the same dilution of 1:2000 in 1% (w/v) BSA/PBS. Nucleus was stained by Hoechst dye (Invitrogen − Molecular Probes) at a dilution of 1:2000 for 5 min at RT. Note that COM crystals were detectable in red by a light reflection at λ633 nm. Finally, coverslips were mounted with 50% glycerol/PBS. Images were taken under ECLIPSE 80i fluorescence microscope (Nikon; Tokyo, Japan).

Knockdown of HSP90 Expression by Small Interfering RNA (siRNA)

To reduce expression of cellular HSP90, macrophages were transfected with HSP90α/β siRNA (siHSP90), whereas siRNA control duplex served as the control for siRNA (siControl). Briefly, macrophages were suspended in antibiotic-free normal growth medium supplemented with 10% FBS and seeded with a density of 2×10^5 cells/mL in 6-well culture plate. The cells were then transfected with 60 pmols siHSP90 or siControl (Santa Cruz Biotechnology) in 800 μL siRNA Transfection Medium (Santa Cruz Biotechnology) at 37 °C in CO_2 incubator for 5 h. After transfection, the cells were added with 1 mL antibiotic-free normal growth medium supplemented with 10% FBS and further incubated for 24 h. The transfected cells were subsequently used within 48 h after completion of the transfection.

Evaluation of siHSP90-induced Altered Levels of HSP90, Phagosome-related Proteins and Cytoskeletal Proteins by Western Blot Analysis

To examine whether the siRNA approach successfully reduced the expression of HSP90, as well as phagosome-related and cytoskeletal proteins, Western blot analysis was performed. A total of 30 μg proteins derived from controlled, siControl and siHSP90 macrophages were separated by 12% SDS-PAGE at 150 V for approximately 2 h using SE260 mini-Vertical Electrophoresis Unit (GE Healthcare). The resolved proteins were then transferred onto a nitrocellulose membrane and nonspecific bindings were blocked with 5% (w/v) skim milk in PBS at RT for 1 h. The membrane was then incubated with mouse monoclonal anti-HSP90α/β (1:1000), anti-α-tubulin (1:1000), anti-β-actin (1:1000), anti-Rab5 (1:1000) or anti-GAPDH (1:2000) as primary antibody. All of these antibodies were purchased from Santa Cruz Biotechnology and diluted in 1% (w/v) skim milk/PBS. After an overnight incubation at 4 °C, the membrane was washed and then further incubated with rabbit anti-mouse IgG conjugated with horseradish peroxidase (Dako) (1:2000−1:4000 in 1% (w/v) skim milk/PBS) at RT for 1 h. Reactive protein bands were then visualized with SuperSignal West Pico chemiluminescence substrate (Pierce Biotechnology, Inc.; Rockford, IL) using an autoradiogram.

Phagocytic Activity Assay

To investigate the phagocytic activity of macrophages after siHSP90, siControl and siHSP90 macrophages were grown on coverslips in a 6-well plate (5×10^5 cells/well) with or without 100 μg/mL COM crystals for 24 h. The controlled cells without (controlled) or with (COM-treated) 100 μg/mL COM crystals served as the internal controls in this experiment. *Staphylococcus aureus* was fluorescently labeled prior to incubation with these macrophages using Cy3-conjugated mouse monoclonal anti-transketolase antibody. Briefly, 1×10^6 CFUs/mL (colony forming units/mL) of *S. aureus* were fixed and permeabilized with 1% (v/v) formaldehyde and 0.1% (v/v) triton X-100, respectively. After a wash with PBS, nonspecific bindings were blocked with 5% (w/v) BSA in PBS at RT for 30 min. The organisms were conjugated with mouse monoclonal anti-transketolase antibody (Santa Cruz Biotechnology) at a dilution of 1:50 in 1% (w/v) BSA/PBS for 1 h. After three washes with PBS, the bacteria were further conjugated with goat anti-mouse IgG conjugated with Cy3 (Dako) at a dilution of 1:2,000 in 1% (w/v) BSA/PBS. Thereafter, the fluorescently labeled bacteria were incubated with individual groups of aforementioned macrophages at 37 °C for 3 h. Macrophages on coverslips were then fixed and permeabilized as aforementioned. After PBS wash, F-actin was stained by Oreagon Green-conjugated phalloidin (Invitrogen Molecular Probes) at a dilution of 1:40 for 1 h at 37 °C and the coverslips were finally mounted with 50% glycerol/PBS. Images were taken under ECLIPSE 80i fluorescence microscope (Nikon; Tokyo, Japan).

Migration Assay

The ability of macrophage to migrate after siHSP90 was evaluated using Transwell culture plates with 5-μm pore size (Corning Life Sciences). Controlled, COM-treated, siControl-COM-treated and siHSP90-COM-treated macrophages (approximately 2×10^5 cells/well) were placed at the upper chamber of Transwell culture plate containing serum-free medium. To provide a chemoattractant gradient, 10% serum-containing medium was added into the lower chamber.[13] After 24-h incubation, the number of macrophages migrated from upper to lower chambers was counted.

dx.doi.org/10.1021/pr4004097 | J. Proteome Res. 2013, 12, 3561−3572

Statistical Analysis

All quantitative data are reported as Mean ± SEM, unless stated otherwise. Statistical analyses were performed using SPSS software version 13.0 (SPSS; Chicago, IL). Comparisons between two sets of data (i.e., controlled vs COM-treated) were performed by unpaired Student's *t* test, whereas multiple comparisons were performed using ANOVA with Tukey's posthoc test. *P* -values less than 0.05 were considered statistically significant.

RESULTS

Morphological Change and Phagocytosis of Macrophages in Response to COM Crystals

To examine the interaction between macrophages and COM crystals, human macrophages were incubated with 100 μg/mL COM crystals for 24 h. Crystal-cell interaction and morphological change of macrophages were examined using an inverted phase-contrast microscope. After 24-h exposure to COM crystals, macrophages stretched pseudopodia to a group of COM crystals, whereas the untreated or controlled cells had no obvious change in their morphology (Supplementary Figure S1, Supporting Information). Laser-scanning confocal microscopy was performed to confirm the phagocytosis of macrophages after induction with COM crystals for 24 h. The property of COM crystals to reflect the light at λ633 nm (in red),[14] fortunately, benefited this set of experiments to visualize the engulfed COM crystals. The cell boundary and phagosome membrane were determined using F-actin as a marker (shown in green), whereas nuclei were stained in blue. The results clearly confirmed that COM crystal was engulfed and surrounded by phogosome membrane inside a macrophage (Figure 1).

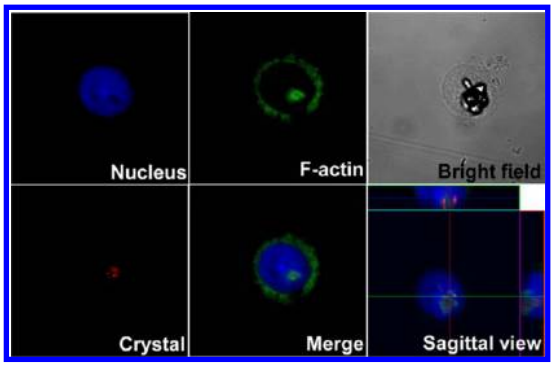


Figure 1. Phagocytosis of COM crystals by macrophages. After an incubation of macrophages with COM crystals (100 μg/mL) for 24 h, the cells were examined by LSM 510 META laser-scanning confocal microscope (Carl Zeiss, Inc.; Oberkochen, Germany) to visualize COM crystals (reflected at λ633 nm in red), cell boundary and phagosome membrane using F-actin as a marker (shown in green) and nucleus (shown in blue). Images were taken with original magnification of 630× and digital zooming 3×. The sagittal view clearly showed that COM crystal was surrounded by phogosome membrane inside a macrophage.

Altered Cellular Proteome of Macrophages after Exposure to COM Crystals

For the cellular proteome study, macrophages were treated with or without 100 μg/mL COM crystals for 24 h before the cellular proteins were extracted. Whole cell lysates derived from the controlled and COM-treated cells (with an equal amount of 150 μg proteins per sample) were then resolved by 2-DE (n = 5 gels derived from individual culture flasks for each condition; a total of 10 gels were analyzed in this study). Using Deep Purple fluorescence dye and Image Master 2D Platinum software (GE healthcare) with highly stringent criteria to detect protein spots, approximately 800 protein spots were visualized in each 2-D gel. Spot matching, quantitative intensity analysis and statistics revealed 18 differentially expressed protein spots in the COM-treated macrophages as compared to the controlled cells (Figure 2). These included 7 spots with increased levels, 7 spots with decreased levels, 3 spots that were present only in the COM-treated macrophages, and 1 spot that was absent in the COM-treated cells. All of these significantly altered proteins were successfully identified by Q-TOF MS and MS/MS analyses. Their details, including identities, methods of identification, percentages of sequence coverage, numbers of matched peptides, isoelectric points, molecular weights, fold changes and p values, are summarized in Table 1. Using UniProt Knowledgebase (Swiss-Prot and TrEMBL entries),

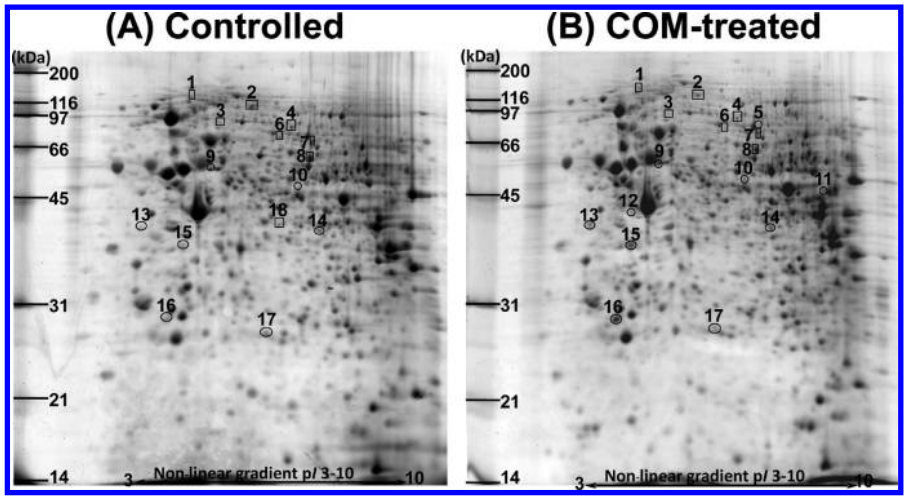


Figure 2. Representative 2-D proteome maps of the significantly altered proteins and their locales in (A) controlled and (B) COM-treated macrophages. A representative 2-D gel (from 5 individual gels for each condition) was selected and created as a map of 18 significantly altered proteins in the controlled vs COM-treated macrophages (p < 0.05). The circles designate the proteins that were increased in their abundance levels or found only in the COM-treated macrophages, whereas rectangles indicate the proteins whose abundance levels were decreased or absent in the COM-treated cells. These significantly altered proteins were successfully identified by Q-TOF MS and MS/MS analyses (see also Table 1).

dx.doi.org/10.1021/pr4004097 | J. Proteome Res. 2013, 12, 3561−3572

Table 1. Summary of Significantly Altered Proteins in Macrophages after Exposure with 100 μg/mL COM Crystals[a]

spot no.	protein name	NCBI ID	identified by	identification scores (MS, MS/MS)	%Cov (MS, MS/MS)	no. of matched peptides (MS, MS/MS)	p*I*	MW (kDa)	spot intensity (arbitrary units) (mean ± SEM) control	spot intensity (arbitrary units) (mean ± SEM) COM-treated	ratio (COM-treated/ control)	*p* value
1	Damage-specific DNA binding protein 1	gil418316	MS, MS/MS	139, 61	27, 1	21, 1	5.14	128.16	0.0400 ± 0.0025	0.0244 ± 0.0034	0.61	0.007
2	Glucosidase, alpha; neutral AB	gil119594451	MS, MS/MS	104, 17	28, 1	18, 1	5.85	104.93	0.1241 ± 0.0096	0.0916 ± 0.0062	0.74	0.031
3	U2 small nuclear ribonucleoprotein auxiliary factor (U2AF) 1	gil6755917	MS	80, NA	28, NA	8, NA	9.12	51.96	0.0272 ± 0.0014	0.0108 ± 0.0054	0.40	0.019
4	Ezrin	gil50881	MS/MS	NA, 86	NA, 1	NA, 2	5.83	69.42	0.0701 ± 0.0043	0.0514 ± 0.0052	0.73	0.030
5	*N*-Ethylmaleimide sensitive fusion protein isoform 5	gil73965161	MS, MS/MS	109, 39	25, 2	14, 1	6.55	83.77	0.0000 ± 0.0000	0.0069 ± 0.0029	#DIV/0	0.042
6	Adenylosuccinate lyase 1	gil126338737	MS	78, NA	27, NA	8, NA	8.49	56.82	0.0399 ± 0.0029	0.0271 ± 0.0038	0.68	0.034
7	5-Aminoimidazole-4-carboxamide ribonucleotide formyltransferase/IMP cyclohydrolase	gil20127454	MS	99, NA	32, NA	14, NA	6.27	65.09	0.0439 ± 0.0039	0.0314 ± 0.0030	0.72	0.046
8	Ezrin	gil31283	MS/MS	NA, 50	NA, 1	NA, 1	5.94	69.47	0.2611 ± 0.0056	0.1958 ± 0.0083	0.75	0.000
9	Heat shock protein 1 (chaperonin)	gil51452	MS	74, NA	32, NA	13, NA	5.48	59.00	0.0988 ± 0.0073	0.1668 ± 0.0249	1.69	0.032
10	Tubulin, alpha, ubiquitous isoform 19	gil109096498	MS	105, NA	41, NA	12, NA	4.94	45.32	0.0061 ± 0.0054	0.0313 ± 0.0087	5.16	0.045
11	Phosphoglycerate kinase	gil202423	MS/MS	NA, 72	NA, 17	NA, 2	7.53	44.91	0.0000 ± 0.0000	0.0238 ± 0.0101	#DIV/0	0.046
12	Beta-actin	gil28336	MS/MS	NA, 157	NA, 16	NA, 4	5.22	42.13	0.0000 ± 0.0000	0.0446 ± 0.0115	#DIV/0	0.005
13	Procollagen-proline, 2-oxoglutarate 4-dioxygenase	gil119610102	MS	75, NA	35, NA	9, NA	4.60	41.07	0.0890 ± 0.0234	0.0783 ± 0.0069	1.73	0.033
14	Elongation factor Tu, mitochondrial	gil704416	MS, MS/MS	104, 167	37, 10	14, 3	7.70	49.85	0.0495 ± 0.0039	0.0783 ± 0.0069	1.58	0.008
15	HSP90AB1 protein	gil29612561	MS, MS/MS	109, 229	22, 9	13, 3	5.02	42.02	0.1460 ± 0.0191	0.2926 ± 0.0419	2.00	0.014
16	HSP90AA1 protein	gil32486	MS, MS/MS	84, 147	25, 10	7, 2	4.59	35.74	0.1532 ± 0.0263	0.2655 ± 0.0205	1.73	0.014
17	Peroxiredoxin 3 isoform a precursor	gil5802974	MS/MS	NA, 127	NA, 9	NA, 2	7.67	28.02	0.0927 ± 0.0187	0.1754 ± 0.0167	1.89	0.015
18	Oxidative stress responsive 1 isoform 2	gil126302907	MS	73, NA	35, NA	8, NA	8.50	32.91	0.0225 ± 0.0094	0.0000 ± 0.0000	0.00	0.043

[a]All these proteins were successfully identified by Q-TOF MS and MS/MS analyses. NCBI = National Center for Biotechnology Information. %Cov = %Sequence coverage [(number of the matched residues/total number of residues in the entire sequence) × 100%]. NA = Not applicable. #DIV/0 = Divided by zero.

dx.doi.org/10.1021/pr400409j | *J. Proteome Res.* 2013, 12, 3561−3572

all these identified proteins were classified based on their major molecular functions, including those involved in cellular structure, carbohydrate metabolism, DNA/RNA processing, protein metabolism, molecular trafficking, and stress response (Table 2). The theoretical subcellular localizations were also predicted.

Table 2. Functional Categories and Subcellular Localization of the Significantly Altered Cellular Proteins in Macrophages Induced by COM Crystals

function/protein name	spot no.	subcellular localization	alteration
Cellular structure			
Alpha-tubulin	10	Cytoplasm, microtubule	Increased
Beta-actin	12	Cytoplasm	Increased[a]
Ezrin	4,8	Cell membrane, Cytoplasm	Decreased
Carbohydrate metabolism			
Glucosidase, alpha	2	Endoplasmic reticulum	Decreased
Phosphoglycerate kinase	11	Cytoplasm	Increased[a]
DNA and mRNA processing			
5-Aminoimidazole-4-carboxamide ribonucleotide formyltransferase/ IMP cyclohydrolase	7	Nucleus	Decreased
Damage-specific DNA binding protein 1	1	Nucleus	Decreased
U2 small nuclear ribonucleoprotein auxiliary factor 1	3	Nucleus	Decreased
Protein metabolism			
Adenylosuccinate lyase 1	6	Cytoplasm	Decreased
Elongation factor Tu, mitochondrial	14	Mitochondria	Increased
Molecular trafficking			
N-Ethylmaleimide sensitive fusion protein	5	Cytoplasm	Increased[a]
Stress response			
Heat shock 60 protein (chaperonin)	9	Cytoplasm	Increased
Heat shock 90 protein AA1	15	Cytoplasm	Increased
Heat shock 90 protein AB1	16	Cytoplasm	Increased
Oxidative stress responsive 1 isoform 2	18	Cytoplasm	Decreased[b]
Peroxiredoxin-3	17	Mitochondria	Increased
Procollagen-proline, 2-oxoglutarate 4-dioxygenase	13	Endoplasmic reticulum lumen	Increased

[a]Proteins that were detectable only in the COM-treated macrophages. [b]Protein that was absent in the COM-treated macrophages.

Confirmation of the Proteomic Data by Western Blot Analysis

Some of the differentially expressed proteins identified by proteomic analysis were randomly selected for subsequent confirmation by conventional immunological method. Western blot analysis confirmed the decreased levels of two forms of ezrin (or villin-2) (spots #4 and #8), with differential molecular masses, in the COM-treated macrophages (Figure 3). Additionally, Western blot data also confirmed the increased levels of α-tubulin (spot #10) and β-actin (spot #12) in the COM-treated macrophages (Figure 3). Glyceraldehyde-3-phosphate dehydrogenase (GAPDH) served as the loading control in this study.

Protein Interaction Network Analysis

We also employed the STRING version 8.3 (http://string.embl.de/)[12] to determine the associations or interactions of all the identified proteins. Accession numbers or identities of these proteins were uploaded through the STRING entry page and the interaction networks were then generated. The analysis revealed three main networks of protein interactions among cytoskeletal proteins, chaperones/stress response proteins, and metabolic proteins (Figure 4). The data also strongly indicated that HSP90 was associated with both β-actin and α-tubulin (Figure 4).

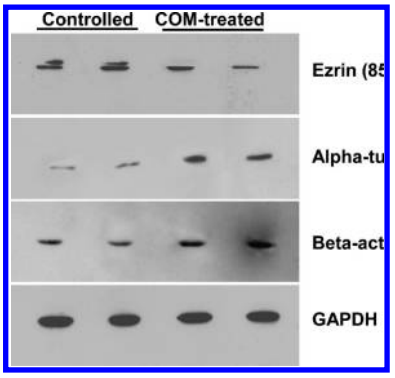


Figure 3. Confirmation of the proteomic data by Western blot analysis. Randomly selected altered proteins (down-regulated ezrin, and up-regulated α-tubulin and β-actin) were confirmed by Western blot analysis (see Supplementary Methods in the Supporting Information for more details). GAPDH served as the loading control.

Confirmation of Associations of HSP90 with Actin and α-Tubulin, and the Role of These Associations in Phagosome Formation

We have demonstrated the triangle of protein interactions among HSP90, β-actin and α-tubulin in our present study (Figure 4). To confirm the associations of these proteins, we performed multiple immunofluorescence stainings of these proteins using Oreagon Green-conjugated phalloidin to stain filamentous form of actin (F-actin), whereas HSP90 and α-tubulin were immunostained with corresponding antibodies conjugated with different fluors (Cy3 and Alexa Flour 488, respectively). The immunofluorescence data confirmed the associations between HSP90 (in red) and F-actin (in green) (Figure 5A), and between HSP90 (in red) and α-tubulin (in green) (Figure 5B). These interactions appeared generalized in macrophages. Several studies have suggested that HSP90 plays an essential role in controlling the stabilization of cytoskeletal proteins through its interactions with F-actin and α-tubulin, resulting to the enhancement of phagocytic activity.[15−18] Moreover, the increased level of heat shock proteins has been reported to enhance F-actin mediated phagosome formation.[19] We thus speculated that their interactions might be important for phagocytic activity of macrophages. However, the data showed that only the association between HSP90 and F-actin was observed on the phagosome membrane (indicated with arrowhead in Figure 5A), whereas the association between HSP90 and α-tubulin was not associated with phagosome (Figure 5B). These data indicated that the association of HSP90 with F-actin, but not with α-tubulin, is important for phagosome formation.

Effects of siHSP90 on Expression of HSP90, Phagosome-related and Cytoskeletal Proteins

According to protein interaction network data, we hypothesized that HSP90 should have a significant role in association with cytoskeletal proteins to mediate phagocytosis and migration of

dx.doi.org/10.1021/pr4004097 | J. Proteome Res. 2013, 12, 3561−3572

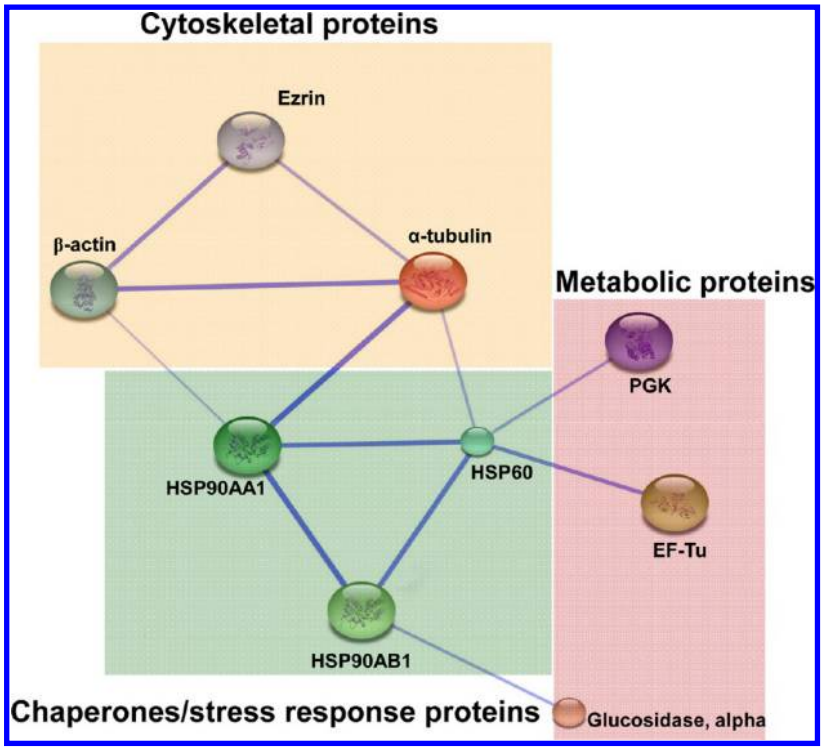


Figure 4. Protein interaction network analysis of the significantly altered proteins in the COM-treated macrophages. Using protein interaction network analysis tool, STRING version 8.3 (http://string-db.org),[12] three networks of the associated proteins were found in all identified proteins that were significantly altered in the COM-treated macrophages. These included the networks for cytoskeletal proteins, chaperones/stress response proteins, and metabolic proteins. The thicker or more intense blue line indicates the stronger association.

macrophages. To address this hypothesis, we introduced small interfering RNA directly against HSP90α/β and investigated the altered levels of HSP90, α-tubulin, β-actin and Rab5 (phagosome marker) by Western blot analysis. The results showed that siHSP90 dramatically reduced expression levels of HSP90, α-tubulin, β-actin and Rab5 as compared to the siControl condition (Figure 6). Taken together, this data implicated that HSP90 might have a significant role in regulating cytoskeletal proteins-mediated phagocytosis and migration of macrophages.

Effects of siHSP90 on Phagocytic Activity of Macrophages

To address the hypothesis that HSP90 had a significant role in phagocytic activity of macrophages, we assessed the capability of macrophages to engulf Cy3-labeled *S. aureus*. Double immunofluorescence study using Oreagon Green-conjugated phalloidin to stain F-actin and to localize the cell boundary revealed that COM-treated macrophages (without siRNA) and siControl-COM-treated macrophages (COM-treated macrophages with siControl) had a large number of intracellular bacteria in each macrophage cell (Figure 7). In contrast, the phagocytic activity was almost completely abolished by siHSP90 in siHSP90-COM-treated macrophages (COM-treated macrophages with siHSP90), which had only a few bacteria remaining intracellularly (Figure 7). These data indicated that HSP90 played an essential role in phagocytic activity of macrophages.

Effects of siHSP90 on Macrophage Migration

In addition to phagocytic activity, the cytoskeletal compartment also promotes macrophage migration, which is an important process in immune response and elimination of foreign materials. Previous studies have suggested that HSP90 plays a critical role in stabilizing cytoskeletal proteins to mediate cell movement.[15,20] To address such role of HSP90 in response to COM crystals, we performed migration assay as detailed in Materials and Methods. The data showed a significant increase in number of migrated macrophages in COM-treated and siControl-COM-treated macrophages as compared to the controlled (untreated) cells (Figure 8). In contrast, siHSP90 caused a significant decrease in number of migrated macrophages as compared to controlled, COM-treated and siControl-COM-treated cells (Figure 8). This study confirmed that HSP90 played a crucial role in macrophage migration.

DISCUSSION

Macrophages are the important immunomodulatory cells with wide-range responses to foreign materials. In kidney stone disease, macrophage infiltration has been frequently found within in the kidney of patients with calcium oxalate kidney stone disease. Several studies have demonstrated the involvement of macrophages to eliminate COM crystals and in inflammatory response.[5−7,21,22] Recently, DNA microarray combining with gene expression network analysis has suggested that inflammatory process occurred in kidney stone disease has been originated from macrophage activity. Okada et al.[21,22] have reported significantly increased expression levels of macrophage-related genes during stone formation associated with the surrounding of COM crystals by macrophages in renal interstitium. In addition, their data have also suggested that the up-regulation of inflammatory response-related genes (*CXCL1*, *CD44* and *MHCII*) might be involved in the phagocytic activity of macrophages through the interaction with osteopontin and fibronectin.[21,22] However, the response of macrophages to COM crystals was not well clarified and under-investigated.

dx.doi.org/10.1021/pr4004097 | J. Proteome Res. 2013, 12, 3561−3572

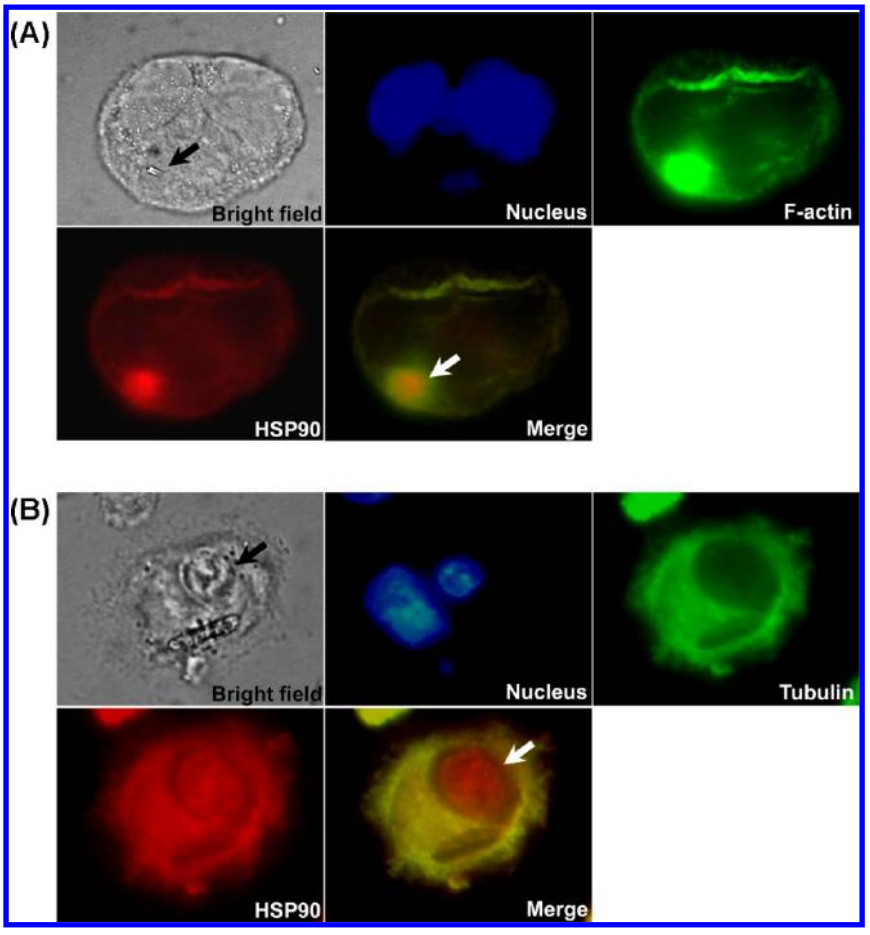


Figure 5. Co-localization of HSP90 and F-actin is important for phagosome formation. After an incubation of macrophages with COM crystals (100 μg/mL) for 24 h, the cells were subjected to multiple immunofluorescence stainings to visualize HSP90 (shown in red) together with F-actin or α-tubulin (shown in green). Nucleus was counter-stained with Hoechst dye (shown in blue). A merged image (last panel) shows colocalizations (as demonstrated by the overlapping of red and green signals that appeared as yellow) of HSP90 with (A) F-actin and with (B) α-tubulin. However, only the association between HSP90 and F-actin was found on the phagosome membrane surrounding COM crystal (A), indicating that the association of HSP90 with F-actin, but not with α-tubulin, is important for phagosome formation. The arrowhead indicates the locale of phagosome. Images were taken using Nikon ECLIPSE 80i fluorescence microscope (Nikon Corp.; Tokyo, Japan) with original magnification 1000×.

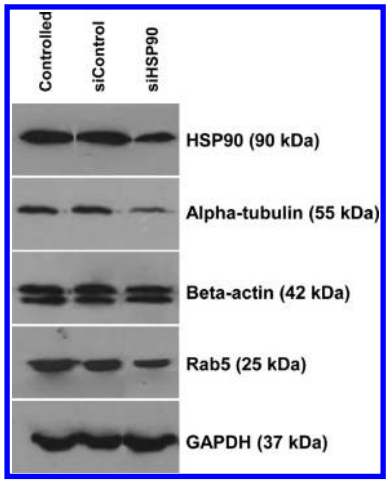


Figure 6. siHSP90 successfully reduced HSP90, phagosome-related and cytoskeletal proteins. An equal amount of 30 μg proteins derived from controlled, siControl and siHSP90 macrophages was loaded into each lane of SDS-PAGE. The resolved proteins were subjected to Western blot analysis of HSP90, α-tubulin, β-actin and Rab5 (phagosome marker) by Western blot analysis (see Materials and Methods for more details). GAPDH served as the loading control.

In our present study, we demonstrated significant changes in levels of 18 proteins in COM-treated macrophages using a proteomics approach (Figure 2, Tables 1 and 2). Functional significances of some of these significantly altered proteins are discussed and highlighted as follows.

COM crystals might induce oxidative stress in macrophages as several chaperones and antioxidant proteins, that is, HSP60, HSP90, peroxiredoxin-3, and procollagen-proline, 2-oxoglutarate 4-dioxygenase (P4Hs), were markedly increased, whereas oxidative stress responsive 1 isoform 2 was absent in the in the COM-treated cells. HSP60 and HSP90 are the molecular chaperones, which regulate the folding of nascent polypeptides and are essential for degradation of misfolded proteins via proteasome.[23] HSP60 and HSP90 have been demonstrated to be increased upon cellular stress conditions (e.g., heat stress, radiation and inflammation).[24] For immune function, HSP60 and HSP90 have been implicated to be related to the pathogenesis of autoimmune diseases, vascular diseases and inflammatory disorders.[25,26] A previous study has demonstrated that HSP60 and HSP90 are the potent activators of macrophages and dendritic cells for stimulating the production of TNF-α and IL-6 cytokines.[27] Peroxiredoxin-3 is a mitochondrial antioxidant and member of ubiquitous enzyme family that plays a crucial role in protecting the

dx.doi.org/10.1021/pr4004097 | J. Proteome Res. 2013, 12, 3561−3572

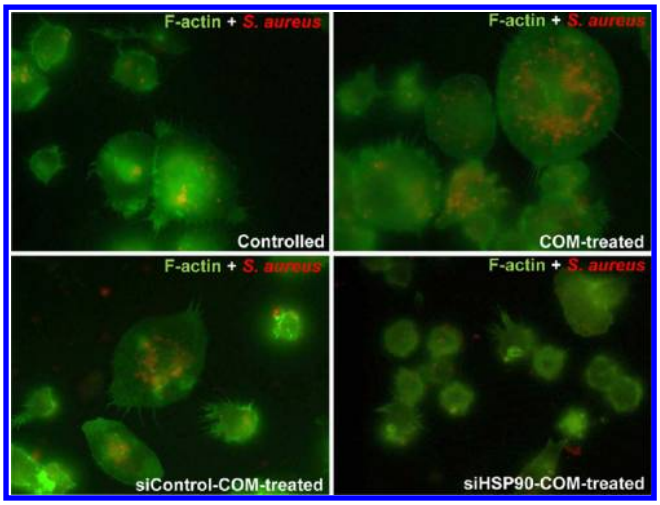


Figure 7. Effects of siHSP90 on phagocytic activity of macrophages. Controlled, COM-treated, siControl-COM-treated, and siHSP90-COM-treated macrophages (5×10^5 cells/well) were incubated with Cy3-labeled *S. aureus* (1×10^6 CFUs/mL) for 3 h. To investigate the phagocytic activity of macrophages, double immunofluorescence study was performed. The cell boundary was stained with Oreagon Green-conjugated phalloidin (shown in green), whereas the Cy3-comjugated microorganisms are shown in red. The phagocytic activity (as demonstrated by a large number of intracellular microorganisms) was observed in COM-treated macrophages, but was almost completely absent in siHSP90-COM-treated macrophages. Similar results were obtained from three independent experiments. Original magnification = 1000×.

cells against ROS and NO-derived products, including peroxynitrite.[28] A previous study has reported that peroxiredoxin was markedly enhanced when macrophages responded to the internalized pathogens and the cells generated high amount of H_2O_2 to restrict the invasion of pathogens.[29] The endoplasmic reticulum chaperone P4Hs has a central role in the biosynthesis of collagen.[30] Additionally, this enzyme contains α_2 and β_2 subunits, in which the β_2 subunit has the same function as protein disulfide isomerase (PDI).[30] Moreover, β_2 subunit of P4Hs acts as the molecular chaperone of fibrillary collagen by preventing the aggregation of the misfolded collagen in endoplasmic reticulum.[31] The present study implicated that macrophages responded to COM crystals by increasing the large amount of respiratory burst molecules, that is, peroxide and ROS, resulting in degradation of cellular proteins. The increased levels of HSP60, HSP90, peroxiredoxin-3 and P4Hs in the COM-treated macrophages found in our present study might be responsible for regulatory mechanisms to cope with oxidative stress condition, as induced by the reduction of oxidative stress responsive 1 isoform 2, and for enhancing the immune response.

Macrophages also induced up-regulations of proteins associated with metabolic pathways. These included proteins in carbohydrate metabolism (e.g., phosphoglycerate kinase; PGK) and protein metabolism (e.g., elongation factor Tu; EF-Tu). PGK catalyzes the interconversion between 1, 3-diphosphate-glycerate and 3-phosphoglycerate, which is the crucial step for generation of ATP. Ryan et al.[32] have suggested that hypoxic tissues could trigger the production of PGK, which in turn facilitates the production of ATP. Thus, the increased level of PGK in response to COM crystals might generate the energy for macrophages to promote cellular activities (e.g., phagocytosis) and reduce the large amount of ROS. EF-Tu plays a role in regulation of translational process in association with aminoacyl-tRNAs.[33] In addition, EF-Tu is also crucial for chaperone activity in refolding the newly synthesized but misfolded polypeptides in mitochondria and prevents the aggregation of the stressed proteins.[34] Under the stress conditions and when the nascent polypeptides fail to insert into the inner membrane, EF-Tu plays an important role in recruitment of the misfolded nascent polypeptides to the degradation process.[34] Taken together, our present study suggested that macrophages increased levels of several metabolic proteins for the immune function and regulation of oxidative stress during the response to COM crystals. The increase of a glycolytic enzyme PGK might provide ATP for maintaining cellular activities, whereas EF-Tu prevented the deleterious effect under such stress condition induced at least in part by mitochondria-mediated stress proteins.

For molecular trafficking, *N*-ethylmaleimide sensitive factor (NSF) is characterized as a member of hexameric ATPase.[35] This enzyme plays an important role in recycling of carrier vesicles in endocytic and exocytic pathways.[36] The vesicular trafficking from cytoplasm to the target membrane is relied on SNARE (soluble-*N*-ethylmaeimide sensitive-factor accessory protein receptor) proteins.[37] In the cells that have multiple cycles of the SNARE-dependent vesicular transport, NSF acts as the crucial enzyme for disaggregate SNARE proteins before they are ready for the next vesicular transport cycle.[37] Previous study has shown that the decrease or inactivation of NSF led to the accumulation of SNARE complex and could further induce cell death.[36] In this study, the increased expression of NSF might be involved in the vesicular transport of macrophages that is crucial for their immune function and phagosome formation.

For cytoskeletal proteins that are important for cellular structure, α-tubulin and β-actin were up-regulated. α-tubulin is a component of microtubule structure that is essential for mitosis, cell migration, cell transport, phagocytic activity and signal transduction.[38] In mammalian cells, α-tubulin can be modified by acetylation for regulating the function of HSP90 pathway.[16] The regulation of HSP90 pathway by α-tubulin is crucial for promoting cell proliferation, cell survival and DNA repairing.[39] Beta-actin, the predominant isoform of actin, plays important roles in many cellular functions. One among these is its crucial role in cell protrusion as well as migration. Therefore, β-actin is commonly found to predominate at the frontal or protruding parts of the moving cells. Assembly of β-actin to form filamentous actin (F-actin) is regulated by the presence of ATP, actin-binding partners and actin-related proteins.[40] Actin polymerization could facilitate the internalization of foreign particles.[41] The stabilization and organization of F-actin is also controlled by HSP90 to maintain the phagocytic function of macrophages.[15,41] Interestingly, the increased level of heat shock proteins has been reported to enhance F-actin-mediated phagosome formation.[19] Furthermore, HSP90 has been proposed to be involved in the assembly of cytoskeletal proteins for migration of cells.[16,39]

In our present study, protein interaction network analysis of these significantly altered proteins revealed three main networks of their interactions, including those of cytoskeletal proteins, chaperones/stress response proteins, and metabolic proteins. Additionally, the interaction networks also pointed out that HSP90 was associated with both β-actin and α-tubulin (Figure 4). Multiple immunofluorescence stainings confirmed such interactions (Figure 5). Although HSP90 and F-actin are

dx.doi.org/10.1021/pr4004097 | *J. Proteome Res.* 2013, 12, 3561−3572

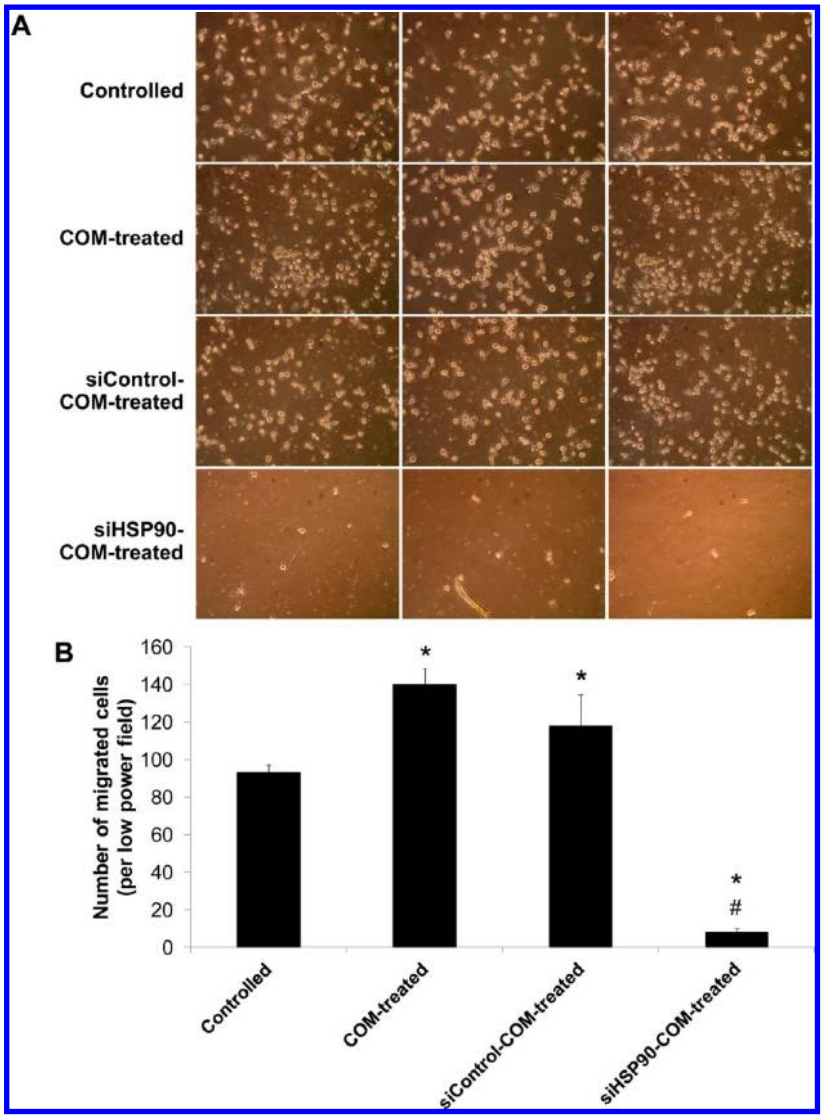


Figure 8. Effects of siHSP90 on macrophage migration. Controlled, COM-treated, siControl-COM-treated, and siHSP90-COM-treated macrophages (2×10^5 cells/well) were inoculated in the upper chamber containing serum-free medium, whereas the lower chamber was added with 10% serum containing medium. After 24-h incubation, the migrated macrophages was (A) imaged using inverted phase-contrast light microscope (Olympus CKX41) with original magnification of 200× and (B) quantitated by Tarosoft Image Frame Work version 0.9.6. The quantitative data are represented as mean ± SD derived from five fields of three independent experiments (B). * = $P < 0.05$ versus controlled macrophages. # = $P < 0.05$ versus COM-treated-macrophages.

generally found in the cytoplasm of cells with many various functions, the role of these proteins has been also implicated to involve in phagocytic activity as well as phagosome formation.[15,19,41] Our data confirmed that the colocalization of HSP90 with F-actin, but not with α-tubulin, was associated with phagosome formation. Moreover, we also confirmed the important role of HSP90 in regulation of cytoskeleton-mediated phagocytic activity and migration in macrophages using siRNA approach (Figures 7 and 8).

In summary, we identified a set of the altered cellular proteins of human macrophages in response to an exposure of COM crystals. These altered proteins were involved in many cellular processes of macrophages, particularly phagocytic activity and migration. Moreover, we also demonstrated that the association of HSP90 with F-actin, but not with α-tubulin, is important for phagosome formation. Moreover, functional validation through siRNA approach confirmed the important role of HSP90 in phagocytosis and migration of macrophages during an exposure to COM crystals. Our data may help in understanding the important role of macrophages in kidney stone disease.

■ ASSOCIATED CONTENT

Supporting Information

Supplementary Methods and Supplementary Figure S1: Morphological change of macrophages in response to COM crystals. This material is available free of charge via the Internet at http://pubs.acs.org.

■ AUTHOR INFORMATION

Corresponding Author

*Phone: +66-2-4192850. E-mail: thongboonkerd@dr.com or vthongbo@yahoo.com.

Notes

The authors declare no competing financial interest.

■ ACKNOWLEDGMENTS

We are grateful to Prof. Shui-Tein Chen and Dr. Supachok Sinchaikul for their assistance on mass spectrometric analyses. This study was supported by the Thailand Research Fund (TRF) Senior Research Scholarship (RTA5380005), Office of the Higher Education Commission and Mahidol University under the National Research Universities Initiative, and Faculty of Medicine Siriraj Hospital. K.S. was supported by Royal Golden Jubilee Ph.D. Program scholarship; V.T. was supported by "Chalermphrakiat" Grant, Faculty of Medicine Siriraj Hospital.

■ ABBREVIATIONS

2-DE, two-dimensional electrophoresis; ACN, acetonitrile; CHAPS, 3-[(3-cholamidopropyl) dimethyl-ammonio]-1-propanesulfonate; CHCA, α-cyano-4-hydroxycinnamic acid; COM, calcium oxalate monohydrate; DTT, dithiothreitol; EDTA, ethylenediamine tetraacetic acid; EF-Tu, elongation factor Tu; GAPDH, glyceraldehyde-3-phosphate dehydrogenase; HSP60, 60 kDa heat shock protein; HSP90, 90 kDa heat shock protein; IEF, isoelectric focusing; IL-6, interleukin-6; MS, mass spectrometry; MS/MS, tandem mass spectrometry; NSF, *N*-ethylmaleimide sensitive factor; P4Hs, procollagen-proline, 2-oxoglutarate 4-dioxygenase; PDI, protein disulfide isomerase; PMA, phorbol-12-myristate-13-acetate; PGK, phosphoglycerate kinase; Q-TOF, quadrupole time-of-flight; ROS, reactive oxygen species; RT, room temperature; siRNA, small interfering RNA; SNARE, soluble-N-ethylmaeimide sensitive-factor accessory protein receptor; TFA, trifluoroacetic acid; TNF-α, tumor necrosis factor-alpha

■ REFERENCES

(1) Flannagan, R. S.; Cosio, G.; Grinstein, S. Antimicrobial mechanisms of phagocytes and bacterial evasion strategies. *Nat. Rev. Microbiol.* **2009**, *7*, 355−366.

(2) Gordon, S.; Taylor, P. R. Monocyte and macrophage heterogeneity. *Nat. Rev. Immunol.* **2005**, *5*, 953−964.

(3) Kinchen, J. M.; Ravichandran, K. S. Phagosome maturation: going through the acid test. *Nat. Rev. Mol. Cell Biol.* **2008**, *9*, 781−795.

(4) Cape, J. L.; Hurst, J. K. The role of nitrite ion in phagocyte function–perspectives and puzzles. *Arch. Biochem. Biophys.* **2009**, *484*, 190−196.

(5) Khan, S. R. Crystal-induced inflammation of the kidneys: results from human studies, animal models, and tissue-culture studies. *Clin. Exp. Nephrol.* **2004**, *8*, 75−88.

(6) de Water, R.; Noordermeer, C.; Houtsmuller, A. B.; Nigg, A. L.; Stijnen, T.; Schroder, F. H.; Kok, D. J. Role of macrophages in nephrolithiasis in rats: an analysis of the renal interstitium. *Am. J Kidney Dis.* **2000**, *36*, 615−625.

(7) de Water, R.; Leenen, P. J.; Noordermeer, C.; Nigg, A. L.; Houtsmuller, A. B.; Kok, D. J.; Schroder, F. H. Cytokine production induced by binding and processing of calcium oxalate crystals in cultured macrophages. *Am. J. Kidney Dis.* **2001**, *38*, 331−338.

(8) Chapman, P. T.; Jamar, F.; Harrison, A. A.; Schofield, J. B.; Peters, A. M.; Binns, R. M.; Haskard, D. O. Characterization of E-selectin expression, leucocyte traffic and clinical sequelae in urate crystal-induced inflammation: an insight into gout. *Br. J. Rheumatol.* **1996**, *35*, 323−334.

(9) Driscoll, K. E.; Carter, J. M.; Hassenbein, D. G.; Howard, B. Cytokines and particle-induced inflammatory cell recruitment. *Environ. Health Perspect.* **1997**, *105* (Suppl5), 1159−1164.

(10) Wuthrich, R. P.; Fan, X.; Ritthaler, T.; Sibalic, V.; Yu, D. J.; Loffing, J.; Kaissling, B. Enhanced osteopontin expression and macrophage infiltration in MRL-Fas(lpr) mice with lupus nephritis. *Autoimmunity* **1998**, *28*, 139−150.

(11) Sintiprungrat, K.; Singhto, N.; Sinchaikul, S.; Chen, S. T.; Thongboonkerd, V. Alterations in cellular proteome and secretome upon differentiation from monocyte to macrophage by treatment with phorbol myristate acetate: insights into biological processes. *J. Proteomics* **2010**, *73*, 602−618.

(12) Jensen, L. J.; Kuhn, M.; Stark, M.; Chaffron, S.; Creevey, C.; Muller, J.; Doerks, T.; Julien, P.; Roth, A.; Simonovic, M.; Bork, P.; von Mering, C. STRING 8–a global view on proteins and their functional interactions in 630 organisms. *Nucleic Acids Res.* **2009**, *37*, D412−D416.

(13) Van Goethem, E.; Poincloux, R.; Gauffre, F.; Maridonneau-Parini, I.; Le, C. V Matrix architecture dictates three-dimensional migration modes of human macrophages: differential involvement of proteases and podosome-like structures. *J. Immunol.* **2010**, *184*, 1049−1061.

(14) Verkoelen, C. F.; van der Boom, B. G.; Houtsmuller, A. B.; Schroder, F. H.; Romijn, J. C. Increased calcium oxalate monohydrate crystal binding to injured renal tubular epithelial cells in culture. *Am. J. Physiol.* **1998**, *274*, F958−F965.

(15) Taiyab, A.; Rao, C. HSP90 modulates actin dynamics: inhibition of HSP90 leads to decreased cell motility and impairs invasion. *Biochim. Biophys. Acta* **2011**, *1813*, 213−221.

(16) Giustiniani, J.; Daire, V.; Cantaloube, I.; Durand, G.; Pous, C.; Perdiz, D.; Baillet, A. Tubulin acetylation favors Hsp90 recruitment to microtubules and stimulates the signaling function of the Hsp90 clients Akt/PKB and p53. *Cell Signal.* **2009**, *21*, 529−539.

(17) Kellermayer, M. S.; Csermely, P. ATP induces dissociation of the 90 kDa heat shock protein (hsp90) from F-actin: interference with the binding of heavy meromyosin. *Biochem. Biophys. Res. Commun.* **1995**, *211*, 166−174.

(18) Williams, N. E.; Nelsen, E. M. HSP70 and HSP90 homologs are associated with tubulin in hetero-oligomeric complexes, cilia and the cortex of Tetrahymena. *J. Cell Sci.* **1997**, *110* (Pt 14), 1665−1672.

(19) Vega, V. L.; De Maio, A. Increase in phagocytosis after geldanamycin treatment or heat shock: role of heat shock proteins. *J. Immunol.* **2005**, *175*, 5280−5287.

(20) Schulz, R.; Marchenko, N. D.; Holembowski, L.; Fingerle-Rowson, G.; Pesic, M.; Zender, L.; Dobbelstein, M.; Moll, U. M. Inhibiting the HSP90 chaperone destabilizes macrophage migration inhibitory factor and thereby inhibits breast tumor progression. *J. Exp. Med.* **2012**, *209*, 275−289.

(21) Okada, A.; Yasui, T.; Hamamoto, S.; Hirose, M.; Kubota, Y.; Itoh, Y.; Tozawa, K.; Hayashi, Y.; Kohri, K. Genome-wide analysis of genes related to kidney stone formation and elimination in the calcium oxalate nephrolithiasis model mouse: detection of stone-preventive factors and involvement of macrophage activity. *J. Bone Miner. Res.* **2009**, *24*, 908−924.

(22) Okada, A.; Yasui, T.; Fujii, Y.; Niimi, K.; Hamamoto, S.; Hirose, M.; Kojima, Y.; Itoh, Y.; Tozawa, K.; Hayashi, Y.; Kohri, K. Renal macrophage migration and crystal phagocytosis via inflammatory-related gene expression during kidney stone formation and elimination in mice: Detection by association analysis of stone-related gene expression and microstructural observation. *J. Bone Miner. Res.* **2010**, *25*, 2701−2711.

(23) Tsan, M. F.; Gao, B. Heat shock proteins and immune system. *J. Leukoc. Biol.* **2009**, *85*, 905−910.

(24) Hartl, F. U. Molecular chaperones in cellular protein folding. *Nature* **1996**, *381*, 571−579.

(25) Pockley, A. G. Heat shock proteins in health and disease: therapeutic targets or therapeutic agents? *Expert Rev. Mol. Med.* **2001**, *3*, 1−21.

(26) van Eden, W.; van der, Z. R.; Prakken, B. Heat-shock proteins induce T-cell regulation of chronic inflammation. *Nat. Rev. Immunol.* **2005**, *5*, 318−330.

(27) Wallin, R. P.; Lundqvist, A.; More, S. H.; von Bonin, A.; Kiessling, R.; Ljunggren, H. G. Heat-shock proteins as activators of the innate immune system. *Trends Immunol.* **2002**, *23*, 130−135.

(28) Abbas, K.; Breton, J.; Drapier, J. C. The interplay between nitric oxide and peroxiredoxins. *Immunobiology* **2008**, *213*, 815−822.

(29) Nathan, C.; Shiloh, M. U. Reactive oxygen and nitrogen intermediates in the relationship between mammalian hosts and microbial pathogens. *Proc. Natl. Acad. Sci. U.S.A.* **2000**, *97*, 8841−8848.
(30) Myllyharju, J. Prolyl 4-hydroxylases, the key enzymes of collagen biosynthesis. *Matrix Biol.* **2003**, *22*, 15−24.
(31) Lamande, S. R.; Bateman, J. F. Procollagen folding and assembly: the role of endoplasmic reticulum enzymes and molecular chaperones. *Semin. Cell Dev. Biol.* **1999**, *10*, 455−464.
(32) Ryan, H. E.; Lo, J.; Johnson, R. S. HIF-1 alpha is required for solid tumor formation and embryonic vascularization. *EMBO J.* **1998**, *17*, 3005−3015.
(33) Nagao, A.; Suzuki, T.; Suzuki, T. Aminoacyl-tRNA surveillance by EF-Tu in mammalian mitochondria. *Nucleic Acids Symp. Ser.* **2007**, 41−42.
(34) Suzuki, H.; Ueda, T.; Taguchi, H.; Takeuchi, N. Chaperone properties of mammalian mitochondrial translation elongation factor Tu. *J. Biol. Chem.* **2007**, *282*, 4076−4084.
(35) Hanson, P. I.; Whiteheart, S. W. AAA+ proteins: have engine, will work. *Nat. Rev. Mol. Cell Biol.* **2005**, *6*, 519−529.
(36) Malsam, J.; Kreye, S.; Sollner, T. H. Membrane fusion: SNAREs and regulation. *Cell. Mol. Life Sci.* **2008**, *65*, 2814−2832.
(37) Stow, J. L.; Manderson, A. P.; Murray, R. Z. SNAREing immunity: the role of SNAREs in the immune system. *Nat. Rev. Immunol.* **2006**, *6*, 919−929.
(38) Gundersen, G. G.; Cook, T. A. Microtubules and signal transduction. *Curr. Opin. Cell Biol.* **1999**, *11*, 81−94.
(39) Whitesell, L.; Lindquist, S. L. HSP90 and the chaperoning of cancer. *Nat. Rev. Cancer* **2005**, *5*, 761−772.
(40) dos Remedios, C. G.; Chhabra, D.; Kekic, M.; Dedova, I. V.; Tsubakihara, M.; Berry, D. A.; Nosworthy, N. J. Actin binding proteins: regulation of cytoskeletal microfilaments. *Physiol. Rev.* **2003**, *83*, 433−473.
(41) Chimini, G.; Chavrier, P. Function of Rho family proteins in actin dynamics during phagocytosis and engulfment. *Nat. Cell Biol.* **2000**, *2*, E191−E196.

JOURNAL OF PROTEOMICS 80 (2013) 55–65



Available online at www.sciencedirect.com

SciVerse ScienceDirect

www.elsevier.com/locate/jprot



Cellular adaptive response of distal renal tubular cells to high-oxalate environment highlights surface alpha-enolase as the enhancer of calcium oxalate monohydrate crystal adhesion

*Rattiyaporn Kanlaya, Kedsarin Fong-ngern, Visith Thongboonkerd**

Medical Proteomics Unit, Office for Research and Development, Faculty of Medicine Siriraj Hospital, Mahidol University, Bangkok, Thailand
Center for Research in Complex Systems Science, Mahidol University, Bangkok, Thailand

ARTICLE INFO

Article history:
Received 26 September 2012
Accepted 7 January 2013

Keywords:
Alpha-enolase
Crystal adhesion
Hyperoxaluria
Kidney stone
Oxalate

ABSTRACT

Hyperoxaluria is one of etiologic factors of calcium oxalate kidney stone disease. However, response of renal tubular cells to high-oxalate environment remained largely unknown. We applied a gel-based proteomics approach to characterize changes in cellular proteome of MDCK cells induced by 10 mM sodium oxalate. A total of 14 proteins were detected as differentially expressed proteins. The oxalate-induced up-regulation of alpha-enolase in whole cell lysate was confirmed by 2-D Western blot analysis. Interaction network analysis revealed that cellular adaptive response under high-oxalate condition involved stress response, energy production, metabolism and transcriptional regulation. Down-regulation of RhoA, which was predicted to be associated with the identified proteins, was confirmed by immunoblotting. In addition, the up-regulation of alpha-enolase on apical surface of renal tubular epithelial cells was also confirmed by immunoblotting of the isolated apical membranes and immunofluorescence study. Interestingly, blockage of alpha-enolase expressed on the cell surface by antibody neutralization significantly reduced the number of calcium oxalate monohydrate (COM) crystals adhered on the cells. These results strongly suggest that surface alpha-enolase plays an important role as the enhancer of COM crystal binding. The increase of alpha-enolase expressed on the cell surface may aggravate kidney stone formation in patients with hyperoxaluria.

© 2013 Elsevier B.V. All rights reserved.

1. Introduction

Many attempts have been made to better understand the initiation of kidney stone formation in patients with hyperoxaluria. Because calcium oxalate is the most common type of crystals found in kidney stones, effects of dicarboxylic anion (oxalate) have received wide attention [1,2]. The supersaturation of oxalate ion can initiate crystalline formation and induce renal cell injury, which promotes crystal adhesion on renal cell surface [3,4]. Oxalate exposure can activate several cellular events, including redistribution of membrane phospholipids, activation of membrane-bound phopholipases, and consequently, lipid signaling that is involved in cellular injury and death [5]. Overloading of oxalate ion can decrease antioxidant activity and increase reactive oxygen species (ROS) production by mitochondria, and ultimately, cell death. However, the increased ROS production and lactate dehydrogenase (LDH) release induced by oxalate are counteracted by several free radical scavengers, including vitamin E, superoxide dismutase (SOD), catalase and iron chelator, suggesting the

* *Corresponding author at:* Medical Proteomics Unit, Office for Research and Development, Director of Center for Research in Complex Systems Science (CRCSS), Siriraj Hospital, Mahidol University, 6th Fl-SiMR Bldg., Siriraj Hospital, 2 Prannok Rd., Bangkoknoi, Bangkok 10700, Thailand. Tel.: +66 2 4192850.
E-mail addresses: thongboonkerd@dr.com, vthongbo@yahoo.com (V. Thongboonkerd).

1874-3919/$ – see front matter © 2013 Elsevier B.V. All rights reserved.
http://dx.doi.org/10.1016/j.jprot.2013.01.001

promising way to prevent oxidative injury and subsequent crystal nucleation [6]. Moreover, oxalate can induce mitochondrial dysfunction as demonstrated in hyperoxaluric rats induced by ethylene glycol (EG) [7]. The results have shown that oxalate could induce permeability transition in this organelle by decreasing activity of mitochondrial respiratory enzyme complexes and increasing mitochondrial swelling [7]. A recent study by Thamilselvan, et al. [8] has demonstrated for the first time that activation of protein kinase C alpha and delta isoforms is the underlying mechanism for oxalate-induced renal epithelial cell injury through the increased ROS production and LDH release. In addition, oxalate exposure increases the production of urinary modulators, e.g. osteopontin (OPN), that can modulate crystal nucleation, growth and aggregation [9]. Moreover, tubular secretion of oxalate has been considered as the key event resulting to hyperoxaluria in calcium stone formers [10].

Nevertheless, response of renal tubular cells to high-oxalate environment remained largely unknown. Daily urinary oxalate excretion can be as high as 0.45–0.50 mg/24 h (equivalent to a concentration of approximately 40–45 mM) in patients with hyperoxaluria [1]. In this study, we investigated the global changes of proteins as a response of distal renal tubular cells under a high-oxalate environment using a gel-based proteomics approach. This *in vitro* condition mimicked hyperoxaluric feature in patients with hyperoxaluria [1,11]. The interacting protein network was then analyzed to obtain biological meanings of the altered proteins. Our findings highlighted alterations of proteins in many cellular processes for adaptation of distal renal tubular cells under a high-oxalate condition. Thereafter, functional analysis was performed to confirm such biological relevance. The functional data revealed that the increased alpha-enolase on apical cell surface played a significant role in enhancement of crystal adhesion induced by high-oxalate.

2. Materials & methods

2.1. Cell cultivation and high-oxalate treatment

MDCK distal renal tubular cells were maintained in Eagle's minimal essential medium (MEM) (Gibco; Grand Island, NY) containing 10% heat inactivated fetal bovine serum (FBS) (Gibco), 2 mM glutamine (Sigma; St.Louis, MO) in the presence of 100 U/ml penicillin G and 100 mg/ml streptomycin (Sigma). Cells were maintained in a humidified incubator at 37 °C with 5% CO_2. For oxalate treatment, sodium oxalate solution was added into the mentioned growth MEM medium to make a final concentration of 10 mM (in 5 ml total volume). This concentration was based on the findings reported previously by Schepers, et al. [11]. The cells were incubated with or without oxalate treatment in a humidified incubator at 37 °C with 5% CO_2 for 72 h, and were then harvested.

2.2. Protein extraction and two-dimensional polyacrylamide gel electrophoresis (2-D PAGE)

Cellular proteins derived from the controlled and oxalate-treated cells were subjected to 2-D PAGE (n=5 gels derived from 5 independent cultures per group; a total of 10 gels were analyzed). Briefly, the cell monolayers were washed three times with PBS and were gently scraped. Whole cell lysates were obtained using a lysis buffer containing 7 M urea, 2 M thiourea, 40 mg/ml 3-[(3-cholamidopropyl) dimethyl-ammonio]-1-propanesulfonate (CHAPS), 120 mM dithiothreitol (DTT), 2% (v/v) ampholytes pH 3–10, and 40 mM Tris-base) at 4 °C for 30 min. Unsolubilized cellular debris and particles were removed by a centrifugation at 13,000×*g* and 4 °C for 5 min. Protein concentrations in the clarified supernatants were determined using Bio-Rad Protein Assay (Bio-Rad Laboratories; Hercules, CA) based on the Bradford method. An equal amount of 150 μg proteins recovered from each sample was loaded for 2-D PAGE detailed in "Supplementary methods". The resolved proteins were stained with SYPRO Ruby fluorescence dye (Invitrogen-Molecular Probes; Eugene, OR) and gel images were captured by using a Typhoon laser scanner (GE Healthcare; Uppsala, Sweden).

2.3. Matching and quantitative analysis of protein spots

Image Master 2D Platinum (GE Healthcare) software (version 6.0) was used for matching and analysis of protein spots visualized in individual gels. Details are provided in "Supplementary methods". Intensity volumes of individual spots were obtained and subjected to statistical analysis. Differentially expressed protein spots were subjected to in-gel tryptic digestion and identification by mass spectrometry.

2.4. Protein identification by quadrupole time-of-flight (Q-TOF) mass spectrometry (MS) and tandem MS (MS/MS)

In-gel tryptic digestion was performed as detailed in "Supplementary methods". The proteolytic samples were premixed 1:1 with the matrix solution (5 mg/ml α-cyano-4-hydroxycinnamic acid (CHCA) in 50% ACN, 0.1% v/v TFA and 2% w/v ammonium citrate) and spotted onto the 96-well sample stage. The samples were analyzed by the Q-TOF Ultima™ mass spectrometer (Micromass; Manchester, UK) (more details are provided in "Supplementary methods"). The MS peptide masses and MS/MS ions were analyzed by the MASCOT search engine (http://www.matrixscience.com) and queried to the NCBI mammalian protein database, assuming that peptides were monoisotopic, oxidized at methionine residues and carbamidomethylated at cysteine residues. Only 1 missed trypsin cleavage was allowed, and peptide mass tolerances of 100 and 50 ppm were used for MS and MS/MS data, respectively.

2.5. Protein network analysis and subcellular localization

The STRING software [12] was adopted to translate expressional proteomic data into biological relevance. This public database weighs and integrates protein–protein interactions from numerous resources, including experimental repositories, computational prediction and published articles [12]. All the significantly altered proteins identified in oxalate-treated MDCK cells were inputted into STRING 8.3 (http://string-db.org) to retrieve the data of (i) protein function, (ii) subcellular localization and (iii) protein interaction/functional connectivity.

2.6. Western blot analysis

2.6.1. 2-D Western blot analysis

A total of 100 μg proteins derived from whole cell lysate of each sample was dissolved in a 2-D gel as aforementioned. The resolved proteins were electro-transferred onto a nitrocellulose membrane. Non-specific bindings were blocked with 5% skim milk in PBS for 1 h. The membrane was then incubated with rabbit polyclonal anti-enolase antibody (Santa Cruz Biotechnology; Santa Cruz, CA) (1:1000 in 1% skim milk/PBS) at 4 °C for 16 h. After washing, the membrane was incubated with goat anti-rabbit IgG conjugated with horseradish peroxidase (HRP) (DAKO) (1:2000 in 1% skim milk/PBS) at 25 °C for 1 h. Immunoreactive protein spots were visualized by SuperSignal West Pico chemiluminescence substrate (Pierce Biotechnology, Inc.; Rockford, IL) and autoradiography.

2.6.2. 1-D Western blot analysis

For apical membrane proteins, apical membranes were isolated from polarized MDCK cells by peeling method as described with details in our previous study [13] (see also "Supplementary methods"). A total of 50 μg proteins derived from whole cell lysate or apical membrane protein fraction from each sample was resolved by 12% SDS-PAGE and transferred onto a nitrocellulose membrane. After blocking non-specific bindings, the membrane was incubated with mouse monoclonal anti-RhoA antibody (Santa Cruz Biotechnology) or rabbit polyclonal anti-enolase antibody (Santa Cruz Biotechnology) (1:1000 in 1% skim milk in PBS) at 4 °C for 16 h. Mouse monoclonal anti-GAPDH (Santa Cruz Biotechnology) was used to detect GAPDH as the loading control (1:2000 in 1% skim milk/PBS). After washing, the membrane was incubated with corresponding secondary antibody conjugated with horseradish peroxidase (HRP) (DAKO) (1:2000–1:4000 in 1% skim milk/PBS) at 25 °C for 1 h. Immunoreactive protein bands were visualized by SuperSignal West Pico chemiluminescence substrate (Pierce Biotechnology) and autoradiography.

2.7. Laser-scanning confocal microscopic examination of apical membrane enolase

MDCK cells were grown on a coverslip and treated with or without 10 mM sodium oxalate as aforementioned. The cells were rinsed with PBS^+ (PBS containing 1 mM $MgCl_2$ and 0.1 mM $CaCl_2$) and then fixed with 3.7% formaldehyde in PBS^+ at 25 °C for 15 min. After washing with PBS^+, the cells were incubated with rabbit polyclonal anti-enolase antibody (Santa Cruz Biotechnology) (1:50 in 1% BSA/PBS) at 37 °C for 1 h. Thereafter, the cells were washed with PBS three times and then incubated with anti-rabbit IgG conjugated with Cy3 (Jackson ImmunoResearch Laboratories; West Grove, PA) containing 0.1 μg/ml Hoechst dye (Invitrogen/Molecular Probes) (for nuclear staining) at 37 °C for 1 h. Three-dimensional planes of X-Y, X-Z and Y-Z scanning were captured under a laser-scanning confocal microscope equipped with an LSM5 Image Browser (LSM 510 Meta, Carl Zeiss; Jena, Germany).

2.8. COM crystal adhesion and neutralization assay

COM crystals were prepared as described previously in our previous study [14,15] (see also "Supplementary methods"). MDCK cells were maintained with or without 10 mM sodium oxalate for 72 h as aforementioned. COM crystals were added into the growth medium (100 μg crystals/ml medium) and further incubated with the cells at 37 °C for 30 min. Thereafter, the unbound crystals were removed and the cells were washed three times with PBS. The remaining crystals adhered on the cell surface were counted at 15 randomized high power fields (HPF) under a phase contrast microscope (Olympus CKX41, Olympus Co. Ltd.; Tokyo, Japan). In parallel, the cells that were pre-incubated with 0.2 μg/ml rabbit polyclonal anti-enolase antibody (Santa Cruz Biotechnology) or non-specific rabbit IgG at 37 °C for 30 min before COM crystal incubation were also evaluated. This experiment was performed in triplicate for all conditions.

2.9. Statistical analysis

Quantitative data are reported as mean ± SEM. Comparisons between the two sets of samples (i.e., controlled vs. oxalate-treated) were performed using unpaired Student's *t* test. P-values less than 0.05 were considered statistically significant.

3. Results

3.1. Proteome changes induced by high-oxalate condition

MDCK cells were maintained with or without 10 mM sodium oxalate for 72 h. Whole cell lysates derived from the controlled (untreated) and oxalate-treated cells were equally loaded (150 μg each) and resolved by 2-D PAGE (n = 5 gels derived from 5 independent cultures per group; a total of 10 gels were analyzed). Spot matching and quantitative intensity analysis of the matched spots revealed 14 differentially expressed protein spots between the two groups (Fig. 1). These significantly altered proteins were successfully identified by Q-TOF MS and/or MS/MS (Table 1). Among these, 8 proteins were down-regulated, whereas other 6 proteins were up-regulated by high-oxalate (1 protein spot was expressed only in the high-oxalate condition). 2-D Western blot analysis was performed to confirm the proteomic data, e.g. the increased level of alpha-enolase (spot #354) in the oxalate-treated MDCK cells (Fig. 2). The increased level and locale in the 2-D map of alpha-enolase were confirmed by 2-D Western blot analysis.

3.2. Network analysis and subcellular localization of the significantly altered proteins

The STRING software was employed to translate the significantly altered proteins into the biological relevance by providing the information about their functions, interactions and subcellular localizations (Fig. 3). In addition to the significantly altered proteins induced by high-oxalate identified in this study (labeled as "colored nodes" with upward or downward arrows for up-regulated or down-regulated

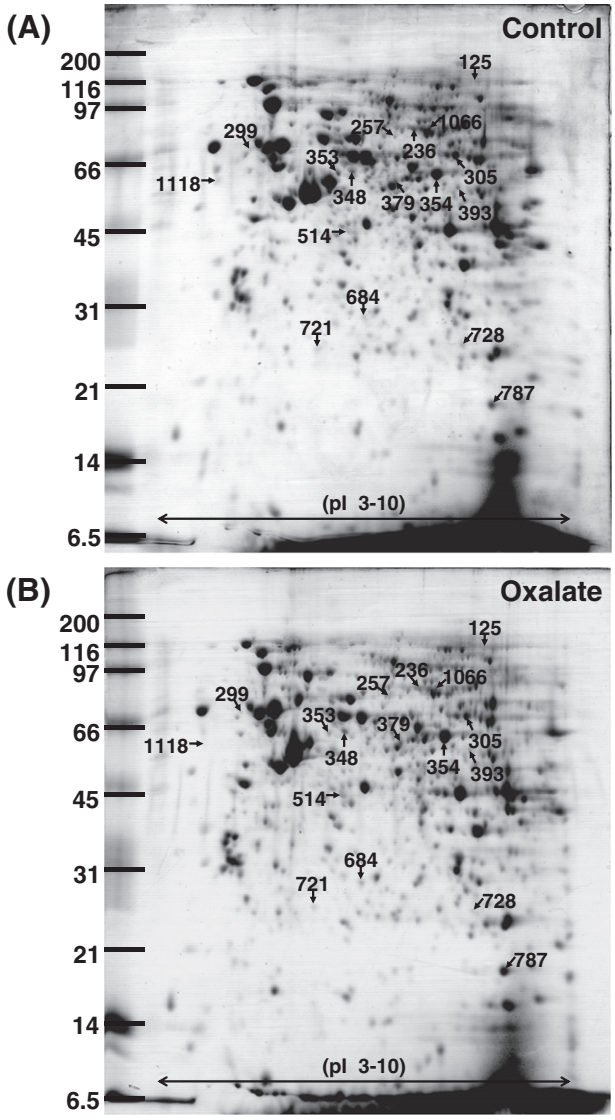


Fig. 1 – Representative 2-D proteome maps of differentially expressed proteins in controlled (A) and oxalate-treated cells (B). MDCK cells were maintained without or with 10 mM sodium oxalate for 72 h and their cellular proteome were analyzed by 2-D PAGE (n = 5 gels derived from 5 independent cultures per group; a total of 10 gels were analyzed). Spot matching and quantitative intensity analysis revealed 14 differentially expressed protein spots, which are labeled as numbers corresponding to those reported in Tables 1 and 2.

proteins, respectively), the interacting proteins predicted from literatures and other databases were labeled as the "white nodes" without arrows. Moreover, each protein node was mapped to its major subcellular localization (Table 2), of which the background image was created by the Pathway Builder Online (*http://www.proteinlounge.com*) (Fig. 3). From this interaction map, RhoA was predicted as an interacting partner of significantly altered proteins identified by proteomic analysis. We then performed 1-D Western blot analysis to examine whether RhoA level was changed by high-oxalate. GAPDH served as the loading control. The data confirmed that RhoA level was decreased in the oxalate-treated MDCK cells (Fig. 4A).

3.3. *Increased surface expression of alpha-enolase induced by high-oxalate*

Network analysis and subcellular localization also suggested that the oxalate-induced increase in expression level of alpha-enolase occurred at apical surface of renal tubular cells. To confirm this data, apical membranes were isolated from polarized MDCK renal tubular epithelial cells using a peeling method described previously by our group [13]. This simple and effective method offers a highly purified apical membrane fraction [13]. 1-D Western blot analysis of alpha-enolase in this apical membrane fraction confirmed that alpha-enolase was expressed in apical membrane of polarized MDCK renal tubular epithelial cells and its expression was increased in apical membrane after an exposure to high-oxalate (Fig. 4B). To further validate this result, immunofluorescence study was performed. The data obtained from laser-scanning confocal microscopy clearly demonstrated that apical surface expression of alpha-enolase was significantly increased in the oxalate-treated cells (Fig. 4C).

3.4. *Effects of high-oxalate on COM crystal adhesion and neutralization of surface alpha-enolase*

We also evaluated the functional significance of the increased expression level of apical surface of alpha-enolase induced by high-oxalate. We hypothesized that high-oxalate could enhance COM crystal adhesion on the cell surface and that the increased expression level of apical surface of alpha-enolase might play significant role in this phenomenon. Our hypothesis was addressed by COM crystal adhesion assay. The data confirmed that high-oxalate significantly increased the number of adherent COM crystals (Fig. 5). Moreover, the data also revealed that neutralization of surface expression of alpha-enolase by specific antibody against this protein dramatically reduced the number of the adherent COM crystals almost to the basal level, whereas neutralization with non-specific IgG derived from the same species as of specific antibody had no effects on the number of adherent COM crystals (Fig. 5).

4. Discussion

Oxalate plays a key role in calcium oxalate kidney stone formation, particularly in hyperoxaluria commonly found in patients with idiopathic calcium oxalate urolithiasis and tubulointerstitial fibrosis [16,17]. However, molecular mechanisms that high-oxalate plays in calcium oxalate kidney stone disease remained unclear. Our present study therefore aimed to characterize changes in cellular proteome of distal renal tubular cells in response to high-oxalate. Our findings have demonstrated that the significantly altered proteins were involved in various biological processes of renal tubular cells, including maintenance of the actin cytoskeletal assembly and nuclear structure (ACTR3, CFL1 and LMNA), signal transduction (PRKAR2A), stress response (HSPB1, ERO1L, SDF2L1 and UQCRC1), energy metabolism (ENO1, GLUD1 and OAT) and

Table 1 – Summary of significantly altered proteins in distal renal tubular (MDCK) cells in response to high-oxalate exposure.

Spot no.	Protein	NCBI entry	Identified by	Identification scores (MS, MS/MS)	%Cov (MS, MS/MS)	No. of matched peptides (MS, MS/MS)	pI	MW (kDa)	Intensity level (Mean ± SEM)		Ratio (Oxalate/control)	p-value
									Control	Oxalate		
	Up-regulated proteins											
514	60S acidic ribosomal protein P0 (L10E) isoform 8	gi|73994699	MS	70, NA	44, NA	7, NA	5.91	32.09	0.0822 ± 0.0149	0.1291 ± 0.0101	1.57	0.031
348	ARP3 actin-related protein 3 homolog	gi|13542701	MS/MS	NA, 143	NA, 14	NA, 4	5.61	47.78	0.1358 ± 0.0052	0.1802 ± 0.0093	1.33	0.003
787	Cofilin 1, non-muscle (18 kDa phosphoprotein)	gi|15012201	MS/MS	NA, 57	NA, 16	NA, 2	8.22	18.72	0.2424 ± 0.0722	0.4816 ± 0.0447	1.99	0.023
354	Enolase 1, (alpha)	gi|12804749	MS/MS	NA, 265	NA, 13	NA, 4	7.01	47.48	1.0128 ± 0.0703	1.3150 ± 0.0502	1.30	0.008
684	Heat shock 27 kDa protein 1	gi|50979116	MS/MS	NA, 87	NA, 20	NA, 3	6.23	22.93	0.0303 ± 0.0187	0.0878 ± 0.0085	2.90	0.023
	Down-regulated proteins											
257	ERO-1like protein alpha precursor (ERO-1lalpha) (Oxidoreductin 1-lalpha)	gi|73963815	MS	108, NA	36, NA	11, NA	5.97	55.18	0.0610 ± 0.0046	0.0336 ± 0.0061	0.55	0.007
305	Glutamate dehydrogenase 1	gi|6980956	MS/MS	NA, 85	NA, 5	NA, 2	8.05	61.72	0.4839 ± 0.0394	0.3107 ± 0.0392	0.64	0.014
236	Lamin A/C	gi|13111979	MS	106, NA	31, NA	13, NA	6.40	65.15	0.1422 ± 0.0235	0.0810 ± 0.0073	0.57	0.038
379	Ornithine aminotransferase, mitochondrial precursor	gi|73998802	MS/MS	NA, 155	NA, 13	NA, 4	6.44	48.75	0.0874 ± 0.0043	0.0656 ± 0.0078	0.75	0.039
1066	Paraspeckle protein 1	gi|20071204	MS/MS	NA, 34	NA, 2	NA, 1	6.26	58.54	0.1041 ± 0.0144	0.0602 ± 0.0082	0.58	0.029
728	Stromal cell-derived factor 2-like protein 1 precursor (SDF2 like protein 1) (PWP1-interacting protein 8)	gi|73996025	MS/MS	NA, 71	NA, 19	NA, 3	10.04	36.73	0.0906 ± 0.0117	0.0330 ± 0.0156	0.36	0.018
393	Thyroid receptor interactor	gi|695370	MS/MS	NA, 83	NA, 8	NA, 2	7.70	45.78	0.0978 ± 0.0063	0.0634 ± 0.0089	0.65	0.013
353	Ubiquinol-cytochrome c reductase core protein I isoform 2	gi|73985642	MS	102, NA	38, NA	11, NA	6.04	53.54	0.1498 ± 0.0124	0.0730 ± 0.0110	0.49	0.002
	Newly expressed proteins											
299	cAMP-dependent protein kinase type II-alpha regulatory subunit	gi|125197	MS/MS	NA, 60	NA, 3	NA, 1	4.80	45.28	0.0000 ± 0.0000	0.0216 ± 0.0015	Divided by 0	<0.001

%Cov = %sequence coverage = [(number of the matched residues/total number of residues in the entire sequence) × 100%].
NA = not applicable.

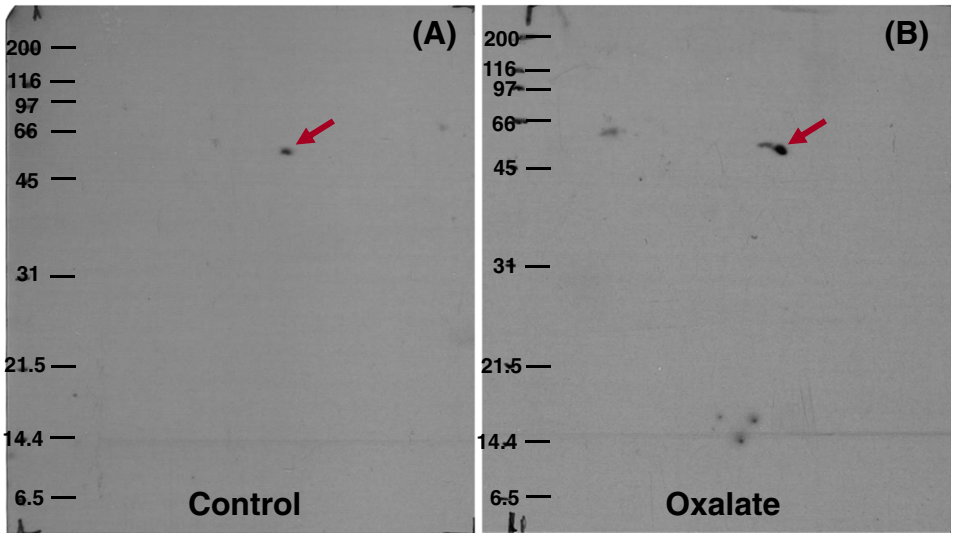


Fig. 2 – Confirmation of the proteome data by 2-D Western blot analysis. Proteins (with an equal amount of 100 μg) derived from whole cell lysate of the controlled (A) and oxalate-treated (B) MDCK cells were resolved by 2-D PAGE and subjected to 2-D Western blot analysis. Primary antibody was rabbit polyclonal anti-enolase antibody (Santa Cruz Biotechnology) (1:1000 in 1% skim milk/PBS), whereas secondary antibody was goat anti-rabbit IgG conjugated with horseradish peroxidase (HRP) (DAKO) (1:2000 in 1% skim milk/PBS).

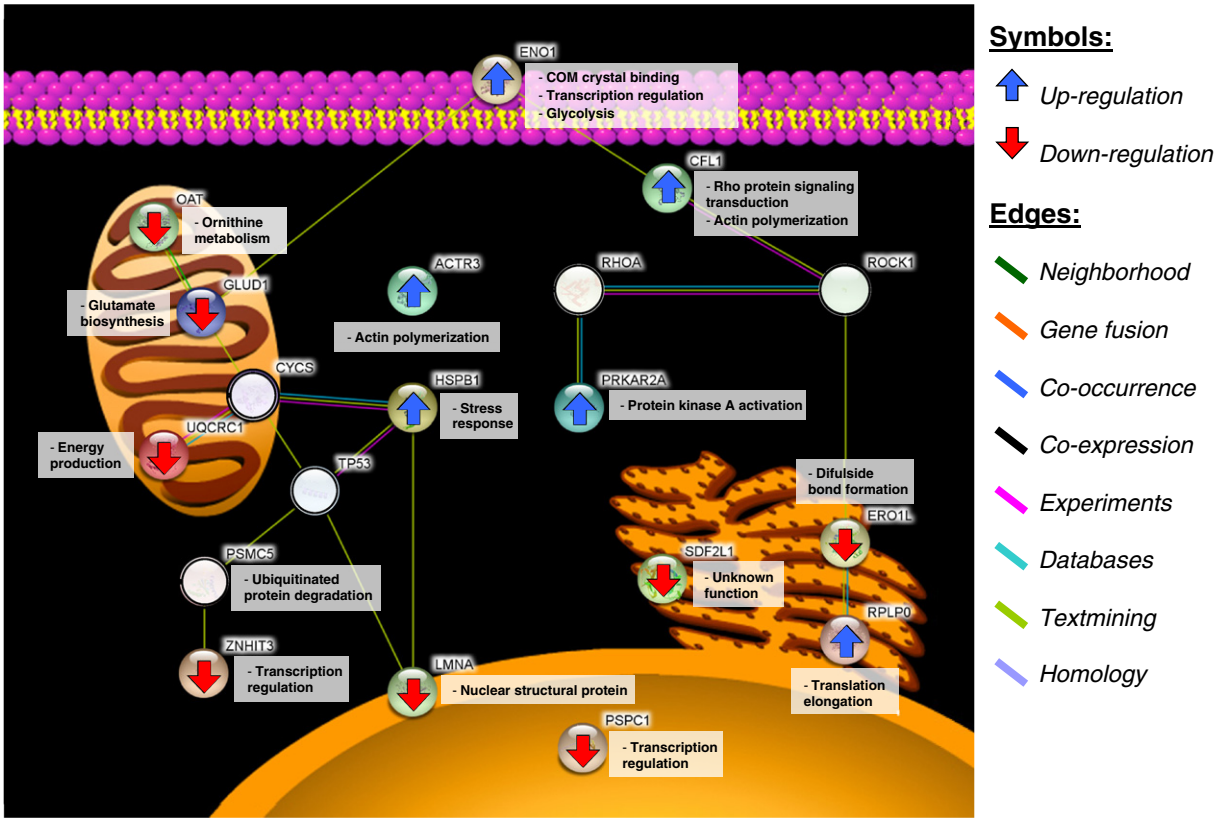


Fig. 3 – Network analysis and subcellular localizations of the significantly altered proteins. Integration of all the significantly altered proteins into the relevant biological meanings was performed by using the STRING software. The network analysis reveals the interactions among proteins, their functions, and subcellular localizations. The "colored nodes" with upward or downward arrows depict the up-regulated or down-regulated proteins, respectively, whereas the "white nodes" without arrows indicate the interacting proteins predicted from literatures and other databases.

Table 2 – Functional classification and subcellular localization of significantly altered proteins in response to high-oxalate exposure and their predicted interacting partners.

Spot no.	Abbreviation	Full protein name	Function(s)	Subcellular localization(s)
Up-regulated proteins				
514	RPLP0	60S acidic ribosomal protein P0 (L10E) isoform 8	Ribosome biogenesis; translational elongation	Cytoplasm; nucleus
348	ACTR3	ARP3 actin-related protein 3 homolog	Actin polymerization	Cytoplasm
787	CFL1	Cofilin 1	Rho protein signaling transduction; actin polymerization	Cytoplasm; nucleus
354	ENO1	Enolase 1	COM crystal binding; transcription regulation; glycolysis	Plasma membrane; cytoplasm; nucleus
684	HSPB1	Heat shock 27 kDa protein 1	Stress response	Cytoplasm; nucleus
299	PRKAR2A	cAMP-dependent protein kinase type II -alpha regulatory subunit	Protein kinase A activation	Cytoplasm
Down-regulated proteins				
257	ERO1L	ERO-1 like protein alpha presursor (ERO-1lalpha)	Disulfide bond formation of proteins	Endoplasmic reticulum
305	GLUD1	Glutamate dehydrogenase 1	Glutamate biosynthesis	Mitochondria
236	LMNA	Lamin A/C	Nuclear structural protein	Nuclear membrane
379	OAT	Ornithine aminotransferase, mitochondrial precursor	Ornithine metabolism	Mitochondria
1066	PSPC1	Paraspeckle protein 1	Transcription regulation	Nucleus
728	SDF2L1	Stromal cell-derived factor 2-like protein 1 precursor	ER stress response	Endoplasmic reticulum
393	ZNHIT3	Thyroid receptor interacting protein 3	Transcription regulation	Cytoplasm
353	UQCRC1	Ubiquinol-cytochrome c reductase core protein I isoform 2	Stress response; Energy metabolism	Mitochondria
Predicted interacting proteins *				
	RHOA	RhoA protein	Rho protein signaling transduction; actin polymerization	Cytoplasm; plasma membrane
	ROCK1	Rho-associated protein kinase 1	Rho protein signaling transduction; actin polymerization	Cytoplasm
	PSPC5	26S protease regulatory subunit 8	Protein degradation by proteasome	Cytoplasm
	CYCS	Cytochrome C	Electron transport chain	Mitochondria
	TP53	Tumor antigen p53	Pro-apoptosis; anti-proliferation	Cytoplasm

* These are the interacting proteins predicted from literatures and other databases using the STRING tool.

transcriptional regulation (PSPC1 and ZNHIT3). The possibilities that these significantly altered proteins played in calcium oxalate kidney stone formation and disease progression are discussed as follows.

Proteins involved in the dynamics of actin cytoskeletal assembly were increased in response to high-oxalate condition. Actin-related protein 3 (ACTR3) is well-characterized as a major component of the ARP2/3 complex lining the cell surface that is essential for maintaining cell shape and motility through actin polymerization. Cofilin1 is necessary for maintaining architecture of podocytes during cell injury [18]. It has been reported that cofilin could interact with ClC-5 and regulates albumin uptake in proximal tubular cells. Phosphorylation of cofilin results in stabilization of actin cytoskeleton and thus inhibits albumin uptake [19]. We hypothesized that the increased levels of ACTR3 and cofilin 1 might be involved in actin remodeling in response to oxalate-induced injury. In contrast, we found the decreased level of a nucleoskeletal protein, lamin A/C, which is the constituent of the nuclear matrix. Hypertonicity could induce expression of lamin A/C and its distribution in the nucleoplasm. Moreover, lamin A/C serves as a scaffold protein by interacting with TonEBP, a transcriptional regulator of gene cassettes contributing in protection against hyperosmolarity [20,21]. We assumed that the decreased level of lamin A/C reflected that the cells might fail to cope with the deteriorate effects induced by high-oxalate.

Type II-alpha regulatory subunit of cAMP-dependent protein kinase (PRKAR2A) was newly expressed under the high-oxalate environment. This protein is involved in signal transduction through protein kinase A (PKA) activation. This regulatory subunit has been shown to regulate protein transport from endosomes to golgi apparatus and endoplasmic reticulum [22]. PRKAR2A also mediates membrane association by binding to a group of PKA anchoring proteins (AKAPs) [23]. Unlike type I PKA, which is highly expressed in proliferating cells, type II PKA is preferentially expressed in the cells that underwent growth arrest [24]. Activation of PKA contributes to oxidative stress found in diabetic rat kidney [25]. Moreover, up-regulation of PRKAR1A has been found in nodular hyperplasia of parathyroid glands in patients with chronic renal failure [26]. Therefore, it is likely that the increase in regulatory subunit of the PKA found in our present study might reflect growth retardation of the cells and oxidative stress induced by PKA activation under the high-oxalate condition.

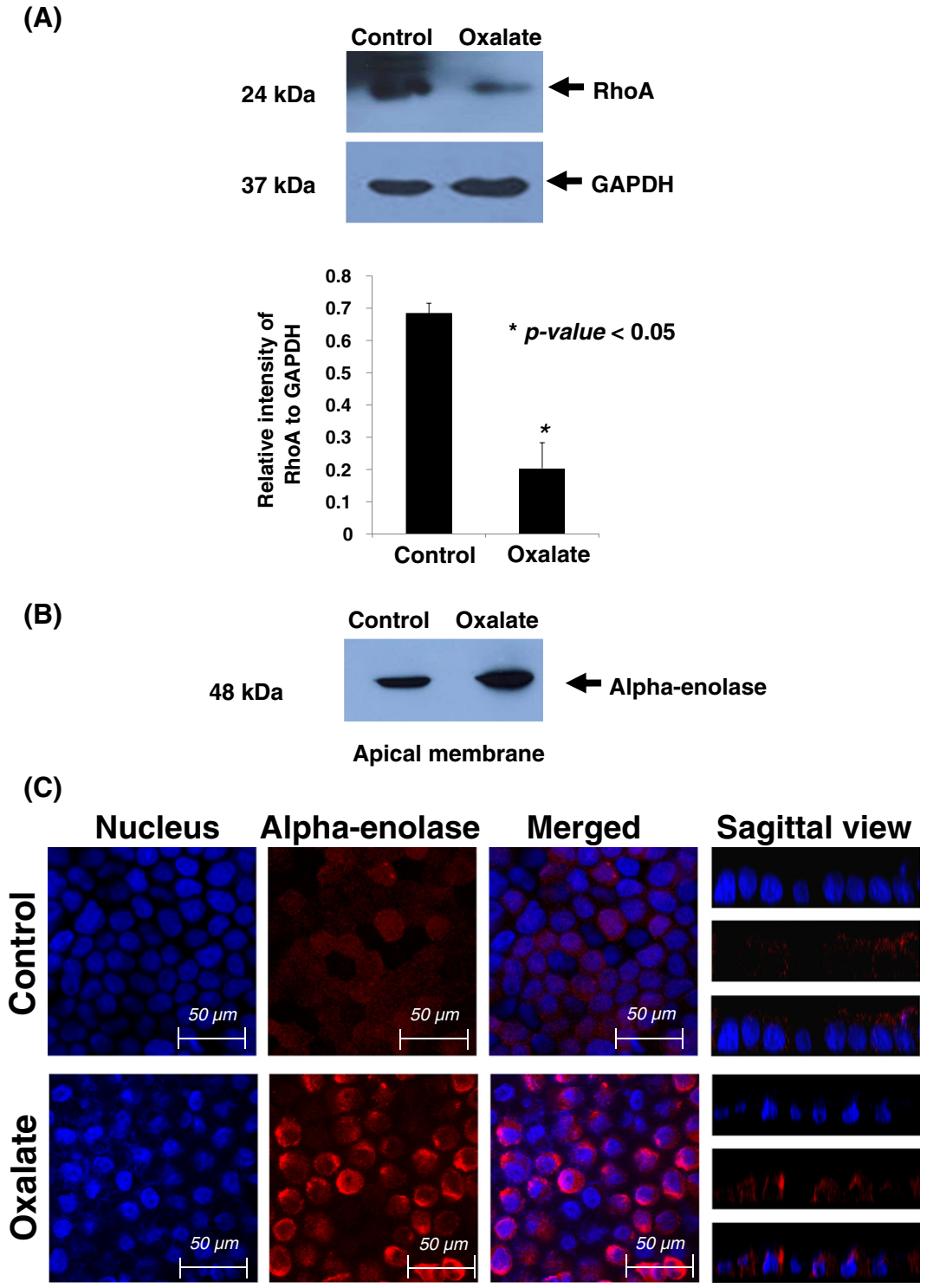


Fig. 4 – Confirmation of the data predicted from network analysis and subcellular localizations using the STRING tool. The decreased level of cytosolic RhoA in oxalate-treated cells was confirmed in whole cell lysate by 1-D Western blot analysis, in which GAPDH served as a loading control (A). 1-D Western blotting was also employed to confirm the increased level of alpha-enolase apical membrane fraction of oxalate-treated cells (B). The latter was also confirmed by immunofluorescence study (C). The fluorescence images were captured under a laser-scanning confocal microscope with 6300× original magnification power (Carl Zeiss; Jena, Germany).

Adaptive response to protect cells during chronic hyperoxaluria by up-regulation of HSP70 has been reported previously [2]. In the present study, we found the increased level of a small heat shock protein. HSP27 (also known as HSPB1 or HSP25) is a small protein with chaperone activity involving in a variety of cellular functions, including thermoresistance,

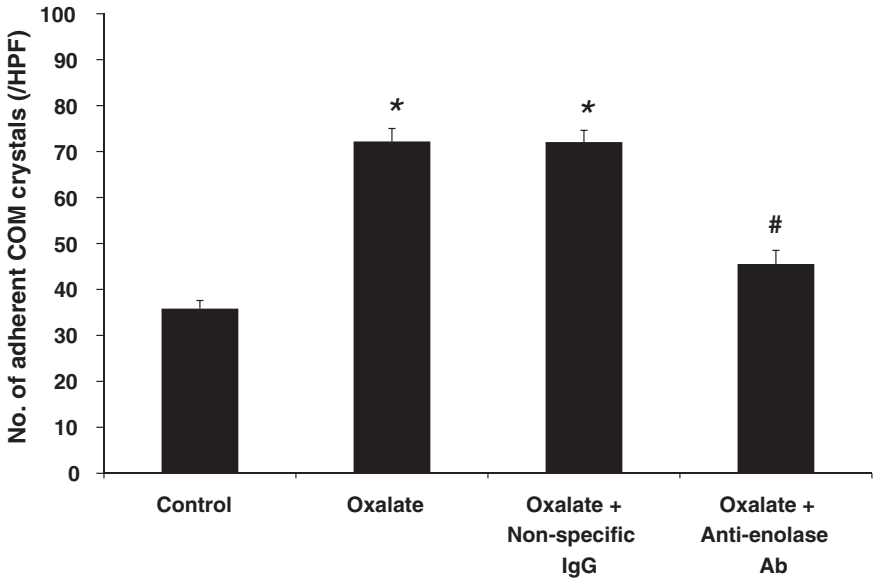


Fig. 5 – COM crystal adhesion and neutralization assay. After MDCK cells were maintained with or without 10 mM sodium oxalate for 72 h, COM crystals were added into the growth medium (100 μg crystals/ml medium) and further incubated with the cells at 37 °C for 30 min. After removing the unbound crystals, the remaining crystals adhered on the cell surface were counted at 15 randomized high power fields (HPF) under a phase contrast microscope (Olympus CKX41). In parallel, the cells that were pre-incubated with 0.2 μg/ml rabbit polyclonal anti-enolase antibody (Santa Cruz Biotechnology) or non-specific rabbit IgG at 37 °C for 30 min before COM crystal incubation were also evaluated. Each bar was constructed from 3 independent experiments. *=$p<0.05$ vs. control; #=$p<0.05$ vs. oxalate-treated cells (without or with non-specific rabbit IgG pretreatment).

inhibition of apoptosis, cell differentiation and signal transduction [27]. A variety of stresses can result to up-regulation of HSP27. We hypothesized that the increase of HSP27 might reflect cellular adaptive response to protect the cells from high-oxalate-induced cell death. In contrast, we also observed the decreased levels of ERO-1 like protein (ERO1L) and stromal cell-derived factor 2-like protein 1 (SDF2L1). ERO1L is an enzyme responsible for disulfide bond formation of proteins [28], whereas SDF2L1 is a component of the endoplasmic reticulum involved in folding of nascent polypeptides in cooperation with other chaperones and members of protein-disulfide family to correct protein folding [29]. Within the endoplasmic reticulum, ERO1 protein family is required for the catalytic activity of protein disulfide isomerase (PDI) [30]. Therefore, the decreased levels of ERO1L and SDF2L1 might aggravate deteriorate effects in the oxalate-treated cells due to accumulation of the misfolded proteins. Another evidence to confirm the induction of oxidative stress response to high-oxalate was the decrease in expression of ubiquinol cytochrome c reductase (UQCRC1 or Cytochrome bc1 complex), which is a subunit of complex III respiratory chain protein with the role in energy production. The loss of UQCRC1 in epithelial cells exposed to H_2O_2 has been reported to worsen cellular oxidative stress through mitochondrial dysfunction [31]. We thus presumed that the reduced UQCRC1 found in our present study reflected mitochondrial dysfunction upon high-oxalate treatment.

The highlight of findings in the present study was the up-regulation of alpha-enolase (enolase 1; ENO1), one of the key glycolytic enzymes. Interestingly, it has been demonstrated that alpha-enolase plays another important role as a plasminogen receptor on many cell types, including monocytes, epithelial cells, and endothelial cells [31–33]. Because plasminogen/plasmin plays a crucial role in extracellular matrix degradation, the up-regulation of alpha-enolase (as a plasminogen receptor) on the cell surface might aggravate crystal invasion under the high-oxalate environment. Network analysis and subcellular localization using the STRING tool revealed that the increased level of alpha-enolase was localized at apical membranes (Fig. 3). Its increased expression at apical membranes was nicely confirmed by Western blot analysis of apical membrane fraction and by immunofluorescence study using laser-scanning confocal microscopic examination (Fig. 4B and C). In addition, our previous study also identified alpha-enolase as one of COM crystal-binding proteins on apical membranes of polarized MDCK cells [34]. Therefore, it is plausible that the increased surface expression of alpha-enolase, as a COM crystal-binding protein, was related to the enhancement of COM crystal adhesion onto renal tubular epithelial cells upon high-oxalate exposure. Our hypothesis was nicely confirmed by a functional assay, which demonstrated that high-oxalate significantly induced COM crystal adhesion and neutralization of surface expression of alpha-enolase successfully prevented such enhancement (Fig. 5).

Our findings indicated that alpha-enolase not only plays a role in regulation of cellular energy but also serves as the binding molecule for COM crystals to enhance COM crystal adhesion under the high-oxalate condition. It would be best to also validate our results in a kidney tissue from hyperoxaluric patients. However, the lack of such tissue is a major limitation in our present study. Moreover, the results also suggested that molecular blocking of surface molecules on renal tubular cells involved in crystal binding may be an effective way to prevent

progression of kidney stone formation in patients with hyperoxaluria. Further clinical studies are required to address this novel therapeutic approach.

In summary, we report herein the adaptive response of distal renal tubular cells to high-oxalate environment. The results revealed that such condition induced many deleterious effects to the cells. In order to complement and maintain several biological functions, the cells altered a set of proteins to cope with this situation. We also demonstrated that high-oxalate could induce surface expression of alpha-enolase to enhance COM crystal adhesion on the cell surface. These data enlighten that the increased expression of alpha-enolase on apical membranes is, at least in part, a crucial mechanism beneath kidney stone formation in patients with hyperoxaluria.

Supplementary data to this article can be found online at http://dx.doi.org/10.1016/j.jprot.2013.01.001.

Acknowledgments

We thank Prof. Shui-Tein Chen, Supachok Sinchaikul and Somchai Chutipongtanate for their technical assistance. This study was supported by the Thailand Research Fund (TRF) (RTA5380005 and TRG5480005), Office of the Higher Education Commission and Mahidol University under the National Research Universities Initiative, and Faculty of Medicine Siriraj Hospital. K.F. was supported by Royal Golden Jubilee Ph.D. Program scholarship, whereas V.T. is also supported by "Chalermphrakiat" Grant, Faculty of Medicine Siriraj Hospital.

REFERENCES

[1] Marengo SR, Romani AM. Oxalate in renal stone disease: the terminal metabolite that just won't go away. Nat Clin Pract Nephrol 2008;4:368–77.
[2] Greene EL, Farell G, Yu S, Matthews T, Kumar V, Lieske JC. Renal cell adaptation to oxalate. Urol Res 2005;33:340–8.
[3] Evan AP. Physiopathology and etiology of stone formation in the kidney and the urinary tract. Pediatr Nephrol 2010;25:831–41.
[4] Khan SR. Renal tubular damage/dysfunction: key to the formation of kidney stones. Urol Res 2006;34:86–91.
[5] Jonassen JA, Cao LC, Honeyman T, Scheid CR. Intracellular events in the initiation of calcium oxalate stones. Nephron Exp Nephrol 2004;98:e61–4.
[6] Thamilselvan S, Khan SR, Menon M. Oxalate and calcium oxalate mediated free radical toxicity in renal epithelial cells: effect of antioxidants. Urol Res 2003;31:3–9.
[7] Veena CK, Josephine A, Preetha SP, Rajesh NG, Varalakshmi P. Mitochondrial dysfunction in an animal model of hyperoxaluria: a prophylactic approach with fucoidan. Eur J Pharmacol 2008;579:330–6.
[8] Thamilselvan V, Menon M, Thamilselvan S. Oxalate-induced activation of PKC-alpha and -delta regulates NADPH oxidase-mediated oxidative injury in renal tubular epithelial cells. Am J Physiol Renal Physiol 2009;297:F1399–410.
[9] Mazzali M, Kipari T, Ophascharoensuk V, Wesson JA, Johnson R, Hughes J. Osteopontin—a molecule for all seasons. QJM 2002;95:3–13.
[10] Bergsland KJ, Zisman AL, Asplin JR, Worcester EM, Coe FL. Evidence for net renal tubule oxalate secretion in patients with calcium kidney stones. Am J Physiol Renal Physiol 2011;300:F311–8.
[11] Schepers MS, van Ballegooijen ES, Bangma CH, Verkoelen CF. Oxalate is toxic to renal tubular cells only at supraphysiologic concentrations. Kidney Int 2005;68:1660–9.
[12] Jensen LJ, Kuhn M, Stark M, Chaffron S, Creevey C, Muller J, et al. STRING 8—a global view on proteins and their functional interactions in 630 organisms. Nucleic Acids Res 2009;37:D412–6.
[13] Fong-ngern K, Chiangjong W, Thongboonkerd V. Peeling as a novel, simple, and effective method for isolation of apical membrane from intact polarized epithelial cells. Anal Biochem 2009;395:25–32.
[14] Thongboonkerd V, Semangoen T, Chutipongtanate S. Factors determining types and morphologies of calcium oxalate crystals: molar concentrations, buffering, pH, stirring and temperature. Clin Chim Acta 2006;367:120–31.
[15] Thongboonkerd V, Chutipongtanate S, Semangoen T, Malasit P. Urinary trefoil factor 1 is a novel potent inhibitor of calcium oxalate crystal growth and aggregation. J Urol 2008;179:1615–9.
[16] Smith LH. Diet and hyperoxaluria in the syndrome of idiopathic calcium oxalate urolithiasis. Am J Kidney Dis 1991;17:370–5.
[17] Khan SR. Pathogenesis of oxalate urolithiasis: lessons from experimental studies with rats. Am J Kidney Dis 1991;17:398–401.
[18] Garg P, Verma R, Cook L, Soofi A, Venkatareddy M, George B, et al. Actin-depolymerizing factor cofilin-1 is necessary in maintaining mature podocyte architecture. J Biol Chem 2010;285:22676–88.
[19] Hryciw DH, Wang Y, Devuyst O, Pollock CA, Poronnik P, Guggino WB. Cofilin interacts with ClC-5 and regulates albumin uptake in proximal tubule cell lines. J Biol Chem 2003;278:40169–76.
[20] Jeon US, Kim JA, Sheen MR, Kwon HM. How tonicity regulates genes: story of TonEBP transcriptional activator. Acta Physiol (Oxf) 2006;187:241–7.
[21] Favale NO, Sterin Speziale NB, Fernandez Tome MC. Hypertonic-induced lamin A/C synthesis and distribution to nucleoplasmic speckles is mediated by TonEBP/NFAT5 transcriptional activator. Biochem Biophys Res Commun 2007;364:443–9.
[22] Wojtal KA, Hoekstra D, van Ijzendoorn SC. Anchoring of protein kinase A-regulatory subunit IIalpha to subapically positioned centrosomes mediates apical bile canalicular lumen development in response to oncostatin M but not cAMP. Mol Biol Cell 2007;18:2745–54.
[23] Foss KB, Solberg R, Simard J, Myklebust F, Hansson V, Jahnsen T, et al. Molecular cloning, upstream sequence and promoter studies of the human gene for the regulatory subunit RII alpha of cAMP-dependent protein kinase. Biochim Biophys Acta 1997;1350:98–108.
[24] Cho-Chung YS. Antisense protein kinase A RI alpha-induced tumor reversion: portrait of a microarray. Biochim Biophys Acta 2004;1697:71–9.
[25] Xu Y, Osborne BW, Stanton RC. Diabetes causes inhibition of glucose-6-phosphate dehydrogenase via activation of PKA, which contributes to oxidative stress in rat kidney cortex. Am J Physiol Renal Physiol 2005;289:F1040–7.
[26] Hibi Y, Kambe F, Tominaga Y, Mizuno Y, Kobayashi H, Iwase K, et al. Up-regulation of the gene encoding protein kinase A type I alpha regulatory subunit in nodular hyperplasia of parathyroid glands in patients with chronic renal failure. J Clin Endocrinol Metab 2006;91:563–8.
[27] de Graauw M, Tijdens I, Cramer R, Corless S, Timms JF, van de WB. Heat shock protein 27 is the major differentially phosphorylated protein involved in renal epithelial cellular

stress response and controls focal adhesion organization and apoptosis. J Biol Chem 2005;280:29885–98.
[28] Sevier CS, Kaiser CA. Ero1 and redox homeostasis in the endoplasmic reticulum. Biochim Biophys Acta 2008;1783: 549–56.
[29] Tongaonkar P, Selsted ME. SDF2L1, a component of the endoplasmic reticulum chaperone complex, differentially interacts with {alpha}-, {beta}-, and {theta}-defensin propeptides. J Biol Chem 2009;284:5602–9.
[30] Shibanuma M, Inoue A, Ushida K, Uchida T, Ishikawa F, Mori K, et al. Importance of mitochondrial dysfunction in oxidative stress response: a comparative study of gene expression profiles. Free Radic Res 2011;45:672–80.
[31] Plow EF, Das R. Enolase-1 as a plasminogen receptor. Blood 2009;113:5371–2.
[32] Seweryn E, Pietkiewicz J, Bednarz-Misa IS, Ceremuga I, Saczko J, Kulbacka J, et al. Localization of enolase in the subfractions of a breast cancer cell line. Z Naturforsch C 2009;64:754–8.
[33] Pancholi V. Multifunctional alpha-enolase: its role in diseases. Cell Mol Life Sci 2001;58:902–20.
[34] Fong-ngern K, Peerapen P, Sinchaikul S, Chen ST, Thongboonkerd V. Large-scale identification of calcium oxalate monohydrate crystal-binding proteins on apical membrane of distal renal tubular epithelial cells. J Proteome Res 2011;10:4463–77.

MONOCLONAL ANTIBODIES IN IMMUNODIAGNOSIS AND IMMUNOTHERAPY
Volume 32, Number 3, 2013
© Mary Ann Liebert, Inc.
DOI: 10.1089/mab.2012.0079

Characterization of Monoclonal Antibodies Against a Human Chondrocyte Surface Antigen

Theerawut Chanmee,[1] Peraphan Phothacharoen,[1] Visith Thongboonkerd,[2] Watchara Kasinrerk,[3] and Prachya Kongtawelert[1]

Chondrocytes express a number of cell-surface molecules that mediate cell-cell or cell-matrix interactions. Identification and full characterization of new chondrocyte surface molecules will lead to a better understanding of the function of the chondrocyte. Researchers used primary human chondrocytes as an immunogen, and various monoclonal antibodies (MAbs) were generated using standard hybridoma technology. A monoclonal antibody named 5D2 was selected for further characterization. The antigen recognized by 5D2 MAb is expressed by primary human chondrocytes, primary synovial fibroblasts, synovial fibroblast cell lines (SW982), primary skin fibroblasts, and osteoblasts, but not expressed in blood cells. Biochemical analysis revealed that the 5D2 antigen is a protein with a molecular weight of approximately 25–35 kDa. Protein identification by mass spectrometry and molecular cloning revealed that 5D2 antigen is identical to the Thy-1 molecule. Furthermore we confirmed this specificity of the antibody by the isolated and cloned Thy-1 gene to the COS-7 and probed it with the 5D2 antibody using Western blot analysis. We examined the role of the Thy-1 molecule in arthritis models and tissue; one was papain-induced rat arthritis, the other was immunohistological staining of osteoarthritic (OA) human articular cartilage. OA cartilage showed a higher expression of Thy-1 as compared with normal tissue in all experimental approaches. The *in vitro* studies showed that the inflammatory cytokine interleukin-1β up-regulated Thy-1 molecule expression in the cartilage tissue. It can be concluded that the Thy-1 might be a potential biomarker for cartilage pathogenesis, degradation, and metabolic turnover.

Introduction

The chondrocyte is the only cell type found in articular cartilage, which synthesizes and secretes extracellular matrix (ECM) molecules such as collagens, polysaccharides, and proteoglycans to ECM.[1] The major degenerative pathology associated with joint and cartilage, which affects the chondrocyte, is arthritis. Arthritis can be subdivided into two major classes: rheumatoid arthritis (RA) and osteoarthritis (OA).

Osteoarthritis (OA) is a group of chronic, painful, disabling conditions affecting articular joints, which occurs from various risk factors such as aging, obesity, and trauma.[2–4] The initial stage of inflammation plays a major role in cartilage degradation leading to osteoarthritis, especially the released interleukin-1β (IL-1β) and tumor necrosis factor alpha (TNF-α).[5] These cytokines act in an autocrine manner, stimulating their own production and inducing chondrocytes to produce proteases, chemokines, nitric oxide, and eicosanoids to drive catabolic pathways, inhibit matrix synthesis, and promote cellular apoptosis.[2]

Chondrocytes regulate the balance between anabolism and catabolism of the extracellular matrix. An alteration in the protein expression pattern of these cells can influence the normal matrix homeostasis. The identification of differentially expressed proteins can help us identify new markers in OA progression and better understand the underlying disease processes.

We have produced monoclonal antibodies (MAb) against chondrocyte surface molecules for use as a research tool and biomarker for cartilage degradation. One of these is considering the practical applications of MAb 5D2. This paper reports (1) the biochemical characterization and cloning of the chondrocyte surface molecule that is recognized by this antibody and (2) its expression level in normal and OA cartilage.

Materials and Methods

Cell culture

Human articular cartilage was obtained (with full informed patient consent) from the arthroscopic diagnosis of a flat pad syndrome patient at Maharaj Nakorn Chiang Mai Hospital (Department of Orthopedics, Faculty of Medicine, Chiang Mai University, Thailand [approval code 070CT111016]). Chondrocytes were isolated by overnight trypsin digestion at

[1]Thailand Excellence Center for Tissue Engineering and Stem Cells, Department of Biochemistry, Faculty of Medicine; [3]Department of Clinical Immunology, Faculty of Associate Medical Science, Chiang Mai University, Chiang Mai, Thailand.
[2]Medical Proteomics Unit, Office for Research and Development, Faculty of Medicine, Siriraj Hospital, Mahidol University, Bangkoknoi, Bangkok, Thailand.

4°C and a subsequent 3 h digestion with collagenase (type IA, Sigma-Aldrich, St. Louis, MO) at 37°C. The cells were washed with PBS and then cultured in DMEM containing 10% FCS as high-density primary monolayer cultures until confluence. Cells were passaged after becoming confluent using 0.05% trypsin/0.02% EDTA.

Generation of monoclonal antibodies against chondrocyte surface antigen

The BALB/c mouse was immunized intraperitoneally three times at 2-week intervals with primary human chondrocyte (1×10^7 cells). Spleen cells were isolated and fused with mouse myeloma P3-X63Ag8.653 cells by standard hybridoma fusion techniques using 50% polyethylene glycol and HAT medium selection. The immunoglobulin isotype of the MAb was determined using an isotyping ELISA kit (Sigma-Aldrich).

Flow cytometric analysis

Human chondrocytes, human synovial fibroblasts, human skin fibroblasts, lymphocytes, monocytes, chondrosarcoma cell lines, SW-982, Daudi, U937, K562, hFOB 1.19, and HepG2 cells were pre-incubated at 4°C for 30 min with 10% human AB serum. Thereafter 5×10^5 cells were stained with 5D2 culture supernatant at 4°C for 30 min. After washing twice with 1%BSA-PBS, the binding of antibody was detected by using FITC-conjugated anti-mouse immunoglobulin antibodies. Cells were incubated with conjugate at 4°C for 30 min. Then, cells were washed three times with 1% BSA-PBS and analyzed by flow cytometer.

Labeling of cells and immunoprecipitation

The primary human chondrocytes were washed with PBS. The cells ($1–5\times10^7$ cells/mL) were incubated with 5 mM sulfo-NHS-LC-Biotin at 4°C for 1 h. The biotinylation was quenched by washing once with 1 mM glycine in PBS first and twice with PBS. Then, labeled cells (1×10^7) were solubilized in 1 mL lysis buffer (5 mM iodoacetamide, protease inhibitor, 1% NP-40, Tris HCl [pH 8.2]) at 4°C for 30 min. The lysate was collected by centrifugation at 10,000 *g*, at 4°C for 20 min. The lysate was mixed with the 5D2 MAb coated CNBr Sepharose beads at 4°C overnight. After immunoprecipitation and SDS–PAGE, biotinylated proteins were transferred to nitrocellulose membrane. The membrane was treated with 5% skim milk in TBS containing 0.05% Tween-20 (TBST) followed by incubation with 5D2 MAb in TBST and subsequent incubation with horseradish peroxidase-conjugated secondary antibody (1:2000 dilution; Amersham Biosciences, Piscataway, NJ) in TBST. The protein was visualized using the enhanced chemiluminescence plus detection system.

Purification and sequencing of 5D2 antigen

Primary human chondrocyte cell lysate was incubated with cyanogen bromide-activated Sepharose coupled with MAb 5D2 overnight at 4°C. After extensive washing with PBS, the bound proteins were eluted with 1x sample buffer (10% glycerol, 1% SDS, 0.1% bromphenol blue, and 0.0625 M Tris-HCl [pH 6.8]). The eluted fractions containing the corresponding MAb 5D2 antigen (determined by immunoblotting) were pooled and separated by SDS-PAGE. The visualized protein bands were excised, washed twice with 200 μL of 50% acetonitrile (ACN)/25 mM NH_4HCO_3 buffer (pH 8.0) at room temperature (RT) for 15 min, and then washed once with 200 μL of 100% ACN. After washing, the samples were extracted and digested with trypsin. Trypsin fragmentation products were analyzed by the Q-TOF Ultima™ mass spectrometer (Micromass, Manchester, United Kingdom). Peptide sequences were compared using the MASCOT search tool.

Molecular cloning of 5D2 molecule

The total mRNA was isolated from the primary human chondrocyte. Thy-1 cDNA was generated by reverse transcription from the isolated mRNA, and the amount of cDNA was increased by RT-PCR. Thy-1 cDNA was cloned into pcDNA3.1 plasmid by using BamH1 and EcoR1 adaptors. The cDNA encoding Thy-1 was transfected to COS-7 cells by using a transfection reagent. $1–3\times10^5$ cells were plated in 35 mm dish, and then added with 1 μg of DNA to GeneJuice reagent/serum-free medium mixture by adding the entire volume of mixture drop-wise to cells in the complete growth medium. The transfection mixture was removed after 2–8 h of incubation and replaced with complete growth medium. After 48 h of cultivation, cells were harvested and the expression of the Thy-1 molecule was detected by indirect immunofluorescence and analyzed by a flow cytometer.

Papain-induced arthritis

Three Wistar rats were injected with a 4% (w/v) papain saline solution into the right knee of each rat on days 1, 4, and 7 of the experimental period. Seven days after the last injection of papain, the animals were sacrificed. The cartilage samples were removed from the tibial plateau in the right knee. The samples were fixed in 4% paraformaldehyde overnight and embedded, then cut into 10 μm thick segments. Some sections were stained with hematoxylin and eosin (H&E) and Safranin O. Animal usage conformed with international and national guidelines for ethical conduct on the care and use of animals.

Immunohistochemical analysis

The expression of Thy-1 was studied during papain-induced OA. The papain model is characterized by a proteoglycan depletion of the articular cartilage. After being deparaffinized, the sections were incubated for 15 min with Chondroitinase ABC and then incubated for 10 min in 3% H_2O_2. After blocking with 3% bovine serum albumin in phosphate-buffered saline (PBS), sections were incubated overnight with the monoclonal antibody. Each slide was stained with sheep anti-mouse IgM (μ chain specific) peroxidase conjugated for 1 h. The color was developed using diaminobenzidine substrate.

Interleukin-1β induced human articular chondrocyte culture

To determine the expression of Thy-1 protein in cultured human chondrocytes, a Western blot analysis was performed. After the cells had grown to 80% confluence, cells were serum starved for 24 h before stimulation with the inflammatory cytokine interleukin-1β (IL-1β, 10 ng/mL). Cells were collected at 0, 24, 48, 72, and 96 h after treatment. The cell lysate was analyzed on 12% SDS-PAGE and transferred to a

Table 1. Flow Cytometry Surface Expression of 5D2 Antigen on Various Cell Types Obtained by Flow Cytometry

Primary cell	
Chondrocyte	+
Synovial fibroblast	+
Skin fibroblast	+
Lymphocyte	−
Monocyte	−
Cell lines	
Chondrosarcoma (SW1353)	−
SW 982	+
Daudi	−
U937	−
K562	−
hFOB 1.19	+
HepG2	−

+, Markers staining positive in more than 98% of cells; −, markers expressed in less than 2% of cells.

nitrocellulose membrane. The membrane was treated with 5% skim milk in TBST containing 0.05% TBST, followed by incubation with the 5D2 MAb in TBST and subsequent incubation with horseradish peroxidase-conjugated secondary antibody (dilution, 1:2000; Amersham Biosciences) in TBST. The expression of Thy-1 protein was visualized using the enhanced chemiluminescence plus detection system.

Results

Cellular distribution of 5D2 antigen

We characterized the molecule recognized by 5D2 MAb on various cell types, including human chondrocytes, human synovial fibroblasts, human skin fibroblasts, lymphocytes, monocytes, chondrosarcoma cell lines, SW-982, Daudi, U937, K562, hFOB 1.19, and HepG2 (Table 1) by the indirect immunofluorescence method. All peripheral blood mononuclear cells and hematopoietic cell lines, including lymphocytes, monocytes, Daudi, U937, and K562, were negative stained with 5D2 MAb. The analysis of cells, which were found in bones and joints including primary human chondrocytes, primary synovial fibroblasts, synovial fibroblast cell lines (SW982), and osteoblast cell lines (hFOB1.19), was strongly positive stained with 5D2 MAb. Its expression was also found in primary skin fibroblasts. On the other hand, neither chondrosarcoma cell lines (SW1353) nor HepG2 cells were recognized. These results indicated that 5D2 antigen is expressed in the cells associated with bones and joints, including human chondrocytes, synovial fibroblasts, and osteoblast cells.

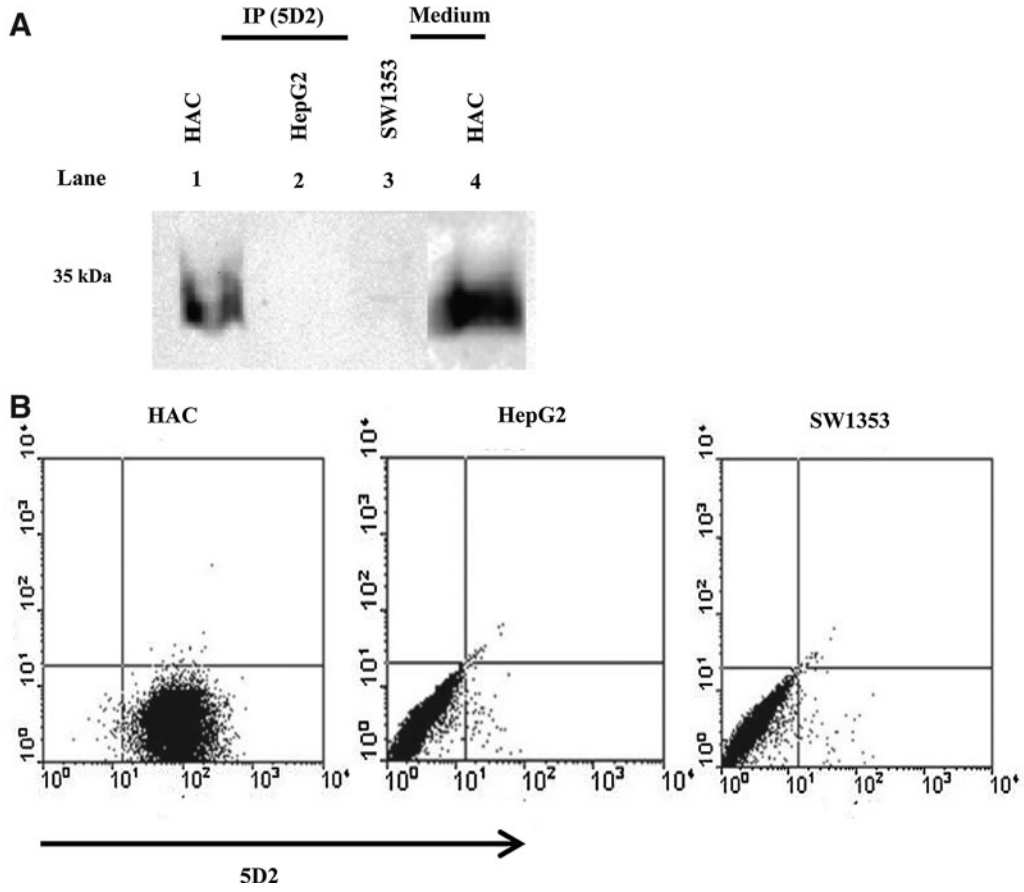


FIG. 1. Biochemical characterization of cell surface molecule recognized by 5D2 MAb. Western blot analysis of immunoprecipitates obtained with either 5D2 MAb from lysates of surface biotin-labeled HAC (lane 1), HepG2 (lane 2), and SW1353 (lane 3). (**A**) The culture media of HAC was subjected to Western blot analysis using 5D2 MAb (lane 4). (**B**) Flow cytometric analysis of 5D2 molecule expression on HAC, HepG2, and SW1353.

TABLE 2. MASS SPECTROMETRIC IDENTIFICATION OF 5D2 MOLECULE

Band no.	Protein name	NCBI ID	Accession no.	Identified by	Identification scores (MS, MS/MS)	%Cov (MS, MS/MS)	No. of matched peptides (MS, MS/MS)	pI	MW (kDa)
c1	Thy-1 (cell surface antigen) [Homo sapiens]	gi|339683	AAA61180	MS, MS/MS	55, 49	31, 18	4, 2	8.96	18.17
c2	Thy-1 (cell surface antigen) [Homo sapiens]	gi|339683	AAA61180	MS/MS	NA, 71	NA, 18	NA, 2	8.96	18.17
c3	Thy-1 (cell surface antigen) [Homo sapiens]	gi|339683	AAA61180	MS, MS/MS	63, 134	31, 18	4, 3	8.96	18.17
c4	Thy-1 (cell surface antigen) [Homo sapiens]	gi|339683	AAA61180	MS/MS	NA, 34	NA, 8	NA, 1	8.96	18.17

NCBI, National Center for Biotechnology Information; %Cov, % sequence coverage [(no. of matched residues/total no. of residues in entire sequence)×100%]; NA, not applicable.
Thy-1 = 100% identities with 5E10 antigen [Homo sapiens] gi|13195770 (AAB26353).
Thy-1 = 80% identities with CD90 protein [Sus scrofa] gi|224697007 (CAM58077).
Thy-1 = 69% identities with CD90.1 [Mus musculus] gi|38325830 (AAR17087).

FIG. 2. Molecular cloning of Thy-1 molecule in COS-7 cell. Expression construct for Thy-1 or mock expression vector (pcDNA3.1) was used to transfect COS-7 cells. After 48 h of transfection, cells were harvested. Western blotting utilized primary antibody to Thy-1 followed by HRP-conjugated secondary antibody and enhanced chemiluminescense for visualization of Thy-1 molecule.

Biochemical characterization of surface molecule recognized by 5D2 MAb

Biochemical studies were performed to characterize the molecule that is recognized by 5D2 MAb using an immunoprecipitation technique. As shown in Figure 1, researchers were able to precipitate a 35 kDa protein from the lysates of surface-biotinylated primary human chondrocytes using 5D2 MAb coupled with cyanogen bromide-activated Sepharose, whereas the antibody did not bind to any protein in cell lysates of HepG2 and SW1353 cell lines (Fig. 1A). These results were confirmed by flow cytometric analysis (Fig. 1B). Furthermore, it was found that the 5D2 molecule can be detected in the culture medium of primary human chondrocytes (Fig. 1A, lane 4).

Mass spectrometric identification of 5D2 molecule

The analysis of 5D2 molecule by mass spectrometry revealed that the 5D2 molecule was significantly matched with Thy-1. Sequence homology search in the NCBI protein database revealed that Thy-1 is 100% identical to the 5D2 antigen [Homo sapiens] (gi|13195770) (AAB26353); 80% identical with the CD90 protein [Sus scrofa] (gi|224697007) (CAM58077); and 69% identical with the CD90.1 [Mus musculus] (gi|38325830) (AAR17087) (Table 2).

To confirm the identification of 5D2 molecule in which the structure has been revealed by mass spectrometry, the cDNA of Thy-1 was inserted via EcoRI and BamHI into the

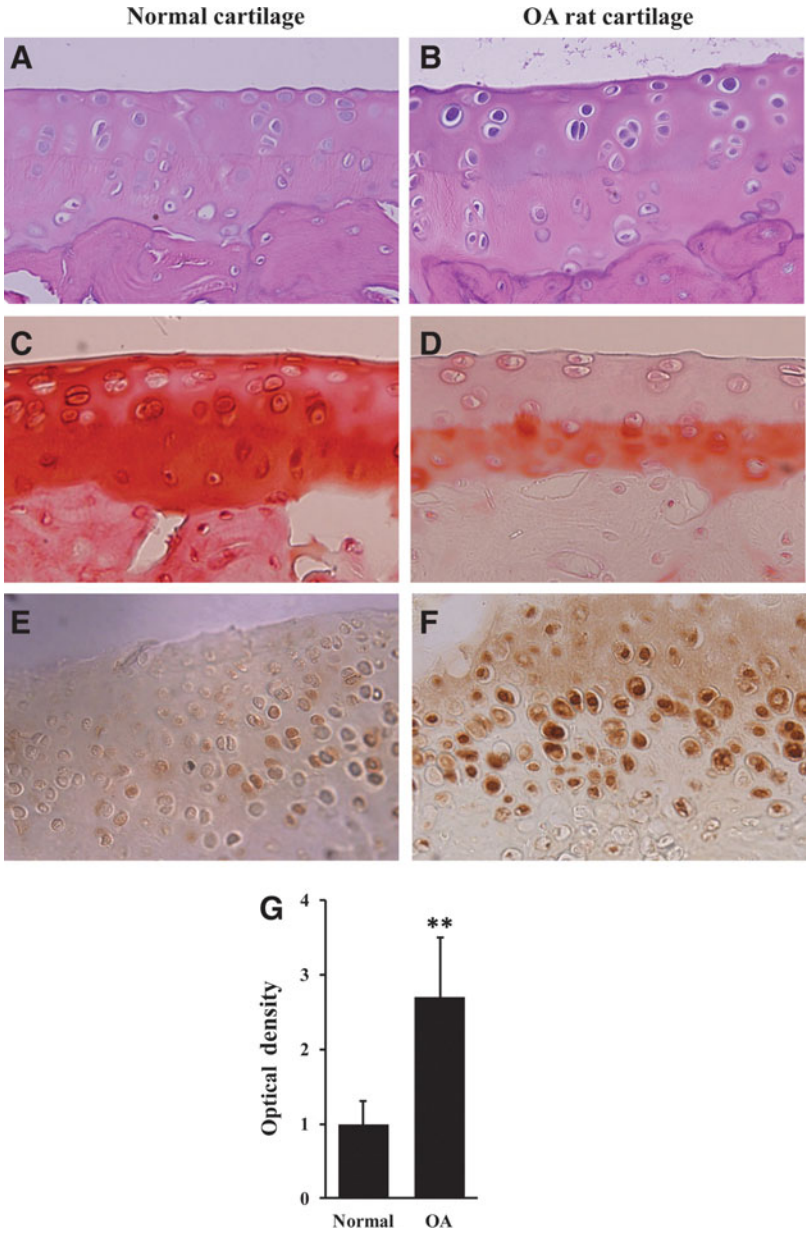


FIG. 3. Histologic analysis of papain-induced osteoarthritis in the knee joints of Wistar rats. Right knee joints were injected with papain solution. The non-injected left knee joints served as internal controls. Sections of articular cartilage from the knee joints of control or OA rats were stained with H&E to visualize cell morphology (**A**,**B**) and stained with Safranin O to detect proteoglycans (**C**,**D**). Expression of Thy-1 molecule was examined by immunohistochemistry (**E**,**F**). H&E staining in normal knee joint (**A**) and after papain injection (**B**). Safranin O staining in normal knee joint (**C**) and after papain injection (**D**). Thy-1 expression in normal knee joint (**E**) and after papain injection (**F**). Average optical density of reaction products was tested by image analysis (**G**). Statistical significance, $^{**}p < 0.01$.

pcDNA3.1 vector and transfected into the COS7 cells, which were subsequently tested for binding of the 5D2 MAb. The transfected COS7 cells expressed Thy-1 molecule, which was observed by Western blot analysis (Fig. 2), demonstrating that the 5D2 antigen is indeed a determinant of the Thy-1 molecule.

Expression of Thy-1 in osteoarthritis

The Thy-1 expression was investigated in the rat model of experimental arthritis using papain-induced arthritis by immunohistological staining. It was found that cartilage in the control rat had a normal chondrocyte structure, showing an intact surface and typical staining of the matrix with Safranin O (Fig. 3A,C). This contrasts with the OA group, which showed marked morphologic changes and the loss of matrix components (Fig. 3B,D). A further investigation of the Thy-1 expression in normal and OA rat cartilage by immunohistochemistry used MAb 5D2, and it was found that the expression of Thy-1 was significantly higher in OA than in normal cartilage (Fig. 3E–G).

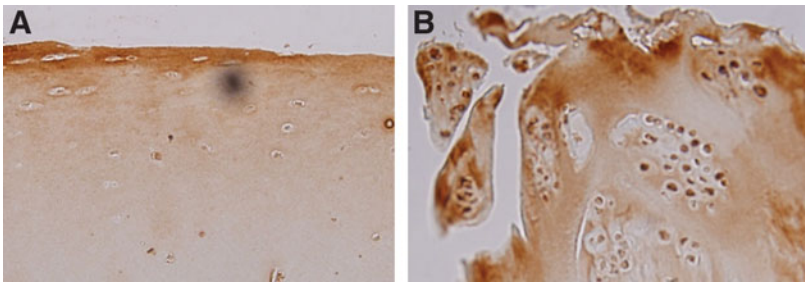


FIG. 4. Thy-1 expression on human normal (**A**) and osteoarthritic cartilage (**B**). Normal and osteoarthritic cartilage sections were stained with 5D2 MAb, which detected the stained antibody by using sheep anti-mouse IgM (μ chain specific) peroxidase conjugated. The color was developed using diaminobenzidine substrate.

Researchers further assessed the expression pattern and determined the precise immunolocalization of Thy-1 in normal and OA human articular cartilage tissue samples. It was found that there was a complete loss of cartilage and chondrocyte aggregation in arthritic lesions in OA samples. In OA tissue samples, clusters of chondrocytes showed strong immunoreactivity with 5D2 antibody compared with normal cartilage (Fig. 4).

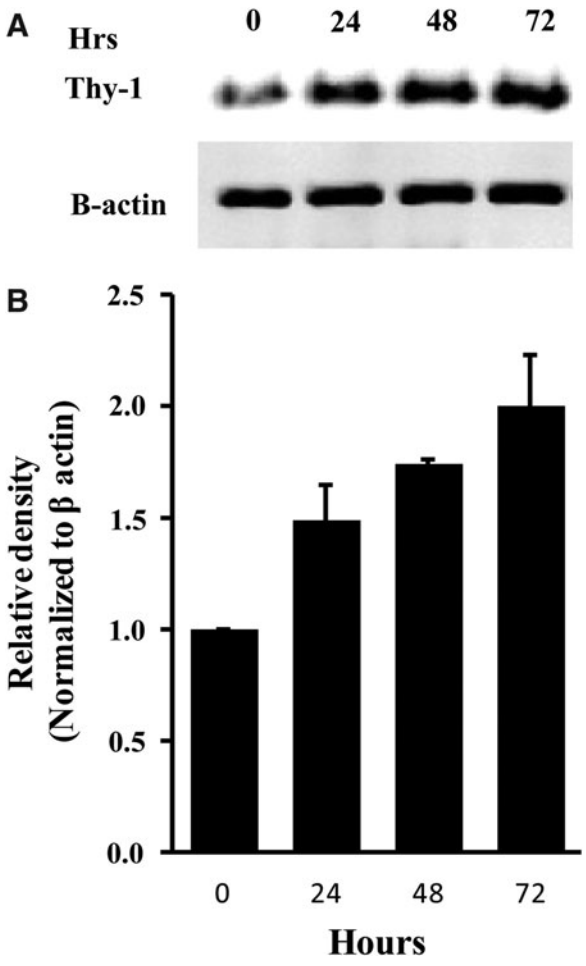


FIG. 5. Expression of Thy-1 protein in cultured human primary chondrocytes. Cells were serum starved for 24 h and incubated with the inflammatory cytokine interleukin-1β (IL-1β, 10 ng/mL). Cells were lysed with sample buffer at 0, 24, 48, and 72 h after treatment. (**A**) Western blot analysis was performed with 5D2 MAb. (**B**) Densitometric analysis of Thy-1 expression.

Because a number of inflammatory cytokines play an important role in osteoarthritis, we then studied the effect of IL-1β on Thy-1 expression in a human articular chondrocyte culture. It was found that there was an increased Thy-1 expression in the cell lysate at 24 h after treatment with the cytokine interleukin-1β (Fig. 5), which was demonstrated by the Western blotting technique.

Discussion

In the present study, monoclonal antibodies were produced against the primary human chondrocyte surface antigen. A MAb named 5D2 was selected for further characterization. It was found that 5D2 antigen was a 25–35 kDa protein that is expressed in many cell types, including chondrocyte, synovial fibroblast, osteoblast, and skin fibroblast. By using a mass spectrometry analysis and cloning system, it was proven that the 5D2 antigen was a determinant on the Thy-1 molecule.

Thy-1 is a 25–37 kDa GPI-anchored cell surface protein that belongs to the immunoglobulin-like supergene family[6] originally described as a marker for thymocyte differentiation in mice.[7] Thy-1 was subsequently found to be expressed in various cell types, including fibroblasts, endothelial cells, neurons, and chondrocytes. Thy-1 has been reported to function in T cell activation,[8,9] neurite outgrowth,[10] apoptosis,[11,12] and tumor suppression.[13] In joint tissue, Thy-1 is also expressed by synovial fibroblast, chondrocyte, and mesenchymal progenitor/stem cells.[14] The precise biological function of Thy-1 in joint tissue is not clear. It has been reported that the expression of Thy-1 in chondrocyte was correlated with its chondrogenic potential. The chondrocyte with higher chondrogenic potential showed the lack of Thy-1 expression.[15] Interestingly, the expression of Thy-1 was increased during monolayer culture, which referred as dedifferentiation of the chondrocyte.[15] There is increasing evidence that interleukin-1β induced chondrocyte dedifferentiation by reducing type II collagen expression.[5,16,17] This event played an important role in OA development.

In an *in vitro* study, the inflammatory cytokines interleukin-1β and tumor necrosis factor-α up-regulated Thy-1 expression in vascular endothelial cells.[18,19] In the present study, we found that interleukin-1β induced Thy-1 expression in human chondrocytes. This demonstrated that Thy-1 was up-regulated in human chondrocyte cells in response to interleukin-1β.

In OA, the production of pro-inflammatory cytokines, such as IL-1β and TNF-α, are increased by articular chondrocytes. The current study was designed to study the expression of Thy-1 in OA disease. The expression of Thy-1 was studied in papain-injected rat joints and compared with normal knee joints using immunohistochemical methods. It was found that in the cartilage of normal knee joints hardly any expression of Thy-1 was observed. After injection of papain, the expression of Thy-1 was enhanced. Similar results were observed in human osteoarthritis cartilage. This result indicated that Thy-1 was increased in OA, which was the outcome of the inflammation cascade. Secreted forms of Thy-1 (sThy-1) have been found to be significantly elevated in synovial fluid of patients with RA.[20] Synovial fluid contains cytokines, matrix degradation products, enzymes, and other factors. The expression of sThy-1 may be induced or enhanced under these conditions and the membrane-bound Thy-1 is shed or cleaved from the cell surface to the synovial fluid.

In summary, the up-regulation of Thy-1 by the inflammatory cytokine interleukin1-β in articular chondrocytes and the increase of Thy-1 in two experimental arthritis conditions, including papain-induced rat arthritis and osteoarthritic human cartilage, suggest that Thy-1 may be a good marker for investigating OA disease.

Acknowledgments

The authors would like to acknowledge the following: the RGJ doctorate program (PHD/0258/2549) for scholarship support (TJ); the Thailand Research Fund (BRG 5180012) (PK); the Thailand Research Fund (RTA5380005); the Office of the Higher Education Commission and Mahidol University under the National Research Universities Initiative (VT); and the NSTDA Research Chair Grant, National Sciences and Technology Development Agency (WK).

Author Disclosure Statement

The authors have no financial interests to disclose.

References

1. Archer CW, and Francis-West P: The chondrocyte. Int J Biochem Cell Biol 2003;35:401–404.
2. Bonnet CS, and Walsh DA: Osteoarthritis, angiogenesis and inflammation. Rheumatology 2005;44:7–16.
3. Loeser RF: Molecular mechanisms of cartilage destruction: mechanics, inflammatory mediators, and aging collide. Arthritis Rheum 2006;54:1357–1360.
4. Martel-Pelletier J, and Pelletier JP: Is osteoarthritis a disease involving only cartilage or other articular tissues? Eklem Hastalik Cerrahisi 2010;21:2–14.
5. Sandell LJ, and Aigner T: Articular cartilage and changes in arthritis. An introduction: cell biology of osteoarthritis. Arthritis Res 2001;3:107–113.
6. Williams AF: Immunoglobulin-related domains for cell surface recognition. Nature 1985;314:579–580.
7. Reif AE, and Allen JM: The Akr thymus antigen and its distribution in leukemias and nervous tissues. J Exp Med 1964;120:413–433.
8. Marmor MD, Bachmann MF, Ohashi PS, Malek TR, and Julius M: Immobilization of glycosylphosphatidylinositol-anchored proteins inhibits T cell growth but not function. Int Immunol 1999;11:1381–1393.
9. Marmor MD, and Julius M: The function of GPI-anchored proteins in T cell development, activation and regulation of homeostasis. J Biol Regul Homeost Agents 2000;14:99–115.
10. Doherty P, Singh A, Rimon G, Bolsover SR, and Walsh FS: Thy-1 antibody-triggered neurite outgrowth requires an influx of calcium into neurons via N- and L-type calcium channels. J Cell Biol 1993;122:181–189.
11. Fujita N, Kodama N, Kato Y, Lee SH, and Tsuruo T: Aggregation of Thy-1 glycoprotein induces thymocyte apoptosis through activation of CPP32-like proteases. Exp Cell Res 1997;232:400–406.
12. Morita H, Isobe K, Cai Z, Miyazaki T, Matsumoto Y, Shinzato T, Yoshikai Y, Kimata K, and Maeda K: Thy-1 antigen mediates apoptosis of rat glomerular cells in vitro and in vivo. Nephron 1996;73:293–298.
13. Lung HL, Bangarusamy DK, Xie D, Cheung AK, Cheng Y, Kumaran MK, Miller L, Liu ET, Guan XY, Sham JS, Fang Y, Li L, Wang N, Protopopov AI, Zabarovsky ER, Tsao SW, Stanbridge EJ, and Lung ML: THY1 is a candidate tumour suppressor gene with decreased expression in metastatic nasopharyngeal carcinoma. Oncogene 2005;24:6525–6532.
14. Campbell DD, and Pei M: Surface markers for chondrogenic determination: a highlight of synovium-derived stem cells. Cells 2012;1:1107–1120.
15. Giovannini S, Diaz-Romero J, Aigner T, Mainil-Varlet P, and Nesic D: Population doublings and percentage of S100-positive cells as predictors of in vitro chondrogenicity of expanded human articular chondrocytes. J Cell Physiol 2010;222:411–420.
16. Hong EH, Yun HS, Kim J, Um HD, Lee KH, Kang CM, Lee SJ, Chun JS, and Hwang SG: Nicotinamide phosphoribosyltransferase is essential for interleukin-1beta-mediated dedifferentiation of articular chondrocytes via SIRT1 and extracellular signal-regulated kinase (ERK) complex signaling. J Biol Chem 2011;286:28619–28631.
17. Peng H, Zhou JL, Liu SQ, Hu QJ, Ming JH, and Qiu B: Hyaluronic acid inhibits nitric oxide-induced apoptosis and dedifferentiation of articular chondrocytes in vitro. Inflamm Res 2010;59:519–530.
18. Lee WS, Jain MK, Arkonac, BM, Zhang, D, Shaw, SY, Kashiki, S, Maemura K, Lee SL, Hollenberg NK, Lee ME, and Haber E: Thy-1, a novel marker for angiogenesis upregulated by inflammatory cytokines. Circ Res 1998;82:845–851.
19. Mason JC, Yarwood H, Tarnok A, Sugars K, Harrison AA, Robinson PJ, and Haskard DO: Human Thy-1 is cytokine-inducible on vascular endothelial cells and is a signaling molecule regulated by protein kinase C. J Immunol 1996;157:874–883.
20. Saalbach A, Wetzig T, Haustein UF, and Anderegg U: Detection of human soluble Thy-1 in serum by ELISA. Fibroblasts and activated endothelial cells are a possible source of soluble Thy-1 in serum. Cell Tissue Res 1999;298:307–315.

Address correspondence to:
Dr. Prachya Kongtawelert
Thailand Excellence Center for Tissue Engineering and Stem Cells Department of Biochemistry
Faculty of Medicine
Chiang Mai University
Chiang Mai 50200
Thailand

E-mail: prachya.kongtawelert@gmail.com

Received: September 6, 2012
Accepted: January 24, 2013

SCIENTIFIC REPORTS



OPEN

SUBJECT AREAS:
INTRACELLULAR SIGNALLING PEPTIDES AND PROTEINS
RENAL CALCULI
MECHANISM OF ACTION
PHOSPHOPROTEINS

Received
20 April 2012

Accepted
6 December 2012

Published
9 January 2013

Correspondence and requests for materials should be addressed to V.T. (thongboonkerd@dr.com)

p38 MAPK mediates calcium oxalate crystal-induced tight junction disruption in distal renal tubular epithelial cells

Paleerath Peerapen[1,2] & Visith Thongboonkerd[1,3]

[1]Medical Proteomics Unit, Office for Research and Development, Faculty of Medicine Siriraj Hospital, Mahidol University, Bangkok, Thailand, [2]Department of Immunology and Immunology Graduate Program, Faculty of Medicine Siriraj Hospital, Mahidol University, Bangkok, Thailand, [3]Center for Research in Complex Systems Science, Mahidol University, Bangkok, Thailand.

We examined whether p38 MAPK plays role in calcium oxalate monohydrate (COM) crystal-induced tight junction disruption. Polarized MDCK cells were pretreated with or without 20 μM SB239063 (p38 MAPK inhibitor) for 2-h, and then incubated with 100 μg/ml COM crystals for up to 48-h. Western blotting showed increased level of phospho-p38, not total p38, in COM-treated cells, whereas SB239063 pretreatment successfully maintained phospho-p38 at its basal level. COM crystals also caused decreased levels of two tight junction proteins, zonula occludens-1 (ZO-1) and occludin. Immunofluorescence study revealed disruption of tight junction, redistribution, and dissociation of ZO-1 and occludin. Moreover, transepithelial resistance (TER) showed defective barrier function, whereas Western blotting for Na^+/K^+-ATPase-α1 revealed defective fence function of tight junction in COM-treated cells. All these expression and functional defects were successfully prevented by SB239063 pretreatment. These findings indicate that COM crystals cause tight junction disruption in distal renal tubular epithelial cells through p38 MAPK activation.

Kidney stone disease is a common health problem worldwide[1,2] with calcium oxalate monohydrate (COM) as the major crystalline composition of kidney stone matrix[3]. Adhesion of COM crystals on renal tubular epithelial cell surface is a crucial mechanism for kidney stone formation[4,5]. This pathogenic process leads to several cellular responses, including overproduction of reactive oxygen species (ROS)[6,7], cellular injury[8], and finally tissue inflammation[9]. Furthermore, our previous study has demonstrated that COM crystals can cause the increased paracellular permeability, loss of cell polarity and disruption of tight junction[10]. However, the cellular signaling involved in COM crystal-induced tight junction disruption remained unknown.

Mitogen-activated protein kinase (MAPK) causes intracellular signaling cascades that cells use to respond to various stimuli. p38 MAPK is one of signaling proteins in MAPK pathway that can be activated by various extracellular stresses, e.g., UV radiation[11], hydrogen peroxide[12], and proinflammatory cytokines[13]. Interestingly, p38 MAPK also plays role in modulation of tight junction function by regulating expression of tight junction proteins in response to several stimuli. In renal tubular cells, p38 MAPK can be activated by tumor necrotic factor α (TNFα) and interferon γ (IFNγ), leading to down-regulation of occludin, zonula occludens-1 (ZO-1) and claudin-2, which contributes to the increase in paracellular permeability[14]. In contrast, inhibition of basal p38 MAPK can enhance the barrier function of tight junction in mammary epithelial cells[15]. On these bases, we hypothesized that COM crystal-induced tight junction disruption may be mediated by p38 MAPK pathway.

This present study is an extended work of our previous report[10] with a specific aim to address whether p38 MAPK plays a significant role in COM- crystal-induced tight junction disruption in polarized Madin-Darby canine kidney (MDCK) cells derived from distal nephron[16,17]. Expression levels of total p38, active form of p38 (phospho-p38), and two main tight junction proteins (occludin and ZO-1) were examined by Western blot analysis, whereas the distribution and co-localization of occludin and ZO-1 were evaluated by immunofluorescence study. In addition, transepithelial resistance (TER) was also measured to examine the barrier function, whereas translocation of Na^+/K^+-ATPase-α1 (a marker for basolateral membrane) to apical membrane was investigated to examine the fence function of tight junction in response to COM crystals. Moreover, a specific inhibitor of p38 MAPK activation, SB239063, was employed to examine whether the inhibition of p38 MAPK pathway could prevent the aforementioned defects of tight junction induced by COM crystals.

Results

Effects of differential doses of COM crystals on cell death. Annexin V/propidium iodide co-staining followed by flow cytometry was performed to examine the effects of differential doses of COM crystals on cell death. After cells were incubated with various doses of COM crystals for 48-h, the data revealed that low doses (50–100 μg/ml) of COM crystals had no effect on cell death, whereas higher doses (500–1000 μg/ml) caused significant increase of cell death in a dose-dependent manner (**Figure 1**).

Effects of differential doses of COM crystals on the integrity of tight junction barrier. Transepithelial resistance (TER) was measured to examine the effects of differential doses of COM crystals on the integrity of tight junction barrier of polarized MDCK cells. The results showed significant decrease of TER in a dose-dependent manner at both 24-h and 48-h after exposure to COM crystals (**Figure 2**).

Based on the data shown in **Figures 1 and 2**, the dosage at 100 μg/ml of COM crystals was used for all subsequent experiments (as we aimed to address the effects of COM crystals on tight junction when the cells were not too toxic).

p38 MAPK in polarized MDCK cells was activated by COM crystals. Western blot analysis for phospho-p38, the active form of p38, was performed to examine the effects of COM crystals on p38 MAPK pathway in polarized MDCK cells. The data revealed that exposure of polarized MDCK cells to COM crystals had caused significantly increased level of phospho-p38 since 3-h until 48-h after COM crystal exposure, whereas the level of total p38 remained unchanged at all time-points (**Figure 3**). Moreover, pretreatment of the cells with a specific inhibitor of p38 MAPK activation, SB239063, successfully maintained phospho-p38 at its basal level (**Figure 3**) at all time-points. These results indicate that p38 MAPK was activated in polarized MDCK cells by COM crystals, and SB239063 could prevent COM crystal-induced p38 MAPK activation. If p38 MAPK pathway is important for regulating COM crystal-induced tight junction disruption, SB239063 should be able to prevent expression and functional defects in tight junction protein complex induced by COM crystals.

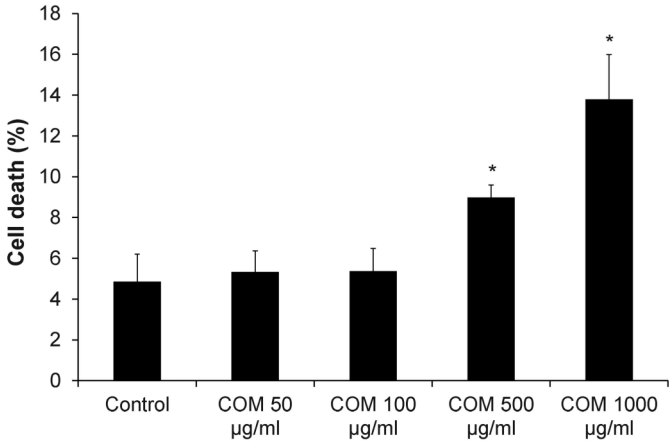


Figure 1 | Cell death assay. Annexin V/propidium iodide co-staining followed by flow cytometry analysis was performed after MDCK cells were exposed to various doses of COM crystals for 48-h. Percentage of total cell death = [(number of both apoptotic and necrotic cells/number of all cells) × 100%]. N = 3 independent experiments for each bar; * = P<0.05 vs. control.

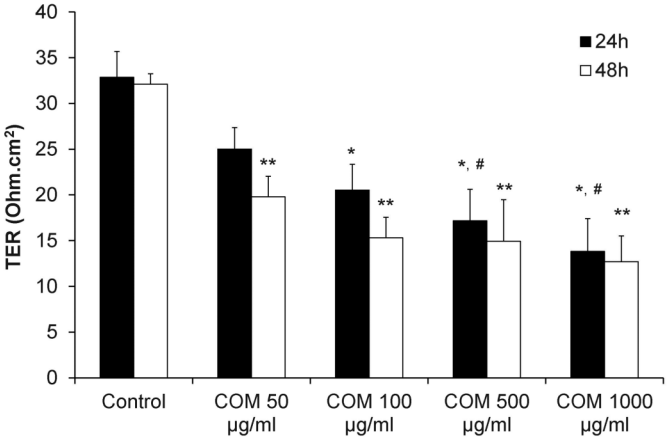


Figure 2 | Measurement of transepithelial resistance (TER) revealed dose-dependent COM-induced decrease of TER. TER was measured after the polarized MDCK cells were exposed to various doses of COM crystals for 24-h and 48-h. N = 3 independent experiments for each bar; * = P<0.01 vs. control at 24-h; ** = P<0.01 vs. control at 48-h; # = P<0.05 vs. 50 μg/ml COM-treated group at 24-h.

Inhibition of p38 MAPK activation successfully prevented the decreased expression levels, redistribution and dissociation of tight junction proteins in polarized MDCK cells induced by COM crystals. We evaluated whether p38 MAPK pathway plays an important role in regulation of COM crystal-induced decreased levels, redistribution and dissociation of two main tight junction proteins, ZO-1 and occludin, in polarized MDCK cells. Western blot analysis revealed that COM crystals significantly reduced expression levels of ZO-1 and occludin, whereas pretreatment with SB239063 successfully maintained the levels of these two tight junction proteins at their basal levels (**Figure 4**). Immunofluorescence study confirmed that COM crystals caused disruption of tight junction, decreased levels, redistribution and dissociation of ZO-1 and occludin in polarized MDCK cells (**Figure 5**). However, pretreatment with SB239063 could preserve tight junction structure, honey comb appearance of expression pattern of ZO-1 and occludin, as well as their co-localization (**Figure 5**).

Effects of COM crystals on adherens junction in polarized MDCK cells. Tight junction formation is also associated with adherens junction. In addition to the investigations on tight junction protein complex, we also evaluated the effects of COM crystals on adherens junction and the role of p38 MAPK pathway in this response. Immunofluorescence study revealed that COM crystals induced disruption of adherens junction and decreased level of epithelial cadherin (E-cadherin) in the polarized MDCK cells (**Figure 5**). And this defect could be partially prevented by pretreatment with SB239063 (**Figure 5**).

Inhibition of p38 MAPK activation partially preserved the barrier function of tight junction in polarized MDCK cells treated with COM crystals. One of the main functions of tight junction is to serve as a paracellular "barrier" to control paracellular transports of water and solutes. We measured TER across polarized MDCK cell monolayer to examine the role of p38 MAPK in COM-induced increase of paracellular permeability. As expected, the results showed that COM crystals led to dramatic decrease in TER (increased permeability) across all time-points (**Figure 6**). Pretreatment with SB239063 partially prevented the defective barrier function of tight junction in polarized MDCK cells induced by COM crystals (**Figure 6**).

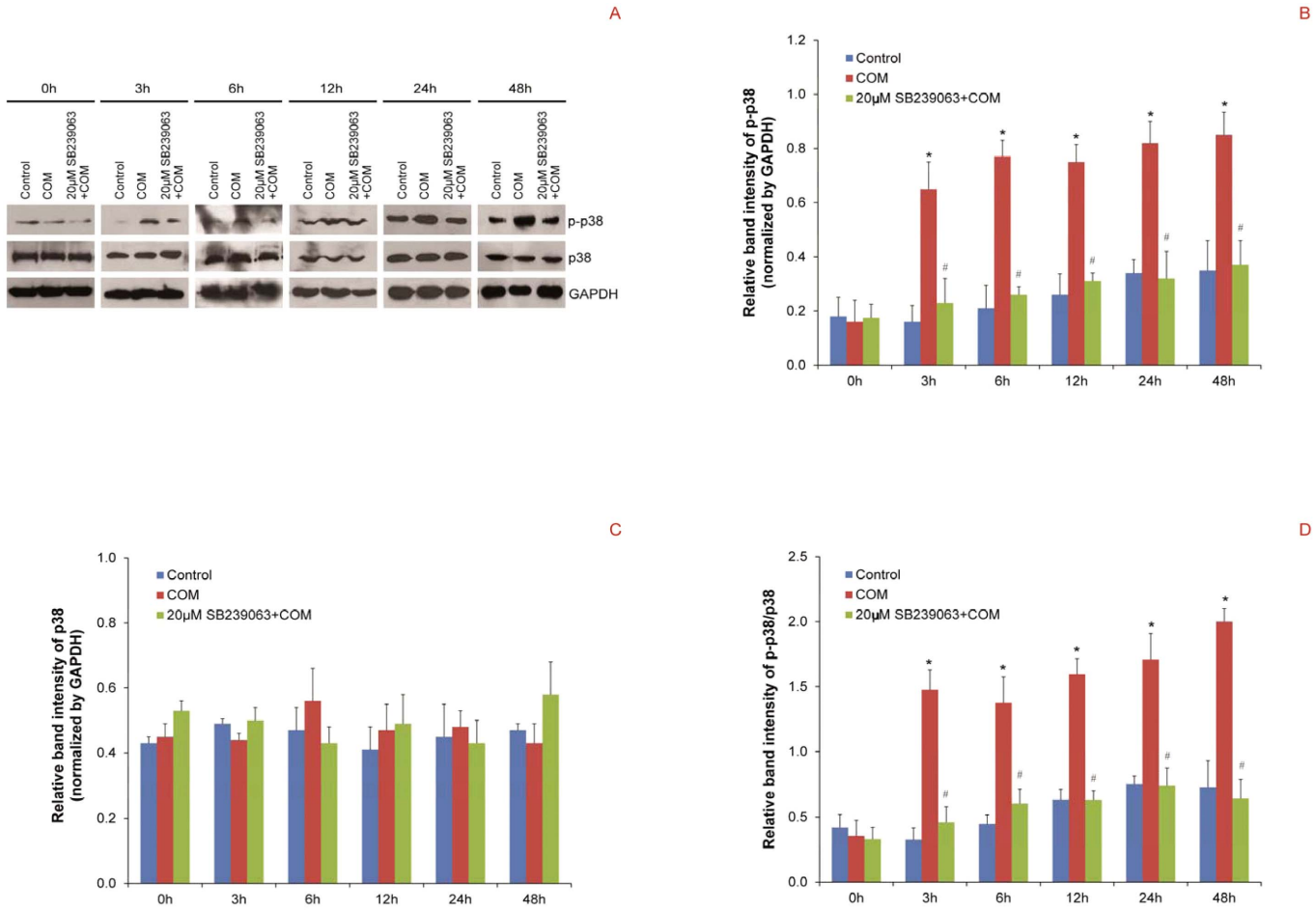


Figure 3 | Western blot analysis revealed that p38 MAPK in polarized MDCK cells was activated by COM crystals. (A) Proteins derived from whole cell lysates of controlled and COM-treated (100 μg/ml) cells at various time-points, without or with 2-h pretreatment by 20 μM SB239063 (an inhibitor of p38 MAPK activation), were equally loaded into each of SDS-PAGE lane (30 μg/lane). The resolved proteins were subjected to Western blot analysis using rabbit polyclonal anti-phospho-p38 or mouse monoclonal anti-p38 antibody as the primary antibody. GAPDH served as the loading control. (B) and (C) Band intensities of phospho-p38 and total p38, respectively, were measured by a densitometer and normalized with that of GAPDH. (D) The ratio of band intensities of phospho-p38 and total p38 (p-p38/p38) was also determined. N = 3 independent experiments for each bar; * = $P<0.05$ vs. control at corresponding time-point; # = $P<0.05$ vs. COM-treated group at corresponding time-point.

Inhibition of p38 MAPK activation successfully prevented defective fence function of tight junction in polarized MDCK cells induced by COM crystals. Another main function of tight junction is to serve as a "fence" to divide epithelial membranes into apical and basolateral membranes. We performed Western blot analysis to examine whether p38 is involved in regulation of defective fence function of tight junction in polarized MDCK cells induced by COM crystals. The data clearly demonstrated that COM crystals induced the translocation of Na^+/K^+-ATPase-α1 (a marker for basolateral membrane) from basolateral to apical membranes (**Figure 7**). However, the COM crystal-induced loss of fence function was attenuated by SB239063 pretreatment (**Figure 7**). Note that the attenuation of defective fence function by SB239063 was not entirely complete as there was a (very) minimal level of Na^+/K^+-ATPase-α1 remained detectable at apical membrane and its expression level at basolateral membrane was still less than the control (**Figure 7**).

Inhibition of p38 MAPK activation partially prevented overproduction of intracellular hydrogen peroxide in polarized MDCK cells induced by COM crystals. The ROS overproduction has been recognized as the p38 activator. We measured the intracellular hydrogen peroxide in polarized MDCK cells to examine the effects of COM crystals on ROS overproduction and the involvement of p38 MAPK. As expected, COM crystals caused the overproduction of the intracellular hydrogen peroxide (**Figure 8**). Interestingly, pretreatment with SB239063 partially prevented the overproduction of intracellular hydrogen peroxide induced by COM crystals (**Figure 8**).

Discussion

Tight junction is the intercellular junction at apicolateral locale of epithelial cells[18]. This junction serves as a "paracellular barrier" to regulate and limit the passage of water, ions, macromolecules and pathogens through the paracellular route. Moreover, it also has a "fence" function to maintain the cell polarity by partitioning epithelial cell membranes into two parts – apical and basolateral membranes[19]. Tight junction protein complex composes of both transmembrane proteins (i.e., occludin[20], claudin[21] and junctional adhesion molecule[22]) and cytoplasmic proteins (i.e., ZO-1[23], ZO-2[24], ZO-3[25] and cingulin[26]). In addition, some proteins in this complex also bind to actin filament through distinct protein domains. Tight junction will function properly when it forms a stable protein complex. Dissociation of this protein complex or down-regulation of some proteins in this complex will lead to disruption and defects of the tight junction. Moreover, tight junction protein complex is also associated with signaling proteins that are involved in regulation of tight junction organization, integrity and functions[27,28].

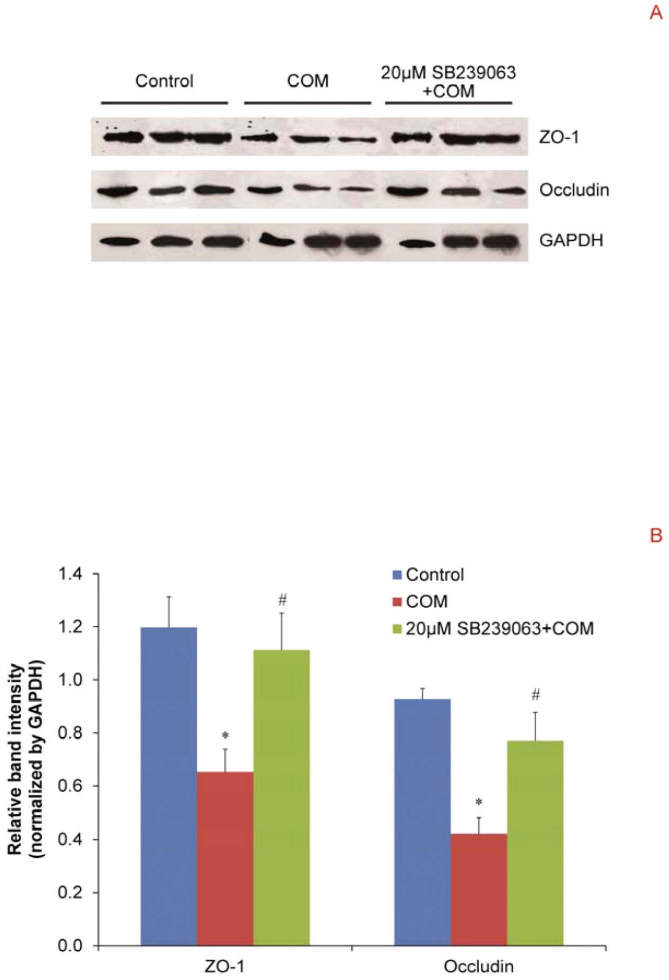


Figure 4 | Western blot analysis revealed that inhibition of p38 MAPK activation successfully prevented the decreased expression levels of tight junction proteins in polarized MDCK cells induced by COM crystals. (A) Proteins derived from whole cell lysate of controlled and COM-treated (100 μg/ml) cells without or with 2-h pretreatment by 20 μM SB239063 were equally loaded into each of SDS-PAGE lane (30 μg/lane). The resolved proteins were then subjected to Western blot analysis for ZO-1 and occludin, whereas GAPDH served as the loading control. (B) Band intensity levels were measured by a densitometer and the relative band intensity levels normalized with GAPDH were compared by one-way ANOVA. N = 3 independent experiments for each bar; * = $P<0.05$ vs. control; # = $P<0.05$ vs. COM-treated group.

Our recent study has shown that COM crystals can induce tight junction disruption[10]. This may, at least in part, explain renal tubulointerstitial injury that frequently occurs in kidney stone disease. Moreover, COM crystal-induced tight junction disruption may be the linkage between intratubular and interstitial (Randall's plaque) theories of kidney stone pathogenesis[10,29,30]. Unfortunately, molecular mechanisms underlying COM crystal-induced tight junction disruption remained unknown. Several studies have suggested that tight junction can be disrupted by various stimuli through MAPK pathway[14,31–33]. A number of previous studies have indicated that p38 MAPK may be activated by oxalate[34,35] and calcium[36], both of which are the compositions of COM crystals. We therefore hypothesized that p38 MAPK might play significant role in COM crystal-induced tight junction disruption. To address our hypothesis, the inhibitor of p38 MAPK activation (SB239063) was employed to examine whether p38 MAPK activation was involved in expression and functional defects in tight junction of polarized MDCK cells induced by COM crystals. We first determined the appropriate dose and condition of COM crystal treatment that could be used to address effects of COM crystals on tight junction complex, as the cellular response to the crystal, not by severe cytotoxicity when the cells are too toxic to cope with the chemical stimulus. Based on the data shown in **Figures 1 and 2**, the dosage of 100 μg/ml COM crystals and 48-h incubation period were used for all subsequent experiments because the defect in tight junction barrier was clearly demonstrated whereas the total cell death remained unchanged. Using this condition, our previous study has reported that approximately 80% of MDCK cells were adhered by COM crystals and another 16% had the internalized COM crystals into the cells[37].

We then examined whether p38 MAPK was activated in polarized MDCK cells upon COM crystal exposure. p38 is a member of MAPK pathway and can be activated by several stimuli, especially extracellular stresses[11–13]. The activated form of p38 MAPK is phosphorylated p38 MAPK[38]. Western blot analysis of time-course expression clearly showed that phospho-p38 level was increased in COM-treated polarized MDCK cells at all time-points, starting at 3-h after COM exposure, whereas total p38 remained unchanged (**Figure 3**). Moreover, SB239063 pretreatment successfully prevented the increased level of phospho-p38 in the COM-treated cells. These data indicated that p38 MAPK was activated in polarized MDCK cells by COM crystals. Furthermore, COM crystals could induce intracellular hydrogen peroxide overproduction, whereas pretreatment with SB239063 partially attenuate this effect (**Figure 8**). Our data were consistent with those reported in several previous studies demonstrating that the phosphorylated form of p38 MAPK was increased in a variety of cells, which were exposed to various stimuli, including oxidative stress[12,33,39].

p38 MAPK is well recognized as a regulator of numerous genes, including transcription factors[38,40]. It plays significant roles in regulation of expression and phosphorylation of proteins. Several lines of evidence have also suggested that the activation of p38 MAPK by proinflammatory cytokines, pathogens and oxidative stress can lead to down-regulation of tight junction proteins, i.e., claudin 2, claudin 11, occludin and ZO-1, in diverse cells[14,31–33]. In addition, activation of p38 MAPK by alcohol can lead to phosphorylation of tight junction proteins and ultimately loss of the barrier function[31]. We thus hypothesized that COM crystal-induced p38 MAPK activation was associated with altered expression of tight junction proteins in polarized MDCK cells. Our hypothesis was addressed by Western blot analysis and immunofluorescence study of ZO-1 and occludin, which are commonly used to demonstrate the disruption of tight junction by various stimuli, e.g., oxidative stress, proinflammatory cytokines and pathogens[41–47]. The data clearly demonstrated that inhibition of p38 MAPK activation by SB239063 pretreatment successfully prevented the decreased expression levels (**Figure 4**), redistribution and dissociation of tight junction proteins in polarized MDCK cells induced by COM crystals (**Figure 5**). These data confirmed the hypothesis that COM crystal-induced p38 MAPK activation was associated with altered expression (i.e., decreased levels, redistribution and dissociation) of tight junction proteins in polarized renal tubular epithelial cells.

Adherens junction has been known as a crucial structure for tight junction formation[48,49]. Furthermore, there is evidence indicating that activation of p38 MAPK can lead to disruption of adherens junction[50]. We therefore hypothesized that COM crystals could also disrupt adherens junction using E-cadherin as the marker. The immunofluorescence study clearly confirmed our hypothesis. The data also revealed that inhibition of p38 MAPK activation by SB239063 pretreatment partially prevented the decreased expression level and disruption of adherens junction induced by COM crystals (**Figure 5**).

In addition to expression study, we also performed functional analyses of the role for p38 MAPK in tight junction functions. As a

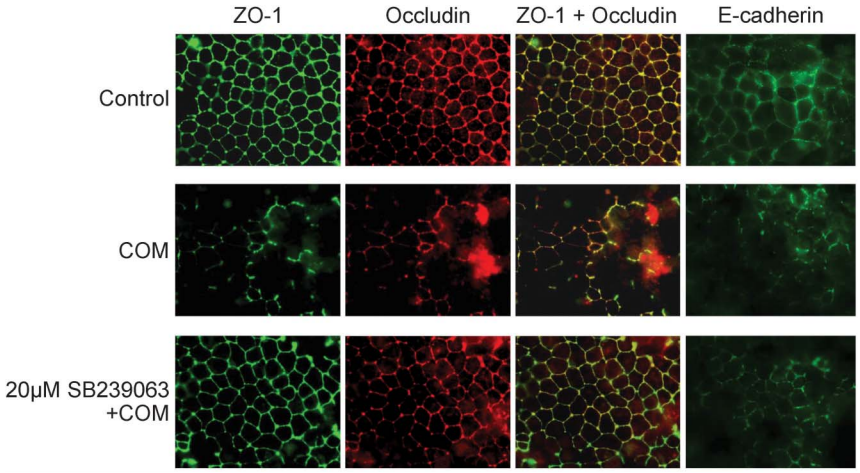


Figure 5 | Immunofluorescence study revealed that inhibition of p38 MAPK activation successfully prevented the decreased expression levels, redistribution and dissociation of tight junction proteins, and partially prevented defects in adherens junction of polarized MDCK cells induced by COM crystals. The polarized MDCK cells were pretreated without or with 20 μM SB239063 for 2-h and then incubated with 100 μg/ml COM crystals for 48-h. Subsequently, the cells were subjected to co-staining for ZO-1(in green, first column) and occludin (in red, second column). The third column shows the merged view of both ZO-1 and occludin, and their co-localization is illustrated in yellow. The cells were also examined for E-cadherin (in green; last column). The polarized MDCK cells grown in COM-free medium served as the controls. Original magnification was 200× for all panels.

"barrier", tight junction regulates the paracellular permeability by regulating the paracellular passage of water, ions, macromolecules and other substances. The impairment of barrier function is associated with leakage of these substances from the intratubular lumen to the interstitial compartment, or *vice versa*, which may eventually lead to cellular injury and tissue inflammation. TER was measured to reflect tight junction integrity and epithelial permeability to ions[51]. The data revealed that TER was dramatically decreased in COM-treated polarized MDCK cells, whereas the inhibition of p38 MAPK activation by SB239063 pretreatment could partially preserve the barrier function of tight junction (**Figure 6**). Our data were consistent

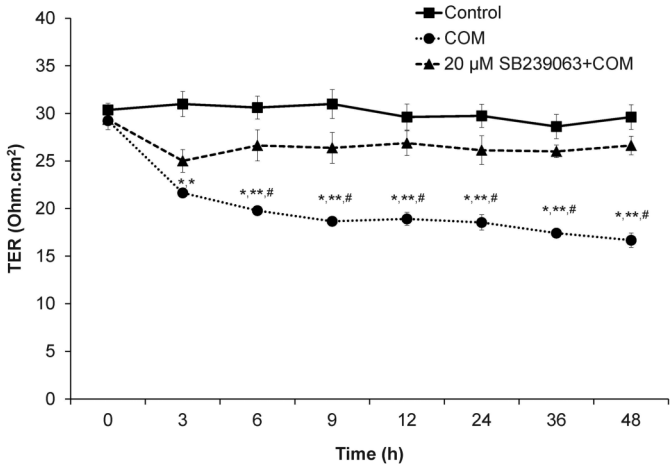


Figure 6 | Measurement of transepithelial resistance (TER) revealed that inhibition of p38 MAPK activation partially preserved the barrier function of tight junction in polarized MDCK cells treated with COM crystals. The polarized MDCK cells grown in Transwells™ were pretreated without or with 20 μM SB239063 for 2-h before incubation with 100 μg/ml COM crystals for up to 48-h. TER was serially measured at 0, 3, 6, 9, 12, 24, 36 and 48-h after COM treatment. The polarized MDCK cells grown in COM-free medium served as the controls. N = 3 independent experiments for each data point; * = $P<0.005$ vs. TER of the controlled cells at the corresponding time-point; ** = $P<0.0005$ vs. the basal TER level; # = $P<0.05$ vs. TER of COM-treated cells pretreated with 20 μM SB239068 at the corresponding time-point.

with those of other previous studies, which have demonstrated that effects of some stimuli on epithelial permeability are less when p38 MAPK activation is inhibited[39,52], and that the inhibition of basal p38 MAPK activity can enhance the epithelial barrier function[15]. As a "fence", tight junction plays critical roles in maintaining epithelial cell polarity and preventing translocation of apical membrane proteins and lipids to basolateral membranes, or *vice versa*. Western blot analysis of basolateral membrane protein, Na^+/K^+-ATPase-α1, revealed that COM crystal-induced translocation of this protein from basolateral to apical membranes of polarized MDCK cells could be prevented (although partially) by inhibition of p38 MAPK activation with SB239063 pretreatment. These data confirmed that the defective barrier and fence functions of tight junction induced by COM crystals were regulated by p38 MAPK pathway.

It should be noted that COM crystal-induced defects in barrier and fence functions of tight junction, as well as overproduction of intracellular hydrogen peroxide, were not completely protected by SB239063 pretreatment (**Figures 6–8**), probably due to two main possibilities. First, the condition for inhibition of p38 MAPK activation might not yet be optimal. The most appropriate dosage and incubation period of pretreatment with SB239063 should be further defined to achieve the optimal yield of such prevention. Second, p38 MAPK might not be the only pathway involved in COM crystal-induced tight junction disruption. There might be some other signaling pathways that also played roles (although not as the major players) in this process.

In conclusion, we have demonstrated for the first time that COM crystals cause disruption and defective barrier and fence functions of tight junction of distal renal tubular epithelial cells through p38 MAPK activation. Our findings add significant information on the pathophysiology of kidney stone disease.

Methods

Cell polarization and treatment with COM crystals with or without pretreatment by a p38 MAPK activation inhibitor. Madin-Darby canine kidney (MDCK) cells were cultivated and polarization was performed as described in **Supplementary Methods**. COM crystals were prepared as described previously[53,54]. The polarized MDCK cells were subjected to pretreatment with or without 20 μM SB239063 (Tocris Bioscience; Bristol, UK), which is a specific inhibitor of p38 MAPK activation, for 2-h. Thereafter, the cells were incubated with COM crystals (by adding COM crystals into the culture medium with a ratio of 100 μg crystals/ml culture medium) for 0, 3, 6, 12, 24 and 48-h. The controlled cells were maintained in COM-free medium that was initially exposed to 100 μg/ml COM crystals (for 30 min), which were then removed from the medium to obtain identical concentrations of free calcium and oxalate ions

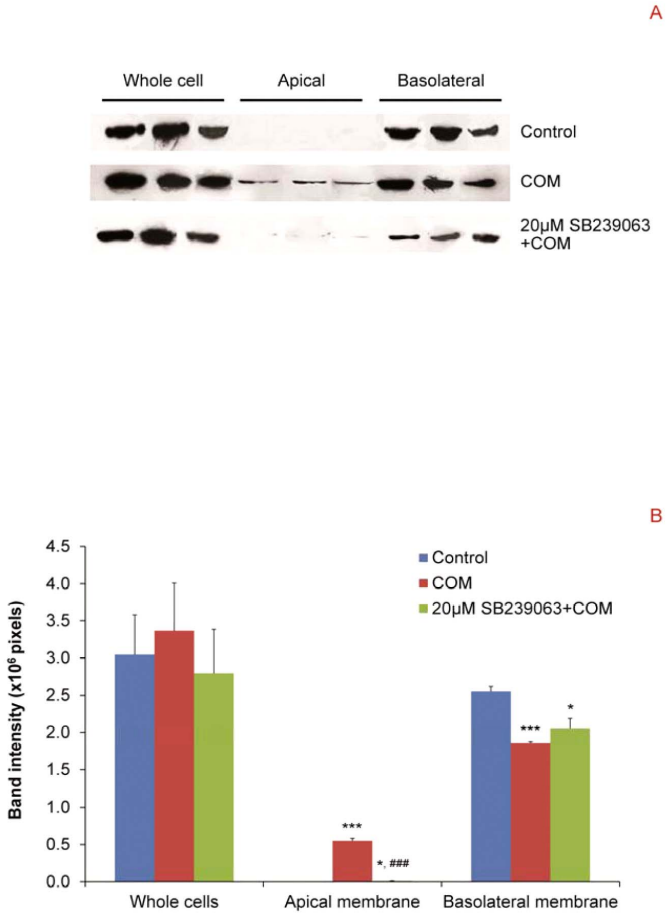


Figure 7 | Western blot analysis revealed that inhibition of p38 MAPK activation successfully prevented defective fence function of tight junction in polarized MDCK cells induced by COM crystals. (A) Proteins derived whole cell lysate, apical and basolateral membranes of controlled and COM-treated (100 μg/ml) cells without or with 20 μM SB239063 pretreatment were subjected to Western blot analysis for Na^+/K^+ATPase-α1, which is a marker of basolateral membrane. Note that equal number of the cells (3.0×10^5 cells) was used for sample preparation of each sample. (B) Band intensity levels were measured by a densitometer and compared by one-way ANOVA. N = 3 independent experiments for each bar; * = P<0.05 vs. control; *** = P<0.0001 vs. control; ### = P<0.001 vs. COM-treated group.

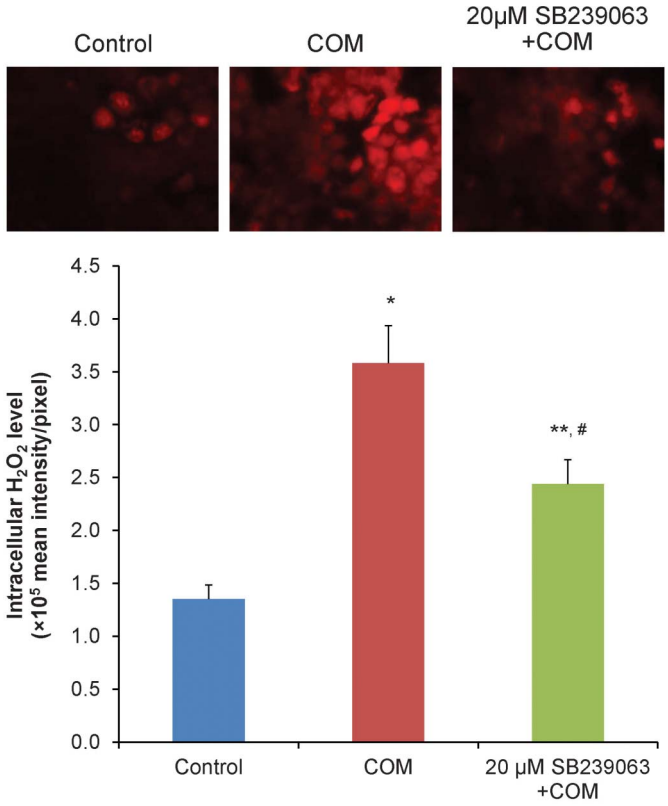


Figure 8 | Semiquantitative fluorescence assay revealed that COM crystals induced intracellular hydrogen peroxide production. The polarized MDCK cells were pretreated without or with 20 μM SB239063 for 2-h and then incubated with 100 μg/ml COM crystals for 48-h. Subsequently, DHR123 was added into the culture medium and the fluorescence signal was detected by fluorescence microscope (upper panels). The mean florescence intensity was then quantitated (lower graph). N = 3 independent experiments of each bar; * = P<0.001 vs. control; ** = P<0.05 vs. control; # = P<0.05 vs. COM-treated group.

in the medium comparing to those of COM crystal-containing medium (as a minimal, but non-negligible, amount of solid COM crystals could be solubilized in the culture medium). The controlled and COM-treated cells were then subjected to the following expression and functional analyses, all of which were done in triplicate.

Isolation of apical and basolateral membranes, and protein extraction. Apical membranes were isolated by a recently established peeling method[55] based on hydrous affinity and ionic interaction between a surface (paper, membrane, or a solid surface) and apical membranes of the cells (additional details for this isolation technique can be found in **Supplementary Methods**). Proteins were extracted from whole cells, apical and basolateral membranes for subsequent Western blot analysis using 1× Laemmli's buffer. Protein concentrations in individual samples were measured by the Bradford method using Bio-Rad Protein Assay (Bio-Rad Laboratories; Hercules, CA).

Western blot analyses. Proteins derived from whole cell lysate with an equal amount of 30 μg/lane were resolved by 10% SDS-PAGE for Western blot analyses of p38 MAPK, phospho-p38, ZO-1, and occludin. For Western blot analysis of Na^+/K^+-ATPase-α1, an equal number of priming cells (3×10^5 cells/sample/lane) was used for isolation of apical and basolateral membranes, and all the recovered proteins derived from each sample were resolved in each lane of 10% SDS-PAGE gel. The resolved proteins were then transferred onto nitrocellulose membranes using a semi-dry transfer apparatus (Bio-Rad; Milano, Italy). Non-specific bindings were blocked with 5% skim milk in PBS for 1-h at room temperature. The membranes were then incubated with mouse monoclonal anti-p38 (Santa Cruz Biotechnology; Santa Cruz, CA), rabbit polyclonal anti-phospho-p38 (Santa Cruz Biotechnology), mouse monoclonal anti-ZO-1 (Zymed; San Francisco, CA), rabbit polyclonal anti-occludin (Santa Cruz Biotechnology), mouse monoclonal anti-Na^+/K^+-ATPase-α1 (Santa Cruz Biotechnology), or mouse monoclonal anti-GAPDH (glyceroldehyde-3-phosphate dehydrogenase) (Santa Cruz Biotechnology) antibody at 4°C overnight. All these primary antibodies were diluted 1 : 1000 with 1% skim milk/PBS. After three washes with PBS, the membranes were incubated with corresponding secondary antibody conjugated with horseradish peroxidase (1 : 2000 in 1% skim milk/PBS) at room temperature for 1-h. Immunoreactive protein bands were then visualized by SuperSignal West Pico chemiluminescence substrate (Pierce Biotechnology; Rockford, IL) and autoradiogram. Band intensity levels were measured by Image Master densitometer (GE Healthcare; Uppsala, Sweden).

Immunofluorescence study. MDCK cells (approximately 5×10^5 cells) were cultivated on cover slips (cleaved mica disk diameter: 9.5 mm, V-1 grade; SPI Supplier; Toronto, Canada). After the cells were pretreated with or without 20 μM SB239063 for 2-h followed by incubation in COM crystal-containing or COM-free medium for 48-h, they were rinsed with ice-cold membrane-preserving buffer. The cells were then fixed with 3.7% formaldehyde for 15-min and permeabilized with 0.1% Triton X-100 for 15-min. For co-staining of ZO1 and occludin, after another washing step with ice-cold membrane-preserving buffer, the cells were incubated with mouse monoclonal anti-ZO1 and rabbit polyclonal anti-occludin (both were purchased from Santa Cruz Biotechnology and diluted 1 : 50 in 1% skim milk/PBS) at 37°C for 1-h. Thereafter, the cells were incubated with AlexaFluor-488-conjugated goat anti-mouse IgG (1 : 5000 in 1% skim milk/PBS; Invitrogen/Molecular Probes; Burlington, Canada), Cy3-conjugated donkey anti-rabbit IgG (1 : 5000 in 1% skim milk/PBS; Jackson ImmunoResearch Laboratories; West Grove, PA) and Hoechst dye (1 : 1000 in PBS for nuclear stain; Invitrogen/Molecular Probes) at 37°C for 1-h. For single staining of E-cadherin after cells were fixed and permeabilized, the cells were incubated with rat monoclonal anti-E-cadherin (1 : 50 in 1% skim milk/PBS; Santa Cruz Biotechnology) at 37°C for 1-h. The cells were then incubated with AlexaFluor-488-conjugated goat anti-rat IgG (1 : 5000 in 1% skim milk/PBS; Invitrogen/

Molecular Probes) and Hoechst dye (1 : 1000 in PBS for nuclear stain; Invitrogen/Molecular Probes) at 37°C for 1-h. The cover slips were then mounted with 50% glyceral/PBS and examined by using a laser-scanning confocal microscope equipped with LSM5 Image Browser (LSM 510 META, Carl Zeiss; Oberkochen, Germany).

Measurement of transepithelial resistance (TER). The resistance across the polarized MDCK cell monolayer was serially measured using Millicell-ERS resistance system (Millipore; Bedford, MA) after the cells were pretreated with or without 20 μM SB239063 followed by incubation in COM crystal-containing or COM-free medium for 0, 3, 6, 9, 12, 24, 36 and 48-h. TER was measured at 3 different sites in each transwell and the background obtained from the blank control was subtracted. The net resistance was multiplied by the membrane area to give the resistance in $Ohm \cdot cm^2$.

Semiquantitative analysis of intracellular hydrogen peroxide by fluorescence microscopy. MDCK cells (approximately 5×10^5 cells) were cultivated on cover slips with or without 2-h pretreatment by 20 μM SB239063 followed by incubation in COM crystal-containing or COM-free medium for 48-h. Thereafter, the cells were rinsed with PBS and then incubated with 10 μM dihydrorhodamine 123 (Sigma; St Louis, MO) at 37°C for 15 min. After the excess dye was removed, the cover slips were mounted with 50% glycerol/PBS and the fluorescence signal was detected using a fluorescence microscope. The quantitative data (fluorescence intensity) was obtained from 15 high power fields (HPF) of each group using ImageJ software (http://rsb.info.nih.gov/ij/).

Statistical analysis. All the experiments were done in triplicate and quantitative data are presented as mean ± SEM. Comparisons of the data among different groups were performed by one-way ANOVA using SPSS software version 13.0 (SPSS; Chicago, IL). P values less than 0.05 were considered statistically significant.

1. Amato, M., Lusini, M. L. & Nelli, F. Epidemiology of nephrolithiasis today. *Urol. Int.* **72 Suppl 1**, 1–5 (2004).
2. Coe, F. L., Evan, A. & Worcester, E. Kidney stone disease. *J Clin. Invest* **115**, 2598–2608 (2005).
3. Schubert, G. Stone analysis. *Urol. Res.* **34**, 146–150 (2006).
4. Evan, A. P., Coe, F. L., Lingeman, J. E. & Worcester, E. Insights on the pathology of kidney stone formation. *Urol. Res.* **33**, 383–389 (2005).
5. Lieske, J. C., Deganello, S. & Toback, F. G. Cell-crystal interactions and kidney stone formation. *Nephron* **81 Suppl 1**, 8–17 (1999).
6. Davalos, M., Konno, S., Eshghi, M. & Choudhury, M. Oxidative renal cell injury induced by calcium oxalate crystal and renoprotection with antioxidants: a possible role of oxidative stress in nephrolithiasis. *J Endourol.* **24**, 339–345 (2010).
7. Thamilselvan, S., Khan, S. R. & Menon, M. Oxalate and calcium oxalate mediated free radical toxicity in renal epithelial cells: effect of antioxidants. *Urol. Res.* **31**, 3–9 (2003).
8. Hackett, R. L., Shevock, P. N. & Khan, S. R. Madin-Darby canine kidney cells are injured by exposure to oxalate and to calcium oxalate crystals. *Urol. Res.* **22**, 197–203 (1994).
9. Khan, S. R. Crystal-induced inflammation of the kidneys: results from human studies, animal models, and tissue-culture studies. *Clin. Exp. Nephrol.* **8**, 75–88 (2004).
10. Peerapen, P. & Thongboonkerd, V. Effects of calcium oxalate monohydrate crystals on expression and function of tight junction of renal tubular epithelial cells. *Lab Invest* **91**, 97–105 (2011).
11. Staples, C. J., Owens, D. M., Maier, J. V., Cato, A. C. & Keyse, S. M. Cross-talk between the p38alpha and JNK MAPK pathways mediated by MAP kinase phosphatase-1 determines cellular sensitivity to UV radiation. *J Biol. Chem.* **285**, 25928–25940 (2010).
12. Cheng, J. C., Klausen, C. & Leung, P. C. Hydrogen peroxide mediates EGF-induced down-regulation of E-cadherin expression via p38 MAPK and snail in human ovarian cancer cells. *Mol. Endocrinol.* **24**, 1569–1580 (2010).
13. Wang, Q. *et al.* Cytokine-induced epithelial permeability changes are regulated by the activation of the p38 mitogen-activated protein kinase pathway in cultured Caco-2 cells. *Shock* **29**, 531–537 (2008).
14. Patrick, D. M., Leone, A. K., Shellenberger, J. J., Dudowicz, K. A. & King, J. M. Proinflammatory cytokines tumor necrosis factor-alpha and interferon-gamma modulate epithelial barrier function in Madin-Darby canine kidney cells through mitogen activated protein kinase signaling. *BMC. Physiol* **6**, 2 (2006).
15. Carrozzino, F., Pugnale, P., Feraille, E. & Montesano, R. Inhibition of basal p38 or JNK activity enhances epithelial barrier function through differential modulation of claudin expression. *Am. J Physiol Cell Physiol* **297**, C775–C787 (2009).
16. Rindler, M. J., Chuman, L. M., Shaffer, L. & Saier, M. H., Jr. Retention of differentiated properties in an established dog kidney epithelial cell line (MDCK). *J Cell Biol.* **81**, 635–648 (1979).
17. Saier, M. H., Jr. Growth and differentiated properties of a kidney epithelial cell line (MDCK). *Am. J Physiol* **240**, C106–C109 (1981).
18. Gonzalez-Mariscal, L., Betanzos, A., Nava, P. & Jaramillo, B. E. Tight junction proteins. *Prog. Biophys. Mol. Biol.* **81**, 1–44 (2003).
19. Matter, K. & Balda, M. S. Functional analysis of tight junctions. *Methods* **30**, 228–234 (2003).
20. Furuse, M. *et al.* Occludin: a novel integral membrane protein localizing at tight junctions. *J Cell Biol.* **123**, 1777–1788 (1993).
21. Morita, K., Furuse, M., Fujimoto, K. & Tsukita, S. Claudin multigene family encoding four-transmembrane domain protein components of tight junction strands. *Proc Natl Acad Sci U S A* **96**, 511–516 (1999).
22. Martin-Padura, I. *et al.* Junctional adhesion molecule, a novel member of the immunoglobulin superfamily that distributes at intercellular junctions and modulates monocyte transmigration. *J Cell Biol.* **142**, 117–127 (1998).
23. Stevenson, B. R., Siliciano, J. D., Mooseker, M. S. & Goodenough, D. A. Identification of ZO-1: a high molecular weight polypeptide associated with the tight junction (zonula occludens) in a variety of epithelia. *J Cell Biol.* **103**, 755–766 (1986).
24. Jesaitis, L. A. & Goodenough, D. A. Molecular characterization and tissue distribution of ZO-2, a tight junction protein homologous to ZO-1 and the Drosophila discs-large tumor suppressor protein. *J Cell Biol.* **124**, 949–961 (1994).
25. Haskins, J., Gu, L., Wittchen, E. S., Hibbard, J. & Stevenson, B. R. ZO-3, a novel member of the MAGUK protein family found at the tight junction, interacts with ZO-1 and occludin. *J Cell Biol.* **141**, 199–208 (1998).
26. Citi, S., Sabanay, H., Jakes, R., Geiger, B. & Kendrick-Jones, J. Cingulin, a new peripheral component of tight junctions. *Nature* **333**, 272–276 (1988).
27. Matter, K. & Balda, M. S. Signalling to and from tight junctions. *Nat. Rev. Mol. Cell Biol.* **4**, 225–236 (2003).
28. Gonzalez-Mariscal, L., Tapia, R. & Chamorro, D. Crosstalk of tight junction components with signaling pathways. *Biochim. Biophys. Acta* **1778**, 729–756 (2008).
29. Evan, A. P. *et al.* Randall's plaque of patients with nephrolithiasis begins in basement membranes of thin loops of Henle. *J Clin. Invest* **111**, 607–616 (2003).
30. Bushinsky, D. A. Nephrolithiasis: site of the initial solid phase. *J Clin. Invest* **111**, 602–605 (2003).
31. Singh, A. K., Jiang, Y. & Gupta, S. Effects of chronic alcohol drinking on receptor-binding, internalization, and degradation of human immunodeficiency virus 1 envelope protein gp120 in hepatocytes. *Alcohol* **41**, 591–606 (2007).
32. Xia, W., Mruk, D. D., Lee, W. M. & Cheng, C. Y. Differential interactions between transforming growth factor-beta3/TbetaR1, TAB1, and CD2AP disrupt blood-testis barrier and Sertoli-germ cell adhesion. *J Biol. Chem.* **281**, 16799–16813 (2006).
33. Lui, W. Y., Wong, C. H., Mruk, D. D. & Cheng, C. Y. TGF-beta3 regulates the blood-testis barrier dynamics via the p38 mitogen activated protein (MAP) kinase pathway: an in vivo study. *Endocrinology* **144**, 1139–1142 (2003).
34. Chaturvedi, L. S. *et al.* Oxalate selectively activates p38 mitogen-activated protein kinase and c-Jun N-terminal kinase signal transduction pathways in renal epithelial cells. *J Biol. Chem.* **277**, 13321–13330 (2002).
35. Han, H. J., Lim, M. J. & Lee, Y. J. Oxalate inhibits renal proximal tubule cell proliferation via oxidative stress, p38 MAPK/JNK, and cPLA2 signaling pathways. *Am. J Physiol Cell Physiol* **287**, C1058–C1066 (2004).
36. Semenova, M. M. *et al.* Rho mediates calcium-dependent activation of p38alpha and subsequent excitotoxic cell death. *Nat. Neurosci.* **10**, 436–443 (2007).
37. Chaiyarit, S. & Thongboonkerd, V. Changes in mitochondrial proteome of renal tubular cells induced by calcium oxalate monohydrate crystal adhesion and internalization are related to mitochondrial dysfunction. *J Proteome. Res.* **11**, 3269–3280 (2012).
38. Ono, K. & Han, J. The p38 signal transduction pathway: activation and function. *Cell Signal* **12**, 1–13 (2000).
39. Oshima, T., Miwa, H. & Joh, T. Aspirin induces gastric epithelial barrier dysfunction by activating p38 MAPK via claudin-7. *Am. J Physiol Cell Physiol* **295**, C800–C806 (2008).
40. Zarubin, T. & Han, J. Activation and signaling of the p38 MAP kinase pathway. *Cell Res.* **15**, 11–18 (2005).
41. Basuroy, S., Seth, A., Elias, B., Naren, A. P. & Rao, R. MAPK interacts with occludin and mediates EGF-induced prevention of tight junction disruption by hydrogen peroxide. *Biochem. J* **393**, 69–77 (2006).
42. Rao, R. K., Baker, R. D., Baker, S. S., Gupta, A. & Holycross, M. Oxidant-induced disruption of intestinal epithelial barrier function: role of protein tyrosine phosphorylation. *Am. J Physiol* **273**, G812–G823 (1997).
43. Sheth, P., Basuroy, S., Li, C., Naren, A. P. & Rao, R. K. Role of phosphatidylinositol 3-kinase in oxidative stress-induced disruption of tight junctions. *J Biol. Chem.* **278**, 49239–49245 (2003).
44. Rodriguez, P., Heyman, M., Candalh, C., Blaton, M. A. & Bouchaud, C. Tumour necrosis factor-alpha induces morphological and functional alterations of intestinal HT29 cl.19A cell monolayers. *Cytokine* **7**, 441–448 (1995).
45. Tazuke, Y., Drongowski, R. A., Teitelbaum, D. H. & Coran, A. G. Interleukin-6 changes tight junction permeability and intracellular phospholipid content in a human enterocyte cell culture model. *Pediatr. Surg. Int.* **19**, 321–325 (2003).
46. Al Sadi, R. M. & Ma, T. Y. IL-1beta causes an increase in intestinal epithelial tight junction permeability. *J Immunol.* **178**, 4641–4649 (2007).
47. Li, Q. *et al.* Disruption of tight junctions during polymicrobial sepsis in vivo. *J Pathol.* **218**, 210–221 (2009).
48. Contreras, R. G. *et al.* E-Cadherin and tight junctions between epithelial cells of different animal species. *Pflugers Arch.* **444**, 467–475 (2002).
49. West, M. R., Ferguson, D. J., Hart, V. J., Sanjar, S. & Man, Y. Maintenance of the epithelial barrier in a bronchial epithelial cell line is dependent on functional E-cadherin local to the tight junctions. *Cell Commun. Adhes.* **9**, 29–44 (2002).

50. Lv, Z. M. *et al.* The role of the p38 MAPK signaling pathway in high glucose-induced epithelial-mesenchymal transition of cultured human renal tubular epithelial cells. *PLoS. One.* **6**, e22806 (2011).
51. Pasternak, A. S. & Miller, W. M. Measurement of trans-epithelial electrical resistance in perfusion: Potential application for in vitro ocular toxicity testing. *Biotechnol. Bioeng.* **50**, 568–579 (1996).
52. Costantini, T. W. *et al.* Role of p38 MAPK in burn-induced intestinal barrier breakdown. *J Surg. Res.* **156**, 64–69 (2009).
53. Thongboonkerd, V., Semangoen, T. & Chutipongtanate, S. Factors determining types and morphologies of calcium oxalate crystals: Molar concentrations, buffering, pH, stirring and temperature. *Clin. Chim. Acta* **367**, 120–131 (2006).
54. Thongboonkerd, V., Chutipongtanate, S., Semangoen, T. & Malasit, P. Urinary trefoil factor 1 is a novel potent inhibitor of calcium oxalate crystal growth and aggregation. *J Urol.* **179**, 1615–1619 (2008).
55. Fong-ngern, K., Chiangjong, W. & Thongboonkerd, V. Peeling as a novel, simple, and effective method for isolation of apical membrane from intact polarized epithelial cells. *Anal. Biochem* **395**, 25–32 (2009).

Acknowledgements

This study was supported by Office of the Higher Education Commission and Mahidol University under the National Research Universities Initiative, and The Thailand Research Fund (RTA5380005) to VT. PP is supported by the Royal Golden Jubilee PhD Program of The Thailand Research Fund, whereas VT is also supported by "Chalermphrakiat" Grant and Faculty of Medicine Siriraj Hospital.

Author contributions

PP and VT designed research; PP performed experiments; PP and VT analyzed data; PP and VT wrote the manuscript.

Additional information

Supplementary information accompanies this paper at http://www.nature.com/scientificreports

Competing financial interests: The authors declare no competing financial interests.

License: This work is licensed under a Creative Commons Attribution-NonCommercial-NoDerivs 3.0 Unported License. To view a copy of this license, visit http://creativecommons.org/licenses/by-nc-nd/3.0/

How to cite this article: Peerapen, P. & Thongboonkerd, V. p38 MAPK mediates calcium oxalate crystal-induced tight junction disruption in distal renal tubular epithelial cells. *Sci. Rep.* **3**, 1041; DOI:10.1038/srep01041 (2013).

World Journal of Gastroenterology

Online Submissions: http://www.wjgnet.com/esps/
wjg@wjgnet.com
doi:10.3748/wjg.v19.i31.5067

World J Gastroenterol 2013 August 21; 19(31): 5067-5075
ISSN 1007-9327 (print) ISSN 2219-2840 (online)
© 2013 Baishideng. All rights reserved.

ORIGINAL ARTICLE

Serum proteins in chronic hepatitis B patients treated with peginterferon alfa-2b

Sunida Kuakarn, Poorichaya SomParn, Pisit Tangkijvanich, Varocha Mahachai, Visith Thongboonkerd, Nattiya Hirankarn

Sunida Kuakarn, Medical Microbiology, Interdisciplinary Program, Graduate School, Chulalongkorn University, Bangkok 10330, Thailand
Poorichaya SomParn, Nattiya Hirankarn, Immunology Unit, Department of Microbiology, Faculty of Medicine, Chulalongkorn University, Bangkok 10330, Thailand
Pisit Tangkijvanich, Department of Biochemistry, Faculty of Medicine, Chulalongkorn University, Bangkok 10330, Thailand
Varocha Mahachai, Department of Medicine, Faculty of Medicine, Chulalongkorn University, Bangkok 10330, Thailand
Visith Thongboonkerd, Medical Proteomics Unit, Office for Research and Development, Faculty of Medicine Siriraj Hospital, Mahidol University, Bangkok 10700, Thailand
Visith Thongboonkerd, Center for Research in Complex Systems Science, Mahidol University, Bangkok 10700, Thailand
Author contributions: Kuakarn S performed the majority of experiments; SomParn P and Thongboonkerd V provided analytical tools and were also involved in editing the manuscript; Tangkijvanich P and Mahachai V provided the collection of samples in addition to providing financial support for this work; Hirankarn N designed the study and wrote the manuscript.
Supported by The 90th Anniversary of Chulalongkorn University Fund (Ratchadaphiseksomphot Endowment Fund); The Thailand Research Fund, No. RMU5180051; The Thailand Research Fund Senior Research Scholarship, No. RTA5380005; The Higher Education Research Promotion and National Research University Project of Thailand, Office of the Higher Education Commission, No. HR1163A; Integrated Innovation Academic Center, Chulalongkorn University Centenary Academic Development Project, No. CU56-HR05, The Liver Research Unit, Chulalongkorn University
Correspondence to: Nattiya Hirankarn, MD, PhD, Immunology Unit, Department of Microbiology, Faculty of Medicine, Chulalongkorn University, 254 Phayathai Road, Pathumwan, Bangkok 10330, Thailand. nattiyap@gmail.com
Telephone: +66-2-2564132 Fax: +66-2-2525952
Received: January 21, 2013 Revised: June 6, 2013
Accepted: June 19, 2013
Published online: August 21, 2013

Abstract

AIM: To study the differential protein profile in serum of hepatitis B patients.

METHODS: Serum samples were obtained from patients with chronic hepatitis B who were receiving peginterferon alfa-2b. The serum samples were subjected to albumin depletion and analyzed by two-dimensional gel electrophoresis (2-DE). Differentially expressed protein spots were identified by electrospray ionization-quadrupole time-of-flight mass spectrometry. Alpha-2-HS-glycoprotein, complement component C3c and CD5 antigen were further analyzed by an enzyme-linked immunosorbent assay and immunonephelometry.

RESULTS: Nineteen patients with HBeAg-positive chronic hepatitis B (CHB) were studied. These patients were followed for at least 1 year after treatment and were classified according to their treatment response: responders (n = 9) and non-responders (n = 10). 2-DE and MS/MS analysis were performed to compare the serum proteins before initiating peginterferon alfa-2b. From the quantitative analysis of the 2-D gel, 7 proteins were detected between the two groups at different levels before treatment. Among these potential candidates, serum levels of alpha-2-HS-glycoprotein, complement component C3c and CD5 antigen-like precursor were further analyzed. In the validation phase, 23 subjects, 9 sustained responders and 14 non-responders, were recruited. Interestingly, the levels of alpha-2-HS-glycoprotein and complement component C3c were elevated in the serum of the non-responders compared to the responders.

CONCLUSION: Serum alpha-2-HS-glycoprotein and

complement component C3c may be potential serum biomarkers in predicting the treatment response of peginterferon alfa-2b in patients with CHB prior to treatment.

© 2013 Baishideng. All rights reserved.

Key words: Proteomics; Peginterferon alfa-2b; Chronic hepatitis B; Alpha-2-HS-glycoprotein; Serum

Core tip: Serum proteins serve as non-invasive biomarkers for several diseases. This is the first report on the potential use of common protein levels in the serum of chronic hepatitis B (CHB) patients to predict treatment responsiveness to peginterferon alfa-2b. We identified 2 potential serum biomarkers, alpha-2-HS-glycoprotein and complement component C3c, that can be used to predict treatment outcome in patients with CHB receiving peginterferon alfa-2b. The identification of these biomarkers prior to treatment is preferable in order to avoid systemic side effects due to interferon therapy.

Kuakarn S, SomParn P, Tangkijvanich P, Mahachai V, Thongboonkerd V, Hirankarn N. Serum proteins in chronic hepatitis B patients treated with peginterferon alfa-2b. *World J Gastroenterol* 2013; 19(31): 5067-5075 Available from: URL: http://www.wjgnet.com/1007-9327/full/v19/i31/5067.htm DOI: http://dx.doi.org/10.3748/wjg.v19.i31.5067

INTRODUCTION

One of the most common health care problems encountered worldwide is hepatitis B virus (HBV) infection which can progress to liver fibrosis, liver cirrhosis and liver cancer (also known as hepatocellular carcinoma). Treatment for chronic hepatitis B includes immunomodulatory agents and antiviral drugs such as nucleoside or nucleotide analogs (NAs). NAs inhibit the replication process of the virus by inhibiting its DNA polymerase[1], whereas immunomodulating therapy mainly includes treatment with interferon-α and pegylated interferon-α. The treatment duration, eradication and lack of drug resistance strains make type 1 interferons ideal for the treatment of chronic HBV[2]. Unfortunately, only 30% of patients will respond to treatment with interferon type 1[3]. The reason for this is because other factors, including the virus and the host, can significantly influence the treatment outcome. Viral factors such as the level of HBV DNA, HBV genotype, levels of hepatitis B surface antigen and hepatitis B core antigen (HBeAg), and HBV viral mutants can affect the outcome of therapy[4,5]. Other factors such as low levels of viral HBV DNA, higher levels of alanine aminotransferase (ALT), older age, being female, and naive to interferon therapy have been shown to be significantly associated with sustainable virological response among HBeAg-positive chronic hepatitis B (CHB) patients[6]. In HBeAg-negative patients, younger age, being female, having high levels of ALT and low levels of viral HBV DNA have been associated with sustainable virological response[7]. In addition, genetic host factors such as human leukocyte antigen (HLA) class Ⅱ (HLA-DRB1*14 allele), presence of polymorphism A (MxA)-88, levels of interleukin-10 and interleukin-12 have been proposed to predict the patient's treatment response after therapy[8-10]. The use of biomarkers is invaluable in predicting treatment response as well as being cost-effective in managing patients with CHB.

Various biomarkers for hepatocellular carcinoma (HCC)[11-13], HBV inflammation, HBV liver cirrhosis[14,15], and hepatitis C virus treatment response[16] have been investigated using proteomics, however, there are no predictive data for the treatment of CHB. One report from MA Hui and colleagues identified a potential serum biomarker for detecting changes after treatment, but was not able to predict the treatment outcome prior to treatment[17]. In the present study, albumin and immunoglobulin G (IgG) depleted serum was subjected to 2-dimensional gel electrophoresis and mass spectrometry. We identified 2 potential serum biomarkers, alpha-2-HS-glycoprotein and complement component C3c, and found that they can be used to predict treatment outcome in patients with CHB receiving peginterferon alfa-2b.

MATERIALS AND METHODS

Serum samples

Serum samples were obtained from patients with CHB who were followed at the King Chulalongkorn Memorial Hospital. All patients received peginterferon alfa-2b (1.5 mg/kg per week) subcutaneously for 48 wk and their responses to this treatment were assessed. These patients were followed for at least 1 year after treatment and were classified as sustained responders or non-responders. Sustained virological response among HBeAg-positive patients was characterized by undetectable HBeAg, detectable anti-HBe (HBeAg seroconversion) and HBV viral load < 2000 IU/mL 48 wk after treatment[18]. Patients without sustained virological response were classified as non-responders. Serum samples were obtained before initiating peginterferon alfa-2b treatment and at 24 wk after treatment.

Study population used to screen for biomarkers

Nineteen patients with HBeAg-positive CHB (9 sustained responders and 10 non-responders) were included in the proteomic study before initiating treatment. After 24 wk of treatment, 6 patients (3 sustained responders and 3 non-responders) were included.

Study population used to validate the system

Another 23 subjects, 9 sustained responders and 14 non-responders, were enrolled in the validation phase of the proteomic study using an enzyme-linked immunosorbent assay (ELISA) and immunonephelometry.

All studies were approved by the Institutional Review Board, Faculty of Medicine, Chulalongkorn University,

Bangkok, Thailand. Informed consent forms were collected from all patients from both phases of the study before any of the procedures were initiated.

Optimization of 2D-gel electrophoresis for pretreatment serum

Albumin and IgG were removed from the patient's serum using the ProteoPrep Blue Albumin Depletion Kit (Sigma: PROTBA) according to the company's protocol. Protein concentrations were measured by the Bio-Rad Bradford total protein assay kit (Biorad Laboratories, Inc., Redmond, WA, United States)[19] using bovine serum albumin (BSA) as the standard curve.

Two-dimensional gel electrophoresis and image analysis

The Immobiline Dry strip (pH 4-7, length 7 cm, Amersham Biosciences, Uppsala, Sweden) was rehydrated with 150 μg protein in 125 μL rehydration buffer containing 9 mol urea, 2% CHAPS, 0.002% w/v bromophenol blue, 0.8% (w/v) DTT, 1% IPG buffer for 14 h at room temperature. Iso-electric focusing (IEF) was performed by IPG ph or IEF apparatus (Amersham Biosciences, Uppsala, Sweden) with a total of 8000 Vhrs. The strip was then equilibrated in equilibration buffer containing 6 mol/L urea, 30% glycerol, 2% SDS, 0.002% bromophenol blue and 50 mmol/L Tris-HCl (pH = 8.8) with 135 mmol/L DTT for 15 min followed by incubation, but replacing with 130 mmol/L iodoacetamide for 15 min. Next, the equilibrated strips were placed on the sodium dodecyl sulfate polyacrylamide gel electrophoresis (SDS-PAGE) composed of 12.5% acrylamide and sealed with 0.5% (w/v) agarose. The SDS-PAGE was run on constant electric field, 15 mA per gel, using the SE 260 Mini-Vertical Units (GE Healthcare, Uppsala, Sweden) until the bromophenol blue tracking dye reached the bottom of the gel. Protein spots were stained with Coomassie Brilliant Blue G-250 stain[20]. The stained gels were scanned with an ImageMaster scanner (GE Healthcare; Uppsala, Sweden). Intensity analysis was carried out using the software, Image Master 2D Platinum (GE Healthcare, Uppsala, Sweden).

Tryptic digestion of the gels

Differentially expressed protein spots were excised from the 2-DE gels and subjected to in-gel tryptic digestion according to the method modified from Katayama *et al*[21]. The gel pieces were destained with 50% methanol and 50 mmol ammonium bicarbonate, and dehydrated with 100% acetonitrile (ACN). The gel pieces were reduced and alkylated in 10 mmol/L of DTT and 100 mmol/L iodoacetamide at room temperature for 1 h. They were then dehydrated twice with 100% ACN for 5 min after alkylation. The gel pieces were subsequently digested in 10 μL trypsin (modified porcine trypsin, sequencing grade, Promega, Madison, WI, United States) solution (20 ng in 10 mmol/L ammonium bicarbonate in 50% ACN) and incubated at room temperature overnight. The peptides were extracted twice by adding 30 μL of solution containing 50% ACN and 0.1% formic acid. The extracted solutions were dried in a heat box at 40 ℃ and kept at -80 ℃ for further analysis by mass spectrometry. Prior to mass spectrometry analysis, the peptide mixtures were reconstituted in 10 μL of 0.1 % formic acid.

Protein identification by LC/MS/MS analysis

Peptide mixtures were analyzed by ultra-performance liquid chromatography (UPLC) (Ultimate 3000, Dionex, united states) coupled to the micrOTOF-Q Ⅱ ™ ESI-Qq-TOF mass spectrometer (Bruker Daltonics, Germany) equipped with an online nanoESI source. The peptide mixture was injected onto a μ-precolumn cartridge (C18 PepMap; 300 μmol/L × 5 mm; 5 μmol/L particle size) composed of peptides, concentrated and then directly separated using a PepMap100 C18 analytical column (5 μm particle size, with 100 Å pore size). The mobile phase was run for each sample using a linear gradient of 10%-55% of 80% ACN in high performance liquid chromatography (HPLC) water for 30 min, with a hold of 15 min at 90% of 80% ACN in HPLC water, followed by a step to 10% of 80% ACN in HPLC water, hold of 20 min. The Q-TOF instrument was operated in positive ionization mode to switch automatically between MS and MS/MS acquisition. The precursor ion (MS) and fragmentation ion (MS/MS) with a mass range were 400-1600 m/z and 50-3000 m/z, respectively. The source parameters were as follows: capillary 2.0 kV, dry gas 0.3 L/min and dry temperature at 150 ℃ . The MS and MS/MS spectrometry data were processed using data analysis software (Bruker Daltonics, Germany) and searched against the NCBInr database using the MASCOT search engine. The parameters were identified using the following set up: species-homo sapiens; enzyme-trypsin; allowed up to 1 missed cleavage; fixed modification-carbamidomethylation on cystenine; variable modification-oxidation on methionines. The peptide mass tolerance and fragment mass tolerance were set at 1.2 Da and 0.6 Da, respectively[15]. A probability-based Mowse score of more than 43 was considered significant ($P < 0.05$).

Validation of the proteomic data by ELISA and immunonephelometry

Validation of the proteomic study was performed in a different population ($n = 23$) composed of 9 sustained responders and 14 non-responders. ELISA was performed according to the company's protocol using the Alpha 2 HS Glycoprotein Human ELISA kit (Abcam, Cambridge, United Kingdom) and human CD5 antigen like (CD5L) ELISA kit (Cusabio Biotech., Ltd., China). Complement component C3c was further validated using immunonephelometry and the BN ProSpec system (Siemens Healthcare Diagnostics Products GmbH, Germany).

Statistical analysis

SPSS version 17.0 (SPSS Inc., Chicago, IL, United States) was used for all statistical analyses. The values of the intensities of the spots are shown as the mean ± SE. In-

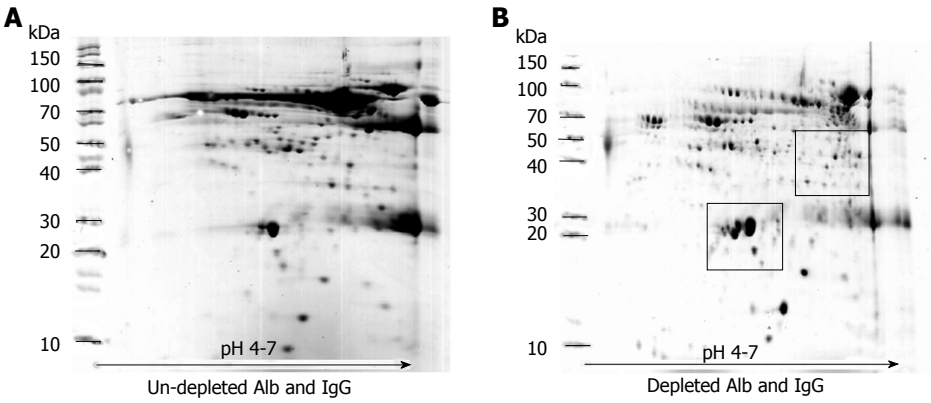


Figure 1 Serum samples from chronic hepatitis B virus-infected patients were run on two-dimensional gels (linear immobilized pH gradients; pH 4-7; 7 cm length). The pictures of the gels show the results before (A) and after (B) treatment using the ProteoPrep Blue Albumin Depletion kit. IgG: Immunoglobulin G; Alb: Albumin.

Table 1 Baseline characteristics of the patients used for screening the biomarkers before initiating chronic hepatitis B therapy (mean ± SE)

	Sustained virological responders (n = 9)	Non-responders (n = 10)	P value
Age (yr)	29.67 ± 8.29	36.90 ± 6.40	0.047
Sex (male:female)	7:2	8:2	0.912
ALT level (U/L)	103.88 ± 105.04	130.50 ± 75.77	0.609
HBV DNA (copies/mL)	(11.07 ± 8.52) × 10^6	(14.35 ± 8.44) × 10^6	0.511
HBeAg	Positive	Positive	NS

HBV: Hepatitis B virus; ALT: Alanine aminotransferase; HBeAg: Hepatitis B e antigen; NS: Not significant.

dependent sample t test was used to evaluate the baseline characteristics of the patients and compare the intensity data of each matched protein spot between the sustained responders and non-responders; the P value cut-off for the independent sample t test was 0.05. Mann-Whitney U test was used to evaluate the different protein expressions between the two groups 24 wk after treatment. For the Mann-Whitney U test, any proteins identified with $P <$ 0.05 were considered significant. The independent sample t test was performed during the validation phase to compare the different levels of alpha-2-HS-glycoprotein. The Mann-Whitney U test was also performed in the validation phase to compare the different levels of complement component C3c and CD5 antigen like proteins. The Pearson correlation was carried out on age and each protein expression value to determine if age had an influence on the expression of the proteins.

RESULTS

Characteristics of the study population in the screening phase

Basic characteristics of the patients are shown in Table 1. The number of men and women, levels of serum ALT and HBV DNA, and presence of HBeAg were comparable between the two groups. However, non-responders were older than the sustained responders.

Optimization of 2D-gel electrophoresis for pretreatment serum

Before performing electrophoresis on the collected serum, the efficiency of the ProteoPrep Blue Albumin Depletion Kit was determined. Figure 1 shows the two representative maps of the serum samples (chronic HBV infection) before and after treatment with the ProteoPrep Blue Albumin Depletion Kit. In the untreated sample, levels of albumin and IgG in serum were approximately 60%-70% and 10%-20%, respectively (Figure 1A). When an equal quantity of protein was pre-treated with ProteoPrep Blue Albumin Depletion Kit, the resolution of the 2D-gels dramatically improved and several spots of other less abundant proteins became visible (Figure 1B).

Comparisons of the expressed proteins between the sustained responders and non-responders before initiating peginterferon alfa-2b treatment

The results of the protein separation by 2D-gel electrophoresis, gel digestion and protein identification by LC/MS/MS are shown in Figure 2. Seven protein spots were detected with various intensities in the patients (Table 2 and Figure 2). Four proteins were significantly detected among the sustained responders: (1) chain A, alpha-1-antitrypsin; (2) albumin, isoform CRA-b; (3) CD5 antigen-like precursor; and (4) albumin. Three proteins were significantly detected among the non-responders: (1) chain A, crystal structure of lipid-free human apolipoprotein A-I; (2) chain C, human complement component C3c; and (3) alpha-2-HS-glycoprotein. Since the sustained responders and non-responders showed significant age differences, the Pearson correlation was used for age and each protein expression value. No significant correlation between age and protein expression was observed; therefore, it is unlikely that age affected protein expression in this study. The identified proteins have the following functions: alpha-1-antitrypsin is a protease inhibitor, serum albumin is a transport and binding protein, alpha-2-HS-glycoprotein is an acute phase response protein, CD5 antigen precursor and complement component C3c are immune protection proteins, and the human apolipoprotein A-I has a role in lipid metabolism

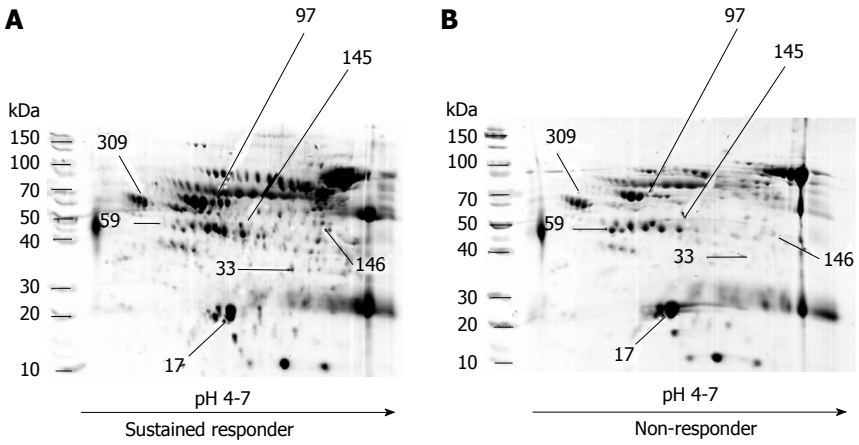


Figure 2 Serum protein spots from the 2-DE gels were significantly different. A: Sustained responders; B: Non-responders before chronic hepatitis B treatment.

Table 2 Proteins found to be significantly different between the sustained responders and non-responders before initiating peginterferon-Interferon alfa-2b treatment

Spot	Protein	NCBI ID	MS score	%cov	pI	MW	Relative intensity (mean ± SE)		SVR/NR	*P* value
							SVR	NR		
Protease inhibitor										
97	Chain A, alpha-1-antitrypsin	Gi|157831596	399	64	5.37	44.28	0.2764 ± 0.0327	0.4275 ± 0.0609	2.34	0.038
Transport protein and protein binding										
33	Albumin, isoform	Gi|119626065	539	38	6.96	61.12	0.0330 ± 0.0121	0.0764 ± 0.0144	2.31	0.033
146	Albumin	Gi|332356380	243	41	5.73	68.48	0.0602 ± 0.0182	0.1516 ± 0.0333	2.52	0.024
Acute phase protein										
309	Alpha-2-HS-glycoprotein	Gi|112910	507	40	5.43	40.09	0.7165 ± 0.0238	0.4782 ± 0.0851	0.67	0.012
Immunity protection										
59	Chain C, human complement C3c	Gi|78101271	513	70	4.79	40.20	0.3969 ± 0.0391	0.2675 ± 0.0403	0.67	0.034
145	CD5 antigen-like precursor	Gi|5174411	443	67	5.28	39.60	0.1086 ± 0.0192	0.1903 ± 0.0197	1.75	0.009
Lipid metabolism										
17	Chain A, crystal structure of lipid-free human apoliprotein A-I	Gi|90108664	1347	78	5.27	28.06	9.4993 ± 0.5044	6.0364 ± 1.0047	0.64	0.005

SVR: Sustained virological response; NR: Non-responder.

Characteristics of the patients from the validation phase of the proteomic study and immunonephelometry

In the validation phase, nine and 14 patients with sustained virological response and nonresponders were enrolled, respectively. The sex ratio, levels of serum and HBV DNA, and HBeAg were not significantly different, but there was a significant difference in age between the groups (Table 3).

Validation of proteins associated with the immune response

We selected 3 proteins (alpha-2-HS-glycoprotein**,** complement component C3c, and CD5 antigen-like proteins) that were significantly different between the 2 groups, and have functions related to immune response for further validation (Figure 3). According to the ELISA results, the serum levels of alpha-2-HS-glycoprotein were significantly elevated among the non-responders when compared to the sustained responders at baseline (Figure 4A). Similarly, the immunonephelometry results showed that serum levels of complement component C3c were significantly elevated in the non-responders when compared to the sustained responders at baseline (Figure 4B), however, the serum levels of CD5 antigen like proteins were comparable between the two groups (Figure 4C). No significant correlation between age and protein expression was observed.

Comparison of the identified proteins after 24 wk of peginterferon alfa-2b treatment

A total of 6 patients, divided into 2 groups, were included in the analysis 24 wk post-treatment. The clinical data were not significantly different between the 2 groups (Table 3). The samples were separated by 2D-gel electrophoresis, and identified by LC/MS/MS. Thirteen protein spots were significantly changed at 24 wk after treatment among the patients in the sustained response group, whereas 6 were found in the non-responders (Table 4). Interestingly, all 13 proteins in the sustained response group which were increased at 24 wk were composed of cholesterol metabolites, proteins from the acute phase response, protease inhibitors, transport proteins and immune protection. Of these, alpha-2-HS-glycoprotein was higher than the baseline level in the responder group. In the non-responder group, levels of proapoliprotein, chain A of human antithrombin Ⅲ complex and alpha-1-B-glycoprotein were higher than the baseline level, whereas

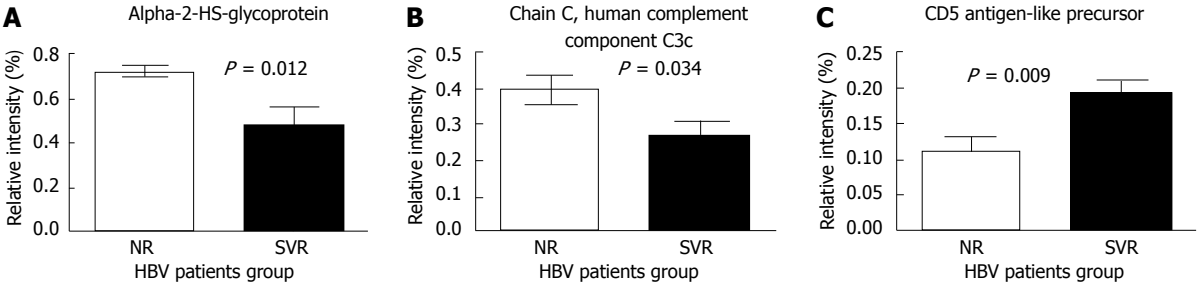


Figure 3 Histograms of the proteomic analysis at different levels. A: Alpha-2-HS-glycoprotein; B: Complement component C3c; C: CD5 antigen-like proteins in sustained responders and non-responders before chronic hepatitis B treatment. The intensity data are presented as mean ± SE (n = 19 gels from all patients and groups). SVR: Sustained virological response; NR: Non-responder.

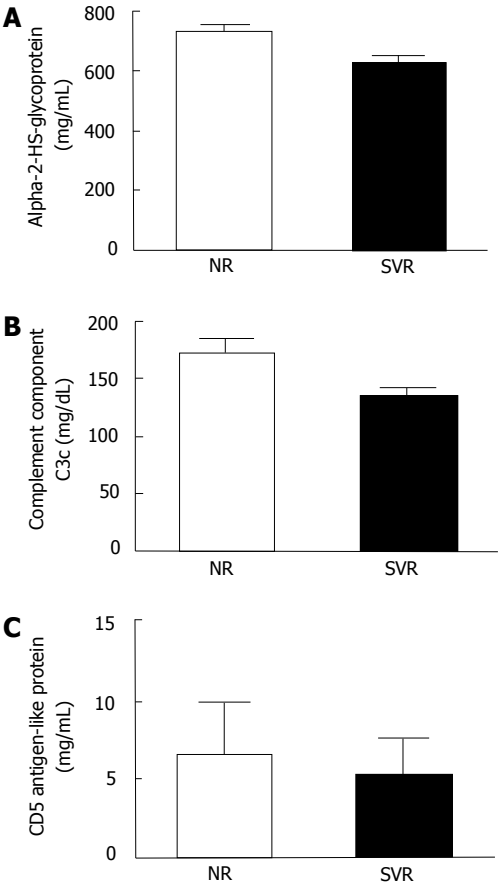


Figure 4 Validation of proteins associated with the immune response. A: Validation by enzyme-linked immunosorbent assay showed that there were elevated levels of alpha-HS-glycoprotein in non-responders before chronic hepatitis B treatment. n = 19 gels from all patients and groups; B: Validation by immunonephelometry showed elevated levels of complement component C3c in non-responders before chronic hepatitis B treatment; C: Validation by immunonephelometry showed elevated levels of CD5 antigen-like proteins in non-responders before chronic hepatitis B treatment. SVR: Sustained virological response; NR: Non-responder.

levels of albumin and alpha-2-HS-glycoprotein decreased 24 wk post-treatment.

DISCUSSION

The proteomic approach is usually used to analyze protein expression. It can be used with various specimens such as tissue, serum, plasma or body fluids. For this study, serum samples were used to identify potential biomarkers that can be further applied to predict the outcome of CHB therapy. Serum was selected because the collection process is non-invasive and proteins from the liver are secreted into the serum. Therefore, serum is an ideal specimen to screen for new proteins or biomarkers. In addition, serum proteomics can be used to detect post-translational modified proteins. 2-DE was used to separate and identify the proteins between 10-200 kDa. The high sensitivity and high throughput of mass spectrometry has resulted in the detection of several new biomarkers in ovarian cancer, prostate cancer, breast cancer and hepatocellular carcinoma. However, it should be noted that 2-DE does have limitations. 2-DE cannot detect low abundant proteins because high abundant proteins such as albumin and IgG can suppress the detection of low abundant proteins. To overcome this obstacle, albumin and IgG were removed from the serum samples before electrophoresis using the ProteoPrep Blue Albumin Depletion Kit. Albumin (-45 mg/mL) and IgG (-10 mg/mL) are the two major protein components of serum, representing 60%-70% and 10%-20% of the total serum protein, respectively[22]. When the high abundant

Table 3 Baseline characteristics of the patients in the validation phase and at 24 wk of treatment (mean ± SE)

	Sustained virological responders	Non-responders	*P* value
Validation phase	(n = 9)	(n = 14)	
Age (yr)	29.56 ± 2.78	37.71 ± 1.97	0.023
Sex (male:female)	7:2	11:3	0.966
ALT level (U/L)	106.88 ± 36.26	130.50 ± 30.93	0.644
HBV DNA (copies/mL)	(11.06 ± 2.84) × 10^6	(13.12 ± 2.45) × 10^6	0.593
HBeAg	Positive	Positive	NS
24 wk	(n = 3)	(n = 3)	
Age (yr)	29.33 ± 6.89	35.67 ± 6.06	NS
Sex (male:female)	Male	Male	NS
ALT level (U/L)	52.33 ± 13.78	253.67 ± 187.74	NS
HBV DNA (copies/mL)	(6.70 ± 6.65) × 10^6	(13.65 ± 6.35) × 10^6	NS
HBeAg	Positive	Positive	NS

HBV: Hepatitis B virus; ALT: Alanine aminotransferase; HBeAg: Hepatitis B e antigen; NS: Not significant.

Table 4 Serum levels of proteins after 24 wk of treatment in the sustained virological responders and non-responders

Spot	Protein Name	NCBI ID	MW/pI	No. of match peptide	MS score	Fold change	Δ relative intensity	Biological function
Sustained virological response								
38	Proapolipoprotein	Gi|178775	28.94/5.50	63	798	↑ 5.17	0.1525[a]	Cholesterolmetabolism
26	Chain A, the structure of pentameric human serum amyloid P	Gi|576259	23.36/6.12	12	174	↑ 6.65	0.0783[a]	Acute phase protein
86	Alpha-2-HS-glycoprotein	Gi|112910	40.098/5.43	32	494	↑ 2.39	0.3773[a]	
309	Alpha-2-HS-glycoprotein	Gi|112910	40.09/5.43	29	507	↑ 2.04	0.4987[a]	
171	Chain A, the intact and cleaved Ⅲ complex as a model for serpin-proteinase interaction	Gi|999513	49.35/5.95	37	396	↑ 9.66	0.1481[b]	
173	Chain A, the intact and cleaved Ⅲ complex as a model for serpin-proteinase interaction	Gi|999513	49.35/5.95	26	210	↑ 8.01	0.0694[a]	Protease inhibitor
149	Serotransferin precursor	Gi|4557871	79.28/6.81	58	650	↑ 3.43	0.1165[a]	
201	PRO2619	Gi|11493459	58.51/5.96	36	278	↑ 4.95	0.0594[a]	Transport protein and proteinbinding
207	Albumin	Gi|332356380	68.48/5.73	48	781	↑ 6.97	0.1653[a]	
280	Albumin	Gi|332356380	68.48/5.73	31	201	↑ 7.33	0.1206[a]	
202	CD5 antigen-like precursor	Gi|5174411	39.60/5.28	11	70	↑ absent at baseline	0.0348[a]	
229	Ig J-chain	Gi|532598	16.04/4.62	3	42	↑ absent at baseline	0.0923[b]	Immunity protection
299	Immunoglobulin light	Gi|218783338	24.16/5.95	26	747	↑ absent at base line	0.1709[b]	
Non-responder								
20	Proapolipoprotein	Gi|178775	28.94/5.45	63	798	↑ absent at base line	0.2383[b]	Cholesterol metabolism
171	Chain A, the intact and cleaved Ⅲ complex as a model for serpine-proteinase interaction	Gi|999513	49.35/5.95	37	396	↑ 2.39	0.0896[a]	Acute phase protein
4	Albumin isoform	Gi|119626066	27.67/6.39	20	660	↓ 0.04	-0.2832[a]	Transport protein and protein binding
264	Serum albumin	Gi|62113341	71.09/5.85	21	115	↓ absent at 24 wk	-0.1196[a]	
123	Alpha-1-B-glycoprotein	Gi|69990	52.47/5.69	27	247	↑ 1.38	0.1610[a]	Serum protein
310	Alpha-2-HS-glycoprotein	Gi|112910	40.09/5.43	30	475	↓ 0.46	-0.4119[a]	Acute phase protein

Relative intensity, [(volume of spot/volume of all the spots in the gel) × 100]. [a]$P < 0.05$, [b]$P < 0.01$ *vs* relative intensity.

proteins were depleted from the serum, this allowed the low abundant protein spots to become visible. However, it is also possible to miss certain low abundant proteins when the high abundant proteins are removed[23]. The reason for this is that low abundant proteins sometimes bind themselves to high abundant proteins. Hence, only albumin and IgG were removed in order to prevent the loss of other important proteins[24]. As expected, in the untreated sample, albumin dominated the gel, obscuring signals from other less abundant proteins. When an equal quantity of protein was pre-treated with the ProteoPrep Blue Albumin Depletion Kit, the resolution of the 2D-gels significantly improved. This process cannot completely eliminate all albumin, but can eliminate enough to allow several protein spots to be clearly visible. Using these techniques, a total of seven protein spots were found to be differentially expressed in the serum of CHB patients, 9 sustained responders and 10 non-responders, before starting peginterferon alfa-2b treatment. Interestingly, four of the proteins were higher in the sustained responders. Of these proteins, only 3 were involved in immune responses: alpha-2-HS-glycoprotein, complement component C3c and CD5 antigen-like proteins. We further validated the proteomic results using the sensitive ELISA and nephelometry assay. In the validation phase of the study, the serum levels of alpha-2-HS-glycoprotein and complement component C3c were significantly higher in the non-responders when compared to the sustained responders. However, the level of CD5 antigen-like protein was not statistically different between the two groups. Since the band intensity of this protein was lower than the other proteins and the level was detected only in the validation phase of the study when the abundant proteins were not depleted, it is possible that the level of CD5 antigen-like protein may have altered when albumin and IgG were removed.

Based on these findings, the authors believe that alpha-2-HS-glycoprotein and complement component C3c are potential serum pre-treatment biomarkers in predicting sustained virological response in CHB patients treated with peginterferon alfa-2b. In this study, the levels of serum alpha-2-HS-glycoprotein were elevated in the non-responders before treatment initiation, whereas the levels were much lower in the sustained responders. In addition, we performed a subsequent serum proteomic analysis in a subset of samples at 24 wk after peginterferon alfa-2b treatment. Serum alpha-2-HS-glycoprotein was also up-regulated in the sustained virological responders, but downregulated in the non-responders. This finding is consistent with the results reported earlier by Ma *et al*[17]. However, a previous study only detected changes after treatment, but was not able to predict the treatment out-

come prior to treatment. The identification of biomarkers prior to treatment is preferable in this case to avoid systemic side effects due to interferon therapy.

Alpha-2-HS-glycoprotein is a high abundant protein produced by the liver and osteoblasts and is usually concentrated in the mineralized tissues. This protein belongs to the cystatin super family[25]. Several studies have reported various levels of alpha-2-HS-glycoprotein in patients with liver diseases[26-28]. Some have found low levels of serum alpha-2-HS-glycoprotein in patients with acute drug-induced hepatitis, alcoholic hepatitis, chronic autoimmune hepatitis, primary biliary cirrhosis, fatty liver and HCC[26,28]. Aside from its multiple functions and ability to affect metabolic diseases, tumor and sepsis[29,30], Dai *et al*[31] reported that it was an independent marker for liver injury and a prognostic marker for CHB. They suggested that the protein may decrease liver inflammation by inhibiting the release of inflammatory factors from activated peripheral blood mononuclear cells[31]. Similarly, Patel *et al*[32] found reduced levels of alpha-2-HS-glycoprotein in chronic hepatitis C patients identified as sustained virological responders before initiating treatment. The reduced levels of alpha-2-HS-glycoprotein in chronic hepatitis C[32] and B patients identified as sustained virological responders before treatment suggest that this protein may potentially be used as a biomarker in predicting the outcome of peginterferon alfa-2b treatment.

Another protein detected in this study was complement component C3c which is the degradation product of complement C3. This protein is important for both the acquired and innate immune systems, especially against microbial infection as it switches the cellular responses from cell death to opsonization[33]. 80%-90% of complement is produced by hepatocytes and is associated with the pathogenesis of many chronic human diseases such as autoimmune diseases, complement-mediated hemolytic anemia, vascular and liver diseases[33,34]. Interestingly, low levels of C3 fragments were detected in HBV and HCC patients compared to normal, healthy controls[11]. According to the results obtained from the screening and validation phases of this study, the expression and levels of complement component C3c were elevated in non-responders before treatment. Thus, complement component C3c may be a possible biomarker in predicting the outcome of peginterferon alfa-2b treatment in patients with CHB.

In conclusion, alpha-2-HS-glycoprotein and complement component C3c proteins were elevated in non-responders indicating that these proteins may be potential biomarkers in predicting the response to peginterferon alfa-2b treatment in patients with CHB prior to treatment. However, external validation is needed to assess the clinical applicability of these two proteins as predictors of anti-HBV treatment outcome.

COMMENTS

Background

The treatment duration, eradication and lack of drug resistance strains make type 1 interferons ideal for the treatment of chronic hepatitis B virus. Unfortunately, only 30% of patients will respond to treatment with interferon type 1. To date, there is no effective predictor of interferon responsiveness.

Research frontiers

The authors identified 2 potential serum biomarkers, alpha-2-HS-glycoprotein and complement component C3c, and determined that they can be used to predict treatment outcome in patients with chronic hepatitis B (CHB) receiving peginterferon alfa-2b.

Innovations and breakthroughs

Serum proteins serve as non-invasive biomarkers for several diseases. This is the first report of the potential use of common protein levels in the serum of CHB patients to predict responsiveness to peginterferon alfa before treatment. The identification of biomarkers prior to treatment is preferable in this case to avoid systemic side effects due to interferon therapy.

Applications

These 2 serum proteins can be added to the list of potential biomarkers to predict responsiveness to peginterferon alfa. However, these findings require further validated using a larger sample size and other independent studies.

Peer review

The authors examined the differential protein profile in serum of hepatitis B patients before treatment with peginteferon-2b. From the quantitative analysis of the 2D-gel and validation step using Enzyme-linked immunosorbent assay and immunonephelometry, serum levels of alpha-2-HS-glycoprotein and complement component C3c were elevated in the serum of the non-responders compared to the responders. This indicated that these 2 serum proteins may be potential serum biomarkers in predicting the treatment response in CHB patients on peginterferon alfa-2b therapy.

REFERENCES

1 **Nguyen T**, Locarnini S. Hepatitis: Monitoring drug therapy for hepatitis B--a global challenge? *Nat Rev Gastroenterol Hepatol* 2009; **6**: 565-567 [PMID: 19789570 DOI: 10.1038/nrgastro.2009.160]

2 **Liu CJ**, Kao JH. Pegylated interferons for the treatment of chronic hepatitis B. *Recent Pat Antiinfect Drug Discov* 2006; **1**: 85-94 [PMID: 18221137]

3 **Leemans W**, Janssen HL, de Man R. Future prospectives for the management of chronic hepatitis B. *World J Gastroenterol* 2007; **13**: 2554-2567 [PMID: 17552002]

4 **Kao JH**. Role of viral factors in the natural course and therapy of chronic hepatitis B. *Hepatol Int* 2007; **1**: 415-430 [PMID: 19669337 DOI: 10.1007/s12072-007-9033-2]

5 **Wong GL**, Chan HL. Predictors of treatment response in chronic hepatitis B. *Drugs* 2009; **69**: 2167-2177 [PMID: 19852523 DOI: 10.2165/11319850-000000000-00000]

6 **Buster EH**, Hansen BE, Lau GK, Piratvisuth T, Zeuzem S, Steyerberg EW, Janssen HL. Factors that predict response of patients with hepatitis B e antigen-positive chronic hepatitis B to peginterferon-alfa. *Gastroenterology* 2009; **137**: 2002-2009 [PMID: 19737568 DOI: 10.1053/j.gastro.2009.08.061]

7 **Bonino F**, Marcellin P, Lau GK, Hadziyannis S, Jin R, Piratvisuth T, Germanidis G, Yurdaydin C, Diago M, Gurel S, Lai MY, Brunetto MR, Farci P, Popescu M, McCloud P. Predicting response to peginterferon alpha-2a, lamivudine and the two combined for HBeAg-negative chronic hepatitis B. *Gut* 2007; **56**: 699-705 [PMID: 17127704 DOI: 10.1136/gut.2005.089722]

8 **Huang YX**, Ma LN, Chen XY, Li Z, Huang YL, Shen CL, Ma B. Genetic polymorphisms of MxA protein and eIF-2a-reg2 and their responses to interferon treatment in patients with chronic hepatitis B. *Zhonghua Ganzangbing Zazhi* 2007; **15**: 187-191 [PMID: 17407708]

9 **Han YN**, Yang JL, Zheng SG, Tang Q, Zhu W. Relationship of human leukocyte antigen class II genes with the susceptibility to hepatitis B virus infection and the response to interferon in HBV-infected patients. *World J Gastroenterol* 2005; **11**: 5721-5724 [PMID: 16237774]

10 **Wu JF**, Wu TC, Chen CH, Ni YH, Chen HL, Hsu HY, Chang MH. Serum levels of interleukin-10 and interleukin-12 predict early, spontaneous hepatitis B virus e antigen seroconversion. *Gastroenterology* 2010; **138**: 165-72.e1-3 [PMID:

19782084 DOI: 10.1053/j.gastro.2009.09.018]
11 **Steel LF**, Shumpert D, Trotter M, Seeholzer SH, Evans AA, London WT, Dwek R, Block TM. A strategy for the comparative analysis of serum proteomes for the discovery of biomarkers for hepatocellular carcinoma. *Proteomics* 2003; **3**: 601-609 [PMID: 12748940 DOI: 10.1002/pmic.200300399]
12 **Feng JT**, Liu YK, Song HY, Dai Z, Qin LX, Almofti MR, Fang CY, Lu HJ, Yang PY, Tang ZY. Heat-shock protein 27: a potential biomarker for hepatocellular carcinoma identified by serum proteome analysis. *Proteomics* 2005; **5**: 4581-4588 [PMID: 16240287 DOI: 10.1002/pmic.200401309]
13 **Yang MH**, Tyan YC, Jong SB, Huang YF, Liao PC, Wang MC. Identification of human hepatocellular carcinoma-related proteins by proteomic approaches. *Anal Bioanal Chem* 2007; **388**: 637-643 [PMID: 17447055 DOI: 10.1007/s00216-007-1263-6]
14 **He QY**, Lau GK, Zhou Y, Yuen ST, Lin MC, Kung HF, Chiu JF. Serum biomarkers of hepatitis B virus infected liver inflammation: a proteomic study. *Proteomics* 2003; **3**: 666-674 [PMID: 12748946 DOI: 10.1002/pmic.200300394]
15 **Marrocco C**, Rinalducci S, Mohamadkhani A, D'Amici GM, Zolla L. Plasma gelsolin protein: a candidate biomarker for hepatitis B-associated liver cirrhosis identified by proteomic approach. *Blood Transfus* 2010; **8** Suppl 3: s105-s112 [PMID: 20606740 DOI: 10.2450/2010.017S]
16 **Paradis V**, Asselah T, Dargere D, Ripault MP, Martinot M, Boyer N, Valla D, Marcellin P, Bedossa P. Serum proteome to predict virologic response in patients with hepatitis C treated by pegylated interferon plus ribavirin. *Gastroenterology* 2006; **130**: 2189-2197 [PMID: 16762639 DOI: 10.1053/j.gastro.2006.02.059]
17 **Ma H**, Wang J, Guo F, Wei L. α-2-HS-glycoprotein is a potential marker predicting hepatitis B e antigen seroconversion in patients with chronic hepatitis B during treatment with pegylated interferon alpha-2b. *Sci China Life Sci* 2011; **54**: 39-47 [PMID: 21253869 DOI: 10.1007/s11427-010-4111-4]
18 **Tangkijvanich P**, Komolmit P, Mahachai V, Sa-nguanmoo P, Theamboonlers A, Poovorawan Y. Low pretreatment serum HBsAg level and viral mutations as predictors of response to PEG-interferon alpha-2b therapy in chronic hepatitis B. *J Clin Virol* 2009; **46**: 117-123 [PMID: 19651540 DOI: 10.1016/j.jcv.2009.07.005]
19 **Bradford MM**. A rapid and sensitive method for the quantitation of microgram quantities of protein utilizing the principle of protein-dye binding. *Anal Biochem* 1976; **72**: 248-254 [PMID: 942051]
20 **Candiano G**, Bruschi M, Musante L, Santucci L, Ghiggeri GM, Carnemolla B, Orecchia P, Zardi L, Righetti PG. Blue silver: a very sensitive colloidal Coomassie G-250 staining for proteome analysis. *Electrophoresis* 2004; **25**: 1327-1333 [PMID: 15174055 DOI: 10.1002/elps.200305844]
21 **Katayama H**, Nagasu T, Oda Y. Improvement of in-gel digestion protocol for peptide mass fingerprinting by matrix-assisted laser desorption/ionization time-of-flight mass spectrometry. *Rapid Commun Mass Spectrom* 2001; **15**: 1416-1421 [PMID: 11507753]
22 **Rengarajan K**, de Smet MD, Wiggert B. Removal of albumin from multiple human serum samples. *Biotechniques* 1996; **20**: 30-32 [PMID: 8770400]
23 **Lu Y**, Liu J, Lin C, Wang H, Jiang Y, Wang J, Yang P, He F. Peroxiredoxin 2: a potential biomarker for early diagnosis of hepatitis B virus related liver fibrosis identified by proteomic analysis of the plasma. *BMC Gastroenterol* 2010; **10**: 115 [PMID: 20939925 DOI: 10.1186/1471-230X-10-115]
24 **Echan LA**, Tang HY, Ali-Khan N, Lee K, Speicher DW. Depletion of multiple high-abundance proteins improves protein profiling capacities of human serum and plasma. *Proteomics* 2005; **5**: 3292-3303 [PMID: 16052620 DOI: 10.1002/pmic.200401228]
25 **Dziegielewska KM**, Møllgård K, Reynolds ML, Saunders NR. A fetuin-related glycoprotein (alpha 2HS) in human embryonic and fetal development. *Cell Tissue Res* 1987; **248**: 33-41 [PMID: 3552239]
26 **Yilmaz Y**, Yonal O, Kurt R, Ari F, Oral AY, Celikel CA, Korkmaz S, Ulukaya E, Ozdogan O, Imeryuz N, Avsar E, Kalayci C. Serum fetuin A/α2HS-glycoprotein levels in patients with non-alcoholic fatty liver disease: relation with liver fibrosis. *Ann Clin Biochem* 2010; **47**: 549-553 [PMID: 20926473 DOI: 10.1258/acb.2010.010169]
27 **Kalabay L**, Gráf L, Vörös K, Jakab L, Benko Z, Telegdy L, Fekete B, Prohászka Z, Füst G. Human serum fetuin A/alpha2HS-glycoprotein level is associated with long-term survival in patients with alcoholic liver cirrhosis, comparison with the Child-Pugh and MELD scores. *BMC Gastroenterol* 2007; **7**: 15 [PMID: 17394649 DOI: 10.1186/1471-230X-7-15]
28 **Kalabay L**, Jakab L, Prohászka Z, Füst G, Benkö Z, Telegdy L, Lörincz Z, Závodszky P, Arnaud P, Fekete B. Human fetuin/alpha2HS-glycoprotein level as a novel indicator of liver cell function and short-term mortality in patients with liver cirrhosis and liver cancer. *Eur J Gastroenterol Hepatol* 2002; **14**: 389-394 [PMID: 11943951]
29 **Sari I**, Kebapcilar L, Taylan A, Bilgir O, Kozaci DL, Yildiz Y, Yuksel A, Gunay N, Akkoc N. Fetuin-A and interleukin-18 levels in ankylosing spondylitis. *Int J Rheum Dis* 2010; **13**: 75-81 [PMID: 20374388 DOI: 10.1111/j.1756-185X.2009.01448.x]
30 **Ix JH**, Sharma K. Mechanisms linking obesity, chronic kidney disease, and fatty liver disease: the roles of fetuin-A, adiponectin, and AMPK. *J Am Soc Nephrol* 2010; **21**: 406-412 [PMID: 20150538 DOI: 10.1681/ASN.2009080820]
31 **Dai XH**, Zhang P, Xiao MF, Zhou RR, Zhang BX, Hu GS, Huang ZB, Fan XG. Protective Role of α2HS-Glycoprotein in HBV-Associated Liver Failure. *Int J Mol Sci* 2011; **12**: 3846-3856 [PMID: 21747711 DOI: 10.3390/ijms12063846]
32 **Patel K**, Lucas JE, Thompson JW, Dubois LG, Tillmann HL, Thompson AJ, Uzarski D, Califf RM, Moseley MA, Ginsburg GS, McHutchison JG, McCarthy JJ. High predictive accuracy of an unbiased proteomic profile for sustained virologic response in chronic hepatitis C patients. *Hepatology* 2011; **53**: 1809-1818 [PMID: 21381069 DOI: 10.1002/hep.24284]
33 **Qin X**, Gao B. The complement system in liver diseases. *Cell Mol Immunol* 2006; **3**: 333-340 [PMID: 17092430]
34 **Qin X**, Krumrei N, Grubissich L, Dobarro M, Aktas H, Perez G, Halperin JA. Deficiency of the mouse complement regulatory protein mCd59b results in spontaneous hemolytic anemia with platelet activation and progressive male infertility. *Immunity* 2003; **18**: 217-227 [PMID: 12594949]

P- Reviewer Genaro MSD **S- Editor** Huang XZ
L- Editor Webster JR **E- Editor** Li JY

百世登
Baishideng®

Published by **Baishideng Publishing Group Co., Limited**
Flat C, 23/F., Lucky Plaza,
315-321 Lockhart Road, Wan Chai, Hong Kong, China
Fax: +852-65557188
Telephone: +852-31779906
E-mail: bpgoffice@wjgnet.com
http://www.wjgnet.com



ISSN 1007-9327
9 771007 932045 31>

© 2013 Baishideng. All rights reserved.

Lai KN, Tang SCW (eds): Diabetes and the Kidney.
Contrib Nephrol. Basel, Karger, 2011, vol 170, pp 172–183

Study of Diabetic Nephropathy in the Proteomic Era

Visith Thongboonkerd

Medical Proteomics Unit, Office for Research and Development, Faculty of Medicine Siriraj Hospital, and Center for Research in Complex Systems Science, Mahidol University, Bangkok, Thailand

Abstract

Diabetic nephropathy (DN) remains a major complication of diabetes leading to end-stage renal disease (ESRD). The number of diabetic patients with ESRD who require renal replacement therapy has been increasing, implicating unsuccessful prevention of diabetic renal complication. This unfavorable outcome reflects insufficient knowledge on pathogenic mechanisms of DN and its detection at late stage. Currently, microalbuminuria is used for diagnosis of DN. However, some patients with microalbuminuria have advanced renal pathological changes indicating that microalbuminuria is not the perfect marker for early detection of DN and a better biomarker is urgently needed. Recently, particularly after the completion of the Human Genome Project, proteomics (systematic analysis of proteins for their identity, quantity and function) has been recognized as an emerging subdiscipline of modern sciences. During the past decade, proteomics has been widely applied to several areas of biomedical research, including the investigation of DN. This chapter summarizes recent progress of proteomics applied to DN with ultimate goals to better understand its pathogenic mechanisms and to search for novel biomarkers for earlier diagnosis.
Copyright © 2011 S. Karger AG, Basel

Despite appropriate treatment, diabetic nephropathy (DN) remains a major complication in diabetic patients and is the leading cause of end-stage renal disease. This unfavorable outcome is most likely due to two main factors. First, the complexity of pathogenic mechanisms of DN is not well understood. Although several previous studies have been conducted to understand this diabetic renal complication, many pieces of the jigsaw of the entire image of its pathogenic mechanisms are still missing. It is not surprising that the prevention of this important diabetic complication is not so successful when this image remains

hazy. Therefore, better understanding of its pathogenesis and pathophysiology is crucial. Second, detection of DN is problematic. Currently, microalbuminuria is the best noninvasive marker available for the diagnosis of DN [1]. However, many patients, who were normoalbuminuric and just recently had positive test for microalbuminuria, have advanced renal histopathological changes [2–4], indicating that microalbuminuria is not the perfect marker for early detection of DN. This may be due to a limitation to measure urinary albumin by conventional laboratory method, which is based on an immunoassay that can detect only the immunoreactive forms of albumin, whereas other forms of albumin remain undetectable. Recently, Candiano et al. [5] reported that there are at least 63 forms or fragments of albumin observed in the urine. To be able to detect all forms of albumin and to search for better biomarkers for earlier diagnosis of DN, an unbiased method that can simultaneously detect all forms of proteins is crucially required.

In the postgenomic era, with the completion of the Human Genome Project, several biotechnologies have been developed to utilize the flooding genomic information to explain biology, (patho)physiology, and pathogenic mechanisms of diseases. One of these postgenomic biotechnologies is proteomics (systematic analysis of proteins for their identity, quantity and function [6]), which emerged after the term 'proteome' (set of proteins encoded by the genome) was coined by Marc Wilkins in 1994 [7]. With the success of protein separation science and mass spectrometry, proteomics can be used for simultaneous analyses of a large number of proteins on the genomic scale. Because proteomics can be used for high-throughput screening of proteins that may be involved in biological phenomena and disease pathogenic mechanisms without any need for their specific antibodies, proteomics is considered as an ideal method to examine both immunoreactive and immunounreactive forms of albumin, as well as other proteins in the urine. In addition, this unbiased method is also useful for biomarker discovery and identification of new therapeutic targets. During the past decade, proteomics has been widely applied to several areas of biomedical research, including the investigation of DN. This chapter summarizes recent progress of proteomics applied to DN with ultimate goals to better understand its pathogenic mechanisms and to search for novel biomarkers for earlier diagnosis.

Brief Overview of Proteomic Technologies: Advantages/Disadvantages of Each Technology

The challenge in proteome analysis is that it involves the complex mixture of proteins, of which physicochemical properties vary and some components are low-abundant proteins. An ideal analytical technique used for proteome analysis should have high resolution, high sensitivity, and high throughput capabilities of protein separation and identification. In the postgenomic biomedical

Table 1. Advantages and disadvantages of various proteomic methodologies

Method	Advantages	Disadvantages
2-DE	available in most of proteomic labs, simple to perform, practical for quantitative analysis of multiple samples	time-consuming, no automation, not applicable for polypeptides/proteins with molecular masses <10 or >200 kDa, limited use for highly hydrophobic proteins
LC-MS/MS	automation, multidimensional, high sensitivity	time-consuming, quantitative analysis is not simple, too sensitive towards interfering compounds
SELDI-TOF MS	easy to use, high throughput, automation, low sample volume required	restricted to selected proteins, low-resolution mass spectrometry, low information content, reproducibility is still problematic, difficult to identify proteins/peptides from SELDI spectra
CE-MS	automation, high sensitivity, multidimensional, low sample volume required	not applicable for proteins with molecular masses >20 kDa, difficult to identify proteins/peptides from CE-MS data
Microarrays	ideal approach, high-throughput, capable of examining low molecular weight and low abundant proteins/peptides	currently does not cover all urinary proteins, conservation of protein functionality during immobilization
Microfluidic technology on a chip	easy to use, automation, high sensitivity, low sample volume required	subsequent identification of the resolved proteins is still limited

research, commonly used proteomic technologies include two-dimensional gel electrophoresis (2-DE), liquid chromatography coupled with tandem mass spectrometry (LC-MS/MS), surface-enhanced laser desorption/ionization time-of-flight mass spectrometry (SELDI-TOF MS), capillary electrophoresis coupled with mass spectrometry (CE-MS), protein microarrays, and microfluidic technology on a chip. Each of these technologies has its own advantages and disadvantages (table 1). Two-dimensional gel electrophoresis is available in most of proteomic laboratories, is simple to perform, and is practical for quantitative analysis of multiple samples. However, it is time-consuming, not applicable for proteins/peptides with molecular masses <10 or >200 kDa, and its utility for highly hydrophobic proteins is still limited [8, 9]. Liquid chromatography coupled with tandem mass spectrometry can be automated with a high sensitivity. However, it is time-consuming and too sensitive for interfering compounds [8, 9]. Moreover, quantitative analysis using LC-MS/MS is not simple and may not

be applicable in a large sample size. Surface-enhanced laser desorption/ionization time-of-flight mass spectrometry is an easy-to-use system with an automation and high-throughput manner. Only a small volume, such as <10 μl, of urine sample is analyzable by SELDI-TOF MS. However, the information obtained from SELDI-TOF MS is restricted only to a particular group of proteins and its reproducibility is still an issue of concern [8, 9]. Moreover, identification of proteins/peptides from SELDI spectra is not easy. Capillary electrophoresis coupled with mass spectrometry is another sensitive system with a high-throughput mode that requires a small volume of urine sample. However, it is not suitable for analysis of proteins with molecular masses >20 kDa [8, 9]. Similar to SELDI-TOF MS, identification of proteins/peptides from CE-MS spectra is not easy. Microarray technology is one of the ideal methods for urinary proteome profiling [10]. This approach allows the high-throughput profiling of multiple proteins in urine samples and offers an opportunity to discover low molecular weight and low abundant biomarkers that may be missed by other (more commonly used) techniques [11]. However, its applications are handicapped by the difficulty to make the arrays to cover all urinary proteins and by the limited availability of antibodies or other ligands [11]. Other limitations include the conservation of protein functionality during immobilization as well as the provision of the required absolute and relative sensitivity [11]. Microfluidic technology on a chip is the latest technology applied to urinary proteome profiling [12]. It is also an easy-to-use system with automation and high throughput. Only 4 μl of urine sample is required for analysis by microfluidic technology on a chip. However, the identification of the resolved proteins is still problematic, as in the case of SELDI-TOF MS and CE-MS (table 1).

Proteomic Analysis of Diabetic Nephropathy

A PubMed search using the keywords 'proteomics' or 'proteomic' or 'proteome' together with 'diabetic nephropathy' retrieved 86 articles published between 2002 and 2010 (fig. 1). This number underscores the great potential of proteomics in the investigation of DN. The following sections summarize some of these recent studies.

Better Understanding of Pathophysiology/Pathogenic Mechanisms of Diabetic Nephropathy by Proteomics Approach

The most commonly used proteomic technique applied to DN is 2-DE, which separates proteins by differential pH in the first dimension and by differential molecular masses in the second dimension. After spot matching and comparative intensity analysis, spots of interest (differentially expressed spots) are excised and subjected to in-gel tryptic digestion and identification by mass spectrometry (mainly matrix-assisted laser desorption/ionization time-of-flight mass

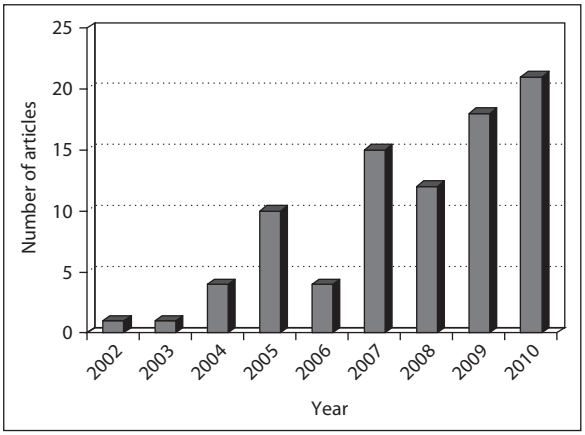


Fig. 1. Number of published articles related to proteomic analysis of DN.

spectrometry or MALDI-TOF MS followed by peptide mass fingerprinting for gel-based proteomic analysis). Thongboonkerd et al. [13] applied a gel-based proteomics approach to examine changes in the renal proteome of OVE26 murine model of type 1 diabetes and observed changes in renal tissue levels of 41 proteins. From these expression data, they focused their attention on the coordinated changes in elastin-elastase pathway. Elastase inhibitor was increased, whereas elastase was decreased. These investigators therefore hypothesized that elastin, which is highly hydrophobic extracellular matrix protein and could not be identified by 2-DE (because of its high hydrophobicity), should be accumulated in diabetic kidney [13]. They then performed immunohistochemical study confirming the hypothesis in both murine and human diabetic kidneys. Elastin was increased in the juxtaglomerular apparatus and renal tubules in the diabetic kidney. This is a good example to demonstrate that proteomics can be used to generate a new hypothesis, which can be confirmed by a conventional method [13].

The same laboratory also identified an increased level of renal calbindin-D28k, which is a vitamin-D-dependent calcium-binding protein, in OVE26 diabetic kidney [14]. The increased level of renal calbindin-D28k was confirmed by Western blot analysis. Immunohistochemistry revealed the increase in renal calbindin-D28k predominately in the distal nephron, implicating its role in tubular reabsorption of calcium during DN. These investigators also extended their study to type 2 diabetes using the *db*/*db* murine model, and found 39 altered renal proteins in this model [15]. Comparing changes identified in both type 1 and type 2 models, it was observed that some proteins had similar changes in both models, which might simply reflect hypoglycemic effects, whereas some other changes were unique in either type 1 or type 2 model, which might be the effects of hypoinsulinemia or hyperinsulinemia

(insulin resistance). Some proteins had contradictory changes, which might be due to several factors (table 2).

Recently, several other groups also applied gel-based proteomics to DN. Tilton et al. [16] examined changes in renal cortical proteome in *db/db* mice and found alterations in the levels of 147 proteins. These altered proteins play significant roles in several biological processes, particularly in metabolic pathways. The investigators also created an interaction map of all the altered proteins, demonstrating that peroxisome proliferator-activated receptor-α was the common node of these protein-protein interactions. Another study by Ramachandra et al. [17] examined changes in membrane and cytosolic subproteomes in human mesangial cells under high-glucose condition. Four proteins were identified as altered proteins in the membrane fraction, whereas five altered proteins were identified in the cytosolic fraction. Among these altered proteins, calmodulin was identified as one of the increased proteins in the cytosolic fraction. Immunostaining confirmed the increase in calmodulin in mesangial cells exposed to high-glucose environment. Moreover, Western blot analysis confirmed the increase in calmodulin not only in high-glucose-exposed mesangial cells but also in rat and mouse diabetic kidney tissues. To address functional significance of calmodulin in diabetic kidney, these investigators examined effect of calmodulin inhibition on glucose uptake in mesangial cells. Functional analysis revealed that inhibition of calmodulin activity by two compounds, W7 and trifluoperazine, completely abolished transforming growth factor-β-induced glucose uptake in mesangial cells. These data indicate that calmodulin plays significant role in glucose transport in mesangial cells [17]. More recently, a similar study was performed by Li et al. [18] to identify changes in cellular proteome of rat mesangial cells upon exposure to high-glucose culture medium. Using 2-DE followed by MALDI-TOF MS, the investigators identified 28 proteins with altered levels in high-glucose condition. Among these, the reduction in proteasome subunit-α type 6 was confirmed not only in rat mesangial cells under the high-glucose condition, but also in streptozotocin-induced diabetic rats and spontaneous OLETF diabetic rat model.

Biomarker Discovery in Diabetic Nephropathy Using Proteomics Approach

An attempt to find urinary biomarkers for DN (and other glomerular diseases such as focal segmental glomerulosclerosis, lupus nephritis class IV, and membranous nephropathy) was made by Varghese et al. [19]. They found no single biomarker could differentiate type or cause of glomerular diseases. However, they used an artificial neural network to create a prediction algorithm and to define disease-specific urinary proteome profile or molecular signature containing multiple markers that could differentiate types of the diseases. They successfully defined such molecular signature containing 21 proteins, which provided a sensitivity of 75–86% and a specificity of 67–92% for the differentiation in a validation set of samples.

Table 2. Comparisons of changes in renal proteome between type 1 and type 2 diabetes

Altered renal proteins	Changes in renal tissue		Hypothesis
	type 1	type 2	
Antithrombin-III	increased	increased	hyperglycemic effects
Calbindin	increased	increased	
Calmodulin	increased	increased	
Complement component 1, q subcomponent-binding protein	increased	increased	
Myosin, light chain, smooth muscle	increased	increased	
Elastase inhibitor	increased	increased	
T-kininogen	increased	increased	
Apolipoprotein A-IV precursor	increased	unchanged	hypoinsulinemic effects
Cellular retinol-binding protein	increased	unchanged	
Contraception-associated protein 1	increased	unchanged	
Crocalbin-like protein	increased	unchanged	
Cytoskeletal tropomyosin	increased	unchanged	
Deoxyribonuclease I	increased	unchanged	
Elastase	decreased	unchanged	
Ferritin heavy chain	increased	unchanged	
Ferritin heavy chain	increased	unchanged	
Hippocampal cholinergic neurostimulating peptide precursor	increased	unchanged	
Histone H3.2	increased	unchanged	
HSPC207	increased	unchanged	
Na-H exchanger, isoform 3 regulator 1	increased	unchanged	
Skeletal muscle tropomyosin	increased	unchanged	
Vimentin	increased	unchanged	
A1AT	unchanged	decreased	hyperinsulinemic effects (or effects from insulin resistance)
Antithrombin-III	unchanged	increased	
Antithrombin-III	unchanged	increased	
Antithrombin-III	unchanged	increased	
Antithrombin-III	unchanged	increased	
ATP synthase delta chain, mitochondrial precursor	unchanged	increased	
Nucleobindin	unchanged	decreased	
Serine protease inhibitor 1-1	unchanged	decreased	
Ferritin light chain 1	increased	decreased	multifactorial
Phosphatidylethanolamine-binding protein	decreased	increased	

Biomarkers were also searched in serum using gel-based proteomics approach. Kim et al. [20] compared serum proteome profile of type 2 diabetic patients with microalbuminuria or end-stage renal disease to normoalbuminuric patients. They found changes in serum levels of 26 proteins in the two groups with renal involvement compared to normoalbuminuric patients. Some of the changes were confirmed by Western blot analysis, e.g. the decrease in extracellular glutathione peroxidase and apolipoprotein E. They also verified their results in a larger, independent set of samples, which clearly confirmed the decrease in glutathione peroxidase in diabetic patients with renal involvement.

Sharma et al. [21] applied gel-based proteomics to DN, but with another technique, the so-called difference in-gel electrophoresis, to find differentially excreted proteins in the urine. Basically, two groups of samples labeled with different dyes were run together within the same gel to avoid gel-to-gel variability. Using this technique, they identified 63 differentially excreted proteins in the urine of patients with long-standing diabetes, impaired renal function and overt proteinuria compared to the controls. One of these differentially excreted proteins was identified by mass spectrometry as α_1-antitrypsin (A1AT). ELISA clearly confirmed the marked increase in A1AT in the urine obtained from diabetic patients. Moreover, immunohistochemical study also revealed the increased tissue expression of A1AT in the diabetic kidney.

Subsequent difference in-gel electrophoresis study by Rao et al. [22] compared the normal urine with that obtained from type 2 diabetic patients with normoalbuminuria, microalbuminuria and macroalbuminuria. Using this technique, they successfully identified several proteins, which had differential levels among the four groups. Interestingly, they found a group of proteins with progressive changes in association with the degree of proteinuria. Surprisingly, they observed the decrease in urinary A1AT in diabetic patients, in contrast to the findings reported by Sharma et al. [21] as discussed above. As A1AT has multiple forms or fragments in the urine, these disparate results might reflect differential forms detected in these two studies.

Capillary electrophoresis coupled with mass spectrometry is another powerful tool for proteome profiling. The system contains capillary loops and electrospray ionization-TOF mass spectrometer. The specific software is used for analyzing the peptide signals and profiles. CE-MS was utilized by Meier et al. [23] to differentiate urinary polypeptide profiles of patients with type 1 diabetes from those of age-matched healthy controls. The analysis revealed that urinary polypeptide pattern of patients with diabetes significantly differed from that of the normal controls. They also performed subgroup analysis and found a pattern of potential biomarkers that could differentiate patients with DN from those without nephropathy. The same group also employed CE-MS to differentiate urinary polypeptide profiles of patients with type 2 diabetes from those of age-matched healthy controls [24]. In the latter study, they also observed specific urinary polypeptide profile for each subgroup based upon the degree of albuminuria.

Surface-enhanced laser desorption/ionization time-of-flight mass spectrometry or ProteinChip technology is widely used for examination of human body fluids. Protein sample is applied onto a chip surface carrying a functional group. After incubation, proteins that do not bind to the surface are removed, and the bound polypeptides or proteins are analyzed by TOF mass spectrometer. Recently, Cho et al. [25] utilized SELDI-TOF MS to search for potential biomarkers in the sera of streptozotocin-induced diabetic rats compared to control animals. They observed eight potential biomarkers in the serum, one of which was identified as C-reactive protein. The increased serum level of C-reactive protein was confirmed by ELISA.

In another study, Dihazi et al. [26] performed SELDI proteome profiling of urine samples obtained from type 2 diabetic patients with nephropathy, compared to those without nephropathy, proteinuric patients from nondiabetic causes, and healthy controls. They identified three protein spectra with mass/charge (or m/z) of 6,188, 11,744, and 14,766 that were differentially excreted among groups. Interestingly, these three spectra could differentiate diabetic patients with nephropathy from those without nephropathy. Subsequently, these SELDI spectra were identified by mass spectrometry as ubiquitin, β_2-microglobulin, and UbA52 ubiquitin ribosomal fusion protein, respectively. Therefore, these proteins may serve as potential biomarkers for the diagnosis of DN. These data were consistent with the findings reported in a subsequent similar study by Papale et al. [27], in which ubiquitin and β_2-microglobulin were identified as potential biomarkers of DN after initial SELDI profiling in a larger number of type 2 diabetic patients.

Additionally, Otu et al. [28] conducted a SELDI study of baseline urine samples collected from Pima Indians with type 2 diabetes 10 years before microalbuminuria occurred. A comparison with those who remained normoalbuminuric after 10 years in the first sample collection, revealed a molecular signature containing 12 SELDI spectra that could differentiate patients who subsequently developed DN from those who remained normoalbuminuric. This is a good work that yielded significant data to predict DN in a long-term follow-up study.

The recent advanced technology applied to urinary proteomics is a microfluidic technology on a chip [29]. Only 4 μl of the untreated urine could be analyzed by this system. Thongboonkerd et al. [29] employed this system to define disease-specific urinary biomarkers for DN and IgA nephropathy. By multiple comparisons, there were significant differences between the normal and diseased urine, and between DN and IgA nephropathy. There were three protein spectra or bands at approximately 12–15, 27–28 and 34–35 kDa that could distinguish DN from IgA nephropathy. Therefore, these differences may serve as the disease-specific biomarkers.

More recently, Merchant et al. [30] differentiated peptidome profiles of patients with type 1 diabetes with microalbuminuria who had normal renal function from those of patients who had declined renal function. Using LC-

MALDI-TOF MS profiling, they identified three peptides that were decreased [including fragments of collagen α_1(IV) and α_1(V) and tenascin-X] and three peptides that were increased (fragments of inositol polyphosphate 2-kinase, zona occludens 3, and FAT tumor suppressor 2) in the urine of patients with declined renal function. Immunohistochemical study also revealed the increased expression levels of tissue polyphosphate 2-kinase and zona occludens 3, consistent with the urinary peptidome data. These peptides may serve as the predictors of DN progression.

Conclusion

Since 2002, proteomics has played a significant role in the study of DN to address its pathophysiology/pathogenic mechanisms and to search for novel biomarkers for its earlier diagnosis. From these proteomic studies, several datasets have been reported to better understand pathophysiology/pathogenic mechanisms of DN, and a large number of biomarker candidates for diagnosis and prediction of DN have been identified. However, the information obtained from these studies remains on bench and is currently not closed to clinical application. To achieve the ultimate goal of clinical application, validation of the proteomic data in a larger sample size with appropriate control groups (i.e. other kidney diseases with similar clinical presentations and laboratory findings that mimic DN) is crucial. Although an attempt has been made in Europe to validate proteomic biomarkers in the urine of patients with DN, this multicenter study [31] limited its scope only to CE-MS data. There should be broader application of the data generated by other proteomic technologies as well. More importantly, translation of all these data to the ready and easy-to-use diagnostic kit(s) is needed. Even with some degree of progression in proteomics applied to DN, the total number of 86 articles published during 2002–2010 is much fewer than anticipated. Urgent attention is required to promote proteomic investigations of DN. It is envisaged that within the next 5–10 years proteomics will be more extensively applied to DN to unravel the complexity of its pathophysiology/pathogenic mechanisms and to define novel biomarkers for more accurate and earlier diagnosis as well as prognosis of DN. Thereafter, bedside application of proteomic data to diabetic patients will be achievable.

Acknowledgements

This work was supported by Office of the Higher Education Commission and Mahidol University under the National Research Universities Initiative, and The Thailand Research Fund (RTA5380005).

References

1 Caramori ML, Fioretto P, Mauer M: The need for early predictors of diabetic nephropathy risk: is albumin excretion rate sufficient? Diabetes 2000;49:1399–1408.

2 Chavers BM, Bilous RW, Ellis EN, Steffes MW, Mauer SM: Glomerular lesions and urinary albumin excretion in type I diabetes without overt proteinuria. N Engl J Med 1989;320:966–970.

3 Fioretto P, Steffes MW, Mauer M: Glomerular structure in nonproteinuric IDDM patients with various levels of albuminuria. Diabetes 1994;43:1358–1364.

4 Bangstad HJ, Osterby R, Dahl-Jorgensen K, Berg KJ, Hartmann A, Nyberg G, Frahm BS, Hanssen KF: Early glomerulopathy is present in young, type 1 (insulin-dependent) diabetic patients with microalbuminuria. Diabetologia 1993;36:523–529.

5 Candiano G, Musante L, Bruschi M, Petretto A, Santucci L, Del Boccio P, Pavone B, Perfumo F, Urbani A, Scolari F, Ghiggeri GM: Repetitive fragmentation products of albumin and alpha1-antitrypsin in glomerular diseases associated with nephrotic syndrome. J Am Soc Nephrol 2006;17:3139–3148.

6 Peng J, Gygi SP: Proteomics: the move to mixtures. J Mass Spectrom 2001;36:1083–1091.

7 Wilkins MR, Sanchez JC, Gooley AA, Appel RD, Humphery-Smith I, Hochstrasser DF, Williams KL: Progress with proteome projects: why all proteins expressed by a genome should be identified and how to do it. Biotechnol Genet Eng Rev 1996;13:19–50.

8 Fliser D, Novak J, Thongboonkerd V, Argiles A, Jankowski V, Girolami MA, Jankowski J, Mischak H: Advances in urinary proteome analysis and biomarker discovery. J Am Soc Nephrol 2007;18:1057–1071.

9 Thongboonkerd V: Recent progress in urinary proteomics. Proteomics Clin Appl 2007;1:780–791.

10 Liu BC, Zhang L, Lv LL, Wang YL, Liu DG, Zhang XL: Application of antibody array technology in the analysis of urinary cytokine profiles in patients with chronic kidney disease. Am J Nephrol 2006;26:483–490.

11 Angenendt P: Progress in protein and antibody microarray technology. Drug Discov Today 2005;10:503–511.

12 Thongboonkerd V, Songtawee N, Sritippayawan S: Urinary proteome profiling using microfluidic technology on a chip. J Proteome Res 2007;6:2011–2018.

13 Thongboonkerd V, Barati MT, McLeish KR, Benarafa C, Remold-O'Donnell E, Zheng S, Rovin BH, Pierce WM, Epstein PN, Klein JB: Alterations in the renal elastin-elastase system in type 1 diabetic nephropathy identified by proteomic analysis. J Am Soc Nephrol 2004;15:650–662.

14 Thongboonkerd V, Zheng S, McLeish KR, Epstein PN, Klein JB: Proteomic identification and immunolocalization of increased renal calbindin-D28k expression in OVE26 diabetic mice. Rev Diab Stud 2005;2:17–24.

15 Thongboonkerd V, Barati MT, McLeish KR, Rovin BH, Pierce WM, Epstein PN, Klein JB: Altered elastase inhibitor and elastin expression in type 2 diabetic kidneys defined by proteomic analysis. J Am Soc Nephrol 2003;14 (suppl):600A.

16 Tilton RG, Haidacher SJ, Lejeune WS, Zhang X, Zhao Y, Kurosky A, Brasier AR, Denner L: Diabetes-induced changes in the renal cortical proteome assessed with two-dimensional gel electrophoresis and mass spectrometry. Proteomics 2007;7:1729–1742.

17 Ramachandra Rao SP, Wassell R, Shaw MA, Sharma K: Profiling of human mesangial cell subproteomes reveals a role for calmodulin in glucose uptake. Am J Physiol Renal Physiol 2007;292:F1182–F1189.

18 Li Z, Zhang H, Dong X, Burczynski FJ, Choy P, Yang F, Liu H, Li P, Gong Y: Proteomic profile of primary isolated rat mesangial cells in high-glucose culture condition and decreased expression of PSMA6 in renal cortex of diabetic rats. Biochem Cell Biol 2010;88:635–648.

19 Varghese SA, Powell TB, Budisavljevic MN, Oates JC, Raymond JR, Almeida JS, Arthur JM: Urine biomarkers predict the cause of glomerular disease. J Am Soc Nephrol 2007;18:913–922.

20 Kim HJ, Cho EH, Yoo JH, Kim PK, Shin JS, Kim MR, Kim CW: Proteome analysis of serum from type 2 diabetics with nephropathy. J Proteome Res 2007;6:735–743.
21 Sharma K, Lee S, Han S, Lee S, Francos B, McCue P, Wassell R, Shaw MA, RamachandraRao SP: Two-dimensional fluorescence difference gel electrophoresis analysis of the urine proteome in human diabetic nephropathy. Proteomics 2005;5:2648–2655.
22 Rao PV, Lu X, Standley M, Pattee P, Neelima G, Girisesh G, Dakshinamurthy KV, Roberts CT Jr, Nagalla SR: Proteomic identification of urinary biomarkers of diabetic nephropathy. Diabetes Care 2007;30:629–637.
23 Meier M, Kaiser T, Herrmann A, Knueppel S, Hillmann M, Koester P, Danne T, Haller H, Fliser D, Mischak H: Identification of urinary protein pattern in type 1 diabetic adolescents with early diabetic nephropathy by a novel combined proteome analysis. J Diabetes Complications 2005;19:223–232.
24 Mischak H, Kaiser T, Walden M, Hillmann M, Wittke S, Herrmann A, Knueppel S, Haller H, Fliser D: Proteomic analysis for the assessment of diabetic renal damage in humans. Clin Sci (Lond) 2004;107:485–495.
25 Cho WC, Yip TT, Chung WS, Leung AW, Cheng CH, Yue KK: Differential expression of proteins in kidney, eye, aorta, and serum of diabetic and non-diabetic rats. J Cell Biochem 2006;99:256–268.
26 Dihazi H, Muller GA, Lindner S, Meyer M, Asif AR, Oellerich M, Strutz F: Characterization of diabetic nephropathy by urinary proteomic analysis: identification of a processed ubiquitin form as a differentially excreted protein in diabetic nephropathy patients. Clin Chem 2007;53:1636–1645.
27 Papale M, Di Paolo S, Magistroni R, Lamacchia O, Di Palma AM, De Mattia A, Rocchetti MT, Furci L, Pasquali S, De Cosmo S, Cignarelli M, Gesualdo L: Urine proteome analysis may allow noninvasive differential diagnosis of diabetic nephropathy. Diabetes Care 2010;33:2409–2415.
28 Otu HH, Can H, Spentzos D, Nelson RG, Hanson RL, Looker HC, Knowler WC, Monroy M, Libermann TA, Karumanchi SA, Thadhani R: Prediction of diabetic nephropathy using urine proteomic profiling 10 years prior to development of nephropathy. Diabetes Care 2007;30:638–643.
29 Thongboonkerd V, Songtawee N, Sritippayawan S: Urinary proteome profiling using microfluidic technology on a chip. J Proteome Res 2007;6:2011–2018.
30 Merchant ML, Perkins BA, Boratyn GM, Ficociello LH, Wilkey DW, Barati MT, Bertram CC, Page GP, Rovin BH, Warram JH, Krolewski AS, Klein JB: Urinary peptidome may predict renal function decline in type 1 diabetes and microalbuminuria. J Am Soc Nephrol 2009;20:2065–2074.
31 Alkhalaf A, Zurbig P, Bakker SJ, Bilo HJ, Cerna M, Fischer C, Fuchs S, Janssen B, Medek K, Mischak H, Roob JM, Rossing K, Rossing P, Rychlik I, Sourij H, Tiran B, Winklhofer-Roob BM, Navis GJ: Multicentric validation of proteomic biomarkers in urine specific for diabetic nephropathy. PLoS One 2010;5:e13421.

Visith Thongboonkerd, MD, FRCPT
Medical Proteomics Unit, Office for Research and Development, Faculty of Medicine Siriraj Hospital, and Center for Research in Complex Systems Science, Mahidol University
12th Floor Adulyadej Vikrom Building, 2 Prannok Road
Bangkoknoi, Bangkok 10700 (Thailand)
Tel./Fax +66 2 4184793, E-Mail thongboonkerd@dr.com